Critical Role of Water to Maintain Protein Stability and Activity in Hydrated Deep Eutectic Solvents and Beyond

A Thesis
Submitted in Partial Fulfillment of the Requirements
for the Degree of

DOCTOR OF PHILOSOPHY

by

TANMOY KHAN

Roll No. 19107312

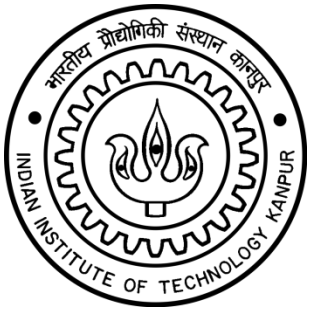

to the

Department of Chemistry
Indian Institute of Technology Kanpur
Kanpur, India

May, 2025

This page left blank intentionally

CERTIFICATE

It is certified that the work reported in the thesis entitled "**Critical Role of Water to Maintain Protein Stability and Activity in Hydrated Deep Eutectic Solvents and Beyond**" has been carried out by **Mr. Tanmoy Khan** under my supervision and has not been submitted elsewhere for a degree.

May 2025
IIT Kanpur

(*Prof. Pratik Sen*)
Thesis Supervisor
Department of Chemistry
Indian Institute of Technology Kanpur
Kanpur, U.P. India- 208016

This page left blank intentionally

DECLARATION

This is to certify that the thesis titled "**Critical Role of Water to Maintain Protein Stability and Activity in Hydrated Deep Eutectic Solvents and Beyond**" has been authored by me. It presents the research conducted by me under the supervision of **Prof. Pratik Sen**.

To the best of my knowledge, it is an original work, both in terms of research content and narrative, and has not been submitted elsewhere, in part or in full, for a degree. Further, due credit has been attributed to the relevant state-of-the-art and collaborations (if any) with appropriate citations and acknowledgements, in line with established norms and practices.

Signature
Name: Tanmoy Khan
Roll No. 19107312
Programme: PhD
Department: Chemistry
Indian Institute of Technology Kanpur
Kanpur 208016

This page left blank intentionally

Department of Chemistry
Indian Institute of Technology Kanpur

Certificate of course work

This is to certify that **Mr. Tanmoy Khan** has satisfactorily completed all the courses required for the Ph.D degree. The courses include:

CHM 629A Principles of Physical Chemistry

CHM 685A Molecule Radiation Interaction

CHM 699A LASER in Chemistry and Biology

CHM 636A Physical Photochemistry

CHM 799 Research

CHM 800A General Seminar

CHM 801A Graduate Seminar

Mr. Tanmoy Khan was admitted to the candidacy of the Ph.D degree in July, 2019 after he successfully completed the written and oral qualifying examinations.

Head
Department of Chemistry
Indian Institute of Technology Kanpur
Kanpur – 208016, India

Convenor, DPGC
Department of Chemistry
Indian Institute of Technology Kanpur
Kanpur – 208016, India

This page left blank intentionally

Dedicated to

Maa and Baba

(মা ও বাবাকে)

This page left blank intentionally

Acknowledgements

At this final stage of my PhD journey, I find that the most difficult and perhaps the most important task is to express my gratitude. In the end, only my name will appear on the cover of this thesis, yet it rests upon the unwavering support of countless individuals without whom this journey would have been unimaginable. Though this thesis marks a defining chapter in my 28 years of life, it is far from the entire story. Einstein once said that both our inner and outer lives are sustained by the contributions of countless others. As I sit down to write these words, memories and faces spanning time and space come flooding back. If I fail to mention anyone, it is a fault of my imperfect memory and the urgency to keep this section concise.

Newton once wrote, "If I have seen further, it is by standing on the shoulders of giants." I borrow his sentiment with humility: the fact that I am submitting this thesis today is something I could scarcely have imagined. Growing up, I never dreamed of becoming a researcher. I never truly believed I could. But there was one person who did — Nilimesh da. I'll come back to him later. But the person who truly sealed that belief, and whose faith, along with Nilimesh da's, carried me this far in academia, is none other than my Sir, my PhD guide, ***Prof. Pratik Sen****.*

I first came to Kanpur during the summer (May-July) of 2018 as an intern. Before I left, Sir told me, "You didn't get the chance to learn all the instruments; come again if you can." And so, I did, returning permanently in 2019, though by then my own ideas about career and life had gone through many shifts. I was still consumed by self-doubt. A few months later, I asked Sir, "Should I even pursue a PhD?" He said, "I have seen many students. You have everything needed to do a PhD — you just need the will." Perhaps it was this small sliver of faith that allowed me to complete the journey. I don't recall a single time I wanted to work on something, and Sir said no. Everyone in the lab will agree that the academic freedom he offered was rare. From the smallest things — plotting a graph — to the intricate details of Solvation Dynamics, from designing a TOC figure to properly representing hydrogen bonds, from the working principle of any random instrument to the details of fluorescence spectroscopy — I have learnt so much from him. He is a great teacher. I never had to hesitate before asking any random questions. And when nothing seemed to be working, I could walk up to him and simply ask for motivation. The environment he built in our lab is a rare treasure. I sincerely thank him from the bottom of my heart and wish the very best to him and his family. This July, I will be completing nearly six long years in Kanpur. It has been a long journey, but it was a happy journey at the same time.

*Coming back now to **Nilimesh da**. Our bond began in May 2018 and has only grown stronger each day since. Everything I have managed to do during my PhD, I have learnt from him. So many times, on so many days, I thought, "This isn't leading anywhere, maybe I should just leave everything and go." The one person who never let me do that, whether through explanation or scolding, was Nilimesh da. From teaching me FCS by holding my hand, showing me how to search papers, read them, write them — grants, paper revisions, designing problems — everything, either he taught me directly or I learnt by watching him. Even today, whatever I write or read, he is my first verifier. But these were just lab matters. He is the true example of what Linus Pauling once said, "If you want to have good ideas, you must have many ideas." Every day over tea or dinner, we discussed and shared our ideas, and almost every day, he would come up with something. It was those brainstorming sessions that made me think about what no one is thinking while observing what everyone is observing.*

Nilimesh isn't just a labmate to me. He is my brother — not by blood, but by life itself. He has become my family. I have discussed every happiness, every sorrow with him, and still do. I have also played an important role in some major decisions in his life. His wife, Shreya di, often says that Nilimesh talks more to me than he does to her! Even now, as I struggle with the fear of applying for postdoc positions, he scolds me at least once a week to push me forward. If I start writing about him, I don't think I will ever be able to stop. He has taught me so much already — and continues to teach — and I have probably absorbed only a tiny fraction. I don't know if these few pages are enough to express just how deeply thankful I am to Sir and to life for giving me such a beautiful gift: a brother for a lifetime.

I must also thank Ejaz da, the co-first author of my first 'first-author' paper. He taught me Solvation Dynamics, the most crucial technique throughout my work. Despite his seniority as a postdoc, he remained the most patient and generous teacher, never allowing his stature to create distance. Beyond science, we wrote songs, discussed poetry, and built memories I will always cherish.

I feel incredibly lucky that I got to work with every single senior in the lab at some point, and there is at least one paper with each of them. But beyond work, the endless chats we had brought me even greater joy. Aritra da, with his love for cricket and football; Shovon da, with endless laughter; Pushpal da, though briefly with us, with shared conversations on music and literature. And I must especially thank Naveen da, he was the first to start work on DES in our lab, and nearly my entire thesis is based on DES systems that he developed. Also, Ishfaq da, another post-doc who

joined just for six months, helped me a lot by synthesizing some fluorophores for protein tagging. I thank him and wish him all the best.

Shreya di and Manjeer di (she stayed for a short time) are the 'didis' I had on this campus. I received a lot of affection from them. Every 'Bhai Phonta', Shreya di would call me early in the morning without fail. Whenever she cooked something, alongside feeding her husband, she would lovingly call me too — I was the other person she insisted on feeding. She is also a meticulous teacher. She patiently tried to teach me protein expression and purification, and whatever little I could learn is entirely to her credit; whatever I could not, the fault lies entirely with me.

When I joined the lab, we were five people who joined together — me, Arghya da, Abhijit, Kuldeep, and Sandeep.

Sandeep and I had worked together even from the summer internship days, later learning FCS side by side. With Kuldeep, after Nilimesh da, I discussed work the most. Every time I struggled with alignments and setups, it was Kuldeep who made my life easier. With him, I spent some good evenings on the badminton court. He is a great friend with a big heart. I wish all the best for him. Abhijit and I joined the lab together — my everyday companion in the lab. We have given our open seminar and submitted our theses around the same time. Through all the phases of academic frustrations, we stood by each other. He remains one of the hardest-working people I have met. Watching his perseverance has been a constant source of inspiration. Arghya da, on the other hand, has always been a figure of deep affection. It's not just the word 'dada' (elder brother), he made me feel the true sense of warmth and care. From pushing me every single day before paper submission to applying for the post-doctoral application now, from sharing late-night lab sessions to countless conversations about life's little details. He is a good listener, and we have shared many moments of both happiness and hardship together. He is one of the most passionate researchers I have met, and that passion is infectious. He always asked me many basic questions and discussed different odd observations from his work, which helped me think beyond my work and helped me strengthen my basics.

Suman joined the lab a year after us, but I never felt he was a junior. He worked on my up-conversion data, for which I owe him heartfelt thanks. Since Abhijit, Suman, and I lived in the same hostel, we ended up doing almost everything together, from coming to the lab, eating meals, playing games, and supporting each other through many personal struggles as well. He is one of the smartest guys in the lab, and I wish he gets the things he deserves.

Recently, two new members, Akash and Harshit, have started working with me. Thanks, and best wishes to them both. Thanks to Dipankar, another dear junior, who helped me in measuring some transient absorption. I need to mention other lab members, Clovis, Subhajit, Patralekha, Bhupendra, and Himanshu. I sincerely apologize to all my lab mates for any hard feelings that may have arisen during my stay.

Bishal was the first MSc student I had the chance to work with. I have rarely seen someone work the way he did. He was truly the kind of student any guide could hope for — anything I asked, he completed it with dedication and precision. He is a wonderful person, and we co-authored three papers together. Later, Soumya and Kuntal joined the lab. After completing their MSc, they stayed an extra year for research. I particularly enjoyed discussing with them and helping them troubleshoot small problems with their data and analysis. Finally, Debojyoti and Swagata — I would like to sincerely thank them as well. Working alongside all these brilliant minds has been an invaluable learning experience for me.

Outside the lab, I must mention some people because it is them who made my life easier. The first would definitely be Aranya. Along with Subhendu, Arnab, Aranya, and our trio (Abhijit, Suman, and I), we enjoyed many cooking sessions together. Special shoutout to all the Saturday nights we spent together. These are the days that will remain with me forever. We have formed a band, "Khaja band", with Arpan (Composer and guitarist), Subhendu (vocalist), Ejaj da (lyricist and vocalist), Suman (vocalist and tech support), Arindam Da (percussion), JD (Ukulele), Manik da (enthusiast leader), and others. The performances and, importantly, the rehearsals are very close to my heart. Apart from them, I would like to thank Subhadip for the precious friendship we share. Hall 8, my hostel, and IIT Kanpur, as well, have given me many close friends, juniors, and seniors like Anjan, Poulami (my sister in the campus), Khoka da, Arindam da, JD, Rajib Da, Manik Da, Panu (Anubrata) da, Nayan da, Soumya, Abir da, Sounak, Soumyadeb, Tamal, Soumya (Roy), Anupam, Sandipan, Saikat da, Payra da, Anubhav, Anindya, Sayantan da, Rajarshi da, and many more. Sincere thanks to all other friends of mine from childhood who are very close to my heart but are not staying in Kanpur. Mansha, Dustu, Dipak, Arindam, Subrata, Mal, Sakshya, Shrutarshi, Sumit, Sankha Das, Arka, Sutanu, Santanu, Pratim, Tamajit, Fadikar, Jeevesh, Bulan, Abhijit Chatterjee, and many more; thank you for existing, it's a bliss to have you all in my life.

This journey would not have been possible without Soumi, the love of my life. Because it was she who had always listened to my frustrations and fears, and

tolerated, motivated me even at the oddest of hours. I first met her just a week before joining IIT Kanpur, and thus, the age of our relationship is as much as my PhD. We have discussed our work, shared each of the moments of joy and loss together, even at a long distance. Whenever I hesitated before doing something, thinking this was not the right time, she was the one who pushed me, saying there would never be the right time until you start. I am grateful to the Almighty for crossing our paths.

I consider myself very lucky as I have encountered many great teachers over time. I have done my higher secondary from Ramakrishna Mission Vidyapith, Purulia. I will be forever grateful to the two pillars of Vidyapith, Shakti da and Swapan da. The time I spent in Narendrapur Ramakrishna Mission Residential College for my B.Sc. has been the highest learning period in my academic journey. I have met many excellent teachers there, AVS Sir, RG Sir, PRG Sir, HKC Sir. I am forever indebted to Naba ka (Nabakumar Bera), because I believe whatever little physical chemistry I have learned in my small life, a large portion is because of him. Another giant of a teacher is Chandan Saha; I am fortunate enough that I have learned a bit of organic chemistry in my B.Sc. from him. His way of teaching and approaching a topic is exceptional, If I could ever become a teacher, I want to follow his style of teaching. All the teachers of my Previous institutions, IIT Hyderabad, Ramakrishna Mission Residential College Narendrapur, Ramakrishna Mission Vidyapith Purulia, Ramharipur Ramakrishna Mission High School, and Harishchandrapur Banshigopal Mahamaya Madhyamik Siksha Kendra, are acknowledged.

I want to take this opportunity to express my gratitude to the unknown reviewers of my papers. It is their questions that helped me learn my work in a better and different way. Many great scientists like Frances Arnold, Ahmed Zewail, Biman Bagchi, Kankan Bhattacharya, etc., whose works inspired me greatly.

I want to thank Kabir Suman and Rabindranath Tagore; without their songs, I could not have written a single line of my paper, a single poem of my sorrow, a single song of life. The works of Satyajit Roy, Narayan Sanyal, Saradindu Bandyopadhyay, Narendranath Mitra, and many others who have written in Bengali -your creations were my refuge. Watching Virat Kohli and Messi taught me to believe in miracles. I am forever grateful to Indian Folk, Indian classical music, and legends like Ustad Zakir Hussain for all the soulful melodies. Thanks to all these great personalities for inspiring millions like me.

I want to take this opportunity to thank all my coursework instructors and chemistry departmental staff for their help. Special thanks to Mr. Somdutta, our departmental CD operator, for running many experiments on my behalf.

*I am grateful to **PMRF** and IIT Kanpur for providing me with the fellowship and infrastructure.*

*Lastly, but most importantly, I want to thank my family, because it is their willpower and hard work that I am standing at this junction of time. The name of my village is Harishchandrapur, a small village in West Bengal, where even today, the mode of travelling is only a cycle or a motorcycle, the connecting bridge to the town has been broken and hanging for more than a year. Forget about a hospital, not a single dispensary is there in the 3-4 villages nearby. I will be the first ever Ph.D. from my village. So, whatever I am and will become is the sacrifice of my mother, **Chintamoni Khan**, and my father, **Manisankar Khan**. It is their dream that I am living in. I want to express my gratitude to my jethu (Gnan Sankar Khan and Siddhartha Sankar Khan) and jethima (Sabitri Khan and Sundari Khan) for their love and care. I want to thank my brother, Shuvo, I love him so much. Thanks to my other cousins, Mejda, Chotda, Rumu di, Banu di, Boumani (Aasmita), and Borda. Thanks to my two little sisters, Khusi and Naisa, for the love they showed me. Thanks to my dadu, dida, masi, meso, mama, suman mama for loving me the way I am. I will be grateful to acknowledge Kaku (Suman Chatterjee) and Kakima (Mousumi Chatterjee) for the love and care they showed me; they are my extended family.*

*Finally, I offer my humble pranams to the Almighty, **Thakur-Maa-Swamiji**, and my guruji, **Late Swami Prabhanandaji Maharaj**.*

Tanmoy Khan

SYNOPSIS

Name of Student:	Tanmoy Khan
Roll No.	19107312
Degree for which submitted:	Ph.D.
Department:	Chemistry
Thesis Title:	**Critical Role of Water to Maintain Protein Stability and Activity in Hydrated Deep Eutectic Solvents and Beyond**
Name of Thesis Supervisor:	Prof. Pratik Sen
Month and year of thesis submission:	May 2025

The thesis is about mechanistic insights into protein behaviour in the deep eutectic solvents (DESs) and crowded media.

Significance of the thesis:

This thesis advances our understanding of protein behavior in complex solvent environments, focusing on deep eutectic solvents (DESs) and crowded media. DESs are emerging as preferred solvents for biocatalysis due to their tunability, low toxicity, simple synthesis, and remarkable ability to stabilize enzymes. However, the mechanisms underlying protein stability and activity in these media remained poorly understood. Starting with a novel non-ionic DES, this work reveals the intrinsic spatial and dynamic heterogeneity of DESs and their role in preserving local microenvironments essential for biomolecular function. By systematically analyzing associated (biological) water dynamics, distinct from bulk solvent effects or conformational changes, this thesis proposes a unifying mechanism considering associated water explaining protein behavior in DESs and other media. For the first time, it is experimentally demonstrated that the modulation of associated water, rather than bulk dynamics, critically governs protein thermal stability and enzymatic activity. This mechanism is validated across different DES systems and a macromolecular crowder (Ficoll-70k), establishing its broader applicability. Moreover, the consistent observation of entropy–enthalpy compensation and its link to hydration dynamics adds a new thermodynamic perspective to protein–solvent interaction studies.

The precision and efficiency of enzymes make biocatalysis an advancing scientific and industrial process. Deep eutectic solvents (DESs) have emerged as promising solvents in this field due to their tunability, non-volatility, low toxicity,

and simple, cost-effective synthesis. Importantly, many enzymes not only retain but also enhance their stability and activity in DESs or hydrated DESs compared to aqueous buffers.

Despite the growing interest and applications of DESs, a critical gap remains: the lack of mechanistic insights into how proteins behave in these complex media and why enzymes remain stable and active therein. Thus, enzyme-DES pair selection in such works largely depends on empirical observations and availability rather than fundamental understanding. To harness the full potential of DESs in biocatalysis, it is crucial to understand what truly governs protein stability and function in these solvents.

From a physical chemistry perspective, research on DESs broadly falls into three categories: (i) synthesis and characterization of the physical properties of DESs and hydrated DESs; (ii) investigations into the structure, dynamics, and molecular-level heterogeneity of DESs; and (iii) studies examining various protein properties such as structure, dynamics, stability, and activity within these media. My approach seeks to integrate these three aspects, aiming to uncover a coherent physical understanding of how enzyme stability and activity are maintained in DES environments.

Central to this exploration is water, the universal biological solvent, which plays an essential role in almost every biophysical process. Particularly, the water molecules that are directly interacting with proteins, known as biological or associated water, exhibits distinct properties from bulk water, such as increased density, lower polarity, and more importantly retarded dynamics. While the importance of associated water in maintaining protein stability and function is axiomatic, how this hydration layer modulates in the presence of DESs remains almost unexplored.

In this thesis, I systematically investigate the dynamics of both associated and bulk water in the presence and absence of enzymes, aiming to delineate the role of water in protein stability and activity within DESs. Using techniques like time-dependent fluorescence Stokes shift (TDFSS), I provide experimental insights into how modulation of associated water dynamics influences protein behavior, laying the

foundation for rational solvent design in biocatalysis. Importantly, by validating these findings across different DESs and macromolecular crowders, this work offers generalized insights that can be applied to understanding protein stability across diverse solvent systems.

1. Multiple evidences for molecular level heterogeneity in a non-ionic biocatalytic deep eutectic solvent

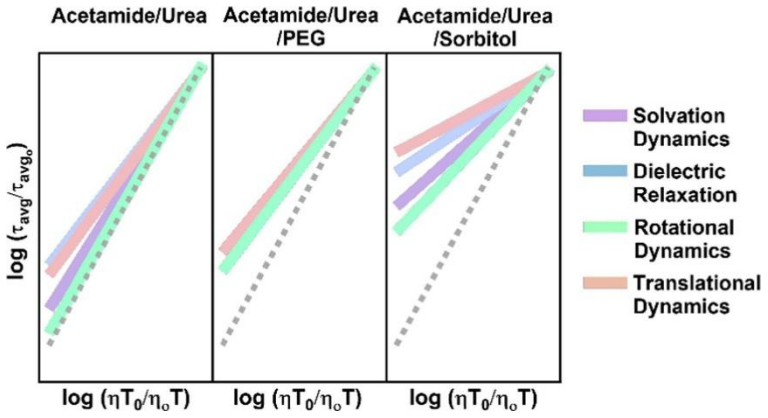

Tanmoy Khan *et al. J. Mol. Liq.* **2023**, 389, 122882

Molecular-level heterogeneity has been identified as an intriguing feature of DESs. In this study, we examine the spatio-temporal heterogeneity of a novel non-ionic DES, acetamide/urea/sorbitol (0.5Ac/0.3Ur/0.2Sor), and the results are compared it with corresponding binary acetamide/urea (0.6Ac/0.4Ur) DES, and another related non-ionic ternary DES (0.55Ac/0.36Ur/0.09PEG). The excitation wavelength-dependent emission measurement suggests an induction of spatial heterogeneity upon sorbitol addition. Dynamic heterogeneity assessed via solvation dynamics, dielectric relaxation, and diffusion studies shows clear length- and timescale dependence, with acetamide/urea/sorbitol exhibiting the highest dynamic heterogeneity. Importantly, the observed viscosity-decoupled dynamics offer insight into how DESs, despite their high viscosity, can still support enzyme stability and activity. Furthermore, component analysis of solvation dynamics reveals an unperturbed immediate solvation shell around the probe. Extending this observation to proteins, where the integrity of the local environment is critical for maintaining

structure and function, suggests that DESs may preserve the hydration shell essential for enzymatic stability and activity.

2. Understanding the intricacy of protein in hydrated deep eutectic solvent: Solvation dynamics, conformational fluctuation dynamics, and stability

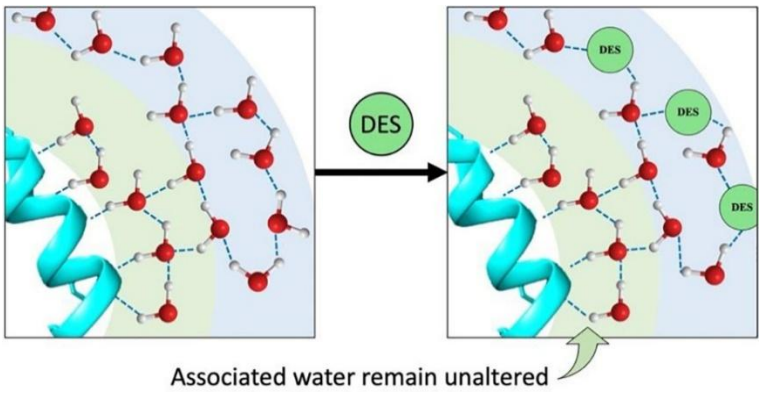

Tanmoy Khan *et al. Int. J. Biol. Macromol.* **2023**, *253*, 127100

In this study, we basically wanted to verify our previous hypothesis of how the presence of DES modulates the hydration layer of the enzyme. Taking human serum albumin (HSA) in varying concentrations of 0.5 Acetamide/0.3 Urea/0.2 Sorbitol (0.5Ac/0.3Ur/0.2Sor) DES, we investigated solvation dynamics, conformational fluctuation dynamics, and thermal stability to understand the intricacy of protein behaviour in DESs. Notably, this represents the first experimental study of the solvation dynamics of a protein in a hydrated DES. Despite a significant increase in bulk viscosity, the associated water dynamics around domain I of HSA slowed only marginally, suggesting that the protein experiences an aqueous-like local environment even in the presence of high concentration of DES. This is probably the first experimental attempt to delineate the role of the associated water structure of the enzyme for maintaining its stability inside DES. However, our results revealed a gradual decrease in side-chain flexibility and an increase in the hydrodynamic radius of HSA at higher DES concentrations, leading to reduced thermal stability. Extending this approach to other proteins, along with proper thermodynamic

analyses, might offer deeper insight into how hydration layer modulation influences protein stability in DESs.

3. Critical Role of Water beyond the Media to Maintain Protein Stability and Activity in Hydrated Deep Eutectic Solvent

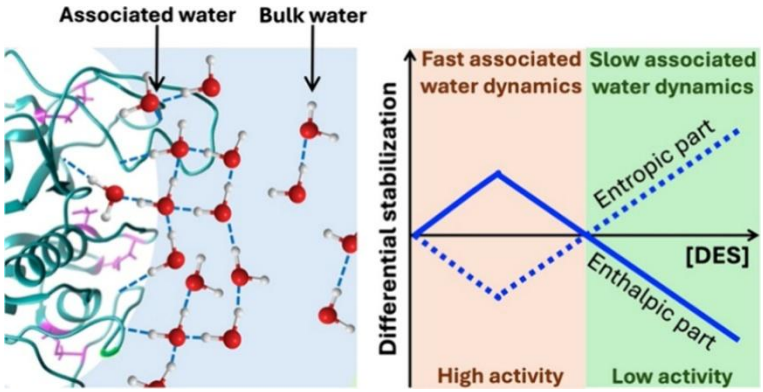

Tanmoy Khan et al. *J. Phys. Chem. B,* **2025**, *129,* 162–175

This study aims to underscore the role of water in governing enzyme stability and activity in DESs. Herein, using bromelain as the model enzyme and 0.5Ac/0.3Ur/0.2Sor as the model DES, we provide experimental evidence that modulation of associated water plays a key role in dictating protein stability and activity in hydrated DES. We specifically termed these findings as the associated water stabilization mechanism (AWSM). Specifically, rigid associated water at higher DES concentrations (beyond 40 % v/v) stabilizes bromelain through entropy but destabilizes it through enthalpy. On the other hand, flexible associated water dynamics at lower DES concentrations result in an opposite thermodynamic outcome. Importantly, the bulk water dynamics cannot explain the stability trend, which emphasizes the critical role of water near the protein surface. Strikingly, associated water dynamics also correlates strongly with bromelain's proteolytic activity. An increasing flexibility of the associated water dynamics leads to the enhancement of the activity. This is the first study to experimentally link associated

water dynamics to enzyme behavior in hydrated DES, offering insights that could guide future developments in solvent engineering for enzyme catalysis.

4. Unravelling the Role of Hydration Dynamics in Enzymatic Stability: A Site-Specific Red Edge Excitation Shift (REES) Study of Human Serum Albumin in Choline Chloride-based Hydrated Deep Eutectic Solvents

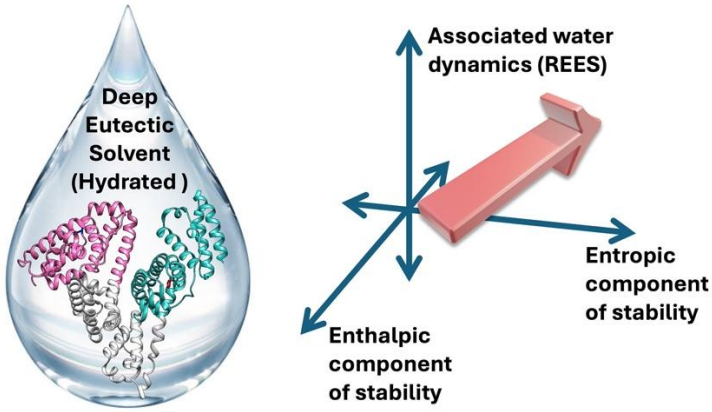

Tanmoy Khan *et al. Biophysical J.,* **2025***, Just accepted*

In this work, we wanted to generalize our hypothesis of the associated water stabilization mechanism (AWSM) in the presence of different DESs. In this study, we explore the role of associated water dynamics in modulating the thermal stability of human serum albumin (HSA) within hydrated ChCl-Glycerol and ChCl-Ethylene Glycol DESs. By employing domain-specific site-selective fluorescence labeling and Red Edge Excitation Shift (REES) measurement, alongside circular dichroism spectroscopy, the study reveals that modulation of hydration dynamics distinctly alters the entropic and enthalpic contributions to protein stability. Flexible hydration enhances enthalpic stabilization but promotes entropic destabilization, while restricted hydration induces the opposite effect, providing a mechanistic basis for entropy–enthalpy compensation. Our findings underscore the necessity of domain-specific stability measurements in multi-domain proteins and highlight the pivotal role of immediate hydration dynamics in protein stabilization within unconventional solvent systems.

5. Role of Associated Water Dynamics on Protein Stability and Activity in Crowded Milieu

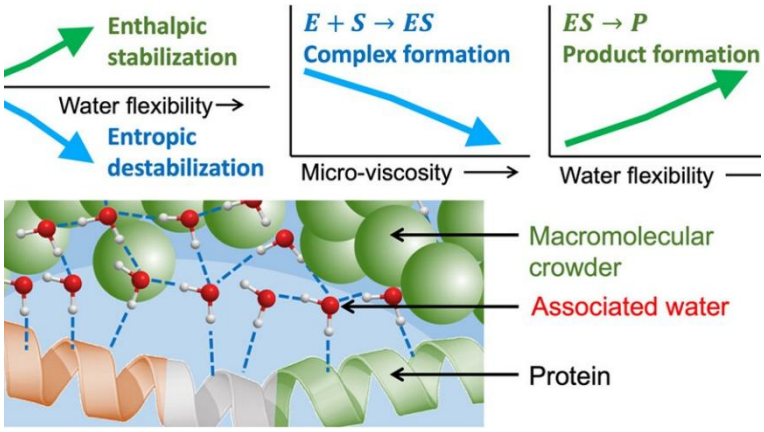

Tanmoy Khan *et al. J. Phys. Chem. B* **2024**, *128,* 8672–8686

To further generalize the hypothesis that associated water modulation governs protein stability and activity beyond DESs, this chapter explores a biologically relevant system under macromolecular crowding. Using bromelain and Ficoll-70 as models, we investigate how associated water dynamics influence protein stability and activity in crowded environments. While traditional crowding theory attributes stability to excluded volume effects and enthalpic interactions, our findings highlight the critical role of hydration layer modulation. In this report, we generalize the conclusion of our previous study and hypothesis, AWSM, i.e., rigid-associated water stabilizes proteins via entropy and destabilizes them via enthalpy, while flexible water has the opposite effect. Additionally, Michaelis–Menten analysis of enzyme activity reveals that micro viscosity (not bulk viscosity) impairs enzyme–substrate (ES) complex formation, while flexible associated water enhances product formation. This study broadens the understanding of protein behavior under crowding and emphasizes the universal role of associated water dynamics across different media.

This page left blank intentionally

Table of Content

Chapter – 2: Experimental 121-198

This page left blank intentionally

Chapter 1

Introduction

A Short Summary

of

Proteins

Deep Eutectic Solvents

Macromolecular Crowding

This page left blank intentionally

Chapter 1

1.1. Proteins: An Overview

Proteins are fundamental components of life, serving as the most abundant biological macromolecules [1,2]. They are involved in almost all essential biological functions, such as facilitating DNA replication, catalyzing biochemical reactions, acting as hormones to regulate physiological processes, transporting drugs and other molecules to specific sites in the body, and many more [1–3].

1.1.1. Structural Features of Proteins:

Proteins consist of long chains of amino acids, called polypeptides, which are connected by peptide bonds. These chains exhibit four distinct levels of structural organization [1–3]:

- **Primary Structure:** This is the linear sequence of amino acids in the polypeptide chain.
- **Secondary Structure:** After synthesis, the polypeptide chain folds into specific shapes, forming regular patterns known as secondary structures. The most common motifs include the α-helix, β-sheet, β-turn, and random coil. The α-helix is the most tightly packed of these structures.
- **Tertiary Structure:** The tertiary structure refers to the three-dimensional arrangement of protein. It forms as the protein folds into its most stable state, known as the native state. It is also the active state of the protein. This structure is stabilized by four types of interactions: disulfide bonds, ionic bonds, hydrogen bonds, and hydrophobic/hydrophilic effect. Disrupting the tertiary structure, often through heat or chemical agents (denaturants), leads to denaturation. This process typically disrupts both the tertiary and secondary structures of the protein. My research explores the thermal denaturation of proteins.

- **Quaternary Structure:** Some proteins are composed of multiple subunits, forming dimeric, trimeric, tetrameric, or oligomeric complexes. The arrangement of these subunits in three-dimensional space is referred to as the quaternary structure.
- **Protein Domains:** Domains are distinct regions within a protein, each having its specific function. The number and size of domains can vary widely among different proteins [4,5].

In my thesis, I have worked mainly with two proteins, plant enzyme bromelain and human serum albumin.

1.1.2. Bromelain

Stem bromelain is a proteolytic enzyme derived from the stem of the pineapple plant. It consists of 212 amino acids and has an isoelectric point (pH) of approximately 9.55, and the 3D structure has been shown in Scheme 1.1.1. Stem bromelain contains seven cysteine residues, including one free cysteine (Cys-26) that plays a significant role in its enzymatic activity [6–8]. This single-domain simple enzyme also includes five tryptophan residues, contributing to its structural stability and function [7,8].

This enzyme has long been used in food processing, particularly for meat tenderizing and protein cleavage, due to its proteolytic properties [9–11]. Beyond its culinary applications, bromelain has found use in the medical field, where it serves as a therapeutic agent for reducing inflammation, treating thrombosis, and managing conditions like arthritis [10,12–17]. Bromelain's ability to break down proteins makes it versatile both in industrial processes and medical treatments, with growing research supporting its efficacy in various health conditions [9,12,14].

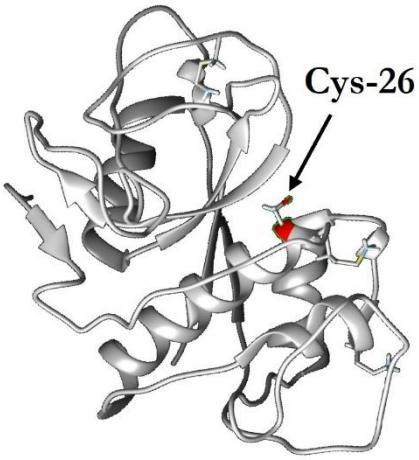

Scheme 1.1.1. 3D-structure of stem bromelain (PDB ID: 1W0Q).

1.1.3. Human Serum Albumin (HSA)

While many biophysical studies focus on single-domain proteins, multi-domain proteins make up more than 70% of proteins in eukaryotes [18]. Human Serum Albumin (HSA) is one of the most studied multi-domain proteins.

HSA, with a molecular weight of ~66.5 kDa, is found in blood plasma and consists of 585 amino acids and 17 disulfide bridges [19,20]. It also contains one free cysteine. Crystallographic studies reveal that HSA is composed of three distinct domains (domain-I, domain-II, and domain-III), each with unique structural characteristics and functions [19,20]. The 3D structure of HSA has been shown in Scheme 1.1.2.

- **Domain-I:** Binds fatty acids and heme, aiding in their transport [21,22].
- **Domain-II:** Specializes in binding and transporting of bulky heterocyclic anions like azapropazone, phentylbutazone, and warfarin [23,24].
- **Domain-III:** Binds aromatic carboxylates such as ibuprofen and is responsible for HSA's esterase activity [23–25].

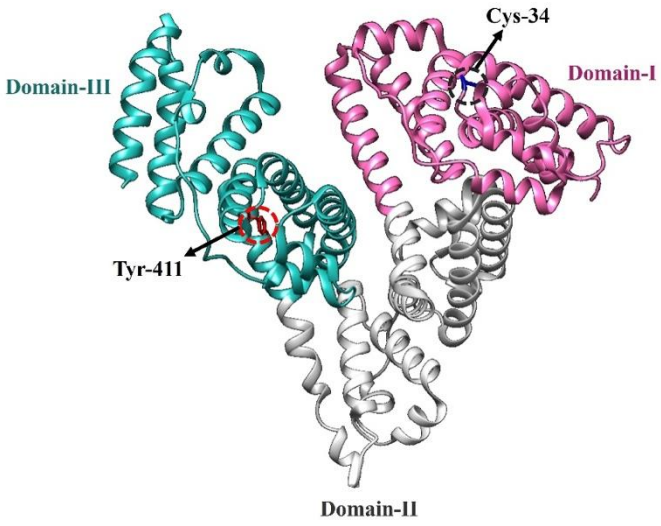

Scheme 1.1.2. 3D-structure of human serum albumin (HSA) (PDB ID: 1HA2).

Each domain behaves differently in response to various external factors. This domain-specific behaviour makes HSA an excellent model for exploring complex biophysical phenomena. The dynamic interactions between these domains could also be crucial for understanding biophysical reactions, positioning HSA as a valuable tool for further research into protein behaviour [20,24].

1.1.4. Thermodynamic Insights into Protein Unfolding:

Protein folding is the process by which a linear chain of amino acids arranges itself into a functional three-dimensional structure [26–31]. This process is essential because a protein must fold correctly to perform its biological functions. Two key questions arise when studying protein folding: (i) How to predict the protein's final structure from its amino acid sequence? (ii) Levinthal's paradox: given the astronomical number of possible conformations, how do proteins fold to the most stable native form so quickly, in mere seconds, rather than millions and millions of years? [32,33]

Christian Anfinsen proposed that the final, functional form of a protein is determined solely by its amino acid sequence [26]. He also demonstrated that proteins could refold

to their native state after being denatured, indicating that the folding information is encoded in the sequence itself [32,34]. The protein folding funnel hypothesis explains the folding process [33,35]. It is a model where the energy landscape of a protein is represented as a funnel. The protein moves from an unfolded, high-energy state at the top of the funnel toward a low-energy, native state at the bottom. Along this path, the protein may pass through several intermediate states, represented by local minima in the funnel (see scheme 1.1.3). The shape and slope of the funnel determine the route and speed of folding. The theory suggests that instead of exploring an overwhelming number of conformations, the folding process is kinetically controlled, allowing it to happen in a biologically relevant timescale [33]. As proteins fold, there is a reduction in both energy and conformational entropy. Unfolding, the reverse process disrupts secondary and tertiary structures due to external disturbances like heat or chemicals.

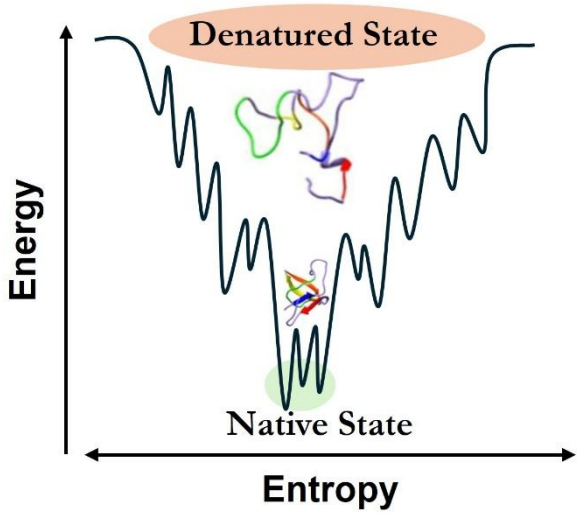

Scheme 1.1.3. Protein folding funnel of free energy. The protein transitions from its denatured state to its native state (global minimum) by passing through several intermediate (local minima) is accompanied by a reduction in conformational entropy.

1.1.4.1. Understanding Free Energy in Protein Unfolding

In thermodynamic terms, protein unfolding can be simplistically considered as a two-state transition:

$N \rightleftharpoons D$

Where N represents the native/folded state, and D represents the denatured/unfolded state. The forward and reverse reactions can be described using forward and backward rate, k_f and k_b respectively.[36]

Forward rate = $k_f[N]$, and backward rate = $k_b[D]$

At equilibrium, forward rate = backward rate

$$\therefore k_f[N] = k_b[D] \quad (1.1.1)$$

At equilibrium, the concentration of the folded and unfolded states reaches a balance, and the equilibrium constant (K) defines this ratio.

$$K = \frac{k_f}{k_b} = \frac{[D]}{[N]} \quad (1.1.2)$$

The free energy change (ΔG) of the reaction can then be written as,

$$\Delta G = -RTlnK = -RTln\frac{[D]}{[N]} \quad (1.1.3)$$

ΔG determines whether the unfolding process is spontaneous ($\Delta G < 0$) or not ($\Delta G > 0$). In protein unfolding, a more positive ΔG indicates that the protein is more stable in its folded state. Now, from an experimental point of view, the determination of ΔG is very important.

1.1.4.2. Calculating Free Energy from Experimental Data

In an unfolding experiment, the response of the protein to perturbation (such as temperature, or denaturant concentration) is tracked by measuring a signal (spectroscopic, in my case) that changes with increasing perturbation. The denaturation of protein is considered a cooperative phenomenon, and thus, the denaturation pathway follows a sigmoidal nature. Initially, the protein remains folded, but as the strength of the perturbation increases, the structure starts to unfold progressively (Scheme 1.1.4). Eventually, the unfolding reaches a saturation point, beyond which no further change is observed in the signal, even if the perturbation continues to increase.

The signal at any given point during the unfolding process can be represented as a linear combination of the signals from both the folded and unfolded states.

Let y_D and y_N represent the signals from the denatured and native states, respectively (see Scheme 1.1.4). The overall signal y can be expressed as a liner combination.[7,37]

$$y = y_N[N] + y_D[D] \qquad (1.1.4)$$

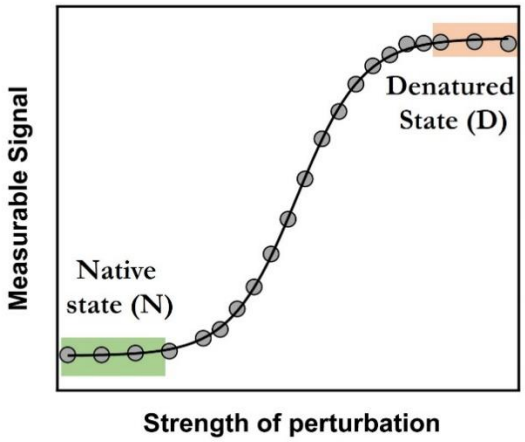

Scheme 1.1.4. A typical unfolding curve of a protein.

From previous equations, we know that the ratio of unfolded to folded protein is represented by the equilibrium constant, K, and thus (from equation 1.1.2),

$$[D] = K[N] \quad (1.1.5)$$

$$\therefore 1 - [N] = K[N] \quad (1.1.6)$$

$$\therefore \ [N] = \frac{1}{1+K} \quad (1.1.7)$$

We can also derive:

$$[D] = \frac{K}{1+K} \quad (1.1.8)$$

Substituting these into the equation 1.1.4:

$$y = y_N \frac{1}{1+K} + \ y_D \frac{K}{1+K}$$

This can be rearranged to solve for K as,

$$K = \frac{y_N - y}{y - y_D} \quad (1.1.9)$$

Since y_N, y_D, and y are measurable quantities, this equation allows for the calculation of K, and a simultaneous determination of the free energy of unfolding is also possible using the equation 1.1.9.

1.1.4.3. Quantifying Entropy and Enthalpy of unfolding

Two components of this change in free energy: entropy (ΔS) and enthalpy (ΔH) which are related through the famous thermodynamic equation,

$$\Delta G = \ \Delta H - T\Delta S \quad (1.1.10)$$

The entropic change of a process talks about the change of randomness in the system and enthalpic terms account for the change in the extent of interactions. From the above

equation, it is clear that a plot of ΔG vs T with a linear fitting can yield entropy and enthalpy as the negative slope and intercept respectively.

I have used this analysis on many occasions in my thesis.

Also, a direct plot of lnK vs. $1/T$ produces a straight line having an intercept of $\frac{\Delta S}{R}$ and slope of $-\frac{\Delta H}{R}$ following the Van't-Hoff equation:

$$lnK = -\frac{\Delta H}{RT} + \frac{\Delta S}{R} \quad (1.1.11)$$

Basically, the equation 1.1.10 and 1.1.11 are same, with the latter calculates the parameters directly from the temperature dependent equilibrium constants.

The thermal unfolding experiment is conducted both in the buffer and in the presence of the perturbation to assess how the perturbation influences the unfolding process. From these experiments, the corresponding changes in free energy, entropy, and enthalpy are calculated. To quantify the effect of any perturbation on the extent of stabilization of the protein, the differential change in free energy, entropy, and enthalpy were calculated as,

$$\Delta\Delta G^0 = \Delta G^0_{perturbation} - \Delta G^0_{buffer} \quad (1.1.12)$$

$$\Delta\Delta H^0 = \Delta H^0_{perturbation} - \Delta H^0_{buffer} \quad (1.1.13)$$

$$\Delta\Delta S^0 = \Delta S^0_{perturbation} - \Delta S^0_{buffer} \quad (1.1.14)$$

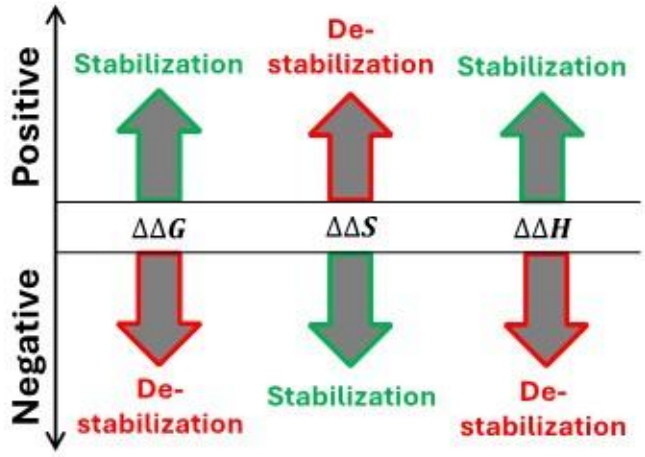

Scheme 1.1.5. Effect of positive/negative free energy, entropy, and enthalpy change of protein unfolding compared to that in the buffer on the overall stability of the protein.

A positive value of $\Delta\Delta G^0$ signifies that the system is likely to be in the native state in the presence of the perturbation compared to the buffer.

As $\Delta\Delta G^0 = \Delta\Delta H^0 - \mathrm{T}\Delta\Delta S^0$, a positive value of $\Delta\Delta H^0$ will be a stabilizing contributor, and a positive value of $\Delta\Delta S^0$ will be destabilizing (see Scheme 1.1.5).

1.1.4.4. Consideration of Heat Capacity into Unfolding Thermodynamics

Note that, in the previous analysis, the temperature dependence of entropy and enthalpy has not been considered. However, it's often found that both enthalpy (ΔH) and entropy (ΔS) can vary with the temperature. This variation is linked to the difference in heat capacities between the folded and unfolded states of the protein, termed the excess heat capacity (ΔC_p). The excess heat capacity is mathematically expressed as the difference between the heat capacity of the unfolded state and the folded state:

$$\Delta C_p = {C_p}^D - {C_p}^N \qquad (1.1.15)$$

Excess heat capacity is related to ΔS and ΔH by

$$\Delta C_p = T\frac{\partial}{\partial t}(\Delta S)_p \qquad (1.1.16)$$

$$\Delta C_p = \frac{\partial}{\partial t}(\Delta H)_p \qquad (1.1.17)$$

Combining equations (1.1.11), (1.1.16), and (1.1.17), one gets a modified version of the Gibbs-Helmholtz equation.[38] The equation considers ΔC_p, which allows for more precise calculations of Gibbs free energy (ΔG) at varying temperatures.[39]

The general form of the equation is:

$$\Delta G\ (T) = \ \Delta H_m \left(1 - \frac{T}{T_m}\right) + \ \Delta C_p[(T - T_m) - Tln(T/T_m)] \qquad (1.1.19)$$

Where:

- $\Delta G\ (T)$ is the Gibbs free energy change at temperature T,
- ΔH_m is the change of enthalpy at the melting temperature T_m,
- ΔC_p is the change in heat capacity,
- T_m is the midpoint temperature of the unfolding transition (where $\Delta G = 0$),
- T is any temperature at which the free energy is being evaluated.
- Also, ΔS is just $\Delta H/T_m$

A deviation from linearity in the Van't-Hoff plot indicates a nonzero change in heat capacity, which can be calculated using the equation 1.1.19. However, in my thesis, I have directly measured entropy and enthalpy and not considered the change in the heat capacity between native and unfolded state. As, in my case considering the ΔC_p while fitting the denaturation curve does not improve the fitting quality much and both the parameters ΔH and ΔS remain similar to the previous model (equation 1.1.10). Figure 1.1.1 is a representative case of the free energy change of bromelain unfolding in the presence of buffer fitted with both equations 1.1.10 and 1.1.19. The maximal deviations from linearity in this case is ~ 200 cal/mol, which demands <10% fractional uncertainties

to observe. This level of accuracy is almost impossible to attain in such measurements. The ability to perform such measurements for excess heat capacity ΔC_p requires the combination of a large temperature range and precise rate-constant measurements. That's why it is a general practice to measure ΔC_p directly by calorimetry measurement. And by fitting the denaturation data ΔC_p is not calculated.

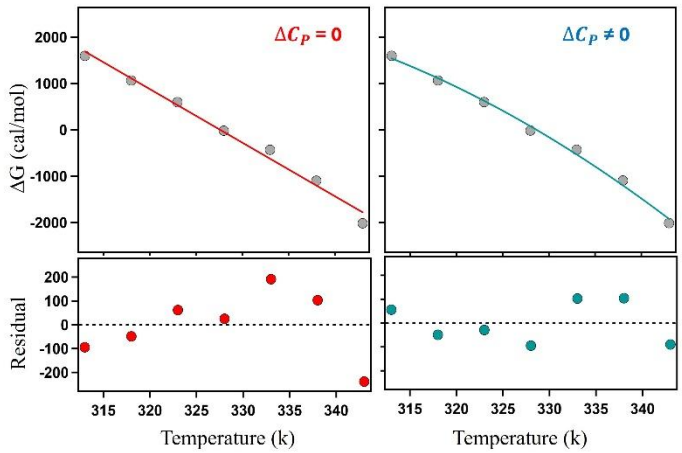

Figure 1.1.1. The free energy change of thermal unfolding of bromelain with temperature. In the left panel, ΔG is fitted with the equation 1.1.10 where ΔC_p is considered 0, that means not considered. However, in the right panel through fitting with equation 1.1.19, a non-zero ΔC_p value was extracted.

1.1.4.5. Physical Insights into Protein Unfolding

The folding funnel hypothesis suggests that the unfolding process is accompanied by increasing randomness in the system which contributes to the feasibility of the process by increasing the change in entropy.[40] On the other hand, the stable interactions (hydrogen bonds, ionic bonds, van der Waals forces, and hydrophobic effect) present in the folded state are disrupted in the unfolded state, which requires energy.[41,42] As a result, heat is absorbed, and the enthalpy of unfolding is typically positive, contributing towards the non-feasibility of the unfolding process.[43] Generally, the total energy difference

between the folded and unfolded states is approximately 20-40 kJ/mol, with the equilibrium constant for a small natural protein typically ranging between 10^4 and 10^7.[44]

1.1.4.6. Role of Water in Protein Unfolding

Water plays an essential role in protein folding and stability, with the modulation of water structure having profound effects on biophysical processes. Proteins carry out their functions in an aqueous environment, and thus, water is central to their behavior. In a typical biophysical experiment, the concentration of the biomolecule is in the micromolar range, while the concentration of water is significantly higher at 55.5 M. This stark difference underscores how even slight changes in water structure can drastically influence the outcome of the experiment. It is well established that the structure of water near a protein's surface differs from that of bulk water, and these water molecules that are in direct interaction with the protein surface are known as associated or biological water.[45–50] The presence of any additives can further modify this structure and thus the unfolding-folding dogma as well.[51–55] Despite this, the critical role of water in protein folding and unfolding remains underexplored.

Pure water consists of a dynamic network of hydrogen-bonded molecules. However, when nonpolar, hydrophobic molecules (such as proteins) are introduced into water, they disrupt this network. Water molecules then form a highly structured shell, or solvation layer, around these hydrophobic groups to maintain optimal hydrogen bonding.[1] This structuring decreases the entropy of the water, meaning the system becomes more ordered and less favourable from a thermodynamic perspective. However, in the process of folding when the hydrophobic groups in a protein are clustered together, the surface area exposed to water decreases, as the unfolded protein is larger in size than the folded protein, thus reducing the extent of the solvation layer and allowing the water molecules to become less structured and more disordered.[1] This increase in entropy is thermodynamically favourable and acts as

the primary driving force for the folding of the protein in water.[1] In short, because of the decrease in the entropy of water molecules (not protein) during unfolding, the natural tendency of water molecules near the protein is to protect the native form of that protein. Any additives that further strengthen the water shell around the protein will impart more stabilization to the system and can be considered as a stabilizing agent to the protein. On the other hand, additives that weaken the water shell will destabilize the protein. Consequently, this strengthening or weakening of the hydrogen bonds leads to an enthalpic change. Specifically, the weakening of the hydrogen-bonded network requires some energy, leading to positive enthalpic changes, whereas in the other case, modulation to a stronger hydrogen bond network, a negative change in enthalpy occurs. Thus, this modulation of the water in the presence of any additive might not only influence the enzyme stability but also may provide a physical basis for the entropy-enthalpy compensation that is observed across many biophysical events.

In my thesis, I have tried to understand the water dynamics modulation in the presence of additives and its impact on protein stability and activity.

1.1.4.7. Entropy-Enthalpy compensation

In many biophysical reactions, there is often a linear relationship observed between entropy (ΔS) and enthalpy (ΔH), a phenomenon known as entropy-enthalpy compensation.[56,57] The famous thermodynamic equation, $\Delta G = \Delta H - T\Delta S$, relates the entropy and enthalpy change of any process. Thus, the entropy-enthalpy compensation appears to be a thermodynamic consequence, and one might think of the existence of a common source. However, the physical reason is not well known. The previous discussion of the role of water somehow portrays the involvement of water in attributing both the change in entropy and enthalpy, and thus it might be

considered a common reason for entropy-enthalpy compensation. In my thesis, I have tried to discuss this in detail.

1.1.5. Dynamics of protein:

As famously remarked by many scientists, the dynamics of biologically active molecules are very important to understand any biological process.[58] The functions of enzymes or proteins, in general, can be comprehended to a great extent by studying their motions. However, it was not until the 1980s that scientists truly began to appreciate the dynamic nature of proteins.[59] Rather than static entities, proteins exist in multiple conformational states, constantly interchanging through various motions, from bond rotations and side-chain shifts to loop movements.[60,61] These conformational changes occur over a variety of timescales, from picoseconds to milliseconds, and involve displacements from as small as 0.01 Å to as large as 10 Å, known as conformational fluctuation dynamics[60,62,63] (Scheme 1.1.6).

Beyond internal motions, proteins exhibit three other essential dynamics within biological environments: **translational motion** (how the protein moves through a solvent media), rotational motion (how the protein rotates in a solvent media), and the **dynamics of water molecules in the immediate vicinity of the protein (scheme 1.1.6)**. The water molecules residing near to protein surface directly make hydrogen bonding with the amino acid residues known as associated or biological water. This **biological water** surrounding proteins has much slower dynamics, and any alteration in its structure or dynamics can significantly impact the protein's stability and activity.[46–48,53,64–67] The viscosity of the solvent media also plays a significant role in controlling the translational and rotational dynamics of the protein.[68,69] In scheme 1.1.6 different dynamics of proteins are represented.

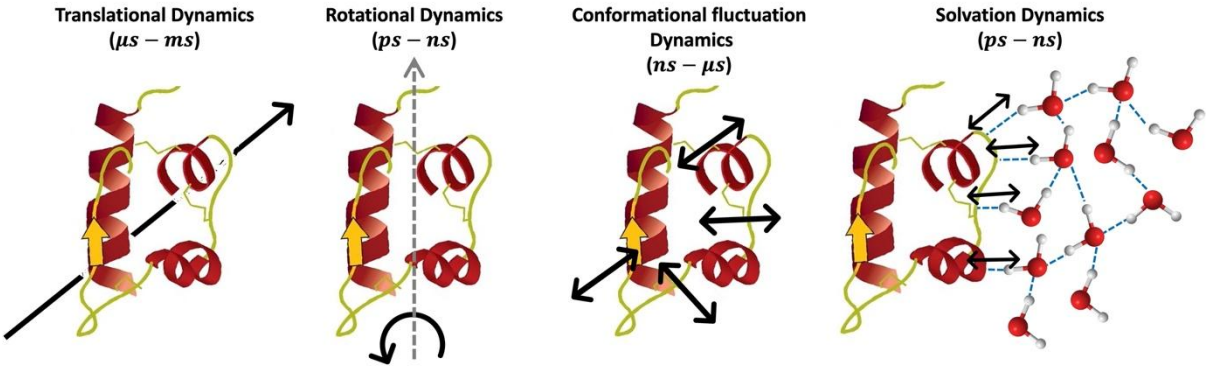

Scheme 1.1.6. Various dynamics of a protein and their tentative timescales.

In my thesis, I have measured the associated water dynamics and conformational dynamics of bromelain and HSA protein in different perturbations (DESs, macromolecular crowder).

1.1.5.1. Conformational dynamics of protein:

Conformational fluctuation dynamics, often referred to as side-chain dynamics, is one of the most important due to its significant role in enzyme function.[70–75] The flexibility of side chains allows proteins to adapt their shapes to accommodate substrates or interact with other biomolecules, thus enhancing specificity and efficiency.[76,77] Moreover, side-chain dynamics contribute to the protein's ability to explore a range of conformations, essential for folding, stability, and interaction with water or other molecules. The timescale of signal transduction, enzymatic activity, and allosteric regulation generally occurs in microseconds, thus observing the microsecond side-chain dynamics is necessary.[74,78,79] Also, probably because of its relative slowness, this side-chain dynamics is studied extensively. Recently, our group also reported a direct correlation of this conformational fluctuation dynamics in influencing the enzymatic activity of bromelain.[75]

The conformational fluctuations in proteins do not occur at the same time or in the same way across a group (ensemble) of protein molecules. Since each protein molecule may undergo conformational changes at different moments or on different timescales, it is challenging to capture a unified or consistent measurement of these fluctuations in experiments. This lack of synchronization makes it difficult to experimentally determine a precise timescale for these dynamic events using an ensemble average technique. This problem can be resolved through single-molecular techniques or at least through techniques at the single-molecular level. In such a scenario, each protein molecule is studied independently, and the fluorescence fluctuation from the protein due to conformational fluctuation can be measured. Among the numerous single-molecule techniques available, two stand out as particularly significant: fluorescence correlation spectroscopy (FCS) and single-molecule fluorescence resonance energy transfer (smFRET).[80–83] Although not a true single molecular technique, FCS offers advantages over sm-FRET, such as avoiding protein immobilization, improved time resolution, and simpler instrumentation.[82,84] FCS has been applied to measure conformational dynamics of various proteins, including cytochrome-c[85,86], lysozyme[87,88], papain[89], prion protein[90], spider silk protein[91], apo myoglobin[92], photosystem-I[93], bromelain[75,94], glutamate receptor[95], human serum albumin (HSA)[96,97], and so on. A detailed understanding of the FCS can be gained through several available review articles and books[98–100].

In my thesis, I have also routinely used FCS and observed the modulation of conformational fluctuation dynamics of proteins in different media.

1.1.5.2. Associated water dynamics of protein:

Generally, the dynamics of a solvent can be measured using many spectroscopic techniques like nuclear magnetic resonance (NMR)[101,102], dielectric relaxation (DR)[45], quasi-elastic neutron scattering (QENS)[103], and time-dependent fluorescence Stokes shift (TDFSS)[66,67,104–107]. However, in the case of a protein

where the immediate surroundings are of utmost importance, the TDFSS method takes the lead due to its unmatched spatial and time resolution.[47,50] In TDFSS, a reporter molecule (fluorescent probe) is excited using a suitable excitation source, and due to its difference in the dipole moment of the ground and excited state, solvent molecules reorganize to stabilize the solute.[100,108] The time taken for this rearrangement is a measure of solvation dynamics.

In a famous article in Nature, 1994, Fleming and his colleagues for the first time using the TDFSS method employing femtosecond fluorescence up-conversion technique with coumarin 343 as the probe, reported the solvation dynamics of water to be ~ 1 ps.[109] A year later Bright and co-workers studied the solvation dynamics of a protein, acrylodan-labeled HSA inside a reverse micelle, and observed a nanosecond relaxation time.[110] After that, the Zewail group, Bhattacharyya group, and many others through a plethora of studies over the years proved the slow solvation dynamics of water in the presence of proteins.[66,67,104–106,111–121]

The theory of this observation of slow solvation dynamics of water is given by Bagchi and co-workers, famously known as the Nandi-Bagchi model.[45] It suggests that the slow solvation dynamics arise because the water molecules near the protein surface behave differently from bulk water, likely forming stronger hydrogen bonds with the protein than those found in bulk water.[45,49] This specialized water, referred to as "biological water" or "associated water," consists of two main components: free water (where water molecules bond only with other water molecules) and bound water (where water molecules are H-bonded to the amino acid residue of protein surface) (see Scheme 1.1.7).[45,46,48,53] These two forms of water continuously exchange, and according to the Nandi-Bagchi model, only free water contributes to the solvation process.[45] However, the timescale of solvation dynamics depends on the equilibrium constant between free and bound water exchange, which is influenced by the difference in the hydrogen bond strength between them.[45,47] The stronger the protein-bound water interaction, the slower the solvation dynamics will be.

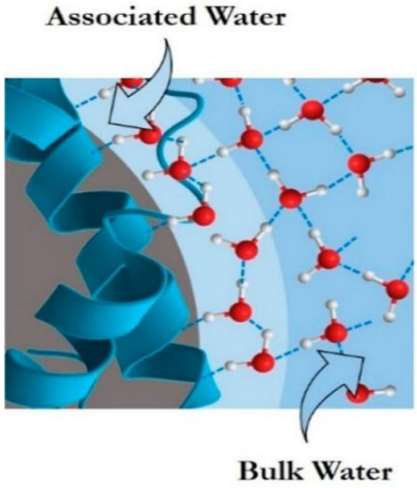

Scheme 1.1.7. Effect of positive/negative free energy, entropy, and enthalpy change of protein unfolding compared to that in the buffer on the overall stability of the protein. This figure is represented from the reference [48].

In the case of protein, the surrounding water that directly interacts with the protein surface is of utmost importance as it influences important protein behaviour like stability and activity.[48,53,66,112,122] Having a site-selective tagging with fluorescent molecules, or if a single tryptophan is present, then the solvation dynamics can give information about the dynamics and structure of the surrounding water molecules (biological water or associated water) of that region of the protein.[47] Therefore, faster dynamics will suggest the presence of free or less strongly bound water around the protein, whereas slower dynamics suggest a rigid or strongly bound water structure around the protein. Due to better spatial and time resolution, TDFSS can report dynamics near the reporter molecule tagged in the protein.[47,123] In contrast, NMR, DR, or QENS captures signals from the whole solution and can give only an average picture.[47] Thus, TDFSS has been extensively used to extract the dynamics of the associated water of various proteins in the presence of different perturbations. Also, the role of this associated water in influencing enzymatic properties like structure, dynamics, stability, and activity is very axiomatic. It is because of the enormous complexity present in the biological systems, delineating the exact role of water in governing enzymatic behavior is still very scarce but of most importance. Attempts

regarding the ability of water to influence stability and activity, are very limited in the literature. In Table 1.1.1, we listed some reports of water structure modulation in the presence of different perturbations.

Table 1.1.1. Water dynamics modulation of proteins in the presence of various perturbations. This is not a comprehensive list of references; many more examples can be found beyond those listed.

Protein	Perturbations	Observation	Year[Ref]
α-Chymotrypsin	inactive state (pH 3.6) and the active state (pH 6.7)	The associated water becomes faster in the active form than in the inactive form of the enzyme	**2002**[66]
Monellin	6M guanidine hydrochloride (GnHCl)	Because of the involvement of the protein backbone motions in the random-coiled state, a retarded hydration dynamics in GnHCl observed than in the buffer	**2002**[111]
Glutaminyl-tRNA synthetase (GlnRS)	1.9 M Urea	The water dynamics at two different sites of the protein modulated differently in urea. The dynamics from covalently attached probes become retarded, but the dynamics extracted through non-specifically attached probes become very flexible.	**2003**[116]
Lysozyme	sodium dodecyl sulfate (SDS)	Solvation dynamics becomes slower in the presence of SDS.	**2003**[113]
HSA	GnHCl	In the unfolded state (6 M GnHCL) the water dynamics becomes very fast with respect to the buffer.	**2004**[112]
Cytochrome C	2 mM SDS and 5 M urea	The water dynamics become more flexible in the presence of both SDS and Urea together than in only SDS	**2005**[105]

HSA	Change of pH (acidic to basic)	With the changes in the pH dependent conformation, the hydration dynamics modulates. The fastest dynamics and the loss of globular structure was observed in the basic pH.	**2006**[67]
GlnRS	l-glutamate+Urea	With the increase in the concentration of urea, the hydration dynamics of the enzyme become progressively faster because of the conformational changes from compact denatured states to fully unfolded states.	**2006**[124]
No protein used	lactose	The hydration dynamics of near lactose become significantly retarded than bulk water.	**2006**[55]
Apomyoglobin	native (pH~6) and molten globule state (pH~4) with mutation at 16 different positions across the whole protein surface	In all the mutant variations of the protein, the associated water becomes more flexible in the molten globule state than in the native state.	**2007**[121]
N-acetyl-leucine-methylamide peptide	Glycerol, DMSO	In glycerol, slower dynamics with two distinguishable relaxation times were observed. However, in the presence of DMSO, the hydration water dynamics become faster and more bulk-like, especially near the hydrophobic regions of the peptide.	**2009**[125]
Flavodoxin	three redox states oxidized form (OX), one-electron reduced	SQ protein has superior stability and retarded water dynamics than OX state. However, in HQ form the solvation becomes faster again	**2010**[126]

	neutral semiquinone (SQ), and two-electron fully reduced anionic hydroquinone (HQ)		
HSA	temperature	Thermal unfolding disrupts this hydration structure, leading to faster, bulk-like water dynamics and irreversible structural destabilization at higher temperatures.	**2011**[127]
α-Chymotrypsin	PEG-400	Water dynamics become more flexible with PEG-400 and correlating well with the activity modulation.	**2011**[128]
HSA	1.5 M [pmim][Br] ionic liquid and 6 M GnHCl	The solvation dynamics become progressively faster from the presence of ionic liquid to GnHCl because of unfolding of the enzyme.	**2012**[115]
HSA	PEG 200 and 400	with PEG concentration, a structured and less mobile hydration shell forms	**2015**[129]
HSA and BSA	Dextran-6k, 40k, 70k; Ficoll-70k; PEG-200, 8k; α-synuclein	Solvation dynamics modulates even at low concentrations of crowder. α-Synuclein slows the associated water dynamics in BSA but speeds up in HSA.	**2015**[130]
γS-Crystallin, γS-G18V (mutant)	Self-crowding	The hydration shell remains dynamic, but mutants show dehydration at lower crowding levels.	**2016**[131]
HSA (Domain-I)	Sucrose and GnHCl	Sucrose mitigates the denaturing impact of guanidine hydrochloride (GnHCl). At lower concentrations	**2016**[117]

		of GnHCl, the presence of sucrose leads to a noticeable slowing of hydration dynamics. However, as the concentration of GnHCl increases, the influence of sucrose on hydration dynamics becomes negligible.	
HSA (Domain-I)	Dextran-6k, 40k, 70k; Ficoll-70k; PEG-200, 8k	Solvation dynamics remain unchanged for small crowders. Larger crowders slow down dynamics beyond 100 gL^{-1}.	**2016**[132]
RNase T1, (SH3) domain of the protein drk	CTAB and AOT reverse micelle with different water pool size	Both proteins experience reduced stability in their respective reverse micelle environments, and the hydration water becomes more ordered and less dynamic	**2018**[133]
Fish eye lens protein γM7-crystallin	Mutation at different positions with different surface exposure	At a more buried probe position the hydration dynamics become more retarded with respect to a exposed position.	**2020**[106]
HSA (Domain-I)	Dextran-6k, 40k, 70k; Ficoll-70k; PEG-8k, urea	Low concentrations induce faster water dynamics; higher concentrations retarded the same.	**2020**[134]
Adenylate kinase	PEG-8k; Dextran-40k, 70k; Ficoll-70k	Water dynamics slows down with crowders. Ficoll-70k has the greatest effect.	**2021**[135]
Adenylate kinase	Ficoll-70k; Dextran-40k, 70k; and PEG-8k	Solvation dynamics slows down with crowders. Dynamics vary across the domains, with a sharp drop at 278-293 K.	**2022**[136]
bovine beta-casein	SDS	With the increase in the SDS concentration, a structural compactness and retardation in the	**2022**[137]

		hydration dynamics of beta casein protein was introduced.	
RNase A	Various osmolytes	Protein-stabilizing osmolytes are typically associated with tightly bound hydration water exhibiting slow dynamics, whereas denaturing osmolytes tend to accelerate the collective rotational motion of surrounding water molecules.	**2022**[51]
HSA (Domain-III & I)	Dextran-40k, Ficoll-70k, PEG-35k	At 100 gL^{-1}, PEG speeds up water dynamics, while dextran and Ficoll slow them down.	**2023**[48]
Mutated adenylate kinase	Urea (0-6 M); Ficoll-70k; Dextran-40k, 70k; PEG-8k	Water dynamics get hindered with an increase in the crowder concentration but show varying effects with urea.	**2023**[138]
Adenylate kinase	Ficoll-70k; Dextran-40k, 70k; PEG-8k	The hydration dynamics of the enzyme is retarded with an increase in the crowder concentration. The water dynamics of the active site of the enzyme is more affected than other positions.	**2024**[139]

Most studies of hydration dynamics modulations are either in the presence of osmolytes or macromolecular crowders. However, almost no studies have tried to correlate this modulation of water dynamics with enzymatic properties like stability and activity. Also, there is a clear lack of experimental evidence and understanding of the modulation of associated water in the presence of DESs or hydrated DESs is there. The term DES was introduced in 2003, and studies of protein behaviours in DES came even after 5-6 years, which might be one of the reasons why no experimental study deciphered the modulation of hydration dynamics of protein in the presence of DESs. However, the previous studies taking osmolytes (many of which are essentially the constituents of DESs) and macromolecular crowders

strongly suggest the crucial role of the associated water in influencing protein stability and activity in the presence of DESs.

1.1.6. Limitations in Enzyme Applications and Directions:

Generally, enzymes or proteins are thought of as the most efficient and effective catalysts because every function going on inside a living body is done by some specific proteins, and the smallest inconvenience in their functions leads to severe disorders and diseases in the body. However, they normally lose their stability and function in conventional organic solvents. Thus, limiting their practical applications in various fields, including medicine, biotechnology, and industrial processes.

Proteins and enzymes are marginally stable in their native state, and thus, with the slightest changes in the native environments (changes in temperature, pH, ionic strength, etc.), enzymes easily lose their structure and function, limiting their use in biocatalysis.

Enzymes have a short shelf life, and long-term storage of enzymes is difficult as they degrade over time, requiring expensive and precise storage conditions like refrigeration and lyophilization.

Addressing these gaps will require advancements in protein engineering and formulation of novel solvents with tunable properties to improve the stability, storage, and effectiveness of proteins and enzymes in various applications.

In my thesis, my work revolved around enzyme behaviour in complex solvents like deep eutectic solvents (DESs), macromolecular crowder, etc. These solvents are believed to be an alternative media where biocatalysis can be performed because of their ability to keep or even increase the stability and activity of the enzymes. I have tried to explore the mechanistic understanding of why protein remains stable and active in such complex solvents.

1.1.7. References:

(1) Nelson, D. L.; Cox, M. M.; Hoskins, A. A. *Lehninger Principles of Biochemistry*; Macmillan Learning: New York, USA, 2021.

(2) Berg, J. M.; Tymoczko, J. L.; Stryer, L. *Biochemistry*, 5th ed.; W.H. Freeman Co.: New York, USA, 2002.

(3) Berezovsky, I. N.; Guarnera, E.; Zheng, Z. Basic Units of Protein Structure, Folding, and Function. *Prog Biophys Mol Biol* **2017**, *128*, 85–99. https://doi.org/10.1016/J.PBIOMOLBIO.2016.09.009.

(4) Ponting, C. P.; Russell, R. R. The Natural History of Protein Domains. *Annu. Rev. Biophys. Biomol. Struct* **2002**, *31*, 45–71. https://doi.org/10.1146/annurev.biophys.31.082901.134314.

(5) Orengo, C. A.; Michie, A. D.; Jones, S.; Jones, D. T.; Swindells, M. B.; Thornton, J. M. CATH – a Hierarchic Classification of Protein Domain Structures. *Structure* **1997**, *5* (8), 1093–1109. https://doi.org/10.1016/S0969-2126(97)00260-8.

(6) Jha, I.; Bisht, M.; Mogha, N. K.; Venkatesu, P. Effect of Imidazolium-Based Ionic Liquids on the Structure and Stability of Stem Bromelain: Concentration and Alkyl Chain Length Effect. *Journal of Physical Chemistry B* **2018**, *122* (30), 7522–7529. https://doi.org/10.1021/ACS.JPCB.8B04661/ASSET/IMAGES/LARGE/JP-2018-04661J_0005.JPEG.

(7) Rani, A.; Venkatesu, P. Insights into the Interactions between Enzyme and Co-Solvents: Stability and Activity of Stem Bromelain. *Int J Biol Macromol* **2015**, *73* (1), 189–201. https://doi.org/10.1016/J.IJBIOMAC.2014.10.068.

(8) Ritonja, A.; Rowan, A. D.; Buttle, D. J.; Rawlings, N. D.; Turk, V.; Barrett, A. J. Stem Bromelain: Amino Acid Sequence and Implications for Weak Binding of Cystatin. *FEBS Lett* **1989**, *247* (2), 419–424. https://doi.org/10.1016/0014-5793(89)81383-3.

(9) Kumar, V.; Mangla, B.; Javed, S.; Ahsan, W.; Kumar, P.; Garg, V.; Dureja, H. Bromelain: A Review of Its Mechanisms, Pharmacological Effects and Potential Applications. *Food Funct* **2023**, *14* (18), 8101–8128. https://doi.org/10.1039/d3fo01060k.

(10) Sahbaz, A.; Aynioglu, O.; Isik, H.; Ozmen, U.; Cengil, O.; Gun, B. D.; Gungorduk, K. Bromelain: A Natural Proteolytic for Intra-Abdominal Adhesion Prevention. *International Journal of Surgery* **2015**, *14*, 7–11. https://doi.org/10.1016/j.ijsu.2014.12.024.

(11) Das, S.; Bhattacharyya, D. Destabilization of Human Insulin Fibrils by Peptides of Fruit Bromelain Derived From Ananas Comosus (Pineapple). *J Cell Biochem* **2017**, *118* (12), 4881–4896. https://doi.org/10.1002/jcb.26173.

(12) Pavan, R.; Jain, S.; Shraddha; Kumar, A. Properties and Therapeutic Application of Bromelain: A Review. *Biotechnol Res Int* **2012**, *2012*, 1–6. https://doi.org/10.1155/2012/976203.

(13) Chobotova, K.; Vernallis, A. B.; Majid, F. A. A. Bromelain's Activity and Potential as an Anti-Cancer Agent: Current Evidence and Perspectives. *Cancer Lett* **2010**, *290* (2), 148–156. https://doi.org/10.1016/j.canlet.2009.08.001.

(14) Varilla, C.; Marcone, M.; Paiva, L.; Baptista, J. Bromelain, a Group of Pineapple Proteolytic Complex Enzymes (Ananas Comosus) and Their Possible Therapeutic and Clinical Effects. a Summary. *Foods* **2021**, *10* (10), 2249. https://doi.org/10.3390/foods10102249.

(15) Debnath, R.; Chatterjee, N.; Das, S.; Mishra, S.; Bose, D.; Banerjee, S.; Das, S.; Saha, K. Das; Ghosh, D.; Maiti, D. Bromelain with Peroxidase from Pineapple Are More Potent to Target Leukemia Growth Inhibition - A Comparison with Only Bromelain. *Toxicology in Vitro* **2019**, *55*, 24–32. https://doi.org/10.1016/j.tiv.2018.11.004.

(16) Metzig, C.; Grabowska, E.; Eckert, K.; Rehse, K.; Maurer, H. R. Bromelain Proteases Reduce Human Platelet Aggregation in Vitro, Adhesion to Bovine Endothelial Cells and Thrombus Formation in Rat Vessels in Vivo. *In Vivo* **1999**, *13* (1), 7–12.

(17) Gläser, D.; Hilberg, T. The Influence of Bromelain on Platelet Count and Platelet Activity in Vitro. *Platelets* **2006**, *17* (1), 37–41. https://doi.org/10.1080/09537100500197489.

(18) Han, J. H.; Batey, S.; Nickson, A. A.; Teichmann, S. A.; Clarke, J. The Folding and Evolution of Multidomain Proteins. *Nature Reviews Molecular Cell Biology 2007 8:4* **2007**, *8* (4), 319–330. https://doi.org/10.1038/nrm2144.

(19) He, X. M.; Carter, D. C. Atomic Structure and Chemistry of Human Serum Albumin. *Nature 1992 358:6383* **1992**, *358* (6383), 209–215. https://doi.org/10.1038/358209a0.

(20) SUDLOW, G.; BIRKETT, D. J.; WADE, D. N. The Characterization of Two Specific Drug Binding Sites on Human Serum Albumin. *Mol Pharmacol* **1975**, *11* (6), 824–832. https://doi.org/10.1016/S0026-895X(25)10691-3.

(21) Curry, S.; Brick, P.; Franks, N. P. Fatty Acid Binding to Human Serum Albumin: New Insights from Crystallographic Studies. *Biochim Biophys Acta* **1999**, *1441* (2–3), 131–140. https://doi.org/10.1016/S1388-1981(99)00148-1.

(22) Curry, S.; Mandelkow, H.; Brick, P.; Franks, N. Crystal Structure of Human Serum Albumin Complexed with Fatty Acid Reveals an Asymmetric Distribution of Binding Sites. *Nature Structural Biology 1998 5:9* **1998**, *5* (9), 827–835. https://doi.org/10.1038/1869.

(23) Lee, P.; Wu, X. Review: Modifications of Human Serum Albumin and Their Binding Effect. *Curr Pharm Des* **2015**, *21* (14), 1862–1865. https://doi.org/10.2174/1381612821666150302115025.

(24) M, H.; Azzazy, E.; Christenson, R. H. All About Albumin: Biochemistry, Genetics, and Medical Applications. Theodore Peters, Jr. San Diego, CA: Academic Press, 1996, 432 Pp, $85.00. ISBN 0-12-552110-3. *Clin Chem* **1997**, *43* (10), 2014a–22015. https://doi.org/10.1093/CLINCHEM/43.10.2014A.

(25) Watanabe, H.; Tanase, S.; Nakajou, K.; Maruyama, T.; Kragh-Hansen, U.; Otagiri, M. Role of Arg-410 and Tyr-411 in Human Serum Albumin for Ligand Binding and Esterase-like Activity. *Biochemical Journal* **2000**, *349* (3), 813–819. https://doi.org/10.1042/BJ3490813.

(26) Anfinsen, C. B. Principles That Govern the Folding of Protein Chains. *Science (1979)* **1973**, *181* (4096), 223–230. https://doi.org/10.1126/SCIENCE.181.4096.223/ASSET/1A648F0F-E322-4108-98DD-B0857103738D/ASSETS/SCIENCE.181.4096.223.FP.PNG.

(27) Daggett, V.; Fersht, A. The Present View of the Mechanism of Protein Folding. *Nature Reviews Molecular Cell Biology 2003 4:6* **2003**, *4* (6), 497–502. https://doi.org/10.1038/nrm1126.

(28) Dill, K. A.; MacCallum, J. L. The Protein-Folding Problem, 50 Years On. *Science (1979)* **2012**, *338* (6110), 1042–1046. https://doi.org/10.1126/SCIENCE.1219021/SUPPL_FILE/1042.MP3.

(29) Rose, G. D.; Fleming, P. J.; Banavar, J. R.; Maritan, A. A Backbone-Based Theory of Protein Folding. *Proc Natl Acad Sci U S A* **2006**, *103* (45), 16623–16633. https://doi.org/10.1073/PNAS.0606843103/ASSET/DEB5B0C7-4897-4F23-BE83-A8DA1580422B/ASSETS/GRAPHIC/ZPQ0440640340005.JPEG.

(30) Englander, S. W.; Mayne, L. The Nature of Protein Folding Pathways. *Proc Natl Acad Sci U S A* **2014**, *111* (45), 15873–15880. https://doi.org/10.1073/PNAS.1411798111/ASSET/439B1B01-761E-4B7B-AE5F-207F13C89AD5/ASSETS/GRAPHIC/PNAS.1411798111FIG06.JPEG.

(31) Dobson, C. M. Protein Folding and Misfolding. *Nature 2003 426:6968* **2003**, *426* (6968), 884–890. https://doi.org/10.1038/nature02261.

(32) Levinthal, C. ARE THERE PATHWAYS FOR PROTEIN FOLDING ? *Extrait du Journal de Chimie Physique* **1968**, *65* (1), 44.

(33) Baldwin, R. L. Protein Folding: Matching Speed and Stability. *Nature* **1994**, *369* (6477), 183–184. https://doi.org/10.1038/369183a0.

(34) ANFINSEN, C. B.; HABER, E.; SELA, M.; WHITE, F. H. The Kinetics of Formation of Native Ribonuclease during Oxidation of the Reduced Polypeptide Chain. *Proc Natl Acad Sci U S A* **1961**, *47* (9), 1309–1314. https://doi.org/10.1073/PNAS.47.9.1309/ASSET/D9AA8804-3797-4BF3-8045-576A3ACD0DE7/ASSETS/PNAS.47.9.1309.FP.PNG.

(35) Dill, K. A.; Chan, H. S. From Levinthal to Pathways to Funnels. *Nature Struct. Biol.* **1997**, *4* (1), 10–19. https://doi.org/10.1038/nsb0197-10.

(36) Shirdel, S. A.; Khalifeh, K. Thermodynamics of Protein Folding: Methodology, Data Analysis and Interpretation of Data. *European Biophysics Journal* **2019**, *48* (4), 305–316. https://doi.org/10.1007/S00249-019-01362-7/FIGURES/7.

(37) Tanford, C. Protein Denaturation. *Adv Protein Chem* **1968**, *23* (C), 121–282. https://doi.org/10.1016/S0065-3233(08)60401-5.

(38) Robertson, A. D.; Murphy, K. P. Protein Structure and the Energetics of Protein Stability. *Chem Rev* **1997**, *97* (5), 1251–1267.

(39) Nicholson, D. A.; Jia, B.; Nesbitt, D. J. Measuring Excess Heat Capacities of Deoxyribonucleic Acid (DNA) Folding at the Single-Molecule Level. *Journal of Physical Chemistry B* **2021**, *125* (34), 9719–9726. https://doi.org/10.1021/ACS.JPCB.1C05555/ASSET/IMAGES/LARGE/JP1C05555_0007.JPEG.

(40) Brady, G. P.; Sharp, K. A. Entropy in Protein Folding and in Protein—Protein Interactions. *Curr Opin Struct Biol* **1997**, *7* (2), 215–221. https://doi.org/10.1016/S0959-440X(97)80028-0.

(41) Privalov, P. L. Thermodynamics of Protein Folding. *J. Chem. Thermodynamics* **1997**, *29*, 447–474.

(42) Pace, C. N.; Fu, H.; Fryar, K. L.; Landua, J.; Trevino, S. R.; Shirley, B. A.; Hendricks, M. M. N.; Iimura, S.; Gajiwala, K.; Scholtz, J. M.; Grimsley, G. R. Contribution of Hydrophobic Interactions to Protein Stability. *J Mol Biol* **2011**, *408* (3), 514–528. https://doi.org/10.1016/J.JMB.2011.02.053.

(43) Hilser, V. J.; Gómez, J.; Freire, E. The Enthalpy Change in Protein Folding and Binding: Refinement of Parameters for Structure-Based Calculations. *Proteins: Structure, Function and Genetics* **1996**, *26* (2), 123–133. https://doi.org/10.1002/(SICI)1097-0134(199610)26:2<123::AID-PROT2>3.0.CO;2-H.

(44) Creighton, T. E. Protein Folding. *Biochemical Journal* **1990**, *270* (1), 1–16. https://doi.org/10.1042/BJ2700001.

(45) Nandi, N.; Bagchi, B. Dielectric Relaxation of Biological Water. *J. Phys. Chem. B* **1997**, *101*, 10954–10961.

(46) Pal, S. K.; Zewail, A. H. Dynamics of Water in Biological Recognition. *Chem Rev* **2004**, *104* (4), 2099–2124. https://doi.org/10.1021/cr020689l.

(47) Bhattacharyya, K. Nature of Biological Water: A Femtosecond Study. *Chemical Communications* **2008**, No. 25, 2848–2857. https://doi.org/10.1039/b800278a.

(48) Das, N.; Tarif, E.; Dutta, A.; Sen, P. Associated Water Dynamics Might Be a Key Factor Affecting Protein Stability in the Crowded Milieu. *J. Phys. Chem. B* **2023**, *127* (14), 3151–3163. https://doi.org/10.1021/acs.jpcb.2c09043.

(49) Bagchi, B. Water Dynamics in the Hydration Layer around Proteins and Micelles. *Chem Rev* **2005**, *105* (9), 3197–3219. https://doi.org/10.1021/cr020661+.

(50) Mondal, S.; Mukherjee, S.; Bagchi, B. Protein Hydration Dynamics: Much Ado about Nothing? *J. Phys. Chem. Lett.* **2017**, *8* (19), 4878–4882. https://doi.org/10.1021/acs.jpclett.7b02324.

(51) Hishida, M.; Anjum, R.; Anada, T.; Murakami, D.; Tanaka, M. Effect of Osmolytes on Water Mobility Correlates with Their Stabilizing Effect on Proteins. *J. Phys. Chem. B* **2022**, *126* (13), 2466–2475. https://doi.org/10.1021/acs.jpcb.1c10634.

(52) Guo, F.; Friedman, J. M. Osmolyte-Induced Perturbations of Hydrogen Bonding between Hydration Layer Waters: Correlation with Protein Conformational Changes. *J. Phys. Chem. B* **2009**, *113* (52), 16632–16642. https://doi.org/10.1021/jp9072284.

(53) Negi, K. S.; Das, N.; Khan, T.; Sen, P. Osmolyte Induced Protein Stabilization: Modulation of Associated Water Dynamics Might Be a Key Factor. *Phys. Chem. Chem. Phys.* **2023**, *25* (47), 32602–32612. https://doi.org/10.1039/d3cp03357k.

(54) Heyden, M.; Bründermann, E.; Heugen, U.; Niehues, G.; Leitner, D. M.; Havenith, M. Long-Range Influence of Carbohydrates on the Solvation Dynamics of Water - Answers from Terahertz Absorption Measurements and Molecular Modeling Simulations. *J. Am. Chem. Soc.* **2008**, *130* (17), 5773–5779. https://doi.org/10.1021/ja0781083.

(55) Heugen, U.; Schwaab, G.; Brü, E.; Heyden, M.; Yu, X.; Leitner, D. M.; Havenith, M. Solute-Induced Retardation of Water Dynamics Probed Directly by Terahertz Spectroscopy. *Proc. Natl. Acad. Sci. USA* **2006**, *103* (33), 12301–12306.

(56) Sharp, K. Entropy--Enthalpy Compensation: Fact or Artifact? *Protein Science* **2001**, *10* (3), 661–667. https://doi.org/10.1110/ps.37801.

(57) Senske, M.; Törk, L.; Born, B.; Havenith, M.; Herrmann, C.; Ebbinghaus, S. Protein Stabilization by Macromolecular Crowding through Enthalpy Rather than Entropy. *J. Am. Chem. Soc.* **2014**, *136* (25), 9036–9041. https://doi.org/10.1021/ja503205y.

(58) Feynman, R. P.; Leighton, R. B.; Sands, M. The Feynman Lectures on Physics; Vol. i. *Am J Phys* **1965**, *33* (9), 750–752.

(59) Wand, A. J. Dynamic Activation of Protein Function: A View Emerging from NMR Spectroscopy. *Nature Structural Biology*. 2001, pp 926–931. https://doi.org/10.1038/nsb1101-926.

(60) Boehr, D. D.; Dyson, H. J.; Wright, P. E. An NMR Perspective on Enzyme Dynamics. *Chem Rev* **2006**, *106* (8), 3055–3079. https://doi.org/10.1021/cr050312q.

(61) Mukherjee, P.; Chandra Singh, P. Experimental Insight into Enzyme Catalysis and Dynamics: A Review on Applications of State of Art Spectroscopic Methods. *Adv Protein Chem Struct Biol* **2020**, *122*, 33–62. https://doi.org/10.1016/bs.apcsb.2020.06.003.

(62) Kahsai, A. W.; Rajagopal, S.; Sun, J.; Xiao, K. Monitoring Protein Conformational Changes and Dynamics Using Stable-Isotope Labeling and Mass Spectrometry. *Nat Protoc* **2014**, *9* (6), 1301–1319. https://doi.org/10.1038/nprot.2014.075.

(63) Grimaldo, M.; Roosen-Runge, F.; Zhang, F.; Schreiber, F.; Seydel, T. Dynamics of Proteins in Solution. *Q Rev Biophys* **2019**, *52* (e7), 1–63. https://doi.org/10.1017/s0033583519000027.

(64) Bellissent-Funel, M. C.; Hassanali, A.; Havenith, M.; Henchman, R.; Pohl, P.; Sterpone, F.; Van Der Spoel, D.; Xu, Y.; Garcia, A. E. Water Determines the Structure and Dynamics of Proteins. *Chem Rev* **2016**, *116* (13), 7673–7697. https://doi.org/10.1021/acs.chemrev.5b00664.

(65) Ball, P. Water as an Active Constituent in Cell Biology. *Chem Rev* **2008**, *108* (1), 74–108. https://doi.org/10.1021/cr068037a.

(66) Pal, S. K.; Peon, J.; Zewail, A. H. Ultrafast Surface Hydration Dynamics and Expression of Protein Functionality: α-Chymotrypsin. *Proc Natl Acad Sci U S A* **2002**, *99* (24), 15297–15302. https://doi.org/10.1073/pnas.242600399.

(67) Qiu, W.; Zhang, L.; Okobiah, O.; Yang, Y.; Wang, L.; Zhong, D.; Zewail, A. H. Ultrafast Solvation Dynamics of Human Serum Albumin: Correlations with Conformational Transitions and Site-Selected Recognition. *J. Phys. Chem. B* **2006**, *110* (21), 10540–10549. https://doi.org/10.1021/jp055989w.

(68) Walser, R.; Gunsteren, W. F. van. Viscosity Dependence of Protein Dynamics. *PROTEINS: Structure, Function, and Genetics* **2001**, *42*, 414–421.

(69) Bashardanesh, Z.; Elf, J.; Zhang, H.; Van Der Spoel, D. Rotational and Translational Diffusion of Proteins as a Function of Concentration. *ACS Omega* **2019**, *4* (24), 20654–20664. https://doi.org/10.1021/ACSOMEGA.9B02835/ASSET/IMAGES/LARGE/AO9B02835_0006.JPEG.

(70) Guo, J.; Zhou, H. X. Protein Allostery and Conformational Dynamics. *Chemical Reviews*. 2016, pp 6503–6515. https://doi.org/10.1021/acs.chemrev.5b00590.

(71) Yon, J. M.; Perahia, D.; Ghélis, C. Conformational Dynamics and Enzyme Activity. *Biochimie* **1998**, *80* (1), 33–42. https://doi.org/10.1016/S0300-9084(98)80054-0.

(72) Gangupomu, V. K.; Wagner, J. R.; Park, I. H.; Jain, A.; Vaidehi, N. Mapping Conformational Dynamics of Proteins Using Torsional Dynamics Simulations. *Biophys J* **2013**, *104* (9), 1999–2008. https://doi.org/10.1016/j.bpj.2013.01.050.

(73) Forest, E.; Man, P. Conformational Dynamics and Interactions of Membrane Proteins by Hydrogen/Deuterium Mass Spectrometry. In *Methods in Molecular Biology*; 2016; Vol. 1432, pp 269–279. https://doi.org/10.1007/978-1-4939-3637-3_17.

(74) Mader, S. L.; Lopez, A.; Lawatscheck, J.; Luo, Q.; Rutz, D. A.; Gamiz-Hernandez, A. P.; Sattler, M.; Buchner, J.; Kaila, V. R. I. Conformational Dynamics Modulate the Catalytic Activity of the Molecular Chaperone Hsp90. *Nat Commun* **2020**, *11* (1), 1–12. https://doi.org/10.1038/s41467-020-15050-0.

(75) Das, N.; Yadav, S.; Negi, K. S.; Tarif, E.; Sen, P. Does Microsecond Active-Site Dynamics Primarily Control Proteolytic Activity of Bromelain? Clues from Single Molecular Level Study with a Denaturant, a Stabilizer and a

Macromolecular Crowder. *BBA Advances* **2022**, *2*, 100041. https://doi.org/10.1016/j.bbadva.2022.100041.

(76) Du, X.; Li, Y.; Xia, Y. L.; Ai, S. M.; Liang, J.; Sang, P.; Ji, X. L.; Liu, S. Q. Insights into Protein–Ligand Interactions: Mechanisms, Models, and Methods. *Int J Mol Sci* **2016**, *17* (2), 144. https://doi.org/10.3390/IJMS17020144.

(77) Lill, M. A. Efficient Incorporation of Protein Flexibility and Dynamics into Molecular Docking Simulations. *Biochemistry* **2011**, *50* (28), 6157. https://doi.org/10.1021/BI2004558.

(78) Choy, M. S.; Li, Y.; Machado, L. E. S. F.; Kunze, M. B. A.; Connors, C. R.; Wei, X.; Lindorff-Larsen, K.; Page, R.; Peti, W. Conformational Rigidity and Protein Dynamics at Distinct Timescales Regulate PTP1B Activity and Allostery. *Mol Cell* **2017**, *65* (4), 644–658. https://doi.org/10.1016/j.molcel.2017.01.014.

(79) Papaleo, E.; Saladino, G.; Lambrughi, M.; Lindorff-Larsen, K.; Gervasio, F. L.; Nussinov, R. The Role of Protein Loops and Linkers in Conformational Dynamics and Allostery. *Chemical Reviews*. 2016, pp 6391–6423. https://doi.org/10.1021/acs.chemrev.5b00623.

(80) Schuler, B. Single-Molecule FRET of Protein Structure and Dynamics - a Primer. *J Nanobiotechnology* **2013**, *11(suppl 1)* (S2), 1–17. https://doi.org/10.1186/1477-3155-11-S1-S2.

(81) Mazal, H.; Haran, G. Single-Molecule FRET Methods to Study the Dynamics of Proteins at Work. *Curr Opin Biomed Eng* **2019**, *12*, 8–17. https://doi.org/10.1016/j.cobme.2019.08.007.

(82) Quast, R. B.; Margeat, E. Studying GPCR Conformational Dynamics by Single Molecule Fluorescence. *Mol Cell Endocrinol* **2019**, *493*, 110469. https://doi.org/10.1016/j.mce.2019.110469.

(83) Petrášek, Z.; Hoege, C.; Mashaghi, A.; Ohrt, T.; Hyman, A. A.; Schwille, P. Characterization of Protein Dynamics in Asymmetric Cell Division by Scanning Fluorescence Correlation Spectroscopy. *Biophys J* **2008**, *95* (11), 5476–5486. https://doi.org/10.1529/biophysj.108.135152.

(84) Briddon, S. J.; Kilpatrick, L. E.; Hill, S. J. Studying GPCR Pharmacology in Membrane Microdomains: Fluorescence Correlation Spectroscopy Comes of Age. *Trends Pharmacol Sci* **2018**, *39* (2), 158–174. https://doi.org/10.1016/j.tips.2017.11.004.

(85) Das, D. K.; Das, A. K.; Mandal, A. K.; Mondal, T.; Bhattacharyya, K. Effect of an Ionic Liquid on the Unfolding of Human Serum Albumin: A Fluorescence Correlation Spectroscopy Study. *ChemPhysChem* **2012**, *13* (7), 1949–1955. https://doi.org/10.1002/cphc.201100421.

(86) Haldar, S.; Mitra, S.; Chattopadhyay, K. Role of Protein Stabilizers on the Conformation of the Unfolded State of Cytochrome c and Its Early Folding Kinetics: Investigation at Single Molecular Resolution. *J. Biol. Chem.* **2010**, *285* (33), 25314–25323. https://doi.org/10.1074/jbc.M110.116673.

(87) Yirdaw, R. B.; McHaourab, H. S. Direct Observation of T4 Lysozyme Hinge-Bending Motion by Fluorescence Correlation Spectroscopy. *Biophys J* **2012**, *103* (7), 1525–1536. https://doi.org/10.1016/j.bpj.2012.07.053.

(88) Pabbathi, A.; Ghosh, S.; Samanta, A. FCS Study of the Structural Stability of Lysozyme in the Presence of Morpholinium Salts. *J. Phys. Chem. B* **2013**, *117* (51), 16587–16593. https://doi.org/10.1021/jp409842d.

(89) Sengupta, B.; Chaudhury, A.; Das, N.; Sen, P. Single Molecular Level Probing of Structure and Dynamics of Papain Under Denaturation. *Prot. Pep. Lett.* **2017**, *24* (11), 1073–1081. https://doi.org/10.2174/0929866524666170811145838.

(90) Goluguri, R. R.; Sen, S.; Udgaonkar, J. Microsecond Sub-Domain Motions and the Folding and Misfolding of the Mouse Prion Protein. *Elife* **2019**, *8*, 44766. https://doi.org/10.7554/eLife.44766.

(91) Ries, J.; Schwarze, S.; Johnson, C. M.; Neuweiler, H. Microsecond Folding and Domain Motions of a Spider Silk Protein Structural Switch. *J. Am. Chem. Soc.* **2014**, *136* (49), 17136–17144. https://doi.org/10.1021/ja508760a.

(92) Chen, H.; Rhoades, E. Fluorescence Characterization of Denatured Proteins. *Curr. Opin. Struct. Biol.* **2008**, *18* (4), 516–524. https://doi.org/10.1016/j.sbi.2008.06.008.

(93) Das, G.; Chattoraj, S.; Nandi, S.; Mondal, P.; Saha, A.; Bhattacharyya, K.; Ghosh, S. Probing the Conformational Dynamics of Photosystem i in Unconfined and Confined Spaces. *Phys. Chem. Chem. Phys.* **2017**, *20* (1), 449–455. https://doi.org/10.1039/c7cp07375e.

(94) Das, N.; Khan, T.; Subba, N.; Sen, P. Correlating Bromelain's Activity with Its Structure and Active-Site Dynamics and the Medium's Physical Properties in a Hydrated Deep Eutectic Solvent. *Phys. Chem. Chem. Phys.* **2021**, *23* (15), 9337–9346. https://doi.org/10.1039/d1cp00046b.

(95) Jensen, M. H.; Sukumaran, M.; Johnson, C. M.; Greger, I. H.; Neuweiler, H. Intrinsic Motions in the N-Terminal Domain of an Ionotropic Glutamate Receptor Detected by Fluorescence Correlation Spectroscopy. *J. Mol. Biol.* **2011**, *414* (1), 96–105. https://doi.org/10.1016/j.jmb.2011.09.037.

(96) Sengupta, B.; Das, N.; Sen, P. Elucidation of Ms Dynamics of Domain-III of Human Serum Albumin during the Chemical and Thermal Unfolding: A Fluorescence Correlation Spectroscopic Investigation. *Biophys Chem* **2017**, *221*, 17–25. https://doi.org/10.1016/j.bpc.2016.11.006.

(97) Yadav, R.; Sengupta, B.; Sen, P. Conformational Fluctuation Dynamics of Domain i of Human Serum Albumin in the Course of Chemically and Thermally Induced Unfolding Using Fluorescence Correlation Spectroscopy. *J. Phys. Chem. B* **2014**, *118* (20), 5428–5438. https://doi.org/10.1021/jp502762t.

(98) Wohland, T.; Maiti, S.; Macháň, R. *An Introduction to Fluorescence Correlation Spectroscopy*; IOP Publishing, 2020. https://doi.org/10.1088/978-0-7503-2080-1.

(99) Haustein, E.; Schwille, P. Ultrasensitive Investigations of Biological Systems by Fluorescence Correlation Spectroscopy. *Methods* **2003**, *29*, 153–166.

(100) Lakowicz, J. R. *Principles of Fluorescence Spectroscopy*; Springer, 2006; pp 1–954. https://doi.org/10.1007/978-0-387-46312-4.

(101) Denisov, V. P.; Jonsson, B. H.; Halle, B. Hydration of Denatured and Molten Globule Proteins. *Nat Struct Biol* **1999**, *6* (3), 253–260. https://doi.org/10.1038/6692.

(102) Otting, G.; Liepinsh, E.; Wüthrich, K. Protein Hydration in Aqueous Solution. *Science (1979)* **1991**, *254* (5034), 974–980. https://doi.org/10.1126/science.1948083.

(103) Russo, D.; Murarka, R. K.; Copley, J. R. D.; Head-Gordon, T. Molecular View of Water Dynamics near Model Peptides. *J. Phys. Chem. B* **2005**, *109* (26), 12966–12975. https://doi.org/10.1021/jp051137k.

(104) Kumar, S.; Peon, J.; Zewail, A. H. Biological Water at the Protein Surface: Dynamical Solvation Probed Directly with Femtosecond Resolution. *Proc. Natl. Acad. Sci. USA* **2002**, *99* (4), 1763–1768.

(105) Sahu, K.; Mondal, S. K.; Ghosh, S.; Roy, D.; Sen, P.; Bhattacharyya, K. Femtosecond Study of Partially Folded States of Cytochrome C by Solvation Dynamics. *J. Phys. Chem. B* **2006**, *110* (2), 1056–1062. https://doi.org/10.1021/jp0538924.

(106) Houston, P.; Macro, N.; Kang, M.; Chen, L.; Yang, J.; Wang, L.; Wu, Z.; Zhong, D. Ultrafast Dynamics of Water-Protein Coupled Motions around the Surface of Eye Crystallin. *J. Am. Chem. Soc.* **2020**, *142* (8), 3997–4007. https://doi.org/10.1021/jacs.9b13506.

(107) Qin, Y.; Wang, L.; Zhong, D. Dynamics and Mechanism of Ultrafast Water-Protein Interactions. *Proc. Natl. Acad. Sci. USA* **2016**, *113* (30), 8424–8429. https://doi.org/10.1073/pnas.1602916113.

(108) Fleming, G. R.; Gijzeman, O. L. J.; Freed, K. F.; Lin, S. H. Theory for Time Resolved Emission Spectra. *Journal of the Chemical Society, Faraday Transactions 2: Molecular and Chemical Physics* **1975**, *71*, 773–780. https://doi.org/10.1039/F29757100773.

(109) Jimenez, R.; Fleming, G. R.; Kumar, P. V.; Maroncelli, M. Femtosecond Solvation Dynamics of Water. *Nature* **1994**, *369* (6480), 471–473. https://doi.org/10.1038/369471a0.

(110) Lundgren, J. S.; Heitz, M. P.; Bright, F. V. Dynamics of Acrylodan-Labeled Bovine and Human Serum Albumin Sequestered within Aerosol-Ot Reverse Micelles. *Anal Chem* **1995**, *67* (20), 3775–3781. https://doi.org/10.1021/AC00116A025.

(111) Peon, J.; Pal, S. K.; Zewail, A. H. Hydration at the Surface of the Protein Monellin: Dynamics with Femtosecond Resolution. *Proceedings of the National Academy of Sciences* **2002**, *99* (17), 10964–10969. https://doi.org/10.1073/pnas.162366099.

(112) Kamal, J. K. A.; Zhao, L.; Zewail, A. H. Ultrafast Hydration Dynamics in Protein Unfolding: Human Serum Albumin. *Proceedings of the National Academy of Sciences* **2004**, *101* (37), 13411–13416. https://doi.org/10.1073/pnas.0405724101.

(113) Dutta, P.; Sen, P.; Halder, A.; Mukherjee, S.; Sen, S.; Bhattacharyya, K. Solvation Dynamics in a Protein–Surfactant Complex. *Chem Phys Lett* **2003**, *377* (1–2), 229–235. https://doi.org/10.1016/S0009-2614(03)01143-6.

(114) Pal, S. K.; Mandai, D.; Sukul, D.; Sen, S.; Bhattacharyya, K. Solvation Dynamics of DCM in Human Serum Albumin. *J. Phys. Chem. B* **2001**, *105* (7), 1438–1441. https://doi.org/10.1021/jp002368o.

(115) Chowdhury, R.; Mojumdar, S. Sen; Chattoraj, S.; Bhattacharyya, K. Effect of Ionic Liquid on the Native and Denatured State of a Protein Covalently Attached to a Probe: Solvation Dynamics Study. *Journal of Chemical Physics* **2012**, *137* (5), 55104. https://doi.org/10.1063/1.4739922/671633.

(116) Sen, P.; Mukherjee, S.; Dutta, P.; Halder, A.; Mandal, D.; Banerjee, R.; Roy, S.; Bhattacharyya, K. Solvation Dynamics in the Molten Globule State of a Protein. *J. Phys. Chem. B* **2003**, *107* (51), 14563–14568. https://doi.org/10.1021/jp036277d.

(117) Yadav, R.; Sengupta, B.; Sen, P. Effect of Sucrose on Chemically and Thermally Induced Unfolding of Domain-I of Human Serum Albumin: Solvation Dynamics and Fluorescence Anisotropy Study. *Biophys Chem* **2016**, *211*, 59–69. https://doi.org/10.1016/j.bpc.2016.02.005.

(118) Mohan, V.; Sengupta, B.; Das, N.; Banerjee, I.; Sen, P. Domain-Specific Stabilization of Structural and Dynamic Responses of Human Serum Albumin by Sucrose. *Protein Pept Lett* **2019**, *26* (4), 287–300. https://doi.org/10.2174/0929866526666190122115702.

(119) Dogra, P.; Arya, S.; Singh, A. K.; Datta, A.; Mukhopadhyay, S. Conformational and Solvation Dynamics of an Amyloidogenic Intrinsically Disordered Domain of a Melanosomal Protein. *Journal of Physical Chemistry B* **2022**, *126* (2), 443–452. https://doi.org/10.1021/ACS.JPCB.1C09304/ASSET/IMAGES/LARGE/JP1C09304_0005.JPEG.

(120) Kistwal, T.; Mukhopadhyay, A.; Dasgupta, S.; Sharma, K. P.; Datta, A. Ultraslow Biological Water-Like Dynamics in Waterless Liquid Protein. *Journal of Physical Chemistry Letters* **2022**, *13* (19), 4389–4393. https://doi.org/10.1021/ACS.JPCLETT.2C00702/ASSET/IMAGES/LARGE/JZ2C00702_0003.JPEG.

(121) Zhang, L.; Wang, L.; Kao, Y.-T.; Qiu, W.; Yang, Y.; Okobiah, O.; Zhong, D. Mapping Hydration Dynamics around a Protein Surface. *Proc. Natl. Acad. Sci. USA* **2007**, *104* (47), 18461–18466.

(122) Kamal, J. K. A.; Xia, T.; Pal, S. K.; Zhao, L.; Zewail, A. H. Enzyme Functionality and Solvation of Subtilisin Carlsberg: From Hours to Femtoseconds. *Chem Phys Lett* **2004**, *387* (4–6), 209–215. https://doi.org/10.1016/j.cplett.2004.02.011.

(123) Maroncelli, M.; Fleming, G. R. Picosecond Solvation Dynamics of Coumarin 153: The Importance of Molecular Aspects of Solvation. *J Chem Phys* **1987**, *86* (11), 6221–6239. https://doi.org/10.1063/1.452460.

(124) Samaddar, S.; Mandal, A. K.; Mondal, S. K.; Sahu, K.; Bhattacharyya, K.; Roy, S. Solvation Dynamics of a Protein in the Pre Molten Globule State. *J Phys Chem B* **2006**, *110* (42), 21210–21215. https://doi.org/10.1021/jp064136g.

(125) Johnson, M. E.; Malardier-Jugroot, C.; Head-Gordon, T. Effects of Co-Solvents on Peptide Hydration Water Structure and Dynamics. *Physical*

Chemistry Chemical Physics **2010**, *12* (2), 393–405. https://doi.org/10.1039/b915888j.

(126) Chang, C. W.; He, T. F.; Guo, L.; Stevens, J. A.; Li, T.; Wang, L.; Zhong, D. Mapping Solvation Dynamics at the Function Site of Flavodoxin in Three Redox States. *J Am Chem Soc* **2010**, *132* (36), 12741–12747. https://doi.org/10.1021/JA1050154/ASSET/IMAGES/LARGE/JA-2010-050154_0006.JPEG.

(127) Luong, T. Q.; Verma, P. K.; Mitra, R. K.; Havenith, M. Do Hydration Dynamics Follow the Structural Perturbation during Thermal Denaturation of a Protein: A Terahertz Absorption Study. *Biophys J* **2011**, *101* (4), 925–933. https://doi.org/10.1016/J.BPJ.2011.05.011/ATTACHMENT/D1C43398-B551-4D7A-A309-48BC549D24DF/MMC1.PDF.

(128) Verma, P. K.; Rakshit, S.; Mitra, R. K.; Pal, S. K. Role of Hydration on the Functionality of a Proteolytic Enzyme α-Chymotrypsin under Crowded Environment. *Biochimie* **2011**, *93* (9), 1424–1433. https://doi.org/10.1016/j.biochi.2011.04.017.

(129) Samanta, N.; Luong, T. Q.; Das Mahanta, D.; Mitra, R. K.; Havenith, M. Effect of Short Chain Poly(Ethylene Glycol)s on the Hydration Structure and Dynamics around Human Serum Albumin. *Langmuir* **2016**, *32* (3), 831–837. https://doi.org/10.1021/acs.langmuir.5b03884.

(130) Mukherjee, S. K.; Gautam, S.; Biswas, S.; Kundu, J.; Chowdhury, P. K. Do Macromolecular Crowding Agents Exert Only an Excluded Volume Effect? A Protein Solvation Study. *Journal of Physical Chemistry B* **2015**, *119* (44), 14145–14156. https://doi.org/10.1021/acs.jpcb.5b09446.

(131) Huang, K. Y.; Kingsley, C. N.; Sheil, R.; Cheng, C. Y.; Bierma, J. C.; Roskamp, K. W.; Khago, D.; Martin, R. W.; Han, S. Stability of Protein-

Specific Hydration Shell on Crowding. *J. Am. Chem.Soci.* **2016**, *138* (16), 5392–5402. https://doi.org/10.1021/jacs.6b01989.

(132) Biswas, S.; Mukherjee, S. K.; Chowdhury, P. K. Crowder-Induced Rigidity in a Multidomain Protein: Insights from Solvation. *J. Phys. Chem. B* **2016**, *120* (49), 12501–12510. https://doi.org/10.1021/acs.jpcb.6b10478.

(133) Senske, M.; Xu, Y.; Bäumer, A.; Schäfer, S.; Wirtz, H.; Savolainen, J.; Weingärtner, H.; Havenith, M. Local Chemistry of the Surfactant's Head Groups Determines Protein Stability in Reverse Micelles. *Physical Chemistry Chemical Physics* **2018**, *20* (13), 8515–8522. https://doi.org/10.1039/c8cp00407b.

(134) Mukherjee, S. K.; Biswas, S.; Rastogi, H.; Dawn, A.; Chowdhury, P. K. Influence of Crowding Agents on the Dynamics of a Multidomain Protein in Its Denatured State: A Solvation Approach. *European Biophysics Journal* **2020**, *49* (3–4), 289–305. https://doi.org/10.1007/s00249-020-01435-y.

(135) Rastogi, H.; Chowdhury, P. K. Understanding Enzyme Behavior in a Crowded Scenario through Modulation in Activity, Conformation and Dynamics. *Biochim Biophys Acta Proteins Proteom* **2021**, *1869* (11), 140699. https://doi.org/10.1016/j.bbapap.2021.140699.

(136) Rastogi, H.; Chowdhury, P. K. Correlating the Local and Global Dynamics of an Enzyme in the Crowded Milieu. *J. Phys. Chem. B* **2022**, *126* (17), 3208–3223. https://doi.org/10.1021/acs.jpcb.1c09759.

(137) Mubashira, K.; Pramanik, U.; Khamari, L.; Mukherjee, S. Monitoring the Effect of SDS on the Solvation Dynamics and Structural Conformation of β-Casein. *Journal of Chemical Sciences* **2022**, *134* (4), 1–9. https://doi.org/10.1007/S12039-022-02092-8/TABLES/2.

(138) Rastogi, H.; Singh, A.; Chowdhury, P. K. Towards the Energy Landscape of Adenylate Kinase in Crowded Milieu: Activity, Conformation, Structure and

Dynamics in Sequence. *Arch Biochem Biophys* **2023**, *743*, 109658. https://doi.org/10.1016/j.abb.2023.109658.

(139) Singh, A.; Gupta, M.; Rastogi, H.; Khare, K.; Chowdhury, P. K. Deeper Insights into Mixed Crowding through Enzyme Activity, Dynamics, and Crowder Diffusion. *J Phys Chem B* **2024**, *128* (22), 5293–5309. https://doi.org/10.1021/acs.jpcb.4c00337.

1.2. Deep Eutectic Solvents (DESs): A brief overview

The field of chemistry has long relied on solvents to facilitate reactions, separations, and other critical processes. However, many traditional solvents are toxic, volatile, and environmentally damaging, driving the search for greener alternatives. Thus, finding safer solvents is one of the most important points among the 12 principles of green chemistry developed by Paul Anastas and John Warner.[1,2] One of the key objectives of green chemistry is to reduce waste generation, and catalysis plays a vital role in achieving this.[3,4] Enzymes, due to their remarkable efficiency and specificity, make biocatalysis a natural choice for industrial processes, offering a sustainable and highly selective approach to chemical reactions.[5–8] However, water is the main solvent for the living world, and most enzymes are stable only in water, limiting the scope of biocatalysis.[9,10]

The approach of using engineered enzymes that are capable of functioning in organic solvents has already been recognized through the Nobel Prize to Frances Arnold.[11–13] However, this approach requires extensive biological expertise and time-consuming trials.[11–14] An alternative approach would be to discover novel solvents that are tunable and can maintain enzyme stability and activity, which would open new possibilities for biocatalysis.[9,10,15] This is where deep eutectic solvents (DESs) show great promise.[10,16–18] DESs offer advantages like simple and atom-efficient synthesis, low vapor pressure, and tunability for product separation and extraction but, most importantly, can keep enzymes/proteins stable and active therein.[19–23] Moreover, many naturally occurring compounds can form deep eutectic solvents (commonly referred to as natural deep eutectic solvent or NaDES) and are thought to be environmentally safer, non-toxic, and biodegradable media than conventionally used organic solvents.[22,24]

1.2.1. Definition of DES

The term ‘deep eutectic solvent’ contains two words, “eutectic” and “deep”, that need to be explained to understand their meaning of it. The term eutectic refers to a mixture of two or more components that, when combined, have a melting point lower than that of any individual component. The word ‘deep’ in DES refers to the significant depression in the melting point, often much lower than that of a simple eutectic mixture.[19,25,26] In 2003, Abott and co-workers pioneered this concept by taking a mixture of choline chloride (with a melting point of 302 ℃) and urea (melting point of 133 ℃) at 1:2 molar ratio, which results in a eutectic mixture with a melting point of only 12 ℃.[27] This ability to dramatically lower the melting point is what distinguishes DESs from ordinary eutectic mixtures, where melting point depression is generally less pronounced (will be clarified in the next sections). This occurs due to the specific interactions between the hydrogen bond donor (HBD) and the hydrogen bond acceptor (HBA), such as choline chloride and urea, which results in forming a liquid that remains stable at a temperature much lower than the melting point of both the constituents.[19,27] The specific interaction between its constituents, generally H-bonding, distinguishes normal eutectic mixtures from deep eutectic solvents.[19,25]

1.2.2. Thermodynamics of Eutectic Mixtures and DESs

Consider a solution that is in equilibrium with pure solid solvent. Then at equilibrium condition [when freezing is occurring],

$$\mu(T, P, x) = \mu_{solid}(T, P) \qquad (1.2.1)$$

Where, $\mu(T, P, x)$ is the chemical potential of the solvent in the solution, $\mu_{solid}(T, P)$ is the chemical potential of the pure solid (as the solid is pure, it does not depend on any composition variable), T is the equilibrium temperature, i.e., the freezing point of the solution, and x is the mole fraction of the solvent in the solution. At constant pressure, the freezing point of a solution is only a function of the composition of the solvent.[28]

For an ideal solution,

$$\mu(T,P,x) = \mu^0(T,P) + RT\ln x \quad (1.2.2)$$

Where, $\mu^0(T,P)$ is the chemical potential of pure liquid solvent

Replacing equation 1.2.2 in equation 1.2.1,

$$\mu^0(T,P) + RT\ln x = \mu_{solid}(T,P) \quad (1.2.3)$$

$$\therefore\ RT\ln x = \mu_{solid}(T,P) - \mu^0(T,P) \quad (1.2.4)$$

$$\therefore\ \ln x = \frac{-\left(\mu^0(T,P) - \mu_{solid}(T,P)\right)}{RT} \quad (1.2.5)$$

As, $\mu^0(T,P)$ is the chemical potential of pure liquid solvent, $\mu^0(T,P) - \mu_{solid}(T,P) = \Delta G_{fusion}$, where the ΔG_{fusion} is the free energy of fusion of the pure solvent.[28]

Then equation 1.2.5 becomes,

$$\ln x = \frac{-\Delta G_{fusion}}{RT} \quad (1.2.6)$$

To discover how T depends on x, we evaluate $\left(\frac{\partial T}{\partial x}\right)$ at constant P,

$$\therefore \frac{\partial}{\partial x}(\ln x) = \frac{\partial}{\partial x}\left[\left(\frac{-\Delta G_{fus}}{RT}\right)\right]_P \quad (1.2.7)$$

$$\therefore \frac{1}{x} = -\frac{1}{R}\left[\frac{\partial}{\partial T}\left(\frac{-\Delta G_{fus}}{T}\right)\left(\frac{\partial T}{\partial x}\right)\right]_P \quad (1.2.8)$$

From Gibbs-Helmholtz equation,

$$\left[\frac{\partial}{\partial T}\left(\frac{\Delta G}{T}\right)\right]_P = -\frac{\Delta H}{T^2} \quad (1.2.9)$$

Then equation 8 becomes,

$$\frac{1}{x} = -\frac{1}{R}\left[-\frac{\Delta H_{fus}}{T^2}\right]\left(\frac{\partial T}{\partial x}\right)_P \quad (1.2.10)$$

$$\frac{1}{x} = \frac{\Delta H_{fus}}{RT^2}\left(\frac{\partial T}{\partial x}\right)_P \quad (1.2.11)$$

ΔH_{fus} = the heat of fusion of the pure solvent

Rearranging and integrating the equation 1.2.11,

$$\int_1^x \frac{dx}{x} = \int_{T_0}^{T} \frac{\Delta H_{fus}}{RT^2}\, dT \quad (1.2.12)$$

When, $x = 1$, the solution is only pure solvent and T_0 is the freezing point of the pure solvent.

Then the equation 1.2.12 becomes,

$$\ln x = -\frac{\Delta H_{fus}}{R}\left(\frac{1}{T} - \frac{1}{T_0}\right) \quad (1.2.13)$$

$$\ln x = \frac{\Delta H_{fus}}{R}\left(\frac{1}{T_0} - \frac{1}{T}\right) \quad (1.2.14)$$

The ideal Solid-Liquid phase diagram for mixtures at different compositions can be determined using Equation 14.[26,28,29]

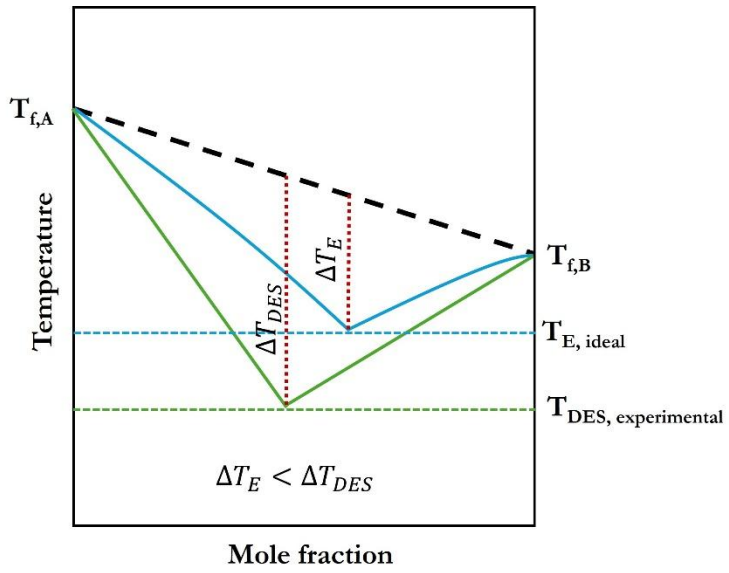

Scheme 1.2.1.: Schematic representation of a simple ideal eutectic mixture (cyan) and a deep eutectic mixture (green) of constituents A and B. $T_{f,A}$ and $T_{f,B}$ are the freezing points of pure A and pure B. In the case of deep eutectic solvent, the depression of the freezing point (ΔT_{DES}) should be higher than the ideal eutectic mixture (ΔT_E).

Eutectic mixtures are characterized by a decrease in melting points. When two compounds mix, it leads to a eutectic point. The ideal phase diagram for such a system is V-shaped rather than a straight line between the melting points of the pure compounds (just a linear combination of the melting points of the two pure constituents, see scheme 1.2.1).[26,29] This V-shape captures the natural melting point depression of the components, signifying an ideal eutectic solvent. By comparing the calculated ideal phase diagram with experimental data, one can assess the system's behavior. If the experimentally observed melting temperatures are significantly lower than those predicted by the ideal model, the mixture qualifies as a deep eutectic solvent (DES).[26,29]

DESs differ from ordinary eutectic mixtures by showing stronger interactions between their components, leading to a greater drop in melting points than the ideal eutectic point.[26,29] This negative deviation from ideal thermodynamics (see scheme 1.2.1) makes a DES “deep”.

1.2.3. Common Misconception regarding DESs

A common misconception is that DESs are a type of ionic liquid. However, Abbott *et al.* clarified that DESs, and ionic liquids are fundamentally different.[19] DESs are mixtures, whereas ionic liquids are pure compounds. Even cholinium chloride (commonly referred to as choline chloride) salt, a common component in DESs, does not qualify as an ionic liquid despite being made of ions.[19,26]

Although the most common description of DESs is that they are simply mixtures of hydrogen bond donors (HBDs) and acceptors (HBAs), a small clarification is required. The acidity differences between the constituents must be small; so that no proton transfer occurs and forms a protic ionic liquid in place of DESs.[26] Smith *et al.* described DESs in their review article as "DESs are systems formed from a eutectic mixture of Lewis or Brønsted acids and bases which can contain a variety of anionic and/or cationic species".[19] This means that not all HBD-HBA mixtures, rather specific acidity differences between constituents enable hydrogen bonding without forming protic ionic liquids, qualify as DESs.[26] Also, the acids and bases must interact in such a way that the melting point drops significantly (negative deviation) beyond what would be predicted if the mixture behaved ideally.[26]

1.2.4. Properties of DESs

Several key features of DES make this solvent a potential game changer in the field of chemistry and biology.

(i) Significant melting point depression: Because of the significant depression in the melting point, most of the deep eutectic solvents remain liquid over a long range of temperatures, especially at room temperature which makes the applicability of DESs wider.[19,25]

(ii) Greenness and biodegradability: Many of the DESs are composed of naturally occurring, biodegradable compounds such as choline chloride, urea, sorbitol, sucrose, etc. The non-toxic and ability to break down into environmentally benign byproducts make DESs a sustainable and green option of chemistry.[22,24]

(iii) Easy and atom-economic synthesis: Simple mixing and heating of an appropriate amount of components can make DES, which makes the synthesis straightforward and atom-economic. However, ionic liquid preparation requires complex synthesis and purification.[30]

(iv) Tunability: The most appealing feature of DESs is their tunability. By adjusting the mole fractions of HBD and HBA, or by varying the types of components used, DESs can be customized to achieve desired solvent properties such as polarity, viscosity, and thermal stability.[19,25,31,32] Also, note that the idea of DESs shouldn't be limited to fixed ratios of HBD and HBA like 1:2, 1:1, etc. Instead, users should be able to adjust the composition of the solvent to achieve the best performance.[26]

(v) High Solubilization Capacity: Depending upon the chemical nature of the constituents, DESs can dissolve a wide range of substances, including polymers, organic compounds, and metal salts, which makes them useful in diverse fields such as chemical synthesis, biocatalysis, and pharmaceuticals.[33,34]

(vi) Safety and Stability: DESs are non-volatile, non-flammable, and also stable both thermally and chemically. This makes them safer for handling, storage, and transport, and ideal for high-temperature or harsh chemical processes like catalysis and metal extraction, where traditional solvents may fail.[19,33]

(vii) Biocompatibility: DESs are particularly attractive in biocatalysis due to their ability to maintain the activity and stability of enzymes. In many cases, enzymes exhibit increased stability and activity in DESs compared to traditional solvents.[23,35–42]

(viii) ***Molecular Heterogeneity of DESs:*** DESs have been extensively characterized to exhibit notable spatial and dynamic heterogeneity at the molecular level, where distinct microenvironments arise due to specific interactions between hydrogen bond acceptor (HBA) and donor (HBD).[43–50]

In one of the chapters, I have identified molecular heterogeneity of the DES; I will be discussing a little bit about heterogeneity here, and then go into the discussion of protein behaviour in DESs and hydrated DESs.

1.2.5. Molecular Heterogeneity of DESs

The presence of molecular-level heterogeneity has been identified as an intriguing feature of DESs.[43–50] Heterogeneity refers to diversity or difference within a system where not all molecules experience the same environment. This is easily observed in mixtures of two solids, but within complex media like liquids, heterogeneity is less perceptible at a macroscopic level. Although most solvent systems appear homogeneous, molecular-level studies often reveal a heterogeneous environment where molecular interactions and forces vary locally.[51–53] This variation stems from force imbalances among molecules due to differences in local interactions. However, confirming the presence of heterogeneity in a system depends strongly on the time and length scale of observation. Most systems will reveal heterogeneity at an atomic scale, yet as the observation scale increases, such heterogeneity becomes "smeared out" and appears homogeneous.

At the molecular level, heterogeneity becomes essential for understanding chemical and biological systems, from solvents to cells and from nanoparticles to bulk solids.[47,54–56] Generally, in literature, one encounters two terms of heterogeneity, namely spatial and dynamic heterogeneity.[51,57] The first one refers to variations in molecular arrangements within a DES, forming distinct microdomains or regions where the composition and interactions of molecules differ (see scheme 1.2.2).[58] The dynamic heterogeneity pertains to variations in molecular motion and relaxation rates across different regions of a DES (see scheme 1.2.2).[58] If there is heterogeneity in dynamics, there must be a difference in structure[51,57], whether we can observe it or not and that is why spatial and dynamic heterogeneity is mainly used in literature as per the methods of observation. Basically, if one can observe heterogeneity in the system through some dynamical measurement, then it is called dynamic heterogeneity and similarly spatial heterogeneity.

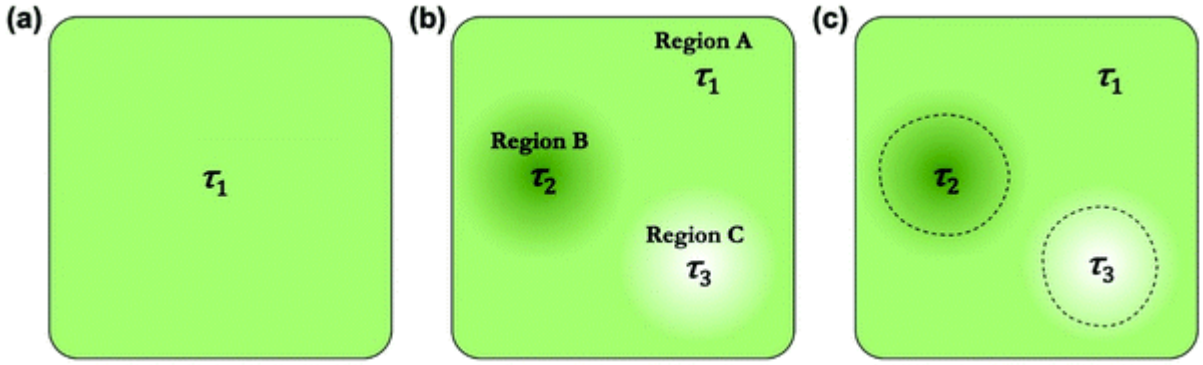

Scheme 1.2.2. (a) Illustration of a homogeneous solvent medium, where all areas have an identical relaxation rate, τ_1, (b) Representation of dynamic heterogeneity, showing Regions B and C with distinct relaxation times (τ_2 and τ_3) compared to the rest of the medium (Region A with τ_1), (c) Depiction of spatial heterogeneity, with boundaries indicating separate dynamic regions. Dynamic heterogeneity suggests that structural differences exist across regions, regardless of whether they are directly observable. This figure has been reprinted from the reference [58].

The go-to technique for detecting spatial heterogeneity in a system is steady-state fluorescence-based red edge excitation shift (REES), because of its easy instrumentation and wide availability.[59–61] Generally, the emission maxima or the quantum yield do not depend upon the excitation wavelength.[62] However, if a heterogeneous distribution of the excitation and emission energy of the indicator fluorophore exists in a solution, excitation at different wavelengths along the absorption spectrum excites different subpopulations.[60,61,63]

The photo-selection is possible only at the red edge because excitation at other positions can also access lower energy states through other transitions.[60,62,63] Individually, Galley and Rubinov, in the year 1970, first proposed this novel edge effect.[64,65] Later, it was extended massively by Azumi in complex liquids and by Demchenko in bio-systems.[66–69] To detect the spatial heterogeneity of DESs or ionic liquids, REES has been extensively used previously.[45,50,59,70–73]

On the other hand, viscosity decoupled dynamics has been taken as a measure of dynamic heterogeneity.[43–45,71,72,74–82] Generally, any dynamics in a media should follow the media viscosity. The translational dynamics and rotational dynamics

depend on the medium's viscosity in a linear manner according to the Stokes-Einstein (SE) and Stokes-Einstein-Debye (SED) relationships, respectively.[58]

$$D_T = \frac{kT}{6\pi\eta r} \qquad \text{(SE relation)}$$

$$D_R = \frac{kT}{8\pi\eta r^3} \qquad \text{(SED relation)}$$

Here, D_T and D_R are the translational and rotational diffusion coefficients, k is the Boltzmann constant, η is the viscosity of the medium, T is the system's temperature, and r is the radius of the molecule considering the sphere. As diffusion coefficients are inversely proportional to the associated relaxation time, it can be linked as $\tau_{T\ or\ R} \propto \frac{\eta}{T}$

Taking log on both sides,

$$\log(\tau_{T\ or\ R}) = \log\left(\frac{\eta}{T}\right) + \log C; \qquad (1.2.15)$$

where $C = \frac{6\pi r}{k}\ or\ \frac{8\pi r^3}{k}$

The relation of dynamics with viscosity is generally expressed in a log-log plot of $\tau_{T\ or\ R}$ and $\frac{\eta}{T}$, producing a straight line with a unitary slope.

Now, if the dynamics depend on the media viscosity fractionally, then

$$\tau_{T\ or\ R} \propto \left(\frac{\eta}{T}\right)^p \qquad (1.2.16)$$

$$\therefore \log(\tau_{T\ or\ R}) = p\log\left(\frac{\eta}{T}\right) + \log C \qquad (1.2.17)$$

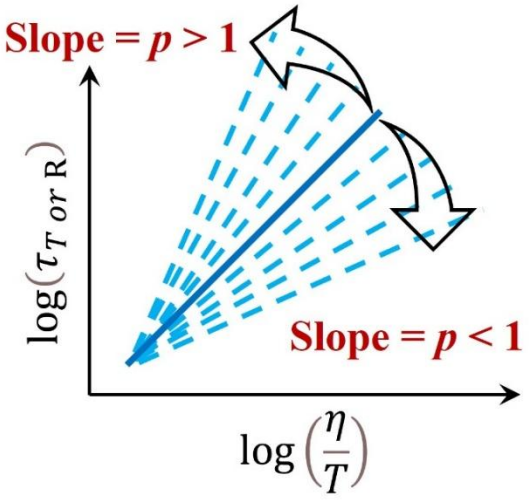

Scheme 1.2.3. (a) Illustration of the log-log plot of relaxation time ($\tau_{T\ or\ R}$) vs temperature reduced viscosity $\left(\frac{\eta}{T}\right)$. The deviation of the slope from unity basically implies the presence of dynamic heterogeneity in the system.

The slope is now denoted as p. A value of $p = 1$ will mean the dynamics strictly follow the media viscosity in a Stokes-Einstein manner. However, $p \neq 1$ indicates that the system no longer adheres to the Stokes-Einstein (SE) or Stokes-Einstein-Debye (SED) relationship, signifying that diffusion is no longer directly coupled with the media viscosity (Scheme 1.2.3).[58] This phenomenon, known as viscosity decoupling, is considered the key indicator of dynamic heterogeneity in the system. Biswas and Co-workers and, subsequently, many other research groups over time identified DESs and hydrated DESs as a dynamically heterogeneous medium.[43,44,50,71,72,74–78,82]

Although DESs are proven to be heterogeneous by different studies, there has been almost no effort to understand the implications of this heterogeneity in other DES-related studies, especially in protein behavior in DESs.

1.2.6. Applications of DESs in Various Fields

By offering advantages over conventional organic solvents, DES has gained recognition as a promising green solvent. A quick search on Scopus with the keyword "deep eutectic solvent" reveals rapid growth in DES-related research, with a high surge in the last 5-6 years (See Figure 1.2.1a). There are many extensive review articles enlisting various applications of DESs and out of the scope of this thesis.[19,20,25,33,83,84] Over the last decade, DESs has garnered substantial attention in biocatalysis, recognized as a potential game changer due to its tunability and exceptional ability to maintain protein stability and activity (See Figure 1.2.1b).[18,21,23,36,85]

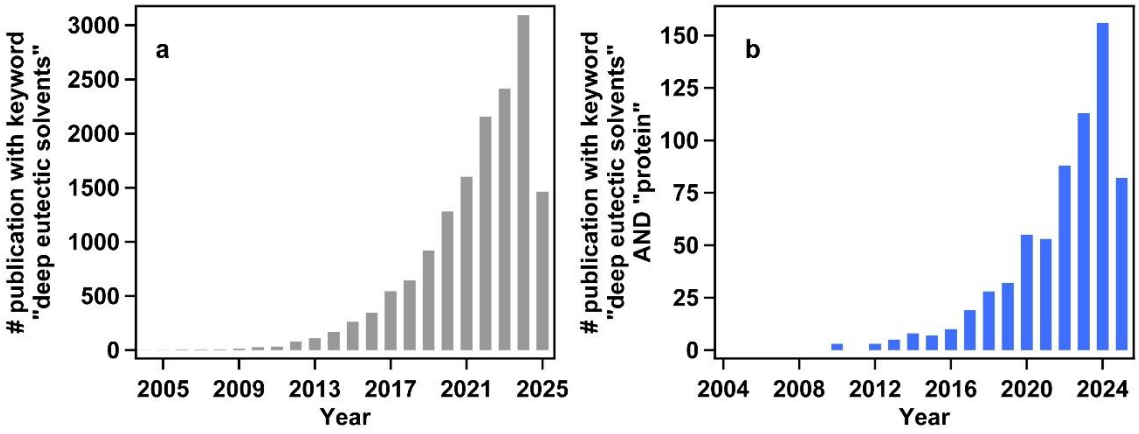

Figure 1.2.1. Number of research articles published each year involving deep eutectic solvents (Source Scopus; Date: 25 April 2025; with Keywords: (a) TITLE-ABS-KEY ("deep eutectic solvents"), (b) TITLE-ABS-KEY ("deep eutectic solvents" AND "protein" OR "enzyme").

Here, I will try to very briefly discuss some of the applications of DESs and then elaborate on the enzyme behaviour in DESs, as that is the primary topic of my thesis.

- **DESs as reaction media:** The most extensive use of DESs was as a reaction media. Many organic reactions, like esterification, polymerization, oxidation, coupling, etc., have been successfully carried out even with better efficiency

and selectivity in DESs.[86–89] A recent review article by Hooshmand *et al.* compiled many cross-coupling reactions along with popular name reactions in DES media and tried to relate the efficiency of the reactions to the nature of DESs.[90] Other articles are available in the literature reporting different classes of organic reactions in DESs.[86–89] Apart from organic reactions, DESs are becoming a popular choice for nanoparticle synthesis media.[91,92] One of the difficult tasks in the case of nanoparticle synthesis is the shape control, which has been done by Liao *et al.* by employing DES as a solvent.[91] More interestingly, they have achieved size control as well just by controlling the amount of water in the media.

- **DESs as extraction media:** In recent times, DESs have shown significant potential in various extraction processes. In desulfurization, DESs like formic acid and tetrabutyl ammonium bromide effectively remove sulfur compounds from fuels, offering a more efficient method than traditional approaches.[93,94] DESs have been successful in metal extraction, like recovering metals such as cadmium from rice flour and enhancing lithium extraction.[95] DESs have also demonstrated efficiency in water purification, extracting micropollutants and heavy metals to provide cleaner water.[96–98] More importantly, DESs outperform conventional solvents in the extraction of bioactive molecules like flavonoids, alkaloids, artemisinin, etc., from natural sources and keep the biomolecules stable therein.[99–102]

- **Greenhouse gas absorption:** Many DESs offer a promising solution for capturing greenhouse gases such as SO_2 and CO_2 due to their ability to form strong interactions with these gases.[103–107] Studies have shown that DESs with appropriate hydrogen bond donors and acceptors can efficiently absorb CO_2, with potential applications in carbon capture and storage technologies.[104–106] The tunability of DESs allows for the optimization of gas absorption capacity,

making them a viable alternative to conventional amine-based CO_2 capture solvents.[108]

- **DESs in electrochemistry**: DESs have gained attention in electrochemistry as both solvents and electrolytes, owing to their high ionic conductivity and ability to dissolve a wide range of electrolytes.[19,109,110] They are used in batteries, supercapacitors, and energy storage devices, where high ion concentration and stability are critical.[111–114] For example, DESs have been used to improve the performance of lithium-ion batteries and supercapacitors, showing enhanced electrochemical properties and better thermal stability compared to traditional electrolytes.[111,112,115]

- **DESs as biocatalytic media:** DESs provide a unique environment that stabilizes enzymes and maintains their activity, making them suitable media for enzymatic reactions.[16,18,21,23,116] Generally, water, due to its poor solubility towards organic solvents, limits the scope of biocatalysis. On the other hand, organic solvents, in most cases, fail to retain the enzymes in their functional state. DESs enable reactions that are difficult to perform in water or organic solvents. Gorke *et al.*, for the first time, used lipase enzyme for the esterification reaction in deep eutectic solvents, which started biocatalysis in DESs.[117] Later, many groups reported that enzymes such as lipase and protease exhibited increased stability and activity in DESs compared to traditional solvents.[36,37,39,41,118–123] This opens new possibilities for industrial biocatalysis, where enzyme-driven reactions can be performed more efficiently and sustainably, employing DES according to requirements. Consequently, growing interest in biocatalysis in DES is clearly visible in the increasing number of publications with time (See Figure 1.2.1b).

  In my thesis, I have worked mainly on the enzymatic behaviour in DESs and tried to provide a physical insight into what actually controls the behaviour.

The following section provides an in-depth analysis of protein behavior in both neat and hydrated deep eutectic solvents.

- **Other uses:** Apart from that, DESs are explored in drug delivery systems for better solubility of poorly soluble drugs.[124–126] Their potential extends to material science, such as biodegradable polymers and sustainable materials, owing to their tunable, non-toxic, and biodegradable properties.[127–130]

1.2.7. Current Understanding of Protein Behaviour in DESs:

As discussed in the previous section, DES has been increasingly identified as a potential biocatalytic medium due to its novel characteristics such as tunability, greenness, and non-denaturant nature.[19,25,30] DES serves as an alternative media, offering unique interactions that may stabilize the protein and/or retain protein activity under certain conditions. The study of protein behavior in deep eutectic solvents (DES) focuses mainly on how these solvents interact with and influence protein stability, structure, and function. Some recent review articles have tabulated almost all the important studies related to DES and protein behavior.[23,116,131] Here, I will only give a list of some important studies along with the most recent reports, which will provide an overview and current understanding of the field.

Table 1.2.1. Modulation of protein stability and activity in the presence of DES or hydrated DES. The references provided are not exhaustive, and numerous additional examples exist in the literature.

Protein	DES	Stability	Activity	Year (ref)
Lipase	Choline chloride (ChCl): urea/glycerol (Gly)	Long-term stability in both choline chloride-urea and glycerol DES.	high activity and selectivity in choline chloride urea and glycerol DES	2012[119]
Lysozyme	ChCl: urea/Gly	Glycerol-based DES stabilized, but urea-based DES destabilized the protein	Activity decreased in neat DES and was restored with buffer dilution.	2013[132]
Lipase	ChCl: urea/Gly	DES act as the media for the enzymatic reaction and kept the enzyme stable	Activity of the enzyme increased in hydrated DES than the neat DES.	2013[41]
Lipase	ChCl: urea	Show good thermal stability with respect to the constituent and buffer solution	Retain the activity	2014[133]

Lipase	24 DES formed using 3 different molar ratios of ChCl, and Choline acetate (ChAc) with urea, glycerol, acetamide, and ethylene glycol (EG)	Enzyme gets more stabilization in cholinium acetate-glycerol DES	Activity increased in ChAc-glycerol and ethylene glycol DES	2014[35]
Lipase	Various choline chloride based binary and ternary DES	half-life time of lipase at 40 °C in hydrated ChCl:glycerol was enhanced, also some DESs provided acid and base stability.	activity of lipase in hydrated ChCl:urea:glycerol DES was 155% higher than that in buffer.	2016[134]
Lysozyme	Trehalose (Tre): ChCl in different molar ratios	Stability increased dramatically in the presence of 75% (w/w) Tre: ChCl(1:3) DES	-	2017[38]
Lysozyme, bovine serum albumin (BSA)	ChCl: Gly/urea	No improvement of thermostability for both the proteins. The partially folded	Neat DES reduces the activity. Hydrated DES restore the enzymatic activity.	2017[135]

		state to more compact native like state transition occurs with water addition in neat DES.		
Lipase	ChCl and N,N-diethyl ethanol ammonium chloride (EAC) based DES	ChCl based DESs were superior to EAC based DESs. DESs showed long term thermal and storage stability.	lipase activity was enhanced in hydrated DES, with the highest activity observed in hydrated ChCl:EG DES.	2017[136]
Lipase	Various choline chloride based binary and ternary DES	ChCl : glycerol : EG (1 : 1 : 1). Showed the highest enzyme stabilization	ChCl–urea–formamide (1 : 1 : 1) showed the highest catalytic activity	2019[137]
Lysozyme	ChCl:Urea	Protein partially unfolds in both neat and hydrated DES, with the lowest stability at 50% (w/w) DES.		2020[138]

Bromelain	Acetamide: urea: sorbitol (0.5:0.3:0.2)	The protein conformation becomes compact at low concentration but become slightly unfolded at higher concentration of DES.	The activity is increased at low DES concentrations than buffer but decreases at higher concentrations. Low viscosity and high polarity influence enhance activity.	2021[39]
Lysozyme	ChCl: Polyols (Gly, erythritol, xylitol, sorbitol) and sugars (xylose, glucose, trehalose)	All DES enhance thermal stability, which increases with the number of OH groups in their constituents.	At 10% (w/w), activity was slightly increased, then declined with higher DES concentrations.	2022[122]
Immunoglobulin G (IgG)	ChCl: Gly/EG/Urea	All DES increased the protein's melting temperature, with ChCl-glycerol showing the greatest effect. They also offered long-term stability for up to 20 days.		2022[139]

BSA, lysozyme, Immunoglobulin G (IgG)	ChCl: Gly/urea	Water addition induces a non-monotonic change in structure and stability. At <10 wt % and >40 wt % H_2O, the protein remains folded or partially folded, while intermediate hydration levels lead to unfolding.		2022[140]
Cellulase and pectinase	ChCl: urea/Gly/EG/1,2-propanediol	Hydrated DES offer greater thermal and storage stability than neat DES, though stability drops at very high-water content.	The activity of the enzyme is retained in both neat and hydrated DES.	2023[141]
Lipase	ChCl: Sorbitol(Sor) /xylitol (Xyl)/Gly/EG/triethylene glycol /urea	DES introduced protein disaggregation.	Activity increased 18-fold in 25% (v/v) ChCl:Sor (2:1) and 10–12-fold in ChCl:Gly	2023[142]

			(1:2), ChCl:EG (1:2), and ChCl:Xyl (2:1) DES.	
Beta-lactoglobulin	Betaine: Sor	The thermal stability in DES is increased with respect to the buffer		2023[143]
Cellulase	ChCl: Gly/EG/lactic acid (LA)	The thermal stability of the enzyme is maintained in ChCl-Gly and ChCl-EG DES but decreases with an increase in ChCl-LA DES.	Activity is improved in the presence of EG-based DES. Also, both the ChCl-Gly and EG DES retain most of the enzyme activity at 50 °C.	2023[144]
Trypsin	Trehalose: betaine with different mole ratio (from 1:3 to 1:9)	Trehalose: betaine (1:7) DES improved the thermal stability of the enzyme. All the DESs gave pH and storage stability.	All the DES improved the activity, and the highest was observed at 50 % (v/v) of trehalose: betaine (1:7) DES.	2023[85]

BSA	ChCl: EG, and benzyltrimethyl ammonium chloride (BTAmCl):EG	While a small amount of BTAmC:lEG fully unfolds the protein, it remains only partially unfolded even at high ChCl:EG DES concentration.		2023[145]
ω-Transaminases (ω-TAs)	10 different ChCl-based DESs (with urea, EG, Gly, etc.)	ChCl: EG:1,2-propanediol DES improves the stability most	the alcohol-based DESs (containing glycerol, ethylene glycol (EG) and 1,2-propanediol (PG)) as HBDs were more potent in enhancing the activity of the enzyme relative to the buffer.	2023[146]
Ubiquitin	Betaine-Gly-water	DES slowed protein torsional dynamics, stabilizing the structure and revealing a non-monotonic folding pattern		2024[147]

		with changing water content.		
Lysozyme	Hybrid Ionic Fluid (HIF) with ChCL: Gly (1:2) DES + 1-Butyl-3-methylimidazolium chloride (BMIM-Cl) or Choline Acetate (Chn-Ac) ionic liquids.	Stabilization was observed with both DES and HIFs; Choline Acetate-based HIF shows higher stabilization than BMIM-Cl.	Choline Acetate-based HIF improves enzymatic activity after incubation; BMIM-Cl shows gradual improvement over time	2024[148]
Lysozyme	Hybrid Ionic Fluid (HIF) with Choline chloride: Malonic acid (1:2) + BMIM-Cl and Chn-Ac ionic liquids.	Stabilization was observed with both DES and HIFs. Choline Acetate-based HIF shows higher stabilization than the other.	Choline Acetate-based HIF improves enzymatic activity more than the other HIF.	2024[149]
β-Glucosidases	Betaine-Gly	Stability enhanced in the presence of DES.	The activity of the enzyme increases with the increase of K_m and V_{max} of the enzyme 13.2% and 57.9%, respectively.	2024[150]

Peroxidase	Betaine: sucrose: water (2:1:10), and betaine: trehalose: water (4:1:14)	Both DESs stabilized the enzyme and retain activity at 75 ℃ and 80 ℃.	The activity of the enzyme enhanced in presence of both DES.	2024[151]
Lipoxygenase	Betaine:Sor:water (1:1:3) [BetSorW], Betaine Glycol (1:3) [BetGly]	Enhanced thermostability at 60°C with BetSorW but minimal improvement with BEtGly.	Activity increased 35% with BetSorW and 40% with BetGly.	2024[152]
Lipase A	ChCl:acetamide, ChCl: EG	Improved thermostability observed in both DES.	Up to 10-fold increase in catalytic efficiency $\left({}^{k_{cat}}/_{K_m}\right)$ for a variant in 30 % (v/v) ChCl-acetamide; and 4.1-fold increase in 95 % (v/v) ChCl: ethylene glycol.	2024[37]
Uricase	Sucrose: fructose: Gly (2:2:4 weight ratio)	At 5% (v/v) of DES, both the enzyme half-life and the T_m increases.	At 5% (v/v) of DES, substrate binding affinity and substrate	2025[153]

			specificity of the enzyme enhanced.	
Lysozyme	ChCl: Gly (1:2)	Lysozyme shows non-monotonic size changes, the radius of gyration (Rg) increases with water up to 40 wt.%, then gradually decreases upon further dilution.		2025[154]
α-chymotrypsin	ChCl or betaine with Gly or Sor	The thermal stability enhanced with increasing concentration of the DESs, with highest observed with ChCl-Sorbitol.	Activity was improved in ChCl based DESs.	2025[155]
Treebean seed protein	ChCl:Gly/ Sor/glucose/ sucrose/fructose	Highest thermal stability was observed in Sorbitol containing DES.	Activity was also improved in sorbitol-based DES	2025[156]

The behavior of many proteins in the presence of different DESs are listed in Table 1.2.1, and the effects are not very generalized. In some cases, a DES shows some positive impact on protein stability and function, and the same DES can show a deleterious effect on another enzyme. For instance, while enzymes like lipase[118,134] and α-chymotrypsin[42], and IgG (Figure 1.2.2b)[139] show improved thermal stability in choline chloride–urea DES, lysozyme appears destabilized in the same solvent system.[122,132,138] On the other hand, different DESs impact the protein differently: glycerol-based DESs generally stabilize lysozyme, whereas urea-based DESs often lead to destabilization, especially at high concentrations.[122,132,138] Kist *et al.* have also shown the deleterious effect of choline chloride-urea DES and the positive effect of choline chloride-glycerol, respectively, taking RNase A as the enzyme (Figure 1.2.2a).[157] The thermal stability of α-chymotrypsin was retained or increased in almost all choline chloride and betaine-based DES (Figure 1.2.2c).[42,155] However, DES's concentration-dependent behavior on protein has been found in some cases. For example, α-chymotrypsin exhibits optimal stability at moderate ChCl-Urea DES concentrations (up to 0.25 $g \cdot mL^{-1}$) but shows decreased stability at higher DES concentrations.[42] The most used enzyme in DES is lipase, which demonstrates enhanced stability and activity in choline chloride-based DESs, particularly those combined with glycerol or urea, and the effect is more pronounced in hydrated forms of DES.[40,41,118,119,133,134,136,137,158–162] Due to providing enhanced thermal stability, DESs, especially choline chloride-based DESs, have been used as long-term storage media for enzymes and other sensitive biomolecules.[139,163,164]

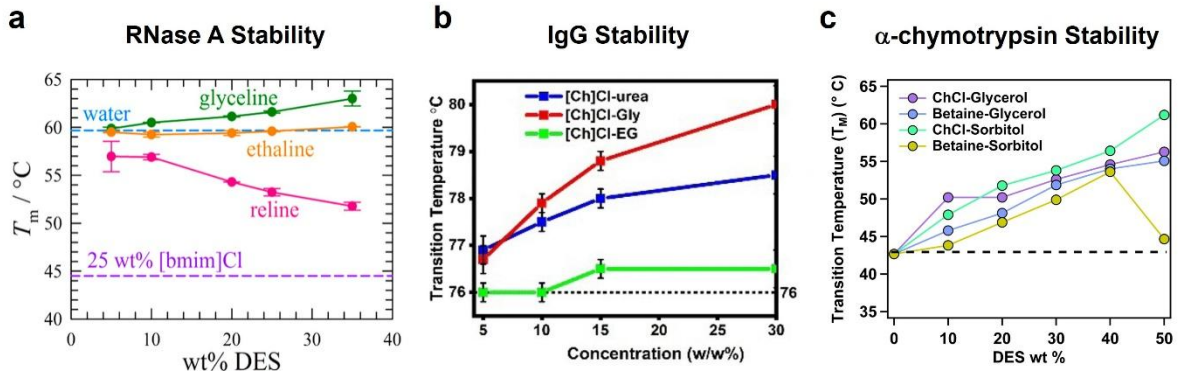

Figure 1.2.2. Some representative examples of enzyme thermal stability in different DES from earlier reports. The name of the enzyme and the DES are mentioned in the plot itself. Note that glyceline, ethaline, and reline are the common names of the choline chloride (ChCl)-glycerol (1:2), ChCl-ethylene glycol (EG) (1:2), and ChCl-urea (1:2) DES, respectively. These figures are represented from the references [139,155,157].

The enzymatic activity in DES also varies in a DES and protein-specific manner. Neat DES formulations often show limited or reduced enzyme activity, which can be restored or enhanced upon dilution with water or buffer.[41,118,132,135,136] The water dilution effect is also not very monotonous; recent studies show the optimal water concentrations for hydrated DES being used as an efficient biocatalytic medium.[37,85,140,153] A very recent study deciphered that very low concentrations of DES even increased the enzymatic activity compared to buffer (Figure 1.2.3b).[165] Toledo *et al.*, in their recent study, evaluated 16 different deep eutectic solvents (DES) formed by combining various hydrogen bond donors—choline chloride (ChCl), choline dihydrogen phosphate (ChDHP), choline dihydrogen citrate (ChDHC), and betaine (Bet)—with hydrogen bond acceptors such as ethylene glycol (EG), glycerol (Gly), erythritol (Ery), and xylitol (Xyl).[36] Their findings revealed that nearly all the DES preserved laccase activity, with the highest activity observed in hydrated ChDHP:Xyl DES. Notably, the activity showed a positive correlation with the increasing number of hydroxyl groups in the polyol component (Figure 1.2.3a).[36] Similar to stability, concentration-dependent activity reversals have been

reported for cytochrome c in multiple DESs, including choline chloride-based systems with ethylene glycol, glycerol, and urea.[166]

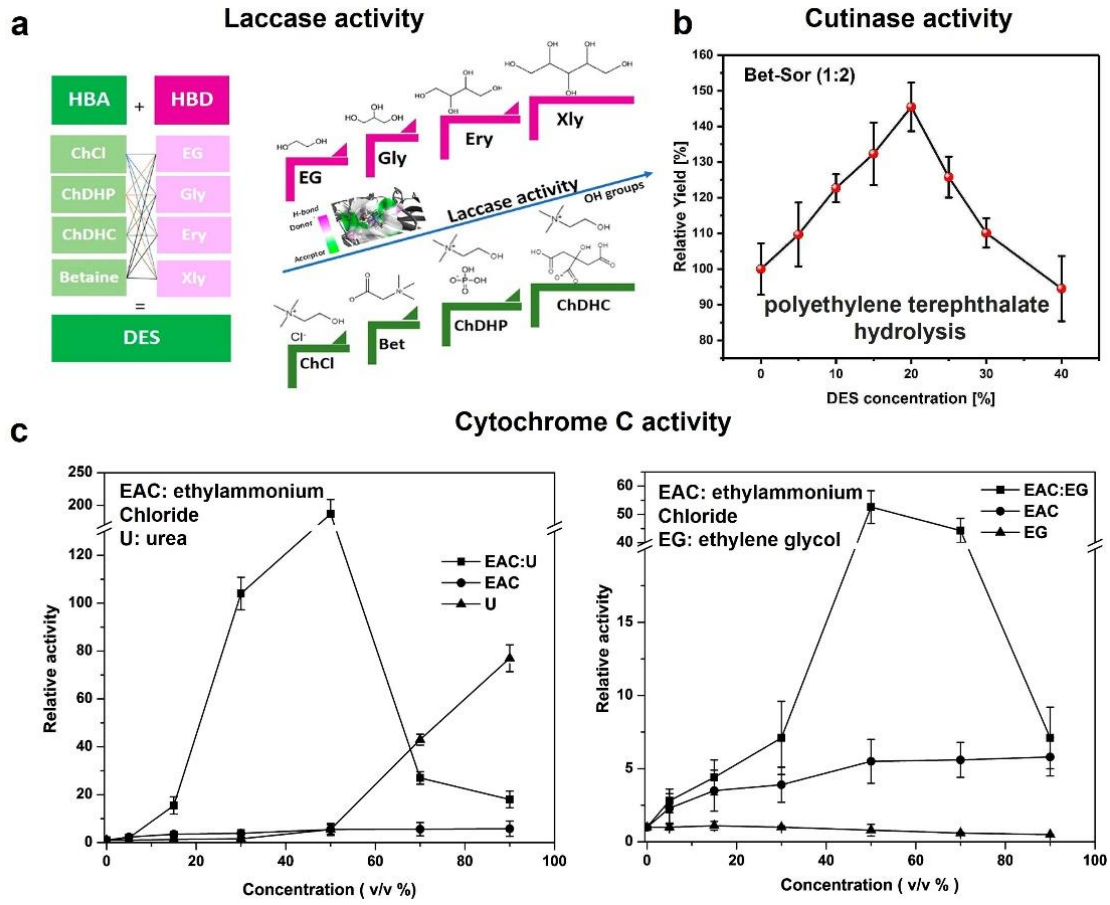

Figure 1.2.3. Some representative examples of enzyme activity in different DES from earlier reports. The name of the enzyme and the DES are mentioned in the plot itself. These figures are represented from the references [36,165,166].

DES formulations with betaine and polyols, such as glycerol, have shown promising thermal stability in proteins like peroxidase, laccase, and β-glucosidases, with activity improvements following rehydration, which also highlights the role of the presence of water for biocatalysis (Figure 1.2.4a).[120] Sun *et al.* recently reported the enzymatic activity of cytochrome p450 is influenced by the physical properties like viscosity, density, and surface tension of the hydrated DES media (Figure

1.2.4b).[121] Proper control experiments with the individual constituents in many studies of the DES further signify the role of DES and hydrated DES (Figure 1.2.3c and 1.2.4c).[35,166]

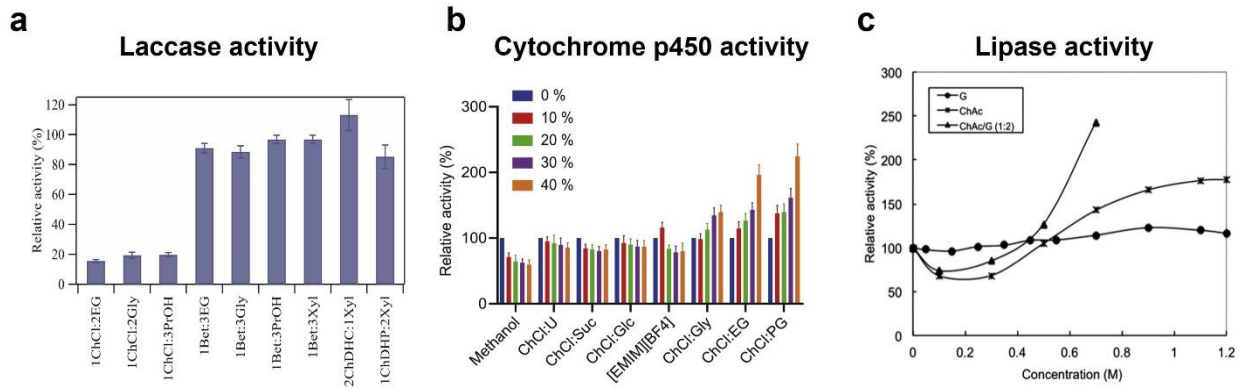

Figure 1.2.4. Some representative examples of enzyme activity in different DES from earlier reports. The name of the enzyme and the DES are mentioned in the plot itself. These figures are represented from references [35,120,121].

Although not included in this thesis, one of my earlier studies serves as a foundational point for the present thesis and warrants mention. In that study, we investigated the behavior of the enzyme bromelain in a novel hydrated DES composed of acetamide, urea, and sorbitol (0.5Ac/0.3Ur/0.2Sor), marking one of the first explorations of protein function in a non-ionic DES system.[39] We correlated bromelain's proteolytic activity with both intrinsic protein characteristics and the physical properties of the hydrated DES medium. Our findings revealed that compact protein conformation and flexibility at the active site enhance enzymatic activity (Figure 1.2.5).[39] Additionally, media with higher polarity and lower viscosity were found to be more conducive to activity (Figure 1.2.5).[39] This study offered mechanistic insight into how enzymatic performance is jointly governed by protein structure and solvent properties, providing valuable guidelines for the rational design of DESs as efficient biocatalytic platforms.

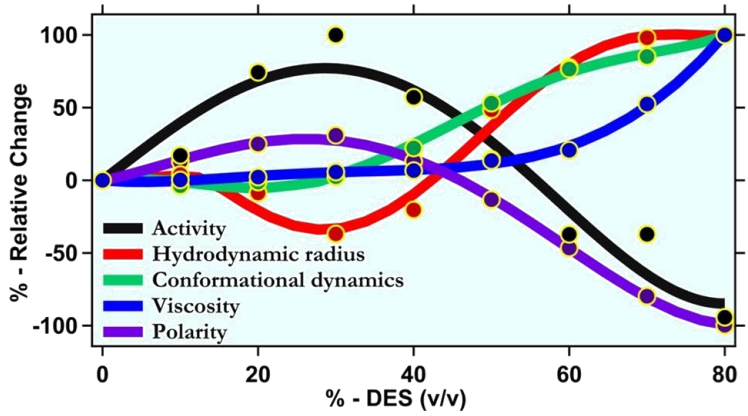

Figure 1.2.5. A more compact structural conformation, higher active-site flexibility, lower viscosity, and higher solvent medium polarity are found to facilitate enzymatic activity of bromelain in a hydrated 0.5Ac/0.3Ur/0.2Sor DES.[39].

Interesting recent examples reveal advancements with hybrid ionic fluids (HIFs), where DESs are combined with ionic liquids to further stabilize enzymes under stress conditions.[148,149] For example, choline acetate-based HIFs demonstrate superior stability and activity in lysozyme and lipase, even at higher temperatures or in extreme pH conditions.[148,149]

However, most of these studies rely on getting a positive result by choosing a pair of DES and protein. The choices are also getting biased by the availability of the proteins and DES constituents. A logical way forward in this field is very much missing because of the lack of mechanistic studies.

1.2.8. Knowledge Gaps in Protein Behavior in DES Systems:

Despite a significant upsurge in the number of reports deciphering protein and enzyme behavior in deep eutectic solvents (DES), there are still several gaps in the understanding of protein stability and activity in DES and hydrated media that need to be addressed:

1. **Limited knowledge of mechanistic interactions:** While many studies demonstrate changes in stability and activity, the underlying mechanisms

through which DES and its components interact with proteins and influence structure, stability, and function are very limited. More in-depth mechanistic studies are necessary to elucidate these interactions at the molecular level.

2. **Bridging Molecular Insights of DES to Enzyme Behavior:** The synthesis and measurement of the physical properties of deep eutectic solvents (DES) have been extensively documented, alongside studies on their structural dynamics and the molecular-level heterogeneity in DES and hydrated DES systems. While these properties are supposed to significantly influence enzyme behavior in DES, there has been little to no effort in correlating these findings to derive a comprehensive mechanistic understanding of enzyme behavior within these systems. Establishing such connections could provide critical insights into the interplay between DES properties and enzymatic behaviour, offering a pathway for advancing DES applications in biocatalysis.
3. **Hydration dynamics and optimal hydration levels:** Although it is axiomatic that the water which is in direct interaction with the enzyme (known as associated water) plays a critical role in influencing enzyme stability and function. Even in many reports regarding protein behavior in DES, it is found that an optimum amount of water is necessary for protein function, indicating the crucial role of water. However, there are no experimental studies reporting the hydration dynamics of a protein in DES and hydrated DES. A deeper understanding of hydration dynamics might lead to better control over enzyme behavior in DES.
4. **Variability across protein-DES types:** Observations show that the effects of DES are highly variable depending on the protein. For instance, the same DES may stabilize one protein but destabilize another. The factors to generalize DES applications for different proteins are necessary.

Addressing these gaps will be essential to fully harness the potential of DES as a versatile medium for protein stabilization and catalysis, paving the way for both

fundamental scientific advancements and practical applications in biotechnology and industry.

In my thesis, I have extensively used the associated water dynamics of proteins and tried to provide mechanistic insight into why proteins remain stable and active in DES or hydrated DES systems.

1.2.9. Objective of the Thesis:

Traditionally, deep eutectic solvents (DESs) have been thought to stabilize proteins primarily through specific interactions between their components and the protein's amino acid residues. These interactions, particularly hydrogen bonding and ionic forces, are believed to reduce electrostatic repulsion among charged residues, thus promoting the maintenance of a near-native structure. Several studies have explored how the nature of DES components and the strength of their intermolecular interactions influence the structural integrity and functional characteristics of various proteins. Recently, Sun *et al.* demonstrated that the physical properties of DES, such as viscosity, density, and refractive index, can modulate both the catalytic efficiency and thermal resilience of enzymes like cytochrome P450.[121] Our own previous work with bromelain further emphasized that protein behavior, including hydrodynamic radius and internal mobility, is closely tied to the physicochemical properties of the DES medium, particularly its polarity and viscosity.[39] Moreover, DESs are frequently proposed to form a protective shell around proteins, offering resistance to thermal denaturation.

However, such generalizations do not fully explain the diverse and sometimes contradictory effects observed across different enzymes, DES types, and DES concentrations.

A careful introspection into the previous literature reveals that enzymes in hydrated DES show superior stability and activity compared to the neat DES. Water is

universally recognized as indispensable in biological function. Water in the immediate vicinity of the protein surface (commonly termed associated or biological water) is believed to govern the protein's stability and activity. For instance, terahertz spectroscopy studies by Heyden *et al.* revealed that less flexible hydration water in the presence of disaccharides correlates with greater protein stability compared to monosaccharides.[167] Our recent research demonstrated that papain stability is enhanced by osmolytes that slow down water dynamics, whereas destabilization is linked with increased hydration mobility.[168] This is consistent with several findings from Zewail's group and others investigating protein stability in crowded environments and non-aqueous solvents via molecular dynamics simulations and theoretical models.[169–177] The general consensus is that a reduction in the flexibility of hydration water surrounding proteins correlates with increased thermal stability, while enhanced water mobility often leads to destabilization.

Collectively, these studies underscore the pivotal role of water dynamics, particularly the behavior of water in the immediate vicinity of the protein, in regulating their behaviour in complex solvent systems. Building on this foundation, I propose that in hydrated DESs, it is not only the DES composition but also the modulation of associated water dynamics that critically influences protein stability and activity (scheme 1.2.4). To support the generalizability of this hypothesis, experiments were conducted using various enzymes and DES systems. Furthermore, to establish the robustness of our findings, my thesis includes a parallel investigation involving a well-known macromolecular crowder, Ficoll-70k. This broader approach demonstrates that our hypothesis concerning the modulation of associated water dynamics extends beyond DESs and is also applicable to systems involving macromolecular crowding and osmolytes.

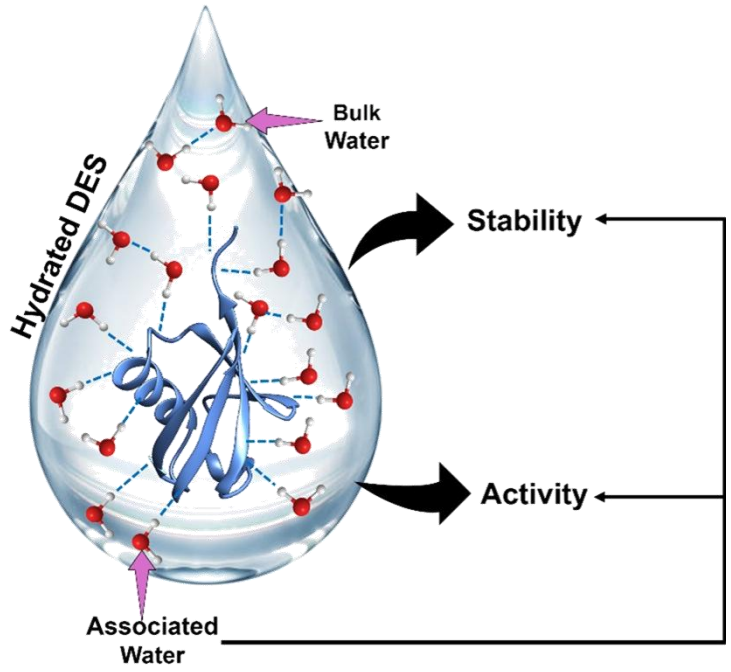

Scheme 1.2.4. Aim of the thesis. Influence of associated water modulation on the modulation of activity and stability of the enzyme in the presence of hydrated DES.

1.2.10. References:

(1) Anastas, P. T.; Warner, J. C. *Green Chemistry: Theory and Practice*; Oxford University Press Inc., New York, USA, 2000.

(2) *12 Principles of Green Chemistry - American Chemical Society*. https://www.acs.org/green-chemistry-sustainability/principles/12-principles-of-green-chemistry.html (accessed 2025-04-24).

(3) Sheldon, R. A. Fundamentals of Green Chemistry: Efficiency in Reaction Design. *Chem Soc Rev* **2012**, *41* (4), 1437–1451. https://doi.org/10.1039/C1CS15219J.

(4) Sheldon, R. A. E Factors, Green Chemistry and Catalysis: An Odyssey. *Chemical Communications* **2008**, *0* (29), 3352–3365. https://doi.org/10.1039/B803584A.

(5) Hauer, B. Embracing Nature's Catalysts: A Viewpoint on the Future of Biocatalysis. *ACS Catal* **2020**, *10* (15), 8418–8427. https://doi.org/10.1021/acscatal.0c01708.

(6) Madhavan, A.; Sindhu, R.; Binod, P.; Sukumaran, R. K.; Pandey, A. Strategies for Design of Improved Biocatalysts for Industrial Applications. *Bioresour Technol* **2017**, *245*, 1304–1313. https://doi.org/10.1016/j.biortech.2017.05.031.

(7) Bommarius, A. S.; Paye, M. F. Stabilizing Biocatalysts. *Chem Soc Rev* **2013**, *42* (15), 6534–6565. https://doi.org/10.1039/c3cs60137d.

(8) Robinson, P. K. Enzymes: Principles and Biotechnological Applications. *Essays Biochem* **2015**, *59*, 1–41. https://doi.org/10.1042/BSE0590001.

(9) van Schie, M. M. C. H.; Spöring, J. D.; Bocola, M.; Domínguez de María, P.; Rother, D. Applied Biocatalysis beyond Just Buffers – from Aqueous to Unconventional Media. Options and Guidelines. *Green Chemistry* **2021**, *23* (9), 3191–3206. https://doi.org/10.1039/D1GC00561H.

(10) Sheldon, R. A.; Woodley, J. M. Role of Biocatalysis in Sustainable Chemistry. *Chem Rev* **2018**, *118* (2), 801–838. https://doi.org/10.1021/ACS.CHEMREV.7B00203/ASSET/IMAGES/LARGE/CR-2017-002034_0025.JPEG.

(11) Arnold, F. H. Protein Engineering for Unusual Environments. *Curr Opin Biotechnol* **1993**, *4*, 450–455.

(12) Arnold, F. H. Directed Evolution: Bringing New Chemistry to Life. *Angewandte Chemie International Edition* **2018**, *57* (16), 4143–4148. https://doi.org/10.1002/ANIE.201708408.

(13) Kan, S. B. J.; Lewis, R. D.; Chen, K.; Arnold, F. H. Directed Evolution of Cytochrome c for Carbon-Silicon Bond Formation: Bringing Silicon to Life.

Science (1979) **2016**, *354* (6315), 1048–1051. https://doi.org/10.1126/SCIENCE.AAH6219/SUPPL_FILE/KAN.SM.PDF.

(14) Chen, K.; Arnold, F. H. Tuning the Activity of an Enzyme for Unusual Environments: Sequential Random Mutagenesis of Subtilisin E for Catalysis in Dimethylformamide. *Proc. Natl. Acad. Sci. USA* **1993**, *90*, 5618–5622.

(15) Stepankova, V.; Bidmanova, S.; Koudelakova, T.; Prokop, Z.; Chaloupkova, R.; Damborsky, J. Strategies for Stabilization of Enzymes in Organic Solvents. *ACS Catal* **2013**, *3* (12), 2823–2836. https://doi.org/10.1021/cs400684x.

(16) Panić, M.; Cvjetko Bubalo, M.; Radojčić Redovniković, I. Designing a Biocatalytic Process Involving Deep Eutectic Solvents. *J. Chem. Technology and Biotechnology* **2021**, *96* (1), 14–30. https://doi.org/10.1002/jctb.6545.

(17) Arnodo, D.; Maffeis, E.; Marra, F.; Nejrotti, S.; Prandi, C. Combination of Enzymes and Deep Eutectic Solvents as Powerful Toolbox for Organic Synthesis. *Molecules 2023, Vol. 28, Page 516* **2023**, *28* (2), 516. https://doi.org/10.3390/MOLECULES28020516.

(18) Xu, P.; Zheng, G. W.; Zong, M. H.; Li, N.; Lou, W. Y. Recent Progress on Deep Eutectic Solvents in Biocatalysis. *Bioresour Bioprocess* **2017**, *4* (1), 1–18. https://doi.org/10.1186/S40643-017-0165-5/METRICS.

(19) Smith, E. L.; Abbott, A. P.; Ryder, K. S. Deep Eutectic Solvents (DESs) and Their Applications. *Chem Rev* **2014**, *114* (21), 11060–11082. https://doi.org/10.1021/cr300162p.

(20) Florindo, C.; Lima, F.; Ribeiro, B. D.; Marrucho, I. M. Deep Eutectic Solvents: Overcoming 21st Century Challenges. *Curr Opin Green Sustain Chem* **2019**, *18*, 31–36. https://doi.org/10.1016/j.cogsc.2018.12.003.

(21) Pätzold, M.; Siebenhaller, S.; Kara, S.; Liese, A.; Syldatk, C.; Holtmann, D. Deep Eutectic Solvents as Efficient Solvents in Biocatalysis. *Trends Biotechnol* **2019**, *37* (9), 943–959. https://doi.org/10.1016/j.tibtech.2019.03.007.

(22) Paiva, A.; Craveiro, R.; Aroso, I.; Martins, M.; Reis, R. L.; Duarte, A. R. C. Natural Deep Eutectic Solvents - Solvents for the 21st Century. *ACS Sustain Chem Eng* **2014**, *2* (5), 1063–1071. https://doi.org/10.1021/sc500096j.

(23) Yadav, N.; Venkatesu, P. Current Understanding and Insights towards Protein Stabilization and Activation in Deep Eutectic Solvents as Sustainable Solvent Media. *Phys. Chem. Chem. Phys.* **2022**, *24* (22), 13474–13509. https://doi.org/10.1039/D2CP00084A.

(24) Usmani, Z.; Sharma, M.; Tripathi, M.; Lukk, T.; Karpichev, Y.; Gathergood, N.; Singh, B. N.; Thakur, V. K.; Tabatabaei, M.; Gupta, V. K. Biobased Natural Deep Eutectic System as Versatile Solvents: Structure, Interaction and Advanced Applications. *Science of The Total Environment* **2023**, *881*, 163002. https://doi.org/10.1016/J.SCITOTENV.2023.163002.

(25) Hansen, B. B.; Spittle, S.; Chen, B.; Poe, D.; Zhang, Y.; Klein, J. M.; Horton, A.; Adhikari, L.; Zelovich, T.; Doherty, B. W.; Gurkan, B.; Maginn, E. J.; Ragauskas, A.; Dadmun, M.; Zawodzinski, T. A.; Baker, G. A.; Tuckerman, M. E.; Savinell, R. F.; Sangoro, J. R. Deep Eutectic Solvents: A Review of Fundamentals and Applications. *Chem Rev* **2021**, *121* (3), 1232–1285. https://doi.org/10.1021/acs.chemrev.0c00385.

(26) Abranches, D. O.; Coutinho, J. A. P. Everything You Wanted to Know about Deep Eutectic Solvents but Were Afraid to Be Told. *Annu Rev Chem Biomol Eng* **2023**, *14* (1), 141–163. https://doi.org/10.1146/annurev-chembioeng-101121-085323.

(27) Abbott, A. P.; Capper, G.; Davies, D. L.; Rasheed, R. K.; Tambyrajah, V. Novel Solvent Properties of Choline Chloride/Urea Mixtures. *Chemical Communications* **2003**, *0* (1), 70–71. https://doi.org/10.1039/B210714G.

(28) Castellan, G. W. *Physical Chemistry*, Third edition.; Sponsoring Editor: Rogers, R. L., Production Editor: Pinette, M., Copy Editor: Moore, J. A., Eds.; Addison-Wesley Publishing Company: Massachusetts, 1983.

(29) Martins, M. A. R.; Pinho, S. P.; Coutinho, J. A. P. Insights into the Nature of Eutectic and Deep Eutectic Mixtures. *J Solution Chem* **2019**, *48* (7), 962–982. https://doi.org/10.1007/S10953-018-0793-1/FIGURES/9.

(30) Płotka-Wasylka, J.; de la Guardia, M.; Andruch, V.; Vilková, M. Deep Eutectic Solvents vs Ionic Liquids: Similarities and Differences. *Microchemical Journal* **2020**, *159*, 105539. https://doi.org/10.1016/j.microc.2020.105539.

(31) Mjalli, F. S.; Ahmed, O. U. Physical Properties and Intermolecular Interaction of Eutectic Solvents Binary Mixtures: Reline and Ethaline. *Asia-Pacific Journal of Chemical Engineering* **2016**, *11* (4), 549–557. https://doi.org/10.1002/apj.1978.

(32) Guo, W.; Hou, Y.; Ren, S.; Tian, S.; Wu, W. Formation of Deep Eutectic Solvents by Phenols and Choline Chloride and Their Physical Properties. *J. Chem. Eng. Data* **2013**, *58* (4), 866–872. https://doi.org/10.1021/je300997v.

(33) El Achkar, T.; Greige-Gerges, H.; Fourmentin, S. Basics and Properties of Deep Eutectic Solvents: A Review. *Environ Chem Lett* **2021**, *19* (4), 3397–3408. https://doi.org/10.1007/S10311-021-01225-8/FIGURES/5.

(34) Shah, P. A.; Chavda, V.; Hirpara, D.; Sharma, V. S.; Shrivastav, P. S.; Kumar, S. Exploring the Potential of Deep Eutectic Solvents in Pharmaceuticals: Challenges and Opportunities. *J Mol Liq* **2023**, *390*, 123171. https://doi.org/10.1016/J.MOLLIQ.2023.123171.

(35) Huang, Z. L.; Wu, B. P.; Wen, Q.; Yang, T. X.; Yang, Z. Deep Eutectic Solvents Can Be Viable Enzyme Activators and Stabilizers. *Journal of Chemical Technology and Biotechnology* **2014**, *89* (12), 1975–1981. https://doi.org/10.1002/jctb.4285.

(36) Toledo, M. L.; Pereira, M. M.; Freire, M. G.; Silva, J. P. A.; Coutinho, J. A. P.; Tavares, A. P. M. Laccase Activation in Deep Eutectic Solvents. *ACS Sustain Chem Eng* **2019**, *7* (13), 11806–11814. https://doi.org/10.1021/acssuschemeng.9b02179.

(37) Wang, X.; Sheng, Y.; Cui, H.; Qiao, J.; Song, Y.; Li, X.; Huang, H. Corner Engineering: Tailoring Enzymes for Enhanced Resistance and Thermostability in Deep Eutectic Solvents. *Angewandte Chemie International Edition* **2024**, *63* (2), e202315125. https://doi.org/10.1002/ANIE.202315125.

(38) Xin, R.; Qi, S.; Zeng, C.; Khan, F. I.; Yang, B.; Wang, Y. A Functional Natural Deep Eutectic Solvent Based on Trehalose: Structural and Physicochemical Properties. *Food Chem* **2017**, *217*, 560–567. https://doi.org/10.1016/j.foodchem.2016.09.012.

(39) Das, N.; Khan, T.; Subba, N.; Sen, P. Correlating Bromelain's Activity with Its Structure and Active-Site Dynamics and the Medium's Physical Properties in a Hydrated Deep Eutectic Solvent. *Phys. Chem. Chem. Phys.* **2021**, *23* (15), 9337–9346. https://doi.org/10.1039/d1cp00046b.

(40) Gorke, J. T.; Srienc, F.; Kazlauskas, R. J. Deep Eutectic Solvents for Candida Antarctica Lipase B-Catalyzed Reactions. In *ACS Symposium Series*; 2010; Vol. 1038, pp 169–180. https://doi.org/10.1021/bk-2010-1038.ch014.

(41) Durand, E.; Lecomte, J.; Baréa, B.; Dubreucq, E.; Lortie, R.; Villeneuve, P. Evaluation of Deep Eutectic Solvent-Water Binary Mixtures for Lipase-

Catalyzed Lipophilization of Phenolic Acids. *Green Chemistry* **2013**, *15* (8), 2275–2282. https://doi.org/10.1039/c3gc40899j.

(42) Yadav, N.; Bhakuni, K.; Bisht, M.; Bahadur, I.; Venkatesu, P. Expanding the Potential Role of Deep Eutectic Solvents toward Facilitating the Structural and Thermal Stability of α-Chymotrypsin. *ACS Sustain Chem Eng* **2020**, *8* (27), 10151–10160. https://doi.org/10.1021/acssuschemeng.0c02213.

(43) Guchhait, B.; Daschakraborty, S.; Biswas, R. Medium Decoupling of Dynamics at Temperatures ∼100 K above Glass-Transition Temperature: A Case Study with (Acetamide + Lithium Bromidenitrate) Melts. *Journal of Chemical Physics* **2012**, *136* (17), 174503. https://doi.org/10.1063/1.4705315.

(44) Guchhait, B.; Das, S.; Daschakraborty, S.; Biswas, R. Interaction and Dynamics of (Alkylamide + Electrolyte) Deep Eutectics: Dependence on Alkyl Chain-Length, Temperature, and Anion Identity. *Journal of Chemical Physics* **2014**, *140* (10), 104514. https://doi.org/10.1063/1.4866178.

(45) Hossain, S. S.; Paul, S.; Samanta, A. Liquid Structure and Dynamics of Tetraalkylammonium Bromide-Based Deep Eutectic Solvents: Effect of Cation Chain Length. *J. Phys. Chem. B* **2019**, *123* (31), 6842–6850. https://doi.org/10.1021/acs.jpcb.9b04955.

(46) Hossain, S. S.; Samanta, A. Solute Rotation and Solvation Dynamics in Deep Eutectic Solvents. *Chemical Physics Impact* **2021**, *3*, 100043. https://doi.org/10.1016/j.chphi.2021.100043.

(47) Töpfer, K.; Pasti, A.; Das, A.; Salehi, S. M.; Vazquez-Salazar, L. I.; Rohrbach, D.; Feurer, T.; Hamm, P.; Meuwly, M. Structure, Organization, and Heterogeneity of Water-Containing Deep Eutectic Solvents. *J Am Chem Soc* **2022**, *144* (31), 14170–14180.

(48) Cui, Y.; Rushing, J. C.; Seifert, S.; Bedford, N. M.; Kuroda, D. G. Molecularly Heterogeneous Structure of a Nonionic Deep Eutectic Solvent Composed of N-Methylacetamide and Lauric Acid. *Journal of Physical Chemistry B* **2019**, *123* (18). https://doi.org/10.1021/acs.jpcb.8b11732.

(49) Spittle, S.; Poe, D.; Doherty, B.; Kolodziej, C.; Heroux, L.; Haque, M. A.; Squire, H.; Cosby, T.; Zhang, Y.; Fraenza, C.; Bhattacharyya, S.; Tyagi, M.; Peng, J.; Elgammal, R. A.; Zawodzinski, T.; Tuckerman, M.; Greenbaum, S.; Gurkan, B.; Dadmun, M.; Maginn, E. J.; Sangoro, J. Evolution of Microscopic Heterogeneity and Dynamics in Choline Chloride-Based Deep Eutectic Solvents. *Nat Commun* **2022**, *13* (1), 219. https://doi.org/10.1038/s41467-021-27842-z.

(50) Subba, N.; Das, N.; Sen, P. Partial Viscosity Decoupling of Solute Solvation, Rotation, and Translation Dynamics in Lauric Acid/Menthol Deep Eutectic Solvent: Modulation of Dynamic Heterogeneity with Length Scale. *J. Phys. Chem. B* **2020**, *124* (31), 6875–6884. https://doi.org/10.1021/acs.jpcb.0c04379.

(51) Ediger, M. D. Spatially Heterogeneous Dynamics in Supercooled Liquids. *Annu Rev Phys Chem* **2000**, *51*, 99–128. https://doi.org/10.1146/annurev.physchem.51.1.99.

(52) MacKowiak, S. A.; Kaufman, L. J. When the Heterogeneous Appears Homogeneous: Discrepant Measures of Heterogeneity in Single-Molecule Observables. *Journal of Physical Chemistry Letters* **2011**, *2* (5), 438–442. https://doi.org/10.1021/JZ1016872/ASSET/IMAGES/LARGE/JZ-2010-016872_0003.JPEG.

(53) Cicerone, M. T.; Ediger, M. D. Relaxation of Spatially Heterogeneous Dynamic Domains in Supercooled Ortho-terphenyl. *J Chem Phys* **1995**, *103* (13), 5684–5692. https://doi.org/10.1063/1.470551.

(54) Kienle, D. F.; Falatach, R. M.; Kaar, J. L.; Schwartz, D. K. Correlating Structural and Functional Heterogeneity of Immobilized Enzymes. *ACS Nano* **2018**, *12* (8), 8091–8103.

(55) Wang, Y. L.; Li, B.; Sarman, S.; Mocci, F.; Lu, Z. Y.; Yuan, J.; Laaksonen, A.; Fayer, M. D. Microstructural and Dynamical Heterogeneities in Ionic Liquids. *Chemical Reviews*. 2020, pp 5798–5877. https://doi.org/10.1021/acs.chemrev.9b00693.

(56) Krahn, J. R.; Lodge, T. P. Spatial Heterogeneity of Solvent Dynamics in Multicomponent Polymer Solutions. *J. Phys. Chem.* **1995**, *99* (20), 8338–8348. https://doi.org/10.1021/j100020a069.

(57) Richert, R. Heterogeneous Dynamics in Liquids: Fluctuations in Space and Time. *Journal of Physics Condensed Matter*. 2002, p R703. https://doi.org/10.1088/0953-8984/14/23/201.

(58) Das, N.; Sen, P. Dynamic Heterogeneity and Viscosity Decoupling: Origin and Analytical Prediction. *Phys. Chem. Chem. Phys.* **2021**, *23* (29), 15749–15757. https://doi.org/10.1039/d1cp01804c.

(59) Hu, Z.; Margulis, C. J. Heterogeneity in a Room-Temperature Ionic Liquid: Persistent Local Environments and the Red-Edge Effect. *Proceedings of the National Academy of Sciences* **2006**, *103* (4), 831–836. https://doi.org/10.1073/pnas.0507364103.

(60) Demchenko, A. P. The Red-Edge Effects: 30 Years of Exploration. *Luminescence*. 2002, pp 19–42. https://doi.org/10.1002/bio.671.

(61) Das, N.; Khan, T.; Sen, P. The Shift of Excitation Spectra at Blue Edge of Emission (BEEmS) as a New Methodology to Probe Heterogeneity. *Chem Phys* **2024**, *577*, 112138. https://doi.org/10.1016/J.CHEMPHYS.2023.112138.

(62) Lakowicz, J. R. *Principles of Fluorescence Spectroscopy*; Springer, 2006; pp 1–954. https://doi.org/10.1007/978-0-387-46312-4.

(63) Demchenko, A. P. Weber's Red-Edge Effect That Changed the Paradigm in Photophysics and Photochemistry. **2016**, 95–141. https://doi.org/10.1007/4243_2016_14.

(64) Galley, W. C.; Purkey, R. M. Role of Heterogeneity of the Solvation Site in Electronic Spectra in Solution*. *Proceedings of the National Academy of Sciences* **1970**, *67* (3), 1116–1121. https://doi.org/10.1073/PNAS.67.3.1116.

(65) Rubinov, A. I.; Tomin, V. I. Bathocromic Luminescence in Solutions of Organic Dyes at Low Temperatures. *Opt. Spektros* **1970**, *29* (6), 1082–1086.

(66) Itoh, K. I.; Azumi, T. Shift of the Emission Band upon Excitation at the Long Wavelength Absorption Edge. II. Importance of the Solute-Solvent Interaction and the Solvent Reorientation Relaxation Process. *J Chem Phys* **1975**, *62* (9), 3431–3438. https://doi.org/10.1063/1.430977.

(67) Azumi, T.; Itoh, K. I.; Shiraishi, H. Shift of Emission Band upon the Excitation at the Long Wavelength Absorption Edge. III. Temperature Dependence of the Shift and Correlation with the Time Dependent Spectral Shift. *J Chem Phys* **1976**, *65* (7), 2550–2555. https://doi.org/10.1063/1.433440.

(68) Demchenko, A. P. On the Nanosecond Mobility in Proteins: Edge Excitation Fluorescence Red Shift of Protein-Bound 2-(p-Toluidinylnaphthalene)-6-Sulfonate. *Biophys Chem* **1982**, *15* (2), 101–109. https://doi.org/10.1016/0301-4622(82)80022-7.

(69) Demchenko, A. P. Fluorescence Molecular Relaxation Studies of Protein Dynamics: The Probe Binding Site of Melittin Is Rigid on the Nanosecond

Time Scale. *FEBS Lett* **1985**, *182* (1), 99–102. https://doi.org/10.1016/0014-5793(85)81162-5.

(70) Jin, H.; Li, X.; Maroncelli, M. Heterogeneous Solute Dynamics in Room Temperature Ionic Liquids. *J. Phys. Chem. B* **2007**, *111* (48), 13473–13478. https://doi.org/10.1021/jp077226.

(71) Das, A.; Biswas, R. Dynamic Solvent Control of a Reaction in Ionic Deep Eutectic Solvents: Time-Resolved Fluorescence Measurements of Reactive and Nonreactive Dynamics in (Choline Chloride + Urea) Melts. *J. Phys. Chem. B* **2015**, *119* (31), 10102–10113. https://doi.org/10.1021/acs.jpcb.5b04936.

(72) Tarif, E.; Mondal, J.; Biswas, R. How Frictional Response during Solute Solvation Controls Solute Rotation in Naturally Abundant Deep Eutectic Solvent (NADES)? A Case Study with Amino Acid Derivative Containing DES. *J Mol Liq* **2020**, *303*, 112451. https://doi.org/10.1016/j.molliq.2020.112451.

(73) Mandal, P. K.; Paul, A.; Samanta, A. Excitation Wavelength Dependent Fluorescence Behavior of the Room Temperature Ionic Liquids and Dissolved Dipolar Solutes. *J Photochem Photobiol A Chem* **2006**, *182* (2), 113–120. https://doi.org/10.1016/J.JPHOTOCHEM.2006.01.003.

(74) Tarif, E.; Mondal, J.; Biswas, R. Interaction and Dynamics in a Fully Biodegradable Glucose-Containing Naturally Abundant Deep Eutectic Solvent: Temperature-Dependent Time-Resolved Fluorescence Measurements. *J. Phys. Chem. B* **2019**, *123* (44), 9378–9387. https://doi.org/10.1021/acs.jpcb.9b06783.

(75) Subba, N.; Tarif, E.; Sen, P.; Biswas, R. Subpicosecond Solvation Response and Partial Viscosity Decoupling of Solute Diffusion in Ionic Acetamide Deep Eutectic Solvents: Fluorescence Up-Conversion and Fluorescence

Correlation Spectroscopic Measurements. *J. Phys. Chem. B* **2020**, *124* (10), 1995–2005. https://doi.org/10.1021/acs.jpcb.0c00061.

(76) Mukherjee, K.; Tarif, E.; Barman, A.; Biswas, R. Dynamics of a PEG Based Non-Ionic Deep Eutectic Solvent: Temperature Dependence. *Fluid Phase Equilib* **2017**, *448*, 22–29. https://doi.org/10.1016/j.fluid.2017.05.003.

(77) Guchhait, B.; Al Rasid Gazi, H.; Kashyap, H. K.; Biswas, R. Fluorescence Spectroscopic Studies of (Acetamide + Sodium/Potassium Thiocyanates) Molten Mixtures: Composition and Temperature Dependence. *J. Phys. Chem. B* **2010**, *114* (15), 5066–5081. https://doi.org/10.1021/jp1001176.

(78) Subba, N.; Polok, K.; Piatkowski, P.; Ratajska-Gadomska, B.; Biswas, R.; Gadomski, W.; Sen, P. Temperature-Dependent Ultrafast Solvation Response and Solute Diffusion in Acetamide-Urea Deep Eutectic Solvent. *J. Phys. Chem. B* **2019**, *123* (43), 9212–9221. https://doi.org/10.1021/ACS.JPCB.9B07794.

(79) Hossain, S. S.; Samanta, A. How Do the Hydrocarbon Chain Length and Hydroxyl Group Position Influence the Solute Dynamics in Alcohol-Based Deep Eutectic Solvents? *Phys. Chem. Chem. Phys.* **2018**, *20* (38), 24613–24622. https://doi.org/10.1039/c8cp04859b.

(80) Barik, S.; Chakraborty, M.; Sarkar, M. How Does Addition of Lithium Salt Influence the Structure and Dynamics of Choline Chloride-Based Deep Eutectic Solvents? *J. Phys. Chem. B* **2020**, *124* (14), 2864–2878. https://doi.org/10.1021/acs.jpcb.9b11947.

(81) Barik, S.; Chakraborty, M.; Mahapatra, A.; Sarkar, M. Choline Chloride and Ethylene Glycol Based Deep Eutectic Solvent (DES) versus Hydroxyl Functionalized Room Temperature Ionic Liquids (RTILs): Assessing the Differences in Microscopic Behaviour between the DES and RTILs.

Physical Chemistry Chemical Physics **2022**, *24* (11), 7093–7106. https://doi.org/10.1039/D1CP05010A.

(82) Barik, S.; Mahapatra, A.; Jena, D.; Sarkar, M. Assessing the Impact of Increase in the Number of Hydroxyl Groups on the Microscopic Behaviors of Ammonium-Based Room Temperature Ionic Liquids: A Combined Fluorescence up-Conversion, Fluorescence Correlation and NMR Spectroscopic Study. *J Photochem Photobiol A Chem* **2023**, *437*, 114505. https://doi.org/10.1016/j.jphotochem.2022.114505.

(83) Perna, F. M.; Vitale, P.; Capriati, V. Deep Eutectic Solvents and Their Applications as Green Solvents. *Curr Opin Green Sustain Chem* **2020**, *21*, 27–33. https://doi.org/10.1016/j.cogsc.2019.09.004.

(84) Jablonský, M.; Škulcová, A.; Šima, J. Use of Deep Eutectic Solvents in Polymer Chemistry–a Review. *Molecules*. 2019. https://doi.org/10.3390/molecules24213978.

(85) Tian, Y.; Zhu, M.; Hu, T.; Liu, C. Natural Deep Eutectic Solvent—A Novel Green Solvent for Protein Stabilization. *Int J Biol Macromol* **2023**, *247*, 125477. https://doi.org/10.1016/J.IJBIOMAC.2023.125477.

(86) Marullo, S.; Meli, A.; D'Anna, F. A Joint Action of Deep Eutectic Solvents and Ultrasound to Promote Diels−Alder Reaction in a Sustainable Way. *ACS Sustain Chem Eng* **2020**, *8* (12), 4889–4899. https://doi.org/10.1021/ACSSUSCHEMENG.0C00193/ASSET/IMAGES/LARGE/SC0C00193_0007.JPEG.

(87) Pawar, P. M.; Jarag, K. J.; Shankarling, G. S. Environmentally Benign and Energy Efficient Methodology for Condensation: An Interesting Facet to the Classical Perkin Reaction. *Green Chemistry* **2011**, *13* (8), 2130–2134. https://doi.org/10.1039/C0GC00712A.

(88) Phadtare, S. B.; Shankarling, G. S. Halogenation Reactions in Biodegradable Solvent: Efficient Bromination of Substituted 1-Aminoanthra-9,10-Quinone in Deep Eutectic Solvent (Choline Chloride : Urea). *Green Chemistry* **2010**, *12* (3), 458–462. https://doi.org/10.1039/B923589B.

(89) Guajardo, N.; Müller, C. R.; Schrebler, R.; Carlesi, C.; Domínguez De María, P. Deep Eutectic Solvents for Organocatalysis, Biotransformations, and Multistep Organocatalyst/Enzyme Combinations. *ChemCatChem* **2016**, *8* (6), 1020–1027. https://doi.org/10.1002/CCTC.201501133.

(90) Hooshmand, S. E.; Afshari, R.; Ramón, D. J.; Varma, R. S. Deep Eutectic Solvents: Cutting-Edge Applications in Cross-Coupling Reactions. *Green Chemistry* **2020**, *22* (12), 3668–3692. https://doi.org/10.1039/D0GC01494J.

(91) Liao, H. G.; Jiang, Y. X.; Zhou, Z. Y.; Chen, S. P.; Sun, S. G. Shape-Controlled Synthesis of Gold Nanoparticles in Deep Eutectic Solvents for Studies of Structure-Functionality Relationships in Electrocatalysis. *Angewandte Chemie - International Edition* **2008**, *47* (47), 9100–9103. https://doi.org/10.1002/ANIE.200803202;REQUESTEDJOURNAL:JOURNAL:15213773;CTYPE:STRING:JOURNAL.

(92) Wagle, D. V.; Zhao, H.; Baker, G. A. Deep Eutectic Solvents: Sustainable Media for Nanoscale and Functional Materials. *Acc Chem Res* **2014**, *47* (8), 2299–2308. https://doi.org/10.1021/AR5000488/ASSET/IMAGES/LARGE/AR-2014-000488_0009.JPEG.

(93) Li, J. J.; Xiao, H.; Tang, X. D.; Zhou, M. Green Carboxylic Acid-Based Deep Eutectic Solvents as Solvents for Extractive Desulfurization. *Energy and Fuels* **2016**, *30* (7), 5411–5418. https://doi.org/10.1021/ACS.ENERGYFUELS.6B00471/ASSET/IMAGES/LARGE/EF-2016-00471C_0013.JPEG.

(94) Chandran, D.; Khalid, M.; Walvekar, R.; Mubarak, N. M.; Dharaskar, S.; Wong, W. Y.; Gupta, T. C. S. M. Deep Eutectic Solvents for Extraction-Desulphurization: A Review. *J Mol Liq* **2019**, *275*, 312–322. https://doi.org/10.1016/J.MOLLIQ.2018.11.051.

(95) Huang, Y.; Feng, F.; Chen, Z. G.; Wu, T.; Wang, Z. H. Green and Efficient Removal of Cadmium from Rice Flour Using Natural Deep Eutectic Solvents. *Food Chem* **2018**, *244*, 260–265. https://doi.org/10.1016/J.FOODCHEM.2017.10.060.

(96) Florindo, C.; Monteiro, N. V.; Ribeiro, B. D.; Branco, L. C.; Marrucho, I. M. Hydrophobic Deep Eutectic Solvents for Purification of Water Contaminated with Bisphenol-A. *J Mol Liq* **2020**, *297*, 111841. https://doi.org/10.1016/J.MOLLIQ.2019.111841.

(97) Florindo, C.; Branco, L. C.; Marrucho, I. M. Development of Hydrophobic Deep Eutectic Solvents for Extraction of Pesticides from Aqueous Environments. *Fluid Phase Equilib* **2017**, *448*, 135–142. https://doi.org/10.1016/J.FLUID.2017.04.002.

(98) Florindo, C.; Lima, F.; Branco, L. C.; Marrucho, I. M. Hydrophobic Deep Eutectic Solvents: A Circular Approach to Purify Water Contaminated with Ciprofloxacin. *ACS Sustain Chem Eng* **2019**, *7* (17), 14739–14746. https://doi.org/10.1021/ACSSUSCHEMENG.9B02658/ASSET/IMAGES/LARGE/SC9B02658_0002.JPEG.

(99) Nam, M. W.; Zhao, J.; Lee, M. S.; Jeong, J. H.; Lee, J. Enhanced Extraction of Bioactive Natural Products Using Tailor-Made Deep Eutectic Solvents: Application to Flavonoid Extraction from Flos Sophorae. *Green Chemistry* **2015**, *17* (3), 1718–1727. https://doi.org/10.1039/C4GC01556H.

(100) Cao, J.; Yang, M.; Cao, F.; Wang, J.; Su, E. Well-Designed Hydrophobic Deep Eutectic Solvents As Green and Efficient Media for the Extraction of

Artemisinin from Artemisia Annua Leaves. *ACS Sustain Chem Eng* **2017**, *5* (4), 3270–3278. https://doi.org/10.1021/ACSSUSCHEMENG.6B03092/ASSET/IMAGES/LARGE/SC-2016-03092D_0006.JPEG.

(101) Duan, L.; Dou, L. L.; Guo, L.; Li, P.; Liu, E. H. Comprehensive Evaluation of Deep Eutectic Solvents in Extraction of Bioactive Natural Products. *ACS Sustain Chem Eng* **2016**, *4* (4), 2405–2411. https://doi.org/10.1021/ACSSUSCHEMENG.6B00091/SUPPL_FILE/SC6B00091_SI_001.PDF.

(102) Cao, J.; Chen, L.; Li, M.; Cao, F.; Zhao, L.; Su, E. Two-Phase Systems Developed with Hydrophilic and Hydrophobic Deep Eutectic Solvents for Simultaneously Extracting Various Bioactive Compounds with Different Polarities. *Green Chemistry* **2018**, *20* (8), 1879–1886. https://doi.org/10.1039/C7GC03820H.

(103) Beni, A. H. N.; Haghbakhsh, R. Sulfur Dioxide Capture by Deep Eutectic Solvents: Proposing Purely Predictive Absorption Models. *J Hazard Mater* **2025**, *490*, 137741. https://doi.org/10.1016/J.JHAZMAT.2025.137741.

(104) Wibowo, H.; Zhong, L.; Huan, Q.; Hu, Q.; Rahim, D. A.; Yan, M. Experimental Study on the Effect of Water Addition to ChCl-MEA DES towards Its Performance in CO2 Removal from Syngas. *Biomass Convers Biorefin* **2022**, *12* (1), 61–71. https://doi.org/10.1007/S13399-021-01673-W/FIGURES/9.

(105) Wang, J.; Cheng, H.; Song, Z.; Chen, L.; Deng, L.; Qi, Z. Carbon Dioxide Solubility in Phosphonium-Based Deep Eutectic Solvents: An Experimental and Molecular Dynamics Study. *Ind Eng Chem Res* **2019**, *58* (37), 17514–17523. https://doi.org/10.1021/ACS.IECR.9B03740/ASSET/IMAGES/LARGE/IE9B03740_0002.JPEG.

(106) Halder, A. K.; Ambure, P.; Perez-Castillo, Y.; Cordeiro, M. N. D. S. Turning Deep-Eutectic Solvents into Value-Added Products for CO2 Capture: A Desirability-Based Virtual Screening Study. *Journal of CO2 Utilization* **2022**, *58*, 101926. https://doi.org/10.1016/J.JCOU.2022.101926.

(107) Yang, D.; Hou, M.; Ning, H.; Zhang, J.; Ma, J.; Yang, G.; Han, B. Efficient SO2 Absorption by Renewable Choline Chloride–Glycerol Deep Eutectic Solvents. *Green Chemistry* **2013**, *15* (8), 2261–2265. https://doi.org/10.1039/C3GC40815A.

(108) Makarov, D. M.; Fadeeva, Y. A.; Golubev, V. A.; Kolker, A. M. Designing Deep Eutectic Solvents for Efficient CO2 Capture: A Data-Driven Screening Approach. *Sep Purif Technol* **2023**, *325*, 124614. https://doi.org/10.1016/J.SEPPUR.2023.124614.

(109) Abbott, A. P. Deep Eutectic Solvents and Their Application in Electrochemistry. *Curr Opin Green Sustain Chem* **2022**, *36*, 100649. https://doi.org/10.1016/J.COGSC.2022.100649.

(110) Nkuku, C. A.; LeSuer, R. J. Electrochemistry in Deep Eutectic Solvents. *Journal of Physical Chemistry B* **2007**, *111* (46), 13271–13277. https://doi.org/10.1021/JP075794J/SUPPL_FILE/JP075794JSI20070723_053920.AVI.

(111) Wang, L.; Deng, Y.; Yan, L. Low-Cost “Water-in-Deep Eutectic Solvent” Electrolyte for High-Performance Zinc Ion Hybrid Supercapacitors. *ACS Appl Energy Mater* **2023**, *6* (20), 10585–10592. https://doi.org/10.1021/ACSAEM.3C01737/ASSET/IMAGES/LARGE/AE3C01737_0005.JPEG.

(112) Ma, G.; Pan, F.; Zhou, X.; Yong, Z.; Wang, X.; Li, C.; Bai, W.; Wang, S. A Flexible Supercapacitor Based on Deep Eutectic Solvent/[EMIM][TFSI] Ionogel with High Energy Density and Wide Temperature Range. *ACS Appl*

Electron Mater **2024**, *6* (2), 1434–1443. https://doi.org/10.1021/ACSAELM.3C01738/ASSET/IMAGES/LARGE/EL3C01738_0007.JPEG.

(113) Hariyanto, Y.; Ng, Y. K.; Siew, Z. Z.; Soon, C. Y.; Fisher, A. C.; Kloyer, L.; Wong, C. W.; Chan, E. W. C. Deep Eutectic Solvents for Batteries and Fuel Cells: Biosubstitution, Advantages, Challenges, and Future Directions. *Energy and Fuels* **2023**, *37* (23), 18395–18407. https://doi.org/10.1021/ACS.ENERGYFUELS.3C02870/ASSET/IMAGES/LARGE/EF3C02870_0003.JPEG.

(114) Azmi, S.; Koudahi, M. F.; Frackowiak, E. Reline Deep Eutectic Solvent as a Green Electrolyte for Electrochemical Energy Storage Applications. *Energy Environ Sci* **2022**, *15* (3), 1156–1171. https://doi.org/10.1039/D1EE02920G.

(115) Tran, M. K.; Rodrigues, M. T. F.; Kato, K.; Babu, G.; Ajayan, P. M. Deep Eutectic Solvents for Cathode Recycling of Li-Ion Batteries. *Nature Energy 2019 4:4* **2019**, *4* (4), 339–345. https://doi.org/10.1038/s41560-019-0368-4.

(116) Sanchez-Fernandez, A.; Jackson, A. J. Proteins in Deep Eutectic Solvents: Structure, Dynamics and Interactions with the Solvent. In *Advances in Botanical Research*; Academic Press Inc., 2021; Vol. 97, pp 69–94. https://doi.org/10.1016/bs.abr.2020.09.003.

(117) Gorke, J. T.; Srienc, F.; Kazlauskas, R. J. Hydrolase-Catalyzed Biotransformations in Deep Eutectic Solvents. *Chemical Communications* **2008**, No. 10, 1235–1237. https://doi.org/10.1039/b716317g.

(118) Durand, E.; Lecomte, J.; Baréa, B.; Villeneuve, P. Towards a Better Understanding of How to Improve Lipase-Catalyzed Reactions Using Deep Eutectic Solvents Based on Choline Chloride. *European Journal of Lipid*

Science and Technology **2014**, *116* (1), 16–23. https://doi.org/10.1002/ejlt.201300246.

(119) Durand, E.; Lecomte, J.; Baréa, B.; Piombo, G.; Dubreucq, E.; Villeneuve, P. Evaluation of Deep Eutectic Solvents as New Media for Candida Antarctica B Lipase Catalyzed Reactions. *Process Biochemistry* **2012**, *47* (12), 2081–2089. https://doi.org/10.1016/j.procbio.2012.07.027.

(120) Delorme, A. E.; Andanson, J. M.; Verney, V. Improving Laccase Thermostability with Aqueous Natural Deep Eutectic Solvents. *Int. J. Biol. Macromol.* **2020**, *163*, 919–926. https://doi.org/10.1016/j.ijbiomac.2020.07.022.

(121) Sun, H.; Xin, R.; Qu, D.; Yao, F. Mechanism of Deep Eutectic Solvents Enhancing Catalytic Function of Cytochrome P450 Enzymes in Biosynthesis and Organic Synthesis. *J Biotechnol* **2020**, *323*, 264–273. https://doi.org/10.1016/j.jbiotec.2020.07.004.

(122) Park, K.; Ham, B. Y.; Li, K.; Kang, S.; Jung, D.; Kim, H.; Liu, Y.; Hwang, I.; Lee, J. Insights into the Enhanced Thermal Stability of Lysozyme with Altered Structure and Activity Induced by Choline Chloride-Based Deep Eutectic Solvents Containing Polyols and Sugars. *J Mol Liq* **2022**, *349*, 118143. https://doi.org/10.1016/j.molliq.2021.118143.

(123) Sheng, Y.; Cui, H.; Wang, X.; Wang, M.; Song, P.; Huang, H.; Li, X. Harnessing Solvation-Guided Engineering to Enhance Deep Eutectic Solvent Resistance and Thermostability in Enzymes. *Green Chemistry* **2024**, *26* (16), 8883–9272. https://doi.org/10.1039/d3gc04933g.

(124) Javed, S.; Mangla, B.; Sultan, M. H.; Almoshari, Y.; Sivadasan, D.; Alqahtani, S. S.; Madkhali, O. A.; Ahsan, W. Pharmaceutical Applications of Therapeutic Deep Eutectic Systems (THEDES) in Maximising Drug

Delivery. *Heliyon* **2024**, *10* (9), e29783. https://doi.org/10.1016/J.HELIYON.2024.E29783.

(125) Shah, P. A.; Chavda, V.; Hirpara, D.; Sharma, V. S.; Shrivastav, P. S.; Kumar, S. Exploring the Potential of Deep Eutectic Solvents in Pharmaceuticals: Challenges and Opportunities. *J Mol Liq* **2023**, *390*, 123171. https://doi.org/10.1016/J.MOLLIQ.2023.123171.

(126) Hayyan, M. Versatile Applications of Deep Eutectic Solvents in Drug Discovery and Drug Delivery Systems: Perspectives and Opportunities. *Asian J Pharm Sci* **2023**, *18* (2), 100780. https://doi.org/10.1016/J.AJPS.2023.100780.

(127) Zhen, A.; Wang, A.; Long, X.; Wang, X.; Sheng, N.; Tang, Q.; Li, J.; Tan, H.; Luo, F.; Li, Z. Designed Amino Acid-Based Deep Eutectic Solvents as a Platform to Functionalize Biomedical Elastomers by Polyaddition Reactions. *Chemical Engineering Journal* **2025**, *512*, 162605. https://doi.org/10.1016/J.CEJ.2025.162605.

(128) Wysokowski, M.; Luu, R. K.; Arevalo, S.; Khare, E.; Stachowiak, W.; Niemczak, M.; Jesionowski, T.; Buehler, M. J. Untapped Potential of Deep Eutectic Solvents for the Synthesis of Bioinspired Inorganic-Organic Materials. *Chemistry of Materials* **2023**, *35* (19), 7878–7903. https://doi.org/10.1021/ACS.CHEMMATER.3C00847/ASSET/IMAGES/LARGE/CM3C00847_0010.JPEG.

(129) Weerasinghe, U. A.; Wu, T.; Chee, P. L.; Yew, P. Y. M.; Lee, H. K.; Loh, X. J.; Dan, K. Deep Eutectic Solvents towards Green Polymeric Materials. *Green Chemistry* **2024**, *26* (15), 8497–8527. https://doi.org/10.1039/D4GC00532E.

(130) García-Argüelles, S.; Serrano, M. C.; Gutiérrez, M. C.; Ferrer, M. L.; Yuste, L.; Rojo, F.; Del Monte, F. Deep Eutectic Solvent-Assisted Synthesis of

Biodegradable Polyesters with Antibacterial Properties. *Langmuir* **2013**, *29* (30), 9525–9534. https://doi.org/10.1021/LA401353R/SUPPL_FILE/LA401353R_SI_001.PDF.

(131) Cao, J.; Wu, R.; Zhu, F.; Dong, Q.; Su, E. Enzymes in Nearly Anhydrous Deep Eutectic Solvents: Insight into the Biocompatibility and Thermal Stability. *Enzyme Microb Technol* **2022**, *157*, 110022. https://doi.org/10.1016/j.enzmictec.2022.110022.

(132) Esquembre, R.; Sanz, J. M.; Wall, J. G.; Del Monte, F.; Mateo, C. R.; Ferrer, M. L. Thermal Unfolding and Refolding of Lysozyme in Deep Eutectic Solvents and Their Aqueous Dilutions. *Phys. Chem. Chem. Phys.* **2013**, *15* (27), 11248–11256. https://doi.org/10.1039/c3cp44299c.

(133) Monhemi, H.; Housaindokht, M. R.; Moosavi-Movahedi, A. A.; Bozorgmehr, M. R. How a Protein Can Remain Stable in a Solvent with High Content of Urea: Insights from Molecular Dynamics Simulation of Candida Antarctica Lipase B in Urea: Choline Chloride Deep Eutectic Solvent. *Phys. Chem. Chem. Phys.* **2014**, *16* (28), 14882–14893. https://doi.org/10.1039/c4cp00503a.

(134) Kim, S. H.; Park, S.; Yu, H.; Kim, J. H.; Kim, H. J.; Yang, Y. H.; Kim, Y. H.; Kim, K. J.; Kan, E.; Lee, S. H. Effect of Deep Eutectic Solvent Mixtures on Lipase Activity and Stability. *J Mol Catal B Enzym* **2016**, *128*, 65–72. https://doi.org/10.1016/j.molcatb.2016.03.012.

(135) Sanchez-Fernandez, A.; Edler, K. J.; Arnold, T.; Alba Venero, D.; Jackson, A. J. Protein Conformation in Pure and Hydrated Deep Eutectic Solvents. *Phys. Chem. Chem. Phys.* **2017**, *19* (13), 8667–8670. https://doi.org/10.1039/c7cp00459a.

(136) Juneidi, I.; Hayyan, M.; Hashim, M. A.; Hayyan, A. Pure and Aqueous Deep Eutectic Solvents for a Lipase-Catalysed Hydrolysis Reaction. *Biochem Eng J* **2017**, *117*, 129–138. https://doi.org/10.1016/j.bej.2016.10.003.

(137) Oh, Y.; Park, S.; Yoo, E.; Jo, S.; Hong, J.; Kim, H. J.; Kim, K. J.; Oh, K. K.; Lee, S. H. Dihydrogen-Bonding Deep Eutectic Solvents as Reaction Media for Lipase-Catalyzed Transesterification. *Biochem Eng J* **2019**, *142*, 34–40. https://doi.org/10.1016/J.BEJ.2018.11.010.

(138) Kumari, P.; Kumari, M.; Kashyap, H. K. How Pure and Hydrated Reline Deep Eutectic Solvents Affect the Conformation and Stability of Lysozyme: Insights from Atomistic Molecular Dynamics Simulations. *Journal of Physical Chemistry B* **2020**, *124* (52), 11919–11927. https://doi.org/10.1021/ACS.JPCB.0C09873/ASSET/IMAGES/LARGE/JP0C09873_0006.JPEG.

(139) Dhiman, D.; Marques, A. S. C.; Bisht, M.; Tavares, A. P. M.; Freire, M. G.; Venkatesu, P. Unveiling the Potential of Deep Eutectic Solvents to Improve the Conformational and Colloidal Stability of Immunoglobulin G Antibodies. *Green Chemistry* **2023**, *25* (2), 650–660. https://doi.org/10.1039/D2GC03415H.

(140) Sanchez-Fernandez, A.; Basic, M.; Xiang, J.; Prevost, S.; Jackson, A. J.; Dicko, C. Hydration in Deep Eutectic Solvents Induces Non-Monotonic Changes in the Conformation and Stability of Proteins. *J. Am. Chem. Soc.* **2022**, *144* (51), 23657–23667. https://doi.org/10.1021/jacs.2c11190.

(141) Guo, J.; Zhao, N.; Zhao, Y.; Jin, H.; Sun, G.; Yu, J.; Zhang, H.; Yu, M.; Yang, D.; Liang, Z. Effect of Deep Eutectic Solvents on the Activity and Stability of Cellulases and Pectinases. *ACS Omega* **2023**, *8* (48), 45678–45686. https://doi.org/10.1021/ACSOMEGA.3C06088/ASSET/IMAGES/LARGE/AO3C06088_0006.JPEG.

(142) Soares, G. A.; Alnoch, R. C.; Alves dos Santos, L.; Mafra, M. R.; Mitchell, D. A.; Krieger, N. High Hydrolytic Activity of the Metagenomic Lipase LipC12 in Deep Eutectic Solvents. *J Mol Liq* **2023**, *391*, 123383. https://doi.org/10.1016/J.MOLLIQ.2023.123383.

(143) Baruah, I.; Borgohain, G. Temperature Dependent Molecular Dynamics Simulation Study to Understand the Stabilizing Effect of NADES on the Protein β-Lactoglobulin. *J Mol Graph Model* **2023**, *125*, 108582. https://doi.org/10.1016/J.JMGM.2023.108582.

(144) Yadav, N.; Chahar, D.; Bisht, M.; Venkatesu, P. Assessing the Compatibility of Choline-Based Deep Eutectic Solvents for the Structural Stability and Activity of Cellulase: Enzyme Sustain at High Temperature. *Int. J. Biol. Macromol.* **2023**, *249*, 125988. https://doi.org/10.1016/j.ijbiomac.2023.125988.

(145) Barik, S.; Mahapatra, A.; Preeyanka, N.; Sarkar, M. Assessing the Impact of Choline Chloride and Benzyltrimethylammonium Chloride-Based Deep Eutectic Solvents on the Structure and Conformational Dynamics of Bovine Serum Albumin: A Combined Steady-State, Time-Resolved Fluorescence and Fluorescence Correlation Spectroscopic Study. *Phys. Chem. Chem. Phys.* **2023**, *25* (29), 20093–20108. https://doi.org/10.1039/d3cp01380d.

(146) Wang, H.; Masuku, M. V.; Tao, Y.; Yang, J.; Kuang, Y.; Lyu, C.; Huang, J.; Yang, S. Improved Stability and Catalytic Efficiency of ω-Transaminase in Aqueous Mixture of Deep Eutectic Solvents. *Molecules* **2023**, *28* (9), 3895. https://doi.org/10.3390/MOLECULES28093895/S1.

(147) Gomes, I.; Martins, G. F.; Galamba, N. Essential Dynamics of Ubiquitin in Water and in a Natural Deep Eutectic Solvent. *Physical Chemistry Chemical Physics* **2024**, *26* (26), 18244–18255. https://doi.org/10.1039/D4CP01773K.

(148) Fatima, U.; Yadav, N.; Venkatesu, P. Sustainable Combination of Ionic Liquid and Deep Eutectic Solvent for Protecting and Preserving of the Protein Structure: The Synergistic Interaction of Enzymes and Eco-Friendly Hybrid Ionic Fluids. *Int J Biol Macromol* **2024**, *268*, 131997. https://doi.org/10.1016/J.IJBIOMAC.2024.131997.

(149) Fatima, U.; Deenadayalu, N.; Venkatesu, P. An Eminent Approach towards next Generation Solvents for Sustainable Packaging and Stability of Enzymes: A Comprehensive Study of Ionic Liquid and Deep Eutectic Solvent Mixtures. *Physical Chemistry Chemical Physics* **2024**, *26* (20), 14766–14776. https://doi.org/10.1039/D4CP00931B.

(150) Meng, F.; Ju, X.; Zhou, Y.; Yan, L.; Chen, Z.; Wu, Y.; Li, L. Balancing the Pretreatment Effect of Deep Eutectic Solvents on Biomass and the Activity of β-Glucosidase Originating from Paenibacillus Sp. LLZ1. *J Mol Liq* **2024**, *400*, 124564. https://doi.org/10.1016/J.MOLLIQ.2024.124564.

(151) Garbe, M.; Lutz, L. U.; Lehmann, L. T.; Strotmann, T.; Berger, R. G.; Ersoy, F. Improving the Stability and Activity of a Dye-Decolourizing Peroxidase Using NADESs. *RSC Sustainability* **2024**, *2* (4), 1058–1066. https://doi.org/10.1039/D3SU00359K.

(152) Garbe, M.; Lehmann, L. T.; Berger, R. G.; Ersoy, F. Improvement in the Stability and Enzymatic Activity of Pleurotus Sapidus Lipoxygenase Dissolved in Natural Deep Eutectic Solvents (NADESs). *Life* **2024**, *14* (2), 271. https://doi.org/10.3390/LIFE14020271/S1.

(153) Soltani-Nezhad, Z.; Zaboli, M.; Mortazavi, M.; Torkzadeh-Mahani, M. Enhancing Stability and Catalytic Activity of Urate Oxidase Using Natural Deep Eutectic Solvent: Insights from Experimental and Computational Approaches. *J Biomol Struct Dyn* **2025**, 1–18. https://doi.org/10.1080/07391102.2025.2486444.

(154) Sarkar, I. Das; Sil, A.; Guchhait, B.; Das, S. Hydrogen-Bond Induced Non-Linear Size Dependence of Lysozyme under the Influence of Aqueous Glyceline. *Journal of Chemical Physics* **2025**, *162* (11), 114506. https://doi.org/10.1063/5.0251283/3340050.

(155) Gajardo-Parra, N. F.; Cea-Klapp, E.; Chandra, A.; Canales, R. I.; Garrido, J. M.; Held, C.; Guajardo, N. Assessing the Effect of Deep Eutectic Solvents on α-Chymotrypsin Thermal Stability and Activity. *ChemSusChem* **2025**, *18* (5), e202401414. https://doi.org/10.1002/CSSC.202401414.

(156) Chakravorty, P.; Das, A. B. Impact of Choline Choride and Sugar Natural Deep Eutectic Solvents on Structure and Functionality of Treebean (Parkia Timoriana) Seed Protein. *Scientific Reports 2025 15:1* **2025**, *15* (1), 1–10. https://doi.org/10.1038/s41598-025-87890-z.

(157) Kist, J. A.; Henzl, M. T.; Bañuelos, J. L.; Baker, G. A. Calorimetric Evaluation of the Operational Thermal Stability of Ribonuclease A in Hydrated Deep Eutectic Solvents. *ACS Sustain Chem Eng* **2019**, *7* (15), 12682–12687. https://doi.org/10.1021/acssuschemeng.9b02585.

(158) Cvjetko Bubalo, M.; Jurinjak Tušek, A.; Vinković, M.; Radošević, K.; Gaurina Srček, V.; Radojčić Redovniković, I. Cholinium-Based Deep Eutectic Solvents and Ionic Liquids for Lipase-Catalyzed Synthesis of Butyl Acetate. *J Mol Catal B Enzym* **2015**, *122*, 188–198. https://doi.org/10.1016/j.molcatb.2015.09.005.

(159) Shehata, M.; Unlu, A.; Sezerman, U.; Timucin, E. Lipase and Water in a Deep Eutectic Solvent: Molecular Dynamics and Experimental Studies of the Effects of Water-In-Deep Eutectic Solvents on Lipase Stability. *J. Phys. Chem. B* **2020**, *124* (40), 8801–8810. https://doi.org/10.1021/acs.jpcb.0c07041.

(160) Nian, B.; Cao, C.; Liu, Y. How Candida Antarctica Lipase B Can Be Activated in Natural Deep Eutectic Solvents: Experimental and Molecular Dynamics Studies. *Journal of Chemical Technology and Biotechnology* **2020**, *95* (1), 86–93. https://doi.org/10.1002/jctb.6209.

(161) Zhou, P.; Wang, X.; Yang, B.; Hollmann, F.; Wang, Y. Chemoenzymatic Epoxidation of Alkenes with Candida Antarctica Lipase B and Hydrogen Peroxide in Deep Eutectic Solvents. *RSC Adv* **2017**, *7* (21), 12518–12523. https://doi.org/10.1039/c7ra00805h.

(162) Chen, G.; Zhang, Q.; Lu, Q.; Feng, B. Protection Effect of Polyols on Rhizopus Chinensis Lipase Counteracting the Deactivation from High Pressure and High Temperature Treatment. *Int J Biol Macromol* **2019**, *127*, 555–562. https://doi.org/10.1016/j.ijbiomac.2019.01.082.

(163) Sanchez-Fernandez, A.; Prevost, S.; Wahlgren, M. Deep Eutectic Solvents for the Preservation of Concentrated Proteins: The Case of Lysozyme in 1 : 2 Choline Chloride : Glycerol. *Green Chemistry* **2022**, *24* (11), 4437–4442. https://doi.org/10.1039/D1GC04378A.

(164) Banerjee, A.; Ibsen, K.; Iwao, Y.; Zakrewsky, M.; Mitragotri, S.; Banerjee, A.; Ibsen, K.; Zakrewsky, M.; Mitragotri, S.; Iwao, Y. Transdermal Protein Delivery Using Choline and Geranate (CAGE) Deep Eutectic Solvent. *Adv Healthc Mater* **2017**, *6* (15), 1601411. https://doi.org/10.1002/ADHM.201601411.

(165) Zheng, X.; Feng, J.; Lu, Y.; Li, R.; Cavaco-paulo, A.; Fu, J. Deep Eutectic Solvent as an Additive to Improve Enzymatic Hydrolysis of Polyethylene Terephthalate (PET). *J Polym Environ* **2024**, *32* (11), 5936–5951. https://doi.org/10.1007/S10924-024-03337-Y/TABLES/3.

(166) Papadopoulou, A. A.; Efstathiadou, E.; Patila, M.; Polydera, A. C.; Stamatis, H. Deep Eutectic Solvents as Media for Peroxidation Reactions Catalyzed

by Heme-Dependent Biocatalysts. *Ind Eng Chem Res* **2016**, *55* (18), 5145–5151. https://doi.org/10.1021/acs.iecr.5b04867.

(167) Heyden, M.; Bründermann, E.; Heugen, U.; Niehues, G.; Leitner, D. M.; Havenith, M. Long-Range Influence of Carbohydrates on the Solvation Dynamics of Water - Answers from Terahertz Absorption Measurements and Molecular Modeling Simulations. *J. Am. Chem. Soc.* **2008**, *130* (17), 5773–5779. https://doi.org/10.1021/ja0781083.

(168) Negi, K. S.; Das, N.; Khan, T.; Sen, P. Osmolyte Induced Protein Stabilization: Modulation of Associated Water Dynamics Might Be a Key Factor. *Phys. Chem. Chem. Phys.* **2023**, *25* (47), 32602–32612. https://doi.org/10.1039/d3cp03357k.

(169) Pal, S. K.; Peon, J.; Zewail, A. H. Ultrafast Surface Hydration Dynamics and Expression of Protein Functionality: α-Chymotrypsin. *Proc Natl Acad Sci U S A* **2002**, *99* (24), 15297–15302. https://doi.org/10.1073/pnas.242600399.

(170) Kamal, J. K. A.; Zhao, L.; Zewail, A. H. Ultrafast Hydration Dynamics in Protein Unfolding: Human Serum Albumin. *Proceedings of the National Academy of Sciences* **2004**, *101* (37), 13411–13416. https://doi.org/10.1073/pnas.0405724101.

(171) Othon, C. M.; Kwon, O.-H.; Lin, M. M.; Zewail, A. H. Solvation in Protein (Un)Folding of Melittin Tetramer-Monomer Transition. *Proc. Natl. Acad. sci. USA* **2009**, *106* (31), 12593–12598.

(172) Qiu, W.; Zhang, L.; Okobiah, O.; Yang, Y.; Wang, L.; Zhong, D.; Zewail, A. H. Ultrafast Solvation Dynamics of Human Serum Albumin: Correlations with Conformational Transitions and Site-Selected Recognition. *J. Phys. Chem. B* **2006**, *110* (21), 10540–10549. https://doi.org/10.1021/jp055989w.

(173) Yadav, R.; Sengupta, B.; Sen, P. Effect of Sucrose on Chemically and Thermally Induced Unfolding of Domain-I of Human Serum Albumin:

Solvation Dynamics and Fluorescence Anisotropy Study. *Biophys Chem* **2016**, *211*, 59–69. https://doi.org/10.1016/j.bpc.2016.02.005.

(174) Mohan, V.; Sengupta, B.; Das, N.; Banerjee, I.; Sen, P. Domain-Specific Stabilization of Structural and Dynamic Responses of Human Serum Albumin by Sucrose. *Protein Pept Lett* **2019**, *26* (4), 287–300. https://doi.org/10.2174/0929866526666190122115702.

(175) Mohan, V.; Sengupta, B.; Acharyya, A.; Yadav, R.; Das, N.; Sen, P. Region-Specific Double Denaturation of Human Serum Albumin: Combined Effects of Temperature and GnHCl on Structural and Dynamical Responses. *ACS Omega* **2018**, *3* (8), 10406–10417. https://doi.org/10.1021/acsomega.8b00967.

(176) Chowdhury, R.; Mojumdar, S. Sen; Chattoraj, S.; Bhattacharyya, K. Effect of Ionic Liquid on the Native and Denatured State of a Protein Covalently Attached to a Probe: Solvation Dynamics Study. *Journal of Chemical Physics* **2012**, *137* (5), 55104. https://doi.org/10.1063/1.4739922/671633.

(177) Samaddar, S.; Mandal, A. K.; Mondal, S. K.; Sahu, K.; Bhattacharyya, K.; Roy, S. Solvation Dynamics of a Protein in the Pre Molten Globule State. *J Phys Chem B* **2006**, *110* (42), 21210–21215. https://doi.org/10.1021/jp064136g.

1.3. Macromolecular Crowders: A Short Overview

Most of our knowledge of biosystems comes from *in vitro* experiments in buffers maintaining the physiological pH [1]. However, the intracellular environment is densely occupied with various biological macromolecules like proteins, protein complexes, nucleic acids, carbohydrates, etc [2–5]. creating a crowded environment [4]. On average, 5-40% of the cellular environment is occupied by crowders, and the concentration of macromolecules varies from 40 to 400 $g.L^{-1}$ inside various cell compartments [5–7]. The viscosity is typically 3-4 times higher than in dilute buffer solutions [8,9]. The biological phenomenon inside such a crowded medium is expected to be different from that in a dilute buffer. It is, therefore, necessary to alter the buffer solution to resemble the cellular environment to understand the correct biology.

Because of the highly intricate architecture of the cellular interior, investigating in-cell crowding or doing *in vitro* research with cell extracts is difficult. Adding inert macromolecules like dextran, ficoll, and polyethylene glycol (PEG) can simulate cellular properties such as limited space and increased viscosity. These studies are essential for understanding the mechanism of crowding-induced alteration of protein's function, structure, and dynamics [10]. Every biological phenomenon (like structure, stability, dynamics, activity, folding, aggregation, association, binding, cell culture, tissue engineering, and so on) is found to be modulated in a crowded environment. As there are many available reviews on these topics [11–20], a very brief discussion on the modulation of protein stability and activity in the presence of crowded environments is given.

1.3.1. Alteration of Protein Stability in the Crowded Milieu

Protein stability is generally characterized as the thermodynamic stability of the protein. It remains stable and active in a particular conformation, known as the native state of the protein. Various factors are responsible for altering this specific form of the protein, and the ability of the protein to retain its original structural parameters

against disruptive forces is called its stability. The more a protein can maintain its specific structural motif against perturbation, the more its stability. Protein stability in the crowded milieu is generally explained in terms of excluded volume theory [21]. This stems from the fact that two solutes cannot access the same space at the same time; thus, in the presence of macromolecular crowder, a protein can access a lesser volume compared to when no macromolecular crowder is present. The excluded volume effect, which is purely entropic, tends to shift protein unfolding toward more compact states, thereby promoting protein stabilization [21–23]. However, instances of protein destabilization observed in the presence of crowding agents have prompted researchers to account for potential direct interactions between the crowder and the protein, which is enthalpic in nature and may contribute to either stabilization or destabilization [24–26]. Overall, the stability of a protein in a crowded environment is now understood to result from a nuanced interplay between entropic forces and enthalpic interactions. The theory considering excluded volume and interaction both can explain most observations except a few, which will be discussed while discussing the unresolved aspect of protein behaviour in the crowded milieu [27–30.] Many recent reviews have described the trends and intricate aspects of the stability of protein in the presence of macromolecular crowders, and it is beyond the scope of this thesis [14,18,20,31,32].

In my thesis, I have tried to explain the enzymatic stability in the crowded milieu in terms of associated water dynamics modulation. This also fulfills the purpose of generalizing the role of associated water modulation in influencing protein stability in the presence of any additive.

1.3.2. Alteration of Enzyme Activity in the Crowded Milieu

Despite numerous reports indicating alterations of protein function in crowded conditions, our understanding of protein activity in such environments remains limited. The very first study of enzymatic reaction in the crowded milieu was done

in 1971 by Laurent [33]. He studied three enzyme systems: (i) degradation of hyaluronic acid by hyaluronate lyase in the presence of PEG; (ii) cleavage of benzoyl DL-arginine p-nitroanilide by trypsin in the presence of HSA and (iii) lactate dehydrogenase reaction in the presence of dextran. He finds that in all these cases, both the Michaelis-Menten constant (K_m) and turnover number (k_{cat}) decrease in the presence of crowders. In 2017, Pielak and coworkers tabulated many works on protein activity in the crowded milieu [34]. Many reports described the activity of proteins in the crowded milieu. Unlike structural and stability modulation, activity modulation does not follow any specific trend. In some reports, the activity increases, whereas in some cases, the activity decreases; even in some cases, the activity remains unaltered [33,35–40]. This is mainly because protein function typically involves several sequential steps, each of which can be influenced by different variables present in the crowded surroundings, making it difficult to pinpoint specific effects.

In my thesis, I have tried to explain the enzymatic activity in the crowded milieu in terms of associated water dynamics modulation.

1.3.3 Expanding the Hypothesis of the Role of Associated Water Beyond Hydrated DES

The central focus of this thesis is to investigate protein behavior within deep eutectic solvents (DESs). Although numerous studies have examined the stability and activity of proteins in DES and hydrated DES environments, mechanistic insights into how these solvents influence protein structure and function remain limited. Drawing inspiration from earlier research, we formulated the hypothesis that modulation of associated water dynamics plays a critical role in determining enzyme stability and activity in the presence of DES. This hypothesis stems from the understanding that associated water (the hydration layer directly interacting with surface residues of proteins) can be modulated by external additives. When this

hydration network is perturbed, it may lead to consequential shifts in protein behavior, including folding, stability, and enzymatic activity. To explore this idea more broadly and test its generalizability beyond DES systems, we incorporated additional solvent environments into our investigation. In particular, I introduced macromolecular crowding agents into our experimental design, as these represent biologically relevant additives known to exert significant influence on protein structure and dynamics. Ficoll-70k, an inert, high-molecular-weight polymer, was selected for its ability to mimic the crowded cellular milieu and provide a platform for probing protein behavior under near-physiological conditions.

Beyond serving as a comparative system, several intriguing observations reported in crowded systems, such as the emergence of a negative entropy component in protein stabilization and the phenomenon of entropy-enthalpy compensation, remain poorly explained by classical crowding theories. In light of these inconsistencies, our group recently proposed that changes in associated water dynamics, induced by crowding agents, could provide a plausible explanation.[41] This perspective is supported by the work of the Pielak and Harries groups, who incorporated non-ideal water–crowder interactions along with classical excluded volume and soft chemical effects into their models [20,42–44].

We hypothesized that the presence of macromolecular crowders could modulate both the entropic and enthalpic components of protein stability by modulating the associated water structure (see Figure 1.3.1). Taking human serum albumin (HSA) in the presence of crowding agents such as Dextran-40k, Ficoll-70k, and PEG-35k, we found that slower water dynamics in the presence of Dextran-40k and Ficoll-70k correlated with entropic stabilization but enthalpic destabilization [41]. Conversely, the presence of PEG-35k led to more flexible hydration dynamics, resulting in the opposite effect [41].

In this thesis, I went a step further to resolve the shortcomings of the previous study, and also tried to give a mechanistic understanding of the enzymatic activity, which was very limited in the literature.

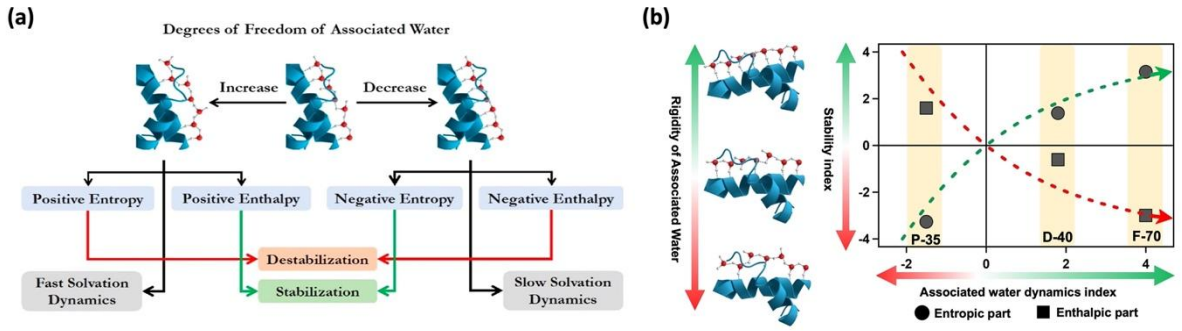

Figure 1.3.1. Associated water dynamics might be key to protein stability in a crowded environment: (a) Water reorganization might be pivotal in managing protein stability in the crowded milieu. Any perturbation that increases the degrees of freedom of associated water results in a positive entropy and enthalpy change. Positive entropy change destabilizes the protein, whereas the positive enthalpic effect has a stabilizing impact. Similarly, when the degrees of freedom of associated water decreases, the protein will be stabilized by negative entropic change and destabilized by negative enthalpic change. One could measure the rigidity of associated water by solvation dynamics measurement. Faster and slower solvation dynamics correlate with how the distortion of associated water modulates the entropy and enthalpy change. This scheme has been reprinted from the reference [41]. (b) Modulation of differential entropic and enthalpic part of thermal denaturation of HSA as a function of associated water dynamics modulation around HSA with various crowders (Dextran-40k, Ficoll-70k, and PEG-35k). With an increase in the rigidity of associated water, the entropic stabilization increases and enthalpic stabilization decreases (*J. Phys. Chem. B* **2023**, *127*, 3151–3163). Figures a and b have been reprinted from the reference [41].

1.3.4. Unresolved Aspects of Protein Behavior in Crowded Milieu:

Apart from extending the hypothesis regarding the role of associated water in enzyme stability and activity beyond hydrated DES, it also provides insights into previously unexplored aspects of macromolecular crowding. Although most of the observations in the presence of macromolecular crowders can be explained using the traditional theories (Excluded volume and soft Interaction), some unresolved questions remain.

Firstly, with individual recognition of entropic and enthalpic components, two interesting observations, namely, negative entropic component and entropy-enthalpy

compensation, cannot be explained by traditional crowding theory (excluded volume effect + interaction).

Secondly, enzymatic activity in the crowded milieu does not follow a proper trend and thus remains a mostly misunderstood parameter.

Thirdly, a concentration-dependent effect of the macromolecular crowding on the enzyme's properties can be found, which was not clearly interpreted.

Moreover, any claim cannot be true without generalizing it to different systems.

In my thesis, taking different DESs and crowder, I have tried to provide a mechanistic insight into enzyme stability and activity.

1.3.5. References:

(1) Ralston, G. B. Effects of "Crowding" in Protein Solutions. *J Chem Educ* **1990**, *67* (10), 857–860. https://doi.org/10.1021/ED067P857.

(2) Zhou, H. X.; Rivas, G.; Minton, A. P. Macromolecular Crowding and Confinement: Biochemical, Biophysical, and Potential Physiological Consequences. *Annu Rev Biophys* **2008**, *37*, 375–397. https://doi.org/10.1146/ANNUREV.BIOPHYS.37.032807.125817.

(3) Gnutt, D.; Ebbinghaus, S. The Macromolecular Crowding Effect--from in Vitro into the Cell. *Biol Chem* **2016**, *397* (1), 37–44. https://doi.org/10.1515/HSZ-2015-0161.

(4) Rivas, G.; Ferrone, F.; Herzfeld, J. Life in a Crowded World. *EMBO Rep* **2004**, *5* (1), 23–27. https://doi.org/10.1038/SJ.EMBOR.7400056.

(5) Fulton, A. B. How Crowded Is the Cytoplasm? *Cell* **1982**, *30* (2), 345–347. https://doi.org/10.1016/0092-8674(82)90231-8.

(6) Zimmerman, S. B.; Trach, S. O. Estimation of Macromolecule Concentrations and Excluded Volume Effects for the Cytoplasm of Escherichia Coli. *J Mol Biol* **1991**, *222* (3), 599–620. https://doi.org/10.1016/0022-2836(91)90499-V.

(7) Ellis, R. J. Macromolecular Crowding: Obvious but Underappreciated. *Trends Biochem Sci* **2001**, *26* (10), 597–604. https://doi.org/10.1016/S0968-0004(01)01938-7.

(8) Puchkov, E. O. Intracellular Viscosity: Methods of Measurement and Role in Metabolism. *Biochem (Mosc) Suppl Ser A Membr Cell Biol* **2013**, *7* (4), 270–279. https://doi.org/10.1134/S1990747813050140/METRICS.

(9) Schreiber, G.; Haran, G.; Zhou, H. X. Fundamental Aspects of Protein-Protein Association Kinetics. *Chem Rev* **2009**, *109* (3), 839–860. https://doi.org/10.1021/CR800373W.

(10) Rivas, G.; Minton, A. P. Macromolecular Crowding In Vitro, In Vivo, and In Between. *Trends Biochem Sci* **2016**, *41* (11), 970–981. https://doi.org/10.1016/J.TIBS.2016.08.013.

(11) Zhou, H. X.; Rivas, G.; Minton, A. P. Macromolecular Crowding and Confinement: Biochemical, Biophysical, and Potential Physiological Consequences. *Annu Rev Biophys* **2008**, *37*, 375–397. https://doi.org/10.1146/ANNUREV.BIOPHYS.37.032807.125817.

(12) Ellis, R. J. Macromolecular Crowding: An Important but Neglected Aspect of the Intracellular Environment. *Curr Opin Struct Biol* **2001**, *11* (1), 114–119. https://doi.org/10.1016/S0959-440X(00)00172-X.

(13) Ellis, R. J. Macromolecular Crowding: Obvious but Underappreciated. *Trends Biochem Sci* **2001**, *26* (10), 597–604. https://doi.org/10.1016/S0968-0004(01)01938-7.

(14) Rivas, G.; Minton, A. P. Macromolecular Crowding In Vitro, In Vivo, and In Between. *Trends Biochem Sci* **2016**, *41* (11), 970–981. https://doi.org/10.1016/J.TIBS.2016.08.013.

(15) Despa, F.; Orgill, D. P.; Lee, R. C. Molecular Crowding Effects on Protein Stability. *Ann N Y Acad Sci* **2006**, *1066*, 54–66. https://doi.org/10.1196/ANNALS.1363.005.

(16) Zimmerman, S. B.; Minton, A. P. Macromolecular Crowding: Biochemical, Biophysical, and Physiological Consequences. *Annu Rev Biophys Biomol Struct* **1993**, *22*, 27–65. https://doi.org/10.1146/ANNUREV.BB.22.060193.000331.

(17) Elcock, A. H. Models of Macromolecular Crowding Effects and the Need for Quantitative Comparisons with Experiment. *Curr Opin Struct Biol* **2010**, *20* (2), 196–206. https://doi.org/10.1016/J.SBI.2010.01.008.

(18) Kuznetsova, I. M.; Turoverov, K. K.; Uversky, V. N. What Macromolecular Crowding Can Do to a Protein. *Int J Mol Sci* **2014**, *15* (12), 23090–23140. https://doi.org/10.3390/IJMS151223090.

(19) Ellis, R. J.; Minton, A. P. Protein Aggregation in Crowded Environments. *Biol Chem* **2006**, *387* (5), 485–497. https://doi.org/10.1515/BC.2006.064.

(20) Speer, S. L.; Stewart, C. J.; Sapir, L.; Harries, D.; Pielak, G. J. Macromolecular Crowding Is More than Hard-Core Repulsions. *Annu Rev Biophys* **2022**, *51*, 267–300. https://doi.org/10.1146/ANNUREV-BIOPHYS-091321-071829.

(21) Minton, A. P. Excluded Volume as a Determinant of Macromolecular Structure and Reactivity. *Biopolymers* **1981**, *20* (10), 2093–2120. https://doi.org/10.1002/bip.1981.360201006.

(22) Rivas, G.; Minton, A. P. Toward an Understanding of Biochemical Equilibria within Living Cells. *Biophys Rev* **2018**, *10* (2), 241–253. https://doi.org/10.1007/S12551-017-0347-6.

(23) Beg, I.; Minton, A. P.; Islam, A.; Hassan, M. I.; Ahmad, F. Comparison of the Thermal Stabilization of Proteins by Oligosaccharides and Monosaccharide Mixtures: Measurement and Analysis in the Context of Excluded Volume Theory. *Biophys. Chem.* **2018**, *237*, 31–37. https://doi.org/10.1016/j.bpc.2018.03.002.

(24) Minton, A. P. Quantitative Assessment of the Relative Contributions of Steric Repulsion and Chemical Interactions to Macromolecular Crowding. *Biopolymers* **2013**, *99* (4), 239–244. https://doi.org/10.1002/bip.22163.

(25) Sarkar, M.; Li, C.; Pielak, G. J. Soft Interactions and Crowding. *Biophys Rev* **2013**, *5* (2), 187–194. https://doi.org/10.1007/s12551-013-0104-4.

(26) Benton, L. A.; Smith, A. E.; Young, G. B.; Pielak, G. J. Unexpected Effects of Macromolecular Crowding on Protein Stability. *Biochemistry* **2012**, *51* (49), 9773–9775. https://doi.org/10.1021/BI300909Q.

(27) Das, N.; Sen, P. Shape-Dependent Macromolecular Crowding on the Thermodynamics and Microsecond Conformational Dynamics of Protein Unfolding Revealed at the Single-Molecule Level. *J. Phys. Chem. B* **2020**, *124* (28), 5858–5871. https://doi.org/10.1021/acs.jpcb.0c03897.

(28) Senske, M.; Törk, L.; Born, B.; Havenith, M.; Herrmann, C.; Ebbinghaus, S. Protein Stabilization by Macromolecular Crowding through Enthalpy Rather than Entropy. *J. Am. Chem. Soc.* **2014**, *136* (25), 9036–9041. https://doi.org/10.1021/ja503205y.

(29) Sung, H. L.; Nesbitt, D. J. Effects of Molecular Crowders on Single-Molecule Nucleic Acid Folding: Temperature-Dependent Studies Reveal

True Crowding vs Enthalpic Interactions. *J. Phys. Chem. B* **2021**, *125* (48), 13147–13157. https://doi.org/10.1021/acs.jpcb.1c07852.

(30) Sharp, K. Entropy--Enthalpy Compensation: Fact or Artifact? *Protein Science* **2001**, *10* (3), 661–667. https://doi.org/10.1110/ps.37801.

(31) Pastore, A.; Temussi, P. A. Crowding Revisited: Open Questions and Future Perspectives. *Trends Biochem Sci* **2022**, *47* (12), 1048–1058. https://doi.org/10.1016/J.TIBS.2022.05.007.

(32) Christiansen, A.; Wang, Q.; Cheung, M. S.; Wittung-Stafshede, P. Effects of Macromolecular Crowding Agents on Protein Folding in Vitro and in Silico. *Biophys Rev* **2013**, *5* (2), 137–145. https://doi.org/10.1007/S12551-013-0108-0.

(33) Laurent, T. C. Enzyme Reactions in Polymer Media. *Eur J Biochem* **1971**, *21* (4), 498–506. https://doi.org/10.1111/j.1432-1033.1971.tb01495.x.

(34) Acosta, L. C.; Perez Goncalves, G. M.; Pielak, G. J.; Gorensek-Benitez, A. H. Large Cosolutes, Small Cosolutes, and Dihydrofolate Reductase Activity. *Protein Science* **2017**, *26* (12), 2417–2425. https://doi.org/10.1002/pro.3316.

(35) Minton, A. P.; Wilf, J. Effect of Macromolecular Crowding upon the Structure and Function of an Enzyme: Glyceraldehyde-3-Phosphate Dehydrogenase. *Biochemistry* **1981**, *20* (17), 4821–4826. https://doi.org/10.1021/bi00520a003.

(36) Minton, A. P.; Wilf, J. Effect of Macromolecular Crowding upon the Structure and Function of an Enzyme: Glyceraldehyde-3-Phosphate Dehydrogenase. *Biochemistry* **1981**, *20* (17), 4821–4826. https://doi.org/10.1021/bi00520a003.

(37) Sierks, M. R.; Sico, C.; Zaw, M. Solvent and Viscosity Effects on the Rate-Limiting Product Release Step of Glucoamylase during Maltose Hydrolysis. *Biotechnol Prog* **1997**, *13* (5), 601–608. https://doi.org/10.1021/bp9700824.

(38) Asaad, N.; Engberts, J. B. F. N. Cytosol-Mimetic Chemistry: Kinetics of the Trypsin-Catalyzed Hydrolysis of p-Nitrophenyl Acetate upon Addition of Polyethylene Glycol and N-Tert-Butyl Acetoacetamide. *J Am Chem Soc* **2003**, *125* (23), 6874–6875. https://doi.org/10.1021/ja034298f.

(39) Derham, B. K.; Harding, J. J. The Effect of the Presence of Globular Proteins and Elongated Polymers on Enzyme Activity. *Biochim Biophys Acta Proteins Proteom* **2006**, *1764* (6), 1000–1006. https://doi.org/10.1016/j.bbapap.2006.01.005.

(40) Jiang, M.; Guo, Z. Effects of Macromolecular Crowding on the Intrinsic Catalytic Efficiency and Structure of Enterobactin-Specific Isochorismate Synthase. *J Am Chem Soc* **2007**, *129* (4), 730–731. https://doi.org/10.1021/ja065064+.

(41) Das, N.; Tarif, E.; Dutta, A.; Sen, P. Associated Water Dynamics Might Be a Key Factor Affecting Protein Stability in the Crowded Milieu. *J. Phys. Chem. B* **2023**, *127* (14), 3151–3163. https://doi.org/10.1021/acs.jpcb.2c09043.

(42) Olgenblum, G. I.; Carmon, N.; Harries, D. Not Always Sticky: Specificity of Protein Stabilization by Sugars Is Conferred by Protein-Water Hydrogen Bonds. *J. Am. Chem. Soc.* **2023**, *145* (42), 23308–23320. https://doi.org/10.1021/jacs.3c08702.

(43) Stewart, C. J.; Olgenblum, G. I.; Propst, A.; Harries, D.; Pielak, G. J. Resolving the Enthalpy of Protein Stabilization by Macromolecular Crowding. *Protein Science* **2023**, *32* (3), e4573. https://doi.org/10.1002/pro.4573.

(44) Sukenik, S.; Sapir, L.; Harries, D. Balance of Enthalpy and Entropy in Depletion Forces. *Curr Opin Colloid Interface Sci* **2013**, *18* (6), 495–501. https://doi.org/10.1016/J.COCIS.2013.10.002.

Chapter 2

Experimental

- **Steady-state Absorption, Emission**
- **Circular Dichroism Spectroscopy**
- **TCSPC**
- **Fluorescence Up conversion**
- **Time-Resolved Emission Spectra**
- **Transient Absorption Spectroscopy**
- **Fluorescence Correlation Spectroscopy**
- **Protein Tagging**
- **DES synthesis**
- **Materials**
- **Sample Preparations**

This page left blank intentionally

2.1 Steady-State Absorption and Emission Spectra:

All the steady-state absorption spectra were recorded using a Shimadzu UV-2450 UV-visible spectrophotometer (Japan). For measuring emission spectra, a Fluoromax-4 spectrofluorometer (Horiba Jobin Yvon) was used. All the emission spectra were corrected for the wavelength-sensitive efficiency of the detector and the monochromator as S_1C/R_1. Here, S_1 is the uncorrected emission intensity, C is the correction factor of the monochromator and detector, and R_1 is the lamp profile. The sample concentration was carefully adjusted to ensure that the absorbance did not exceed the value of 0.2, minimizing inner filter effects and self-quenching. Also, proper control (blank) spectra are taken and subtracted when required. In the case of temperature-dependent absorption/emission experiments, an external Peltier-based temperature controller (TCC-100, Shimadzu, Japan) with an accuracy of 0.5 ºC was connected to the spectrophotometer/ spectrofluorimeter.

2.1.1. Estimation of Red edge excitation shift (REES)

REES is measured by scanning emission spectra along with the absorption profile. The shift in the emission maxima with the change in the excitation wavelength is quantified as the REES (Scheme 2.1) [1,2]. However, one major concern for REES is how much longer wavelength (red edge) one should excite so that total REES can be measured. Azumi *et al.* suggested that the absolute value of REES can be obtained by taking the emission spectra at very high temperatures where all the emissions are expected to originate from a completely solvated state [3,4]. I have taken this approach in the case of REES measurement in DES in the absence of protein (Chapter 3).

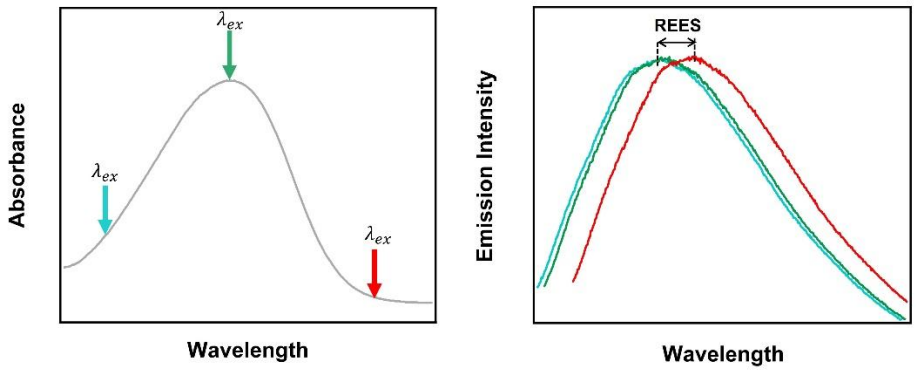

Scheme 2.1. Quantification of REES. Measuring emission spectra by exciting at different wavelengths across the absorption spectrum and the shift in the emission maxima.

However, this approach is not very useful for systems like proteins and micelles, as they can transform into different structural arrangements at very high temperatures [5]. Given this challenge, I ensured consistency throughout the experiments with such systems. In all experiments with protein, the emission was recorded up to ~10% of the absorption spectrum intensity, as data quality significantly deteriorates beyond this point. And this 10% threshold was set as the limit. Although changing the limiting range would affect the value of REES, the overall trend with respect to any perturbations remains consistent.

2.1.2. Mechanistic Basis of REES

The molecular origin of Red-Edge Excitation Shift (REES) lies in the heterogeneous distribution of excitation and emission energies of the fluorophore coupled with the dynamic nature of solvent-fluorophore interactions [1,2,6]. In such a scenario, excitation at different wavelengths across the absorption spectrum selectively promotes distinct subpopulations of fluorophores to different excited states. Under red-edge excitation, fluorophores in highly solvated environments are preferentially excited [6]. In contrast, when excitation occurs at the peak or blue edge of the absorption spectrum, emission from the most populated state dominates, and the

emission spectrum represents an average over all excited states [6]. This phenomenon results in an excitation wavelength-dependent shift in emission maxima, known as REES [1,6]. The occurrence of REES depends on the timescale of solvent relaxation relative to the fluorescence lifetime [4,6]. When the stabilization of the excited state by the surrounding solvent occurs faster than its fluorescence lifetime ($\tau_S < \tau_f$), emission predominantly takes place from the fully solvated state, regardless of the excitation wavelength, and no REES is observed (Scheme 2.2). However, if solvent relaxation is slower than the excited-state lifetime ($\tau_S > \tau_f$), emission occurs before complete solvent stabilization, and REES can be observed (Scheme 2.2) [6].

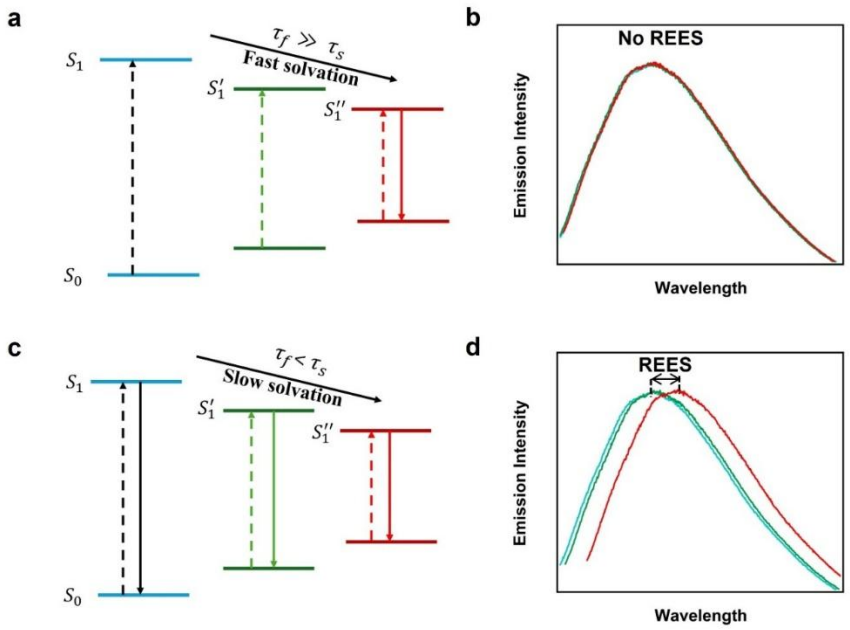

Scheme 2.2. Schematic representation of red edge excitation shift (REES). In a heterogeneous distribution of the environment around the fluorophore, photoexcitation at different wavelengths excites molecules to different excited states (S_1, S_1', S_1''). (a) When the solvation dynamics (τ_s) is faster than the emission lifetime (τ_f), irrespective of the excitation wavelength, emission originates from the completely solvent-relaxed state, and emission maxima are independent of the excitation wavelength. Consequently, (b) no REES can be observed. (c) When the solvation dynamics is slower than the emission lifetime, it does not permit the solvent dipolar realignment before the emission, and in this case, the emission originates from a partially solvent-relaxed state for the high-energy excitation and a fully solvent-relaxed state for low-energy excitation. As a result, (d) red-shifted emission spectra and REES can be observed.

Since REES only manifests under conditions of restricted solvent mobility, it serves as a sensitive probe for hydration dynamics around a fluorophore [7–9]. Additionally, changes in the magnitude of REES in the presence of an additive suggest modulation of solvation dynamics within the system. Specifically, increased REES indicates slower solvation dynamics, revealing critical insights into solvent-mediated interactions [9].

2.2. Circular Dichroism Spectroscopy

Circular dichroism (CD) spectra were recorded using a commercial J-815 CD spectrometer (Jasco, Japan) with a 0.2 cm pathlength cuvette. A corresponding blank (containing all components except the protein) was measured and subtracted from the sample spectra. Each spectrum represents the average of three accumulations.

The principle of CD lies in the fact that chiral molecules absorb left- and right-circularly polarized light to different extents, producing a distinct CD signal [10]. This technique is particularly useful for measuring the secondary and tertiary structure of proteins and nucleic acids, as different secondary structures (α-helices, β-sheets, and random coils) exhibit characteristic CD spectra [11]. For instance, an α-helix exhibits characteristic negative bands at 208 nm and 222 nm [12,13]. In contrast, a β-sheet is identified by a negative band at 218 nm and a positive band at 195 nm [13,14]. Several well-established methods are available for extracting secondary structural parameters from CD data. In my thesis, I have used freely available software, CDNN, to analyze the CD spectra for quantifying the presence of different secondary structural motifs in a protein [15]. Additionally, the thermal evolution of the CD signal at 222 nm has been taken as an indicator of the modulation of α-helicity, and consequently, all the thermodynamic analyses have been done.

2.3. Time-resolved fluorescence Measurement using Time-Correlated Single Photon Counting (TCSPC)

Time-resolved fluorescence measurements are performed to determine the average duration a molecule remains in its excited state, commonly referred to as its fluorescence lifetime. Several techniques can be employed for fluorescence lifetime measurements, including time-correlated single-photon counting (TCSPC), fluorescence up-conversion, and streak camera methods. For my research, I utilized a TCSPC instrument with a temporal resolution of ~160 picoseconds.

2.3.1. Brief Theory of TCSPC

One of the most widely used techniques for time-resolved fluorescence measurements is TCSPC, with several dedicated books available on the subject [16–18]. This method records the arrival time (t) of the first photon detected after each pulsed excitation. The likelihood of capturing this photon at a specific time, t, corresponds to the fluorescence intensity at that instant.

Since fluorescence is a random process, photons are released from different relaxation stages from the Franck-Condon state, leading to a time-dependent distribution of emitted photons, known as fluorescence decay. By accumulating numerous single-photon events post-excitation, the fluorescence decay profile is reconstructed. This decay pattern is then analyzed to determine the average duration a fluorophore remains in its excited state.

2.3.2. Schematic Representation of the TCSPC Setup

A schematic representation of the Time-Correlated Single-Photon Counting (TCSPC) setup is illustrated in Scheme 2.3. This technique measures the arrival time of emitted photons following sample excitation with a pulsed light source. Upon

excitation, a signal is generated and processed through electronic components, beginning with the constant fraction discriminator (CFD), which precisely determines the pulse's arrival time. The CFD then triggers the time-to-amplitude converter (TAC), initiating a linear voltage ramp within a capacitor. Simultaneously, the detector captures fluorescence photons, and the corresponding signal is sent to the CFD, which instructs the TAC to halt the voltage increase. A monochromator (MC) directs the emitted photons to a multichannel plate photomultiplier tube (MCP PMT) for single-photon detection. Accurately measuring photon arrival times in TCSPC is complex due to amplitude jitter in the detector signal and instability in the excitation source, leading to a time jitter that impacts the instrument response function (IRF). To address this, the CFD splits the incoming signal into two components—one is delayed, while the other is inverted. These are then recombined, ensuring that the zero-crossing point remains unaffected by amplitude variations of the pulse [19].

In TCSPC measurements, conditions are optimized to ensure that, on average, only one photon is detected per 100 excitation pulses. The voltage output from the TAC, which is proportional to the time difference between excitation and emission events, is amplified and digitized via an analog-to-digital converter (ADC). This digital value is recorded as a single detection event. The photons are then sorted into different time bins by a multichannel analyzer (MCA) based on their arrival times. The instrument used in this thesis supports up to 4096 channels, offering a time resolution of 4.88 picoseconds per channel for a TAC range of 20 nanoseconds.

To achieve high-precision fluorescence lifetime measurements, a histogram is generated by compiling photon count data against time. This histogram represents the fluorescence intensity decay curve. For accurate lifetime determination, the emission polarizer is positioned at the magic angle (54.9°) relative to the excitation polarizer. In my thesis, all measurements were performed using a commercial TCSPC system (LifeSpec II, Edinburgh Instruments, U.K.).

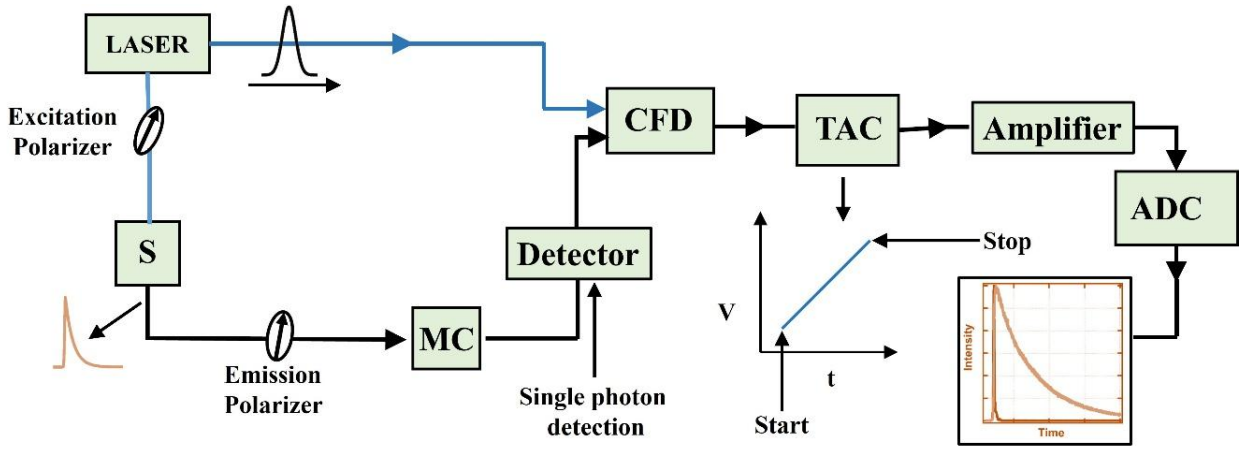

Scheme 2.3. A schematic representation of the TCSPC instrument. Abbreviations: CFD: Constant Fraction Discriminator, S: Sample holder, TAC: Time to Amplitude Converter, MC: Monochromator, ADC: Analogue to digital converter.

2.3.3. TCSPC data analysis

The fluorescence intensity decay profile obtained from TCSPC measurements can be analyzed using appropriate models to extract the fluorescence lifetime of a sample. However, before fitting the data, it is crucial to correct for the influence of the excitation laser pulse and any errors arising from the finite response time of the electronic components. Ideally, fluorescence decay analysis assumes that the laser pulse acts as an instantaneous delta function, but in reality, it has a finite width.

To account for this, the instrument response function (IRF) is recorded using a scattering medium, such as colloidal silica (Ludox solution) or milk, which acts as a zero-lifetime reference. This IRF is then deconvoluted from the fluorescence decay profile of the sample to correct for distortions. The deconvolution process assumes that the finite-width excitation pulse can be represented as a sum of multiple delta pulses of varying amplitudes. Consequently, the overall fluorescence intensity at a given time (t) is modeled as the cumulative response of the sample to all these delta pulses, mathematically expressed as [16,18]:

$$N(t) = \int_0^t L(t')I(t-t')\,dt' \qquad (2.1)$$

where, $I(t-t')$ represents the fluorescence intensity of the sample at time t, resulting from an excitation pulse of amplitude $L(t')$ at time t'. This equation, known as the convolution integral, forms the basis for determining the best-fitting decay function for the measured data. Single-exponential decay models are straightforward to fit, whereas multi-exponential decay functions add complexity. Higher-order exponential fitting should only be attempted when simpler models fail to provide an accurate representation.

Deconvolution follows an iterative least-squares regenerative convolution approach [16,17,19]. After acquiring both the IRF and the fluorescence decay profile, a projected decay function is combined with the IRF to generate a new reconvoluted function. This function is then compared with the recorded decay to calculate the χ^2 value which quantifies the goodness of fit:

$$\chi^2 = \sum_{k=0}^{n} \frac{1}{\sigma_k^2} [F(t_k) - F_P(t_k)]^2 \qquad (2.2)$$

where, $F(t_k)$ and $F_P(t_k)$ represent the experimental and projected fluorescence intensities at two different times, n is the number of data points and σ_k is the standard deviation of each data point. Since TCSPC follows Poisson statistics, the standard deviation is given by

$$\sigma_k = [N(t_k)]^{\frac{1}{2}} \qquad (2.3)$$

Where, N is taken as the number of channels used for measurement.

The reconvolution process and χ^2 calculations continue iteratively until successive iterations yield negligible improvement. Once the fitting process converges, a reduced chi-square value (χ_r) is computed as:

$$\chi_r^2 = \frac{\chi^2}{n-f} = \frac{\chi^2}{\nu} \qquad (2.4)$$

where ν is the degree of freedom, which is the difference between the number of data points (n) and the floating parameters (f). The software, FAST (provided by the

instrument manufacturer), has been used in this thesis to analyze and extract the time components of the fluorescence transients measured by TCSPC.

2.4. Time-resolved fluorescence Measurement using Fluorescence up-conversion Spectroscopy:

Femtosecond fluorescence up-conversion, also known as fluorescence optical gating, is a powerful technique that allows for the investigation of ultrafast photophysical and photochemical processes. This method provides a unique opportunity to study the dynamics of excited-state molecules with sub-picosecond time resolution, offering insights into fundamental processes such as energy transfer, charge separation, and relaxation mechanisms. In one of my works (Chapter 5), Fluorescence up-conversion with a femtosecond resolution (IRF~300 fs) has been used.

2.4.1. Basic principle of Fluorescence up-conversion

The basic principle of femtosecond fluorescence up-conversion relies on the nonlinear optical process of sum-frequency generation [20–22]. The second harmonic of a femtosecond oscillator (a mode-locked Ti:Sapphire laser) operating at frequency (ω_1) is used to excite the sample [20–23]. This time at which the pulse excites the sample marked as time zero which generates an emitted light (ω_2) from the sample itself.

A second pulse (a portion of the fundamental pulse), referred to as the gate pulse, is temporally delayed (arriving at the time, $t = \tau$) and then combined with the fluorescence emission from the sample. The two pulses interact in a nonlinear beta barium borate (BBO) crystal, resulting in the up-conversion of the fluorescence (sum frequency, ω_3, generation) to a higher-energy photon that can be detected.

$$\omega_1 + \omega_2 = \omega_3 \qquad (2.5)$$

A mechanical delay stage controls the time of arrival of the gate pulse to the non-linear crystal. As fluorescence intensity is a function of its lifetime, the intensity of the emitted light and, consequently, the intensity of the sum frequency light will also be proportional to that. Mathematically, the intensity of the sum frequency light (I_{sum}) is proportional to both the intensity of the fluorescence (I_{fl}) and of the gate pulse (I_{gate}) as[22],

$$I_{sum} \propto \int_{-\infty}^{+\infty} I_{fl}(t) I_{gate}(t-\tau) dt \qquad (2.6)$$

The sum frequency light is only generated when both the fluorescence and the gate pulse are present in the crystal.

2.4.2. Schematic Representation and a Brief Explanation of the Fluorescence Up-conversion Setup

The femtosecond fluorescence up-conversion setup typically includes a femtosecond laser, a mechanical delay stage to control the temporal delay between the excitation and gate pulses, a nonlinear crystal, and a detection system, such as a monochromator and a photomultiplier tube or a CCD camera (see scheme 2.4).

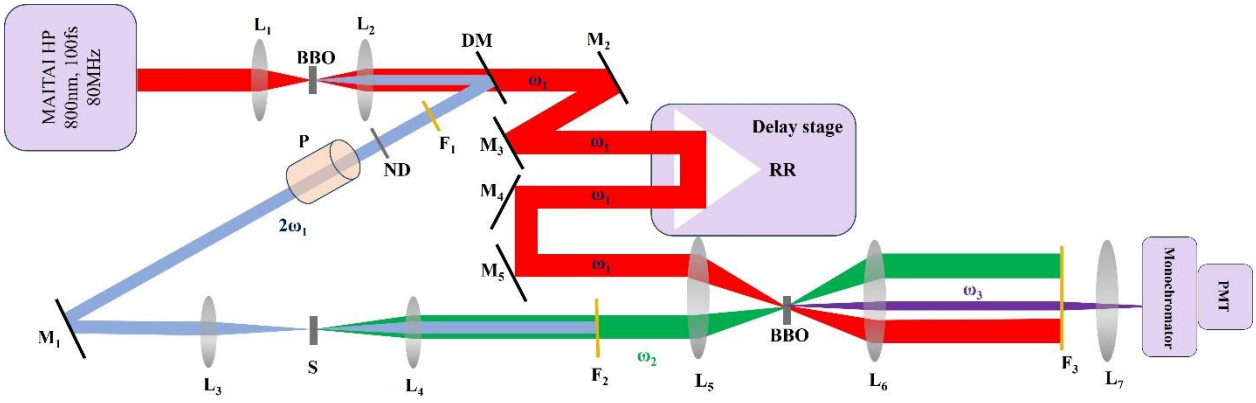

Scheme 2.4. A schematic representation of the fluorescence up-conversion instrument. Abbreviations: L_1, L_2, L_3, L_4, L_5, L_6, L_7: Lens, BBO: β-barium borate crystal, DM: Dichroic mirror/ Dichroic beamsplitter, M_1, M_2, M_3, M_4, M_5: Mirror, RR: roto reflector used to control delay, F_1, F_2, F_3: Filter to cut light of certain wavelength, ND: neutral density filter, P: Berek polarizer to adjust excitation light's polarization, S: Sample, PMT: Photomultiplier tube, ω_1: fundamental (excitation) light, ω_2: emitted light from the sample, ω_3: Sum frequency light.

The experiment begins with a mode-locked Ti:Sapphire laser (Mai-Tai HP, Spectra Physics, USA), which emits ultrafast pulses wavelength (ω_1). This laser operates at an 80 MHz repetition rate, with a 100 fs pulse duration, providing high temporal resolution for capturing fluorescence events. The fundamental light (ω_1) is directed to a 0.2 mm thick β-barium borate (BBO) crystal through the lens (L_1), which doubles the frequency to generate the second harmonic ($2\omega_1$). This second harmonic ($2\omega_1$) light is used as the excitation source to excite the sample. The second harmonic ($2\omega_1$) passes through a lens (L_2) and a dichroic mirror (DM), which splits the light into two beams, namely the excitation beam and a gate beam. The excitation beam is further refined by passing through a cut-off filter (F_1) to remove the remaining excitation light, a neutral density (ND) filter for controlling the intensity, and a Berek polarizer (P) to adjust the polarization of the excitation pulse. This excitation light is then guided and focused through mirror (M_1) and lens (L_3) to the rotating sample cell. When the sample absorbs the excitation pulse ($2\omega_1$), it moves to an excited state and then emits fluorescence at a longer wavelength (ω_2) which is

collected by lens L_4 and passes through a cut-off filter (F_2) to remove any excitation light ($2\omega_1$).

The gate pulse (ω_1) is directed separately using mirrors (M_2 and M_3) to a retro-reflector (RR) on a mechanical delay stage controlled using software, which allows precise control over when the gate pulse meets the fluorescence. Both the fluorescence (ω_2) and the delayed gate pulse (ω_1) are focused together on a second BBO crystal using lens L_5. In this nonlinear BBO crystal, the two beams mix to generate a new signal with a sum frequency ($\omega_1 + \omega_2 = \omega_3$). To ensure only the sum-frequency light reaches the detector, I used a lens (L_6), an appropriate cut-off filter (F_3), and an iris (not shown in the scheme) to eliminate any remaining excitation and gate beam components. The sum-frequency light (ω_3) is then focused into a monochromator using lens L_7. The monochromator selects the desired wavelength and directs it to a photomultiplier tube (PMT) coupled with a photon-counting device for detection. The entire system, including data acquisition, monochromator control, and optical delay adjustment, is managed by LUMEX software (CDP Corp).

2.4.3. Data analysis of fluorescence up-conversion

To accurately determine fluorescence lifetimes, it is necessary to characterize the IRF of the experimental setup. The IRF represents the system's temporal response and accounts for pulse-broadening effects introduced by optical components.

The IRF was measured using the Raman scattering signal of water, which appears at a frequency shift of ~3300 cm^{-1} from the excitation wavelength [23–25]. Replacing the sample cell with a water cell, the system recorded the IRF at a chosen wavelength. Raman scattering is an instantaneous process with zero intrinsic time delay, making it an ideal reference. By measuring the sum-frequency signal generated from the Raman signal of water and the gate pulse, the temporal profile of the excitation and detection pulses was obtained. The IRF was best described by a Gaussian function

with a full-width at half-maximum (FWHM) of approximately 300 fs. Mathematically, the IRF is represented as,

$$G(x) = \frac{1}{\sigma\sqrt{2\pi}} e^{-(x-\mu)^2/2\sigma^2} \quad (2.7)$$

Where, σ represents the width parameter of the Gaussian function, μ is the x-axis position (mean) of the function. The FWHM of this Gaussian function can be calculated as, $H = 2\sigma\sqrt{2\ ln2} \sim 2.3548\ \sigma$.

The excitation pulse is assumed to occur at zero time, so for data analysis, the function is simplified by setting $\mu = 0$.

In femtosecond fluorescence up-conversion spectroscopy, the recorded fluorescence intensity decay is not a direct representation of the actual molecular relaxation. Instead, the measured decay curve is modified due to the finite-width IRF. Thus, analyzing fluorescence lifetime, especially for those in the sub-picosecond range, it is crucial to apply deconvolution techniques to extract the correct decay parameters. To extract the fluorescence lifetimes, the experimental decay data were fitted using a convolution function of the IRF with a sum of exponential decay functions. Relaxation of multiple exponentials can be extended easily from this.

The convolution function is,

$$I(t) = G(x) * S(x) \quad (2.8)$$

Where, $S(x) = \exp\left(-\frac{x}{\tau}\right)$, τ is the lifetime.

$$I(t) = \frac{1}{\sigma\sqrt{2\pi}} \int_0^\infty exp\left(-\frac{x}{t}\right) exp\left(-(t-x)^2/2\sigma^2\right) dx \quad (2.9)$$

$$\therefore I(t) = \frac{1}{\sigma\sqrt{2\pi}} \int_0^\infty exp\left(-\frac{\left(x^2+t^2+\frac{2\sigma^2 x}{\tau}-2tx\right)}{2\sigma^2}\right) dx \quad (2.10)$$

Let's assume,

$$z = \frac{\left(x - \left(t - \frac{\sigma^2}{\tau}\right)\right)}{\sigma\sqrt{2}} \tag{2.11}$$

$$\therefore \frac{\left(x^2 + t^2 + \frac{2\sigma^2 x}{\tau} - 2tx\right)}{2\sigma^2} = z^2 + \frac{1}{\tau}\left[t - \frac{\sigma^2}{2\tau}\right] \tag{2.12}$$

Using equations 2.11 and 2.12 in equation 2.10, we get,

$$I(t) = \frac{1}{\sqrt{\pi}} exp\left(\frac{\sigma^2}{2\tau^2} - \frac{t}{\tau}\right) \int_{-\left(\frac{t - \frac{\sigma^2}{\tau}}{\sigma\sqrt{2}}\right)}^{\infty} exp(-z^2)dz \tag{2.13}$$

The error function can be introduced as,

$$erf(x) = \frac{2}{\sqrt{\pi}} \int_0^x exp(-z^2)dz \tag{2.14}$$

Also, as error function is an odd function, $erf(-x) = -erf(x)$ can be written.

By introducing this error function in equation 2.13, we get,

$$I(t) = \frac{1}{\sqrt{\pi}} exp\left(\frac{\sigma^2}{2\tau^2} - \frac{t}{\tau}\right)\left(1 - erf\left(\frac{\sigma^2 - t\tau}{\sqrt{2}.\sigma t}\right)\right) \tag{2.15}$$

The above equation is used in my works to fit a fluorescence transient recorded using (femtosecond) fluorescence up-conversion. Although the equation involves only a mono exponential decay, practically in my case multiexponential function has been used. As convolution is a linear operation, the distributive and additive property of convolution has been used in the case of multiexponential data fitting. Equation 2.15 was expanded in terms of summation of different exponential lifetime components convoluted with the same gaussian function with definite weightage coefficients. All the fittings of the transients have been done using IGOR Pro (WaveMetrics, Inc.) software.

2.5. Basics of Time-Resolved Emission Spectra (TRES)

Time-resolved emission Spectra (TRES) can be indirectly reconstructed using wavelength-dependent fluorescence decay measurements [16,19]. This method is based on the fundamental principle that, upon excitation, the probe molecule experiences a substantial change in its dipole moment [19]. As a result, the surrounding solvent molecules reorganize to stabilize this new dipole moment. This reorientation process is experimentally observed through a time-dependent red shift of the emission maximum, known as the Stokes shift, which continues until the solvent reaches equilibrium (refer to Scheme 2.5) [19,26].

To generate TRES, fluorescence decay measurements are recorded at multiple wavelengths across the steady-state emission spectrum. These decay profiles are analyzed using the previously discussed methods. The intensity of TRES at a given time t and wavelength λ is expressed as the product of two independent functions:

$$I(\lambda, t) = A(\lambda)B(t) \tag{2.16}$$

The steady-state fluorescence spectrum (I_{SS}) is obtained by integrating $I(\lambda, t)$ over time and can be written as,

$$I_{SS} = \int_0^\infty I(\lambda, t)dt \tag{2.17}$$

Substituting Equation 2.16 into Equation 2.17:

$$I_{SS} = \int_0^\infty A(\lambda)B(t)dt \tag{2.18}$$

Since A(λ) is independent of time, it can be taken out of the integral:

$$I_{SS} = A(\lambda) \int_0^\infty B(t)dt \tag{2.19}$$

Here, B(t) represents the fluorescence decay, which is typically modeled as a sum of exponentials. Therefore,

$$B(t) = \sum_i \alpha_i \exp\left(-\frac{t}{\tau_i}\right) \quad (2.20)$$

Where the pre-exponential factors satisfy the condition, $\sum_i a_i(\lambda) = 1$

we obtain,

$$I_{SS} = A(\lambda) \sum_i \alpha_i \tau_i \quad (2.21)$$

$$A(\lambda) = \frac{I_{SS}}{\sum_i \alpha_i \tau_i} \quad (2.22)$$

Therefore,

$$I(\lambda, t) = \frac{I_{SS}}{\sum_i \alpha_i \tau_i} \sum_i \alpha_i \exp\left(-\frac{t}{\tau_i}\right) \quad (2.23)$$

This equation describes the intensity distribution across different wavelengths at a given time. A widely used approach to track the temporal evolution of TRES is by monitoring the time-dependent shift in the emission peak, commonly referred to as the Stokes shift. This shift, ν(t), can be modeled using the lognormal function:

$$g(\nu) = g_0 exp\left[-\ln(2)\left(\frac{\ln\left[1+\frac{2b(\nu-\nu_p)}{\Delta}\right]}{b}\right)^2\right] \quad (2.24)$$

for $\alpha > 1$, $g(\nu) = 0$ (2.25)

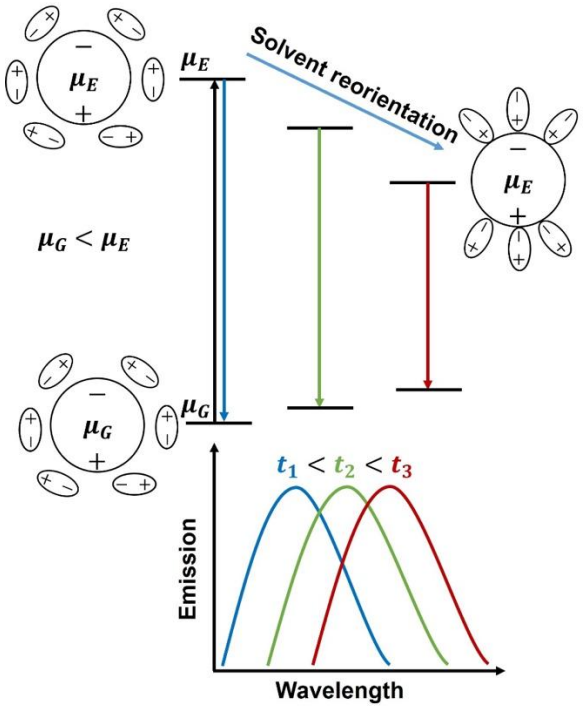

Scheme 2.5. The scheme illustrates the concept of solvation dynamics (upper panel) alongside the progression of time-resolved fluorescence Stokes shift (lower panel). Following optical excitation to the Franck–Condon (FC) state, and vibrational relaxation, the surrounding solvent begins to reorganize to accommodate the altered electronic distribution of the excited molecule because of the dipole moment difference between the ground (μ_G) and excited (μ_E) state. This relaxation with a more favorable solvent arrangement towards the excited state dipole leads to a decrease in the overall energy of the system. As a result, the emitted fluorescence undergoes a red shift over time, each corresponding to emission at different stages of solvent reorganization. The lower panel of the graph shows how the emission maximum shifts toward longer wavelengths (from t_1 to t_3), reflecting the time-dependent nature of the Stokes shift as solvation proceeds toward equilibrium.

for $\alpha < 1$, where $\alpha = \frac{2b(\nu - \nu_p)}{\Delta}$ (2.26)

To facilitate comparison, the peak frequency shift $\nu(t)$ is often converted into a solvent response (normalized) function $C(t)$ as,

$$C(t) = \frac{\nu(t) - \nu(\infty)}{\nu(0) - \nu(\infty)} \quad (2.16)$$

The function $C(t)$ is typically modeled using either a single exponential or a sum of exponentials to determine the average solvation time ($\langle\tau_s\rangle$).

2.6. Transient Absorption Spectroscopy (TA)

In my thesis, transient absorption spectroscopy is minimally used. The solvation dynamics of the buffer and different concentrations of hydrated DES (in the absence of protein) were only investigated using transient absorption (TA) spectroscopy. Since the relaxation times in both pure buffer and hydrated DES fall within the 1–30 ps range, they cannot be accurately captured by TCSPC. While fluorescence up-conversion could, in principle, resolve such ultrafast processes, our TA setup offers a superior temporal resolution of approximately 70–80 fs that is significantly faster than the 300 fs instrument response of our up-conversion system. Additionally, the data curation in TA is much faster, and solvation dynamics can be extracted more directly through the stimulated emission profiles, which directly yield time-resolved emission spectra (TRES) without the complex analysis involved in fluorescence up-conversion [27].

2.6.1. Fundamental Concept of TA

Transient absorption (TA) spectroscopy, a classic pump-probe technique, enables the observation of excited-state dynamics with ultrafast time resolution. In this method, an ultrashort laser pulse (typically in the order of tens of femtoseconds) initiates a non-equilibrium population in the system. A second pulse, referred to as the probe, monitors the subsequent evolution of this transient state at a controlled time delay [28–30]. By choosing a sufficiently short excitation pulse (e.g., 50 fs), it becomes possible to resolve most of the primary events occurring on ultrafast timescales in the excited state [28–30].

The setup I used has a pump pulse operating at 400 nm, which selectively excites a fraction of the molecular population to the electronically excited state. The probe is a broadband white-light continuum spanning the visible region (450–750 nm), which intersects the same region of the sample at variable time delays. These delays are introduced via a computer-controlled mechanical delay stage. The probe intensity is intentionally kept low to minimize the possibility of inducing nonlinear effects or multiphoton absorption (see Scheme 2.6).

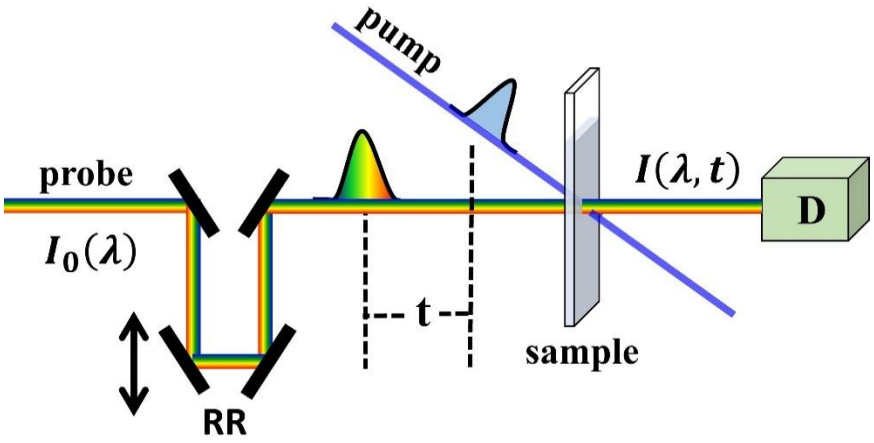

Scheme 2.6. Simplified illustration of the transient absorption spectroscopy setup.

Detection is performed spectrally across the entire range of the probe beam at each chosen delay time, and the process is repeated for successive delays to construct a time-resolved picture. As TA is fundamentally an absorption-based method, the principles of the Lambert-Beer law are applicable to describe how the probe intensity changes upon interaction with the sample.

$$I(\lambda, t) = I_0(\lambda) \times 10^{-\varepsilon(\lambda)N(t)l} \qquad (2.17)$$

Where, $I_0(\lambda)$ is the initial probe intensity at a given wavelength and $I(\lambda, t)$ is the transmitted intensity at a time delay t. Note that the time zero corresponds to the point where the pump and probe pulses arrive at the sample simultaneously. $\varepsilon(\lambda)$ is the molar extinction coefficient at the wavelength λ, $N(t)$ denotes the time-dependent population of the absorbing state, and l is the optical path length of the sample.

From Equation 2.17, the absorbance $A(\lambda, t)$ at any wavelength and time can be expressed as,

$$A(\lambda, t) = log \frac{I_0(\lambda)}{I(\lambda,t)} = \varepsilon(\lambda) N(t) l \tag{2.18}$$

However, in TA measurements, what is typically observed is the difference in absorbance between the excited and unexcited states of the sample. This differential absorbance is denoted as:

$$\Delta A(\lambda, t) = A(\lambda, t) - A(\lambda) \tag{2.19}$$

$$\Delta A(\lambda, t) = log \frac{I_0(\lambda)}{I(\lambda,t)} - log \frac{I_0(\lambda)}{I(\lambda)} = log \frac{I(\lambda)}{I(\lambda,t)} \tag{2.20}$$

Equation 2.20 indicates that the measurable parameter is the change in probe intensity with and without the excitation by the pump. Hence, it simplifies to,

$$\Delta A(\lambda, t) = log \frac{I^{probe}}{I^{probe}_{pump}} \tag{2.21}$$

In equation 2.21, the quantity I^{probe} represents the intensity measured when the pump is blocked (usually using a mechanical chopper). I^{probe}_{pump} is the intensity when both pump and probe interact with the sample.

As the excited-state population $N(t)$ changes with time due to relaxation processes, the differential absorbance $\Delta A(\lambda, t)$ evolves accordingly, thereby encoding the dynamics of the system following photoexcitation.

Being an absorption-based method, transient absorption spectroscopy can simultaneously track both radiative and non-radiative relaxation processes, depending on the spectral features being probed [29,30]. This makes it an extremely versatile tool for studying a wide range of ultrafast photo-physical and photochemical events.

2.6.2. Insights from TA

Transient absorption (TA) spectroscopy provides access to several distinct photo-physical processes, four of which are commonly detected and are illustrated in Scheme 2.7. and described below.

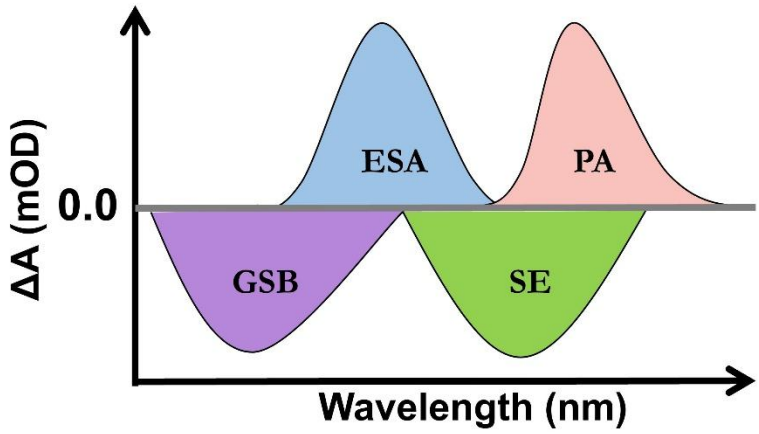

Scheme 2.7. Representative contributions of various transient signals observed in TA spectra.

Ground state bleaching (GSB): - When a sample is excited by the pump pulse, a portion of the molecules is elevated from the ground electronic state to an excited state. As a result, the ground-state population is partially depleted, leading to reduced absorption of the probe light at wavelengths corresponding to ground-state transitions. Since less probe light is absorbed compared to the unpumped state (i.e., $I^{probe} < I^{probe}_{pump}$) the absorbance change ΔA becomes negative. This decrease in signal, known as ground-state bleaching, reduces over time as the molecules relax back to the ground state, typically through radiative or non-radiative pathways.

Stimulated Emission (SE): - Molecules in the excited state can return to the ground state by emitting photons. While spontaneous emission occurs randomly, if the probe pulse contains photons with energies matching the emission transition, it can induce stimulated emission. These stimulated photons travel in phase and direction with the probe beam, increasing the overall probe intensity at those wavelengths. Thus, similar to GSB, $I^{probe} < I^{probe}_{pump}$ and a negative ΔA signal appears. The spectral shape of the SE contribution often mirrors the molecule's fluorescence spectrum and appears red-shifted relative to the GSB band. SE intensity also decays over time in sync with the depletion of the excited-state population. Importantly, the probe intensity is kept low enough to avoid significantly perturbing the excited-state population.

***Excited-state absorption (ESA)**:* - After excitation by the pump, some molecules reside in an excited state, from which they may absorb additional photons from the probe pulse to reach higher electronic states. This process leads to excited-state absorption. As the probe photons are absorbed only when the pump creates an excited state, the transmitted probe intensity decreases in the presence of pump

excitation, and $I^{probe} > I^{probe}_{pump}$ in this case. This will result in a positive ΔA signal. The appearance and evolution of ESA bands provide insights into higher-lying excited-state structures and their dynamics. Finding this information is one of the strengths of transient absorption which was typically inaccessible through fluorescence methods.

Product absorption (PA)*:* - Upon photoexcitation, molecules can undergo various secondary processes, including photochemical transformations, electron or proton transfer, or structural rearrangements, resulting in the formation of new transient species. These reaction products may possess their own absorption characteristics and can interact with the probe light. Since these new species are not present prior to excitation, their absorption leads to a positive change in the probe spectrum ($I^{probe} > I^{probe}_{pump}$), contributing to a positive PA signal.

The ability to simultaneously observe all these processes with a single instrument is what makes TA spectroscopy very powerful in the field of physics and chemistry. However, it is important to recognize certain factors, such as limited spectral coverage of the probe pulse and the temporal resolution defined by the instrument response function, and analyzing a complex spectrum containing much information altogether can restrict the ability to resolve all these processes simultaneously.

2.6.3. Instrumentation of TA setup

All transient absorption experiments in this work were carried out using a commercially available femtosecond broadband transient absorption system (Femto-Frame-II, IB Photonics, Bulgaria). The complete optical configuration is depicted in Scheme 2.8. The system is powered by a Ti:Sapphire regenerative amplifier (Spitfire

Pro XP, Spectra-Physics, USA), which delivers pulses at 800 nm with a duration of approximately 80 fs and a repetition rate of 1 kHz. This amplifier is pumped by a 20 W Q-switched Nd:YLF laser (Empower, Spectra-Physics) and seeded by a femtosecond oscillator (MaiTai SP, Spectra-Physics). The pulse width was confirmed using a commercial autocorrelator.

The output beam at 800 nm is divided into two parts using a beamsplitter (BS1). One portion is directed to generate the pump pulse, while the other is used to produce the probe. Pump generation is carried out within a JANOS tripler module provided by the same manufacturer. The incoming 800 nm light first passes through a BBO crystal to generate the second harmonic at 400 nm. This 400 nm light, along with the residual 800 nm, passes through a half-wave plate and enters a second BBO crystal where third harmonic generation (266 nm) occurs. The three harmonics (800, 400, 266 nm) are then separated using dichroic mirrors, and depending on the requirement, either 400 nm or 266 nm is selected for sample excitation using mirrors M6 and M7. The other arm of the fundamental 800 nm light, after reflection off mirror M5, is routed through a series of mirrors (MB1–MB3) into a retroreflector (RR) mounted on a mechanical translation stage. This stage allows for delay generation of up to 2 nanoseconds between the pump and probe pulses. A small fraction of this beam is deflected by BS2 to fall onto a photodiode (PD), which regulates the mechanical chopper controlling pump modulation. The remaining portion of the 800 nm beam is attenuated via a neutral density filter (ND1), shaped with an iris, and then focused by lens L4 onto a 0.3 mm sapphire crystal to produce a white light continuum (WLC), covering ~450–750 nm. The characteristics of the WLC strongly depend on the incident beam profile and energy, which are tuned using the ND filter and iris. This continuum is collected using a parabolic mirror (MB5), passed through two notch filters (N1, N2) to remove residual 800 nm light, and redirected via mirrors MB6 and MB7. It is then focused onto the sample using another parabolic mirror (MB10). Meanwhile, the pump pulse, after passing through a chopper for modulation, has its polarization adjusted with a half-wave plate to

minimize anisotropic interference. The intensity is regulated by a rotating neutral density filter (ND2), and the beam is focused onto the same location as the probe using lens L3 and mirror MB12. The typical excitation spot diameter at the sample position ranges from 100–200 μm. The chopper periodically blocks the pump to enable acquisition of both pump-on and pump-off conditions, essential for calculating differential absorbance. The probe light, after transmission through the sample, is focused onto a 200 μm fiber optic cable using mirror MB11. A final neutral density filter (ND3) ensures the intensity reaching the detector is within operational limits. Detection is performed using a CCD-based spectrograph, where the dispersed probe beam is analyzed using a set of diffraction gratings. Due to a slight angular difference between the pump and probe beams at the sample, only the probe reaches the detection system. Time-zero calibration is carried out using a reference material (Coumarin 152 in ethanol) by monitoring the rise of the known signal and tuning the delay stage accordingly. The entire instrument is operated via software developed on the LabVIEW platform. Throughout the experiments, pump power was maintained around 10–15 μW to prevent photodegradation. To verify sample integrity, steady-state absorption spectra were recorded before and after each measurement session.

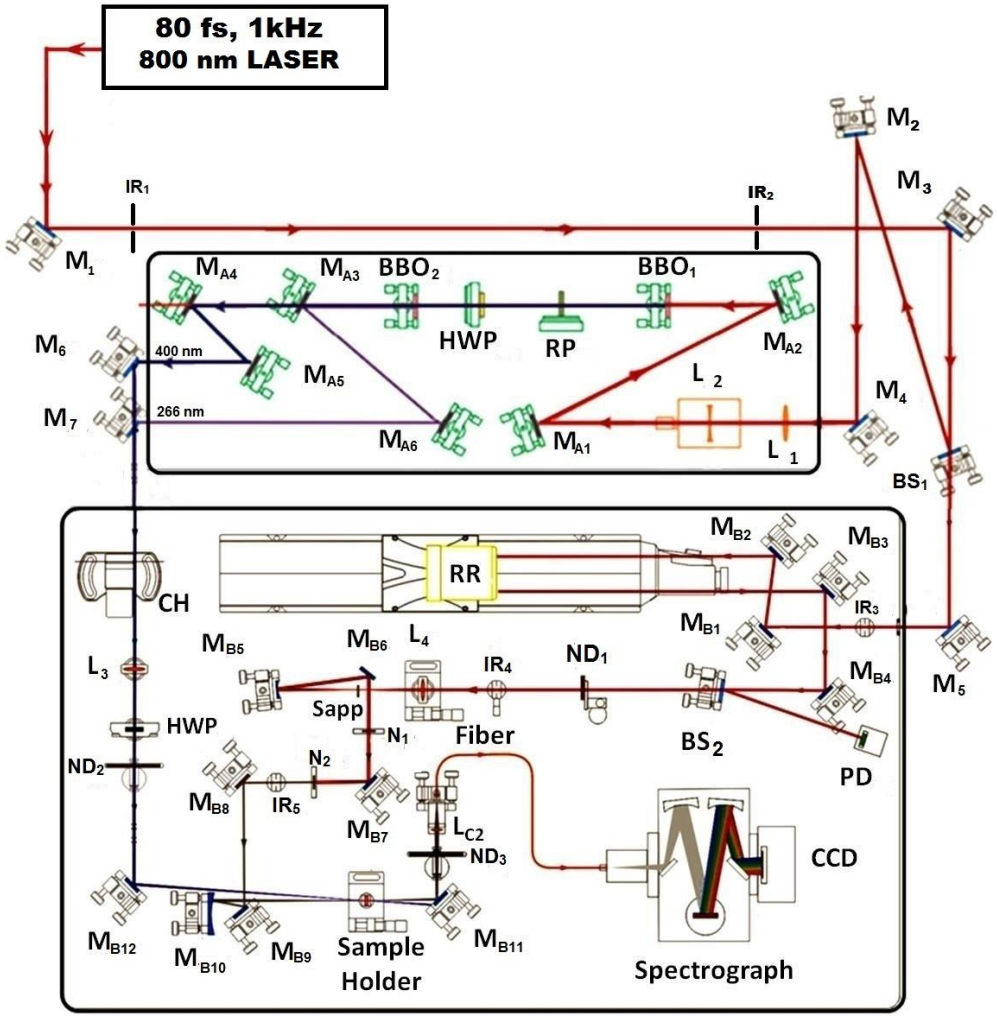

Scheme 2.8. Detailed optical schematic of the femtosecond transient absorption spectrometer

2.6.4. TA data analysis

In this thesis, the application of transient absorption (TA) spectroscopy has been totally limited to probing solvation dynamics [27]. Specifically, the focus has been on the 450–550 nm spectral range, where the differential absorbance spectra for C-343 in both buffer and hydrated DESs predominantly display stimulated emission (SE) features. The use of C-343 to measure the solvation dynamics is purely based on the solubility of the dye in both buffer and hydrated DES.

Unlike fluorescence lifetime measurements using TCSPC and fluorescence up conversion, where the time-resolved emission spectrum needs to be reconstructed

from decay traces, TA offers the advantage of directly yielding time-resolved emission spectra in terms of evolution of SE signal (provided the SE band is well-separated and not significantly influenced by overlapping contributions such as ESA or PA). To extract the precise SE peak positions at each time point, the corresponding ΔA spectra were individually fitted using a log-normal function restricted to the SE-dominated region. By monitoring the temporal evolution of these maxima of the SE signal, the solvent response function was constructed using equation 2.16. Subsequently, solvation times were determined by fitting the solvent response with a multiexponential function.

Because of the complications stated above (overlapping of another signal to SE signal) and limited availability of the instrument, TA is very minimally applied to extract solvation dynamics [27,30–35]. The study by Poizat *et al.* (2002), is one of the earliest demonstrations of solvation dynamics measurement using TA [36]. Since then, only a limited number of publications have adopted this technique for such studies. However, recent work by Xia *et al.* has shown that the solvation times obtained from TA [33] are in strong agreement with those derived by Maroncelli and coworkers using conventional time-resolved emission spectroscopy (TRES) [37]. These findings support the idea that with careful experimental design and minimal signal interference, TA can provide a valuable complementary route for accessing solvation dynamics.

2.7. Fluorescence Correlation Spectroscopy (FCS)

This thesis incorporates fluorescence measurements at the single-molecule level, offering insights that conventional ensemble average technique, such as steady-state absorption/emission or time-resolved fluorescence spectroscopy, often misses out. While these traditional methods, such as steady-state absorption, CD, and emission or time-resolved fluorescence spectroscopy, are well-suited for uniform, isotropic systems, they miss out important information when the system exhibits

heterogeneity in molecular properties or behavior. In such cases, observing and analyzing individual molecules becomes critical to unravel the underlying complexity.

Certain dynamic or structural features of biomolecules, particularly those related to conformational fluctuations, can only be probed meaningfully through single-molecule approaches [38–42]. In addition to their analytical advantages, these techniques provide a major experimental benefit: they operate effectively at extremely low concentrations, typically in the nanomolar to picomolar range [43,44]. This is particularly advantageous where higher concentrations (in the micromolar range) might lead to aggregation of the protein.

2.7.1. A short theory of FCS

Fluorescence Correlation Spectroscopy (FCS) was first introduced by Elliot L. Elson, Douglas Magde, and Watt. W. Webb in the year 1972 [45–48]. FCS is centered on analyzing time-dependent fluctuations in fluorescence intensity within a confined optical volume [44,46,47]. These fluctuations predominantly originate from molecular diffusion. However, contributions from photophysical transitions, chemical reactions, or conformational changes occurring on comparable or faster timescales than diffusion are also significant [43,44]. FCS interprets such fluctuations using temporal correlation functions, autocorrelation, and cross-correlation to extract kinetic and dynamic parameters relevant to the fluorescent species under study [44].

2.7.2. Mathematical Foundation: Fluctuations and Correlation

'An Introduction to Fluorescence Correlation Spectroscopy' by Prof. Wohland, Maiti, and Machan has nicely covered this part. This part is essentially taken from that book [44].

2.7.2.1. Fluctuations

FCS aims at extracting information about molecular processes that are occurring in a system. The system can be a simple buffer solution, complex mixtures like proteins or enzymes, live cells or organisms, etc.[45,49–52]. Any molecular process in such a system is constituted by molecular events that lead to changes in some observable parameters. The temporal deviations in the observable parameter from the average value are called fluctuations. In Fluorescence Correlation Spectroscopy (FCS), fluctuations refer to the temporal deviations in fluorescence intensity from its average value, observed within a very small detection volume [44,45].

These fluctuations are caused by a) Brownian diffusion of molecules in and out of the observation volume, b) Photophysical transitions, such as triplet state blinking, c) Chemical reactions or conformational changes affecting fluorophore brightness.

If $F(t)$ is the fluorescence intensity at time t, then the fluctuation ($\delta F(t)$) is defined as:

$$\delta F(t) = F(t) - \langle F(t) \rangle \tag{2.22}$$

Average of the fluctuation,

$$\langle \delta F(t) \rangle = \langle F(t) - \langle F(t) \rangle \rangle = 0 \tag{2.23}$$

Even in systems that appear to be in equilibrium, molecular motion and reactions continue to occur, producing subtle variations around the average state. These fluctuations are not just background noise; they encode valuable information about the kinetics, mobility, and interactions of molecules and are the foundation upon which the analytical power of FCS is built [44].

2.7.2.2. Idea of Correlation and Correlation Function

To explore how these fluctuations are analyzed to uncover molecular-level processes, it is essential to introduce the concept of correlation.

In general terms, the correlation between two variables implies that the value of one is, to some degree, influenced by or linked to the value of the other. The strength of this dependency reflects the degree of correlation [44]. In cases of perfect correlation, the value of one variable can be predicted precisely from the other. A classic example is the relationship between mass and volume for a solid under standard conditions—if the mass of the solid is increased or reduced, its volume changes proportionally, reflecting a direct and predictable dependency [44].

To define correlation mathematically, let's consider two variables, a and b, each of which depends on some general coordinate or parameter u.

According to the mathematical definition, two variables are said to be correlated if the average of their product is not equal to the product of their individual averages.[44] In other words:

$$\langle a(u).b(u)\rangle \neq \langle a(u)\rangle.\langle b(u)\rangle \tag{2.24}$$

The correlation coefficient is defined as,

$$g = \frac{\langle a(u).b(u)\rangle}{\langle a(u)\rangle.\langle b(u)\rangle} \tag{2.25}$$

Whenever, $g > 1$: the data is correlated, $g < 1$: the data is anti-correlated, and $g = 1$: the data is not correlated [44].

Correlation fundamentally refers to the degree of similarity or association between quantities. In the context of this thesis, the focus is on the autocorrelation function, which specifically describes the correlation of a signal with a time-shifted version of itself. More precisely, autocorrelation evaluates how the value of a variable at one

point in time relates to its value at a later time, separated by a defined time interval [44].

In Fluorescence Correlation Spectroscopy (FCS), the variable under study is the fluorescence intensity, which changes over time as molecules move in and out of the detection volume [44]. This intensity corresponds to the number of emitted photons detected from a minute confocal volume. When a fluorescent molecule is within this volume, its emission is captured efficiently by the detector; once it diffuses out, the signal contribution from that molecule vanishes. These fluctuations in detected photon count form the basis for calculating the autocorrelation function, allowing insight into molecular motion and dynamics at single-molecule sensitivity [44,50].

If $F(t)$ is the fluorescence intensity at time t, and if we want to write the autocorrelation function after a time $t + \tau$,

$$G(\tau) = \frac{\langle F(t).F(t+\tau)\rangle}{\langle F(t)\rangle.\langle F(t+\tau)\rangle} \quad (2.26)$$

We can simplify this equation as we measure only in an equilibrium condition (stationary process) i.e. process in which the time of measurement does not alter the observation or the average value of the observable, and thus, $\langle F(t)\rangle = \langle F(t+\tau)\rangle$

$$G(\tau) = \frac{\langle F(t).F(t+\tau)\rangle}{\langle F(t)\rangle^2} \quad (2.27)$$

This can be easily shown that autocorrelation function is an even function,

$G(\tau) = G(-\tau)$.

Up to this point, it's important to note that the correlation function is defined in terms of the fluorescence intensity rather than the fluctuations themselves. This is logical, as the signal, i.e., the time-dependent fluorescence intensity, is the actual observable collected during the experiment and is directly available for correlation analysis. However, since fluctuations are defined as deviations from the average signal,

computing them requires prior calculation of the mean fluorescence intensity. Only then can the autocorrelation of these fluctuations be determined.

As the definition of fluctuation is deviation from the mean, fluctuation ($\delta F(t)$) can be written as[44],

$$\delta F(t) = F(t) - \langle F(t) \rangle \tag{2.28}$$

The average of the fluctuation is (from equation 2.28),

$$\langle \delta F(t) \rangle = \langle F(t) - \langle F(t) \rangle \rangle = \langle F(t) \rangle - \langle \langle F(t) \rangle \rangle = \langle F(t) \rangle - \langle F(t) \rangle = 0$$

From equation 2.28, we can express the signal $F(t)$ in terms of fluctuation,

$$F(t) = \delta F(t) + \langle F(t) \rangle \tag{2.29}$$

If we substitute this equation 2.29 into the autocorrelation function of the signal (equation 2.27),

$$G(\tau) = \frac{\langle (\delta F(t) + \langle F(t) \rangle)(\delta F(t+\tau) + \langle F(t+\tau) \rangle) \rangle}{\langle F(t) \rangle^2} \tag{2.30}$$

$$= \frac{\langle \delta F(t).\delta F(t+\tau) + \delta F(t).\langle F(t+\tau) \rangle + \langle F(t) \rangle.\delta F(t+\tau) + \langle F(t) \rangle.\langle F(t+\tau) \rangle \rangle}{\langle F(t) \rangle^2} \tag{2.31}$$

We have already shown the average over fluctuation $\langle \delta F(t) \rangle = 0$. Also, for the stationary processes, $\langle F(t) \rangle = \langle F(t+\tau) \rangle$.

That means,

$$\langle \delta F(t).\langle F(t+\tau) \rangle \rangle = \langle \delta F(t) \rangle.\langle F(t+\tau) \rangle = 0 \tag{2.32}$$

$$\langle \langle F(t) \rangle.\delta F(t+\tau) \rangle = \langle F(t) \rangle.\langle \delta F(t+\tau) \rangle = 0 \tag{2.33}$$

Thus the equation 2.31 becomes,

$$G(\tau) = \frac{\langle \delta F(t).\delta F(t+\tau) + \langle F(t) \rangle.\langle F(t+\tau) \rangle \rangle}{\langle F(t) \rangle^2}$$

$$\therefore G(\tau) = \frac{\langle \delta F(t).\delta F(t+\tau) + \langle F(t)\rangle^2 \rangle}{\langle F(t)\rangle^2}$$

$$\therefore G(\tau) = \frac{\langle \delta F(t).\delta F(t+\tau)\rangle + \langle F(t)\rangle^2}{\langle F(t)\rangle^2}$$

$$\therefore G(\tau) = \frac{\langle \delta F(t).\delta F(t+\tau)\rangle}{\langle F(t)\rangle^2} + 1$$

That means we have proved that,

$$G(\tau) = \frac{\langle F(t).F(t+\tau)\rangle}{\langle F(t)\rangle^2} = \frac{\langle \delta F(t).\delta F(t+\tau)\rangle}{\langle F(t)\rangle^2} + 1 \qquad (2.34)$$

This analysis leads to the conclusion that the autocorrelation function (ACF) calculated from the raw signal and the one derived from the fluctuations share the same functional form. The only distinction between them is a constant offset of 1.

Therefore, aside from this offset, both functions, whether by correlating the signal or its fluctuations, contain identical information about the system's dynamics. By convention, the correlation function derived directly from the signal is denoted as $G(\tau)$, while the autocorrelation of the fluctuations is represented as $g(\tau)$.

$$\therefore G(\tau) = \frac{\langle F(t).F(t+\tau)\rangle}{\langle F(t)\rangle^2} = g(\tau) + 1 \qquad (2.35)$$

And, $g(\tau) = \frac{\langle \delta F(t)\delta F(t+\tau)\rangle}{\langle F(t)\rangle^2}$ (2.36)

At $\tau = 0$, $g(0) = \frac{\langle \delta F(t)^2\rangle}{\langle F(t)\rangle^2}$

And at any $\tau \neq 0$, $g(\tau) = \frac{\langle \delta F(t)\delta F(t+\tau)\rangle}{\langle F(t)\rangle^2}$

$\langle \delta F(t)\rangle^2$ is always positive as it is a square term, however $\langle \delta F(t)\delta F(t+\tau)\rangle$ can be both larger and smaller than zero, which is expected for fluctuations.

Thus,

$\langle \delta F(t)^2 \rangle \geq \langle \delta F(t) \delta F(t+\tau) \rangle$ as the term "$\langle \delta F(t) \delta F(t+\tau) \rangle$" will have negative contributions. Therefore, the correlation function (either signal or fluctuation) will have the highest value at $\tau = 0$. And at a very long time ($\tau \to \infty$) $g(\tau)$ will become 0. This means a plot of $g(\tau)$ versus τ will give us a decay curve of self-similarity with time.

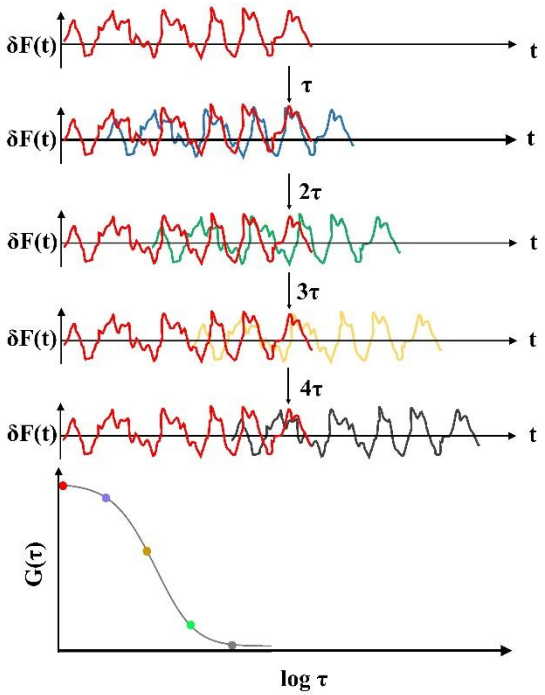

Scheme 2.9. Scheme 2.9. Conceptual illustration of how the autocorrelation function is constructed. Autocorrelation quantifies the self-similarity of a fluctuating fluorescence signal over time. In this schematic, the same fluorescence fluctuation trace is compared with its time-shifted versions at increasing lag times ($\tau, 2\tau, 3\tau, 4\tau$). As the lag time increases, the overlap between the original and shifted traces decreases, leading to a reduction in correlation. Eventually, at large lag times, no meaningful similarity remains, and the autocorrelation value approaches zero. The plot at the bottom shows the decay of the autocorrelation function $g(\tau)$ as a function of lag time on a logarithmic scale.

Previously in FCS, to detect the fluorescence signal or the fluctuations of the fluorescence intensity, one detector was used. Thus, the autocorrelation function

needs to be generated to extract information about the processes that caused fluctuations in the intensity, which is, in general, free diffusion of the fluorophore through the detection volume [44]. However, with the modernization of the instrument, two detectors with a 50:50 beam splitter are used. Basically, the fluorescence is split equally into two channels using the beam splitter and detected separately but simultaneously using two detectors. In this way, the signal-to-noise ratio was improved a lot by eliminating detector-specific noise, which is uncorrelated across the two channels [44].

This allows the measurement of a cross-correlation function between the two independently recorded fluorescence signals, $F_1(t)$ and $F_2(t)$ as[44],

$$G_{12} = \frac{\langle F_1(t).F_2(t+\tau)\rangle}{\langle F_1(t)\rangle.\langle F_2(t+\tau)\rangle} \quad (2.37)$$

Scheme 2.9 visually demonstrates how the autocorrelation function decreases with increasing lag time. A similar curve is expected for cross-correlation as well. To interpret this decay meaningfully, particularly in terms of molecular diffusion or any other dynamic process that drives fluorescence fluctuations, it is essential to have a well-defined understanding of both the optical detection volume and the system under study. The mathematical model used for curve fitting must be carefully chosen to reflect the underlying source of the fluctuations. Only then can the resulting fit yield accurate and physically relevant parameters that describe the system's behavior.

2.7.3. Fitting Function of the Fluorescence Autocorrelation Function

In Fluorescence Correlation Spectroscopy (FCS), the analysis is based on recording a time-dependent fluorescence intensity trace, F(t), that originates from a confined observation volume. Several spatial and optical parameters influence the

fluorescence signal detected at any given time. Let 'r' represent the position in space and 't' time. The key factors determining the signal include[44]:

(a) The excitation intensity distribution ($I(r,t)$), which describes how the excitation light is spatially distributed. For most practical cases in FCS, this intensity is considered time-independent, reducing to $I(r)$.
(b) The collection efficiency function (CEF) of the optical system, which reflects how effectively emitted photons are captured at different locations in space. In confocal FCS, this function is largely governed by the microscope's point spread function (PSF) and the geometry of the pinhole, which restricts out-of-focus light.
(c) The factor k which encompasses the molecular brightness of the fluorophore. This includes its absorption cross-section, quantum yield, and overall detection efficiency—accounting for photon losses through the optical path and the efficiency of the detector.
(d) $S(r)$, defines the spatial extent of the fluorescent sample being investigated.
(e) The spatiotemporal distribution of fluorophores, represented by $C(r,t)$which varies as molecules diffuse through or react within the detection volume.

The intensity fluctuations, which are basically due to concentration fluctuation in the observation volume, can be defined as[44]

$$\delta F(t) = \int I(r).CEF(r).S(r).\delta C(r,t)dr \tag{2.38}$$

As we already know, from equation 2.36,

$$g(\tau) = \frac{k^2 \int\int I(r).I(r')CEF(r).CEF(r')S(r)S(r')\langle \delta C(r,t)\delta C(r',t+\tau)\rangle dr dr'}{k^2\langle \int I(r).CEF(r).S(r).C(r,t)dr\rangle^2} \tag{2.39}$$

Assuming the sample is much larger than the observation volume, $S(r) = 1$. Also, in the denominator only the concentration term is affected by time, and a time integral over that concentration term will result in average concentration, $\langle C\rangle$. Thus, we can write,

$$\therefore g(\tau) = \frac{\int\int I(r).I(r')CEF(r).CEF(r')S(r)S(r')\langle\delta C(r,t)\delta C(r',t+\tau)\rangle drdr'}{\langle c\rangle^2\langle\int I(r).CEF(r).S(r).dr\rangle^2} \quad (2.40)$$

In confocal fluorescence correlation spectroscopy (FCS), the combined effect of the excitation focus and the spatial filtering imposed by the pinhole can be approximated using a three-dimensional Gaussian profile. This simplification is widely adopted because it closely resembles the actual shape of the detection volume, especially when a tightly focused laser beam is used in conjunction with a confocal pinhole.

If P denote the laser power, the spatial profile of the detection volume, denoted as $W(r)$, is given by the product of the excitation intensity distribution ($I(r)$) and the collection efficiency function ($CEF(r)$) [44]. Under the 3D Gaussian approximation, this function can be written as[44]:

$$W(r) = I(r).CEF(r) = \frac{2P}{\pi w_0} e^{\frac{-2x^2}{{w_0}^2}.\frac{-2y^2}{{w_0}^2}.\frac{-2z^2}{{z_0}^2}} \quad (2.41)$$

For pure diffusion, the fluctuations in concentration can be written (the details can be found in the book[44] mentioned above) as,

$$\langle\delta C(r,t)\delta C(r',t+\tau)\rangle = \langle C\rangle.\frac{e^{\frac{-(x-x')^2+(y-y')^2+(z-z')^2}{4D\tau}}}{8(\pi D\tau)^{3/2}} \quad (2.42)$$

Replacing these equations (2.41, 2.42) into the autocorrelation function,

$$g(\tau) = \frac{\int\int\int\int\int\int e^{\frac{-2\left(x^2+x'^2\right)}{{w^2}_0}} e^{\frac{-2\left(y^2+y'^2\right)}{{w^2}_0}} e^{\frac{-2\left(z^2+z'^2\right)}{{z^2}_0}}.\frac{e^{\frac{-(x-x')^2+(y-y')^2+(z-z')^2}{4D\tau}}}{8(\pi D\tau)^{3/2}} dxdx'dydy'dzdz'}{\langle C\rangle\left(\int\int\int e^{\frac{-2x^2}{{w^2}_0}} e^{\frac{-2y^2}{{w^2}_0}} e^{\frac{-2z^2}{{z^2}_0}} dxdydz\right)^2} \quad (2.43)$$

Integrating and simplifying, we get,

$$g(\tau) = \frac{1}{\langle C \rangle \pi^{3/2} {w_0}^2 z_0} \left(1 + \frac{4D\tau}{{w_0}^2}\right)^{-1/2} \left(1 + \frac{4D\tau}{{w_0}^2}\right)^{-1/2} \left(1 + \frac{4D\tau}{{z_0}^2}\right)^{-1/2} \quad (2.44)$$

Diffusion in each direction has one term in this equation 2.44. As the system is rotationally symmetric, the two terms coming from x and y direction are essentially the same, and thus the function becomes,

$$g(\tau) = \frac{1}{N} \left(1 + \frac{\tau}{\tau_D}\right)^{-1} \left(1 + \frac{\tau}{K^2 \tau_D}\right)^{-1/2} \quad (2.45)$$

In this equation,

$N = \langle C \rangle \pi^{3/2} w_0^2 z_0 = \langle C \rangle . V_{eff}$,

$\tau_D = diffusion\ time = \frac{w_0^2}{4D}$; $K = structure\ factor = \frac{z_0}{w_0}$

Most importantly, the effective detection volume of the FCS (V_{eff}) is represented as,

$$V_{eff} = \pi^{3/2} w_0^2 z_0 \quad (2.46)$$

At $\tau = 0$, the equation 2.45 becomes, $g(0)$, which is the inverse of the average particle number in the observation volume and is expressed as,

$$g(0) = \frac{1}{N} = \frac{1}{V_{eff} \langle C \rangle} \quad (2.47)$$

So, equation 2.45 can be rewritten as,

$$g(\tau) = g(0) \cdot \left(1 + \left(\frac{\tau}{\tau_D}\right)\right)^{-1} \cdot \left(1 + \left(\frac{1}{K}\right)^2 \cdot \frac{\tau}{\tau_D}\right)^{-\frac{1}{2}} \quad (2.48)$$

In the case where $\tau = \tau_D$, the function (equation 2.48) will become,

$$g(\tau_D) = g(0) \cdot \left(1 + \left(\frac{\tau_D}{\tau_D}\right)\right)^{-1} \cdot \left(1 + \left(\frac{1}{K}\right)^2 \cdot \frac{\tau_D}{\tau_D}\right)^{-\frac{1}{2}}$$

$$\therefore g(\tau_D) = g(0).\frac{1}{2\sqrt{1+K^{-2}}}$$

Replacing a typical value of K in a confocal FCS setup, $K \sim 5$, in $g(\tau_D)$,

$$g(\tau_D) \approx \frac{g(0)}{2.04} \approx \frac{1}{2.04\ N}$$

So, τ_D is the time at which the amplitude of the correlation becomes half of its initial value. This simple way can be qualitatively used to estimate the comparative nature of diffusion, i.e., faster or slower than the other.

Up to this point, the derivation of the autocorrelation function assumes that the fluorophore's fluorescence intensity only fluctuates due to translational diffusion within the observation volume. However, in actual experimental conditions, this is rarely the case. Photophysical or chemical processes, triplet state transitions, or conformational changes can also contribute significantly to the overall fluctuation pattern [43,44,50].

To account for such non-diffusive contributions, an additional multiplicative factor is incorporated into the autocorrelation function. The total ACF is now expressed as,

$$g_{total}(\tau) = g_{total}(\tau) \cdot X_{kinetics}(\tau) \quad (2.49)$$

In cases where the fluorophore undergoes reversible transitions such as entering a non-fluorescent triplet state, the kinetic contribution can be modeled using a simple exponential decay function

$$X_R(\tau) = 1 - A + A \cdot e^{-\frac{\tau}{\tau_R}} \tag{2.50}$$

Where A is the fractional contribution of the photophysical process to the overall fluorescence fluctuation, τ_R is the characteristic time constant of the process (e.g., triplet lifetime). For convenience, this function can be normalized by the non-fluctuating component $(1 - A)$, leading to the simplified form

$$X_R(\tau) = 1 + a \cdot e^{-\frac{\tau}{\tau_R}} \tag{2.51}$$

Where, $a = {}^{A}/_{1 - A}$.

When both diffusion and a reversible photophysical process contribute to fluorescence fluctuations, the final form of the autocorrelation function can be written as,

$$g(\tau) = \frac{1}{V_{eff}\langle C\rangle} \cdot \frac{1}{\left(1+\left(\frac{\tau}{\tau_D}\right)\right)} \cdot \frac{1}{\sqrt{1+\left(\frac{1}{K}\right)^2 \cdot \frac{\tau}{\tau_D}}} \cdot \left(1 + a \cdot e^{-\frac{\tau}{\tau_R}}\right)$$

$$\therefore g(\tau) = g(0) \cdot \left(1 + \left(\frac{\tau}{\tau_D}\right)\right)^{-1} \cdot \left(1 + \left(\frac{1}{K}\right)^2 \cdot \frac{\tau}{\tau_D}\right)^{-\frac{1}{2}} \cdot \left(1 + a \cdot e^{-\frac{\tau}{\tau_R}}\right) \tag{2.52}$$

In some cases, anomalous diffusion (e.g., hindered or subdiffusive motion in crowded environments) must be considered [53–55]. This is accounted for by introducing an anomaly exponent α, modifying the autocorrelation function as[54,56],

$$g(\tau) = g(0) \cdot \left(1 + \left(\frac{\tau}{\tau_D}\right)^{\alpha}\right)^{-1} \cdot \left(1 + \left(\frac{1}{K}\right)^2 \cdot \left(\frac{\tau}{\tau_D}\right)^{\alpha}\right)^{-\frac{1}{2}} \quad (2.53)$$

'α' is a measure of the extent of deviation from normal diffusion. The diffusion is referred to as subdiffusion for 0 < α < 1, normal diffusion for α = 1, and super diffusion for α > 1 [54,56].

For more than one particle diffusing normally (i.e. $\alpha = 1$), the ACF can be written as[44]

$$G(\tau) = \frac{1}{(\sum_i N_i)^2} \sum_i N_i D_i(\tau)\,;\; D_i(\tau) = \left(1 + \frac{\tau}{\tau_{D_i}}\right)^{-1} \left(1 + \frac{1}{K^2}\frac{\tau}{\tau_{D_i}}\right)^{-\frac{1}{2}} \quad (2.54)$$

2.7.4. Structural Information Extraction Employing FCS

Once the diffusion time (τ_D) is obtained by fitting the autocorrelation curves using appropriate models (discussed above), and diffusion coefficient (D_t) of the particle is determined, one can extract structural information, the hydrodynamic radius (r_H), of the particle by applying the Stokes-Einstein equation [57,58]. The Stokes-Einstein equation describes the diffusion of a spherical particle of hydrodynamic radius (r_H) undergoing Brownian motion in a viscous fluid at a constant temperature. The mathematical form of the equation is,

$$r_H = \frac{k_B T}{6\pi\eta D_t} \quad (2.55)$$

where k_B is the Boltzmann constant, T is the absolute temperature and η is the viscosity of the medium, D_t is the translational diffusion coefficient.

To calibrate our system and accurately determine the confocal volume (specifically, K), we performed a series of FCS measurements using Rhodamine 6G (R6G) at varying concentrations in water. The autocorrelation curves were fitted globally, and the value of K was extracted under the assumption that the diffusion coefficient of R6G in water is known, $D_t = 4.14 \times 10^{-6}\ cm^2 s^{-1}$ [59]. Once calibrated, the parameter 'K' kept fixed for all subsequent fittings of a particular set of experimental data using any appropriate fitting models.

2.7.5. Accounting for Medium-induced Refractive Index and Viscosity Alterations

When external perturbations such as temperature shifts, some additives like DES, or macromolecular crowders are introduced, they can significantly alter the viscosity and refractive index of the solution. To isolate the viscosity-induced effects from those due to molecular size or structure, we implemented a control experiment at every condition tested by using Rhodamine 6G (R6G) as a reference fluorophore. R6G is a small, rigid dye whose structure remains unaffected by environmental changes such as the addition of DES or crowding and changes in temperature. Thus, any shift in its measured diffusion time reflects solely the change in solution viscosity.

Using the known hydrodynamic radius of R6G (r_H^{R6G}) in buffer, and its measured diffusion time under the same experimental conditions, we calculated the hydrodynamic radius of the protein or any dye at every experimental point according to the following equation.

$$r_H^{protein} = r_H^{R6G} \times \frac{\tau_D^{protein}}{\tau_D^{R6G}} \quad (2.56)$$

FCS is routinely used by researchers to monitor the conformational change of protein in the presence of various external perturbations like desaturating agents, heat, DES, crowder, confinement, and so forth [40,51,52,60–67].

Regarding refractive index variations, we compensated for these changes by adjusting the objective collar. At each experimental condition, the collar was fine-tuned to maximize the $G(0)$ value, which ensures the smallest effective observation volume and consistent optical alignment across all measurements.

2.7.6. FCS Setup

One of the primary challenges in single-molecule fluorescence detection is eliminating interference from background signals, such as Raman scattering from the solvent [19]. The solution lies in minimizing the observation volume to the femtoliter scale, which drastically reduces background noise and enhances signal specificity. Achieving such a confined detection volume is the central goal of Fluorescence Correlation Spectroscopy (FCS) instrumentation [19]. This can be realized through two major optical approaches: (i) confocal microscopy, and (ii) total internal reflection geometry (TIRF) [44,68].

In this thesis, a home-built confocal FCS setup has been used for performing single molecular level fluorescence experiments (see scheme 2.10).

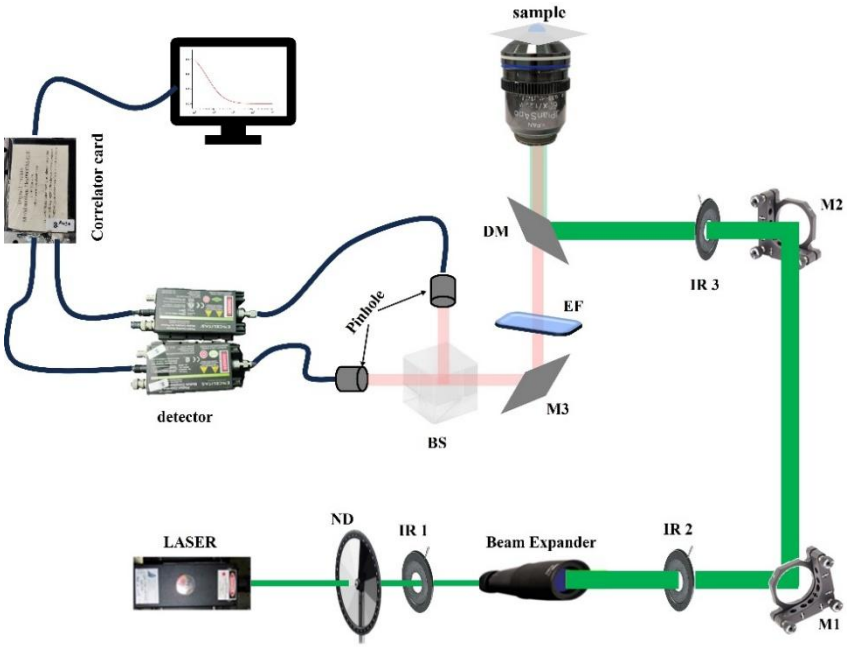

Scheme 2.10. A schematic diagram of a home-built FCS. (Abbreviations: IR, iris; M, mirror; DM, dichroic mirror; ND, neutral density filter; EF, emission filter). The sample cells are specially designed glass cells with a water jacket surrounding them. In the water jacket, there are one inlet and one outlet for water circulation. Labocon LLCB-202 temperature controller unit has been used to circulate water of a specific temperature through the water jacket to control the temperature of the sample cell.

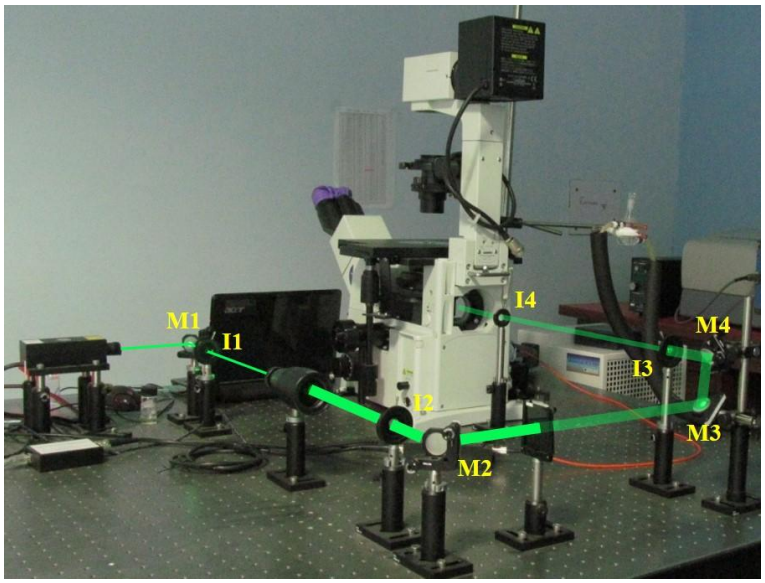

Figure 2.1. Image of home-built FCS setup.

The schematic diagram has been shown as scheme 2.10. and the photograph of the actual setup has been shown in Figure 2.1.

To facilitate understanding, the entire setup is divided into three major functional components such as (a) excitation unit, (b) detection unit, and (c) data analysis unit, and they are discussed in the following paragraphs.

(a) Excitation unit: The excitation unit comprises the laser source, a beam expander (telescope), a sequence of mirrors (M1–M4), and irises (I1–I4). The laser delivers a collimated beam with an initial diameter of 2.5 mm. Since forming a small focal spot requires a broader input beam, the laser beam is expanded nearly 8-fold using the telescope before being directed into the microscope using strategically positioned mirrors. To regulate excitation intensity, a neutral density (ND) filter is placed in the optical path. The beam width is finely adjusted using an iris positioned just before entering the microscope, and maintained nearly at 10 mm, optimized for the objective's aperture. The collimated beam is then directed through a dichroic mirror, which reflects the excitation light toward the objective lens. The objective is actually a collection of lenses which is used to focus the collimated beam onto the sample that is placed on a clean coverslip mounted on the microscope stage.

(b) Detection unit: Following excitation, the sample emits fluorescence, which is collected only from the portion directed back into the objective lens. These photons are collimated by the same objective, transmitted through the dichroic mirror and an emission filter to cut any excitation light mixed with the emitted light, and finally fall onto a cubic (50:50) beamsplitter. This emitted light is then focused into two pinholes placed perpendicular to each other. These pinholes (realized via a fiber tip) plays a critical role by acting as a spatial filter, ensuring that only photons originating from the focal volume are detected. Photons emitted from outside this volume are

effectively blocked, thus maintaining confocality. The pinhole size directly controls the effective observation volume (see Scheme 2.11 and Scheme 2.12 for illustration).

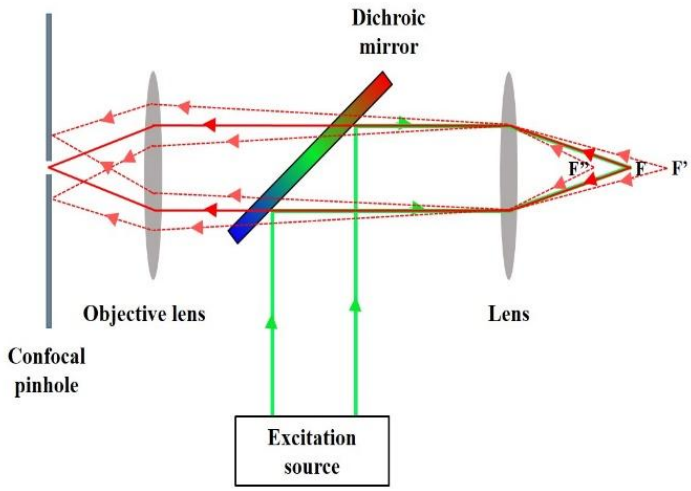

Scheme 2.11. Schematic representation of the confocal detection system.

The optical fiber, held in place by a five-axis positioner, precisely guides the photons to a single-photon avalanche photodiode (APD), which converts them into an electronic signal suitable for time-resolved detection.

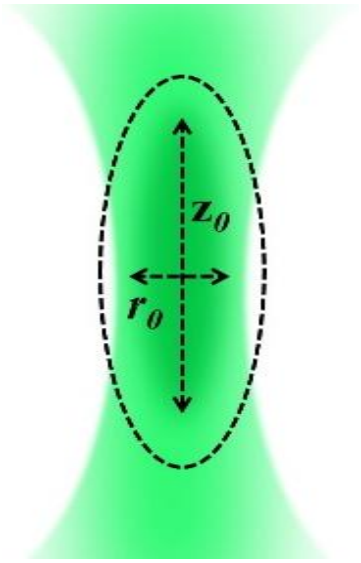

Scheme 2.12. Gaussian-shaped observation volume.

(c) Analysis unit: The detected fluorescence signal through the two pinholes and optical fibre, in the form of photon counts, is transmitted from the avalanche photodiodes (APD) to the autocorrelator card. This card's primary function is to segment the intensity time trace into discrete bins and compute the degree of cross-correlation within the two signals detected by two APDs based on varying time delays (lag times). The autocorrelation curve of fluorescence intensity collected through each APD can also be observable just by switching off the other detector.

To form the correlation curve, it first determines the mean fluorescence intensity of one channel $\langle F_1(t)\rangle$ and the corresponding fluctuation $\delta F_1(t)$. The fluctuation profile of the other channel, $\delta F_2(t)$ is then shifted incrementally in time, with the magnitude of the shift defined by the time resolution capabilities of the correlator hardware.

In our setup, the correlator card supports a minimum lag time resolution of 0.2 microseconds, allowing it to resolve events as fast as 0.2 μs. Its maximum lag time extends up to approximately 3435969984 microseconds, which is equivalent to nearly one hour, enabling the observation of dynamic processes across a broad temporal window. The range of dynamic events that can be studied is inherently bound by these minimum and maximum lag values.

Once the correlation curve is computed, the result is transferred to a graphical user interface based on the LabVIEW platform, where it can be visualized in real time. The data is simultaneously saved in ASCII format, which facilitates further quantitative analysis and model fitting using Igor Pro software.

2.7.6.1. Specification of the Components of the FCS setup

Laser: MGL-III-532-5mW (532 nm), CNI, China

Telescope: BE10M-A, Thorlabs, USA

Mirrors: KM100, Thorlabs, USA

Microscope: Inverted confocal microscope, IX-71, Olympus, Japan

Objective lens: 60X water immersion objective with numerical aperture 1.2, working distance 0.28 mm, Olympus.

Dichroic mirror: ZT532RDC, Chroma, USA.

Bandpass filters: ET605/70m

Neutral density filters: NDC-50C-4M - Mounted Continuously Variable ND Filter, Thorlabs, USA

Cubic Beam Splitter: BS010 - 50:50 Non-Polarizing Beamsplitter Cube, 400 - 700 nm, Thorlabs, USA

Fibre patch chord: M43L01, M42L01, M67L01, Thorlabs, USA

Detector: SPCM-AQRH-13-FC-24420, Excelitas technologies

Correlator card: Flex 990EM-12E,

Opto-mechanics: Post, rods, iris, and holders are from Thorlabs, USA, and Holmarc, India.

2.7.6.2. Calibration of the Instrument

Fitting the experimental auto/cross correlation curves yields the diffusion time of molecules through the detection volume. However, this diffusion time is influenced by several factors such as the observation volume and the medium's viscosity, making it an extensive property [43,44]. Therefore, to extract meaningful size-related information from the diffusion time, calibration of the focal volume is essential. Additionally, the theoretical models used to analyze FCS data assume a Gaussian

excitation beam profile. For this reason, proper calibration of the system is a prerequisite before starting any measurements.

Alignment of the Detector:

The fiber patch cord, which also functions as the confocal pinhole, must be precisely positioned at the focal point of the emitted photons to ensure accurate photon detection from the defined Gaussian volume. This alignment is achieved using a five-axis positioner, which allows adjustment in x, y, and z directions as well as angular tilts in two planes. It is aligned as follows:

(i) Initial Alignment: A concentrated dye solution is placed in the sample chamber, and the fiber is coarsely aligned until the fluorescence becomes visible at the fiber's output.

(ii) Fine Alignment: A dilute dye solution (~1–5 nM) is then used, and the fiber position is adjusted carefully using the screws of five-axis to maximize photon count at the detector, ensuring that it is perfectly aligned with the focused emission path.

Before taking any data for an unknown sample, the photon count from a standard dye like rhodamine 6G (R6G) is checked. If the signal is lower than expected, the alignment and calibration procedure is repeated.

Achieving the minimal Detection Volume

Once proper alignment is ensured, the next objective is to reduce the volume of excitation to the smallest possible extent. This is crucial for improving spatial resolution and signal-to-noise ratio. The diameter of the excitation beam plays a key role in defining the focal volume, and larger beam diameters result in tighter focal volumes (see Scheme 2.13). The calibration involves recording the diffusion time of

a low-concentration dye solution (~1-5 nM) while systematically varying the objective collar setting and adjusting the focal plane height above the coverslip.

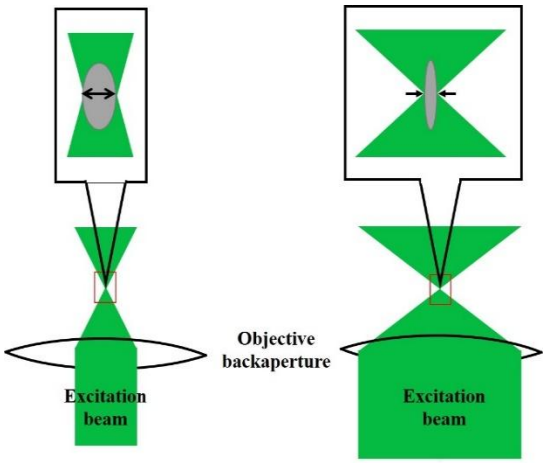

Scheme 2.13. Illustration of focal volume control via excitation beam diameter and objective overfilling.

The collar ring of the objective allows correction for spherical aberrations due to mismatches in refractive indices between the immersion medium, the cover glass, and the sample. It is essential to determine the optimal collar position for each refractive index and excitation wavelength. Figure 2.2 illustrates how the diffusion time of rhodamine 6G in aqueous solution changes with collar position.

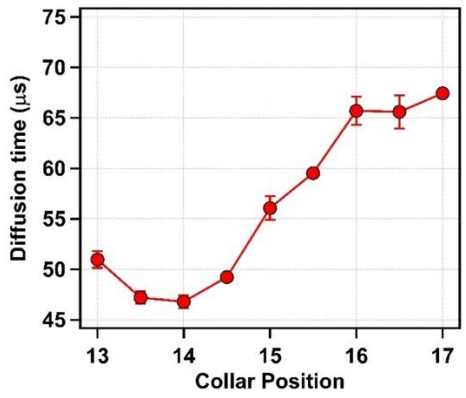

Figure 2.2. Dependence of rhodamine 6G diffusion time on the objective collar setting.

As evident from the figure, the shortest diffusion time is attained at collar position ~13.5-14, indicating optimal alignment and minimal focal volume.

The vertical control (z-axis) of the focal plane is provided in the microscope as a rotating knob. The height of the focal point from the surface of the cover slip can be controlled by the knob provided in the microscope to vary the z-axis of the objective. Both the upper and lower surfaces of the cover slip can be located by finding a sudden jump in the detected photon counts. The upper and lower interfaces of the coverslip can be identified by a sudden increase in detected photon counts. For consistent measurements, the focal plane is typically positioned about 40 μm above the coverslip surface to avoid optical interference, which has been found optimal in the system used in this thesis.

Measurement of the dimension of the observation volume

The observation volume, typically Gaussian-shaped (Scheme 2.12), is determined using a dye (R6G in most cases) with a known diffusion coefficient. Several autocorrelation curves are recorded at different dye concentrations (Figure 2.3). The parameter 'K' is defined as the ratio of the axial to radial dimensions of the observation volume, which characterizes the volume and remains constant across all concentration-dependent measurements. Only the number of particles within the observation volume varies with dye concentration. The resulting autocorrelation curves are globally fitted (from 1 μs) using a one-component diffusion model, incorporating an additional exponential term to account for the known triplet-state photo physics of the rhodamine dye. However, the characteristic timescale for this photophysical process in buffer is approximately 1–2 μs. Thus, fitting the autocorrelation curves from 10 μs onward effectively eliminates any contribution from photo physics and then can be fitted with only a one-component diffusion

model. Importantly, the observation volume parameters obtained in these two ways remain consistent.

The global fitting yields the diffusion time (which is independent of the concentration and hence the same for all the curves) and the instrumental parameter 'K' which is the ratio of the axial and radial diameters of the observation volume, $K = \frac{z_0^2}{w_0^2}$.

The known diffusion coefficient of R6G dye in the buffer is 4.14 x 10^{-6} cm^2 sec^{-1} [59]. The value of the transverse radius (r) is can then be calculated using the equation, $D = \frac{w_0^2}{4\tau_D}$. By employing another equation, $V_{eff} = \pi^{3/2} w_0^2 z_0$, the effective observation volume of our setup was estimated to be ~ 0.7-0.9 fL.

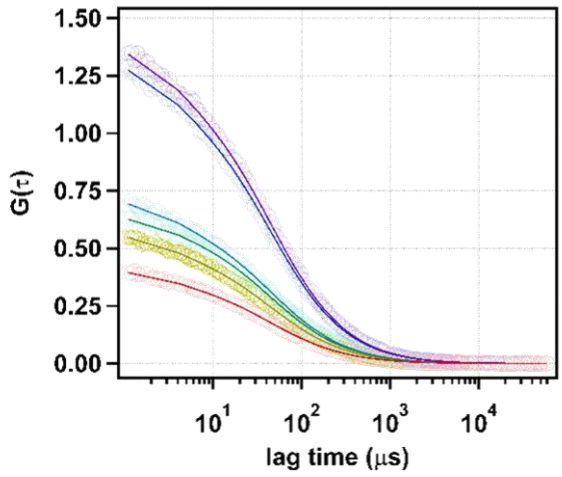

Figure 2.3. Global fitting of autocorrelation curves using equation 2.52 in order to measure the dimensions of the observation volume.

Checking the effect of power

Fluorescence correlation spectroscopy (FCS) is highly sensitive to fluctuations in fluorescence intensity. However, at elevated excitation powers, additional sources of fluctuation, such as photobleaching and transitions to non-emissive triplet states

can distort the signal and complicate data interpretation. To minimize such artifacts, the excitation power must be carefully tuned prior to data acquisition.

To determine the optimal laser intensity, a preliminary power-dependence check is conducted. The sample system is exposed to a range of excitation powers, and the resulting fluorescence autocorrelation curves are recorded and compared. Robust fluorophores like rhodamine 6G exhibit high resistance to power-induced effects, showing minimal distortion in their correlation curves across a wide power range. In contrast, more sensitive systems like tagged proteins show deviations in the correlation profiles once a certain power threshold is crossed. For these less photostable systems, all subsequent measurements are performed at an excitation power slightly below this previously optimized critical threshold, ensuring minimal photophysical interference while maintaining adequate signal strength.

Temperature-Controlled FCS Measurements

To enable FCS measurements at varying temperatures, our group developed a custom-designed thermal chamber [40,52,64]. Temperature-dependent FCS studies are relatively uncommon, and to the best of my knowledge, such configurations are not widely implemented in other laboratories. In one of the investigations for this thesis, I employed this setup to explore thermally induced changes in molecular diffusion and structural dynamics.

The temperature-controlled unit comprises a sample-holding chamber enclosed by a water jacket (Scheme 2.14). This jacket features inlet and outlet ports to allow continuous water circulation. The bottom of the sample chamber is in direct contact with a microscope-compatible coverslip on which the fluorescent sample is placed. The temperature of the circulating water—and hence the sample—is precisely regulated using a programmable water circulator (Lab Companion, JEIO TECH, Billerica, MA, USA). This setup ensures stable and uniform thermal conditions

across the detection volume during FCS measurements, allowing reliable analysis of temperature-dependent molecular behavior.

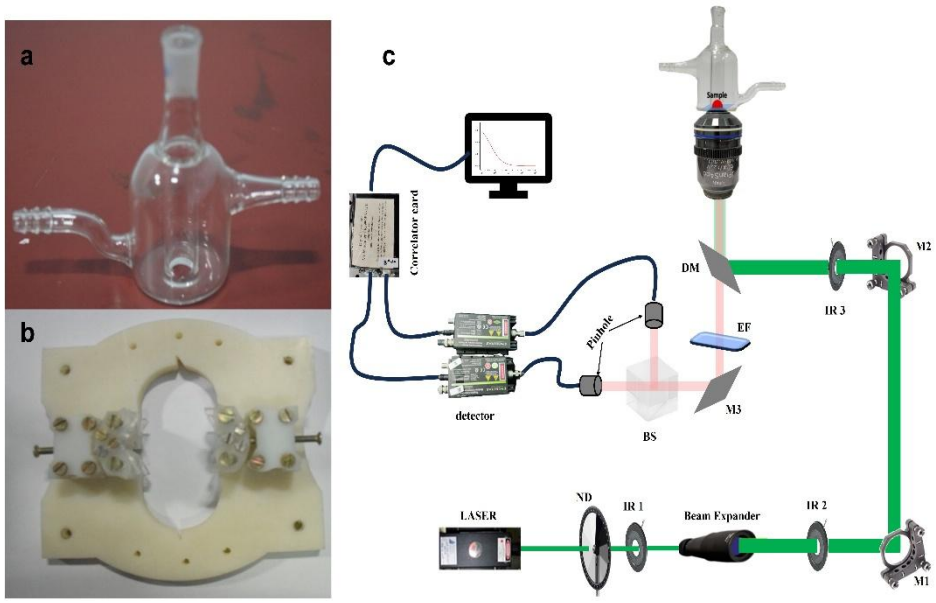

Scheme 2.14. Temperature-dependent FCS. (a) sample cell, (b) holder, (c) temperature cell attached to the FCS setup. DM: dichroic mirror, EF: emission filter, IR: iris, M: mirror, BS: beam splitter, ND: neutral density filter.

2.8. Other Instruments

In addition to the primary techniques discussed in detail, a few supplementary instruments were employed on a limited scale. To begin with, the dynamic viscosity of both the prepared deep eutectic solvents (DESs) and their hydrated counterparts was assessed using a rolling-ball viscometer (Lovis 2000 M, Anton Paar, Austria), which features a built-in temperature regulation system. Moreover, as DESs are typically composed of hygroscopic materials, it is a standard practice to evaluate their inherent water content. For this purpose, we utilized Karl Fischer titration (KAFI LABINDIA KF Titrator) to accurately quantify the moisture present in the DES samples. For freshly prepared (from overnight vacuum dried constituents)

0.5Ac/0.3Ur/0.2Sor DES, the water content is measured to be 0.3 % (w/w), whereas for 0.55Ac/0.36Ur/0.09PEG DES, the water content is found to be 0.4 % (w/w).

2.9. Protein Tagging

In this thesis, two proteins, Human Serum Albumin (HSA) and Bromelain, were studied. Site-specific fluorescent tagging was carried out to probe distinct structural and dynamical features of these proteins. Both of these proteins were tagged following previously published reports [69–73].

For HSA, selective labeling was achieved in two distinct regions (Scheme 2.15):

Domain I (free cysteine residue) was labeled with CPM (7-diethylamino-3-(4'-maleimidylphenyl)-4-methylcoumarin), and TMR (tetramethylrhodamine-5-maleimide) according to requirement.

Domain III (tyrosine residue) was tagged using the fluorophore NPCE.

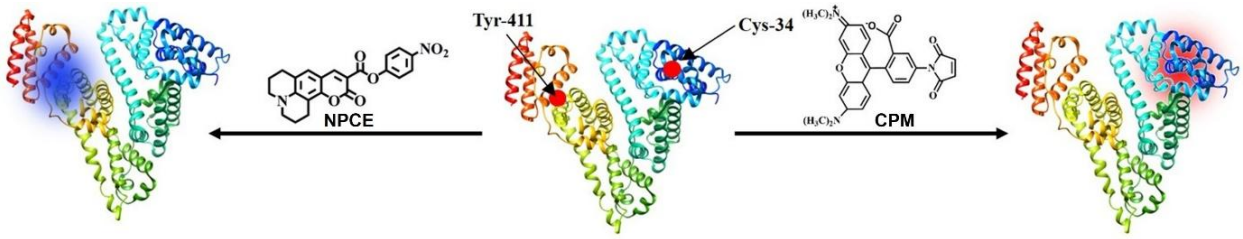

Scheme 2.15. Schematic representation of labelling of Cys-34 (domain-I), and Tyr-414 (domain-III) of HSA by CPM and NPCE fluorophore.

However, the bromelain enzyme possesses a single free cysteine (Cys-26) at its catalytic site (Scheme 2.16). This thiol group served as a labeling site, and CPM was employed for site-specific conjugation.

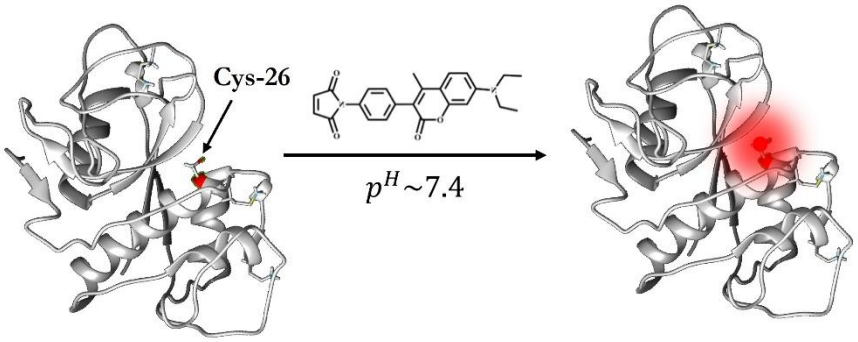

Scheme 2.16. Schematic representation of labeling of Cys-26 of bromelain by TMR fluorophore.

Generally, for the FCS study, I have used TMR-tagged proteins. However, in other fluorescence experiments like emission spectra and time-resolved emission, I have used CPM or NPCE-tagged proteins as per the requirement of the study.

Labeling of HSA with CPM/TMR

Cys-34 of HSA was covalently tagged to CPM and TMR following the previously described method. Briefly, two 10 ml, 90 μM stock solutions of HSA in the buffer of pH 7.4 were taken in round-bottom flasks. Separately, each of the labeling dyes was prepared in DMSO and was added dropwise to one of the HSA solutions under stirring conditions such that in the final solution, the molar ratio became HSA: dye = 1:1.2. The reaction mixtures were then stirred for 12 h at 25 °C. Two reaction mixtures were then separately dialyzed against 1:20 (V/V) DMSO: buffer solution at 5 °C. The dialysis medium was changed 3 times a day for 4 days and then twice in 24 h till the complete removal of untagged dye (as measured by the absorption spectrum of the dialysis medium). The labeled proteins were concentrated using a 10 kDa centrifugal filtration unit. The site-selectivity of the tagging is confirmed through control experiments. The tagging efficiency of TMR-tagged HSA and CPM-tagged HSA is calculated to be ~72%, and ~ 88 % from the ratio of the concentration

of HSA to dye in the CPM tagged-HSA, using ϵ_{HSA}^{280}, ϵ_{TMR}^{555} and ϵ_{CPM}^{390} values of 36,500 $M^{-1}cm^{-1}$, 75,000 $M^{-1}cm^{-1}$, and 33,000 $M^{-1}cm^{-1}$, respectively [69].

Labelling of HSA with NPCE

40 mg of HSA was dissolved in 9 mL of 50 mM phosphate buffer (pH=8.0), and 1 mL of NPCE in DMSO was added slowly into it such that the molar ratio of protein and dye in the reaction mixture is 1:0.9. There are altogether 19 tyrosine residues present in HSA. However, Tyr-411 is the most accessible one at pH 8 for the esterification reaction owing to its considerably low p^{Ka} value. The ratio of the protein and the dye (NPCE) is taken as 1:0.9 to avoid tagging of NPCE at multiple sites. The reaction mixture was then stirred at room temperature for 24 hrs. Upon completion of the reaction, the reaction mixture was dialyzed against DMSO:buffer mixture (having the same DMSO: buffer ratio as in the reaction mixture) at 4°C to remove the unreacted dye. The dialysis solution was replaced four times in two days. Then the solution was replaced with pure phosphate buffer (50 mM, pH 7.4) several times during the next week. The dialysis solution was checked through absorption and emission studies each time for the presence of unreacted dye molecules. When the dialysis solution was found free of any dye, dialysis was stopped, and the labelled protein was collected from the tubes. The labelled protein was further washed and concentrated using the 10 kDa cutoff centrifugal filtration unit and lyophilized to obtain the solid labelled protein. The tagging efficiency was calculated to be 70% using the standard procedure [71,72].

Labeling of Bromelain with CPM

Briefly, 192 mg of bromelain was dissolved in 19 mL phosphate buffer (50 mM, pH 7.4). Following continuous stirring, 3.8 mg of CPM in 0.5 mL of DMSO was added dropwise to the protein solution. The reaction mixture was stirred for 12 h at 20 °C,

followed by dialysis at 5 °C using 1000 mL of phosphate buffer (50 mM, pH 7.4) and the same concentration of DMSO as in the reaction mixture. The dialysis medium was changed four times a day for the first 4 days, and after that, dialysis was carried out with two times medium change until the dialyzed solution showed no appreciable fluorescence. The CPM-tagged bromelain was then concentrated using the 10 kDa-cutoff centrifugal filtration unit. The tagging efficiency is calculated to be ~70%, from the ratio of the concentration of bromelain to dye in the CPM tagged bromelain, using $\epsilon^{280}_{bromelain}$ and ϵ^{390}_{CPM} values of 63,500 $M^{-1}cm^{-1}$ and 33,000 $M^{-1}cm^{-1}$, respectively [69].

2.10. Some Control Experiments Related to Tagging:

2.10.1. Confirmation, Site-selectivity, and Perturbation Related to Tagging of Fluorophores to HSA:

Human serum albumin contains 35 cysteine residues. However, only Cys-34 in domain I is free, and all the others are connected through a disulfide bond with another cysteine residue. Thus, a site-specific tagging of CPM or TMR to the Cys-34 residue is very much possible. For this purpose, we have used HSA and dye in a 1:1.2 ratio for efficient tagging. The absorption spectra of CPM do not change upon tagging to HSA. CPM itself is a very weakly fluorescent molecule with its emission maximum lying around 480 nm. When tagged to HSA, it shows a blue shift of 17 nm (Figure 2.4). This hints that upon tagging CPM goes inside the protein core.

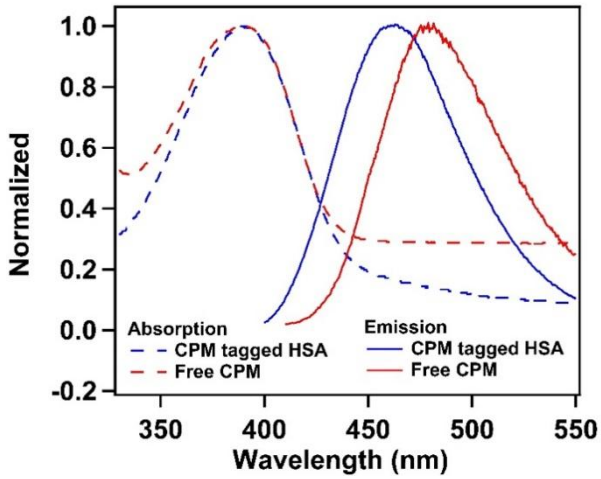

Figure 2.4. Intensity-normalized absorption and emission spectra of free CPM and CPM tagged to HSA.

Due to considerable absorption of the acetamide-urea-sorbitol DES in the absorption region (~400 nm) of the dye CPM, single molecular measurement with that probe was not possible. Thus, to measure the FCS, we have used a different probe TMR. TMR is not a solvatochromic dye, so after it covalently binds to cys-34 of HSA, the absorption and emission spectra of the dye do not change observably. However, this non solvatochromicity of the TMR dye is not a problem for conducting experiments through FCS. Also, the confirmation of TMR tagging has been done using FCS itself (see Figure 2.6). This change of probe is not going to alter our observations as the probe TMR is attaching to the protein in the exact same place where CPM is covalently bound. To be sure about that, we have measured the thermal stability of unlabelled HSA, TMR-tagged HSA, and CPM-tagged HSA using CD spectroscopy (Figure 2.5). All the CD signals and the nature of melting curves are very much similar, confirming the same.

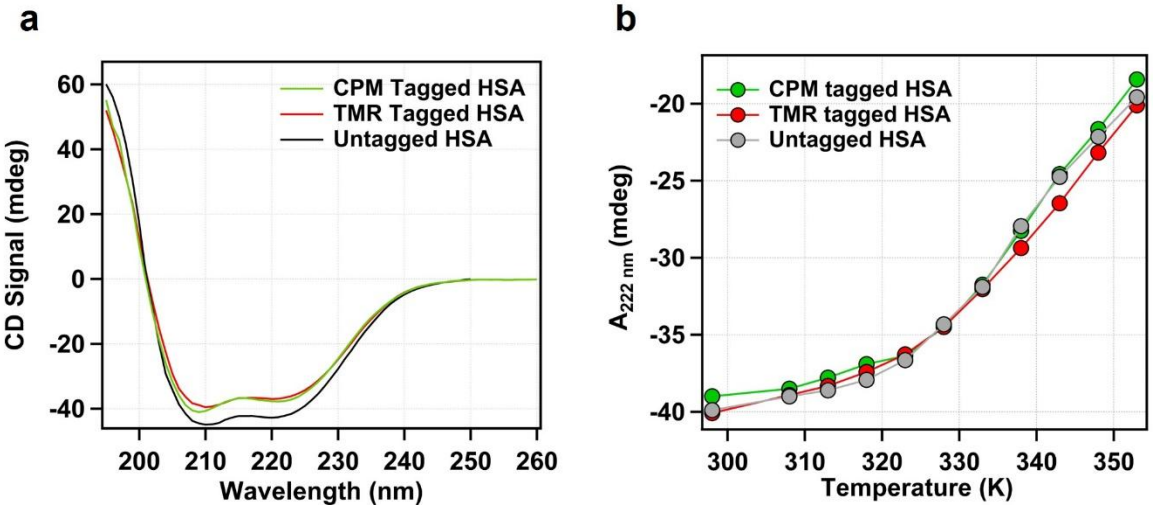

Figure 2.5. (a) Circular dichroism spectra of untagged, TMR tagged, and CPM tagged HSA at room temperature (298 K), (b) Melting curves of untagged, TMR tagged, and CPM tagged HSA

Table 2.1. Secondary structural parameters from CD spectra of untagged HSA, TMR tagged HSA and CPM tagged HSA at room temperature (calculated using CDNN software).

	%- of secondary structural contents			
	α- helicity	β- sheet	β- turn	Random coil
Untagged HSA	67.1	5.7	12.8	14.4
TMR tagged HSA	65.5	5.4	13.0	16.1
CPM tagged HSA	66.8	6.0	12.5	14.7

Now, we measured the diffusion time of free TMR dye and TMR tagged HSA, and the diffusion time came as 45μs and 228 μs, respectively. (Figure 2.6) This increments in the diffusion times while attaching with the protein also confirms the attachment of the probe with the protein under investigation. A similar FCS experiment (as that of free TMR and TMR tagged HSA) with free CPM and CPM

tagged to HSA suggests the tagging, and we have already proved that in our previous publications.

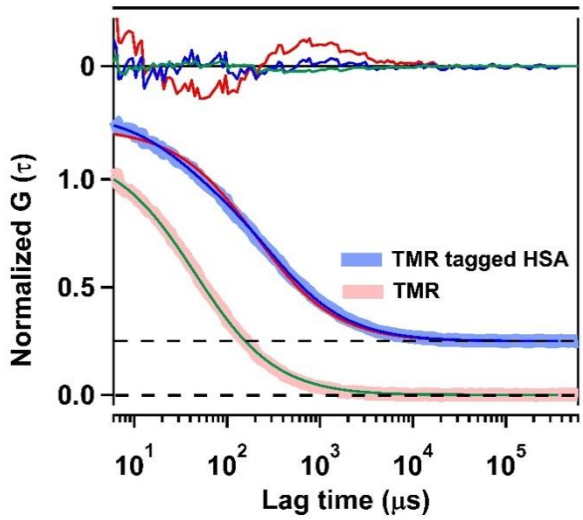

Figure 2.6. Fluorescence intensity autocorrelation curve of free TMR, and TMR tagged to HSA in phosphate buffer. The autocorrelation function of TMR fits well with equation 3. The fitting lines and the residuals are shown in the figure. The autocorrelations of TMR tagged to HSA cannot be fitted with equation 3 satisfactorily, but an extra relaxation term is required and can be fitted by equation 4 (see the fitting lines and residual). Autocorrelation trace of TMR-HSA was fitted from 5 μs due to the known inherent photo physics of rhodamine dye in a 1 μs timescale.

2.10.2. Conformation and perturbation related to tagging of fluorophores to bromelain:

Bromelain possesses a total of five cysteine residues, among which two form disulfide bridges, leaving a single cysteine, Cys-26, in its unbound, reactive form, which is labeled using the fluorophore CPM. Interestingly, as this free Cys-26 is located within the enzyme's active site, any site-specific information will be from the active site of the enzyme.

The fluorescent probe CPM exhibits minimal fluorescence in aqueous environments, typically emitting at around 482 nm (Figure 2.7b). Upon binding to bromelain,

however, its fluorescence becomes significantly more intense, with the emission peak shifting slightly towards the blue region at 476 nm (Figure 2.7b). This spectral shift and enhanced emission are likely due to the limited rotational freedom of the 7-diethylamino group when nestled within the protein's hydrophobic interior, indicating successful conjugation. However, the absorbance characteristics of CPM remain largely unchanged after tagging (Figure 2.7a). Prior research on proteins such as human serum albumin and β-lactoglobulin has used CPM emission behavior to infer structural details near the labeling site. To extract any such information employing this labeled protein, one needs to confirm that the labeling process does not compromise the structural integrity of bromelain. For that, we analyzed the circular dichroism spectra of both the untagged and CPM-tagged bromelain. The nearly overlapping CD profiles confirm that the overall secondary structure remains intact following the modification (Figure 2.7c).

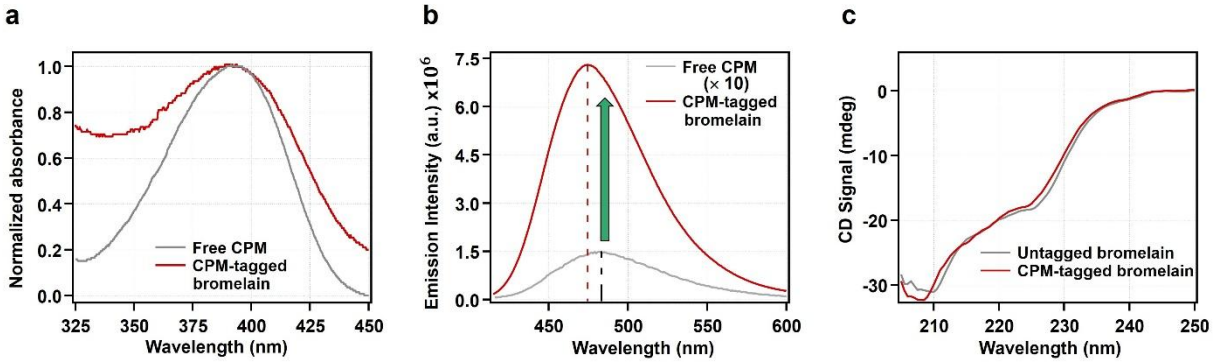

Figure 2.7. (a) normalized absorption, (b) emission spectra, and (c) circular dichroism spectra of free CPM (grey) and CPM tagged to Bromelain (red). Although absorption spectra (in a) do not alter with labelling, a huge increment in the intensity and blue shift of the emission spectra (in b) confirms the labelling of CPM dye to the enzyme bromelain. The CD spectra (in c) confirm no significant alteration in the conformation after tagging.

2.11. DESs Preparation

2.11.1. Acetamide-Urea-Sorbitol DES preparation

Acetamide and urea were dried under vacuum for overnight before the synthesis. Sorbitol was used as received commercially. Acetamide/urea/sorbitol DES was prepared by mixing the appropriate amounts (mole fractions, 0.5 Ac, 0.3 Ur, and 0.2 Sor) of the constituents in a sealed container and slowly heating to 75 °C while stirring. After one hour of heating and stirring, a clear solution of DES was obtained, which remained liquid even at 280 K and was used for all the experiments. Precautions for external water incorporation were always taken care of.

2.11.2. Acetamide-Urea-PEG DES preparation

Acetamide, urea and PEG-300 with a molar ratio of 0.55:0.36:0.09 was used to form the (0.55Ac/0.36Ur/0.09PEG) DES following the published procedure [69,74]. This DES is not liquid at room temperature (at 298 K) and becomes solid, however, at the experimental temperature range, a clear liquid state was observed.

2.11.3. Choline chloride (ChCl)- Glycerol (Gly) /Ethylene glycol (EG) DES preparation

Choline chloride was recrystallized in hot ethanol (60 ℃) and vacuum dried because of its highly hygroscopic nature before use. For both the ChCl-Gly (1:2) and ChCl-EG (1:2), the constituents in appropriate amount have been taken in a glass container with a magnetic bead and then sealed immediately. The mixture was then heated at 80 ℃ for around 1-2 hours until the clear liquid was observed.

2.12. Materials Used

Here I have provided a list of materials used in this thesis along with their purity and suppliers' information.

Table 2.2. List of materials used in this thesis

Material	**Supplier**	**Purity**
Acetamide	Sigma Aldrich	>99%
Urea	Sigma Aldrich	>99%
Sorbitol	Sigma Aldrich	>98%
Choline chloride	Sigma Aldrich	≥98%
Glycerol	Sigma Aldrich	≥99.0%
Ethylene glycol	Sigma Aldrich	~99.8%
Rhodamine 6G (R6G)	Sigma Aldrich	Dye content 99.0%
PEG-300	TCI	No data available
Coumarin 153 (C153)	Exciton	No data available
7-diethylamino-3-(4'-maleimidylphenyl)-4-methylcoumarin (CPM)	Sigma Aldrich	≥95% purity (HPLC)
tetramethylrhodamine-5-maleimide (TMR),	Sigma Aldrich	≥85% (HPLC)
coumarin 343 (C343)	Sigma Aldrich	Dye content 97 %
Bromelain	Sigma Aldrich	≥3 units/mg protein
Human Serum Albumin (HSA)	Sigma Aldrich	≥98%
Ficoll-70	Sigma Aldrich	No data available
4-nitro-phenylacetic acid (pNPA)	Sigma Aldrich	99%
disodium hydrogen phosphate dihydrate ($Na_2HPO_4.2H_2O$)	Merck, India	≥ 99.0 %
sodium dihydrogen phosphate dihydrate ($NaH_2PO_4.2H_2O$)	Merck, India	≥ 99.0 %
Dialysis membrane tubing (12 kDa cutoff)	Sigma Aldrich	-
Centrifugal filter units (Amicon Ultra, 10kDa cutoff)	Merck Millipore, Germany	-

dimethyl sulfoxide (DMSO)	Sisco Research Laboratories Pvt. Ltd.	HPLC grade (99.8%)
casein	Sigma Aldrich	87-94%

2.13. Sample Preparation

Our experiments were done in phosphate buffer (of concentration 50 mM) of pH 7.4 which was prepared by mixing the appropriate amount of disodium hydrogen phosphate and sodium dihydrogen phosphate solution in double distilled water. All the protein samples were prepared in this buffer and incubated overnight to reach equilibrium before measurement. In the case of steady state fluorescence, steady state absorption, CD experiment, and time resolved fluorescence experiment, the protein concentrations were kept around ~5 μM. For steady state fluorescence study of bromelain, both untagged protein and CPM tagged were used. Similarly for HSA, both the CPM tagged and NPCE tagged HSA were used depending upon the requirement. For CD experiments of both the proteins, untagged proteins were used. In the case of time resolved fluorescence measurement, always the tagged proteins were used. In single molecular level experiments employing FCS, the concentration were kept ~5 nM. In all the cases the concentrations were measured by using the reported molar extinction value of the protein at 280 nm. In experiments with DES, I used % v/v concentration scale and prepared the sample by mixing the synthesized DES with required amount of buffer. For experiments involving macromolecular crowder, Ficoll-70k, a concentrated stock solution was prepared at 300 gL^{-1} in the buffer solution of pH 7.4. Throughout my thesis, the concentrations of the Ficol-70k have been consistently reported in units of $g \cdot L^{-1}$. It is important to note that representing crowder concentrations in grams per liter rather than molarity or normality is a widely accepted convention in the field.

In the case of heterogeneity study of acetamide-urea-sorbitol DES (chapter 3), a portion of the synthesized DES is transferred into a quartz-cuvette (path length 1

cm) pre-stained with the required dye (R6G or coumarin-153) and is sealed immediately. We took care to ensure the complete dissolution of the dye into DES. In the case of Transient Absorption measurement of hydrated DES (chapter 4), the concentration of the fluorophore, coumarin 343 is kept much higher. We maintained OD~0.5 at 400 nm wavelength in a 1 mm pathlength cuvette.

2.14. References

(1) Demchenko, A. P. The Red-Edge Effects: 30 Years of Exploration. *Luminescence*. 2002, pp 19–42. https://doi.org/10.1002/bio.671.

(2) Demchenko, A. P. Weber's Red-Edge Effect That Changed the Paradigm in Photophysics and Photochemistry. **2016**, 95–141. https://doi.org/10.1007/4243_2016_14.

(3) Azumi, T.; Itoh, K. I.; Shiraishi, H. Shift of Emission Band upon the Excitation at the Long Wavelength Absorption Edge. III. Temperature Dependence of the Shift and Correlation with the Time Dependent Spectral Shift. *J Chem Phys* **1976**, *65* (7), 2550–2555. https://doi.org/10.1063/1.433440.

(4) Itoh, K. I.; Azumi, T. Shift of the Emission Band upon Excitation at the Long Wavelength Absorption Edge. II. Importance of the Solute-Solvent Interaction and the Solvent Reorientation Relaxation Process. *J Chem Phys* **1975**, *62* (9), 3431–3438. https://doi.org/10.1063/1.430977.

(5) Nelson, D. L.; Cox, M. M.; Hoskins, A. A. *Lehninger Principles of Biochemistry*; Macmillan Learning: New York, USA, 2021.

(6) Das, N.; Khan, T.; Sen, P. The Shift of Excitation Spectra at Blue Edge of Emission (BEEmS) as a New Methodology to Probe Heterogeneity. *Chem*

Phys **2024**, *577*, 112138. https://doi.org/10.1016/J.CHEMPHYS.2023.112138.

(7) Chattopadhyay, A.; Haldar, S. Dynamic Insight into Protein Structure Utilizing Red Edge Excitation Shift. *Acc Chem Res* **2014**, *47* (1), 12–19. https://doi.org/10.1021/ar400006z.

(8) More, S. R.; Jha, S. K. Multi-Site Red-Edge Excitation Shift Reveals the Residue-Specific Solvation Dynamics during the Native to Amyloid-like Transition of an Amyloidogenic Protein. *Journal of Physical Chemistry B* **2024**. https://doi.org/10.1021/acs.jpcb.4c07067.

(9) Brahma, R.; Raghuraman, H. Novel Insights in Linking Solvent Relaxation Dynamics and Protein Conformations Utilizing Red Edge Excitation Shift Approach. *Emerg Top Life Sci* **2021**, *5* (1), 89–101. https://doi.org/10.1042/ETLS20200256.

(10) Whitmore, L.; Wallace, B. A. Protein Secondary Structure Analyses from Circular Dichroism Spectroscopy: Methods and Reference Databases. *Biopolymers* **2008**, *89* (5), 392–400. https://doi.org/10.1002/BIP.20853,.

(11) Johnson, W. C. Secondary Structure of Proteins through Circular Dichroism Spectroscopy. *Annu Rev Biophys Biophys Chem* **1988**, *17*, 145–166. https://doi.org/10.1146/ANNUREV.BB.17.060188.001045,.

(12) Wei, Y.; Thyparambil, A. A.; Latour, R. A. Protein Helical Structure Determination Using CD Spectroscopy for Solutions with Strong Background Absorbance from 190-230 Nm. *Biochim Biophys Acta* **2014**, *1844* (12), 2331. https://doi.org/10.1016/J.BBAPAP.2014.10.001.

(13) Greenfield, N. J. Using Circular Dichroism Spectra to Estimate Protein Secondary Structure. *Nat Protoc* **2007**, *1* (6), 2876–2890. https://doi.org/10.1038/nprot.2006.202.

(14) Greenfield, N.; Fasman, G. D. Computed Circular Dichroism Spectra for the Evaluation of Protein Conformation. *Biochemistry* **1969**, *8* (10), 4108–4116. https://doi.org/10.1021/BI00838A031/ASSET/BI00838A031.FP.PNG_V03.

(15) Bohm, G.; Muhr, R.; Jaenicke, R. Quantitative Analysis of Protein Far UV Circular Dichroism Spectra by Neural Networks. *Protein Eng* **1992**, *5* (3), 191–195.

(16) Fleming, G. R. *Chemical Applications of Ultrafast Spectroscopy*; Oxford University Press: New York, 1986.

(17) Becker, W. *Advanced Time-Correlated Single Photon Counting Techniques*; Castleman, A. W., Toennies, J. P., Zinth, W., Eds.; Springer Series in Chemical Physics; Springer Berlin Heidelberg: Berlin, Heidelberg, 2005; Vol. 81. https://doi.org/10.1007/3-540-28882-1.

(18) O' Connor, D. V.; Phillips, D. *Time Correlated Single Photon Counting*; Academic Press, New York, USA: New York, 1984.

(19) Lakowicz, J. R. *Principles of Fluorescence Spectroscopy*; Springer, 2006; pp 1–954. https://doi.org/10.1007/978-0-387-46312-4.

(20) Hallidy, L. A.; Topp, M. R. Picosecond Luminescence Detection Using Type-II Phase-Matched Frequency Conversion. *Chem Phys Lett* **1977**, *46* (1), 8–14. https://doi.org/10.1016/0009-2614(77)85153-1.

(21) Chosrowjan, H.; Taniguchi, S.; Tanaka, F. Ultrafast Fluorescence Upconversion Technique and Its Applications to Proteins. *FEBS J* **2015**, *282* (16), 3003–3015. https://doi.org/10.1111/FEBS.13180.

(22) Kahlow, M. A.; Jarzęba, W.; DuBruil, T. P.; Barbara, P. F. Ultrafast Emission Spectroscopy in the Ultraviolet by Time-gated Upconversion.

Review of Scientific Instruments **1988**, *59* (7), 1098–1109. https://doi.org/10.1063/1.1139734.

(23) Xu, J.; Knutson, J. R. Ultrafast Fluorescence Spectroscopy via Upconversion: Applications to Biophysics. *Methods Enzymol* **2008**, *450*, 159–183. https://doi.org/10.1016/S0076-6879(08)03408-3.

(24) Y.R., S. *The Principles of Nonlinear Optics*; John Wiley, New York, 1984.

(25) Zernike, F.; Midwinter, J. E. *Applied Nonlinear Optics*; John Wiley & Sons, Ltd., 1973.

(26) Fleming, G. R.; Gijzeman, O. L. J.; Freed, K. F.; Lin, S. H. Theory for Time Resolved Emission Spectra. *Journal of the Chemical Society, Faraday Transactions 2: Molecular and Chemical Physics* **1975**, *71*, 773–780. https://doi.org/10.1039/F29757100773.

(27) Changenet-Barret, P.; Choma, C. T.; Gooding, E. F.; Degrado, W. F.; Hochstrasser, R. M. Ultrafast Dielectric Response of Proteins from Dynamics Stokes Shifting of Coumarin in Calmodulin. *J. Phys. Chem. B* **2000**, *104* (39), 9322–9329. https://doi.org/10.1021/jp001634v.

(28) *Femtosecond Laser Pulses*; Rullière, C., Ed.; Advanced Texts in Physics; Springer New York: New York, NY, 2005. https://doi.org/10.1007/B137908.

(29) Ruckebusch, C.; Sliwa, M.; Pernot, P.; de Juan, A.; Tauler, R. Comprehensive Data Analysis of Femtosecond Transient Absorption Spectra: A Review. *Journal of Photochemistry and Photobiology C: Photochemistry Reviews* **2012**, *13* (1), 1–27. https://doi.org/10.1016/J.JPHOTOCHEMREV.2011.10.002.

(30) Berera, R.; van Grondelle, R.; Kennis, J. T. M. Ultrafast Transient Absorption Spectroscopy: Principles and Application to Photosynthetic

Systems. *Photosynth Res* **2009**, *101* (2–3), 105–118. https://doi.org/10.1007/s11120-009-9454-y.

(31) Buzády, A.; Savolainen, J.; Erostyák, J.; Myllyperkiö, P.; Somogyi, B.; Korppi-Tommola, J. Femtosecond Transient Absorption Study of the Dynamics of Acrylodan in Solution and Attached to Human Serum Albumin. *J. Phys. Chem. B* **2003**, *107* (5), 1208–1214. https://doi.org/10.1021/jp027107o.

(32) McGregor, S. K. M.; Govind, C.; Wood, M. K. R.; Shukla, A.; Lim, H.; Lepage, R. J.; Krenske, E. H.; K. N., N. U.; Ajayaghosh, A.; Karunakaran, V.; Namdas, E. B.; Lo, S.-C. Structural Integration of Carbazole and Tetraphenylethylene: Ultrafast Excited-State Relaxation Dynamics and Efficient Electroluminescence. *Adv Photonics Res* **2021**, *2* (4), 2000144. https://doi.org/10.1002/adpr.202000144.

(33) Zhu, H.; Li, M.; Hu, J.; Wang, X.; Jie, J.; Guo, Q.; Chen, C.; Xia, A. Ultrafast Investigation of Intramolecular Charge Transfer and Solvation Dynamics of Tetrahydro[5]-Helicene-Based Imide Derivatives. *Sci Rep* **2016**, *6*, 24313. https://doi.org/10.1038/srep24313.

(34) Chowdhury, P. K.; Halder, M.; Sanders, L.; Calhoun, T.; Anderson, J. L.; Armstrong, D. W.; Song, X.; Petrich, J. W. Dynamic Solvation in Room-Temperature Ionic Liquids. *J. Phys. Chem. B* **2004**, *108* (29), 10245–10255. https://doi.org/10.1021/jp0376828.

(35) Gupta, S.; Rafiq, S.; Sen, P. Dynamics of Solvent Response in Methanol-Chloroform Binary Solvent Mixture: A Case of Synergistic Solvation. *J. Phys. Chem. B* **2015**, *119* (7), 3135–3141. https://doi.org/10.1021/jp5120338.

(36) Tan, X.; Gustafson, T. L.; Lefumeux, C.; Burdzinski, G.; Buntinx, G.; Poizat, O. Solvation Dynamics Probed by Femtosecond Transient

Absorption Spectroscopy: Vibrational Cooling and Conformational Relaxation in S1 Trans-4,4′-Diphenylstibene. *J. Phys. Chem. A* **2002**, *106* (14), 3593–3598. https://doi.org/10.1021/jp013176b.

(37) Horng, M. L.; Gardecki, J. A.; Papazyan, A.; Maroncelli, M. Subpicosecond Measurements of Polar Solvation Dynamics: Coumarin 153 Revisited. *J. Phys. Chem.* **1995**, *99* (48), 17311–17337. https://doi.org/10.1021/J100048A004.

(38) Schuler, B. Single-Molecule FRET of Protein Structure and Dynamics - a Primer. *J Nanobiotechnology* **2013**, *11(suppl 1)* (S2), 1–17. https://doi.org/10.1186/1477-3155-11-S1-S2.

(39) Petrášek, Z.; Hoege, C.; Mashaghi, A.; Ohrt, T.; Hyman, A. A.; Schwille, P. Characterization of Protein Dynamics in Asymmetric Cell Division by Scanning Fluorescence Correlation Spectroscopy. *Biophys J* **2008**, *95* (11), 5476–5486. https://doi.org/10.1529/biophysj.108.135152.

(40) Yadav, R.; Sengupta, B.; Sen, P. Conformational Fluctuation Dynamics of Domain i of Human Serum Albumin in the Course of Chemically and Thermally Induced Unfolding Using Fluorescence Correlation Spectroscopy. *J. Phys. Chem. B* **2014**, *118* (20), 5428–5438. https://doi.org/10.1021/jp502762t.

(41) Sengupta, B.; Acharyya, A.; Sen, P. Elucidation of the Local Dynamics of Domain-III of Human Serum Albumin over the Ps–Ms Time Regime Using a New Fluorescent Label. *Phys. Chem. Chem. Phys.* **2016**, *18* (41), 28548–28555. https://doi.org/10.1039/C6CP05743H.

(42) Quast, R. B.; Margeat, E. Studying GPCR Conformational Dynamics by Single Molecule Fluorescence. *Mol Cell Endocrinol* **2019**, *493*, 110469. https://doi.org/10.1016/j.mce.2019.110469.

(43) Rigler, R.; Elson, E. S. *Fluorescence Correlation Spectroscopy*; Springer Series in Chemical Physics; Springer Berlin Heidelberg: Berlin, Heidelberg, 2001; Vol. 65. https://doi.org/10.1007/978-3-642-59542-4.

(44) Wohland, T.; Maiti, S.; Macháň, R. *An Introduction to Fluorescence Correlation Spectroscopy*; IOP Publishing, 2020. https://doi.org/10.1088/978-0-7503-2080-1.

(45) Elson, E. L. Fluorescence Correlation Spectroscopy: Past, Present, Future. *Biophys J* **2011**, *101* (12), 2855–2870. https://doi.org/10.1016/j.bpj.2011.11.012.

(46) Magde, D.; Elson, E.; Webb, W. W. Thermodynamic Fluctuations in a Reacting System—Measurement by Fluorescence Correlation Spectroscopy. *Phys Rev Lett* **1972**, *29* (11), 705. https://doi.org/10.1103/PhysRevLett.29.705.

(47) Magde, D.; Elson, E. L.; Webb, W. W. Fluorescence Correlation Spectroscopy. II. An Experimental Realization. *Biopolymers* **1974**, *13* (1), 29–61. https://doi.org/10.1002/BIP.1974.360130103,.

(48) Maiti, S.; Haupts, U.; Webb, W. W. Fluorescence Correlation Spectroscopy: Diagnostics for Sparse Molecules. *Proc Natl Acad Sci U S A* **1997**, *94* (22), 11753. https://doi.org/10.1073/PNAS.94.22.11753.

(49) Krieger, J. W.; Singh, A. P.; Bag, N.; Garbe, C. S.; Saunders, T. E.; Langowski, J.; Wohland, T. Imaging Fluorescence (Cross-) Correlation Spectroscopy in Live Cells and Organisms. *Nature Protocols 2015 10:12* **2015**, *10* (12), 1948–1974. https://doi.org/10.1038/nprot.2015.100.

(50) Macháň, R.; Wohland, T. Recent Applications of Fluorescence Correlation Spectroscopy in Live Systems. *FEBS Lett* **2014**, *588* (19), 3571–3584. https://doi.org/10.1016/J.FEBSLET.2014.03.056.

(51) Das, N.; Sen, P. Structural, Functional, and Dynamical Responses of a Protein in a Restricted Environment Imposed by Macromolecular Crowding. *Biochemistry* **2018**, *57* (42), 6078–6089. https://doi.org/10.1021/acs.biochem.8b00599.

(52) Das, N.; Sen, P. Shape-Dependent Macromolecular Crowding on the Thermodynamics and Microsecond Conformational Dynamics of Protein Unfolding Revealed at the Single-Molecule Level. *J. Phys. Chem. B* **2020**, *124* (28), 5858–5871. https://doi.org/10.1021/acs.jpcb.0c03897.

(53) Feder, T. J.; Brust-Mascher, I.; Slattery, J. P.; Baird, B.; Webb, W. W. Constrained Diffusion or Immobile Fraction on Cell Surfaces: A New Interpretation. *Biophys J* **1996**, *70* (6), 2767–2773. https://doi.org/10.1016/S0006-3495(96)79846-6.

(54) Höfling, F.; Franosch, T. Anomalous Transport in the Crowded World of Biological Cells. *Reports on Progress in Physics* **2013**, *76* (4), 046602. https://doi.org/10.1088/0034-4885/76/4/046602.

(55) Banks, D. S.; Tressler, C.; Peters, R. D.; Höfling, F.; Fradin, C. Characterizing Anomalous Diffusion in Crowded Polymer Solutions and Gels over Five Decades in Time with Variable-Lengthscale Fluorescence Correlation Spectroscopy. *Soft Matter* **2016**, *12* (18), 4190–4203. https://doi.org/10.1039/c5sm01213a.

(56) Tabatabaei, F.; Lenz, O.; Holm, C. Simulational Study of Anomalous Tracer Diffusion in Hydrogels. *Colloid Polym Sci* **2011**, *289* (5–6), 523–534. https://doi.org/10.1007/S00396-011-2393-0/FIGURES/11.

(57) Einstein, A. Über Die von Der Molekularkinetischen Theorie Der Wärme Geforderte Bewegung von in Ruhenden Flüssigkeiten Suspendierten Teilchen. *Ann Phys* **1905**, *322* (8), 549–560. https://doi.org/10.1002/ANDP.19053220806.

(58) Das, N.; Sen, P. Dynamic Heterogeneity and Viscosity Decoupling: Origin and Analytical Prediction. *Phys. Chem. Chem. Phys.* **2021**, *23* (29), 15749–15757. https://doi.org/10.1039/d1cp01804c.

(59) Müller, C. B.; Loman, A.; Pacheco, V.; Koberling, F.; Willbold, D.; Richtering, W.; Enderlein, J. Precise Measurement of Diffusion by Multi-Color Dual-Focus Fluorescence Correlation Spectroscopy. *EPL* **2008**, *83* (4), 46001. https://doi.org/10.1209/0295-5075/83/46001.

(60) Das, N.; Sen, P. Macromolecular Crowding: How Shape and Interaction Affect the Structure, Function, Conformational Dynamics and Relative Domain Movement of a Multi-Domain Protein. *Phys. Chem. Chem. Phys.* **2022**, *24* (23), 14242–14256. https://doi.org/10.1039/D1CP04842B.

(61) Khan, T.; Das, N.; Negi, K. S.; Bhowmik, S.; Sen, P. Understanding the Intricacy of Protein in Hydrated Deep Eutectic Solvent: Solvation Dynamics, Conformational Fluctuation Dynamics, and Stability. *Int. J. Biol. Macromol.* **2023**, *253*, 127100. https://doi.org/10.1016/j.ijbiomac.2023.127100.

(62) Hossain, S. S.; Paul, S.; Samanta, A. Structural Stability and Conformational Dynamics of Cytochrome c in Hydrated Deep Eutectic Solvents. *J. Phys. Chem. B* **2021**, *125* (22), 5757–5765. https://doi.org/10.1021/acs.jpcb.1c01975.

(63) Pabbathi, A.; Ghosh, S.; Samanta, A. FCS Study of the Structural Stability of Lysozyme in the Presence of Morpholinium Salts. *J. Phys. Chem. B* **2013**, *117* (51), 16587–16593. https://doi.org/10.1021/jp409842d.

(64) Sengupta, B.; Das, N.; Sen, P. Elucidation of Ms Dynamics of Domain-III of Human Serum Albumin during the Chemical and Thermal Unfolding: A Fluorescence Correlation Spectroscopic Investigation. *Biophys Chem* **2017**, *221*, 17–25. https://doi.org/10.1016/j.bpc.2016.11.006.

(65) Sengupta, B.; Chaudhury, A.; Das, N.; Sen, P. Single Molecular Level Probing of Structure and Dynamics of Papain Under Denaturation. *Prot. Pep. Lett.* **2017**, *24* (11), 1073–1081. https://doi.org/10.2174/0929866524666170811145838.

(66) Sengupta, B.; Das, N.; Singh, V.; Thakur, A. K.; Sen, P. Fluorescence Correlation Spectroscopy as a Tool to Investigate the Directionality of Proteolysis. *Int. J. Biol. Macromol.* **2020**, *164*, 2524–2534. https://doi.org/10.1016/j.ijbiomac.2020.08.103.

(67) Halder, B.; Ghosh, S.; Khan, T.; Pal, S.; Das, N.; Sen, P. Tracking Heterogenous Protein Aggregation at Nanoscale through Fluorescence Correlation Spectroscopy. *Photochem Photobiol* **2024**, *100*, 989–999. https://doi.org/10.1111/php.14004.

(68) White, D. S.; Smith, M. A.; Chanda, B.; Goldsmith, R. H. Strategies for Overcoming the Single-Molecule Concentration Barrier. *ACS Measurement Science Au* **2023**, *3* (4), 239. https://doi.org/10.1021/ACSMEASURESCIAU.3C00002.

(69) Das, N.; Khan, T.; Subba, N.; Sen, P. Correlating Bromelain's Activity with Its Structure and Active-Site Dynamics and the Medium's Physical Properties in a Hydrated Deep Eutectic Solvent. *Phys. Chem. Chem. Phys.* **2021**, *23* (15), 9337–9346. https://doi.org/10.1039/d1cp00046b.

(70) Das, N.; Yadav, S.; Negi, K. S.; Tarif, E.; Sen, P. Does Microsecond Active-Site Dynamics Primarily Control Proteolytic Activity of Bromelain? Clues from Single Molecular Level Study with a Denaturant, a Stabilizer and a Macromolecular Crowder. *BBA Advances* **2022**, *2*, 100041. https://doi.org/10.1016/j.bbadva.2022.100041.

(71) Das, N.; Sahu, S.; Khan, T.; Sen, P. Site-Specific Heterogeneity of Multi-Domain Human Serum Albumin and Its Origin: A Red Edge Excitation Shift

Study. *Photochem Photobiol* **2023**, *99* (2), 538–546. https://doi.org/10.1111/php.13712.

(72) Das, N.; Tarif, E.; Dutta, A.; Sen, P. Associated Water Dynamics Might Be a Key Factor Affecting Protein Stability in the Crowded Milieu. *J. Phys. Chem. B* **2023**, *127* (14), 3151–3163. https://doi.org/10.1021/acs.jpcb.2c09043.

(73) Das, N.; Sen, P. Size-Dependent Macromolecular Crowding Effect on the Thermodynamics of Protein Unfolding Revealed at the Single Molecular Level. *Int J Biol Macromol* **2019**, *141*, 843–854. https://doi.org/10.1016/j.ijbiomac.2019.09.029.

(74) Subba, N.; Sahu, P.; Das, N.; Sen, P. Rational Design, Preparation and Characterization of a Ternary Non-Ionic Room-Temperature Deep Eutectic Solvent Derived from Urea, Acetamide, and Sorbitol. *Journal of Chemical Sciences* **2021**, *133* (1), 25. https://doi.org/10.1007/s12039-020-01866-2.

Chapter 3

Multiple Evidences of Molecular Level Heterogeneity in a Non-ionic Biocatalytic Deep Eutectic Solvent

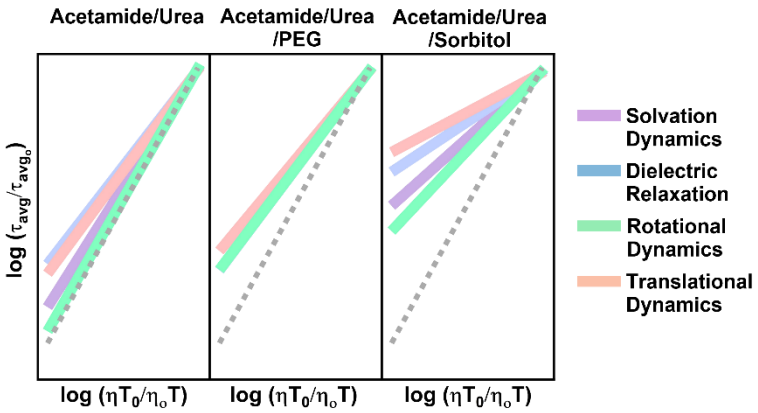

Tanmoy Khan, Ejaj Tarif, Yuto Awano, Lou Serafin Lozada, Nilimesh Das, Keisuke Tominaga, and Pratik Sen

J. Mol. Liq. **2023**, *389*, 122882.

Abstract:

Deep eutectic solvents (DESs) are new-generation solvents with exquisite and tuneable properties. Molecular-level heterogeneity has been identified as an intriguing feature of such solvents. Herein, we examined the spatio-temporal heterogeneity of a potential non-ionic biocatalytic DES, acetamide/urea/sorbitol (0.5Ac/0.3Ur/0.2Sor), and compared the result with corresponding binary acetamide/urea (0.6Ac/0.4Ur) DES, and another related non-ionic ternary DES (0.55Ac/0.36Ur/0.09PEG). The effect of the addition of a third component on the spatio-temporal heterogeneity of a DES was investigated. The excitation wavelength-dependent emission measurement suggests an introduction of spatial heterogeneity in acetamide/urea/sorbitol compared to spatially homogenous acetamide/urea and acetamide/urea/PEG. The dynamic heterogeneity measurements in terms of solvation dynamics, dielectric relaxation, and rotational and translational diffusion dynamics indicate a length and timescale dependency. Overall, acetamide/urea/sorbitol is dynamically more heterogenous than the other two related DESs.

3.1. Introduction

Structure and dynamics control chemistry and biology. Modern science has identified molecular level heterogeneity as one of the intriguing aspects of structure and dynamics [1–4]. The heterogeneity of a medium is relative to the observation dimension. For the sub-atomic length scale of observation, every system will appear to be heterogeneous and with a bigger dimension of observation this heterogeneity will tend to smear out as unobservable.

In the literature, one would invariably encounter two terms, spatial and dynamic heterogeneity, which are often used interchangeably [5,6]. Heterogeneity mainly originates from the presence of different interactions in terms of spatial arrangement or relaxation rates. The first one is defined as spatial heterogeneity, and the latter is described as dynamic heterogeneity [5–7].

The molecular-level picture of heterogeneity both in terms of structure and dynamics mainly comes from studies of glass-forming liquid that shows viscosity decoupled relaxation rates near glass transition temperature (T_g) due to microdomain formation [8–12]. These locally preferred clusters facilitate local structural relaxation but do not facilitate the relaxation of the entire system [11,13,14]. Even if the Stokes-Einstein (SE) relationship is locally satisfied within these microdomains and bulk, their spatial averages might indicate a deviation from the SE relationship due to preferential sampling from the microdomains [15]. A unique breakthrough in this field comes when viscosity decoupled relaxation rates were identified for polar and non-polar liquids at a much higher temperature than the T_g [16]. In the case of polar and H-bonded solvents, minimal decoupling was observed [16]. Consequent research proved that such dynamic heterogeneity, even at ambient room temperature might well be a common phenomenon for ILs and DESs [17–25].

DESs are already touted as the next game-changer in various fields of chemistry and biology owing to their green character, easy and atom-economic synthesis, exceptional tunability, biocompatibility, low volatility, etc [26–29]. Many

recent reviews are available that summarise various uses of DES in many different fields [26,27,30–35]. However, from the viewpoint of a physical chemist, we are more interested in the molecular level insight of such systems. Most of the works in this direction are with ionic DESs. Only a handful of reports are available deciphering the structure and dynamics of non-ionic DESs [36–39].

Biswas group has explored various acetamide-based ionic DESs, and they showed the presence of substantial dynamic and spatial heterogeneity in these systems [17,18,40–44]. Replacement of electrolytes by the non-ionic urea makes the system almost homogeneous, both in relaxation rates and spatial arrangement [19,38,45]. However, this DES is not liquid at room temperature, thus limiting its use. Recently, a third component (PEG-300) is added to the acetamide/urea DES to lower its freezing point down to 303 K [20]. Moreover, this system is spatially homogeneous, but its rotational relaxation shows considerable viscosity decoupling [20].

In this context, herein we have chosen sorbitol as the third component, which itself is solid. The ternary 0.5Ac/0.3Ur/0.2Sor DES is liquid even at 253 K, making it an interesting non-ionic DES for practical applications [46]. We have already shown the positive effect of 0.5Ac/0.3Ur/0.2Sor DES on protein structure and activity [47]. Herein we employed steady-state/time-resolved fluorescence and fluorescence correlation spectroscopy covering a broad range of lengths and time scales to decipher the microscopic heterogeneity of this DES. We have also used dielectric relaxation spectroscopy to understand the inherent medium dynamics and associated heterogeneity of the system. Our results demonstrate that the system is highly heterogenous both spatially and dynamically, and the extent of heterogeneity depends on the length scale of the measurement. We also compared the heterogeneity of this DES with the corresponding binary acetamide/urea (0.6Ac/0.4Ur) DES, and another similar non-ionic ternary DES (0.55Ac/0.36Ur/0.09PEG), and investigate the effect of the addition of a third component on the spatio-temporal heterogeneity.

3.2. Results and Discussion:

3.2.1. Steady-state Measurements

At 298 K, the absorption and emission maxima of C153 in 0.5Ac/0.3Ur/0.2Sor non-ionic DES were measured to be 433.7 nm (23057.4 cm^{-1}) and 534.5 nm (18709.1 cm^{-1}), respectively. Interestingly, with an increase in the temperature (298 K to 343 K) we observed a very small blue shift of ~1.5 nm in the absorption spectra (Figure 1a and Table 1). Such a surprising blue shift with increasing temperature might be due to decreasing dielectric constant of the medium with increasing temperature [48,49]. Similar observations were also made with other ionic liquids and DESs [17]. In the emission spectrum, we observed a red shift of 9.5 nm with the increase in the temperature (298 K to 343 K) (Figure 1b, Table 1).

Table 1: Temperature dependent absorption and emission maxima of coumarin 153 in 0.5Ac/0.3Ur/0.2Sor DES.

Temperature (K)	Absorption Maximum (nm)	Absorption Maximum (cm^{-1})	Emission maximum (nm)	Emission maximum (cm^{-1})
298	433.7	23057.4	534.5	18709.1
303	433.2	23084.0	536.6	18635.8
308	433.0	23094.7	538.4	18573.5
313	433.0	23094.7	539.8	18525.4
318	432.7	23110.7	541.2	18477.4
323	432.5	23121.4	542.0	18450.2
328	432.3	23132.1	542.7	18426.4
333	432.2	23137.4	543.1	18412.8
338	432.0	23148.1	543.6	18395.9
343	431.9	23153.5	544.0	18382.4

The observation could be explained as follows. The medium here is highly viscous (Table 1). At low temperatures, emission originates from an incomplete solvated state. But with an increase in temperature, viscosity decreases, and emission is

expected to originate from a more solvated state with a gradual red shift, which is nothing but the origin of the red edge excitation shift (REES) [50,51]. Furthermore, a competition between solvation time and probe lifetime critically controls the detection of heterogeneity through REES [52–54].

We measured the excitation wavelength (λ_{ex}) dependent emission maxima (λ_{em}) of C153 dissolved in 0.5Ac/0.3Ur/0.2Sor DES and observed a REES of 10 nm (346.3 cm^{-1}) at 303 K (Figure 1c and section S4 of Supplementary Material). However, as the transition did not get saturated, it was difficult to comment on the actual value of REES. Azumi *et al.* suggested that the absolute value of REES can be obtained by taking the emission spectra at very high temperatures where all the emissions are expected to originate from a completely solvated state [55,56]. In this way, a REES of ~11.5 nm (~400 cm^{-1}) was calculated for C153 in 0.5Ac/0.3Ur/0.2Sor DES that indicated the presence of moderate spatial heterogeneity, with respect to the lifetime of C153 at 303 K (Table 2).

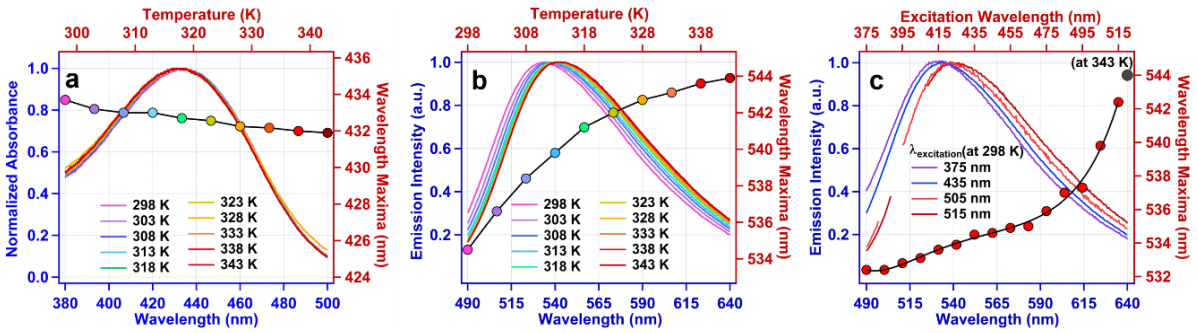

Figure 1. Steady-state (a) absorption and (b) emission spectra of C153 dissolved in 0.5Ac/0.3Ur/0.2Sor DES. (c) Excitation wavelength-dependent emission of C153 in this DES at 298K. Here axes are colour-coded. Similar colour axes imply the respective X and Y axis for the data plotted. In the case of excitation wavelength-dependent emission, the red data points are plotted concerning red axes.

Table 2: Excitation dependent emission maxima of coumarin 153 in 0.5Ac/0.3Ur/0.2Sor DES.

λ_{ex} (nm)	λ_{em}^{max} (nm)	$\bar{\nu}_{em}^{max}$ (cm^{-1})
375	532.4	18782.9
385	532.4	18782.9
395	532.8	18768.8
405	533.1	18758.2
415	533.6	18740.6
425	533.9	18730.1
435	534.5	18709.1
445	534.6	18705.6
455	534.9	18695.1
465	535.0	18691.6
475	535.9	18660.2
485	537.0	18622.0
495	537.3	18611.6
505	539.8	18525.4
515	542.4	18436.6

3.2.2. Solvation dynamics study: We constructed time-resolved emission spectra (TRES) from the collected wavelength-dependent fluorescence decays (see Figure 2). We measured the solvent response of C153 in 0.5Ac/0.3Ur/0.2Sor DES at different temperatures using the time-dependent fluorescence Stokes shift (TDFSS) method.

TRES in two representative temperatures are shown in Figures 3a and 3b. The calculated $S(t)$ at different temperatures along with the bi-exponential fitting are shown in Figure 3c, and the parameters are tabulated in Table 3.

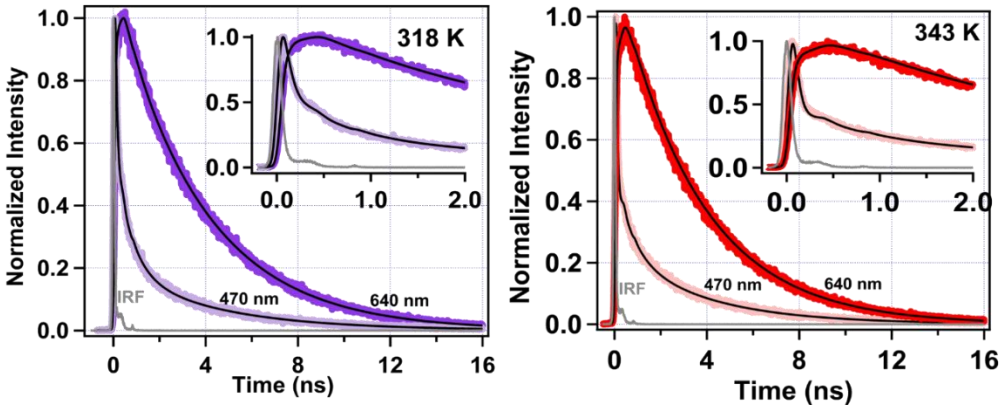

Figure 2: Fluorescence transients at the blue and red edge of steady-state emission of C153 in 0.5Ac/0.3Ur/0.2Sor DES at two extreme experimental temperatures.

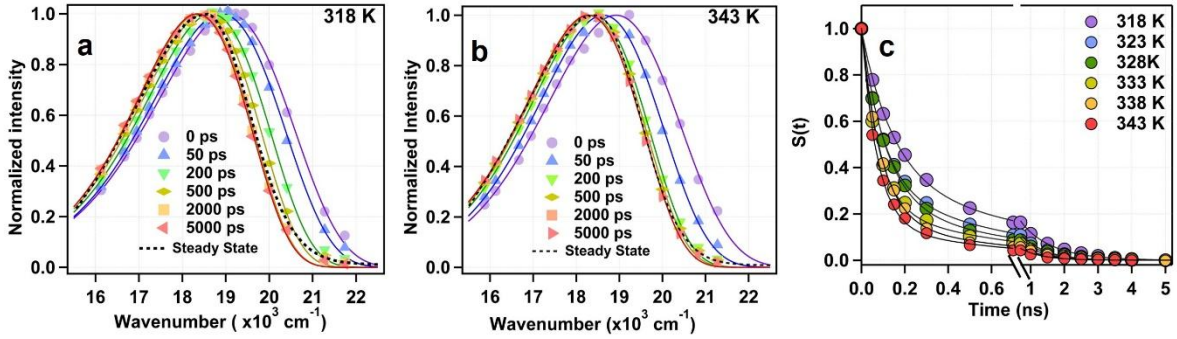

Figure 3. Representative time-resolved emission spectra at (a) 318 K and (b) 343 K. Emission spectra at various times are colour-coded and mentioned in the respective plots. Each steady-state emission spectra at that temperature exciting at the same wavelength as the time-resolved study are represented with a black dashed line. (c) Solvent response functions at different temperatures. Solid lines represent fittings by a bi-exponential function.

Table 3. Bi-exponential fitting parameters of solvent response function $S(t)$ of 0.5Ac/0.3Ur/0.2Sor DES and its viscosities at different temperatures. Note that SS means stokes shift.

Temp (K)	b_1	τ_{S1} (ps)	b_2	τ_{S2} (ps)	$\langle\tau_S\rangle$ (ps)	SS (cm^{-1})	η (cP)	% missed
318	0.65±0.02	150±40	0.35±0.02	950±40	430±50	670±70	482.3±9	47
323	0.67±0.02	100±20	0.33±0.02	690±30	280±30	760±70	307.2±5	41
328	0.75±0.02	110±20	0.25±0.02	730±30	265±35	670±60	202.0±8	51
333	0.77±0.02	80±10	0.23±0.02	670±20	215±25	770±80	141.0±8	44
338	0.83±0.02	90±10	0.17±0.02	670±10	190±20	650±50	90.3±6	53

343	0.85±0.02	70±10	0.15±0.02	640±10	155±20	650±60	66.3±8	54

The average solvation time of 0.5Ac/0.3Ur/0.2Sor DES at 318 K was found to be 430 ps, which decreases to 156 ps at 343 K. The solvent responses are characterized by a fast component (~150-70 ps) with 65-85 % contribution and a relatively slower component (~950-640 ps) with 15-35% contribution. The amplitude of the fast component increases, whereas the slow component decreases with an increase in temperature. The missing percent, calculated from the Fee-Maronceli method [57], was around 40-50 % for temperature values. Previously, DESs were also reported with a missing percentage in this range or higher using the picosecond TDFSS method [53,54,58]. The estimated large missing percentage is probably due to the presence of ultrafast solvation component in 0.5Ac/0.3Ur/0.2Sor DES. Measurement with better time resolution may catch the information that was missed here.

It can be observed from Figure 3c that with an increase in temperature, the temporal decay of solvent response function becomes faster, which may be thought to be solely associated with the viscosity drop of the medium. However, solvation time decreases about 2.7 times on raising the temperature from 318 K to 343 K, while viscosity decreases ~7.3 times. It hints that the medium viscosity does not solely control the solvation of C153 in 0.5Ac/0.3Ur/0.2Sor DES. To see the relationship between medium viscosity and solvation time, we plotted the average solvation time as a function of temperature-reduced viscosity in a double logarithmic fashion, and the slope (*p*-value) is 0.45 (Figure 4a). If simple diffusion controls the solvation, then a near unity *p*-value should have been observed. That is the case when Jin *et al.* examined the solvation dynamics of C153 in normal H-bonded solvents and 21 room-temperature ionic liquids [59]. In the present case, a pronounced fractional viscosity dependence indicates the existence of dynamic heterogeneity in the medium. We also estimated the activation energy (E_s^a) associated with the solvation dynamics as 33.27 kJ mol^{-1} (Figure 4b), which is ~2.2 times less than the

activation energy of viscous flow (E_η^a = 72.35 kJ mol^{-1}) (Figure 4c). This result also shows the deviation of solvation dynamics from the medium viscosity.

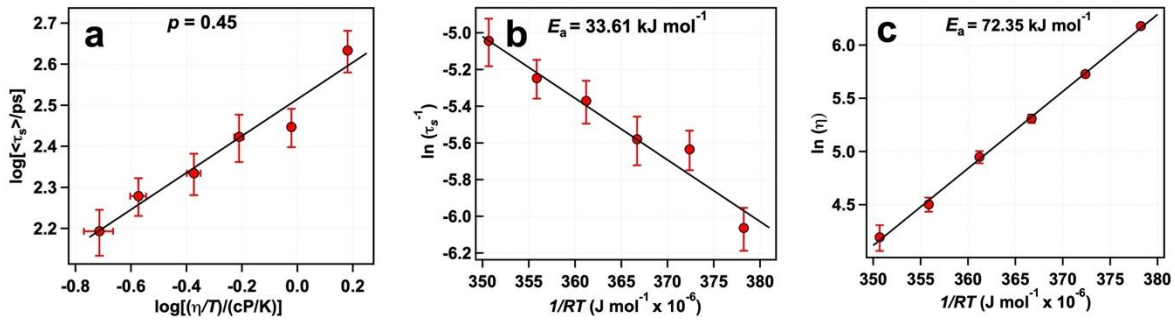

Figure 4. (a) Log-log plot of average solvation time ($\langle\tau_s\rangle$) vs temperature-reduced viscosity, $\left(\frac{\eta}{T}\right)$, with a linear fit (solid black line). (b) Arrhenius plot of average solvation time and (c) activation energy of viscous flow plot.

3.2.3. Dielectric relaxation study

Dielectric relaxation spectroscopy (DRS) is an extensively used technique to measure the frequency-dependent dielectric response of a dipolar system by applying an external electric field. The interaction of the electric field with a dipolar system in the broad frequency range gives information about the collective reorientation dynamics. DRS is a non-invasive technique and complements fluorescence spectroscopic results in a better way. We have performed temperature-dependent (318-343 K) DRS measurements to collect information about the relaxation dynamics of the dipolar constituents of 0.5Ac/0.3Ur/0.2Sor DES system in the GHz region.

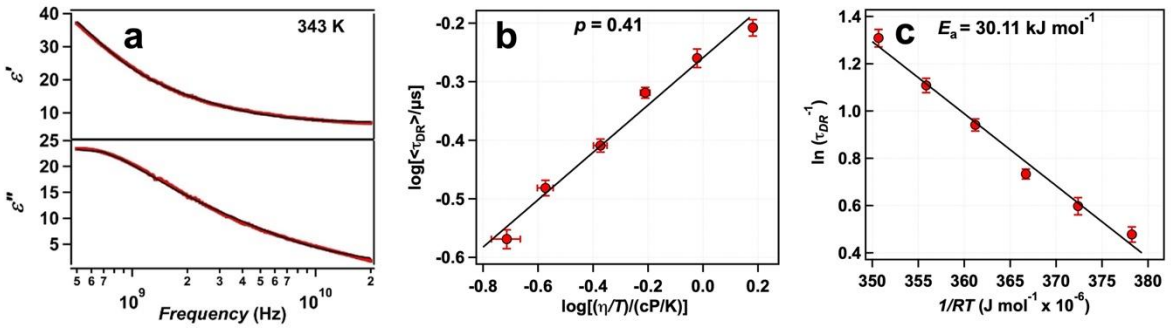

Figure 5. (a) Representative real (ε') and imaginary (ε'') parts of the complex dielectric spectra of 0.5Ac/0.3Ur/0.2Sor DES at 343 K with 2-Debye fit (solid black lines). (b) Log-log plot of average DR time $\langle\tau_{DR}\rangle$ vs temperature-reduced viscosity, $\left(\frac{\eta}{T}\right)$ with the linear fit represented by the solid black line. (c) Arrhenius plot of average DR time.

As representative data, we show the real (ε') and imaginary (ε'') parts of the complex dielectric spectra at 343 K with a 2-Debye fitting in Figure 5a. All the temperature dependent dielectric spectra along with their respective 2-Debye fitting lines are given in Figure 6.

The necessary parameters obtained are summarized in Table 4. Two-time components are obtained from the fitting, one in the range of sub-nanosecond (τ_1) and another in the picosecond (τ_2). As expected, the long-time component dominates the relaxation (amplitude ~90%) and decreases with increasing temperature. The short-time component is found to be temperature insensitive. The average DR time also decreases with temperature, and to explore the relationship with the medium viscosity we plotted it against temperature-reduced viscosity in a log-log graph in Figure 5b. The obtained *p*-value 0.41 indicates substantial dynamic heterogeneity. The estimated activation energy (E_{DR}^{a}) associated with the dielectric relaxation dynamics is 30.1 kJ mol^{-1} (Figure 5c), which is ~2.4 times less than the activation energy of viscosity (E_{η}^{a} = 72.3 kJ mol^{-1}). This difference in activation energy associated with reorientational dynamics (DR dynamics) and viscosity is reflected in the *p*-value as well.

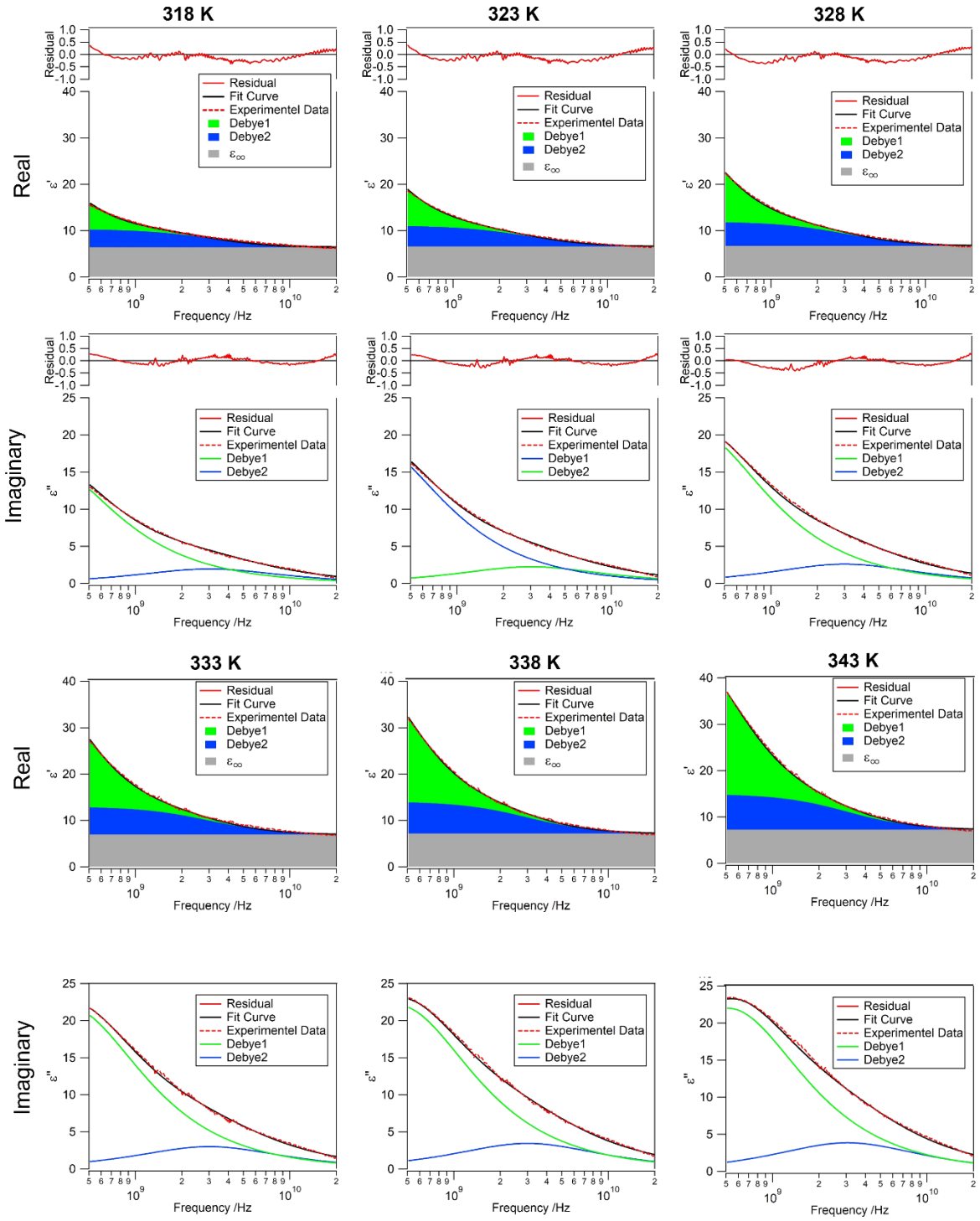

Figure 6: Fitting of real (ε') and imaginary (ε'') part of the complex dielectric spectra of 0.5Ac/0.3Ur/0.2Sor DES at different temperatures with the 2-Debye fit. The upper panel for each temperature represents the real part whereas the lower is the imaginary part.

Table 4. Temperature-dependent fitting parameters obtained from simultaneous 2-Debye fits to real (ε') and imaginary (ε'') components of the measured DR spectra for 0.5Ac/0.3Ur/0.2Sor DES.

Temp (K)	$\Delta\varepsilon_1$	τ_1 (ns)	$\Delta\varepsilon_2$	τ_2 (ns)	$\langle\tau_{DR}\rangle$ (ns)	ε_∞
318	33.6 ±0.19	0.69±0.02	3.9 ±0.16	0.053±0.002	0.62±0.02	6.37
323	38.5 ±0.08	0.61±0.02	4.5 ±0.12	0.053±0.002	0.55±0.02	6.54
328	41.7 ±0.08	0.53±0.01	5.2 ±0.08	0.053±0.001	0.48±0.01	6.68
333	43.8 ±0.25	0.44±0.01	6.0 ±0.08	0.053±0.001	0.39±0.01	6.89
338	44.2 ±0.26	0.37±0.01	6.9 ±0.09	0.053±0.001	0.33±0.01	7.10
343	44.0 ±0.12	0.31±0.01	7.7 ±0.09	0.052±0.001	0.27±0.01	7.19

3.2.4. Rotational dynamics study:

Temperature ($318\,K \leq T \leq 343\,K$) dependent fluorescence anisotropy decays ($r(t)$) of C153 in 0.5Ac/0.3Ur/0.2Sor DES along with its fitting line with a bi-exponential function, $r(t) = c_1 e^{\frac{-t}{\tau_{r1}}} + c_2 e^{\frac{-t}{\tau_{r2}}}$, are depicted in Figure 7a and the fitting parameters are tabulated in Table 5. The initial anisotropy value of C153 was taken as 0.376 [16]. $r(t)$ is characterized by a fast sub-nanosecond time component and a dominant slow component (~90%) of a few nanoseconds. With an increase in the temperature, both the amplitude and the component of the faster time constant increase, while, the slower time component and its amplitude decrease. As a result, with increasing temperature, the average rotational time ($< \tau_r >$) decreases from ~5 ns to ~1.5 ns from 318 K to 343 K.

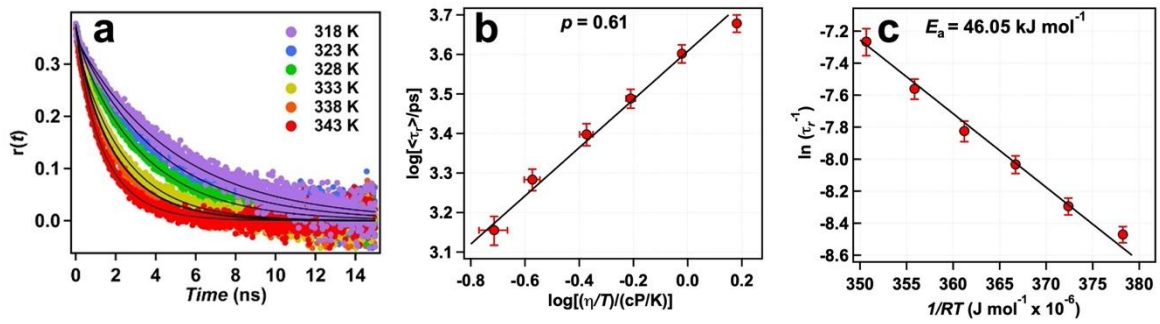

Figure 7. (a) Fluorescence anisotropy decays of C153 in 0.5Ac/0.3Ur/0.2Sor DES at different temperatures with a bi-exponential fit (solid black lines). (b) Log-log plot of average rotational diffusion time (τ_r) vs temperature-reduced viscosity (η/T) with the linear fit represented by a solid black line. (c) Arrhenius plot of average probe rotational time.

Table 5. Biexponential fitting parameters of fluorescence anisotropy decays *r(t)* in 0.5Ac/0.3Ur/0.2Sor DES at different temperatures.

Temp (K)	c_1	τ_{r_1} (ps)	c_2	τ_{r_2} (ps)	$\langle\tau_r\rangle$ (ps)
318	0.04±0.02	110±40	0.96±0.02	4960±150	4770±240
323	0.04±0.02	110±30	0.96±0.02	4160±130	4000±210
328	0.09±0.02	290±60	0.91±0.02	3360±110	3080±170
333	0.08±0.02	220±40	0.92±0.02	2700±120	2500±160
338	0.16±0.02	580±30	0.84±0.02	2170±100	1920±120
343	0.20±0.02	610±20	0.80±0.02	1640±120	1430±120

We plotted the average rotational time $\langle\tau_r\rangle$ as a function of temperature-reduced viscosity $\left(\eta/T\right)$ in log-log fashion (Figure 7b) to identify how extensively the medium viscosity controls the solute (C153) rotation in 0.5Ac/0.3Ur/0.2Sor DES. Interestingly, we found a substantial decoupling of rotational motion from the viscosity with p≈0.61. Such fractional viscosity dependence might arise from various factors like the non-spherical shape of the probe molecule, the non-continuum nature of the solvent medium, specific interaction between solvent and

solute, and non-Brownian motion like large angle jumps and inertia-driven motion especially in a viscous liquid, apart from the dynamical heterogeneous characteristics of the media. Normally, the formation of DES is explained by strong H-bond formation between its constituents [26,27]. In the present case, where all the constituents are non-ionic, the solvent could be identified as an H-bonded solvent. For typical H-bonding solvents, Horng *et al.* demonstrated that the rotation of C153 exhibits a power-law dependency on the viscosity with p=0.96 [16]. This study eliminates the possibility of non-sphericity and specific interaction induced break down on SED relationship. In another study, Jin *et al.* demonstrated that there is no specific interaction between C153 and 21 ionic liquids [59]. Using these data, Guchhait *et al.* calculated a near unity p-value of the system [44]. This observation somewhat eliminates the probability of fractional dependence of viscous liquids (like in our case) due to non-Brownian motion. Although it is very difficult to ascertain how much of the decoupling between average rotational time and viscosity originates from the violation of the assumptions stated in the SED relationship or from the underlying microscopic heterogeneity, the preceding discussion strongly hints toward the presence of dynamic heterogeneity in corresponding length (nm) and time (ns) scale.

The estimated activation energy (E_r^a) associated with rotational dynamics of C153 is ~46 kJ mol^{-1} (Figure 7c), which is ~1.6 times smaller than the activation energy (E_η^a) associated with the viscous flow of the system. This observation also supports that the fractional viscosity dependency of rotational dynamics leads to the dynamic heterogeneity of the medium.

3.2.5. Translational dynamics study

We measured the fluorescence intensity autocorrelation function of R6G in 0.5Ac/0.3Ur/0.2Sor DES at various temperatures (318 K to 343 K) (Figure 8) to investigate translational diffusion dynamics through FCS [60,61]. To begin with, we

fitted our data by simple Stokes-Einstein diffusion (normal diffusion model with one diffusion coefficient). The fitting quality is found to be reasonably good, and the fitting parameters are tabulated in Table 6.

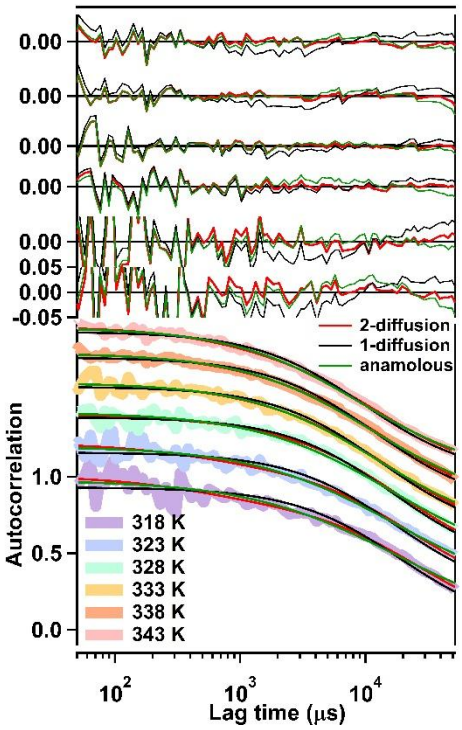

Figure 8. Translational dynamics via single molecular level FCS. Normalized fluorescence intensity autocorrelation curve of R6G in 0.5Ac/0.3Ur/0.2Sor DES at different temperatures. Fitting lines using the model of single-particle normal diffusion, single-particle anomalous diffusion, and two-component normal diffusion are shown by solid black, green, and red lines, respectively. The respective residuals of fittings are also shown with the same colours.

Table 6: Fitting parameter of fluorescence intensity autocorrelation function of R6G in 0.5Ac/0.3Ur/0.2Sor DES at different temperatures with single component diffusion model and anomalous diffusion model.

Temp (K)	τ_{1D} (μs)	$\tau_{anamolous}$ (μs)	α
318	19043	17670	0.73
323	17838	16830	0.76
328	16500	16000	0.8

333	13345	12726	0.85
338	11992	11303	0.85
343	9671	9027	0.86

In this case, the observed *p*-value from the log-log plot of the average translational diffusion time ($\langle\tau_D\rangle$) and temperature-reduced viscosity (see Figure 9) is 0.33, which is quite low compared to the *p*-value obtained from solvation dynamics, dielectric relaxation, and fluorescence anisotropy studies. This suggests the existence of higher decoupling in translational dynamics in 0.5Ac/0.3Ur/0.2Sor DES.

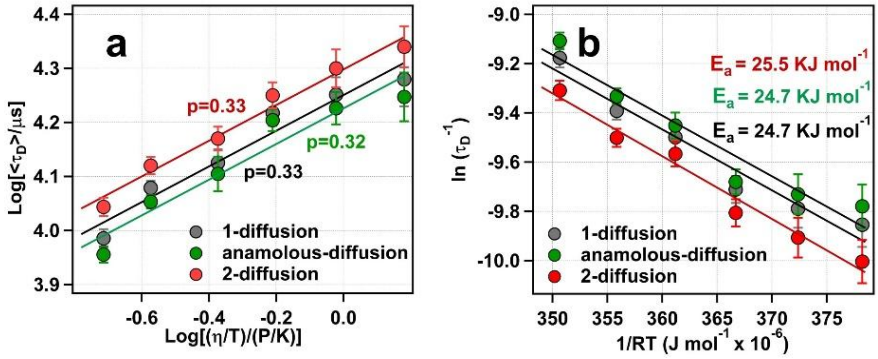

Figure 9. (a) Log-log plot of average translational diffusion time (τ_D) obtained using different fitting models vs temperature-reduced viscosity (η/T) with the linear fit represented by a solid black line. (b) Arrhenius plot of average probe diffusion time obtained from different fittings.

One self-contradicting point is that the fitting parameters that are used in *p*-value calculation are obtained from normal diffusion, yet the *p*-value showed a significant deviation from normal diffusion. A close inspection of the fitting lines and fit residues reveals that the fitting is not perfect. Generally, diffusion in a complex environment is described by anomalous diffusion. For such diffusion, another parameter known as anomalous coefficient is required to describe the autocorrelation traces. The fitting results with anomalous diffusion are shown in

Table 6. As can be seen, the introduction of the anomalous coefficient does not significantly improve the quality of the fitting (Figure 8). Except for the first two experimental temperatures, the values of anomalous exponent are also close to 1, hinting that the diffusion is primarily normal SE diffusion. The *p*-value obtained in this way (0.32, Figure 9a) is also very similar to what was obtained using the normal diffusion model (0.33, Figure 9a). In the case of heterogeneous distribution, a probe can show multi-diffusion phenomena. This is not rare in complex liquid systems [41,62–64]. Inspired by this fact, we fitted our autocorrelation functions with a two-diffusion equation (described in the experimental section) (see Figure 8 for the fitting result and Table 7 for the fitting parameters).

Table 7. Fitting parameters of fluorescence intensity autocorrelation functions of R6G in 0.5Ac/0.3Ur/0.2Sor DES at different temperatures with two component diffusion model.

Temp (K)	τ_{D1} (µs)	N_1	τ_{D2} (µs)	N_2	$\langle\tau_D\rangle$ (µs)
318	500±60	0.18±0.02	26900±1400	0.82±0.02	22150±1700
323	520±50	0.15±0.02	23500±1200	0.85±0.02	20050±1500
328	1000±90	0.07±0.02	19400±600	0.93±0.02	18110±930
333	1430±120	0.14±0.02	17000±500	0.86±0.02	14820±760
338	1200±30	0.14±0.02	15400±400	0.86±0.02	13410±630
343	980±60	0.17±0.02	13100±300	0.83±0.02	11040±500

It is clear that the fitting quality improved greatly. The slower diffusion component is very much like what we obtained from the fitting by one diffusion equation and shows somewhat similar temperature dependence. Another diffusion component is fast and surprisingly remains more or less constant with changes in temperature/viscosity (Table 7). The log-log plot with the average diffusion time vs temperature-reduced viscosity yielded a similar *p*-value of 0.33 (Figure 9a). Arrhenius's analysis with the average diffusion time also yielded similarl $E_\eta^a = 25.5\, kJ\, mol^{-1}$ as in the case of average diffusion times with 1-diffusion and

anomalous fitting ($E_\eta^a \sim 24.7\ kJ\ mol^{-1}$, Figure 9b). To the best of our knowledge, the origin of the two-time constant cannot be assigned confidently. However, the need for the second diffusion component might have arisen from the inherent heterogeneity of the system, which was reflected in the excitation wavelength dependence of the fluorescence emission in this DES. This kind of bimodal diffusion was observed in various ILs [62–64]. Patra *et al.* reported a similar kind of bimodal diffusion in methylimidazolium ILs of different chain lengths and commented on the presence of dynamic heterogeneity therein [62]. Hu *et al.* showed the presence of spatial heterogeneity in IL with the help of an excitation wavelength-dependent emission study [65]. With the help of MD simulation, Wang *et al.* proved such different domain formations in IL lead to heterogeneous environment formation, which smears out in the higher temperature range and behaves homogeneously [4]. Our data also somehow follows this kind of behaviour as with the increase in temperature the ACFs become better fitted with one diffusion than the lower temperature ACFs. In a work by Guo *et al.* with [C$_n$MPy][Tf$_2$N] RTILs of varying alkyl chain length two diffusion components were observed using FCS [64]. The authors argued that mesostructure heterogeneity is responsible for this phenomenon following the analogy that the translational diffusion rate of R6G differs depending upon the spatial region of the RTIL the probe molecule is experiencing [64].

The significant deviation of the *p*-value from unity suggests a breakdown of hydrodynamic viscosity dependence of solute diffusion. This deviation may be attributed to dynamic heterogeneity resulting either from spatially different diffusive relaxation rates due to inhomogeneous solution structure or from accessing the nonhydrodynamic modes owing to large angular jump, hopping, etc [66–69]. In 2018, Gan *et al.* showed that the breakdown of SE relationship in supercooled water can arise from the temperature dependency of the effective hydrodynamic radius instead of being a constant as assumed in the SE model [70]. Very recently Shao *et al.* also showed that the deviation of SE relationship in aqueous ionic solution might be appreciated by accounting the change of hydrodynamic radius of the ions [71].

However, keeping aside the reason for such viscosity decoupling, one needs to be sure if the decoupled diffusion dynamics is a characteristic feature of DES or can be invariably seen in other molecular liquids as well. In a cross-experiment previously reported by our group with DMF [41], a decoupled diffusion with a *p*-value of 0.82 was obtained. The aspherical positively charged nature of R6G dye and DMF not being a structureless continuum was suggested for such observation [41]. In the present case, the *p*-value is much lower than 0.82, which can be taken as an indication of the presence of dynamic heterogeneity in the system. Overall, this high decoupling (p~0.33) in the case of translational motion of the dye in this medium hints that the dye molecule does not feel the medium viscosity while diffusing. This result can be extended to understand the enzyme/substrate diffusion in case of enzymatic activity inside such viscous DES media or any alternative media in general.

3.2.6. Comparison with Similar DESs

We collected results from various acetamide-based DESs because a comparison might provide additional insight. Many acetamide-based ionic DESs were studied previously, and all of them showed considerable spatial and dynamic heterogeneity[17,18,40–44] unlike 0.6Ac/0.4Ur DES [19,38]. Replacing urea with electrolytes introduces substantial heterogeneity both in terms of spatial and dynamical arrangement [17,18,40–44]. Recently, Mukherjee *et al.* studied the microscopic heterogeneity of a DES made of acetamide, urea, and PEG-300 (0.55Ac/0.36Ur/0.09PEG) [20]. The introduction of PEG-300 introduces a mild dynamic heterogeneity in the system [20]. Here, for the comparison between non-ionic acetamide-based DESs, we have taken the previously reported data and measured them, if needed, and introduced all of them in a normalized log-log plot to show the extent of deviation in terms of dynamic heterogeneity with the present system. We have measured temperature-dependent solvation dynamics of 0.55Ac/0.36Ur/0.09PEG DES, which was previously absent in the literature. The

details of those temperature-dependent solvation dynamics measurements are provided in Figure 10 and Table 8.

The log-log plot of average solvation time ($\langle\tau_s\rangle$) *vs* $\frac{\eta}{T}$ of the two acetamide-based non-ionic DESs along with the presently studied system is shown in Figure 12a. From the figure, it is clear that solvation dynamics is almost coupled with medium viscosity in 0.6Ac/0.4Ur DES (p=0.85), but the introduction of PEG-300 (in 0.55Ac/0.36Ur/0.09PEG DES) induces a mild decoupling (p=0.74) which become more pronounced (*p*=0.45) in the case of addition of sorbitol (in 0.5Ac/0.3Ur/0.2Sor DES).

The extent of decoupling in the case of inherent dynamics (in GHz region) for all three DESs follows a similar trend as in solvation dynamics (Figure 12b). In the case of 0.55Ac/0.36Ur/0.09PEG DES, the previous work reported the decoupling in dielectric relaxation using only the first component of relaxation time [20]. To keep the uniformity in the comparison, we plotted the first component of relaxation time τ_1 (using the 2-Debye model) instead of $\langle\tau_{DR}\rangle$ in Figure 12b. However, in our case, the *p*-value obtained for $\langle\tau_{DR}\rangle$ or τ_1 are almost similar.

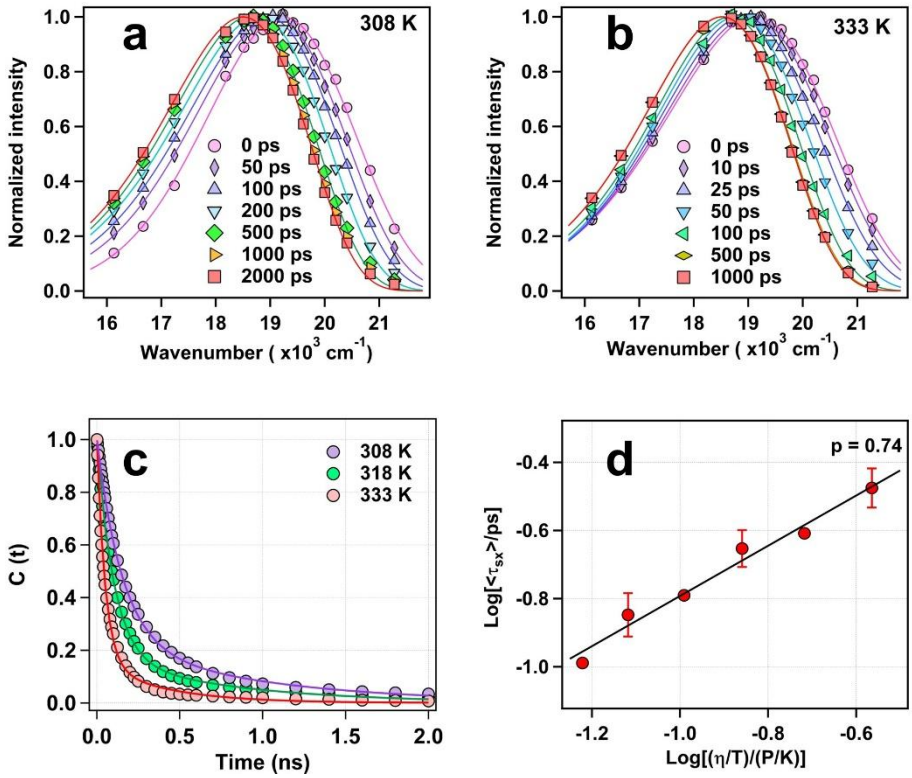

Figure 10. Representative time-resolved emission spectra of 0.55Ac/0.36Ur/0.09PEG DES at (a) 308 K and (b) 333 K. Emission spectra at various times are colour-coded and mentioned in the respective plots. (c) Representative solvent response functions at different temperatures are shown in color-coded manner. Solid lines represent fittings by a bi-exponential function. (d) Log-Log plot of average solvation time $\langle\tau_s\rangle$ vs temperature reduced viscosity, $\left(\frac{\eta}{T}\right)$, with a linear fit (solid black line).

Table 8: Biexponential fitting parameters of solvent response function S(t) of 0.55Ac/0.36Ur/0.09PEG DES and its viscosity at different temperatures.

Temp (K)	b_1	τ_{S1} **(ps)**	b_2	τ_{S2} **(ps)**	$\langle\tau_S\rangle$ **(ps)**	η **(cP)**
318	0.76±0.02	151±50	0.24±0.02	920±70	335±44	84
323	0.80	101	0.20	820	246	60
328	0.82±0.03	102±20	0.18±0.03	780±50	222±28	44
333	0.86	78	0.14	700	162	33
338	0.87±0.03	67±10	0.13±0.03	660±50	142±21	25

343	0.85	50	0.15	400	103	20

The heterogeneity in terms of rotational dynamics for 0.55Ac/0.36Ur/0.09PEG DES is characterized by p=0.74, which is substantially lower compared to the 0.6Ac/0.4Ur DES (p=0.96, Figure 12c). In the case of 0.5Ac/0.3Ur/0.2Sor DES, we estimated p=0.61 from fluorescence anisotropy. We had to measure the temperature-dependent translational dynamics of the 0.55Ac/0.36Ur/0.09PEG DES employing FCS. Related normalized intensity autocorrelation functions with fitting and the time components extracted can be found in Figure 11 and Table 9.

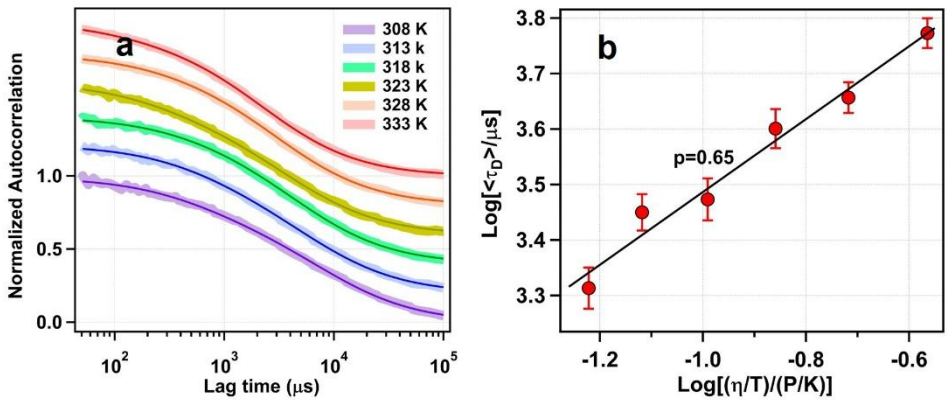

Figure 11: Translational dynamics via single molecular level FCS. (a) Normalized fluorescence intensity autocorrelation curve of R6G in 0.55Ac/0.36Ur/0.09PEG DES at different temperatures. Fitting lines are shown by solid lines. (b) log-log plot of average translational diffusion time (τ_D) vs temperature reduced viscosity (η/T) with the linear fit represented by the solid black line.

Table 9: Fitting parameters of fluorescence intensity autocorrelation function of R6G in 0.55Ac/0.36Ur/0.09PEG DES at different temperatures with two component diffusion model.

Temperature (K)	N_1	N_2	τ_{D1} (μs)	τ_{D2} (μs)	$\langle\tau_D\rangle$ (μs)
308	0.34±0.02	0.66±0.02	687±50	8585±500	5926±368

313	0.33±0.02	0.67±0.02	811±60	6396±400	4534±290
318	0.22±0.02	0.78±0.02	662±50	4937±400	3987±323
323	0.29±0.02	0.71±0.02	339±40	4056±350	2972±259
328	0.19±0.02	0.81±0.02	400±40	3368±250	2817±212
333	0.15±0.02	0.85±0.02	150±20	2390±200	2056±176

The viscosity decoupling, in this case, is pronounced compared to 0.6Ac/0.4Ur DES but less compared to the system under investigation (Figure 12d). Taken together, one sees that the introduction of a non-ionic third component to an already known DES introduces substantial microscopic heterogeneity.

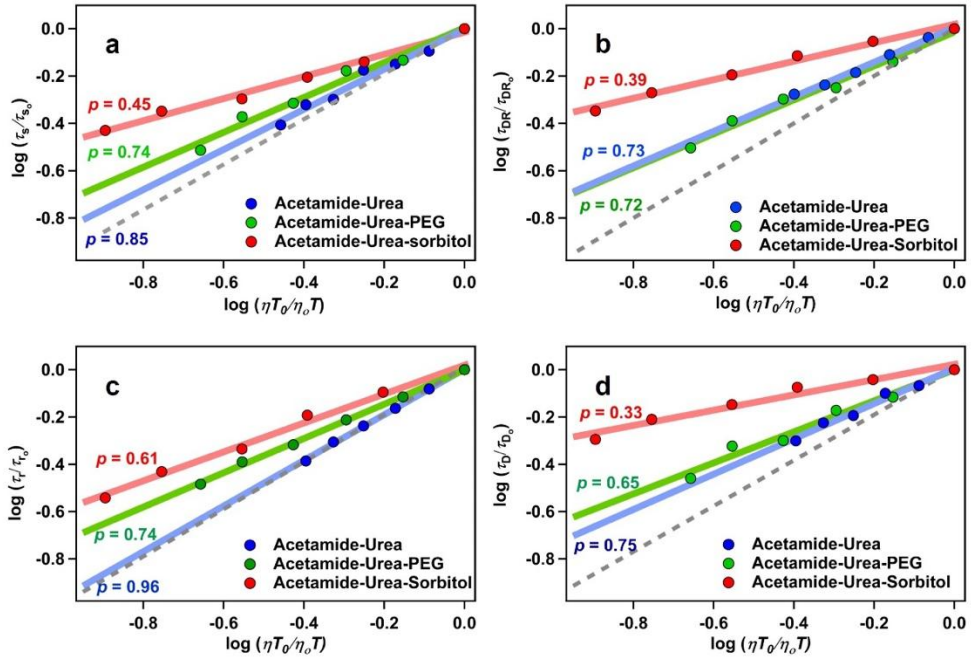

Figure 12. Log-log plots of normalized (a) average solvation time, (b) average DR time, (c) average rotational time, and (d) average diffusion time, with temperature-reduced normalized viscosity. Here normalization has been done by taking the lowest experimental temperature; average time and viscosities at that respective lowest investigated temperature. Grey broken lines indicate the dynamics guided by the Stokes-Einstein equation(i.e. p=1).

Overall, an additive-induced heterogeneity is somehow prominent in this study. One very interesting but contradicting study from the Abbott group needs to be cited here where they have investigated diffusion in ethaline (0.33 choline chloride / 0.66 ethylene glycol) DES in presence of various additives [72]. They have chosen the additives as glucose, 1-pentanol, and phenol among which glucose is a room temperature solid and pentanol is a liquid and phenol is a liquid only above 313 K. The interesting finding was that adding glucose increases the bulk viscosity of the system whereas the other two additives reduce it. The addition of glucose to the DES makes the choline ion (Ch^+) diffusion Stokesian type, whereas, in the case of both phenol and 1-pentanol Ch^+ diffuses in a phase that is more viscous than the bulk viscosity, indicating heterogeneities in the mixture. In the case of phenol, a change in the slope for the diffusion trend after 313 K has also been observed [72]. This finding suggests that solid additives favour the formation of a homogenous mixture, whereas liquid additives favour the formation of a heterogeneous mixture. The authors assumed that the hydrogen bonding strength between the solute and the solvent (DES) has a major role to play. A similar study by Agostino *et al.* showed that when water was added to ethaline, a heterogeneous liquid was formed [73]. In the present case, both sorbitol (solid additive) and PEG-300 (liquid additive) induce a higher heterogeneity in the Ac/Ur DES, though, in the case of sorbitol, the heterogeneity is much more prominent than that of PEG-300. However, such a conclusion cannot be conjectured from the smaller number of available studies, and more research is needed.

3.3. Potential Implications of Dynamic Heterogeneity in Reactions/Biocatalysis inside DES:

Our report deciphers the molecular-level heterogeneity of the non-ionic 0.5Ac/0.3Ur/0.2Sor DES in various lengths and timescales. Though such heterogeneity has been routinely observed for many ILs and DESs for many years, implications of such studies in explaining biocatalysis or any reaction are uncommon

in the literature. As we already showed this DES to be a potential biocatalytic medium[74], we tried to contemplate if this study has some implications in explaining the enzyme's activity in such a medium. All the dynamics measured in this medium are very much decoupled from the medium viscosity and the most pronounced decoupling can be observed in the case of diffusion dynamics. Normally, biocatalysis involves the reaction of large biomolecules, which is mainly guided by the diffusion of enzymes and substrates towards each other. The less *p*-value (~0.33) in the case of translational motion of the dye in this medium hints that the molecule does not feel the medium viscosity as such. This result can be extended to the enzyme/substrate to explain the enzymatic activity inside viscous DES media. On the other hand, solvation dynamics tells how fast the probe is being solvated by the medium. For a reaction, especially in the case of biocatalysis, it is thought that the associated water dynamics plays a major role in controlling the enzymatic activity [75,76]. In the present case, the biocatalytic medium shows a strong viscosity decoupled solvation dynamics (p=0.45), suggesting that the probe is surrounded by much flexible solvent molecules compared to what one expects from the bulk viscosity.

To have a better insight we estimated the viscosity decoupling of the two solvation components individually (Figure 13). Normally, the origin of the short component is believed to be from the immediate solvation shell of the probe, whereas the contribution from the extended solvation shell reflects upon a long component of the solvation dynamics. Our analysis reveals that the faster time components are severely viscosity decoupled (p=0.16) suggesting that the first solvation shell remains almost intact in this DES (Figure 13c). It might have a huge implication as to why DES, being so viscous, can still be so efficient as a solvent media for various reactions. In the case of the other two DESs under investigation (Ac/Ur and Ac/Ur/PEG), the p-values for individual components are given in Figures 13a and 13b. One can see that the p-value of the first component is more viscosity decoupled than the second one in all cases. However, the extent of decoupling is much less in these cases compared to Ac/Ur/Sor DES. It suggests that 0.5Ac/0.3Ur/0.2Sor DES

might be a better choice as a potential reaction/biocatalytic media than the other two as the probe is experiencing much lesser viscosity than the other two DESs. Obviously, more work is needed in this regard, especially in understanding these systems in the presence of enzymes. Our future studies, taking actual enzymes, may provide further useful insights into this speculation.

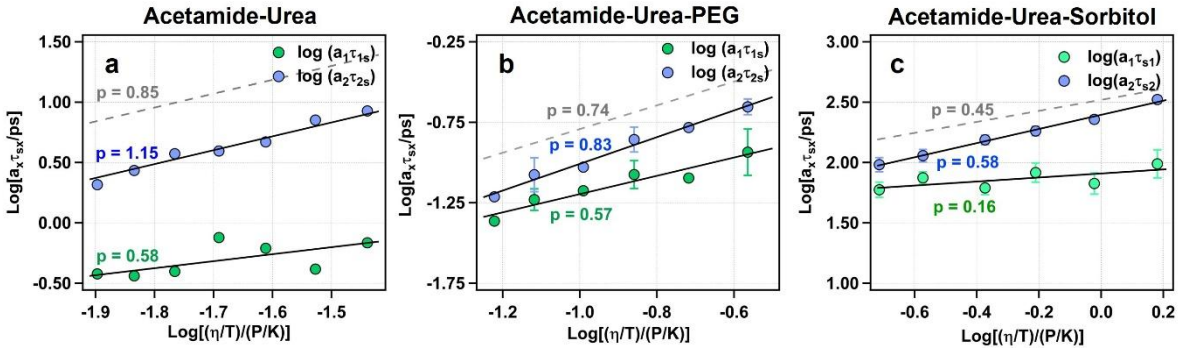

Figure 13. Log-log plots of time components of solvation dynamics along with its contribution vs temperature reduced viscosity (η/T), with a linear fit (solid black line) for (a) 0.6Ac/0.4Ur DES, (b) 0.55Ac/0.36Ur/0.09PEG DES, and (c) 0.5Ac/0.3Ur/0.2Sor DES. The black dashed line here represents the fitting line with average solvation time and the corresponding p-value is written in the same colour.

3.4. Conclusion

One important way to fine-tune DESs properties is the addition of a third component in binary DESs. The addition of sorbitol in the binary acetamide/urea DES forms a ternary 0.5Ac/0.3Ur/0.2Sor DES that has a much lower melting point [46]. and is found suitable for practical application [47]. The present work demonstrates spatial and dynamic heterogeneity in 0.5Ac/0.3Ur/0.2Sor DES using steady-state, time-resolved fluorescence, dielectric relaxation, and single molecular level FCS studies.

We observed a considerable shift in the excitation wavelength-dependent emission maxima of a solvatochromic dye (C153) suggests that the system possesses considerable spatial heterogeneity. The fractional viscosity decoupling (p~0.4) of average solvation time suggests the presence of dynamic heterogeneity in the system

in the length (nm) and time (ps-ns) scale of solvation dynamics. The inherent dynamics of the medium explored using DR measurement also show a substantial decoupled dynamic (p~0.62). The average rotational time of the probe also shows a medium viscosity decoupling (p~0.6) suggesting a definitive but probably weaker dynamic heterogeneity in the length (10 nm) and time (ns) scale of anisotropy measurement. For translational dynamics, which provides information at a much larger length (μm) and timescale (μs-ms), we observed the strongest decoupling (p~0.3) from medium viscosity suggesting a very strong dynamic heterogeneity at this higher length and time scale. Using the Arrhenius equation, we determined the activation energy of viscous flow and various dynamics that also reinforce the conclusion of strong dynamic heterogeneity of the system, which depends on the length and timescale of the measurement. The addition of PEG instead of sorbitol introduces mild dynamic heterogeneity both in translational (p~0.41) and rotational (p~0.74) motion, but no spatial heterogeneity. One possible reason might be the physical state of the third component (sorbitol is solid, while PEG is liquid). Future studies are necessary to understand the actual reason for the differential behaviour of these two additives, in which neutron scattering and MD simulation might help immensely. Overall, the present study might be beneficial to understand the transition of binary to ternary DESs and how the addition of a third component controls the macroscopic and microscopic properties of the DESs.

3.5. References

(1) Töpfer, K.; Pasti, A.; Das, A.; Salehi, S. M.; Vazquez-Salazar, L. I.; Rohrbach, D.; Feurer, T.; Hamm, P.; Meuwly, M. Structure, Organization, and Heterogeneity of Water-Containing Deep Eutectic Solvents. *J. Am. Chem. Soc.* **2022**, *144* (31), 14170–14180.

(2) Krahn, J. R.; Lodge, T. P. Spatial Heterogeneity of Solvent Dynamics in Multicomponent Polymer Solutions. *J. Phys. Chem.* **1995**, *99* (20), 8338–8348. https://doi.org/10.1021/j100020a069.

(3) Kienle, D. F.; Falatach, R. M.; Kaar, J. L.; Schwartz, D. K. Correlating Structural and Functional Heterogeneity of Immobilized Enzymes. *ACS Nano* **2018**, *12* (8), 8091–8103.

(4) Wang, Y. L.; Li, B.; Sarman, S.; Mocci, F.; Lu, Z. Y.; Yuan, J.; Laaksonen, A.; Fayer, M. D. Microstructural and Dynamical Heterogeneities in Ionic Liquids. *Chem. Rev.* 2020, pp 5798–5877. https://doi.org/10.1021/acs.chemrev.9b00693.

(5) Ediger, M. D. Spatially Heterogeneous Dynamics in Supercooled Liquids. *Annu. Rev. Phys. Chem.* **2000**, *51*, 99–128. https://doi.org/10.1146/annurev.physchem.51.1.99.

(6) Richert, R. Heterogeneous Dynamics in Liquids: Fluctuations in Space and Time. *J. Phys.: Condens. Matter* **2002**, *14* (23), R703. https://doi.org/10.1088/0953-8984/14/23/201.

(7) Jin, H.; Li, X.; Maroncelli, M. Heterogeneous Solute Dynamics in Room Temperature Ionic Liquids. *J. Phys. Chem. B* **2007**, *111* (48), 13473–13478. https://doi.org/10.1021/jp077226.

(8) Hoshino, T.; Fujinami, S.; Nakatani, T.; Kohmura, Y. Dynamical Heterogeneity near Glass Transition Temperature under Shear Conditions. *Phys. Rev. Lett.* **2020**, *124* (11), 118004. https://doi.org/10.1103/PhysRevLett.124.118004.

(9) Sillescu, H. Heterogeneity at the Glass Transition: A Review. *J. Non-Cryst. Solids* **1999**, *243* (2–3), 81–108. https://doi.org/10.1016/S0022-3093(98)00831-X.

(10) Deschenes, L. A.; Vanden Bout, D. A. Single-Molecule Studies of Heterogeneous Dynamics in Polymer Melts near the Glass Transition. *Science (1979)* **2001**, *292* (5515). https://doi.org/10.1126/science.1056430.

(11) Kumar, P.; Buldyrev, S. V.; Becker, S. R.; Poole, P. H.; Starr, F. W.; Stanley, H. E. Relation between the Widom Line and the Breakdown of the Stokes-Einstein Relation in Supercooled Water. *Proc. Natl. Acad. Sci. USA* **2007**, *104* (23), 9575–9579. https://doi.org/10.1073/pnas.0702608104.

(12) Berthier, L.; Biroli, G.; Bouchaud, J. P.; Cipelletti, L.; El Masri, D.; L'Hôte, D.; Ladieu, F.; Pierno, M. Physics: Direct Experimental Evidence of a Growing Length Scale Accompanying the Glass Transition. *Science (1979)* **2005**, *310* (5755). https://doi.org/10.1126/science.1120714.

(13) Kivelson, D.; Kivelson, S. A.; Zhao, X.; Nussinov, Z.; Tarjus, G. A Thermodynamic Theory of Supercooled Liquids. *Physica A Stat. Mech. Appl.* **1995**, *219* (1–2), 27–38. https://doi.org/10.1016/0378-4371(95)00140-3.

(14) Chen, S. H.; Mallamace, F.; Mou, C. Y.; Broccio, M.; Corsaro, C.; Faraone, A.; Liu, L. The Violation of the Stokes-Einstein Relation in Supercooled Water. *Proc. Natl. Acad. Sci. USA* **2006**, *103* (35), 12974–12978. https://doi.org/10.1073/pnas.0603253103.

(15) Das, N.; Sen, P. Dynamic Heterogeneity and Viscosity Decoupling: Origin and Analytical Prediction. *Phys. Chem. Chem. Phys.* **2021**, *23* (29), 15749–15757. https://doi.org/10.1039/d1cp01804c.

(16) Horng, M. L.; Gardecki, J. A.; Maroncelli, M. Rotational Dynamics of Coumarin 153: Time-Dependent Friction, Dielectric Friction, and Other Nonhydrodynamic Effects. *Journal of Physical Chemistry A* **1997**, *101* (6). https://doi.org/10.1021/jp962921v.

(17) Guchhait, B.; Das, S.; Daschakraborty, S.; Biswas, R. Interaction and Dynamics of (Alkylamide + Electrolyte) Deep Eutectics: Dependence on Alkyl Chain-Length, Temperature, and Anion Identity. *J. Chem. Phys.* **2014**, *140* (10), 104514. https://doi.org/10.1063/1.4866178.

(18) Guchhait, B.; Daschakraborty, S.; Biswas, R. Medium Decoupling of Dynamics at Temperatures ∼100 K above Glass-Transition Temperature: A Case Study with (Acetamide + Lithium Bromidenitrate) Melts. *J. Chem. Phys.* **2012**, *136* (17), 174503. https://doi.org/10.1063/1.4705315.

(19) Das, A.; Das, S.; Biswas, R. Density Relaxation and Particle Motion Characteristics in a Non-Ionic Deep Eutectic Solvent (Acetamide + Urea): Time-Resolved Fluorescence Measurements and All-Atom Molecular Dynamics Simulations. *J. Chem. Phys.* **2015**, *142* (3), 034505. https://doi.org/10.1063/1.4906119.

(20) Mukherjee, K.; Tarif, E.; Barman, A.; Biswas, R. Dynamics of a PEG Based Non-Ionic Deep Eutectic Solvent: Temperature Dependence. *Fluid Phase Equilib.* **2017**, *448*, 22–29. https://doi.org/10.1016/j.fluid.2017.05.003.

(21) Hossain, S. S.; Paul, S.; Samanta, A. Liquid Structure and Dynamics of Tetraalkylammonium Bromide-Based Deep Eutectic Solvents: Effect of Cation Chain Length. *J. Phys. Chem. B* **2019**, *123* (31), 6842–6850. https://doi.org/10.1021/acs.jpcb.9b04955.

(22) Hossain, S. S.; Samanta, A. How Do the Hydrocarbon Chain Length and Hydroxyl Group Position Influence the Solute Dynamics in Alcohol-Based Deep Eutectic Solvents? *Phys. Chem. Chem. Phys.* **2018**, *20* (38), 24613–24622. https://doi.org/10.1039/c8cp04859b.

(23) Mahapatra, A.; Chakraborty, M.; Barik, S.; Sarkar, M. Comparison between Pyrrolidinium-Based and Imidazolium-Based Dicationic Ionic Liquids: Intermolecular Interaction, Structural Organization, and Solute Dynamics.

Physical Chemistry Chemical Physics **2021**, *23* (37). https://doi.org/10.1039/d1cp02790e.

(24) Barik, S.; Chakraborty, M.; Sarkar, M. How Does Addition of Lithium Salt Influence the Structure and Dynamics of Choline Chloride-Based Deep Eutectic Solvents? *J. Phys. Chem. B* **2020**, *124* (14), 2864–2878. https://doi.org/10.1021/acs.jpcb.9b11947.

(25) Hossain, S. S.; Samanta, A. Solute Rotation and Solvation Dynamics in Deep Eutectic Solvents. *Chem. Phys. Impact* **2021**, *3*, 100043. https://doi.org/10.1016/j.chphi.2021.100043.

(26) Smith, E. L.; Abbott, A. P.; Ryder, K. S. Deep Eutectic Solvents (DESs) and Their Applications. *Chem Rev* **2014**, *114* (21), 11060–11082. https://doi.org/10.1021/cr300162p.

(27) Hansen, B. B.; Spittle, S.; Chen, B.; Poe, D.; Zhang, Y.; Klein, J. M.; Horton, A.; Adhikari, L.; Zelovich, T.; Doherty, B. W.; Gurkan, B.; Maginn, E. J.; Ragauskas, A.; Dadmun, M.; Zawodzinski, T. A.; Baker, G. A.; Tuckerman, M. E.; Savinell, R. F.; Sangoro, J. R. Deep Eutectic Solvents: A Review of Fundamentals and Applications. *Chem Rev* **2021**, *121* (3), 1232–1285. https://doi.org/10.1021/acs.chemrev.0c00385.

(28) Florindo, C.; Lima, F.; Ribeiro, B. D.; Marrucho, I. M. Deep Eutectic Solvents: Overcoming 21st Century Challenges. *Curr. Opin. Green Sustain. Chem.* **2019**, *18*, 31–36. https://doi.org/10.1016/j.cogsc.2018.12.003.

(29) Paiva, A.; Craveiro, R.; Aroso, I.; Martins, M.; Reis, R. L.; Duarte, A. R. C. Natural Deep Eutectic Solvents - Solvents for the 21st Century. *ACS Sustainable Chem. Eng.* **2014**, *2* (5), 1063–1071. https://doi.org/10.1021/sc500096j.

(30) Perna, F. M.; Vitale, P.; Capriati, V. Deep Eutectic Solvents and Their Applications as Green Solvents. *Curr. Opin. Green Sustain. Chem.* **2020**, *21*, 27–33. https://doi.org/10.1016/j.cogsc.2019.09.004.

(31) Jablonský, M.; Škulcová, A.; Šima, J. Use of Deep Eutectic Solvents in Polymer Chemistry–a Review. *Molecules*. 2019. https://doi.org/10.3390/molecules24213978.

(32) Padwal, C.; Pham, H. D.; Jadhav, S.; Do, T. T.; Nerkar, J.; Hoang, L. T. M.; Kumar Nanjundan, A.; Mundree, S. G.; Dubal, D. P. Deep Eutectic Solvents: Green Approach for Cathode Recycling of Li-Ion Batteries. *Adv. Energ. Sustain. Res.* **2022**, *3* (1), 2100133. https://doi.org/10.1002/aesr.202100133.

(33) Yadav, N.; Venkatesu, P. Current Understanding and Insights towards Protein Stabilization and Activation in Deep Eutectic Solvents as Sustainable Solvent Media. *Phys. Chem. Chem. Phys.* **2022**, *24* (22), 13474–13509. https://doi.org/10.1039/D2CP00084A.

(34) Cunha, S. C.; Fernandes, J. O. Extraction Techniques with Deep Eutectic Solvents. *TrAC - Trends Anal. Chem.* 2018, pp 225–239. https://doi.org/10.1016/j.trac.2018.05.001.

(35) Liu, P.; Hao, J. W.; Mo, L. P.; Zhang, Z. H. Recent Advances in the Application of Deep Eutectic Solvents as Sustainable Media as Well as Catalysts in Organic Reactions. *RSC Adv.* **2015**, *5* (60), 48675–48704. https://doi.org/10.1039/C5RA05746A.

(36) Abranches, D. O.; Martins, M. A. R.; Silva, L. P.; Schaeffer, N.; Pinho, S. P.; Coutinho, J. A. P. Phenolic Hydrogen Bond Donors in the Formation of Non-Ionic Deep Eutectic Solvents: The Quest for Type v Des. *Chemical Communications* **2019**, *55* (69). https://doi.org/10.1039/c9cc04846d.

(37) Subba, N.; Das, N.; Sen, P. Partial Viscosity Decoupling of Solute Solvation, Rotation, and Translation Dynamics in Lauric Acid/Menthol Deep Eutectic

Solvent: Modulation of Dynamic Heterogeneity with Length Scale. *J. Phys. Chem. B* **2020**, *124* (31), 6875–6884. https://doi.org/10.1021/acs.jpcb.0c04379.

(38) Subba, N.; Polok, K.; Piatkowski, P.; Ratajska-Gadomska, B.; Biswas, R.; Gadomski, W.; Sen, P. Temperature-Dependent Ultrafast Solvation Response and Solute Diffusion in Acetamide-Urea Deep Eutectic Solvent. *J. Phys. Chem. B* **2019**, *123* (43), 9212–9221. https://doi.org/10.1021/ACS.JPCB.9B07794.

(39) Cui, Y.; Rushing, J. C.; Seifert, S.; Bedford, N. M.; Kuroda, D. G. Molecularly Heterogeneous Structure of a Nonionic Deep Eutectic Solvent Composed of N-Methylacetamide and Lauric Acid. *Journal of Physical Chemistry B* **2019**, *123* (18). https://doi.org/10.1021/acs.jpcb.8b11732.

(40) Mukherjee, K.; Das, S.; Rajbangshi, J.; Tarif, E.; Barman, A.; Biswas, R. Temperature-Dependent Dielectric Relaxation in Ionic Acetamide Deep Eutectics: Partial Viscosity Decoupling and Explanations from the Simulated Single-Particle Reorientation Dynamics and Hydrogen-Bond Fluctuations. *Journal of Physical Chemistry B* **2021**, *125* (45). https://doi.org/10.1021/acs.jpcb.1c07299.

(41) Subba, N.; Tarif, E.; Sen, P.; Biswas, R. Subpicosecond Solvation Response and Partial Viscosity Decoupling of Solute Diffusion in Ionic Acetamide Deep Eutectic Solvents: Fluorescence Up-Conversion and Fluorescence Correlation Spectroscopic Measurements. *J. Phys. Chem. B* **2020**, *124* (10), 1995–2005. https://doi.org/10.1021/acs.jpcb.0c00061.

(42) Mukherjee, K.; Das, A.; Choudhury, S.; Barman, A.; Biswas, R. Dielectric Relaxations of (Acetamide + Electrolyte) Deep Eutectic Solvents in the Frequency Window, $0.2 \leq \nu/\mathrm{GHz} \leq 50$: Anion and Cation Dependence. *Journal of Physical Chemistry B* **2015**, *119* (25). https://doi.org/10.1021/acs.jpcb.5b01502.

(43) Gazi, H. A. R.; Guchhait, B.; Daschakraborty, S.; Biswas, R. Fluorescence Dynamics in Supercooled (Acetamide + Calcium Nitrate) Molten Mixtures. *Chem. Phys. Lett.* **2011**, *501* (4–6), 358–363. https://doi.org/10.1016/j.cplett.2010.12.003.

(44) Guchhait, B.; Al Rasid Gazi, H.; Kashyap, H. K.; Biswas, R. Fluorescence Spectroscopic Studies of (Acetamide + Sodium/Potassium Thiocyanates) Molten Mixtures: Composition and Temperature Dependence. *J. Phys. Chem. B* **2010**, *114* (15), 5066–5081. https://doi.org/10.1021/jp1001176.

(45) Mukherjee, K.; Das, S.; Tarif, E.; Barman, A.; Biswas, R. Dielectric Relaxation in Acetamide + Urea Deep Eutectics and Neat Molten Urea: Origin of Time Scales via Temperature Dependent Measurements and Computer Simulations. *J. Chem. Phys.* **2018**, *149* (12), 124501. https://doi.org/10.1063/1.5040071.

(46) Subba, N.; Sahu, P.; Das, N.; Sen, P. Rational Design, Preparation and Characterization of a Ternary Non-Ionic Room-Temperature Deep Eutectic Solvent Derived from Urea, Acetamide, and Sorbitol. *J. Chem. Phys.* **2021**, *133* (1), 25. https://doi.org/10.1007/s12039-020-01866-2.

(47) Das, N.; Khan, T.; Subba, N.; Sen, P. Correlating Bromelain's Activity with Its Structure and Active-Site Dynamics and the Medium's Physical Properties in a Hydrated Deep Eutectic Solvent. *Phys. Chem. Chem. Phys.* **2021**, *23* (15), 9337–9346. https://doi.org/10.1039/d1cp00046b.

(48) Hunger, J.; Stoppa, A.; Schrödle, S.; Hefter, G.; Buchner, R. Temperature Dependence of the Dielectric Properties and Dynamics of Ionic Liquids. *ChemPhysChem* **2009**, *10* (4), 723–733. https://doi.org/10.1002/cphc.200800483.

(49) Petrowsky, M.; Freeh, R. Application of the Compensated Arrhenius Formalism to Dielectric Relaxation. *J. Phys. Chem. B* **2009**, *113* (50), 16118–16123. https://doi.org/10.1021/jp907018s.

(50) Demchenko, A. P. The Red-Edge Effects: 30 Years of Exploration. *Luminescence*. 2002, pp 19–42. https://doi.org/10.1002/bio.671.

(51) Das, N.; Sahu, S.; Khan, T.; Sen, P. Site-Specific Heterogeneity of Multi-Domain Human Serum Albumin and Its Origin: A Red Edge Excitation Shift Study. *Photochem. Photobiol.* **2023**, *99* (2), 538–546.

(52) Lakowicz, J. R. *Principles of Fluorescence Spectroscopy*; Springer, 2006; pp 1–954. https://doi.org/10.1007/978-0-387-46312-4.

(53) Das, A.; Biswas, R. Dynamic Solvent Control of a Reaction in Ionic Deep Eutectic Solvents: Time-Resolved Fluorescence Measurements of Reactive and Nonreactive Dynamics in (Choline Chloride + Urea) Melts. *J. Phys. Chem. B* **2015**, *119* (31), 10102–10113. https://doi.org/10.1021/acs.jpcb.5b04936.

(54) Tarif, E.; Mondal, J.; Biswas, R. How Frictional Response during Solute Solvation Controls Solute Rotation in Naturally Abundant Deep Eutectic Solvent (NADES)? A Case Study with Amino Acid Derivative Containing DES. *J. Mol. Liq.* **2020**, *303*, 112451. https://doi.org/10.1016/j.molliq.2020.112451.

(55) Azumi, T.; Itoh, K. I.; Shiraishi, H. Shift of Emission Band upon the Excitation at the Long Wavelength Absorption Edge. III. Temperature Dependence of the Shift and Correlation with the Time Dependent Spectral Shift. *J. Chem. Phys.* **1976**, *65* (7), 2550–2555. https://doi.org/10.1063/1.433440.

(56) Itoh, K. I.; Azumi, T. Shift of the Emission Band upon Excitation at the Long Wavelength Absorption Edge. II. Importance of the Solute-Solvent

Interaction and the Solvent Reorientation Relaxation Process. *J. Chem. Phys.* **1975**, *62* (9), 3431–3438. https://doi.org/10.1063/1.430977.

(57) Fee, R. S.; Maroncelli, M. Estimating the Time-Zero Spectrum in Time-Resolved Emmsion Measurements of Solvation Dynamics. *Chem Phys* **1994**, *183* (2–3), 235–247. https://doi.org/10.1016/0301-0104(94)00019-0.

(58) Tarif, E.; Mondal, J.; Biswas, R. Interaction and Dynamics in a Fully Biodegradable Glucose-Containing Naturally Abundant Deep Eutectic Solvent: Temperature-Dependent Time-Resolved Fluorescence Measurements. *J. Phys. Chem. B* **2019**, *123* (44), 9378–9387. https://doi.org/10.1021/acs.jpcb.9b06783.

(59) Jin, H.; Baker, G. A.; Arzhantsev, S.; Dong, J.; Maroncelli, M. Solvation and Rotational Dynamics of Coumarin 153 in Ionic Liquids: Comparisons to Conventional Solvents. *J. Phys. Chem. B* **2007**, *111* (25), 7291–7302. https://doi.org/10.1021/jp070923h.

(60) Wohland, T.; Maiti, S.; Macháň, R. An Introduction to Fluorescence Correlation Spectroscopy. *An Introduction to Fluorescence Correlation Spectroscopy* **2020**. https://doi.org/10.1088/978-0-7503-2080-1.

(61) Schwille, P.; Korlach, J.; Webb, W. W. Fluorescence Correlation Spectroscopy with Single-Molecule Sensitivity on Cell and Model Membranes. *Cytometry* **1999**, *36* (3), 176–182.

(62) Patra, S.; Samanta, A. Microheterogeneity of Some Imidazolium Ionic Liquids as Revealed by Fluorescence Correlation Spectroscopy and Lifetime Studies. *J. Phys. Chem. B* **2012**, *116* (40), 12275–12283. https://doi.org/10.1021/jp3061202.

(63) Wu, E. C.; Kim, H. J.; Peteanu, L. A. Spectroscopic and MD Study of Dynamic and Structural Heterogeneities in Ionic Liquids. *J. Phys. Chem. B* **2017**, *121* (5), 100–1107. https://doi.org/10.1021/acs.jpcb.6b10678.

(64) Guo, J.; Baker, G. A.; Hillesheim, P. C.; Dai, S.; Shaw, R. W.; Mahurin, S. M. Fluorescence Correlation Spectroscopy Evidence for Structural Heterogeneity in Ionic Liquids. *Phys. Chem. Chem. Phys.* **2011**, *13* (27), 12395–12398. https://doi.org/10.1039/c1cp20929a.

(65) Hu, Z.; Margulis, C. J. Heterogeneity in a Room-Temperature Ionic Liquid: Persistent Local Environments and the Red-Edge Effect. *Proc. Natl. Acad. Sci. USA* **2006**, *103* (4), 831–836. https://doi.org/10.1073/pnas.0507364103.

(66) Dueby, S.; Daschakraborty, S. Size Dependence of Solute's Translational Jump-Diffusion in Solvent: Relationship between Trapping and Jump-Diffusion. *Chem. Phys. Lett.* **2022**, *806*, 140059.

(67) Becker, S. R.; Poole, P. H.; Starr, F. W. Fractional Stokes-Einstein and Debye-Stokes-Einstein Relations in a Network-Forming Liquid. *Phys. Rev. Lett.* **2006**, *97* (5), 055901.

(68) Daschakraborty, S.; Dubey, V. Breakdown of the Stokes−Einstein Relation in Supercooled Water/ Methanol Binary Mixtures: Explanation Using the Translational Jump-Diffusion Approach. *J. Phys. Chem. B* **2020**, *124* (46), 10398–10408.

(69) Xu, L.; Mallamace, F.; Yan, Z.; Starr, F. W.; Buldyrev, S. V.; Eugene Stanley, H. Appearance of a Fractional Stokes–Einstein Relation in Water and a Structural Interpretation of Its Onset. *Nat. Phys.* **2009**, *5* (8), 565–569. https://doi.org/10.1038/nphys1328.

(70) Ren, G.; Chen, L.; Wang, Y. Dynamic Heterogeneity in Aqueous Ionic Solutions. *Phys. Chem. Chem. Phys.* **2018**, *20* (33), 21313–21324. https://doi.org/10.1039/c8cp02787k.

(71) Shao, Y.; Hellström, M.; Yllö, A.; Mindemark, J.; Hermansson, K.; Behler, J.; Zhang, C. Temperature Effects on the Ionic Conductivity in Concentrated

Alkaline Electrolyte Solutions. *Phys. Chem. Chem. Phys.* **2020**, *22* (19), 10426–10430. https://doi.org/10.1039/c9cp06479f.

(72) Häkkinen, R.; Alshammari, O.; Timmermann, V.; D'Agostino, C.; Abbott, A. Nanoscale Clustering of Alcoholic Solutes in Deep Eutectic Solvents Studied by Nuclear Magnetic Resonance and Dynamic Light Scattering. *ACS Sustainable Chem. Eng.* **2019**, *7* (17), 15086–15092. https://doi.org/10.1021/acssuschemeng.9b03771.

(73) D'Agostino, C.; Gladden, L. F.; Mantle, M. D.; Abbott, A. P.; Ahmed, E. I.; Al-Murshedi, A. Y. M.; Harris, R. C. Molecular and Ionic Diffusion in Aqueous-Deep Eutectic Solvent Mixtures: Probing Inter-Molecular Interactions Using PFG NMR. *Phys. Chem. Chem. Phys.* **2015**, *17* (23), 15297–15304. https://doi.org/10.1039/c5cp01493j.

(74) Das, N.; Khan, T.; Subba, N.; Sen, P. Correlating Bromelain's Activity with Its Structure and Active-Site Dynamics and the Medium's Physical Properties in a Hydrated Deep Eutectic Solvent. *Phys. Chem. Chem. Phys.* **2021**, *23* (15), 9337–9346. https://doi.org/10.1039/d1cp00046b.

(75) Verma, P. K.; Rakshit, S.; Mitra, R. K.; Pal, S. K. Role of Hydration on the Functionality of a Proteolytic Enzyme α-Chymotrypsin under Crowded Environment. *Biochimie* **2011**, *93* (9), 1424–1433. https://doi.org/10.1016/j.biochi.2011.04.017.

(76) Khan, T.; Halder, B.; Das, N.; Sen, P. Role of Associated Water Dynamics on Protein Stability and Activity in Crowded Milieu. *J Phys Chem B* **2024**, *128*, 8672–8686. https://doi.org/10.1021/acs.jpcb.4c04337.

This page left blank intentionally

Chapter 4

Understanding the Intricacy of Protein in Hydrated Deep Eutectic Solvent: Solvation Dynamics, Conformational Fluctuation Dynamics, and Stability

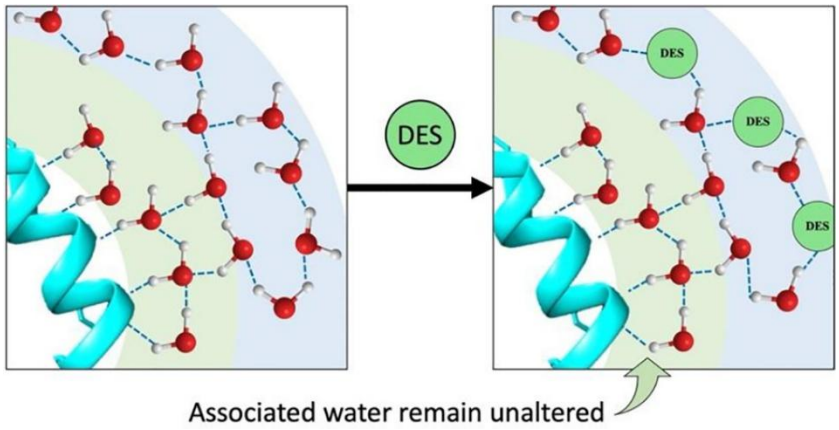

Tanmoy Khan, Nilimesh Das, Kuldeep Singh Negi, Suman Bhowmik and Pratik Sen*

Int. J. Biol. Macromol. **2023**, 253, 127100.

Abstract:

Deep eutectic solvents (DESs) are potential biocatalytic media due to their easy preparation, fine-tuneability, biocompatibility, and most importantly, due to their ability to keep protein stable and active. However, there are many unanswered questions and gaps in our knowledge about how proteins behave in these alternate media. Herein, we investigated solvation dynamics, conformational fluctuation dynamics, and stability of human serum albumin (HSA) in 0.5 Acetamide/0.3 Urea/0.2 Sorbitol (0.5Ac/0.3Ur/0.2Sor) DES of varying concentrations to understand the intricacy of protein behaviour in DES. Our result revealed a gradual decrease in the side-chain flexibility and thermal stability of HSA beyond 30% DES. On the other hand, the associated water dynamics around domain-I of HSA decelerate only marginally with increasing DES content, although viscosity rises considerably. We propose that even though macroscopic solvent properties are altered, a protein feels only an aqueous type of environment in the presence of DES. This is probably the first experimental study to delineate the role of the associated water structure of the enzyme for maintaining its stability inside DES. Although considerable effort is necessary to generalize such claims, it might serve as the basis for understanding why proteins remain stable and active in DES.

4.1. Introduction

Enzymes are the most efficient and selective catalysts that play a significant role in diverse biochemical transformations and industrial processes [1–4]. However, the utilization of the enzymes is limited as they are only stable in water. Targeted enzyme mutation can overcome this issue to some extent [5–9]. Further, obtaining designer solvents that can keep enzymes stable and active is also very important for industrial applications [10–12]. Ionic liquids (ILs), owing to their non-volatility, high thermal stability, and a broad spectrum of solutes dissolving capabilities, become the most studied solvents in this regard [11,13–16]. More importantly, IL can be engineered by changing the constituent cations and anions [17,18]. However, in recent times, deep eutectic solvents (DESs) have been identified as the new choice for biocatalysis because of their additional advantages over ILs in terms of cost-effectiveness, easy (only through mixing and heating and no further purification required) and atom-economic preparation [19–21]. A huge number of naturally occurring/synthetic constituents and their different mole fractions can form DES, which provides a broad spectrum of engineered solvent media [22,23]. Many recent reports and review articles have highlighted that proteins remain stable and active in DESs [24–30]. However, incorporation of proteins into neat DES is very difficult as their solubilization rate is extremely slow, and also incorporation through heating is inappropriate owing to the thermolabile character of proteins [31–33]. Adding water to the DES system in order to overcome this hindrance was found to be quite fruitful as it also offers an extra degree of freedom for tailoring solvent properties like viscosity and polarity that improves the dissolution rate of macromolecules [34,35]. More interestingly, the stability and activity of some enzymes are reported to get enhanced in hydrated DES media compared to that in the buffer [36–45]. This makes hydrated DESs an exciting choice as a biocatalytic medium.

However, most of the research in this field relies on getting a positive result by choosing a pair of DES and protein. The choices are also getting biased on the availability of the proteins and constituents of DES. A logical way forward in this field is very much missing. Nevertheless, some recent reports proposed that DESs

properties like H-bond strength, interaction strength between DES constituents and protein, solvent polarity, viscosity, and density might influence the enzymatic activity and stability in such media [46,47]. Our group contributed to this understanding by carrying out the proteolytic activity of bromelain in the presence of a DES at various degrees of hydration [45]. We suggested that compact structural conformation, flexible active site dynamics of the enzyme, lower viscosity, and higher polarity of the solvent media primarily affect the biocatalytic activity of bromelain [45].

However, the mechanistic understanding of why proteins/enzymes are stable and active in these alternate media (DES) is still in its infancy. One aspect that has been completely ignored in the literature is how the associated water dynamics of an enzyme is modulated in the presence of a DES. It is well proven that the water in the immediate vicinity of an enzyme (known as associated water) is quite different from the normal bulk water [48–51]. This associated water is directly hydrogen bonded to the protein surface, making it dynamically retarded [48,49,51–53] and can influence many cellular processes [50,54–57]. The role of water dynamics in influencing protein properties has mainly been reported in the case of osmolytes [58–60]. Although there are some reports through MD simulation/theoretical studies in the case of different non-aqueous solvents pointing out the role of hydration [61–65], to the best of our knowledge, there are no experimental studies in DESs.

A variety of techniques are available to measure the dynamics of associated water, namely, NMR [66,67], dielectric relaxation (DR) [68], quasi-electron neutron scattering (QENS) [69], and time-dependent fluorescence Stokes shift (TDFSS) [50,53,55,56,70–74]. However, in the case of proteins, where the immediate surrounding is essential, the fluorescence-based TDFSS method becomes of utmost importance due to its unmatched spatial resolution [48,75]. It can report dynamics in the immediate vicinity of the reporter molecule tagged in the protein. In contrast, NMR, DR, or QENS captures signals from the whole solution and can give only an average picture [48]. In addition to associated water dynamics around the protein, internal protein dynamics is also a controlling factor of various cellular phenomena [76–81]. Among these, microsecond protein dynamics is one of the most important factors in controlling

enzymatic activity and signal transduction. However, its modulation in DESs is scarcely studied in the literature [45,47].

Herein, we aimed to understand the intricacy of protein behavior in a DES as a part of our ongoing effort to achieve a holistic physical insight into why proteins remain stable and active in DESs. We have chosen human serum albumin (HSA) as a model protein that has been extensively characterized in the native state and under different conditions of chemical and thermal stress [13,70,82–85] and can be site-selectively tagged to observe site-specific information [86,87]. HSA is the major transport protein in the human circulatory system [88], making the choice of HSA even more relevant. In the past, most of the experiments carried out to understand protein behaviour in DESs were done in ionic DESs [28,36,39,41,89,90]. However, for many practical purposes involving hydrophobic solutes, ionic DESs will not be a good choice. Non-ionic DESs can overcome this problem, and in recent years, such non-ionic DESs have gained attention in various fields [91–93]. Therefore, understanding protein behaviour in non-ionic DESs is important. DES formed by acetamide, and urea is one of the most studied non-ionic DES [94,95], but it is not liquid at room temperature which limits its applicability [96]. We have reported earlier that adding sorbitol as a third component lowers the freezing point of the system [97]. This ternary DES with a composition of 0.5Ac/0.3Ur/0.2Sor remains in a liquid state even at 280 K. Because of this, we chose 0.5Ac/0.3Ur/0.2Sor DES for the present study.

In this work, we measured the solvation dynamics around the domain-I of HSA in 0.5Ac/0.3Ur/0.2Sor DES as a function of the degree of hydration using the TDFSS method. Analysis concerning individual components of solvation, water contents, and viscosity modulation is discussed, which might provide physical insight into enzymatic behavior in DES. Secondly, we reported microsecond side-chain dynamics of domain-I of HSA with DES at various degrees of hydration. Thirdly, we have measured the thermal stability of HSA in the DES as a function of water content. More importantly, some control experiments with constituent solutions give us much-needed information regarding the retention of the DES structure with water dilution.

4.2. Results and Discussion:

4.2.1. Hydrated DES or aqueous solution of DES constituents

There are debates in the literature on the preservation of the DES network in the presence of water [34,98–100]. Generally, for high water content, DESs lose their typical structure and become a simple aqueous solution of the constituents [98–100]. Hence, it is important to investigate if the hydrated DES in this study is merely an aqueous solution of its constituents. We separately prepared the hydrated DES solution and mixed all three constituents of DES in water, maintaining the same component concentrations as in hydrated DES. From 70% (v/v), the constituents were found to be insoluble in the required amount of water. This simple observation implies that from 70% (v/v) onwards, DES in the water system is not merely an aqueous solution of the DES constituents, but rather a hydrated DES with the retention of the DES network. Next, we measured the translational diffusion of rhodamine 6G (R6G) in both the hydrated DES and aqueous solution of DES constituents using fluorescence correlation spectroscopy. From the measured translational diffusion time (τ_D) we calculated microviscosity using the Stokes-Einstein equation ($D_t = \frac{k_B T}{6\pi\eta R}$; where '$D_t$' is the translational diffusion coefficient, 'k_B' is the Boltzmann's constant, 'T' is the temperature, 'R' is the molecular radius of the probe, and 'η' is the viscosity, and, $\tau_D \propto {}^{1}/_{D_t}$).

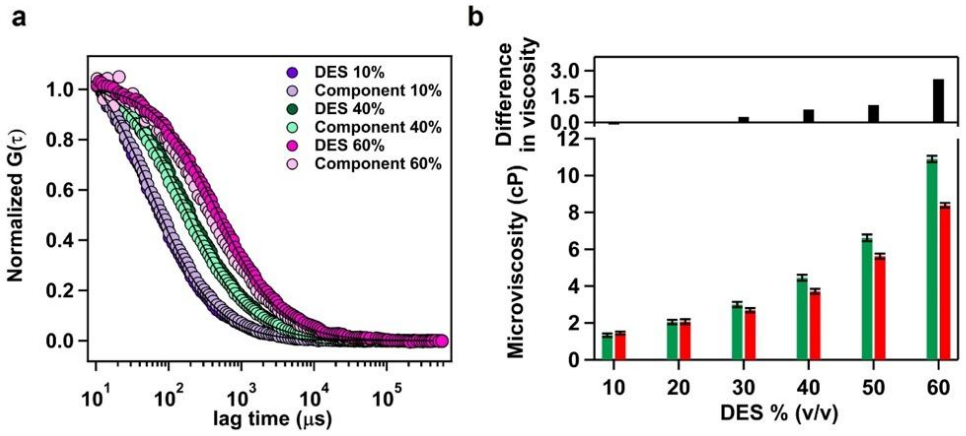

Figure 1. (a) Representative fluorescence intensity autocorrelation curves of R6G in hydrated DES and component solution of the same concentration as in hydrated DES, (b) Micro viscosity of the hydrated DES (green) and constituent solution (red) keeping the same concentration as in hydrated DES. Black bars are representing the differences between the viscosity of hydrated DES and component solution. The error bar represents the standard deviation of the mean of three independent experiments.

Figure 1 depicts that up to 30 % (v/v) DES in water, the microviscosity remains similar to that in the solution of constituents in water. However, from 30 % (v/v), a clear difference in the microviscosity of the hydrated DES and the component solution is visible. This experiment suggests that up to 30 % (v/v) DES in water is probably an aqueous solution of the constituents of the DES. However, beyond that, it is surely a hydrated DES where the property cannot be achieved just by mixing the solution of DES constituents. We have earlier compared the proteolytic activity of bromelain in both hydrated 0.5Ac/0.3Ur/0.2Sor DES and aqueous component solution and observed a significant enhancement of activity at lower concentration (up to 40% v/v) in the former case [45]. However, a slight increase in the proteolytic activity compared to pure buffer at lower concentrations of DES constituent solution was also observed [45]. Therefore, there is a hint that a synergistic action from the individual components might also play a role. Nevertheless, the significant positive effects on bromelain activity in hydrated DES probably arise due to the hydrogen-bonded network of the DES which might still exist even at such low concentrations of DES. Similar retention of the network-like structure of choline chloride/urea and

choline chloride/1,2-propane-di-ol DES was found up to 83 mol% and 50 % (v/v) of water, respectively [98,100]. Thus the structure retainment in the case of hydrated DES depends on the nature of the constituents. In our case, probably some portions of network-like DES structure maintain their integrity even at very low concentrations (~20-30% v/v) of DES [45].

4.2.2. Solvation dynamics of hydrated DESs using transient absorption spectroscopy:

It is well known that dynamics of solvent play a significant role in many chemical and biological processes. However, experimental studies on the solvation dynamics of hydrated DES are limited in the literature [101,102]. Having established that the properties of hydrated DES cannot be achieved just by mixing the solution of DES constituents (at least beyond 30% v/v DES), we measured solvation dynamics at various concentrations of the DES in water using the solvatochromic coumarin 343 probe with femtosecond transient absorption spectroscopy in the absence of the protein. We could not go beyond 70% (v/v) DES concentration as the data quality becomes very poor due to scattering in the sample. The representative time-resolved stimulated emission spectra for different concentrations of the DES can be found in Figure 2.

From the collected data we constructed the solvent response function (see Figure 3a) using the equation mentioned in the Figure 3a. The solvent response functions were well described by a bi-exponential function ($S(t) = a_1 e^{\frac{-t}{\tau_1}} + a_2 e^{\frac{-t}{\tau_2}}$) yielding the faster ($\tau_1$) and the slower time components (τ_2) of solvation as 190 fs and 1.4 ps, respectively, in the case of buffer (Figure 3c, 3d). We observed a gradual slowdown of average solvation dynamics with increasing DES concentration (Figure 3b). This is expected as the viscosity increases with the addition of DES in water (Figure 3e). However, the faster time component remains almost unchanged. We have quantified

the extent of viscosity dependence on solvation dynamics (τ_s) using the Stoke-Einstein relation as

$$\tau_s \propto \left(\frac{\eta}{T}\right)^p \quad (1)$$

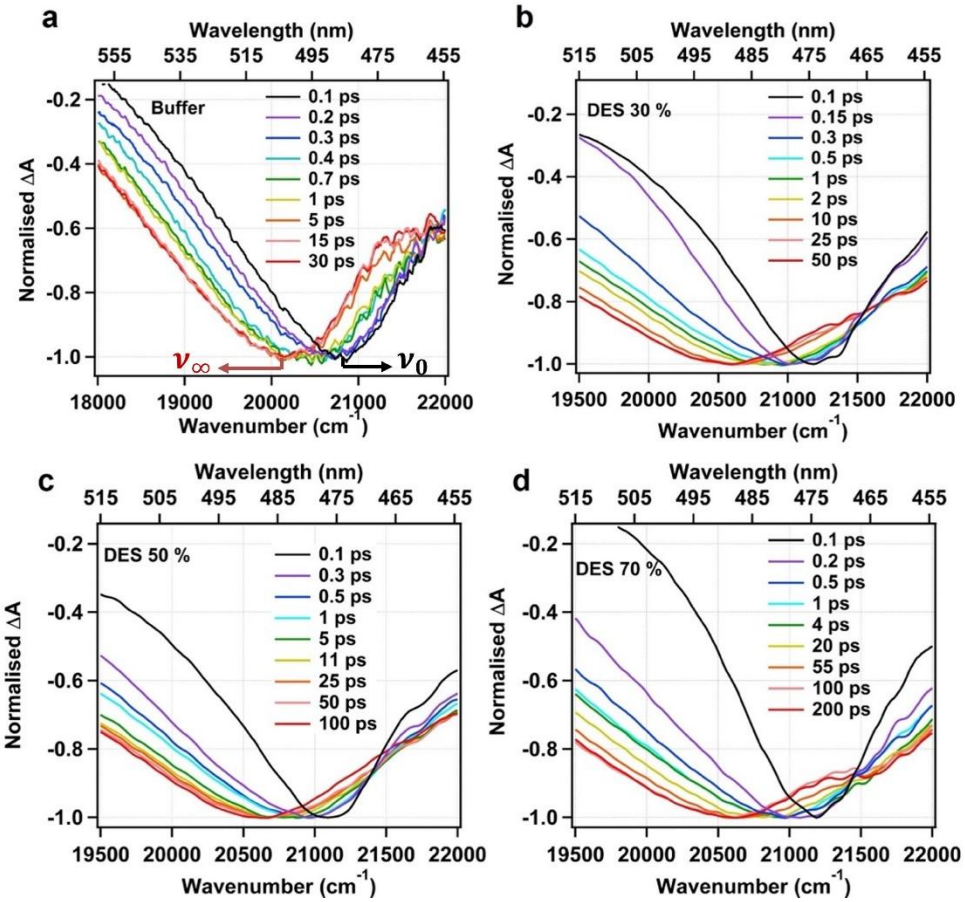

Figure 2. Time-resolved stimulated emission spectra of C 343 in (a) buffer, (b) 30% (v/v), (C) 50% (v/v), and (d) 70% (v/v) hydrated DES concentrations.

where, η is the viscosity and T is the temperature of the medium [103]. p value signifies the coupling of the dynamics to the viscosity of the medium [104,105], which can be readily obtained from the log-log plot, as per equation 2.

$$\log(\tau_x) = p \log\left(\frac{\eta}{T}\right) + \log C \qquad (2)$$

Expectedly, the average solvation time follows the medium viscosity (p~1). Component analysis reveals that the slower component of solvation is also viscosity coupled (p~1). However, the faster time component remains almost unchanged (p~0). (Figure 3c, 3f, and Table 1).

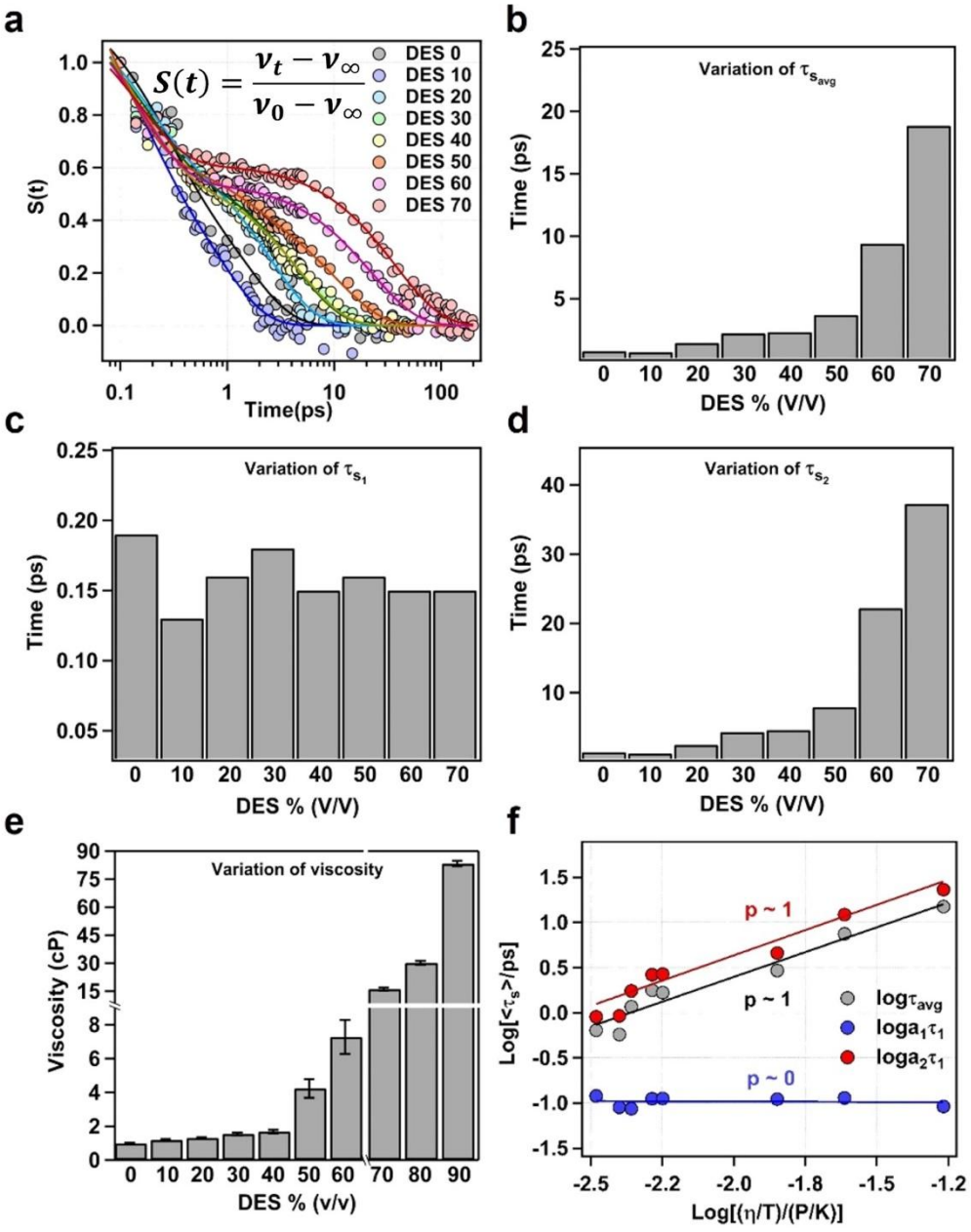

Figure 3. (a) Solvent response function of C 343; and variation of (b) average solvation times, (c) faster time components, (d) slower time components with different degrees of hydrated 0.5Ac\0.3Ur\0.2Sor DES in the absence of protein, (e) viscosity of different concentrations of 0.5Ac/0.3Ur/0.2Sor DES in the buffer, (f) log-log plot of individual timescales of solvation dynamics of hydrated 0.5Ac\0.3Ur\0.2Sor DES with the temperature reduced viscosity.

Table 1. Biexponential fitting parameters of the solvent response function, S(t), of C-343 in the presence of different concentrations of hydrated 0.5Ac/0.3Ur/0.2Sor DES.

DES concentration	a_1(%)	τ_{S_1} (ps)	a_2 (%)	τ_{S_2} (ps)	τ_{avg} (ps)
0	49.6	0.19	50.4	1.41	0.80
10	49.3	0.13	50.7	1.30	0.72
20	43.2	0.16	56.8	2.46	1.47
30	50.4	0.18	49.6	4.32	2.23
40	56.4	0.15	43.6	4.62	2.10
50	54.3	0.16	45.7	7.91	3.70
60	58.0	0.15	42.0	22.2	9.41
70	49.6	0.15	50.4	37.3	18.85

This result suggests that a bulk water-like ambiance around the probe might still exist even in the presence of 70% (v/v) DES, where the viscosity is very high. At the same time, the addition of DES to the buffer significantly alters medium properties (like microviscosity, average solvation time, etc.). The impact of this result can be extended in the case of protein where the immediate water near the protein surface which is in direct interaction with the protein can influence many important enzymatic properties like stability and activity [53,55,56]. We hypothesized that although biological observations are always system-specific, one general way of keeping

protein stable and active in viscous DESs might be through retaining this unperturbed portion of water around it.

4.2.3. Associated Water Dynamics of HSA with Increasing DES content:

To understand the associated water dynamics around the protein, we measured the solvation dynamics of CPM tagged to HSA in buffer, and in the presence of different concentrations of 0.5Ac/0.3Ur/0.2Sor DES. The time-resolved emission spectra (TRESs) at different DES concentrations are shown in Figure 4. The solvent response function and the average solvation time are shown in Figure 5, and the time components are tabulated in Table 2.

The average solvation time of CPM-tagged HSA in water is ~2.2 ns, which gradually increases upon the addition of DES and becomes ~3.4 ns for 90% (v/v) DES in water (Figure 5b). Initially, we thought that it might be a direct/straightforward consequence of increasing medium viscosity with increasing DES concentration. However, the viscosity change for the 90% DES is ~83 times (from ~1 cP in water to ~83 cP in 90% DES) (see Table 2). Therefore, the extent of the increase in the solvation time with increasing DES concentration is negligible compared to that of the viscosity increment. It hints that HSA can maintain the associated water structure around it even in the presence of high concentrations of DES.

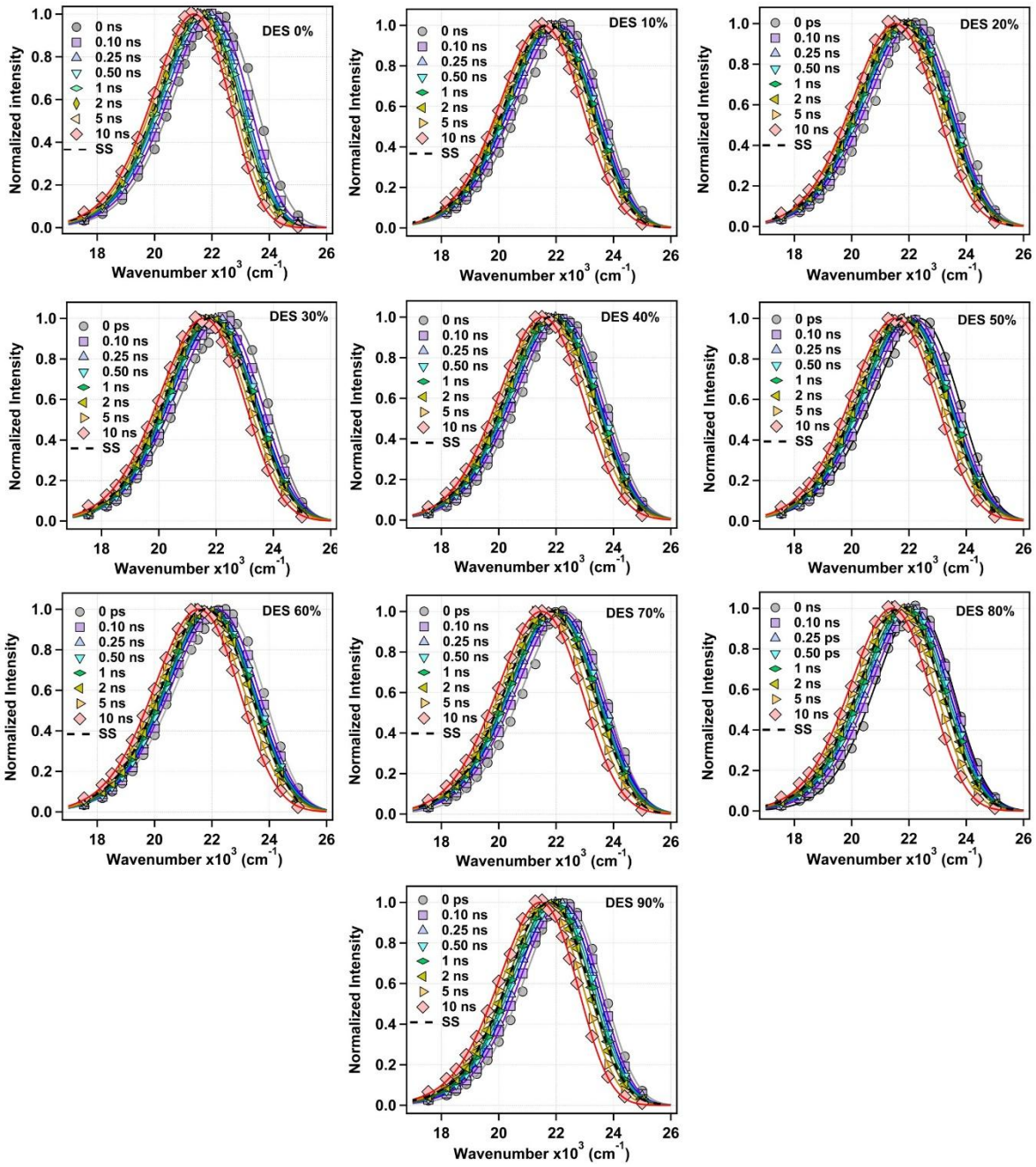

Figure 4. Time resolved emission spectra (TRES) of CPM labelled HSA with different degrees of hydrated (0.5Ac\0.3Ur\0.2Sor) DES. Black dashed line represents the steady state (SS) emission spectra of CPM labelled HSA at the respective DES concentration.

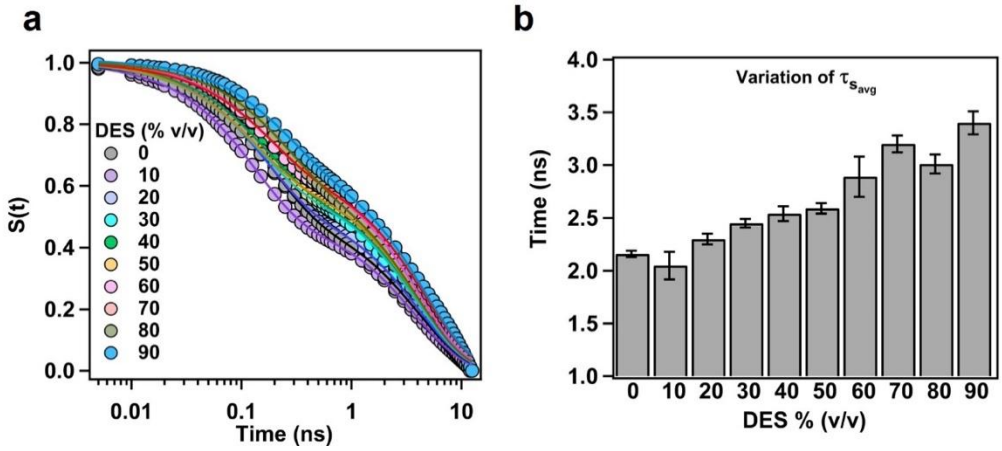

Figure 5. (a) Solvent response function and (b) average solvation time of CPM labeled HSA in buffer and different concentrations of 0.5Ac/0.3Ur/0.2Sor DES. The error bar represents the standard deviation of the mean of three independent experiments.

Table 2: Biexponential fitting parameters of the solvent response function, S(t), of CPM, tagged HSA in the presence of different concentrations of 0.5Ac/0.3Ur/0.2Sor DES and the viscosity of different concentrations of 0.5Ac/0.3Ur/0.2Sor DES in the buffer.

DES concentration %(V/V)	a_1	τ_{S_1} (ps)	a_2	τ_{S_2} (ns)	$\tau_{S_{avg}}$ (ns)	**Viscosity (cP)**
0	0.49	170±10	0.51	4.08±0.10	2.16±0.03	0.98±0.04
10	0.51	160±15	0.49	4.02±0.24	2.05±0.13	1.19±0.05
20	0.46	160±10	0.54	4.13±0.22	2.30±0.05	1.31±0.04
30	0.40	130±20	0.60	4.00±0.10	2.45±0.04	1.54±0.08
40	0.40	150±10	0.60	4.14±0.17	2.54±0.07	1.68±0.10
50	0.38	130±20	0.62	4.09±0.10	2.58±0.05	4.23±0.55
60	0.34	160±10	0.66	4.29±0.10	2.89±0.19	7.27±1.00
70	0.33	170±10	0.67	4.68±0.15	3.20±0.08	16.14±0.80
80	0.37	230±20	0.63	4.65±0.20	3.01±0.09	30.16±1.00
90	0.31	250±20	0.69	4.81±0.22	3.40±0.11	83.30±1.50

4.2.4. Component analysis suggests the first solvation shell remains unperturbed with DESs:

A deeper insight could be gained from the individual component analysis. In the experimental result, the bi-exponential solvent response functions were comprised of a sub-nanosecond (130-250 ps) and a few nanoseconds (3-5 ns) time components. The faster sub-nanosecond time component originates from the water molecules residing in the immediate vicinity of the protein surface, commonly termed biological water [49,51,53,106,107]. The longer timescale represents the contribution from polar residues of the protein, coupled motion between the amino acid side-chain fluctuations and water molecules, and the overall tumbling motion of the protein [48,49,51,107]. The variation of faster (τ_{S_1}) and slower (τ_{S_2}) time components of solvation are represented in Figure 6a and Figure 6b. Like in the case of solvation dynamics of hydrated DES in the absence of protein, here also the faster time component remains unaltered up to 70% DES. It suggests an unperturbed first solvation shell around HSA up to 70% DES. Beyond that, the associated water dynamics gets slightly affected. However, these changes are also insignificant concerning the significant viscosity change of the medium.

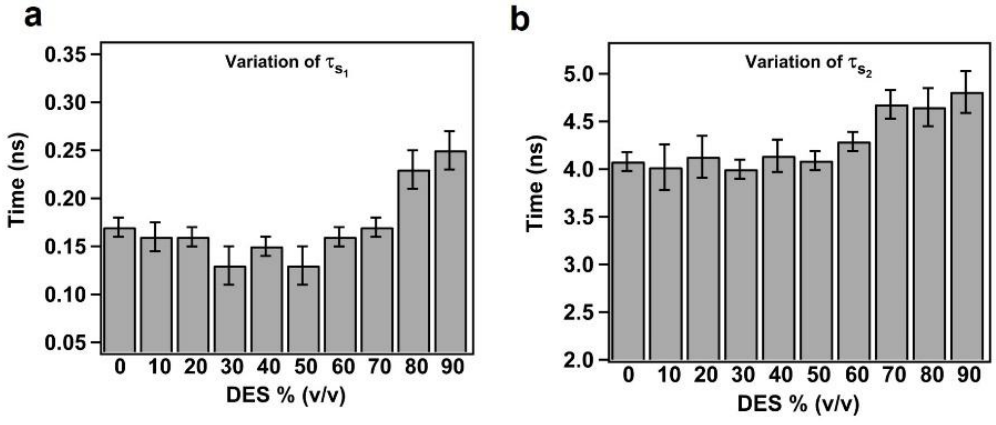

Figure 6. The variation of (a) faster time component and (b) slower time component of CPM tagged HSA in the presence of different concentrations of 0.5Ac/0.3Ur/0.2Sor DES in the buffer. The error bar represents the standard deviation of the mean of at least two independent experiments.

To quantify how much the solvation dynamics and its individual components are coupled to the viscosity of the medium, here also we have constructed the log-log plot (see Figure 7). The slope of the log-log plot for the fast component is almost zero, implying this to be viscosity independent. This means that the associated water dynamics around the protein is not modulated at all with the addition of DES. The slow component also shows a very weak viscosity coupling.

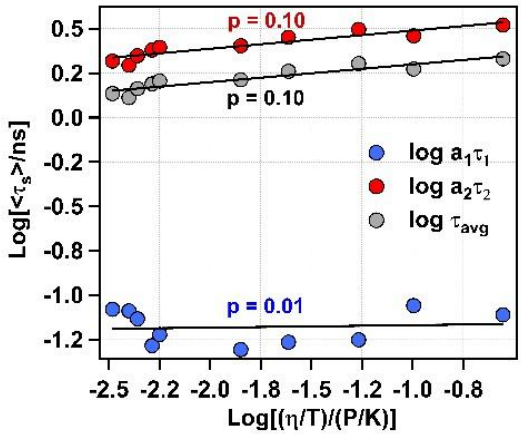

Figure 7. Log-log plot of individual timescales and average solvation time of CPM labeled HSA with the temperature-reduced viscosity of different concentrations of 0.5Ac/0.3Ur/0.2Sor DES in the buffer.

This result is remarkable. It suggests that at least in the first solvation shell, water structure is maintained at least up to 70% (v/v) of DES. Protein, therefore, feels only an aqueous environment, even at this concentration of DES, where the macroscopic properties of the system, like viscosity, change drastically (up to 16 times at 70% DES). It is almost axiomatic that water plays an important role in dictating every protein property. Especially, the associated water, which directly interacts with a protein, should have a huge effect on protein properties [48,50,53,55]. Our result implies that the character of this associated water remains unperturbed in the presence of DES. It might have an enormous implication in the field of biocatalysis and provides a clue that enzymes remain active and stable in DES by keeping its associated water

structure intact. Previously, Hayyan's group suggested a similar mechanism to explain the stability and activity of an enzyme in the DES using MD simulation [29]. Our findings likely represent the first experimental support in favour of such a mechanism.

4.2.5. Associated water dynamics of HSA in component solution:

We also measured the solvation dynamics of HSA in the aqueous solutions of DES's constituents and compared the results with hydrated DES. All the time-resolved emission spectra (TRESs) can be found in Figure 8.

As the microviscosity (Figure 1b) in the case of hydrated DES is more than the same concentration of aqueous solution of constituents, the dynamics are expected to be affected less in the latter case compared to the former. We observed a monotonous slowing down of solvation dynamics with an increase in the constituent concentration, though the faster time component, which represents the associated water dynamics around HSA, remains unaltered (Figure 9 and Table 3). The extent of slowing down in the solvation dynamics is almost similar to that in hydrated DES. This observation is very surprising considering that at least above 30% (v/v) hydrated DES is different from the aqueous solution of DES components in terms of macroscopic and microscopic properties (Section 3.1.).

We propose that DES or hydrated DES keep protein stable and active by maintaining the associated water around it and at the same time providing an alternate media where the physical properties can be fine-tuned as per the requirement. Proteins also remain stable and active in the presence of various osmolytes, ILs, and macromolecular crowders. In a previous report, we have shown that associated water dynamics play a key role in controlling protein stability in the crowded milieu [50]. We suggest that associated water property might be one of the principal governing factors in controlling protein behavior in the presence of any additives.

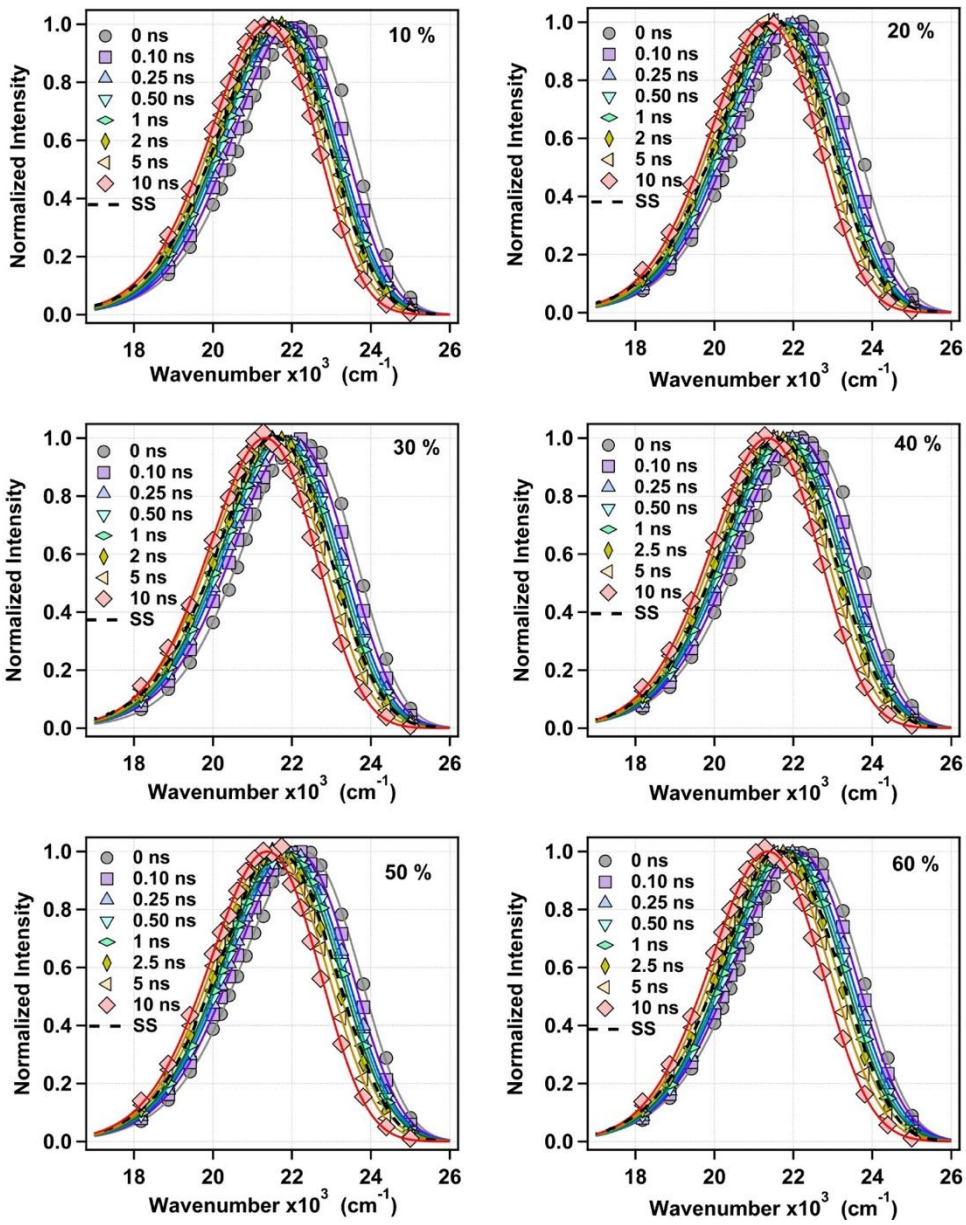

Figure 8. Time-resolved emission spectra (TRES) of CPM labelled HSA in the presence of different concentrations of constituent's solution of 0.5Ac/0.3Ur/0.2Sor DES.

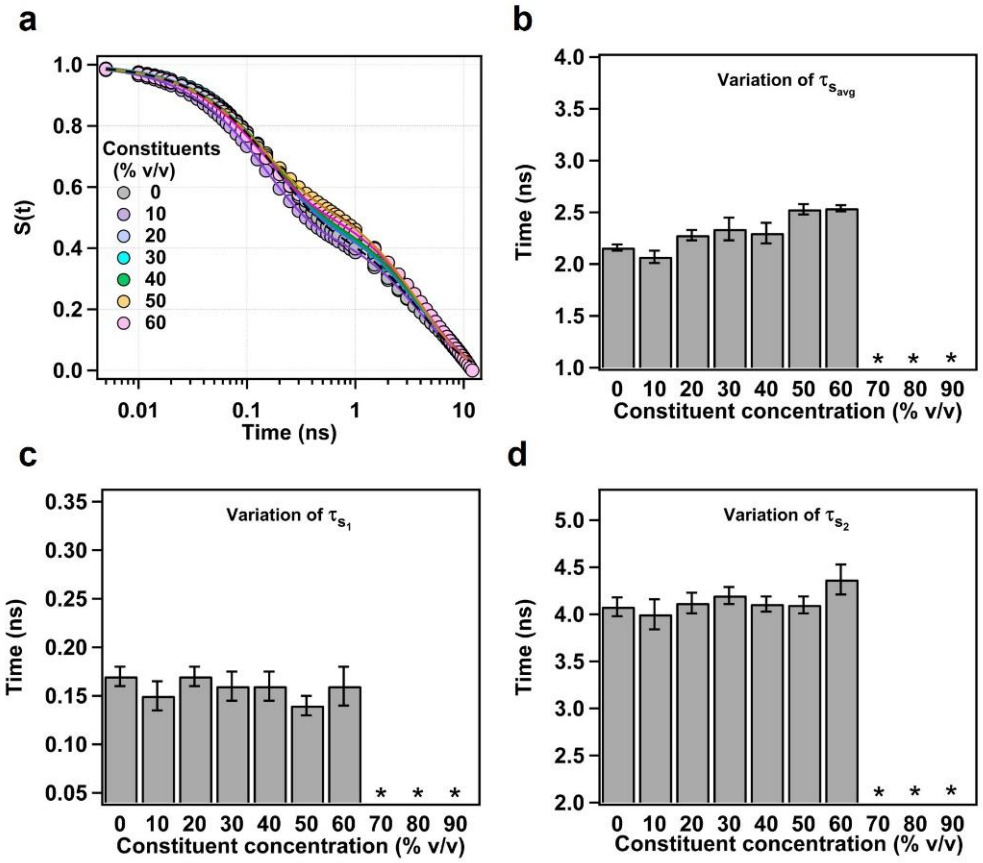

Figure 9. (a) Solvent response function, (b)variation of average solvation time, (c) variation of faster time component and (d) variation of the slower time component of CPM tagged HSA in the presence of buffer and different concentrations of constituent's solution of 0.5Ac/0.3Ur/0.2Sor DES. Solid lines in (a) represent fitting by a bi-exponential function. "* (Asterix)" points could not be measured as the constituents remain insoluble at those concentrations. The error bar represents the standard deviation of the mean of at least two independent experiments.

Table 3. Biexponential fitting parameters of the solvent response function, S(t) of CPM, tagged HSA in the presence of different concentrations of constituent solution of 0.5Ac/0.3Ur/0.2Sor DES.

DES concentration %(V/V)	a_1	τ_{S_1} (ps)	a_2	τ_{S_2} (ns)	$\tau_{S_{avg}}$ (ns)
0	0.49	170±10	0.51	4.08±0.10	2.16±0.03
10	0.50	140±15	0.50	4.11±0.16	2.12±0.02
20	0.47	160±10	0.53	4.17±0.11	2.28±0.02
30	0.46	160±15	0.54	4.20±0.09	2.34±0.09

40	0.46	170±15	0.54	4.25±0.08	2.37±0.04
50	0.40	140±10	0.60	4.00±0.09	2.45±0.05
60	0.34	155±20	0.66	4.37±0.16	2.94±0.03

4.2.6. Protein structural modulation and solvation dynamics

One may debate whether the constancy of solvation dynamics results merely from the conservation of the HSA's associated water structure in the presence of DES or whether the water structure and protein structure are regulated to keep the solvation dynamics constant. When a protein changes its conformation or structure, the bulk water molecules are expected to interact with the hydration layer to a different extent, resulting in a change in the solvation dynamics. To investigate if such an alteration plays a key role in the modulation of solvation dynamics, we performed a steady-state emission study of CPM attached to HSA that provides the local environment around it and estimated the hydrodynamic radii of HSA with the addition of DES using FCS. We also presented previously reported changes in the emission maximum and hydrodynamic size of CPM-tagged to HSA with the addition of guanidinium hydrochloride (GnHCl) [85,87], as a control to understand the extent of change in the presence of DES. GnHCl is a common denaturing agent, and with an increase in the concentration, it destabilizes the native conformation of any protein [108]. The effect of GnHCl-induced denaturation of HSA is well reported in the literature by various groups, including ours [83–85,87,109,110]. The change in the emission maximum and hydrodynamic radius with GnHCl concentration is plotted here to show the extent of the effect exerted by DES on the structure of HSA in comparison to a common denaturing agent, which is supposed to unfold the protein. Our experiment shows a slight blue shift in the emission spectrum in the presence of different concentrations of DES (Figure 10a, 10c, and Table 4). While a blue shift can indicate minor structural compaction, it is also plausible that this shift is due to the presence of the less polar DES components in the immediate solvation shell of the protein. Also, there is virtually no change in the hydrodynamic radii of HSA up

to 30% of DES. However, beyond that, the size of the protein increases with an increase in the DES content of the medium (Figure 10d and Table 4). This observed increase in the hydrodynamic radius likely suggests a combination of factors; firstly, a partial disruption of the HSA structure, and secondly, the potential association of some bulkier DES components with the protein's surface. The emission and FCS-related raw data can be found in Figures 10a and 10b. This increase in the size of HSA suggests a disruption of HSA structure with the addition of DES, although the change is not much (39 Å in the buffer to 49 Å in 80% DES) compared to the chemical denaturation (63 Å in 6 M GnHCl). This means although the hydrodynamic radius of HSA starts to increase around 40% (v/v) DES, it surely does not reach the completely unfolded state even in the presence of the highest concentration of the DES used here.

Obviously, the alteration of protein conformation at the higher DES concentration might affect its solvation dynamics. However, when a protein opens up due to its structural alterations, more bulk water molecules are expected to interact with the hydration layer of the protein surface, thus accelerating the process [87,111]. On the other hand, for higher DES concentrations, the water dynamics in the present case did not speed up. This suggests that despite a slight but definitive structural alteration, it does not severely affect the water structure modulation.

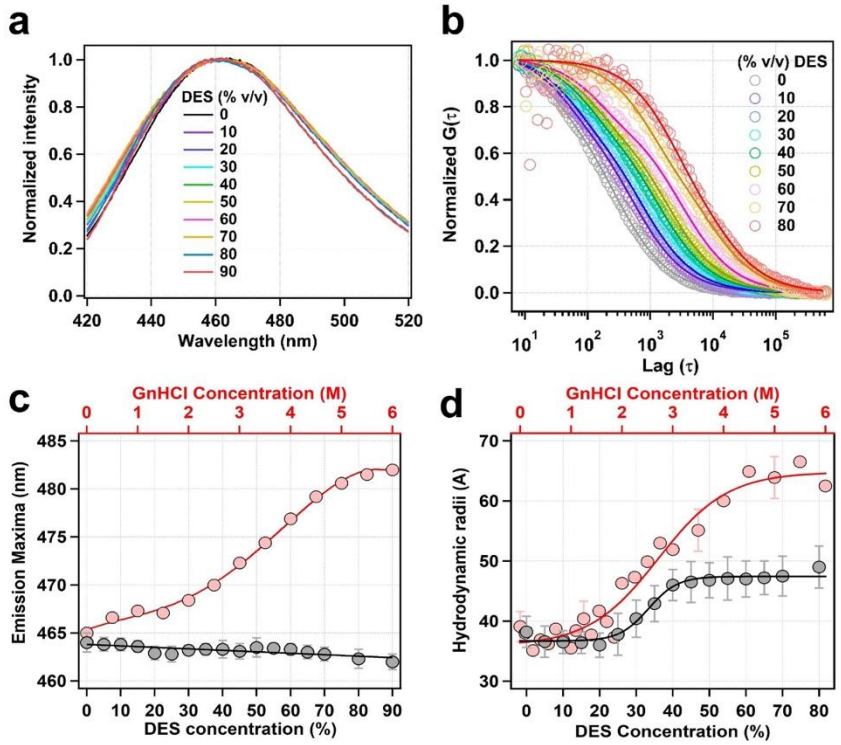

Figure 10. (a) Intensity normalized emission spectra of CPM tagged to HSA in the presence of hydrated 0.5Ac\0.3Ur\0.2Sor DES. (b) Normalized fluorescence intensity autocorrelation curve of TMR tagged HSA in the presence of differently hydrated 0.5Ac\0.3Ur\0.2Sor DES. (c) Steady-state emission maxima of CPM labeled HSA in different concentrations of 0.5Ac/0.3Ur/0.2Sor DES in buffer (grey). (d) Hydrodynamic radius of HSA with DES concentrations (grey). The data points shown in red have been taken from REF-[85] and [87] and represent the emission maxima and hydrodynamic radius with GnHCl concentration in the respective figures. The error bar represents the standard deviation of the mean of three independent experiments.

Table 4. Steady-state emission maxima of CPM-tagged HSA, hydrodynamic radii (see Supplementary Material for calculation), and conformational fluctuation time of TMR-tagged HSA in different concentrations of 0.5Ac/0.3Ur/0.2Sor DES in buffer.

DES concentration (% V/V)	Emission Maxima (nm)	Hydrodynamic Radii (Å)	Conformational Fluctuation time (τ_R) (µs)
0	463.0± 1.0	38.2±2.6	27.0±6.6
5	462.8±0.7	36.6±2.6	32.4±3.7
10	462.8±0.6	36.5±1.9	32.0±4.8

15	462.6±0.6	36.4±1.8	36.0±7.9
20	461.9±0.7	36.0±2.0	31.8±6.7
25	461.8±0.8	37.8±3.5	34.0±5.1
30	462.2±0.5	40.4±3.1	29.0±6.9
35	462.3±0.6	42.9±3.0	32.0±7.2
40	462.3±0.9	46.0±2.6	45.0±9.1
45	462.1±0.8	46.5±3.4	60.0±10.4
50	462.5±1.0	46.8±2.9	71.0±9.6
55	462.4±0.5	47.1±3.6	80.0±7.0
60	462.3±0.6	47.0±3.0	85.0±9.7
65	462.0±0.7	47.2±2.8	90.0±6.3
70	461.8±0.7	47.5±3.3	95.0±7.9
80	461.3±1.0	49.0±3.5	110±10.0
90	461.0±0.8	*	*

* We could not measure the hydrodynamic radius and τ_R at 90% DES, as the data quality of HSA becomes very poor at this concentration

4.2.7. Conformational fluctuation of HSA in the presence of hydrated DESs

Besides the water dynamics, the intrinsic protein dynamics or conformational fluctuation dynamics can also play a role in dictating protein properties [76,77,79,80]. It is well-accepted that the protein structure is not rigid, instead, it is an average of several closely related structural conformations [112]. The interconversion timescale between these conformations is known as conformational fluctuation time. Many studies confirmed the role of such inherent dynamics on enzymatic activity [77,80,112,113]. Experimentally, the conformational fluctuation dynamics of proteins in the presence of DES have not been explored in detail. There are few studies of the conformational fluctuation dynamics of proteins in ILs [13,114], but probably only one or two studies reported the conformational dynamics of a protein in the case of DES

[47,115]. In our previous work, we correlated the flexible active site dynamics of bromelain to the superior proteolytic activity in the presence of a DES [45].

For the present case, we also have analyzed the conformational fluctuation dynamics from the FCS autocorrelation function (see Figure 10b). This fluctuation is a very local phenomenon and represents the ease of the concerted chain motion dynamics.[84,85,116] Because of this dynamics, the electron-rich amino acid residues around TMR (tagged in the domain-I of HSA) move close and away from the probe, thus modulating its fluorescence behaviour, and can be observed in the FCS experiment.[82,85] In the buffer, the measured value of conformational fluctuation time is 27 μs, which is following the previous report [85]. With the addition of DES, the conformational fluctuation dynamics become progressively slower (see figure 11 and table 4), significantly beyond ~30% DES. There could be various reasons for such modulations. Firstly, with increasing DES concentration, the viscosity of the medium increases, and this increased friction might slow down the side chain dynamics. However, the extent of slowing down of conformational dynamics involving domain-1 of HSA (~4 times) is much less than the increment of viscosity (~30 times) as we move from buffer to 80% DES. Secondly, the size of HSA increases (especially beyond 30% DES), so the surrounding electron-rich residues that quench TMR fluorescence now need to move a greater distance, and it might increase the timescale of such movement. However, in our previous publications, we showed that such a relationship between protein size and conformational time scale might not always hold [78,117,118]. At this stage, it is tough to predict the exact reason for such a trend, but it might have a key implication on its behaviour [77,119]. To note, a similar modulation of conformational flexibility was observed for another protein: bromelain in the same DES [45].

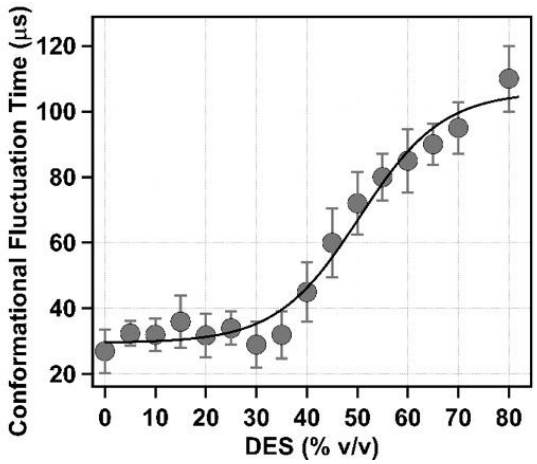

Figure 11. The variation of conformational fluctuation time of HSA as a function of 0.5Ac/0.3Ur/0.2Sor DES concentration in the buffer. The error bar represents the standard deviation of the mean of three independent experiments.

The conformational fluctuation dynamics and solvation dynamics are two very different information about protein and its surrounding solvent, respectively. Obviously, the internal protein dynamics depend on the rigidity of the surrounding solvent (associated water) and therefore there might be a correlation between them. Previously, a correlation has been established between internal protein dynamics in nanosecond timescale and solvation dynamics [120]. However, the correlation between microsecond conformational fluctuation and solvation is not known. Apparently, the rigid associated water structure should hinder side-chain dynamics, therefore an increase in the conformational fluctuations time should be associated with an increase in solvation time. Our results also indicate the same. Up to 40% DES, both parameters remain almost constant. However, beyond that there is an increase in both the solvation and conformational fluctuations time. Moreover, the dependence of conformational fluctuations on DES concentration (~ 4 times increment from 0 to 80% DES) is much steeper than that of the solvation time (~1.5 times increment from 0 to 90% DES). At this point, it is very difficult to ascertain the reason behind this. One possible explanation could be that both these parameters depend strongly on the protein structural modulation in the presence of DES. At higher DES concentrations, HSA is somewhat unfolded. For unfolded protein because the

exchange channel between associated and bulk water increases, solvation time decreases. However, for unfolded protein, because the distance between the tagged dye and the neighbouring amino acids increases, the conformational fluctuations time might increase. Another possibility may lie in the time scale and length scale of the dynamics. Solvation dynamics occur in the sub-picosecond to the nanosecond time scale and in the sub-nanometre length scale, whereas conformational fluctuations occur in the microsecond time scale and nanometre length scale. This difference in the time and length scale of these two dynamics might respond to a perturbation (viscosity change for example) differently.

4.2.8. Effect of DES content on the stability of HSA

Next, to understand the stability of HSA in the presence of DES, we have used steady-state fluorescence spectra of CPM-tagged HSA to obtain the melting curve of HSA (see Figures 12) in the presence of different DES contents. Generally, with denaturation, the protein becomes unfolded, and as a signature, any solvatochromic probe attached to the protein shows a red shift in the emission maximum. Representative steady-state fluorescence spectra are provided in Figures 12a-c. From the shift of emission spectra, we have calculated the fraction unfolded at each temperature using the equation, $f_U = \frac{\lambda^{em} - \lambda_N^{em}}{\lambda_U^{em} - \lambda_N^{em}}$. In this equation, λ^{em} is the emission maxima of CPM-tagged HSA at any temperature; λ_N^{em} and λ_U^{em} are the emission maxima of the native and unfolded state of HSA, respectively. As the thermal unfolding curve of HSA was not saturating, choosing the unfolded state from those data is very difficult. However, the GnHCl-induced chemical denaturation curve of HSA shows a hint of saturation and reached a totally unfolded state at 6 M GnHCl. So, we constructed the normalized melting curves (fraction unfolded) at each degree of hydrated DES (Figure 12), considering the lowest emission maxima as the native and the emission maxima of the 6 M GnHCl as the unfolded state of HSA. The temperature at which the fraction unfolded and folded becomes equal, i.e., fraction

unfolded = 0.5, can be considered as melting temperature. However, we restrained ourselves from extracting any melting temperature or thermodynamic entity from these curves, as the curves do not get saturated and reached the plateau, even at the highest temperature (373 K) used in this study. From the melting curves (Figure 12g), one could conclude that at low concentrations of DES (up to 30%), the change in the stability is less, but beyond that, a significant decrease in the stability is observed. Such decreasing stability can be a direct consequence of structural alteration of the HSA at higher DES concentration. We have seen an increase in the hydrodynamic radius of the HSA beyond 30% of DES. However, at the lower DES concentration, where the structure remains unperturbed and associated water dynamics do not change much, DES retains most of the stability of HSA. At very high concentrations of DES (80-90%) the associated water dynamics also slightly get perturbed along with the protein structure, which is probably responsible for the significant stability loss.

Next, we also measured the thermal stability of HSA in the constituent aqueous solution keeping the concentrations of each of the constituents same as in hydrated DES. Representative raw data and the melting curves are presented in Figures 12d-f and 12h. We found that at lower concentrations (up to 40%) the thermal stability curves of HSA both in the hydrated DES and component solution match well. However, after 40% the stability is a little higher in the case of hydrated DES than in component solutions (see Figure 12i). Probably the network-like structure of DES, which surely exists in the higher DES concentrations, has some protective role towards HSA.

Recently, we experimentally showed a strong correlation between protein stability and associated water structure modulation [50]. A pre-requisite of such correlation is that the added perturbation does not change the structure much. As this condition is not fulfilled in this case, any direct correlation of stability with associated water dynamics is not possible at this stage. In the future project, we will examine whether

a correlation between stability and associated water structure holds good in DES medium.

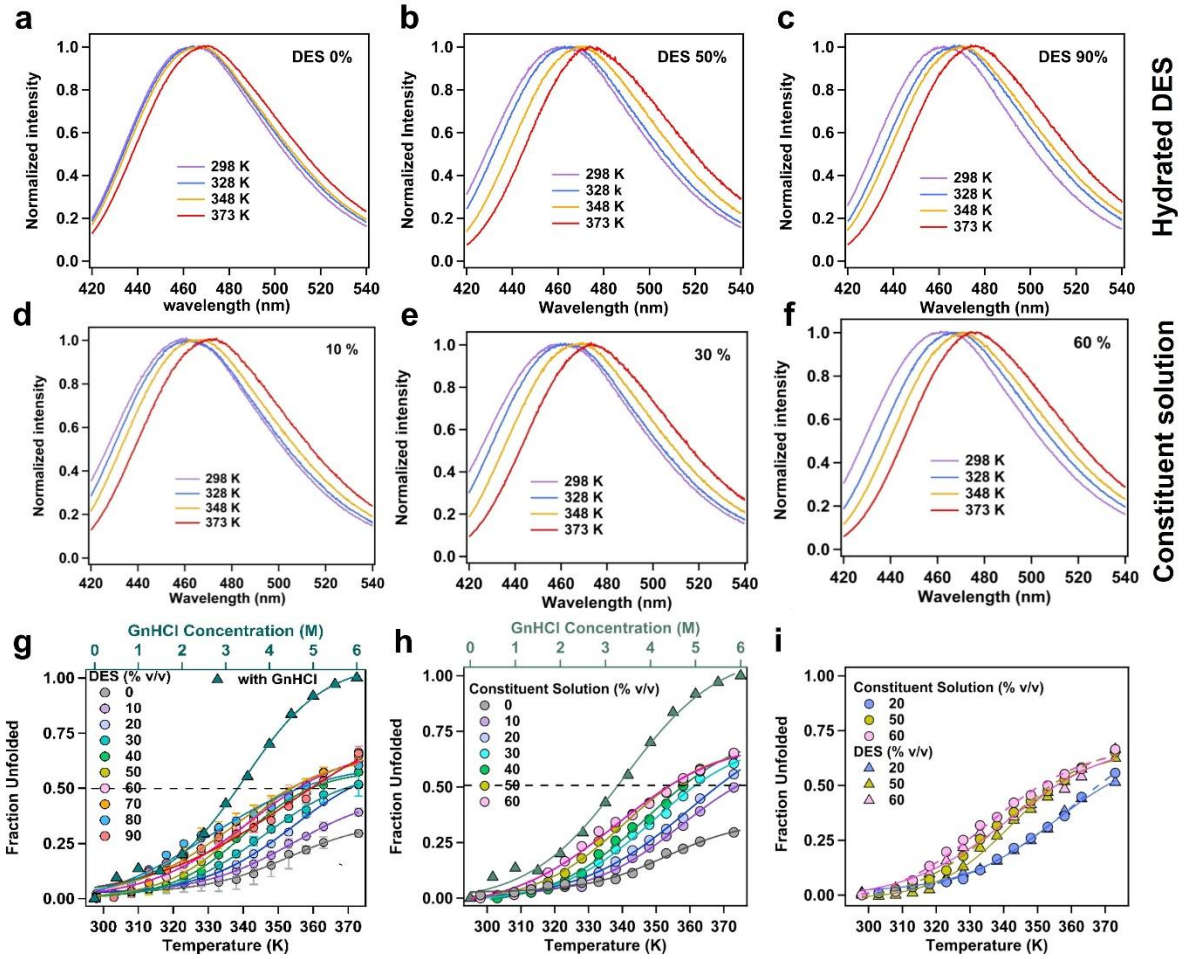

Figure 12. Representative intensity normalized temperature-dependent emission spectra of CPM tagged to HSA in the presence of, (a)-(c) differently hydrated 0.5Ac\0.3Ur\0.2Sor DES; and (d)-(f) solution of constituents of 0.5Ac\0.3Ur\0.2Sor DES. Melting curves in terms of fraction unfolded of CPM-tagged HSA at, (g) different concentrations of 0.5Ac/0.3Ur/0.2Sor DES in the buffer, and (h) different concentrations of constituent's solution in buffer. The solid lines are the eye guides. Note that emission maxima in the presence of 6M GnHCl have been taken as the totally unfolded state in calculating fraction unfolded curves at each DES concentration. Variation of the fraction unfolded with increasing concentration of GnHCl (dark green) was plotted with respect to the similar colour-coded top axis (green). The error bar represents the standard deviation of the mean of three independent experiments. (i) Comparison of melting curves of HSA in presence of similar concentrations of hydrated DES (circle and solid lines) and in its component's solution (triangle and broken lines).

4.3. Comparison of Our Results in the Light of Previous Literature:

The most thoroughly studied enzyme in DES is probably lipase [16,28–30,39–41,43,61,62,65,121]. The biocatalysis by lipase in DES has been first reported by Gorke *et al.* [39]. It was found that 12% urea led to a loss of 70% enzymatic activity of lipase. However, in choline chloride/urea (containing 66% urea) DES, merely less than 1% of enzymatic activity is lost and the stability of the enzyme was found to be higher in the DES than in the corresponding component solution [39]. Monhemi *et al.* with the help of MD simulation pointed out that an alteration of hydrogen bonding of water with the protein surface might have a role in modulating the enzyme stability and activity in such urea-based DESs [65]. Durand *et al.* observed that the addition of up to 20% water improves the lipase activity at least 10 times in choline chloride/urea DES [40]. However, in another study, Zhou *et al.* reported the deleterious effect of choline chloride/urea DES on *Candida antarctica* lipase B catalyzed epoxidation reaction, whereas choline chloride/sorbitol DES stood out as an efficient media for the same reaction [122]. These hints that activity and stability depend very much on the nature of protein and DES. Esquembre *et al.* were the first to examine the concentration effect of hydrated choline chloride/urea and choline chloride/glycerol DESs on hen egg lysozyme and found that aqueous dilution from the neat DES leads to refolding of the thermally denatured state of lysozyme and the activity was also recovered [36]. On the other hand, Zeng *et al.* reported refolding of thermally unfolded lysozyme with increasing betaine/urea DES concentration [123]. Various other experimental and simulation studies delineated the superiority of hydrated DESs over neat DESs [36–38,42–44,124,125]. There are few reports on bovine serum albumin (BSA) in urea-based DESs as well. The extraction efficiency of BSA in hydrated choline chloride/urea and betaine/urea DES was found to be more than in ILs and these DESs also keep the conformation of the protein intact [126]. However, the effect of neat DES on BSA was found to be detrimental [32]. Venkatesu and co-workers have recently reported BSA in a solvent system comprised of macromolecular crowders and DES together. Interestingly the combination of

choline chloride/urea with polyethylene glycol showed an elevated melting temperature of BSA than individual crowder or DES [127]. However, to the best of our knowledge, there is no report deciphering the enzymatic properties of HSA in any DES. Here we used a non-ionic DES (0.5Ac/0.3 Ur/ 0.2 Sor) at different degrees of hydration. Previously the structure, activity, and dynamics of proteolytic enzyme bromelain were reported in this same hydrated DES by our group [45]. We found that at all DES concentrations, enzymatic activity was retained. Moreover, at lower DES concentrations (up to 30% v/v) the proteolytic activity even increases compared to that in buffer and then it decreases with a further increase in the DES concentration. In this report, we measured the solvation dynamics of HSA in the same hydrated DES. To the best of our knowledge, this is probably the first experimental report on the solvation dynamics of any protein in DES. We found that associated water around the protein does not alter up to 70% v/v DES. We also found that the thermal stability of HSA does not change much up to 30% DES and then decreases with increasing DES concentration. This study provides a clue that enzymes remain active and stable in DES by keeping their associated water structure intact. However, any direct correlation of stability with associated water dynamics is not possible at this stage because structural alteration of the HSA at higher DES concentration (beyond 30%) can also influence the stability. An increment in protein hydrodynamic radius with DES addition was reported in the case of cellulase enzyme in the presence of ChCl-lactic acid DES [128]. Previously, Kist *et al.* also found a similar deleterious effect on the thermal stability of ribonuclease A with increasing concentration of choline chloride/urea DES [129]. Overall, the enzymatic property in DES depends on both the nature of DES constituents and proteins. Through this study, we want to emphasize considering associated water dynamics modulation in order to understand the protein behaviour in hydrated DES. Also, the associated water property might be one of the principal governing factors in controlling protein behavior in the presence of any additives.

4.4. Overall Understanding and Conclusions

Herein, we contemplated the modulation of solvation dynamics/conformational fluctuation dynamics around domain-I of HSA and the thermal stability of HSA in 0.5Ac/0.3Ur/0.2Sor DES with varying degrees of hydration to understand the intricacy of protein behaviour in DES. Also, from control experiments, we proved that at least beyond 30 % (v/v) DES it is surely a hydrated DES, the properties of which cannot be achieved just by mixing the solution of DES constituents.

The main findings can be summarised as follows: (i) We have measured the solvation dynamics of the hydrated DES system in the absence of protein using transient absorption spectroscopy and found that the average solvation time follows the medium viscosity but a portion of water remains bulk-like. (ii) Solvation dynamics around domain-I of HSA with increasing DES content slows down very slightly with respect to the huge viscosity increment (~83 times at 90% DES). Component analysis of solvation dynamics suggests that the first solvation shell remains unperturbed at least up to 70% DES. (iii) Although the mixture of individual components differs from hydrated DES in terms of microviscosity, the alteration of solvation dynamics of domain-I of HSA shows similar behaviour to that in hydrated DES. (iv) The microsecond conformational fluctuation dynamics of domain-I of HSA is unperturbed up to ~30% DES, and beyond that, it becomes gradually slower. (v) The thermal stability of HSA gradually decreases with the addition of DES. The effect is more prominent in the DES constituent's solution than in the same concentration of hydrated DES. Probably the network-like structure of DES plays some protective role against thermal stress.

Overall, this report is a part of our ongoing effort to achieve a holistic physical insight into why proteins remain stable and active in DES. The significance of water in any biophysical event is nearly beyond dispute. Especially, the biological water that directly interacts with the protein is a critical controlling factor. Herein, we showed that HSA maintains the associated water structure around it in the hydrated DES. Singularly, the first solvation shell around HSA remains unperturbed. Protein,

therefore, feels only an aqueous environment in the presence of DES, although the macroscopic properties of the solvent change significantly. We feel that this result is not expected considering current knowledge. Our result is probably the first experimental proof that protein remains stable and active in DES by keeping its associated water structure intact. We understand that a huge effort is necessary to generalize our claim by taking different DESs and proteins. We also acknowledge that a comparison of complete solvation dynamics, thermodynamic stability parameters, and enzymatic activity are essential. Our future works are aimed at this.

4.5. References:

(1) Hauer, B. Embracing Nature's Catalysts: A Viewpoint on the Future of Biocatalysis. *ACS Catal* **2020**, *10* (15), 8418–8427. https://doi.org/10.1021/acscatal.0c01708.

(2) Madhavan, A.; Sindhu, R.; Binod, P.; Sukumaran, R. K.; Pandey, A. Strategies for Design of Improved Biocatalysts for Industrial Applications. *Bioresour Technol* **2017**, *245*, 1304–1313. https://doi.org/10.1016/j.biortech.2017.05.031.

(3) Bommarius, A. S.; Paye, M. F. Stabilizing Biocatalysts. *Chem. Soc. Rev.* **2013**, *42* (15), 6534–6565. https://doi.org/10.1039/c3cs60137d.

(4) Robinson, P. K. Enzymes: Principles and Biotechnological Applications. *Essays Biochem* **2015**, *59*, 1–41. https://doi.org/10.1042/BSE0590001.

(5) Chen, K.; Arnold, F. H. Tuning the Activity of an Enzyme for Unusual Environments: Sequential Random Mutagenesis of Subtilisin E for Catalysis in Dimethylformamide. *Proc. Natl. Acad. Sci. USA* **1993**, *90*, 5618–5622.

(6) Arnold, F. H. Protein Engineering for Unusual Environments. *Curr. Opin. Biotechnol.* **1993**, *4*, 450–455.

(7) Fasan, R.; Chen, M. M.; Crook, N. C.; Arnold, F. H. Engineered Alkane-Hydroxylating Cytochrome P450BM3 Exhibiting Nativelike Catalytic Properties. *Angew. Chem. Int. Ed.* **2007**, *46* (44), 8414–8418. https://doi.org/10.1002/anie.200702616.

(8) Zaks, A.; Klibanov, A. M. Enzymatic Catalysis in Organic Media at 100°C. *Science (1979)* **1984**, *224* (4654), 1249–1251. https://doi.org/10.1126/science.6729453.

(9) Klibanov, A. M. Improving Enzymes by Using Them in Organic Solvents. *Nature* **2001**, *409*, 241–246.

(10) Panić, M.; Cvjetko Bubalo, M.; Radojčić Redovniković, I. Designing a Biocatalytic Process Involving Deep Eutectic Solvents. *J. Chem. Technology and Biotechnology* **2021**, *96* (1), 14–30. https://doi.org/10.1002/jctb.6545.

(11) van Rantwijk, F.; Sheldon, R. A. Biocatalysis in Ionic Liquids. *Chem. Rev.* **2007**, *107* (6), 2757–2785. https://doi.org/10.1021/cr050946x.

(12) Stepankova, V.; Bidmanova, S.; Koudelakova, T.; Prokop, Z.; Chaloupkova, R.; Damborsky, J. Strategies for Stabilization of Enzymes in Organic Solvents. *ACS Catal* **2013**, *3* (12), 2823–2836. https://doi.org/10.1021/cs400684x.

(13) Das, D. K.; Das, A. K.; Mandal, A. K.; Mondal, T.; Bhattacharyya, K. Effect of an Ionic Liquid on the Unfolding of Human Serum Albumin: A Fluorescence Correlation Spectroscopy Study. *ChemPhysChem* **2012**, *13* (7), 1949–1955. https://doi.org/10.1002/cphc.201100421.

(14) Murador, D. C.; de Souza Mesquita, L. M.; Vannuchi, N.; Braga, A. R. C.; de Rosso, V. V. Bioavailability and Biological Effects of Bioactive Compounds Extracted with Natural Deep Eutectic Solvents and Ionic

Liquids: Advantages over Conventional Organic Solvents. *Curr Opin Food Sci* **2019**, *26*, 25–34. https://doi.org/10.1016/j.cofs.2019.03.002.

(15) Sheldon, R. A. Biocatalysis in Ionic Liquids: State-of-the-Union. *Green Chem.* **2021**, *23* (21), 8406–8427. https://doi.org/10.1039/d1gc03145g.

(16) Schöfer, S. H.; Kaftzik, N.; Wasserscheid, P.; Kragl, U. Enzyme Catalysis in Ionic Liquids: Lipase Catalysed Kinetic Resolution of 1-Phenylethanol with Improved Enantioselectivity. *Chem. Commun.* **2001**, 425–426. https://doi.org/10.1039/b009389k.

(17) Bara, J. E.; Finotello, A.; Magee, J. W.; Qian, S.; O'Harra, K. E.; Dennis, G. P.; Noble, R. D. 110th Anniversary: Properties of Imidazolium-Based Ionic Liquids Bearing Both Benzylic and n-Alkyl Substituents. *Ind. Eng. Chem. Res.* **2019**, *58* (38), 17956–17964. https://doi.org/10.1021/acs.iecr.9b03159.

(18) Liu, Y.; Chen, X.; Men, S.; Licence, P.; Xi, F.; Ren, Z.; Zhu, W. The Impact of Cation Acidity and Alkyl Substituents on the Cation-Anion Interactions of 1-Alkyl-2,3-Dimethylimidazolium Ionic Liquids. *Phys. Chem. Chem. Phys.* **2019**, *21* (21), 11058–11065. https://doi.org/10.1039/c9cp01381d.

(19) Płotka-Wasylka, J.; de la Guardia, M.; Andruch, V.; Vilková, M. Deep Eutectic Solvents vs Ionic Liquids: Similarities and Differences. *Microchemical Journal* **2020**, *159*, 105539. https://doi.org/10.1016/j.microc.2020.105539.

(20) Smith, E. L.; Abbott, A. P.; Ryder, K. S. Deep Eutectic Solvents (DESs) and Their Applications. *Chem Rev* **2014**, *114* (21), 11060–11082. https://doi.org/10.1021/cr300162p.

(21) Domínguez de María, P.; Maugeri, Z. Ionic Liquids in Biotransformations: From Proof-of-Concept to Emerging Deep-Eutectic-Solvents. *Curr. Opin. Chem. Biol.* **2011**, *15* (2), 220–225. https://doi.org/10.1016/j.cbpa.2010.11.008.

(22) Mjalli, F. S.; Ahmed, O. U. Physical Properties and Intermolecular Interaction of Eutectic Solvents Binary Mixtures: Reline and Ethaline. *Asia-Pacific Journal of Chemical Engineering* **2016**, *11* (4), 549–557. https://doi.org/10.1002/apj.1978.

(23) Guo, W.; Hou, Y.; Ren, S.; Tian, S.; Wu, W. Formation of Deep Eutectic Solvents by Phenols and Choline Chloride and Their Physical Properties. *J. Chem. Eng. Data* **2013**, *58* (4), 866–872. https://doi.org/10.1021/je300997v.

(24) Yadav, N.; Venkatesu, P. Current Understanding and Insights towards Protein Stabilization and Activation in Deep Eutectic Solvents as Sustainable Solvent Media. *Phys. Chem. Chem. Phys.* **2022**, *24* (22), 13474–13509. https://doi.org/10.1039/D2CP00084A.

(25) Pätzold, M.; Siebenhaller, S.; Kara, S.; Liese, A.; Syldatk, C.; Holtmann, D. Deep Eutectic Solvents as Efficient Solvents in Biocatalysis. *Trends Biotechnol* **2019**, *37* (9), 943–959. https://doi.org/10.1016/j.tibtech.2019.03.007.

(26) Kist, J. A.; Zhao, H.; Mitchell-Koch, K. R.; Baker, G. A. The Study and Application of Biomolecules in Deep Eutectic Solvents. *J Mater Chem B* **2021**, *9* (3), 536–566. https://doi.org/10.1039/d0tb01656j.

(27) Almeida, J. S.; Capela, E. V.; Loureiro, A. M.; Tavares, A. P. M.; Freire, M. G. An Overview on the Recent Advances in Alternative Solvents as Stabilizers of Proteins and Enzymes. *ChemEngineering* **2022**, *6* (4), 51. https://doi.org/10.3390/chemengineering6040051.

(28) Kim, S. H.; Park, S.; Yu, H.; Kim, J. H.; Kim, H. J.; Yang, Y. H.; Kim, Y. H.; Kim, K. J.; Kan, E.; Lee, S. H. Effect of Deep Eutectic Solvent Mixtures on Lipase Activity and Stability. *J. Mol. Catal. B Enzym.* **2016**, *128*, 65–72. https://doi.org/10.1016/j.molcatb.2016.03.012.

(29) Juneidi, I.; Hayyan, M.; Hashim, M. A.; Hayyan, A. Pure and Aqueous Deep Eutectic Solvents for a Lipase-Catalysed Hydrolysis Reaction. *Biochem Eng J* **2017**, *117*, 129–138. https://doi.org/10.1016/j.bej.2016.10.003.

(30) Nian, B.; Cao, C.; Liu, Y. How Candida Antarctica Lipase B Can Be Activated in Natural Deep Eutectic Solvents: Experimental and Molecular Dynamics Studies. *Journal of Chemical Technology and Biotechnology* **2020**, *95* (1), 86–93. https://doi.org/10.1002/jctb.6209.

(31) Sanchez-Fernandez, A.; Basic, M.; Xiang, J.; Prevost, S.; Jackson, A. J.; Dicko, C. Hydration in Deep Eutectic Solvents Induces Non-Monotonic Changes in the Conformation and Stability of Proteins. *J. Am. Chem. Soc.* **2022**, *144* (51), 23657–23667. https://doi.org/10.1021/jacs.2c11190.

(32) Sanchez-Fernandez, A.; Edler, K. J.; Arnold, T.; Alba Venero, D.; Jackson, A. J. Protein Conformation in Pure and Hydrated Deep Eutectic Solvents. *Phys. Chem. Chem. Phys.* **2017**, *19* (13), 8667–8670. https://doi.org/10.1039/c7cp00459a.

(33) Sanchez-Fernandez, A.; Jackson, A. J. Proteins in Deep Eutectic Solvents: Structure, Dynamics and Interactions with the Solvent. In *Advances in Botanical Research*; Academic Press Inc., 2021; Vol. 97, pp 69–94. https://doi.org/10.1016/bs.abr.2020.09.003.

(34) Ma, C.; Laaksonen, A.; Liu, C.; Lu, X.; Ji, X. The Peculiar Effect of Water on Ionic Liquids and Deep Eutectic Solvents. *Chem. Soc. Rev.* **2018**, *47* (23), 8685–8720. https://doi.org/10.1039/c8cs00325d.

(35) Dai, Y.; Witkamp, G. J.; Verpoorte, R.; Choi, Y. H. Tailoring Properties of Natural Deep Eutectic Solvents with Water to Facilitate Their Applications. *Food Chem* **2015**, *187*, 14–19. https://doi.org/10.1016/j.foodchem.2015.03.123.

(36) Esquembre, R.; Sanz, J. M.; Wall, J. G.; Del Monte, F.; Mateo, C. R.; Ferrer, M. L. Thermal Unfolding and Refolding of Lysozyme in Deep Eutectic Solvents and Their Aqueous Dilutions. *Phys. Chem. Chem. Phys.* **2013**, *15* (27), 11248–11256. https://doi.org/10.1039/c3cp44299c.

(37) Xin, R.; Qi, S.; Zeng, C.; Khan, F. I.; Yang, B.; Wang, Y. A Functional Natural Deep Eutectic Solvent Based on Trehalose: Structural and Physicochemical Properties. *Food Chem* **2017**, *217*, 560–567. https://doi.org/10.1016/j.foodchem.2016.09.012.

(38) Niknaddaf, F.; Shahangian, S. S.; Heydari, A.; Hosseinkhani, S.; Sajedi, R. H. Deep Eutectic Solvents as a New Generation of Chemical Chaperones. *ChemistrySelect* **2018**, *3* (38), 10603–10607. https://doi.org/10.1002/slct.201802235.

(39) Gorke, J. T.; Srienc, F.; Kazlauskas, R. J. Deep Eutectic Solvents for Candida Antarctica Lipase B-Catalyzed Reactions. In *ACS Symposium Series*; 2010; Vol. 1038, pp 169–180. https://doi.org/10.1021/bk-2010-1038.ch014.

(40) Durand, E.; Lecomte, J.; Baréa, B.; Dubreucq, E.; Lortie, R.; Villeneuve, P. Evaluation of Deep Eutectic Solvent-Water Binary Mixtures for Lipase-Catalyzed Lipophilization of Phenolic Acids. *Green Chem.* **2013**, *15* (8), 2275–2282. https://doi.org/10.1039/c3gc40899j.

(41) Durand, E.; Lecomte, J.; Baréa, B.; Villeneuve, P. Towards a Better Understanding of How to Improve Lipase-Catalyzed Reactions Using Deep Eutectic Solvents Based on Choline Chloride. *European Journal of Lipid Science and Technology* **2014**, *116* (1), 16–23. https://doi.org/10.1002/ejlt.201300246.

(42) Huang, Z. L.; Wu, B. P.; Wen, Q.; Yang, T. X.; Yang, Z. Deep Eutectic Solvents Can Be Viable Enzyme Activators and Stabilizers. *Journal of*

Chemical Technology and Biotechnology **2014**, *89* (12), 1975–1981. https://doi.org/10.1002/jctb.4285.

(43) Cvjetko Bubalo, M.; Jurinjak Tušek, A.; Vinković, M.; Radošević, K.; Gaurina Srček, V.; Radojčić Redovniković, I. Cholinium-Based Deep Eutectic Solvents and Ionic Liquids for Lipase-Catalyzed Synthesis of Butyl Acetate. *J. Mol. Catal. B Enzym.* **2015**, *122*, 188–198. https://doi.org/10.1016/j.molcatb.2015.09.005.

(44) Yadav, N.; Bhakuni, K.; Bisht, M.; Bahadur, I.; Venkatesu, P. Expanding the Potential Role of Deep Eutectic Solvents toward Facilitating the Structural and Thermal Stability of α-Chymotrypsin. *ACS Sustain Chem Eng* **2020**, *8* (27), 10151–10160. https://doi.org/10.1021/acssuschemeng.0c02213.

(45) Das, N.; Khan, T.; Subba, N.; Sen, P. Correlating Bromelain's Activity with Its Structure and Active-Site Dynamics and the Medium's Physical Properties in a Hydrated Deep Eutectic Solvent. *Phys. Chem. Chem. Phys.* **2021**, *23* (15), 9337–9346. https://doi.org/10.1039/d1cp00046b.

(46) Sun, H.; Xin, R.; Qu, D.; Yao, F. Mechanism of Deep Eutectic Solvents Enhancing Catalytic Function of Cytochrome P450 Enzymes in Biosynthesis and Organic Synthesis. *J Biotechnol* **2020**, *323*, 264–273. https://doi.org/10.1016/j.jbiotec.2020.07.004.

(47) Hossain, S. S.; Paul, S.; Samanta, A. Structural Stability and Conformational Dynamics of Cytochrome c in Hydrated Deep Eutectic Solvents. *J. Phys. Chem. B* **2021**, *125* (22), 5757–5765. https://doi.org/10.1021/acs.jpcb.1c01975.

(48) Bhattacharyya, K. Nature of Biological Water: A Femtosecond Study. *Chemical Communications* **2008**, No. 25, 2848–2857. https://doi.org/10.1039/b800278a.

(49) Bagchi, B. Water Dynamics in the Hydration Layer around Proteins and Micelles. *Chem Rev* **2005**, *105* (9), 3197–3219. https://doi.org/10.1021/cr020661+.

(50) Das, N.; Tarif, E.; Dutta, A.; Sen, P. Associated Water Dynamics Might Be a Key Factor Affecting Protein Stability in the Crowded Milieu. *J. Phys. Chem. B* **2023**, *127* (14), 3151–3163. https://doi.org/10.1021/acs.jpcb.2c09043.

(51) Mondal, S.; Mukherjee, S.; Bagchi, B. Protein Hydration Dynamics: Much Ado about Nothing? *J. Phys. Chem. Lett.* **2017**, *8* (19), 4878–4882. https://doi.org/10.1021/acs.jpclett.7b02324.

(52) Qin, Y.; Wang, L.; Zhong, D. Dynamics and Mechanism of Ultrafast Water-Protein Interactions. *Proc. Natl. Acad. Sci. USA* **2016**, *113* (30), 8424–8429. https://doi.org/10.1073/pnas.1602916113.

(53) Pal, S. K.; Peon, J.; Bagchi, B.; Zewail, A. H. Biological Water: Femtosecond Dynamics of Macromolecular Hydration. *J. Phys. Chem. B* **2002**, *106* (48), 12376–12395. https://doi.org/10.1021/jp0213506.

(54) Bellissent-Funel, M. C.; Hassanali, A.; Havenith, M.; Henchman, R.; Pohl, P.; Sterpone, F.; Van Der Spoel, D.; Xu, Y.; Garcia, A. E. Water Determines the Structure and Dynamics of Proteins. *Chem Rev* **2016**, *116* (13), 7673–7697. https://doi.org/10.1021/acs.chemrev.5b00664.

(55) Pal, S. K.; Peon, J.; Zewail, A. H. Ultrafast Surface Hydration Dynamics and Expression of Protein Functionality: α-Chymotrypsin. *Proc. Natl. Acad. Sci. USA* **2002**, *99* (24), 15297–15302. https://doi.org/10.1073/pnas.242600399.

(56) Verma, P. K.; Rakshit, S.; Mitra, R. K.; Pal, S. K. Role of Hydration on the Functionality of a Proteolytic Enzyme α-Chymotrypsin under Crowded Environment. *Biochimie* **2011**, *93* (9), 1424–1433. https://doi.org/10.1016/j.biochi.2011.04.017.

(57) Ball, P. Water as an Active Constituent in Cell Biology. *Chem Rev* **2008**, *108* (1), 74–108. https://doi.org/10.1021/cr068037a.

(58) Shukla, N.; Pomarico, E.; Chen, L.; Chergui, M.; Othon, C. M. Retardation of Bulk Water Dynamics by Disaccharide Osmolytes. *J. Phys. Chem. B* **2016**, *120* (35), 9477–9483. https://doi.org/10.1021/acs.jpcb.6b07751.

(59) Guo, F.; Friedman, J. M. Osmolyte-Induced Perturbations of Hydrogen Bonding between Hydration Layer Waters: Correlation with Protein Conformational Changes. *J. Phys. Chem. B* **2009**, *113* (52), 16632–16642. https://doi.org/10.1021/jp9072284.

(60) Hishida, M.; Anjum, R.; Anada, T.; Murakami, D.; Tanaka, M. Effect of Osmolytes on Water Mobility Correlates with Their Stabilizing Effect on Proteins. *J. Phys. Chem. B* **2022**, *126* (13), 2466–2475. https://doi.org/10.1021/acs.jpcb.1c10634.

(61) Trodler, P.; Pleiss, J. Modeling Structure and Flexibility of Candida Antarctica Lipase B in Organic Solvents. *BMC Struct. Biol.* **2008**, *8*. https://doi.org/10.1186/1472-6807-8-9.

(62) Shehata, M.; Unlu, A.; Sezerman, U.; Timucin, E. Lipase and Water in a Deep Eutectic Solvent: Molecular Dynamics and Experimental Studies of the Effects of Water-In-Deep Eutectic Solvents on Lipase Stability. *J. Phys. Chem. B* **2020**, *124* (40), 8801–8810. https://doi.org/10.1021/acs.jpcb.0c07041.

(63) Wedberg, R.; Abildskov, J.; Peters, G. H. Protein Dynamics in Organic Media at Varying Water Activity Studied by Molecular Dynamics Simulation. *J. Phys. Chem. B* **2012**, *116* (8), 2575–2585. https://doi.org/10.1021/jp211054u.

(64) Bittner, J. P.; Zhang, N.; Huang, L.; Domínguez De María, P.; Jakobtorweihen, S.; Kara, S. Impact of Deep Eutectic Solvents (DESs) and

Individual Des Components on Alcohol Dehydrogenase Catalysis: Connecting Experimental Data and Molecular Dynamics Simulations. *Green Chem.* **2022**, *24* (3), 1120–1131. https://doi.org/10.1039/d1gc04059f.

(65) Monhemi, H.; Housaindokht, M. R.; Moosavi-Movahedi, A. A.; Bozorgmehr, M. R. How a Protein Can Remain Stable in a Solvent with High Content of Urea: Insights from Molecular Dynamics Simulation of Candida Antarctica Lipase B in Urea: Choline Chloride Deep Eutectic Solvent. *Phys. Chem. Chem. Phys.* **2014**, *16* (28), 14882–14893. https://doi.org/10.1039/c4cp00503a.

(66) Denisov, V. P.; Jonsson, B. H.; Halle, B. Hydration of Denatured and Molten Globule Proteins. *Nat Struct Biol* **1999**, *6* (3), 253–260. https://doi.org/10.1038/6692.

(67) Otting, G.; Liepinsh, E.; Wüthrich, K. Protein Hydration in Aqueous Solution. *Science (1979)* **1991**, *254* (5034), 974–980. https://doi.org/10.1126/science.1948083.

(68) Nandi, N.; Bhattacharyya, K.; Bagchi, B. Dielectric Relaxation and Solvation Dynamics of Water in Complex Chemical and Biological Systems. *Chem Rev* **2000**, *100* (6), 2013–2045. https://doi.org/10.1021/cr980127v.

(69) Russo, D.; Murarka, R. K.; Copley, J. R. D.; Head-Gordon, T. Molecular View of Water Dynamics near Model Peptides. *J. Phys. Chem. B* **2005**, *109* (26), 12966–12975. https://doi.org/10.1021/jp051137k.

(70) Qiu, W.; Zhang, L.; Okobiah, O.; Yang, Y.; Wang, L.; Zhong, D.; Zewail, A. H. Ultrafast Solvation Dynamics of Human Serum Albumin: Correlations with Conformational Transitions and Site-Selected Recognition. *J. Phys. Chem. B* **2006**, *110* (21), 10540–10549. https://doi.org/10.1021/jp055989w.

(71) Rastogi, H.; Chowdhury, P. K. Correlating the Local and Global Dynamics of an Enzyme in the Crowded Milieu. *J. Phys. Chem. B* **2022**, *126* (17), 3208–3223. https://doi.org/10.1021/acs.jpcb.1c09759.

(72) Pal, S. K.; Mandai, D.; Sukul, D.; Sen, S.; Bhattacharyya, K. Solvation Dynamics of DCM in Human Serum Albumin. *J. Phys. Chem. B* **2001**, *105* (7), 1438–1441. https://doi.org/10.1021/jp002368o.

(73) Houston, P.; Macro, N.; Kang, M.; Chen, L.; Yang, J.; Wang, L.; Wu, Z.; Zhong, D. Ultrafast Dynamics of Water-Protein Coupled Motions around the Surface of Eye Crystallin. *J. Am. Chem. Soc.* **2020**, *142* (8), 3997–4007. https://doi.org/10.1021/jacs.9b13506.

(74) Zhang, L.; Wang, L.; Kao, Y.-T.; Qiu, W.; Yang, Y.; Okobiah, O.; Zhong, D. Mapping Hydration Dynamics around a Protein Surface. *Proc. Natl. Acad. Sci. USA* **2007**, *104* (47), 18461–18466.

(75) Maroncelli, M.; Fleming, G. R. Picosecond Solvation Dynamics of Coumarin 153: The Importance of Molecular Aspects of Solvation. *J. Chem. Phys.* **1987**, *86* (11), 6221–6239. https://doi.org/10.1063/1.452460.

(76) Das, N.; Sen, P. Structural, Functional, and Dynamical Responses of a Protein in a Restricted Environment Imposed by Macromolecular Crowding. *Biochemistry* **2018**, *57* (42), 6078–6089. https://doi.org/10.1021/acs.biochem.8b00599.

(77) Das, N.; Yadav, S.; Negi, K. S.; Tarif, E.; Sen, P. Does Microsecond Active-Site Dynamics Primarily Control Proteolytic Activity of Bromelain? Clues from Single Molecular Level Study with a Denaturant, a Stabilizer and a Macromolecular Crowder. *BBA Advances* **2022**, *2*, 100041. https://doi.org/10.1016/j.bbadva.2022.100041.

(78) Das, N.; Sen, P. Macromolecular Crowding: How Shape and Interaction Affect the Structure, Function, Conformational Dynamics and Relative

Domain Movement of a Multi-Domain Protein. *Phys. Chem. Chem. Phys.* **2022**, *24* (23), 14242–14256. https://doi.org/10.1039/D1CP04842B.

(79) Yon, J. M.; Perahia, D.; Ghélis, C. Conformational Dynamics and Enzyme Activity. *Biochimie* **1998**, *80* (1), 33–42. https://doi.org/10.1016/S0300-9084(98)80054-0.

(80) Guo, J.; Zhou, H. X. Protein Allostery and Conformational Dynamics. *Chemical Reviews*. 2016, pp 6503–6515. https://doi.org/10.1021/acs.chemrev.5b00590.

(81) Torgeson, K. R.; Clarkson, M. W.; Granata, D.; Lindorff-Larsen, K.; Page, R.; Peti, W. Conserved Conformational Dynamics Determine Enzyme Activity. *Sci Adv* **2022**, *8* (31), eabo5546. https://doi.org/10.1126/sciadv.abo5546.

(82) Nandy, A.; Chakraborty, S.; Nandi, S.; Bhattacharyya, K.; Mukherjee, S. Structure, Activity, and Dynamics of Human Serum Albumin in a Crowded Pluronic F127 Hydrogel. *J. Phys. Chem. B* **2019**, *123* (16), 3397–3408. https://doi.org/10.1021/acs.jpcb.9b00219.

(83) Shil, S.; Das, N.; Sengupta, B.; Sen, P. Sucrose-Induced Stabilization of Domain-II and Overall Human Serum Albumin against Chemical and Thermal Denaturation. *ACS Omega* **2018**, *3* (12), 16633–16642. https://doi.org/10.1021/acsomega.8b01832.

(84) Sengupta, B.; Das, N.; Sen, P. Elucidation of Ms Dynamics of Domain-III of Human Serum Albumin during the Chemical and Thermal Unfolding: A Fluorescence Correlation Spectroscopic Investigation. *Biophys Chem* **2017**, *221*, 17–25. https://doi.org/10.1016/j.bpc.2016.11.006.

(85) Yadav, R.; Sengupta, B.; Sen, P. Conformational Fluctuation Dynamics of Domain i of Human Serum Albumin in the Course of Chemically and Thermally Induced Unfolding Using Fluorescence Correlation

Spectroscopy. *J. Phys. Chem. B* **2014**, *118* (20), 5428–5438. https://doi.org/10.1021/jp502762t.

(86) Sengupta, B.; Acharyya, A.; Sen, P. Elucidation of the Local Dynamics of Domain-III of Human Serum Albumin over the Ps–Ms Time Regime Using a New Fluorescent Label. *Phys. Chem. Chem. Phys.* **2016**, *18* (41), 28548–28555. https://doi.org/10.1039/C6CP05743H.

(87) Das, N.; Sahu, S.; Khan, T.; Sen, P. Site-Specific Heterogeneity of Multi-Domain Human Serum Albumin and Its Origin: A Red Edge Excitation Shift Study. *Photochem. Photobiol.* **2023**, *99* (2), 538–546.

(88) Curry, S.; Mandelkow, H.; Brick, P.; Franks, N. Crystal Structure of Human Serum Albumin Complexed with Fatty Acid Reveals an Asymmetric Distribution of Binding Sites. *Nature Structural Biology 1998 5:9* **1998**, *5* (9), 827–835. https://doi.org/10.1038/1869.

(89) Gorke, J. T.; Srienc, F.; Kazlauskas, R. J. Hydrolase-Catalyzed Biotransformations in Deep Eutectic Solvents. *Chemical Communications* **2008**, No. 10, 1235–1237. https://doi.org/10.1039/b716317g.

(90) Toledo, M. L.; Pereira, M. M.; Freire, M. G.; Silva, J. P. A.; Coutinho, J. A. P.; Tavares, A. P. M. Laccase Activation in Deep Eutectic Solvents. *ACS Sustain Chem Eng* **2019**, *7* (13), 11806–11814. https://doi.org/10.1021/acssuschemeng.9b02179.

(91) Cao, J.; Su, E. Hydrophobic Deep Eutectic Solvents: The New Generation of Green Solvents for Diversified and Colorful Applications in Green Chemistry. *J. Clean. Prod.* **2021**, *314*, 127965. https://doi.org/10.1016/j.jclepro.2021.127965.

(92) Van Osch, D. J. G. P.; Dietz, C. H. J. T.; Warrag, S. E. E.; Kroon, M. C. The Curious Case of Hydrophobic Deep Eutectic Solvents: A Story on the

Discovery, Design, and Applications. *ACS Sustain Chem Eng* **2020**, *8* (29), 10591–10612. https://doi.org/10.1021/acssuschemeng.0c00559.

(93) Van Osch, D. J. G. P.; Dietz, C. H. J. T.; Van Spronsen, J.; Kroon, M. C.; Gallucci, F.; Van Sint Annaland, M.; Tuinier, R. A Search for Natural Hydrophobic Deep Eutectic Solvents Based on Natural Components. *ACS Sustain Chem Eng* **2019**, *7* (3), 2933–2942. https://doi.org/10.1021/acssuschemeng.8b03520.

(94) Subba, N.; Polok, K.; Piatkowski, P.; Ratajska-Gadomska, B.; Biswas, R.; Gadomski, W.; Sen, P. Temperature-Dependent Ultrafast Solvation Response and Solute Diffusion in Acetamide-Urea Deep Eutectic Solvent. *J. Phys. Chem. B* **2019**, *123* (43), 9212–9221. https://doi.org/10.1021/ACS.JPCB.9B07794.

(95) Mukherjee, K.; Das, S.; Tarif, E.; Barman, A.; Biswas, R. Dielectric Relaxation in Acetamide + Urea Deep Eutectics and Neat Molten Urea: Origin of Time Scales via Temperature Dependent Measurements and Computer Simulations. *J. Chem. Phys.* **2018**, *149* (12), 124501. https://doi.org/10.1063/1.5040071.

(96) Suriyanarayanan, S.; Olsson, G. D.; Kathiravan, S.; Ndizeye, N.; Nicholls, I. A. Non-Ionic Deep Eutectic Liquids: Acetamide–Urea Derived Room Temperature Solvents. *Int. J. Mol. Sci.* **2019**, *20* (12), 2857. https://doi.org/10.3390/ijms20122857.

(97) Subba, N.; Sahu, P.; Das, N.; Sen, P. Rational Design, Preparation and Characterization of a Ternary Non-Ionic Room-Temperature Deep Eutectic Solvent Derived from Urea, Acetamide, and Sorbitol. *J. Chem. Phys.* **2021**, *133* (1), 25. https://doi.org/10.1007/s12039-020-01866-2.

(98) Hammond, O. S.; Bowron, D. T.; Edler, K. J. The Effect of Water upon Deep Eutectic Solvent Nanostructure: An Unusual Transition from Ionic Mixture

to Aqueous Solution. *Angew. Chem. Int. Ed.* **2017**, *129* (33), 9914–9917. https://doi.org/10.1002/ange.201702486.

(99) El Achkar, T.; Fourmentin, S.; Greige-Gerges, H. Deep Eutectic Solvents: An Overview on Their Interactions with Water and Biochemical Compounds. *J. Mol. Liq.* **2019**, *288*, 111028. https://doi.org/10.1016/j.molliq.2019.111028.

(100) Dai, Y.; Witkamp, G. J.; Verpoorte, R.; Choi, Y. H. Tailoring Properties of Natural Deep Eutectic Solvents with Water to Facilitate Their Applications. *Food Chem* **2015**, *187*, 14–19. https://doi.org/10.1016/j.foodchem.2015.03.123.

(101) D'Agostino, C.; Gladden, L. F.; Mantle, M. D.; Abbott, A. P.; Ahmed, E. I.; Al-Murshedi, A. Y. M.; Harris, R. C. Molecular and Ionic Diffusion in Aqueous-Deep Eutectic Solvent Mixtures: Probing Inter-Molecular Interactions Using PFG NMR. *Phys. Chem. Chem. Phys.* **2015**, *17* (23), 15297–15304. https://doi.org/10.1039/c5cp01493j.

(102) Dugoni, G. C.; Di Pietro, M. E.; Ferro, M.; Castiglione, F.; Ruellan, S.; Moufawad, T.; Moura, L.; Costa Gomes, M. F.; Fourmentin, S.; Mele, A. Effect of Water on Deep Eutectic Solvent/β-Cyclodextrin Systems. *ACS Sustain Chem Eng* **2019**, *7* (7), 7277–7285. https://doi.org/10.1021/acssuschemeng.9b00315.

(103) Schiller, R. THE STOKES-EINSTEIN LAW BY MACROSCOPIC ARGUMENTS. *Int. J. Radiat. Appl. Instrum* **1991**, *37* (3), 549–550.

(104) Das, N.; Sen, P. Dynamic Heterogeneity and Viscosity Decoupling: Origin and Analytical Prediction. *Phys. Chem. Chem. Phys.* **2021**, *23* (29), 15749–15757. https://doi.org/10.1039/d1cp01804c.

(105) Das, N.; Subba, N.; Sen, P. Viscosity Decoupling Does Not Guarantee Dynamic Heterogeneity: A Way Out. *J. Photochem. Photobiol. A: Chem.* **2023**, *436*, 114361. https://doi.org/10.1016/J.JPHOTOCHEM.2022.114361.

(106) Mukherjee, S.; Mondal, S.; Bagchi, B. Distinguishing Dynamical Features of Water inside Protein Hydration Layer: Distribution Reveals What Is Hidden behind the Average. *J. Chem. Phys.* **2017**, *147* (2), 024901. https://doi.org/10.1063/1.4990693.

(107) Mondal, S.; Mukherjee, S.; Bagchi, B. Origin of Diverse Time Scales in the Protein Hydration Layer Solvation Dynamics: A Simulation Study. *J. Chem. Phys.* **2017**, *147* (15), 154901. https://doi.org/10.1063/1.4995420.

(108) Wingfield, P. T. Use of Protein Folding Reagents. *Curr Protoc Protein Sci* **2016**, *2016*, A.3A.1-A.3A.8. https://doi.org/10.1002/0471140864.psa03as84.

(109) Heller, W. T. Comparison of the Thermal Denaturing of Human Serum Albumin in the Presence of Guanidine Hydrochloride and 1-Butyl-3-Methylimidazolium Ionic Liquids. *J. Phys. Chem. B* **2013**, *117* (8), 2378–2383. https://doi.org/10.1021/jp400079p.

(110) Ahmad, B.; Ahmed, M. Z.; Haq, S. K.; Khan, R. H. Guanidine Hydrochloride Denaturation of Human Serum Albumin Originates by Local Unfolding of Some Stable Loops in Domain III. *Biochim Biophys Acta Proteins Proteom* **2005**, *1750* (1), 93–102. https://doi.org/10.1016/j.bbapap.2005.04.001.

(111) Mohan, V.; Sengupta, B.; Acharyya, A.; Yadav, R.; Das, N.; Sen, P. Region-Specific Double Denaturation of Human Serum Albumin: Combined Effects of Temperature and GnHCl on Structural and Dynamical Responses. *ACS Omega* **2018**, *3* (8), 10406–10417. https://doi.org/10.1021/acsomega.8b00967.

(112) Kahsai, A. W.; Rajagopal, S.; Sun, J.; Xiao, K. Monitoring Protein Conformational Changes and Dynamics Using Stable-Isotope Labeling and Mass Spectrometry. *Nat Protoc* **2014**, *9* (6), 1301–1319. https://doi.org/10.1038/nprot.2014.075.

(113) Gangupomu, V. K.; Wagner, J. R.; Park, I. H.; Jain, A.; Vaidehi, N. Mapping Conformational Dynamics of Proteins Using Torsional Dynamics Simulations. *Biophys J* **2013**, *104* (9), 1999–2008. https://doi.org/10.1016/j.bpj.2013.01.050.

(114) Mojumdar, S. Sen; Chowdhury, R.; Chattoraj, S.; Bhattacharyya, K. Role of Ionic Liquid on the Conformational Dynamics in the Native, Molten Globule, and Unfolded States of Cytochrome C: A Fluorescence Correlation Spectroscopy Study. *J. Phys. Chem. B* **2012**, *116* (40), 12189–12198. https://doi.org/10.1021/jp307297s.

(115) Barik, S.; Mahapatra, A.; Preeyanka, N.; Sarkar, M. Assessing the Impact of Choline Chloride and Benzyltrimethylammonium Chloride-Based Deep Eutectic Solvents on the Structure and Conformational Dynamics of Bovine Serum Albumin: A Combined Steady-State, Time-Resolved Fluorescence and Fluorescence Correlation Spectroscopic Study. *Phys. Chem. Chem. Phys.* **2023**, *25* (29), 20093–20108. https://doi.org/10.1039/d3cp01380d.

(116) Haldar, S.; Mitra, S.; Chattopadhyay, K. Role of Protein Stabilizers on the Conformation of the Unfolded State of Cytochrome c and Its Early Folding Kinetics: Investigation at Single Molecular Resolution. *J. Biol. Chem.* **2010**, *285* (33), 25314–25323. https://doi.org/10.1074/jbc.M110.116673.

(117) Das, N.; Sen, P. Size-Dependent Macromolecular Crowding Effect on the Thermodynamics of Protein Unfolding Revealed at the Single Molecular Level. *Int. J. Biol. Macromol.* **2019**, *141*, 843–854. https://doi.org/10.1016/j.ijbiomac.2019.09.029.

(118) Das, N.; Sen, P. Shape-Dependent Macromolecular Crowding on the Thermodynamics and Microsecond Conformational Dynamics of Protein Unfolding Revealed at the Single-Molecule Level. *J. Phys. Chem. B* **2020**, *124* (28), 5858–5871. https://doi.org/10.1021/acs.jpcb.0c03897.

(119) Sen, S.; Kumar, H.; Udgaonkar, J. B. Microsecond Dynamics During the Binding-Induced Folding of an Intrinsically Disordered Protein. *J. Mol. Biol.* **2021**, *433* (22), 167254. https://doi.org/10.1016/j.jmb.2021.167254.

(120) Jha, A.; Ishii, K.; Udgaonkar, J. B.; Tahara, T.; Krishnamoorthy, G. Exploration of the Correlation between Solvation Dynamics and Internal Dynamics of a Protein. *Biochemistry* **2011**, *50* (3), 397–408. https://doi.org/10.1021/bi101440c.

(121) Durand, E.; Lecomte, J.; Baréa, B.; Piombo, G.; Dubreucq, E.; Villeneuve, P. Evaluation of Deep Eutectic Solvents as New Media for Candida Antarctica B Lipase Catalyzed Reactions. *Process Biochemistry* **2012**, *47* (12), 2081–2089. https://doi.org/10.1016/j.procbio.2012.07.027.

(122) Zhou, P.; Wang, X.; Yang, B.; Hollmann, F.; Wang, Y. Chemoenzymatic Epoxidation of Alkenes with Candida Antarctica Lipase B and Hydrogen Peroxide in Deep Eutectic Solvents. *RSC Adv* **2017**, *7* (21), 12518–12523. https://doi.org/10.1039/c7ra00805h.

(123) Zeng, C. X.; Qi, S. J.; Xin, R. P.; Yang, B.; Wang, Y. H. Synergistic Behavior of Betaine-Urea Mixture: Formation of Deep Eutectic Solvent. *J. Mol. Liq.* **2016**, *219*, 74–78. https://doi.org/10.1016/j.molliq.2016.02.076.

(124) Delorme, A. E.; Andanson, J. M.; Verney, V. Improving Laccase Thermostability with Aqueous Natural Deep Eutectic Solvents. *Int. J. Biol. Macromol.* **2020**, *163*, 919–926. https://doi.org/10.1016/j.ijbiomac.2020.07.022.

(125) Harifi-Mood, A. R.; Ghobadi, R.; Divsalar, A. The Effect of Deep Eutectic Solvents on Catalytic Function and Structure of Bovine Liver Catalase. *Int. J. Biol. Macromol.* **2017**, *95*, 115–120. https://doi.org/10.1016/j.ijbiomac.2016.11.043.

(126) Zeng, Q.; Wang, Y.; Huang, Y.; Ding, X.; Chen, J.; Xu, K. Deep Eutectic Solvents as Novel Extraction Media for Protein Partitioning. *Analyst* **2014**, *139* (10), 2565–2573. https://doi.org/10.1039/c3an02235h.

(127) Bhakuni, K.; Yadav, N.; Venkatesu, P. A Novel Amalgamation of Deep Eutectic Solvents and Crowders as Biocompatible Solvent Media for Enhanced Structural and Thermal Stability of Bovine Serum Albumin. *Phys. Chem. Chem. Phys.* **2020**, *22* (42), 24410–24422. https://doi.org/10.1039/d0cp04397d.

(128) Yadav, N.; Chahar, D.; Bisht, M.; Venkatesu, P. Assessing the Compatibility of Choline-Based Deep Eutectic Solvents for the Structural Stability and Activity of Cellulase: Enzyme Sustain at High Temperature. *Int. J. Biol. Macromol.* **2023**, *249*, 125988. https://doi.org/10.1016/j.ijbiomac.2023.125988.

(129) Kist, J. A.; Henzl, M. T.; Bañuelos, J. L.; Baker, G. A. Calorimetric Evaluation of the Operational Thermal Stability of Ribonuclease A in Hydrated Deep Eutectic Solvents. *ACS Sustain Chem Eng* **2019**, *7* (15), 12682–12687. https://doi.org/10.1021/acssuschemeng.9b02585.

Chapter 5

Critical Role of Water beyond the Media to Maintain Protein Stability and Activity in Hydrated Deep Eutectic Solvent

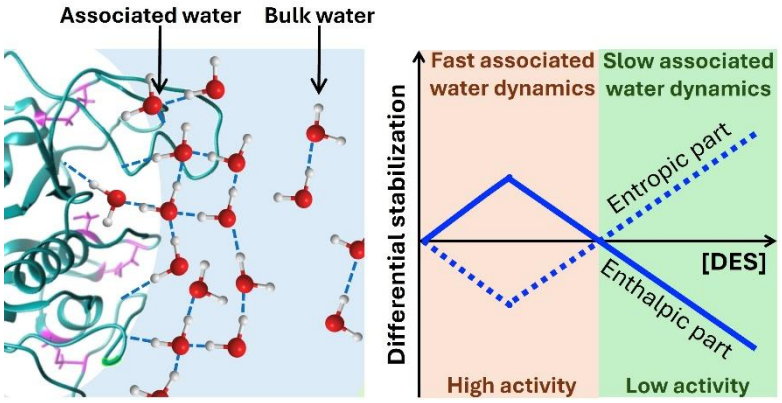

Tanmoy Khan, Nilimesh Das, Suman Bhowmik, Kuldeep Singh Negi, and Pratik Sen*

J. Phys. Chem. B **2025**, 129, 162-175.

Abstract

Hydrated deep eutectic solvents (DESs) are recognized for their potential in biocatalysis due to their tunability, biocompatibility, greenness, and ability to keep protein stable and active. However, the mechanisms governing enzyme stability and activity in DESs remain poorly understood. Herein, using bromelain as the model enzyme and acetamide(0.5)/urea(0.3)/sorbitol(0.2) as the model DES, we provide experimental evidence that modulation of associated water plays a key role in dictating protein stability and activity in hydrated DES. Specifically, rigid associated water at higher DES concentrations (beyond 40% v/v) stabilizes bromelain through entropy but destabilizes it through enthalpy. On the other hand, flexible associated water dynamics at lower DES concentrations result in an opposite thermodynamic outcome. Importantly, the bulk water dynamics cannot explain the stability trend, which emphasizes the critical role of water near the protein surface. Strikingly, associated water dynamics also correlates strongly with bromelain's proteolytic activity. An increasing flexibility of the associated water dynamics leads to the enhancement of the activity. This is the first study to experimentally link associated water dynamics to enzyme behaviour in hydrated DES, offering insights that could guide future developments in solvent engineering for enzyme catalysis.

5.1. Introduction

Until mid-1980s, it was believed that proteins remained stable and active only in aqueous media, thus limiting their use in biocatalysis [1,2,5]. This paradigm shifted with the success of engineered enzymes, using directed evolution, which maintained stability and activity in organic solvents [2–5]. In addition to protein engineering, environmental/solvent engineering may also lead to the tailored performance of specific enzymes for biocatalysis [1,6–8]. Deep eutectic solvents (DESs) have emerged as promising biocatalytic media due to their unique characteristics, such as ease of synthesis, greenness, tunability (making extraction and product isolation easier), and biocompatibility (Scheme 1) [9–15]. Furthermore, many conceivable combinations of constituents result in a huge library of deep eutectic systems, indicating that DES has the potential to revolutionize this field [16]. Numerous reports show that apart from the aqueous medium, proteins remain stable and active in such media as well [12,15,17–31]. and even sometimes show superior activity over the buffer [15,19,24,28,32–35]. However, only a handful of reports delve into the mechanism behind retained protein stability and activity in DESs, and a thorough understanding is very much missing in the literature [36–39].

It was believed that DES stabilizes proteins primarily through unique interactions between its components and amino acids of the protein through the formation of a hydrogen-bond network and ionic interactions [36,40,41]. These interactions can reduce electrostatic repulsion between charged amino acid residues to maintain a native-like structure [38,42]. A recent report utilized DES-protein interaction to precisely control the conformational landscape of proteins [43]. Some reports discussed the influence of constituents' nature and the hydrogen bonding strength between constituents on the structural and functional properties of some proteins [24,36,38,44]. DES media might provide a unique microenvironment that maintains the enzyme's native-like state through specific interactions between its components [36,38,39,44,45]. Some DESs might enhance enzyme stability due to their specific thermal properties [46–48]. A recent study by Sun *et al.* found that the physical properties of the DES, like density, viscosity, refractive index, etc., affect the catalytic activity and thermal

stability of the cytochrome P450 enzyme [29]. Our group also reported that protein properties like hydrodynamic radius and internal dynamics, along with media properties like polarity and viscosity, profoundly affect the enzymatic activity of bromelain [28].

A careful introspection into the previous literature reveals that enzymes in hydrated DESs show superior stability and activity than the neat DESs [26–28,30,33,49]. Moreover, hydrated DES also overcomes the challenges of protein incorporation in predominantly viscous DES (Scheme 1), along with offering an edge for tailoring solvent properties [27,50,51]. The necessity of water in almost all biological processes is axiomatic, and studies have established the role of water[52–56], mainly the water near the protein surface (which is commonly termed associated or biological water), in governing proteins' stability and activity [57–64]. For example, using terahertz spectroscopy, Heyden *et al.* showed that less flexible water dynamics with disaccharides lead to higher stability compared to monosaccharides [65]. We recently showed that the stabilization of papain by osmolytes is associated with slowing down water dynamics, whereas faster water dynamics accompany destabilization [58]. Similar results were obtained by Hishida *et al* [56]. Zewail group also published many reports in this same line [53,59,62,66,67]. There are a few reports that considered water dynamics modulation in the presence of macromolecular crowder as well to explain the stability of a protein [57,61,63,68,69]. Generally, it is observed that flexible hydration dynamics around the protein lead to a loss in protein stability and vice versa [58,62,66,70]. Moreover, many reports hypothesized the presence of a protection layer by DES around protein, which protects the protein from thermal stress [25,36,38,44].

In addition to the immense role of water in protein's stability, the role of water is necessary for its function [59,61,63,67]. Few studies in the literature tried to correlate enzyme activity with the water structure [59,61,63,67,71,72]. For example, a study on α-chymotrypsin in the presence of poly-ethylene glycol crowder revealed that flexible hydration dynamics is linked to the enzyme's active state [61]. Sykora *et al.* used protein engineering on haloalkane dehalogenase and found that water dynamics is a key to its function despite successful structural changes [73]. A mechanistic study

reveals that flexible water dynamics favor product formation from the enzyme-substrate complex for bromelain in the presence of a macromolecular crowder [63]. Many reports even showed that a small amount of water dramatically improves the functionality of enzymes inside anhydrous DES [30,37,41,74]. This further highlights the importance of water modulation around protein surfaces. Therefore, we proposed that the consideration of associated water dynamics is essential in understanding protein behavior in DESs, hydrated DESs, or any other medium.

However, the modulation of water structure and dynamics in the case of DESs is almost unexplored. Our group was the first to experimentally observe the associated water dynamics around a protein (human serum albumin, HSA) in the hydrated DES [20]. We showed that associated water dynamics remain largely unaltered with the change in hydration level, although the solvent properties like viscosity and polarity change drastically [20]. We hypothesized that this unperturbed associated water might be responsible for protein stability and activity inside hydrated DES, in general [20.] In this report, we move one step ahead, to measure the stability and activity of a proteolytic enzyme, bromelain, in acetamide/urea/sorbitol DES as a function of hydration level and establish a novel relationship between protein stability and activity with associated water dynamics (Scheme 1). This ternary DES, composed of acetamide, urea, and sorbitol, was chosen for its non-ionic nature, ability to remain liquid even at 280 K, and the molecular-level understanding established in our earlier reports [20,28,75,76]. Here, we used the fluorescence based time-dependent fluorescence Stokes shift (TDFSS) method to study associated water dynamics in the immediate vicinity of the protein [52,77,78]. No note, other routinely used techniques to measure water dynamics, like nuclear magnetic resonance (NMR), dielectric relaxation (DR), and quasi-elastic neutron scattering (QENS), capture signals from the entire system, and can only give an average picture [79–81].

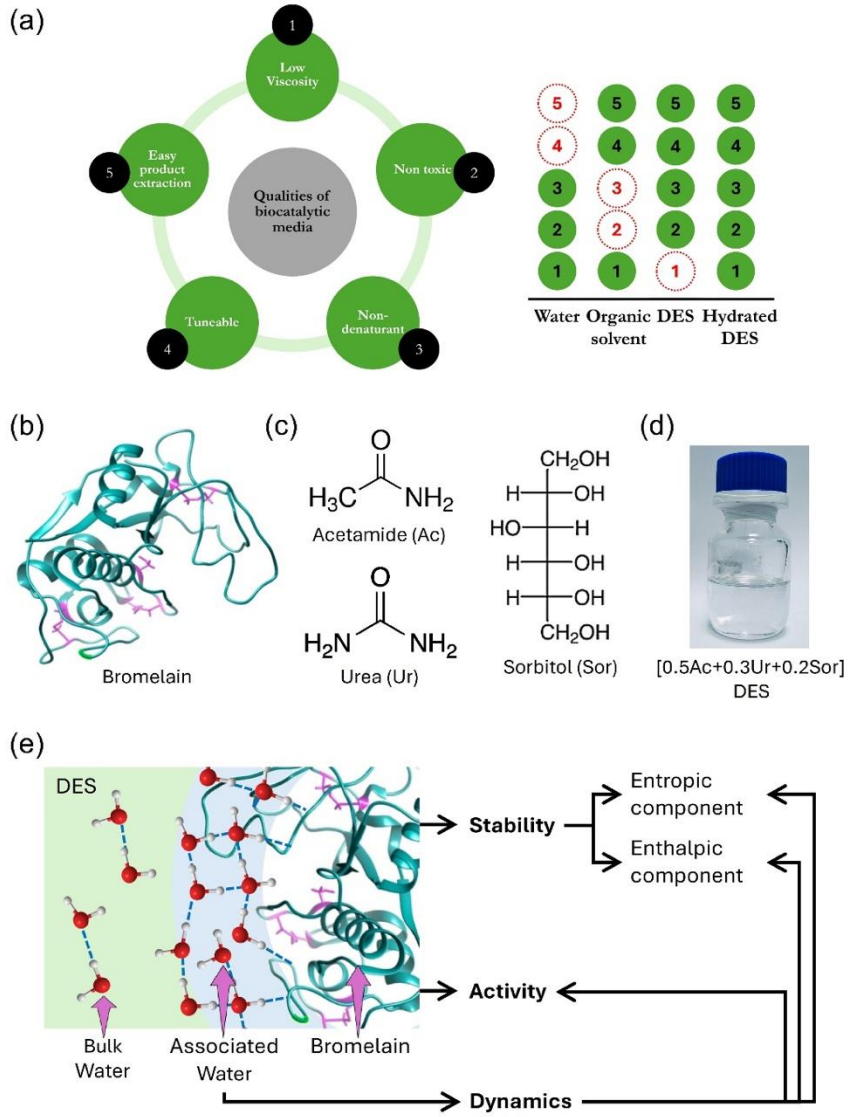

Scheme 1. (a) The desirable properties of a biocatalytic media. Apart from the low viscosity, DES can achieve all the properties that either water or the organic solvent could not. Going from the DES to hydrated DES, low viscosity and more tunability can be achieved, making hydrated DES a better candidate for a biocatalytic medium. (b) Three-dimensional structure of bromelain (PDB ID 1W0Q). (c) Chemical structure of the constituents of the used DES. (d) Photograph of prepared DES (0.5 Ac + 0.3 Ur + 0.2 Sor) at room temperature. (e) The aim of the present work. Measurement of activity and recognition of the entropic and enthalpic components of stability; and the influence of associated water modulation on both.

5.2. Results and discussion

5.2.1. Thermal stability of bromelain with hydrated DESs

The emission maximum of tryptophan is highly sensitive to its environment [82,83]. Buried tryptophan residues in hydrophobic regions exhibit a blue-shifted emission, whereas exposed residues show a red-shifted emission, which is due to tryptophan's

higher excited-state dipole moment than the ground state [82,83]. This makes tryptophan fluorescence a valuable indicator of the protein's folding and unfolding [82,83]. Bromelain contains five tryptophan residues and exhibits intrinsic fluorescence, which has been recorded at various temperatures to monitor the thermal denaturation in buffer and in the presence of various amounts of acetamide(0.5)/urea(0.3)/sorbitol(0.2) (Ac/Ur/Sor) DES (see Figure 1).

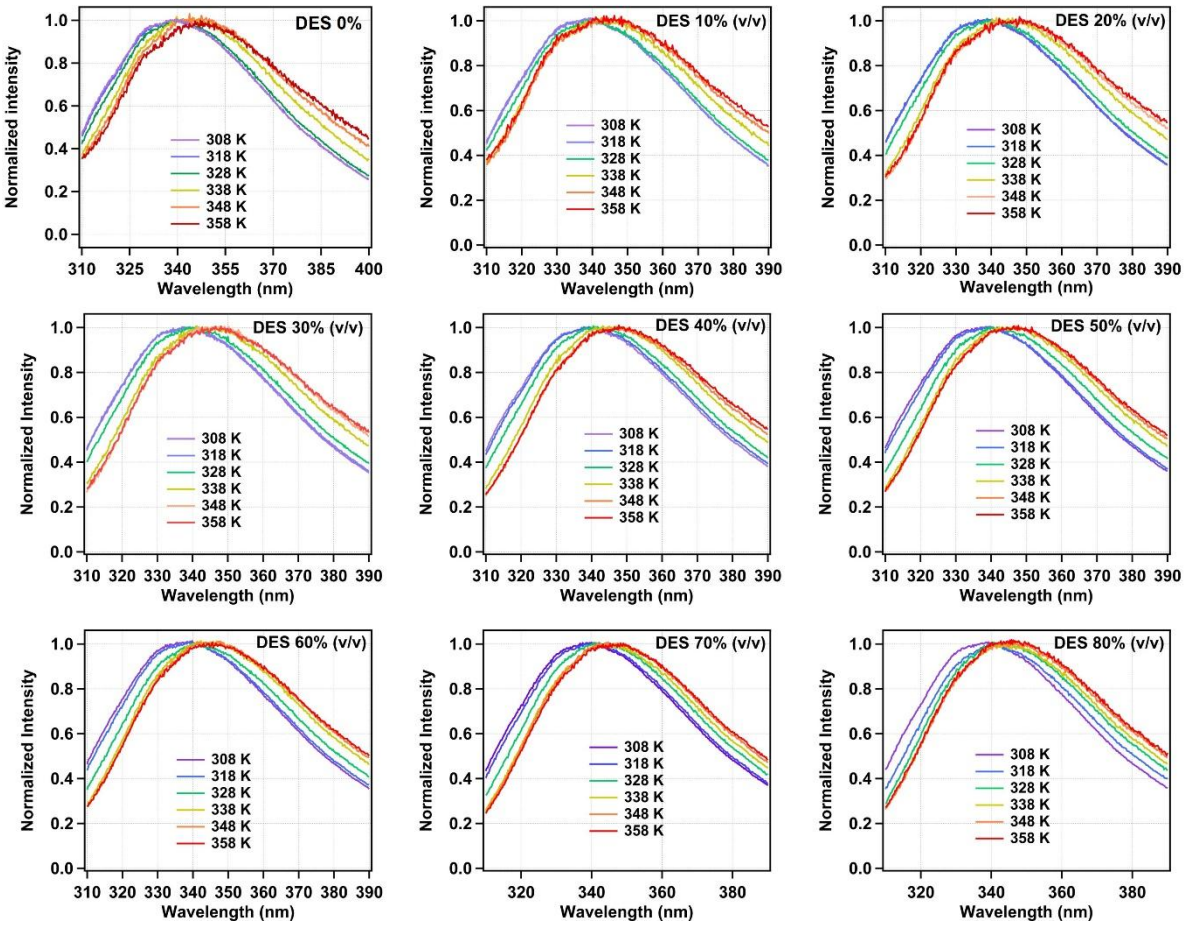

Figure 1. Temperature-dependent fluorescence emission spectra of bromelain in the presence of various concentrations of hydrated 0.5Ac/0.3Ur/0.2Sor DES.The concentrations of the hydrated DES are mentioned in the respective figures.

In Figure 2, we have shown the stepwise measurement of melting temperature from fluorescence spectra. From the thermal fluorescence spectra of bromelain in the buffer in Figure 2a, emission maxima at each temperature were measured by fitting with a log-normal function and represented as a function of the temperature in

Figure 2b. Figure 2c represents the fraction unfolded (f_u) of bromelain in buffer and in the presence of various amounts of DES, which are calculated through, $f_u = \frac{\lambda-\lambda_N}{\lambda_D-\lambda_N}$, where λ_N and λ_D are the emission maximum of the native and denatured states, respectively, obtained from the measured data, as shown in Figure 2b. Bromelain in the presence of various amounts of DES have been calculated similarly and presented in Figure 2d. The melting temperature (T_m) is the temperature where $f_u = 0.5$, which has been plotted in Figure 2e for bromelain in buffer and in the presence of various amounts of Ac/Ur/Sor DES. In the buffer, bromelain's T_m is found to be ~335 K, which is consistent with the previous report [58]. At low DES concentrations (up to 40% V/V), bromelain's stability remained largely intact, while at higher DES concentrations, bromelain's thermal stability reduced significantly, which is similar to the findings with human serum albumin in the same DES [20].

Generally, it is believed that interaction between the components of DES and the amino acids of the enzyme influences the stability of the enzyme [24,38,44]. Previously, we have proved that this DES with different hydration levels cannot be considered as merely an aqueous solution of its components [20]. This implies that the specific interaction between DES components and bromelain is not essential for maintaining bromelain's stability and also nullifies the denaturant effect of urea, which is one of the components of the used DES. Additionally, viscosity-driven stabilization is also not a factor in this case, as higher DES content reduces the protein stability, though it leads to an increase in the viscosity. The effect of charge screening and salt bridge formation can also be ruled out, as the DES in the present case is non-ionic [75,76]. However, the hydrophobic effect, dispersion forces, or more general Van der Waals interactions in the case of non-ionic DES might influence enzymatic behaviour and introduce some destabilization.

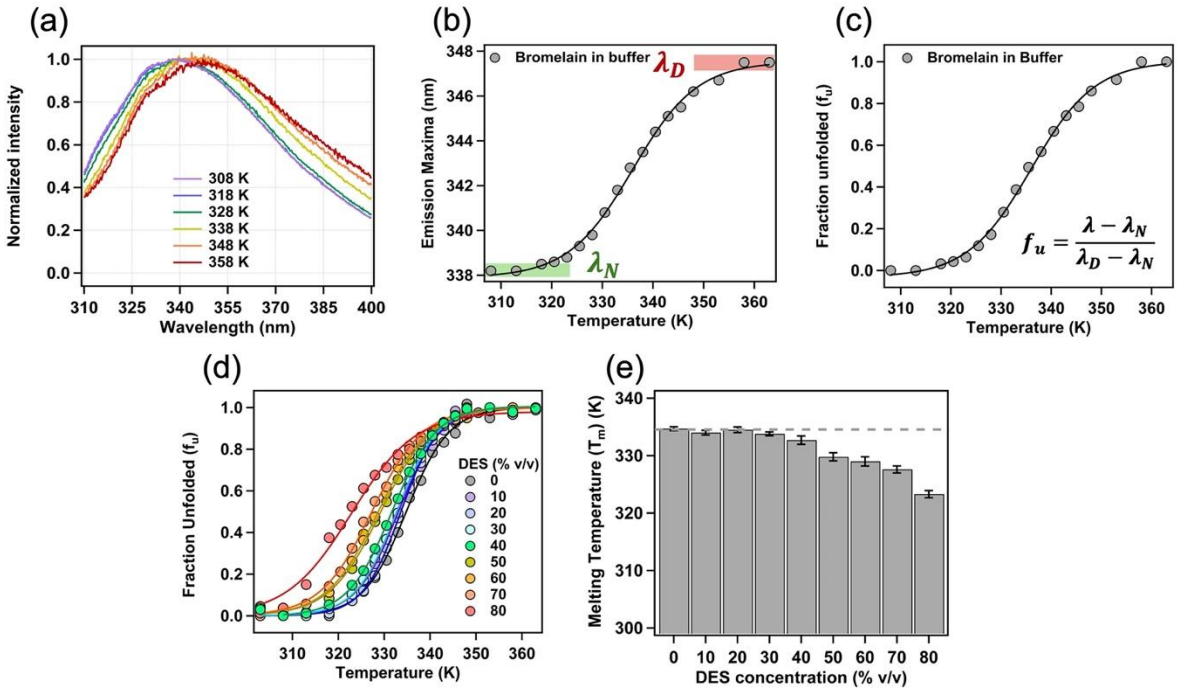

Figure 2. Thermal stability of bromelain in the presence of different concentrations of hydrated DES. (a) Representative steady-state fluorescence spectra of bromelain in buffer at different temperatures. (b) Variation of emission maxima of bromelain in the buffer as a function of temperature. (c) Variation of fraction unfolded (f_u), which has been calculated using the equation mentioned in the inset, as a function of temperature. (d) Comparison of the thermal unfolding curve for different concentrations of hydrated Ac/Ur/Sor DES. Each curve was fitted using the sigmoidal function (equation 10). (e) Comparison of the melting temperature (T_m) of bromelain in the presence of differently hydrated Ac/Ur/Sor DES.

Several reports on protein stability in DES hypothesized that the network-like structure in DES forms a unique solvation shell around the protein that acts as a protective layer leading to enhanced stability [36–38,84]. However, except for some theoretical studies, there is no experimental evidence for this [36,37,41]. In our recent report, for the first time, we have experimentally shown that human serum albumin feels an unperturbed immediate solvation environment even in the presence of a high concentration of hydrated acetamide/urea/sorbitol (the same DES used here) DES, whereas the viscosity and solvation dynamics of the bulk media change drastically [20]. We proposed that the unperturbed associated water might be responsible for maintaining the stability and activity of the protein inside hydrated DES [20]. As this associated water is in direct interaction with the protein surface, it should profoundly affect the stability of the enzyme. To check the validity of the proposal we have measured the associated water dynamics.

5.2.2. Associated water dynamics of bromelain in hydrated DESs

Various methods like NMR, neutron scattering, and terahertz spectroscopy can measure water dynamics, but they offer an average picture [79–81]. Our prime interest is the associated water, which interacts directly with the protein surface, as discussed above [57,63]. Thus, we have used the time-dependent fluorescence Stokes shift (TDFSS) method to decipher the modulation of associated water. This method has superior spatial and time resolution over other techniques [52,66,77]. TDFSS employs a solvatochromic probe, which undergoes a change in the dipole moment upon photoexcitation. This induces the surrounding solvent molecules to rearrange themselves for stabilization of the excited state of the solvatochromic probe. This rearrangement time is a measure of the solvation time. In the case of the solvatochromic probe labeled to the protein, TDFSS will give information on the associated water dynamics of the protein [85,86].

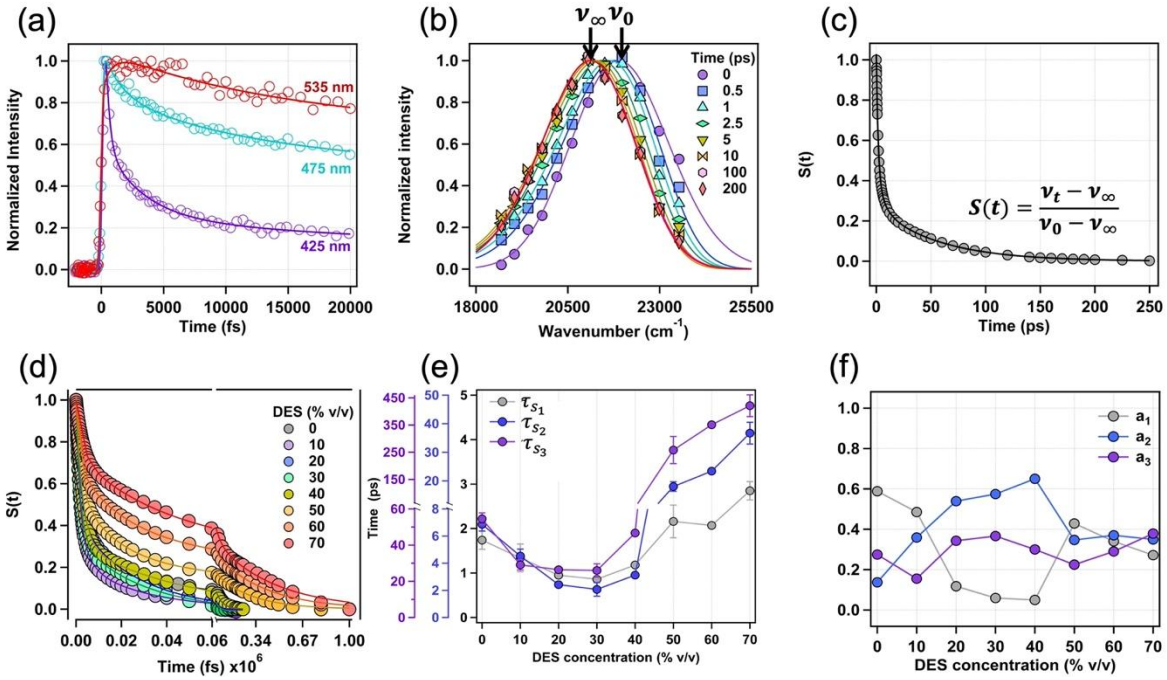

Figure 3. Solvation dynamics around bromelain in the presence of various Ac/Ur/Sor DES concentrations. (a) Time-resolved emission spectra (TRES) of CPM-tagged bromelain in buffer (only a few representative time points have been shown to provide clear visualization). (b) Time-dependent shift of emission maxima of CPM-tagged bromelain in the buffer. (c) Solvent correlation function, S(t), of CPM-tagged bromelain in the buffer. The equation used to form the function is mentioned in the inset. (d) Comparison of S(t)s in the presence of

different DES concentrations. The dynamics in the case of 80% DES could not be measured as it become too slow to be captured using the time window of 1 ns of fs-fluorescence up conversion setup. The variation of (e) solvation time components and respective (f) amplitudes of associated water dynamics of bromelain in the presence of different concentrations of DES. The error bars represent the standard deviation of the mean of three independent experiments.

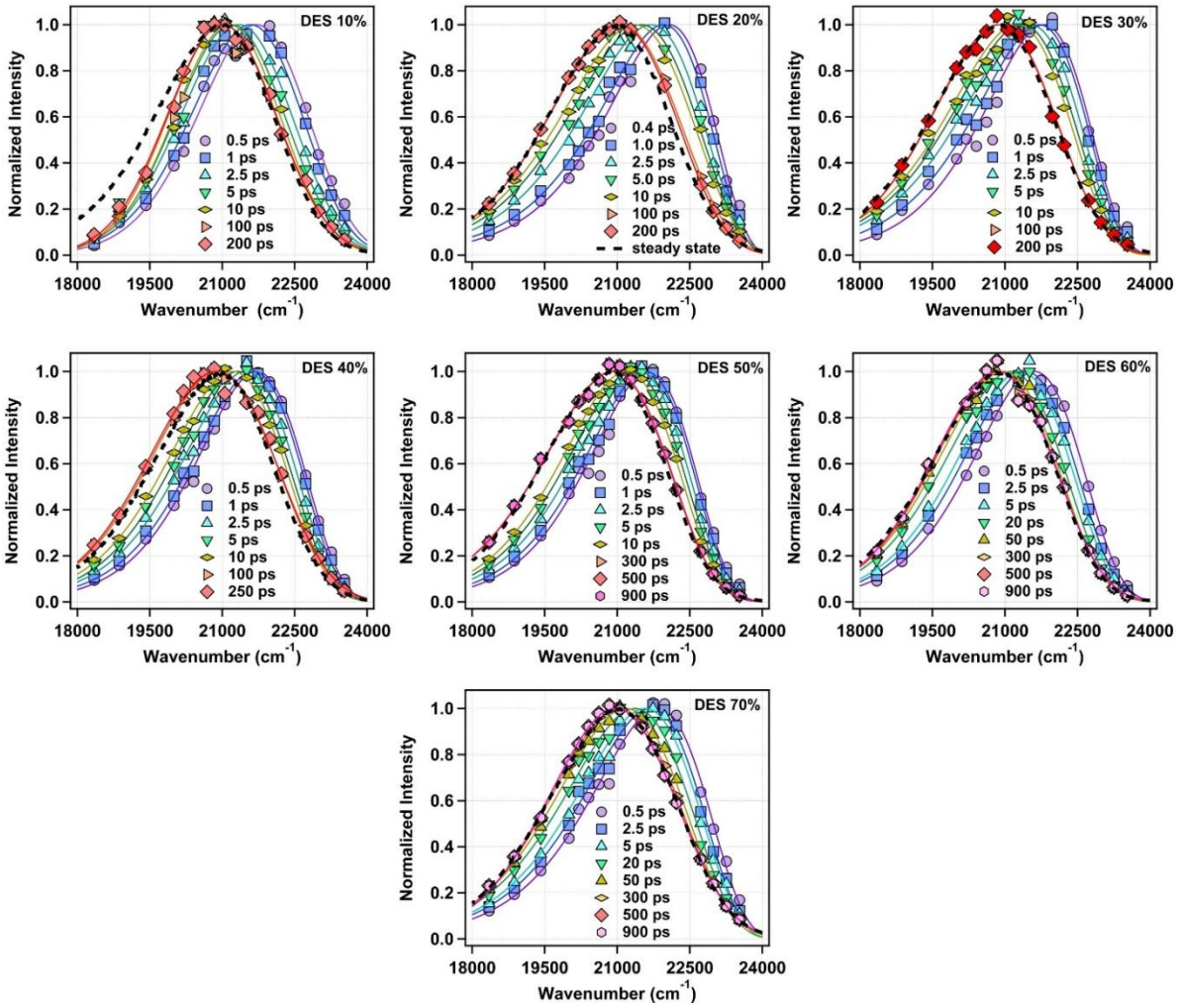

Figure 4. Time-resolved emission spectra (TRES) of CPM-tagged bromelain in the presence of various concentrations of hydrated 0.5Ac/0.3Ur/0.2Sor DES. The concentrations of the hydrated DES are mentioned in the respective figures.

In the present case, we site selectively tagged bromelain with a coumarin-based (solvatochromic) fluorescent molecule, 7-diethylamino-3-(4′-maleimidylphenyl)-4-methylcoumarin (CPM), to measure the associated water dynamics. We constructed time-resolved emission spectra (TRES) from the collected wavelength-dependent fluorescence decays (see Figures 3a, 3b), and evaluated the time-dependent shift of the emission maximum of CPM-tagged bromelain in buffer and in the presence of

various concentrations of DES. All the TRES of CPM-tagged bromelain in different concentrations of DES are given in Figure 4. The solvent response function, *S*(t)is then derived and presented in Figures 3c and 3d, respectively. All the obtained solvent correlation functions are best fitted with a tri-exponential function, yielding three-time components. The faster time component is in the order of 1-2 ps (τ_1), the second one is around 3-30 ps (τ_2), and the slowest time component is observed to be 30-400 ps (τ_3). The variation of time components and their contributions are shown in Figures 3e, 3f, and Table 1. All three components (τ_1, τ_2 and τ_3), become flexible up to 30% DES and then slow down (see Figure 3e) with an increase in the DES concentration.

Table 1: Fitting parameters of the solvent correlation function of CPM-tagged bromelain (associated water) using femtosecond fluorescence up-conversion technique.

DES (% v/v)	**Observed Stokes shift (cm^{-1})**	**τ_1(ps)**	**a_1**	**τ_2(ps)**	**a_2**	**τ_3(ps)**	**a_3**
0	730	1.74±0.20	0.60	6.86±0.50	0.14	54.5±3.34	0.26
10	815	1.34±0.31	0.55	4.53±0.51	0.24	29.1±2.81	0.22
20	815	0.95	0.11	2.42	0.48	26.4	0.41
30	790	0.86±0.25	0.11	2.07±0.50	0.54	26.0±3.68	0.35
40	650	1.18	0.10	3.12	0.59	46.7	0.30
50	820	2.16±0.37	0.43	18.0±1.66	0.36	258±50	0.21
60	760	2.07	0.31	23.4	0.37	351	0.31
70	850	2.85±0.20	0.26	36.7±3.80	0.37	421±40	0.37

Although a fair amount of debate exists in assigning the origin of different time components of the water dynamics, the most accepted theory is provided by Bagchi and co-workers [87–89]. According to that theory, the less than 1 ps time component usually originates from the free water present near the fluorophore. The component in the range of 2-50 ps comes from the water reorientation in the protein hydration layer (i.e. the associated water). As a result of coupling between associated water and the side-chain dynamics of the protein, another slower time component in the range of 50-300 ps might also be observed [87,89].

In the present study, we observed two time components, τ_1 and τ_2, in the time range of 1-30 ps, and assigned both of them to the dynamics of associated water in the protein hydration layer. The slowest component in the range of 30-400 ps is probably arising due to the coupling between associated water and side-chain protein dynamics. As the time scales of different components are not very distinct, the mixing of contributions from different sources is a possibility. Thus, the observed τ_1 might have some contribution from the free water near the fluorescent tag. Previously, Zhong and coworkers reported the timescale of associated water dynamics of different proteins in similar timescale ranges using the TDFSS technique [78,90,91]. Overall, our result indicates that in the low DES concentration (up to 30% v/v), the associated water dynamics becomes flexible, and at higher DES concentrations (after 40% v/v), the associated water becomes increasingly rigid.

5.2.3. The relationship between thermal stability and associated water dynamics cannot be explained by traditional theory

Examining Figure 2e, it can be found that bromelain's thermal stability remains almost the same up to 30% DES, while the flexibility of the associated water dynamics increased (Figure 3e). Interestingly, beyond 30% DES, bromelain stability drops significantly, while associated water becomes slower (Figure 3e). Prior literature, including ours, makes it abundantly evident that proteins typically have higher stability when associated water dynamics becomes slower (see Figure 5b) [56,58,62,70,92,93]. For example, papain's stability increased with more rigid associated

water.[58] However, in the present study, we observed exactly the opposite behaviour beyond 40% (v/v) DES (Figure 5a), challenging the existing hypothesis (Figure 5b). This suggests a need to re-evaluate stability in terms of entropic and enthalpic contributions rather than overall stability, as we recently suggested [57,63].

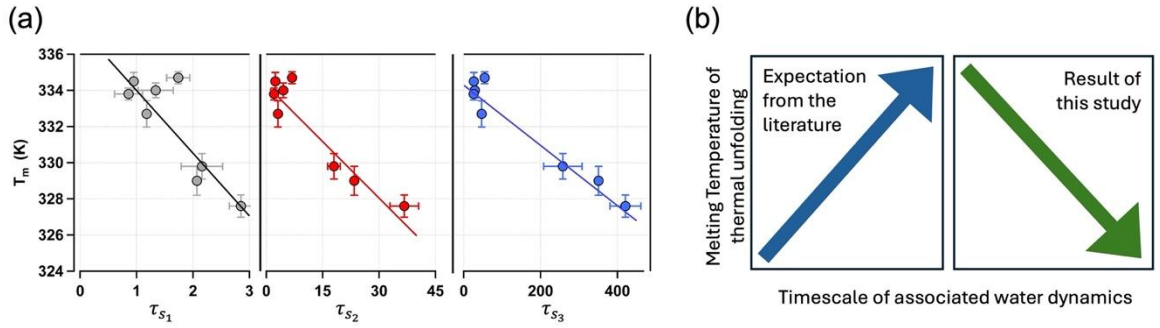

Figure 5. The relation between associated water dynamics modulation and thermal stability of the enzyme. (a) The plot of the melting temperature of bromelain with different components of associated water dynamics, τ_{S1} , τ_{S2}, and τ_{S3}. (b) Plot of melting temperature with modulation of associated water dynamics has been conceptualized based on the consensus present in the literature. According to the literature, the melting temperature of an enzyme increases with the rigidity of associated water dynamics. The right panel is from the present study, where rigid associated water dynamics decrease the melting temperature of bromelain. The error bars represent the standard deviation of the mean of three independent experiments.

5.2.4. Recognition of individual entropic and enthalpic contributions of thermal stability

From the thermal unfolding data, we determined the free energy of the unfolding of bromelain in various DES concentrations using the equations mentioned in Figure 6a. Using the Gibbs-Helmholtz equation, we recognized the individual entropic and enthalpic terms of the thermal unfolding of bromelain in buffer (Figure 6b) and various DES concentrations (Figure 6c). Taking the thermal denaturation of bromelain in the buffer as the baseline, the entropic and enthalpic contributions to the stability of bromelain due to DES can be calculated using equations 5.1 and 5.2.

$$\Delta\Delta H^0 = \Delta H^0_{DES} - \Delta H^0_{buffer} \quad (5.1)$$

$$\Delta\Delta S^0 = \Delta S^0_{DES} - \Delta S^0_{buffer} \quad (5.2)$$

A positive value of $\Delta\Delta H^0$ implies that DES provides stabilization to bromelain relative to buffer, whereas a positive value of $\Delta\Delta S^0$ imparts destabilization (Figure 6d). Differential entropy and enthalpy values relative to the buffer (Figure 6e) revealed that low concentrations of DES cause entropic destabilization to bromelain, which shifts to stabilization at higher DES levels. Similarly, enthalpic stabilization of bromelain has been seen for lower DES concentrations, which becomes destabilizing in nature for higher DES concentrations. Perhaps, we observed a clear entropy–enthalpy relationship in the DES-induced stability of bromelain, a common phenomenon known as entropy–enthalpy compensation (Figure 6f) [94–96]. Further, the linear trend of the $T\Delta\Delta S$ versus $\Delta\Delta H$ (at 300 K) plot with a slope of 0.88 indicates that the overall stability of bromelain with DES at various concentrations is dominated by the enthalpic contribution (Figure 6f).

The entropy–enthalpy compensation seems like a natural consequence of thermodynamics: $\Delta G = \Delta H - T\Delta S$. The question that remains is its physical origin. It seems that some common factor modulates both the entropic and the enthalpic terms. Water is present in almost all biochemical processes and strongly interacts with protein [53–55,88]. Considering water's colossal role, it is intuitive to think that this common factor might be water. In fact, in our previous report, we demonstrated that modulation of water–protein hydrogen bonds can originate in compensating entropy and enthalpy in the crowded milieu [57,63]. Following this, we propose that modulation of water-protein hydrogen bonds could explain the entropic and enthalpic terms of bromelain stability in DES.

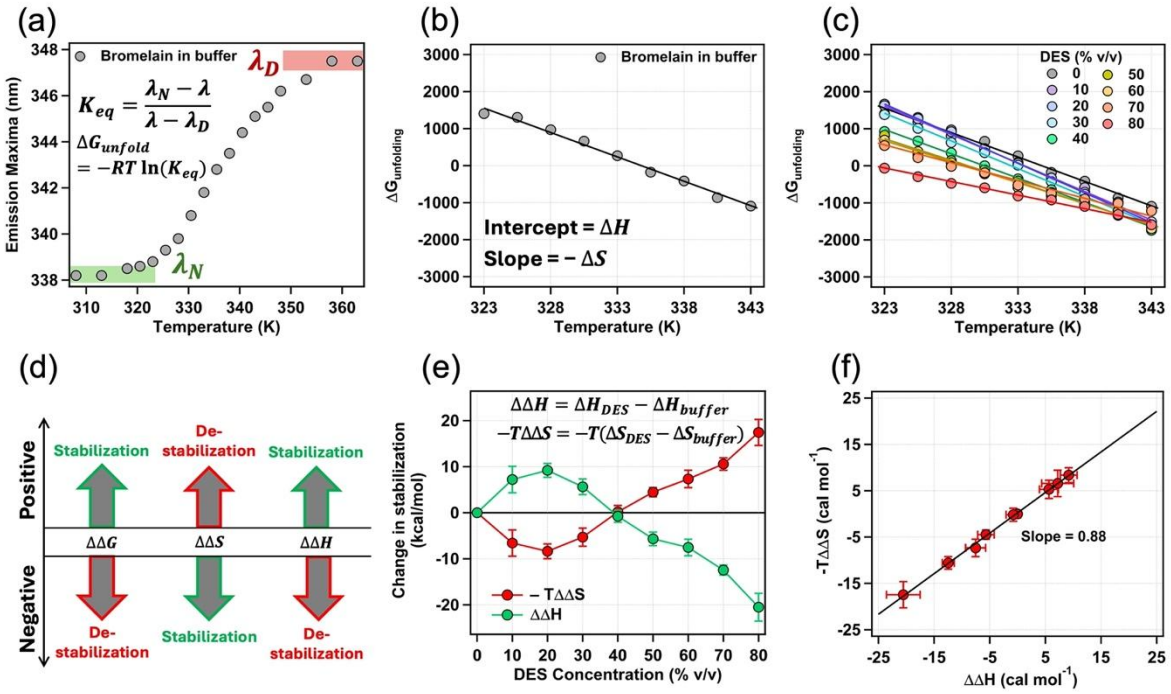

Figure 6: Individual entropic and enthalpic components of thermal stabilization of bromelain in hydrated DES. (a) Variation of bromelain's emission maximum as a function of temperature. The equation for calculating the equilibrium constant and the native and denatured state signals is given in the inset of the figure. (b) Schematic for estimating the change in the entropy and the enthalpy from the slope and the intercept, respectively, from the unfolding free energy of bromelain in buffer. (c) Plot of unfolding free energy of bromelain in the presence of various concentrations of AC/Ur/Sor DES as a function of the temperature. (d) Effect of positive/negative free energy, entropy, and enthalpy change of protein unfolding compared to that in the buffer on the overall stability of the protein. (e) Differential entropic component ($-T\Delta\Delta S$), where $-T\Delta\Delta S = -T(\Delta S_{DES} - \Delta S_{buffer})$ and enthalpic component ($\Delta\Delta H$), where, $\Delta\Delta H = \Delta H_{DES} - \Delta H_{buffer}$ for thermal unfolding of bromelain in the presence of different concentrations of AC/Ur/Sor DES. (f) Plot of entropic and enthalpic terms of bromelain stability. The black line is a linear fit, indicating entropy–enthalpy compensation. The error bars represent the standard deviation of the mean of three independent experiments.

5.2.5. Relationship between associated water structure and individual entropic and enthalpic contribution of thermal stability:

To quantitatively determine the relationship between associated water structure and individual entropic and enthalpic contribution of thermal stability, we compared differential entropy and enthalpy change of unfolding of bromelain against DES concentrations with the changes in the time components ($\Delta\tau_1$, $\Delta\tau_2$ and $\Delta\tau_3$) of the associated water dynamics of bromelain in Figure 7. An entropic destabilization with enthalpic stabilization at lower DES concentrations coincides with more flexible

water dynamics, while entropic stabilization with enthalpic destabilization at higher DES concentrations aligns with rigid water dynamics.

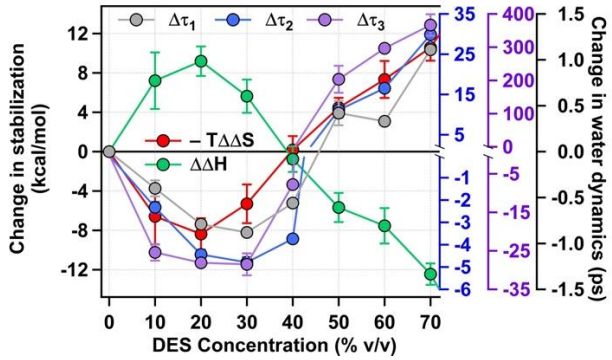

Figure 7. Differential entropy and enthalpy change of bromelain's unfolding along with the changes in the time components ($\Delta\tau_1, \Delta\tau_2$ and $\Delta\tau_3$) of associated water dynamics of bromelain with varying DES concentrations. The error bars represent the standard deviation of the mean of three independent experiments.

Further analysis of entropic and enthalpic changes as functions of $\Delta\tau_1$ (Figure 8a), $\Delta\tau_2$ (Figure 8b) and $\Delta\tau_3$ (Figure 8c), shows strong correlations between the modulation of the second and third components of the associated water dynamics and differential entropic (adjusted R^2~0.80 and 0.83, respectively) or enthalpic (adjusted R^2 ~ 0.80 and 0.82, respectively) components of the stability. However, the correlation is slightly weaker (adjusted R^2 ~ 0.76 and 0.77 for the entropic and enthalpic terms, respectively) for the fastest time component modulation ($\Delta\tau_1$), likely due to contributions from the free/bulk-like water in the measured fastest time component.

However, one needs to be assured that such water modulation does not come from other sources like conformational changes of the protein. Generally, when a protein unfolds, more bulk water molecules are expected to interact with the hydration layer of the protein surface [70,97–100]. Thus, the overall solvation dynamics is expected to be faster [97–100]. Our previous work showed that bromelain's conformation remained stable up to 40% v/v Ac/Ur/Sor DES, with only a slight reduction in hydrodynamic radius [28]. This indicates that up to 40% v/v Ac/Ur/Sor DES, where the media viscosity also notably increases compared to buffer, a more rigid water dynamics is

anticipated. However, our experiment revealed faster-associated water dynamics, confirming that the change in the associated water dynamics is not due to the structural alterations of bromelain [28]. Similarly, at higher DES concentrations, while bromelain slightly unfolds [28], water dynamics surprisingly become more rigid, further indicating no prominent role of structural alteration in the modulation of associated water dynamics. Therefore, this result suggests that the associated water of protein (i.e. those water molecules that are interacting with protein in the protein hydration layer) plays a key role in determining the stability of bromelain in DES.

Basically, at low DES concentrations, the water around bromelain becomes more flexible, indicating a weaker hydrogen-bond network. In such cases, the water molecules gain higher degrees of freedom, and thus the entropy is gained ($\Delta\Delta S = +ve$), leading to entropic destabilization. Simultaneously, the weakening of the hydrogen-bonded network requires some energy ($\Delta\Delta H = +ve$), leading to enthalpic stabilization. At higher DES concentrations, the situation is completely opposite. The water around bromelain in such condition becomes rigid, suggesting DES-induced strengthening of the protein-water hydrogen-bond network, leading to entropic loss of the medium ($\Delta\Delta S = -ve$) and a negative enthalpic change ($\Delta\Delta H = -ve$), resulting in entropic stabilization and enthalpic destabilization, respectively.

Up to this, we have established a correlation between the associated water dynamics and protein stability in hydrated DES through experiments. However, a key question remains: does this effect stem solely from changes in associated water? Since associated water dynamics reflect the H-bond strength difference between surface-bound and free-water [76,99], any change in free water could influence the bound water, as well [80,101]. Additionally, the protein itself strongly affects the associated water, while free water modulation likely depends on the specific perturbation. To explore this, we investigated if there is any correlation between bulk dynamics and bromelain stability. In our previous report, using transient absorption spectroscopy, we presented the dynamics of Ac/Ur/Sor DES at varying hydration levels without protein, focusing on bulk water behaviour, and observed two time components [20].

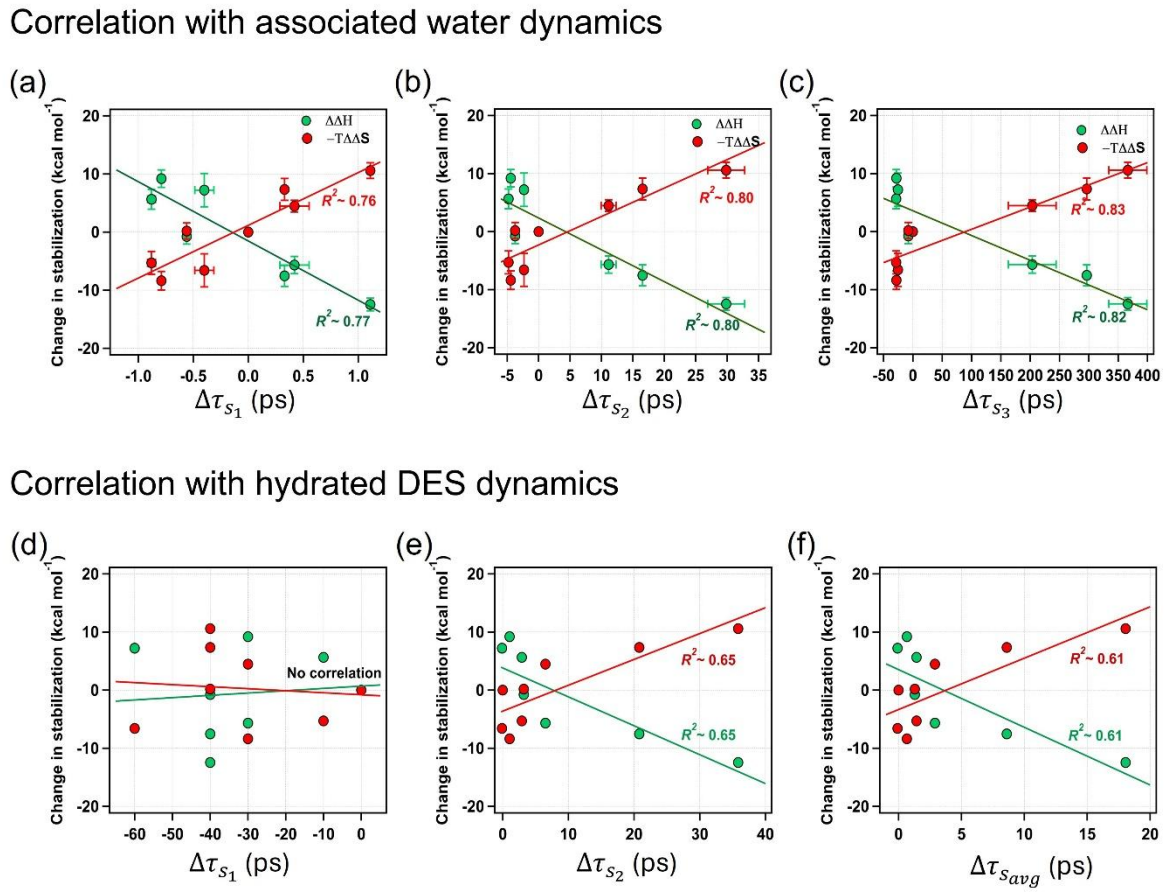

Figure 8. In the upper panel the correlation between differential entropic and enthalpic terms with a change in the (a) first time component ($\Delta\tau_{S1}$), (b) second time component ($\Delta\tau_{S2}$) and (c) third time component ($\Delta\tau_{S3}$) of the associated water dynamics is shown. In the lower panel the correlation between differential entropic and enthalpic terms with a change in the (d) first time component ($\Delta\tau_{S1}$), (e) second time component ($\Delta\tau_{S2}$), and (f) average solvation time ($\Delta\tau_{avg}$) of the bulk solvation dynamics of hydrated DES in the absence of protein is given. The adjusted R^2, which tells about the goodness of the correlation, has been mentioned in the respective plots. The error bars represent the standard deviation of the mean of three independent experiments.

The faster time components remain almost unperturbed up to 70% (v/v) DES, whereas the longer time components increase with the increase in the DES concentration [20]. Note that with the increase in the DES concentration, the average solvation time of the hydrated DES (in the absence of bromelain) also becomes progressively slower. Here, we plot bromelain's differential entropy and enthalpy of unfolding against the time components ($\Delta\tau_1, \Delta\tau_2, \Delta\tau_{avg}$) of solvation dynamics of hydrated DES at different concentrations. The observed low value of R^2 in

Figures 8d, 8e, and 8f indicate no significant link between the stability and bulk dynamics of the DES media.

Overall, our results show that in hydrated DES, the associated water dynamics might be rigid or flexible depending on the DES concentration. Rigid-associated water imparts entropic stabilization and enthalpic destabilization to the protein, whereas flexible water imparts entropic destabilization and enthalpic stabilization (Scheme 2). This enhances our knowledge of why proteins might be stable in DES. Strikingly, such stability cannot be explained in terms of the modulation of overall water structure, highlighting the critical role of water molecules in the vicinity of the protein surface.

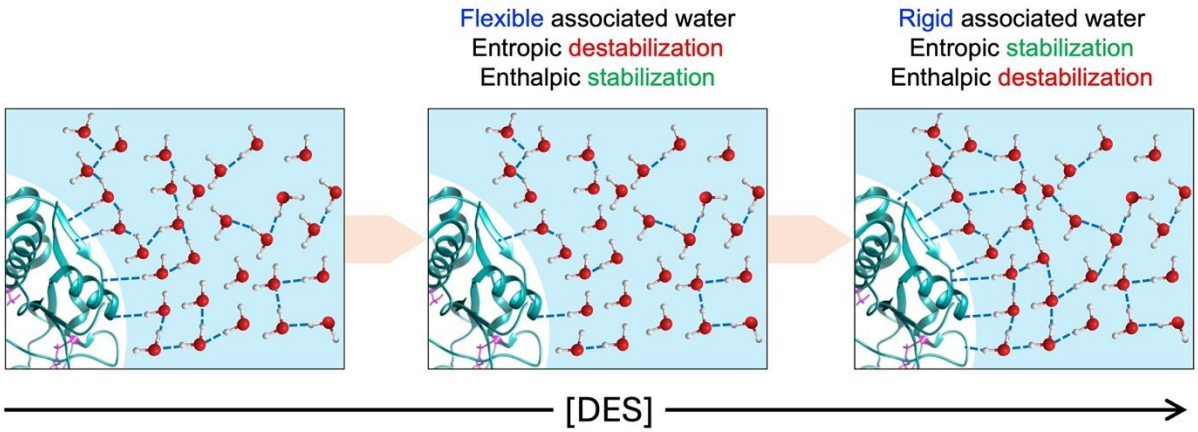

Scheme 2. Associated water dynamics modulation explains bromelain stability across DES concentrations. At initial concentrations of the DES, the associated water becomes more flexible, destabilized bromelain through entropy, which is compensated by stabilizing enthalpy. Whereas, at higher DES concentrations, the associated water becomes more rigid, stabilized bromelain through entropy with a concomitant enthalpic destabilization.

5.2.6. Relationship between associated water dynamics and enzymatic activity:

Enzyme activity is influenced by many factors like protein structure, conformational dynamics, media's viscosity/polarity, etc. Identifying the major factors that influence an enzymatic reaction is very difficult as the reaction involves many steps, and many factors combinedly control them [28,102–113]. Mechanistic studies on how enzymatic activity is controlled in DESs are very limited in the literature [19,28,42,114].

Some reports suggest that interactions present between DES components affect enzyme structure and function, particularly if the enzyme interacts with the hydrogen bonding sites of the DES constituents [41,115,116]. Previously, we have shown that along with the compact enzyme conformation and flexible active site dynamics of bromelain, the physical properties like viscosity and polarity of the hydrated DES play a key role in influencing the enzymatic activity [28]. The consensus regarding the correlation of protein activity with water dynamics suggests that flexible associated water dynamics might influence enzymatic reactions [61,63,67]. Experimentally, very few reports are available where a correlation between activity and dynamics has been made [59,61,67]. Verma *et al.* have shown flexible water dynamics with increasing crowder concentration reflects better enzymatic activity [61]. Reports from the Zewail group also follow a similar trend [59,67]. However, in the presence of deep eutectic solvents, such a correlation has never been made.

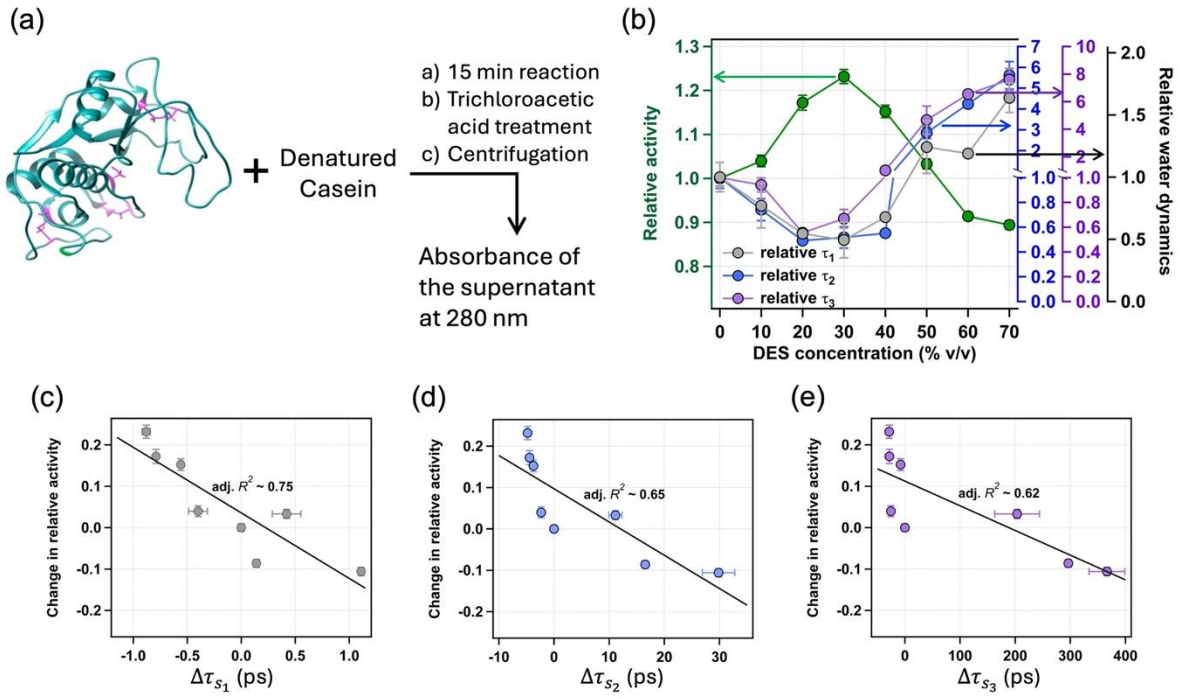

Figure 9. (a) Schematic representation of the proteolytic activity of bromelain using denatured casein as a substrate. (b) A plot of the relative activity of bromelain and the relative time components of associated water dynamics of bromelain against DES concentration. Correlation between change in relative activity with a change in the (c) first time component ($\Delta\tau_{S1}$), (d) second time component ($\Delta\tau_{S2}$), and (e) third time component ($\Delta\tau_{S3}$) of the associated water

dynamics of bromelain. The error bars represent the standard deviation of the mean of three independent experiments.

In our earlier report, the proteolytic activity of bromelain in the presence of Ac/Ur/Sor DES was found to increase at lower DES concentrations and then gradually decrease with DES concentration after 40% (v/v) DES [28]. Here, we tried to see if there is any correlation present between associated water dynamics and enzymatic activity of bromelain in the presence of DES. For that, we remeasured the proteolytic activity of bromelain (see Figure 9a) in the presence of Ac/Ur/Sor DES of varying concentrations, and the trend of activity with DES concentrations matches completely with our previous report [28]. At lower DES concentrations, where the water is more flexible, the activity was found to be more than in the buffer. At higher DES concentrations, the activity drops with an increase in the rigidity of the associated water (Figure 9b). Importantly, the relative change of proteolytic activity correlates well with the changes in the components of associated water dynamics (Figures 9c, 9d, 9e) with an adjusted R^2 values of 0.75 and 0.65, and 0.62 for $\Delta\tau_1$, $\Delta\tau_2$, and $\Delta\tau_3$ respectively.

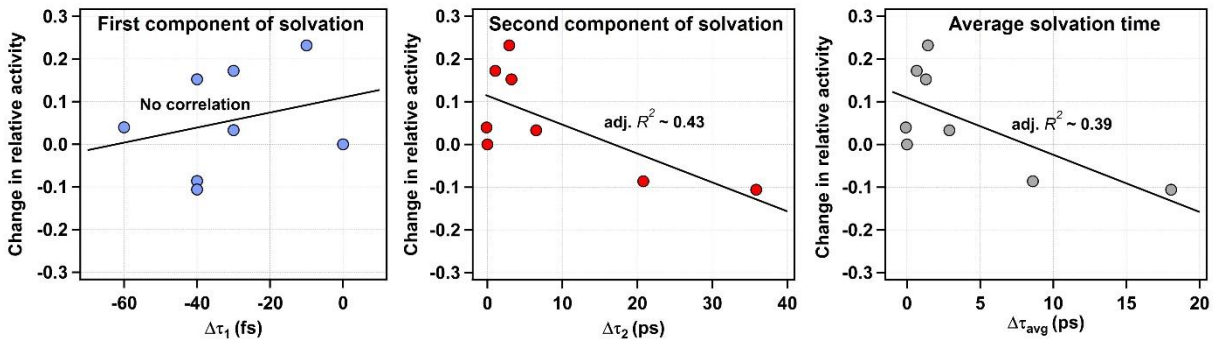

Figure 10. Correlation between the relative change of bromelain's proteolytic activity with the change in time components of bulk solvation dynamics of hydrated Ac/Ur/Sor DES (in the absence of protein).

However, this correlation does not hold at all when we plot the relative change of proteolytic activity with solvation dynamics of the hydrated DES media in the absence of protein (Figure 10), which delineates the important role of associated water in influencing enzyme function. However, the correlation of the associated

water dynamics with activity is somewhat poorer than with stability. At this point, it is extremely difficult to point out the specific reason. However, as many properties of enzymes and media control the activity might lead to a poor correlation.

Physically, one can think that to digest the substrate (we used casein in the present study), both the enzyme (bromelain) and the substrate need to diffuse towards each other to make the enzyme-substrate complex. Thus, media viscosity must play an important role. With an increase in the DES concentration, the viscosity of the media constantly increases [20], which predicts a constant decrease in the activity. However, interestingly that has not been observed here. Another important step in the enzymatic reaction is the dissociation of the enzyme-substrate complex into the final product, and an increase in the rate of product formation leads to an increase in the overall activity [117,118]. In our recent study, we have shown that in the presence of macromolecular crowder the product formation from the enzyme-substrate complex correlates strongly with the associated water dynamics of the enzyme [63]. In the present case also, the flexible associated water around the enzyme at low DES concentration might facilitate the product formation and thus enhance the overall activity. For the low concentrations of DES where enhanced activity was observed, the media polarity also increased a little, which might also facilitate the enzymatic reaction [28]. Thus, further studies are needed to justify such claims, and our future studies will be more focused on that. The observation of enhanced enzymatic activity in hydrated DES is fairly common, but until now, no explanation has been provided [19,29,39,41,119]. The present study correlates the same with associated water dynamics, which might give a logical heads-up to such observations.

5.3. Summary and conclusions

DESs and hydrated DESs have all the potential to be fantastic biocatalytic media. However, little is understood about how they keep proteins stable and active. Through MD simulation, Monhemi *et al.* proposed that DES creates a protective microenvironment around proteins through hydrogen bonding [36], which lacks any experimental validation until the present work. Here we showed that the DES-

mediated change in the protective water layer modulates bromelain's stability and activity. Using femtosecond time-resolved fluorescence Stokes shift, we explored the impact of associated water dynamics on bromelain in Ac/Ur/Sor DES. Up to 30% DES, the water becomes flexible and then rigidifies with an increase in the DES concentration. We observed that low DES concentrations destabilize bromelain entropically and stabilize it enthalpically, while higher concentrations reverse this. We propose that flexible associated water stabilizes bromelain via enthalpy and destabilizes via entropy, with the opposite effect for rigid associated water. Crucially, the observed stability trends cannot be attributed to bulk water dynamics, highlighting the pivotal role of associated/biological water. Moreover, bromelain's proteolytic activity increases at low DES but declines above 40%, which aligns well with the change in the associated water dynamics. This report offers a novel perspective on how water dynamics influence protein stability and activity, with implications for understanding enzyme behavior in DES. Importantly, our hypothesis can explain both the positive and negative effects imparted by the DES and might also effectively predict the enzyme-specific effects. While more research is needed to generalize these findings, our work lays the foundation for future studies.

5.4. References:

(1) Stepankova, V.; Bidmanova, S.; Koudelakova, T.; Prokop, Z.; Chaloupkova, R.; Damborsky, J. Strategies for Stabilization of Enzymes in Organic Solvents. *ACS Catal* **2013**, *3* (12), 2823–2836. https://doi.org/10.1021/cs400684x.

(2) Serdakowski, A. L.; Dordick, J. S. Enzyme Activation for Organic Solvents Made Easy. *Trends Biotechnol* **2008**, *26* (1), 48–54. https://doi.org/10.1016/j.tibtech.2007.10.007.

(3) Arnold, F. H. Protein Engineering for Unusual Environments. *Curr Opin Biotechnol* **1993**, *4*, 450–455.

(4) Chen, K.; Arnold, F. H. Tuning the Activity of an Enzyme for Unusual Environments: Sequential Random Mutagenesis of Subtilisin E for Catalysis in Dimethylformamide. *Proc. Natl. Acad. Sci. USA* **1993**, *90*, 5618–5622.

(5) Zaks, A.; Klibanov, A. M. Enzymatic Catalysis in Organic Media at 100°C. *Science (1979)* **1984**, *224* (4654), 1249–1251. https://doi.org/10.1126/science.6729453.

(6) Panić, M.; Cvjetko Bubalo, M.; Radojčić Redovniković, I. Designing a Biocatalytic Process Involving Deep Eutectic Solvents. *J. Chem. Technology and Biotechnology* **2021**, *96* (1), 14–30. https://doi.org/10.1002/jctb.6545.

(7) van Rantwijk, F.; Sheldon, R. A. Biocatalysis in Ionic Liquids. *Chem Rev* **2007**, *107* (6), 2757–2785. https://doi.org/10.1021/cr050946x.

(8) Sheldon, R. A. Biocatalysis in Ionic Liquids: State-of-the-Union. *Green Chemistry* **2021**, *23* (21), 8406–8427. https://doi.org/10.1039/d1gc03145g.

(9) Smith, E. L.; Abbott, A. P.; Ryder, K. S. Deep Eutectic Solvents (DESs) and Their Applications. *Chem Rev* **2014**, *114* (21), 11060–11082. https://doi.org/10.1021/cr300162p.

(10) Domínguez de María, P.; Maugeri, Z. Ionic Liquids in Biotransformations: From Proof-of-Concept to Emerging Deep-Eutectic-Solvents. *Curr. Opin. Chem. Biol.* **2011**, *15* (2), 220–225. https://doi.org/10.1016/j.cbpa.2010.11.008.

(11) Florindo, C.; Lima, F.; Ribeiro, B. D.; Marrucho, I. M. Deep Eutectic Solvents: Overcoming 21st Century Challenges. *Curr Opin Green Sustain Chem* **2019**, *18*, 31–36. https://doi.org/10.1016/j.cogsc.2018.12.003.

(12) Pätzold, M.; Siebenhaller, S.; Kara, S.; Liese, A.; Syldatk, C.; Holtmann, D. Deep Eutectic Solvents as Efficient Solvents in Biocatalysis. *Trends*

Biotechnol **2019**, *37* (9), 943–959. https://doi.org/10.1016/j.tibtech.2019.03.007.

(13) Perna, F. M.; Vitale, P.; Capriati, V. Deep Eutectic Solvents and Their Applications as Green Solvents. *Curr Opin Green Sustain Chem* **2020**, *21*, 27–33. https://doi.org/10.1016/j.cogsc.2019.09.004.

(14) Paiva, A.; Craveiro, R.; Aroso, I.; Martins, M.; Reis, R. L.; Duarte, A. R. C. Natural Deep Eutectic Solvents - Solvents for the 21st Century. *ACS Sustain Chem Eng* **2014**, *2* (5), 1063–1071. https://doi.org/10.1021/sc500096j.

(15) Huang, Z. L.; Wu, B. P.; Wen, Q.; Yang, T. X.; Yang, Z. Deep Eutectic Solvents Can Be Viable Enzyme Activators and Stabilizers. *Journal of Chemical Technology and Biotechnology* **2014**, *89* (12), 1975–1981. https://doi.org/10.1002/jctb.4285.

(16) Hansen, B. B.; Spittle, S.; Chen, B.; Poe, D.; Zhang, Y.; Klein, J. M.; Horton, A.; Adhikari, L.; Zelovich, T.; Doherty, B. W.; Gurkan, B.; Maginn, E. J.; Ragauskas, A.; Dadmun, M.; Zawodzinski, T. A.; Baker, G. A.; Tuckerman, M. E.; Savinell, R. F.; Sangoro, J. R. Deep Eutectic Solvents: A Review of Fundamentals and Applications. *Chem Rev* **2021**, *121* (3), 1232–1285. https://doi.org/10.1021/acs.chemrev.0c00385.

(17) Sanchez-Fernandez, A.; Jackson, A. J. Proteins in Deep Eutectic Solvents: Structure, Dynamics and Interactions with the Solvent. In *Advances in Botanical Research*; Academic Press Inc., 2021; Vol. 97, pp 69–94. https://doi.org/10.1016/bs.abr.2020.09.003.

(18) Yadav, N.; Venkatesu, P. Current Understanding and Insights towards Protein Stabilization and Activation in Deep Eutectic Solvents as Sustainable Solvent Media. *Phys. Chem. Chem. Phys.* **2022**, *24* (22), 13474–13509. https://doi.org/10.1039/D2CP00084A.

(19) Toledo, M. L.; Pereira, M. M.; Freire, M. G.; Silva, J. P. A.; Coutinho, J. A. P.; Tavares, A. P. M. Laccase Activation in Deep Eutectic Solvents. *ACS Sustain Chem Eng* **2019**, *7* (13), 11806–11814. https://doi.org/10.1021/acssuschemeng.9b02179.

(20) Khan, T.; Das, N.; Negi, K. S.; Bhowmik, S.; Sen, P. Understanding the Intricacy of Protein in Hydrated Deep Eutectic Solvent: Solvation Dynamics, Conformational Fluctuation Dynamics, and Stability. *Int. J. Biol. Macromol.* **2023**, *253*, 127100. https://doi.org/10.1016/j.ijbiomac.2023.127100.

(21) Delorme, A. E.; Andanson, J. M.; Verney, V. Improving Laccase Thermostability with Aqueous Natural Deep Eutectic Solvents. *Int. J. Biol. Macromol.* **2020**, *163*, 919–926. https://doi.org/10.1016/j.ijbiomac.2020.07.022.

(22) Gorke, J. T.; Srienc, F.; Kazlauskas, R. J. Hydrolase-Catalyzed Biotransformations in Deep Eutectic Solvents. *Chemical Communications* **2008**, No. 10, 1235–1237. https://doi.org/10.1039/b716317g.

(23) Sanchez-Fernandez, A.; Edler, K. J.; Arnold, T.; Alba Venero, D.; Jackson, A. J. Protein Conformation in Pure and Hydrated Deep Eutectic Solvents. *Phys. Chem. Chem. Phys.* **2017**, *19* (13), 8667–8670. https://doi.org/10.1039/c7cp00459a.

(24) Xin, R.; Qi, S.; Zeng, C.; Khan, F. I.; Yang, B.; Wang, Y. A Functional Natural Deep Eutectic Solvent Based on Trehalose: Structural and Physicochemical Properties. *Food Chem* **2017**, *217*, 560–567. https://doi.org/10.1016/j.foodchem.2016.09.012.

(25) Nian, B.; Cao, C.; Liu, Y. How Candida Antarctica Lipase B Can Be Activated in Natural Deep Eutectic Solvents: Experimental and Molecular

Dynamics Studies. *Journal of Chemical Technology and Biotechnology* **2020**, *95* (1), 86–93. https://doi.org/10.1002/jctb.6209.

(26) Esquembre, R.; Sanz, J. M.; Wall, J. G.; Del Monte, F.; Mateo, C. R.; Ferrer, M. L. Thermal Unfolding and Refolding of Lysozyme in Deep Eutectic Solvents and Their Aqueous Dilutions. *Phys. Chem. Chem. Phys.* **2013**, *15* (27), 11248–11256. https://doi.org/10.1039/c3cp44299c.

(27) Sanchez-Fernandez, A.; Basic, M.; Xiang, J.; Prevost, S.; Jackson, A. J.; Dicko, C. Hydration in Deep Eutectic Solvents Induces Non-Monotonic Changes in the Conformation and Stability of Proteins. *J. Am. Chem. Soc.* **2022**, *144* (51), 23657–23667. https://doi.org/10.1021/jacs.2c11190.

(28) Das, N.; Khan, T.; Subba, N.; Sen, P. Correlating Bromelain's Activity with Its Structure and Active-Site Dynamics and the Medium's Physical Properties in a Hydrated Deep Eutectic Solvent. *Phys. Chem. Chem. Phys.* **2021**, *23* (15), 9337–9346. https://doi.org/10.1039/d1cp00046b.

(29) Sun, H.; Xin, R.; Qu, D.; Yao, F. Mechanism of Deep Eutectic Solvents Enhancing Catalytic Function of Cytochrome P450 Enzymes in Biosynthesis and Organic Synthesis. *J Biotechnol* **2020**, *323*, 264–273. https://doi.org/10.1016/j.jbiotec.2020.07.004.

(30) Durand, E.; Lecomte, J.; Baréa, B.; Villeneuve, P. Towards a Better Understanding of How to Improve Lipase-Catalyzed Reactions Using Deep Eutectic Solvents Based on Choline Chloride. *European Journal of Lipid Science and Technology* **2014**, *116* (1), 16–23. https://doi.org/10.1002/ejlt.201300246.

(31) Barik, S.; Mahapatra, A.; Preeyanka, N.; Sarkar, M. Assessing the Impact of Choline Chloride and Benzyltrimethylammonium Chloride-Based Deep Eutectic Solvents on the Structure and Conformational Dynamics of Bovine Serum Albumin: A Combined Steady-State, Time-Resolved Fluorescence

and Fluorescence Correlation Spectroscopic Study. *Phys. Chem. Chem. Phys.* **2023**, *25* (29), 20093–20108. https://doi.org/10.1039/d3cp01380d.

(32) Gorke, J. T.; Srienc, F.; Kazlauskas, R. J. Deep Eutectic Solvents for Candida Antarctica Lipase B-Catalyzed Reactions. In *ACS Symposium Series*; 2010; Vol. 1038, pp 169–180. https://doi.org/10.1021/bk-2010-1038.ch014.

(33) Durand, E.; Lecomte, J.; Baréa, B.; Dubreucq, E.; Lortie, R.; Villeneuve, P. Evaluation of Deep Eutectic Solvent-Water Binary Mixtures for Lipase-Catalyzed Lipophilization of Phenolic Acids. *Green Chemistry* **2013**, *15* (8), 2275–2282. https://doi.org/10.1039/c3gc40899j.

(34) Yadav, N.; Bhakuni, K.; Bisht, M.; Bahadur, I.; Venkatesu, P. Expanding the Potential Role of Deep Eutectic Solvents toward Facilitating the Structural and Thermal Stability of α-Chymotrypsin. *ACS Sustain Chem Eng* **2020**, *8* (27), 10151–10160. https://doi.org/10.1021/acssuschemeng.0c02213.

(35) Yadav, N.; Halanur, M.; Bisht, M.; Nataraj, S. K.; Venkatesu, P.; Mondal, D. Multifunctional Solvothermal Carbon Derived from Alginate Using "water-in-Deep Eutectic Solvents" for Enhancing Enzyme Activity. *Chemical Communications* **2020**, *56* (67), 9659–9662. https://doi.org/10.1039/d0cc03866k.

(36) Monhemi, H.; Housaindokht, M. R.; Moosavi-Movahedi, A. A.; Bozorgmehr, M. R. How a Protein Can Remain Stable in a Solvent with High Content of Urea: Insights from Molecular Dynamics Simulation of Candida Antarctica Lipase B in Urea: Choline Chloride Deep Eutectic Solvent. *Phys. Chem. Chem. Phys.* **2014**, *16* (28), 14882–14893. https://doi.org/10.1039/c4cp00503a.

(37) Shehata, M.; Unlu, A.; Sezerman, U.; Timucin, E. Lipase and Water in a Deep Eutectic Solvent: Molecular Dynamics and Experimental Studies of the Effects of Water-In-Deep Eutectic Solvents on Lipase Stability. *J. Phys. Chem. B* **2020**, *124* (40), 8801–8810. https://doi.org/10.1021/acs.jpcb.0c07041.

(38) Cao, J.; Wu, R.; Zhu, F.; Dong, Q.; Su, E. Enzymes in Nearly Anhydrous Deep Eutectic Solvents: Insight into the Biocompatibility and Thermal Stability. *Enzyme Microb Technol* **2022**, *157*, 110022. https://doi.org/10.1016/j.enzmictec.2022.110022.

(39) Mamashli, F.; Badraghi, J.; Delavari, B.; Lanjanian, H.; Sabbaghian, M.; Hosseini, M.; Saboury, A. A. Improvement of Versatile Peroxidase Activity and Stability by a Cholinium-Based Ionic Liquid. *J Mol Liq* **2018**, *272*, 597–608. https://doi.org/10.1016/j.molliq.2018.09.128.

(40) Zeng, C. X.; Qi, S. J.; Xin, R. P.; Yang, B.; Wang, Y. H. Synergistic Behavior of Betaine-Urea Mixture: Formation of Deep Eutectic Solvent. *J. Mol. Liq.* **2016**, *219*, 74–78. https://doi.org/10.1016/j.molliq.2016.02.076.

(41) Juneidi, I.; Hayyan, M.; Hashim, M. A.; Hayyan, A. Pure and Aqueous Deep Eutectic Solvents for a Lipase-Catalysed Hydrolysis Reaction. *Biochem Eng J* **2017**, *117*, 129–138. https://doi.org/10.1016/j.bej.2016.10.003.

(42) Khodaverdian, S.; Dabirmanesh, B.; Heydari, A.; Dashtban-moghadam, E.; Khajeh, K.; Ghazi, F. Activity, Stability and Structure of Laccase in Betaine Based Natural Deep Eutectic Solvents. *Int J Biol Macromol* **2018**, *107*, 2574–2579. https://doi.org/10.1016/j.ijbiomac.2017.10.144.

(43) Sanchez-Fernandez, A.; Poon, J.-F.; Leung, A. E.; Prévost, S. F.; Dicko, C. Stabilization of Non-Native Folds and Programmable Protein Gelation in Compositionally Designed Deep Eutectic Solvents. *ACS Nano* **2024**, *18* (28), 18314–18326. https://doi.org/10.1021/acsnano.4c01950.

(44) Park, K.; Ham, B. Y.; Li, K.; Kang, S.; Jung, D.; Kim, H.; Liu, Y.; Hwang, I.; Lee, J. Insights into the Enhanced Thermal Stability of Lysozyme with Altered Structure and Activity Induced by Choline Chloride-Based Deep Eutectic Solvents Containing Polyols and Sugars. *J Mol Liq* **2022**, *349*, 118143. https://doi.org/10.1016/j.molliq.2021.118143.

(45) Chen, G.; Zhang, Q.; Lu, Q.; Feng, B. Protection Effect of Polyols on Rhizopus Chinensis Lipase Counteracting the Deactivation from High Pressure and High Temperature Treatment. *Int J Biol Macromol* **2019**, *127*, 555–562. https://doi.org/10.1016/j.ijbiomac.2019.01.082.

(46) Fan, J.; Gao, D.; Song, F. Experimental Study on Thermophysical Property of Deep Eutectic Solvents as Heat Transfer Fluid. *Case Studies in Thermal Engineering* **2023**, *50*, 103426. https://doi.org/10.1016/j.csite.2023.103426.

(47) Naser, J.; Mjalli, F. S.; Gano, Z. S. Molar Heat Capacity of Selected Type III Deep Eutectic Solvents. *J Chem Eng Data* **2016**, *61* (4), 1608–1615. https://doi.org/10.1021/acs.jced.5b00989.

(48) Mackowiak, A.; Galek, P.; Fic, K. Deep Eutectic Solvents for High-Temperature Electrochemical Capacitors. *ChemElectroChem* **2021**, *8* (21), 4028–4037. https://doi.org/10.1002/celc.202100711.

(49) Bhakuni, K.; Yadav, N.; Venkatesu, P. A Novel Amalgamation of Deep Eutectic Solvents and Crowders as Biocompatible Solvent Media for Enhanced Structural and Thermal Stability of Bovine Serum Albumin. *Phys. Chem. Chem. Phys.* **2020**, *22* (42), 24410–24422. https://doi.org/10.1039/d0cp04397d.

(50) Dai, Y.; Witkamp, G. J.; Verpoorte, R.; Choi, Y. H. Tailoring Properties of Natural Deep Eutectic Solvents with Water to Facilitate Their Applications. *Food Chem* **2015**, *187*, 14–19. https://doi.org/10.1016/j.foodchem.2015.03.123.

(51) Ma, C.; Laaksonen, A.; Liu, C.; Lu, X.; Ji, X. The Peculiar Effect of Water on Ionic Liquids and Deep Eutectic Solvents. *Chem Soc Rev* **2018**, *47* (23), 8685–8720. https://doi.org/10.1039/c8cs00325d.

(52) Bhattacharyya, K. Nature of Biological Water: A Femtosecond Study. *Chemical Communications* **2008**, No. 25, 2848–2857. https://doi.org/10.1039/b800278a.

(53) Pal, S. K.; Zewail, A. H. Dynamics of Water in Biological Recognition. *Chem Rev* **2004**, *104* (4), 2099–2124. https://doi.org/10.1021/cr020689l.

(54) Ball, P. Water as an Active Constituent in Cell Biology. *Chem Rev* **2008**, *108* (1), 74–108. https://doi.org/10.1021/cr068037a.

(55) Bellissent-Funel, M. C.; Hassanali, A.; Havenith, M.; Henchman, R.; Pohl, P.; Sterpone, F.; Van Der Spoel, D.; Xu, Y.; Garcia, A. E. Water Determines the Structure and Dynamics of Proteins. *Chem Rev* **2016**, *116* (13), 7673–7697. https://doi.org/10.1021/acs.chemrev.5b00664.

(56) Hishida, M.; Anjum, R.; Anada, T.; Murakami, D.; Tanaka, M. Effect of Osmolytes on Water Mobility Correlates with Their Stabilizing Effect on Proteins. *J. Phys. Chem. B* **2022**, *126* (13), 2466–2475. https://doi.org/10.1021/acs.jpcb.1c10634.

(57) Das, N.; Tarif, E.; Dutta, A.; Sen, P. Associated Water Dynamics Might Be a Key Factor Affecting Protein Stability in the Crowded Milieu. *J. Phys. Chem. B* **2023**, *127* (14), 3151–3163. https://doi.org/10.1021/acs.jpcb.2c09043.

(58) Negi, K. S.; Das, N.; Khan, T.; Sen, P. Osmolyte Induced Protein Stabilization: Modulation of Associated Water Dynamics Might Be a Key Factor. *Phys. Chem. Chem. Phys.* **2023**, *25* (47), 32602–32612. https://doi.org/10.1039/d3cp03357k.

(59) Pal, S. K.; Peon, J.; Zewail, A. H. Ultrafast Surface Hydration Dynamics and Expression of Protein Functionality: α-Chymotrypsin. *Proc Natl Acad Sci U S A* **2002**, *99* (24), 15297–15302. https://doi.org/10.1073/pnas.242600399.

(60) Pal, S. K.; Peon, J.; Bagchi, B.; Zewail, A. H. Biological Water: Femtosecond Dynamics of Macromolecular Hydration. *J. Phys. Chem. B* **2002**, *106* (48), 12376–12395. https://doi.org/10.1021/jp0213506.

(61) Verma, P. K.; Rakshit, S.; Mitra, R. K.; Pal, S. K. Role of Hydration on the Functionality of a Proteolytic Enzyme α-Chymotrypsin under Crowded Environment. *Biochimie* **2011**, *93* (9), 1424–1433. https://doi.org/10.1016/j.biochi.2011.04.017.

(62) Qiu, W.; Zhang, L.; Okobiah, O.; Yang, Y.; Wang, L.; Zhong, D.; Zewail, A. H. Ultrafast Solvation Dynamics of Human Serum Albumin: Correlations with Conformational Transitions and Site-Selected Recognition. *J. Phys. Chem. B* **2006**, *110* (21), 10540–10549. https://doi.org/10.1021/jp055989w.

(63) Khan, T.; Halder, B.; Das, N.; Sen, P. Role of Associated Water Dynamics on Protein Stability and Activity in Crowded Milieu. *J Phys Chem B* **2024**, *128*, 8672–8686. https://doi.org/10.1021/acs.jpcb.4c04337.

(64) Das, N.; Khan, T.; Halder, B.; Ghosh, S.; Sen, P. Macromolecular Crowding Effects on Protein Dynamics. *Int J Biol Macromol* **2024**, *281*, 136248. https://doi.org/10.1016/j.ijbiomac.2024.136248.

(65) Heyden, M.; Bründermann, E.; Heugen, U.; Niehues, G.; Leitner, D. M.; Havenith, M. Long-Range Influence of Carbohydrates on the Solvation Dynamics of Water - Answers from Terahertz Absorption Measurements and Molecular Modeling Simulations. *J. Am. Chem. Soc.* **2008**, *130* (17), 5773–5779. https://doi.org/10.1021/ja0781083.

(66) Kumar, S.; Peon, J.; Zewail, A. H. Biological Water at the Protein Surface: Dynamical Solvation Probed Directly with Femtosecond Resolution. *Proc. Natl. Acad. Sci. USA* **2002**, *99* (4), 1763–1768.

(67) Kamal, J. K. A.; Xia, T.; Pal, S. K.; Zhao, L.; Zewail, A. H. Enzyme Functionality and Solvation of Subtilisin Carlsberg: From Hours to Femtoseconds. *Chem Phys Lett* **2004**, *387* (4–6), 209–215. https://doi.org/10.1016/j.cplett.2004.02.011.

(68) Mukherjee, S. K.; Gautam, S.; Biswas, S.; Kundu, J.; Chowdhury, P. K. Do Macromolecular Crowding Agents Exert Only an Excluded Volume Effect? A Protein Solvation Study. *Journal of Physical Chemistry B* **2015**, *119* (44), 14145–14156. https://doi.org/10.1021/acs.jpcb.5b09446.

(69) Majumdar, S.; Rastogi, H.; Chowdhury, P. K. Bridging Soft Interaction and Excluded Volume in Crowded Milieu through Subtle Protein Dynamics. *J. Phys. Chem. B* **2024**, *128* (3), 716–730. https://doi.org/10.1021/acs.jpcb.3c07266.

(70) Mohan, V.; Sengupta, B.; Acharyya, A.; Yadav, R.; Das, N.; Sen, P. Region-Specific Double Denaturation of Human Serum Albumin: Combined Effects of Temperature and GnHCl on Structural and Dynamical Responses. *ACS Omega* **2018**, *3* (8), 10406–10417. https://doi.org/10.1021/acsomega.8b00967.

(71) Eisenmesser, E. Z.; Millet, O.; Labeikovsky, W.; Korzhnev, D. M.; Wolf-Watz, M.; Bosco, D. A.; Skalicky, J. J.; Kay, L. E.; Kern, D. Intrinsic Dynamics of an Enzyme Underlies Catalysis. *Nature* **2005**, *438* (7064), 117–121. https://doi.org/10.1038/nature04105.

(72) Fenimore, P. W.; Frauenfelder, H.; Mcmahon, B. H.; Young, R. D. Bulk-Solvent and Hydration-Shell Fluctuations, Similar to-and-Fluctuations in

Glasses, Control Protein Motions and Functions. *Proc. Natl. Acad. Sci. USA* **2004**, *101* (40), 14408–14413.

(73) Sykora, J.; Brezovsky, J.; Koudelakova, T.; Lahoda, M.; Fortova, A.; Chernovets, T.; Chaloupkova, R.; Stepankova, V.; Prokop, Z.; Smatanova, I. K.; Hof, M.; Damborsky, J. Dynamics and Hydration Explain Failed Functional Transformation in Dehalogenase Design. *Nat Chem Biol* **2014**, *10* (6), 428–430. https://doi.org/10.1038/nchembio.1502.

(74) Choi, Y. H.; van Spronsen, J.; Dai, Y.; Verberne, M.; Hollmann, F.; Arends, I. W. C. E.; Witkamp, G. J.; Verpoorte, R. Are Natural Deep Eutectic Solvents the Missing Link in Understanding Cellular Metabolism and Physiology? *Plant Physiol* **2011**, *156* (4), 1701–1705. https://doi.org/10.1104/pp.111.178426.

(75) Khan, T.; Tarif, E.; Awano, Y.; Lozada, L. S.; Das, N.; Tominaga, K.; Sen, P. Multiple Evidences for Molecular Level Heterogeneity in a Non-Ionic Biocatalytic Deep Eutectic Solvent. *J Mol Liq* **2023**, *389*, 122882. https://doi.org/10.1016/j.molliq.2023.122882.

(76) Subba, N.; Sahu, P.; Das, N.; Sen, P. Rational Design, Preparation and Characterization of a Ternary Non-Ionic Room-Temperature Deep Eutectic Solvent Derived from Urea, Acetamide, and Sorbitol. *Journal of Chemical Sciences* **2021**, *133* (1), 25. https://doi.org/10.1007/s12039-020-01866-2.

(77) Jimenez, R.; Fleming, G. R.; Kumar, P. V.; Maroncelli, M. Femtosecond Solvation Dynamics of Water. *Nature* **1994**, *369* (6480), 471–473. https://doi.org/10.1038/369471a0.

(78) Zhang, L.; Wang, L.; Kao, Y.-T.; Qiu, W.; Yang, Y.; Okobiah, O.; Zhong, D. Mapping Hydration Dynamics around a Protein Surface. *Proc. Natl. Acad. Sci. USA* **2007**, *104* (47), 18461–18466.

(79) Denisov, V. P.; Jonsson, B. H.; Halle, B. Hydration of Denatured and Molten Globule Proteins. *Nat Struct Biol* **1999**, *6* (3), 253–260. https://doi.org/10.1038/6692.

(80) Nandi, N.; Bagchi, B. Dielectric Relaxation of Biological Water. *J. Phys. Chem. B* **1997**, *101*, 10954–10961.

(81) Russo, D.; Murarka, R. K.; Copley, J. R. D.; Head-Gordon, T. Molecular View of Water Dynamics near Model Peptides. *J. Phys. Chem. B* **2005**, *109* (26), 12966–12975. https://doi.org/10.1021/jp051137k.

(82) Moon, C. P.; Fleming, K. G. Using Tryptophan Fluorescence to Measure the Stability of Membrane Proteins Folded in Liposomes. *Methods Enzymol* **2011**, *492*, 189–211. https://doi.org/10.1016/B978-0-12-381268-1.00018-5.

(83) Shil, S.; Das, N.; Sengupta, B.; Sen, P. Sucrose-Induced Stabilization of Domain-II and Overall Human Serum Albumin against Chemical and Thermal Denaturation. *ACS Omega* **2018**, *3* (12), 16633–16642. https://doi.org/10.1021/acsomega.8b01832.

(84) Sheng, Y.; Cui, H.; Wang, X.; Wang, M.; Song, P.; Huang, H.; Li, X. Harnessing Solvation-Guided Engineering to Enhance Deep Eutectic Solvent Resistance and Thermostability in Enzymes. *Green Chemistry* **2024**, *26* (16), 8883–9272. https://doi.org/10.1039/d3gc04933g.

(85) Lakowicz, J. R. *Principles of Fluorescence Spectroscopy*; Springer, 2006; pp 1–954. https://doi.org/10.1007/978-0-387-46312-4.

(86) Maroncelli, M.; Fleming, G. R. Picosecond Solvation Dynamics of Coumarin 153: The Importance of Molecular Aspects of Solvation. *J Chem Phys* **1987**, *86* (11), 6221–6239. https://doi.org/10.1063/1.452460.

(87) Mondal, S.; Mukherjee, S.; Bagchi, B. Origin of Diverse Time Scales in the Protein Hydration Layer Solvation Dynamics: A Simulation Study. *J. Chem. Phys.* **2017**, *147* (15), 154901. https://doi.org/10.1063/1.4995420.

(88) Bagchi, B. Water Dynamics in the Hydration Layer around Proteins and Micelles. *Chem Rev* **2005**, *105* (9), 3197–3219. https://doi.org/10.1021/cr020661+.

(89) Mondal, S.; Mukherjee, S.; Bagchi, B. Protein Hydration Dynamics: Much Ado about Nothing? *J. Phys. Chem. Lett.* **2017**, *8* (19), 4878–4882. https://doi.org/10.1021/acs.jpclett.7b02324.

(90) Houston, P.; Macro, N.; Kang, M.; Chen, L.; Yang, J.; Wang, L.; Wu, Z.; Zhong, D. Ultrafast Dynamics of Water-Protein Coupled Motions around the Surface of Eye Crystallin. *J. Am. Chem. Soc.* **2020**, *142* (8), 3997–4007. https://doi.org/10.1021/jacs.9b13506.

(91) Qin, Y.; Wang, L.; Zhong, D. Dynamics and Mechanism of Ultrafast Water-Protein Interactions. *Proc. Natl. Acad. Sci. USA* **2016**, *113* (30), 8424–8429. https://doi.org/10.1073/pnas.1602916113.

(92) Guo, F.; Friedman, J. M. Osmolyte-Induced Perturbations of Hydrogen Bonding between Hydration Layer Waters: Correlation with Protein Conformational Changes. *J. Phys. Chem. B* **2009**, *113* (52), 16632–16642. https://doi.org/10.1021/jp9072284.

(93) Yadav, R.; Sen, P. Mechanistic Investigation of Domain Specific Unfolding of Human Serum Albumin and the Effect of Sucrose. *Protein Science* **2013**, *22* (11), 1571–1581. https://doi.org/10.1002/pro.2357.

(94) Sharp, K. Entropy--Enthalpy Compensation: Fact or Artifact? *Protein Science* **2001**, *10* (3), 661–667. https://doi.org/10.1110/ps.37801.

(95) Senske, M.; Törk, L.; Born, B.; Havenith, M.; Herrmann, C.; Ebbinghaus, S. Protein Stabilization by Macromolecular Crowding through Enthalpy Rather than Entropy. *J. Am. Chem. Soc.* **2014**, *136* (25), 9036–9041. https://doi.org/10.1021/ja503205y.

(96) Das, N.; Sen, P. Shape-Dependent Macromolecular Crowding on the Thermodynamics and Microsecond Conformational Dynamics of Protein Unfolding Revealed at the Single-Molecule Level. *J. Phys. Chem. B* **2020**, *124* (28), 5858–5871. https://doi.org/10.1021/acs.jpcb.0c03897.

(97) Yadav, R.; Sengupta, B.; Sen, P. Effect of Sucrose on Chemically and Thermally Induced Unfolding of Domain-I of Human Serum Albumin: Solvation Dynamics and Fluorescence Anisotropy Study. *Biophys Chem* **2016**, *211*, 59–69. https://doi.org/10.1016/j.bpc.2016.02.005.

(98) Mohan, V.; Sengupta, B.; Das, N.; Banerjee, I.; Sen, P. Domain-Specific Stabilization of Structural and Dynamic Responses of Human Serum Albumin by Sucrose. *Protein Pept Lett* **2019**, *26* (4), 287–300. https://doi.org/10.2174/0929866526666190122115702.

(99) Kamal, J. K. A.; Zhao, L.; Zewail, A. H. Ultrafast Hydration Dynamics in Protein Unfolding: Human Serum Albumin. *Proceedings of the National Academy of Sciences* **2004**, *101* (37), 13411–13416. https://doi.org/10.1073/pnas.0405724101.

(100) Samaddar, S.; Mandal, A. K.; Mondal, S. K.; Sahu, K.; Bhattacharyya, K.; Roy, S. Solvation Dynamics of a Protein in the Pre Molten Globule State. *J Phys Chem B* **2006**, *110* (42), 21210–21215. https://doi.org/10.1021/jp064136g.

(101) Nandi, N.; Bhattacharyya, K.; Bagchi, B. Dielectric Relaxation and Solvation Dynamics of Water in Complex Chemical and Biological

Systems. *Chem Rev* **2000**, *100* (6), 2013–2045. https://doi.org/10.1021/cr980127v.

(102) Rastogi, H.; Singh, A.; Chowdhury, P. K. Towards the Energy Landscape of Adenylate Kinase in Crowded Milieu: Activity, Conformation, Structure and Dynamics in Sequence. *Arch Biochem Biophys* **2023**, *743*, 109658. https://doi.org/10.1016/j.abb.2023.109658.

(103) Rastogi, H.; Chowdhury, P. K. Understanding Enzyme Behavior in a Crowded Scenario through Modulation in Activity, Conformation and Dynamics. *Biochim Biophys Acta Proteins Proteom* **2021**, *1869* (11), 140699. https://doi.org/10.1016/j.bbapap.2021.140699.

(104) Nandy, A.; Chakraborty, S.; Nandi, S.; Bhattacharyya, K.; Mukherjee, S. Structure, Activity, and Dynamics of Human Serum Albumin in a Crowded Pluronic F127 Hydrogel. *J. Phys. Chem. B* **2019**, *123* (16), 3397–3408. https://doi.org/10.1021/acs.jpcb.9b00219.

(105) Yon, J. M.; Perahia, D.; Ghélis, C. Conformational Dynamics and Enzyme Activity. *Biochimie* **1998**, *80* (1), 33–42. https://doi.org/10.1016/S0300-9084(98)80054-0.

(106) Vöpel, T.; Makhatadze, G. I. Enzyme Activity in the Crowded Milieu. *PLoS One* **2012**, *7* (6), e39418. https://doi.org/10.1371/journal.pone.0039418.

(107) Tzeng, S. R.; Kalodimos, C. G. Protein Activity Regulation by Conformational Entropy. *Nature* **2012**, *488* (7410), 236–240. https://doi.org/10.1038/nature11271.

(108) Acosta, L. C.; Perez Goncalves, G. M.; Pielak, G. J.; Gorensek-Benitez, A. H. Large Cosolutes, Small Cosolutes, and Dihydrofolate Reductase Activity. *Protein Science* **2017**, *26* (12), 2417–2425. https://doi.org/10.1002/pro.3316.

(109) Kim, S. H.; Park, S.; Yu, H.; Kim, J. H.; Kim, H. J.; Yang, Y. H.; Kim, Y. H.; Kim, K. J.; Kan, E.; Lee, S. H. Effect of Deep Eutectic Solvent Mixtures on Lipase Activity and Stability. *J Mol Catal B Enzym* **2016**, *128*, 65–72. https://doi.org/10.1016/j.molcatb.2016.03.012.

(110) Mader, S. L.; Lopez, A.; Lawatscheck, J.; Luo, Q.; Rutz, D. A.; Gamiz-Hernandez, A. P.; Sattler, M.; Buchner, J.; Kaila, V. R. I. Conformational Dynamics Modulate the Catalytic Activity of the Molecular Chaperone Hsp90. *Nat Commun* **2020**, *11* (1), 1–12. https://doi.org/10.1038/s41467-020-15050-0.

(111) Xu, S.; Wang, J.; Dong, J. Nonspecific Interaction and Overlap Concentration Influence Macromolecular Crowding Effect on Glucose Oxidase Activity. *Int. J. Biol. Macromol.* **2023**, *241*, 124525. https://doi.org/10.1016/j.ijbiomac.2023.124525.

(112) Derham, B. K.; Harding, J. J. The Effect of the Presence of Globular Proteins and Elongated Polymers on Enzyme Activity. *Biochim Biophys Acta Proteins Proteom* **2006**, *1764* (6), 1000–1006. https://doi.org/10.1016/j.bbapap.2006.01.005.

(113) Das, N.; Yadav, S.; Negi, K. S.; Tarif, E.; Sen, P. Does Microsecond Active-Site Dynamics Primarily Control Proteolytic Activity of Bromelain? Clues from Single Molecular Level Study with a Denaturant, a Stabilizer and a Macromolecular Crowder. *BBA Advances* **2022**, *2*, 100041. https://doi.org/10.1016/j.bbadva.2022.100041.

(114) Weibels, S.; Syguda, A.; Herrmann, C.; Weingärtner, H. Steering the Enzymatic Activity of Proteins by Ionic Liquids. A Case Study of the Enzyme Kinetics of Yeast Alcohol Dehydrogenase. *Physical Chemistry Chemical Physics* **2012**, *14* (13), 4635. https://doi.org/10.1039/c2cp24041f.

(115) Wu, B.-P.; Wen, Q.; Xu, H.; Yang, Z. Insights into the Impact of Deep Eutectic Solvents on Horseradish Peroxidase: Activity, Stability and Structure. *J Mol Catal B Enzym* **2014**, *101*, 101–107. https://doi.org/10.1016/j.molcatb.2014.01.001.

(116) Zhao, H.; Baker, G. A.; Holmes, S. Protease Activation in Glycerol-Based Deep Eutectic Solvents. *J Mol Catal B Enzym* **2011**, *72* (3–4), 163–167. https://doi.org/10.1016/j.molcatb.2011.05.015.

(117) Rodriguez, J. M. G.; Hux, N. P.; Philips, S. J.; Towns, M. H. Michaelis-Menten Graphs, Lineweaver-Burk Plots, and Reaction Schemes: Investigating Introductory Biochemistry Students' Conceptions of Representations in Enzyme Kinetics. *J. Chem. Educ.* **2019**, *96* (9), 1833–1845. https://doi.org/10.1021/acs.jchemed.9b00396.

(118) Silverstein, T. P. When Both Km and Vmax Are Altered, Is the Enzyme Inhibited or Activated? *Biochemistry and Molecular Biology Education* **2019**, *47* (4), 446–449. https://doi.org/10.1002/bmb.21235.

(119) Papadopoulou, A. A.; Efstathiadou, E.; Patila, M.; Polydera, A. C.; Stamatis, H. Deep Eutectic Solvents as Media for Peroxidation Reactions Catalyzed by Heme-Dependent Biocatalysts. *Ind Eng Chem Res* **2016**, *55* (18), 5145–5151. https://doi.org/10.1021/acs.iecr.5b04867.

This page left blank intentionally

Chapter 6

Site-Specific Water Dynamics Drives Protein Stability in Hydrated Deep Eutectic Solvents

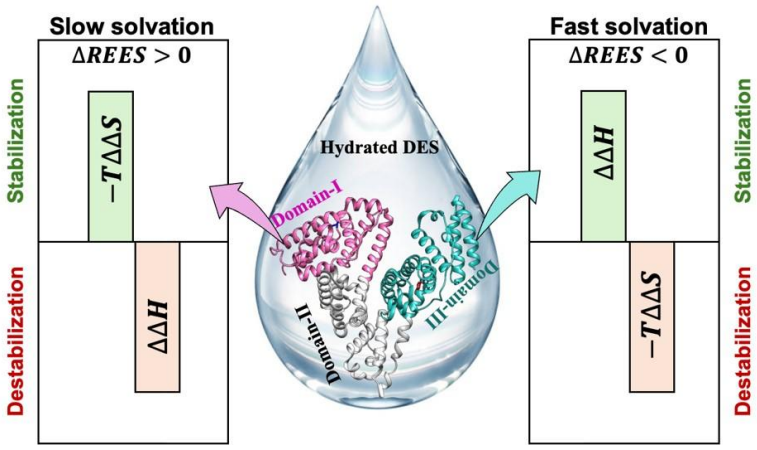

Tanmoy Khan, Kuntal Debnath, Kuldeep Singh Negi, and Pratik Sen*

Biophysical J., **2025,** 124, 1-18

Abstract:

Deep eutectic solvents (DESs) have gained prominence as promising biocatalytic media owing to their tunability, cost-effectiveness, and biocompatibility. However, a comprehensive mechanistic understanding of protein behavior in such environments remains elusive. In this study, we explore the role of associated water dynamics in modulating the thermal stability of human serum albumin within hydrated choline chloride-glycerol and choline chloride-ethylene glycol DESs. By employing domain-specific site-selective fluorescence labelling and red edge excitation shift (REES) measurement, alongside circular dichroism spectroscopy, we reveal that modulation of associated water dynamics distinctly alters the entropic and enthalpic contributions to protein stability. Flexible associated water enhances enthalpic stabilization but promotes entropic destabilization, while restricted associated water induces the opposite effect, providing a mechanistic basis for the entropy–enthalpy compensation. Our findings underscore the necessity of domain-specific stability measurements in multi-domain proteins and highlight the pivotal role of immediate hydration dynamics in protein stabilization within unconventional solvent systems. This study offers valuable insights for the rational design of DES-based biocatalytic systems.

6.1. Introduction:

Biocatalysis and deep eutectic solvents (DESs): Two key strategies for efficient biocatalysis involve either suitable engineering of the enzyme to keep it stable and active in conventional organic solvents or utilizing tunable solvents that inherently support the native enzyme's stability and activity [1]. The first approach, named directed evolution [2,3], was recognized with the 2018 Nobel Prize in chemistry. On the other hand, ionic liquids (IL) and deep eutectic solvents (DESs), owing to their versatile characteristics, have recently been found to keep enzymes stable and active therein [4–9]. Among these two, DES has certain edges over ILs regarding easy, cost-effective, and atom-economical synthesis [8,10,11]. Because of all these superior qualities, there has been an upsurge in studies exploring enzymatic behaviour in DESs and hydrated DESs in recent times [5,12–18]. However, most reports focus on enzyme stability and activity in DESs without investigating the underlying reasons for enzyme stabilization in these unconventional media.

Theories of enzyme stability in DES: Enzyme stability in DESs is often attributed to the network-like structure of DESs, which is primarily formed through extensive hydrogen bonding [14,19,20]. Such a structure creates a protective environment that sustains enzyme stability and activity [19,21–23]. Additionally, the high viscosity of DESs may restrict enzymes' conformational flexibility, preserving their structural integrity [24–26]. Specific hydrogen bonding and ionic interactions between DES components and amino acid residues of an enzyme further influence enzyme conformation and stability [14,19,20]. Recently, Fernandez *et al.* reported that bovine serum albumin and lysozyme can adopt compact globular folds, intermediate states, or unfolded chains depending on the chemical composition of the DES [27]. Few reports even suggest that various physical properties such as polarity, density, refractive index, and surface tension of the DES can also contribute to enzyme thermal stability and catalytic activity [28,29].

Limitations of the current understandings: Although the above understandings are insightful and can explain certain results, they fail to fully account for DES-specific, protein-specific, and DES concentration-dependent stability and activity of enzymes. For instance, lipase, immunoglobulin G, and α-chymotrypsin show higher thermal stability in ChCl-urea DES; yet lysozyme is destabilized in the same DES [21,30–32]. Moreover, in ChCl-urea DES, α-chymotrypsin stabilizes up to 0.25 $g.mL^{-1}$; but its thermal stability decreases at higher DES concentrations [33]. Cytochrome C, studied by Papadopoulou *et al.* exhibits a concentration-dependent activity reversal in several DESs, including in ChCl-EG, ChCl-Gly, and ChCl-urea DESs [34]. Our group has also reported DES concentration-dependent thermal stability and activity of the enzymes [29,35,36]. These observations challenge traditional stability explanations in DES media and indicate the need for a deeper mechanistic understanding.

Role of water dynamics modulation in DES-protein milieu: A closer examination of the literature highlights that hydrated DESs are generally more effective in maintaining enzyme stability and activity compared to anhydrous DESs [14,30,37–39]. Multiple studies have shown that even minimal amounts of water can restore enzyme functionality that is otherwise absent in anhydrous DESs [38–40]. In fact, several reports further highlight that an optimal level of water is crucial for enhancing enzyme function within DESs [18,41,42]. Very recently, Fernandez *et al.* demonstrated that water modulates enzyme behavior in a non-monotonic fashion, with optimal hydration levels favoring specific conformations [43]. Collectively, these findings emphasize the critical role of water in regulating enzyme behaviour in hydrated DES media. Specifically, water in the immediate surroundings that directly interacts with the protein surface, referred to as associated water (which is also known as bound water, biological water, and hydration layer), is known to play a crucial role in maintaining protein stability and activity [44–50]. Inspired by these findings, we hypothesize that modulation of associated water dynamics could significantly impact enzyme stability and activity in hydrated DESs [35,36].

Previous studies and their shortcomings: Very recently, we have experimentally shown that less flexible associated water in the presence of hydrated acetamide-urea-sorbitol DES stabilizes an enzyme (bromelain) through the entropic component but destabilizes it through the enthalpic component [35]. The flexible associated water dynamics influence the thermal stability of bromelain in exactly the opposite way [35]. Our hypothesis explained both the positive and negative effects of DES on bromelain [35]. However, to generalize this hypothesis, further investigations involving different enzymes and DES compositions are necessary.

Objectives of this study: In this study, we examine human serum albumin (HSA) in the presence of two choline chloride (ChCl) based DES, ChCl-glycerol [1:2] (ChCl-Gly) and ChCl-ethylene glycol [1:2] (ChCl-EG), to extend our previous findings on enzyme stability in hydrated DESs. By selecting DESs with different hydrogen bond donors (glycerol vs. ethylene glycol) (Scheme 1), we may be able to determine their specific influence (if any) on enzyme thermal stability. To probe hydration dynamics, we employ a steady-state fluorescence technique popularly termed as red-edge excitation shift (REES), which has been used as an indicator of water dynamics [51–54]. Given HSA's multidomain structure, site-specific fluorescence labeling allowed us a unique opportunity to examine different domains individually (Scheme 1) [55–57]. We have also studied domain-specific thermal stability. Our findings establish a strong correlation between individual entropy and enthalpy contributions to the domain-specific stability and the domain-specific REES, offering insights that could be valuable for biocatalysis in DESs.

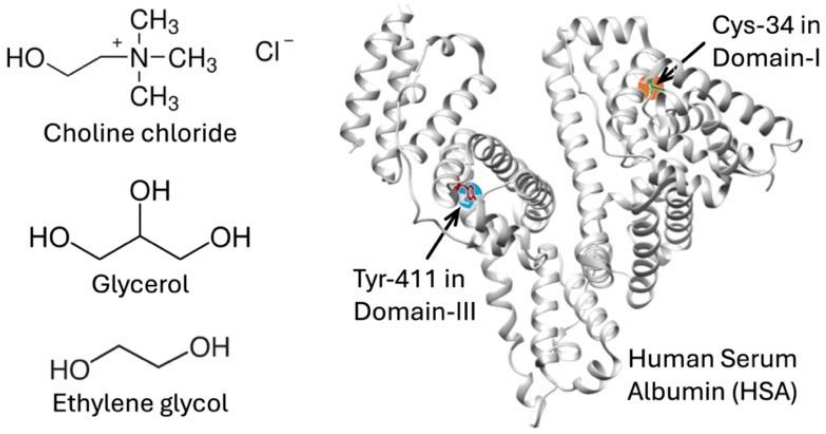

Scheme 1. (a) The chemical structures of hydrogen bond donors and acceptors of the used DESs (choline chloride-ethylene glycol and choline chloride-glycerol). (b) 3D structure of human serum albumin, where different domains are represented with different colours. Additionally, the specific sites where fluorescence labelling has been done are shown with red and black circles.

6.2. Results and Discussion:

6.2.1. Thermal Stability of HSA in the Presence of Choline Chloride-based Hydrated DESs: To investigate the thermal stability of human serum albumin (HSA) in the presence of hydrated choline chloride-based deep eutectic solvents (DESs), choline chloride–ethylene glycol [1:2] (ChCl-EG) and choline chloride–glycerol [1:2] (ChCl-Gly), we performed temperature-dependent circular dichroism (CD) spectroscopic measurements. The CD spectra of HSA in buffer (Figure 1a) display a clear temperature-dependent shift, with a minima (negative peak) at 222 nm. Temperature-dependent CD spectra of HSA in the presence of different concentrations of DES are represented in Figure 2. Monitoring the CD signal at 222 nm against temperature (Figure 1b) allowed us to compute the fraction of unfolded protein (f_u) (Figure 1c) using equation 6.1 and consequently the melting temperature using equation 6.2.

$$f_u = \frac{A_{222} - A_{222}^N}{A_{222}^U - A_{222}^N} \tag{6.1}$$

where, A_{222}^N and A_{222}^U represent the absorbance value at 222 nm of the native and fully denatured states of the protein, respectively, which are taken as the lowest and

highest values of the absorbance in the thermal denaturation experiment. The melting temperature is defined as the temperature at which half the protein population is unfolded, i.e., $f_u = 0.5$, which was determined by fitting the data to the following equation.

$$y = y_N + \frac{y_N - y_U}{1 + e^{(T_m - T)/d}} \quad (6.2)$$

In the above equation, y_N represents signal corresponding to the native (folded) state of the protein at low temperature, which is taken as 0 (i.e., f_U=0), y_U represents signal corresponding to the unfolded state of the protein at high temperature and taken as 1 (i.e., f_U=1). T_m represents the melting temperature and indicates the stability of the enzyme, and d is the slope or cooperativity factor. It describes how sharply the transition occurs. Smaller d values mean a steeper, more cooperative unfolding transition, while larger values indicate a broader transition.

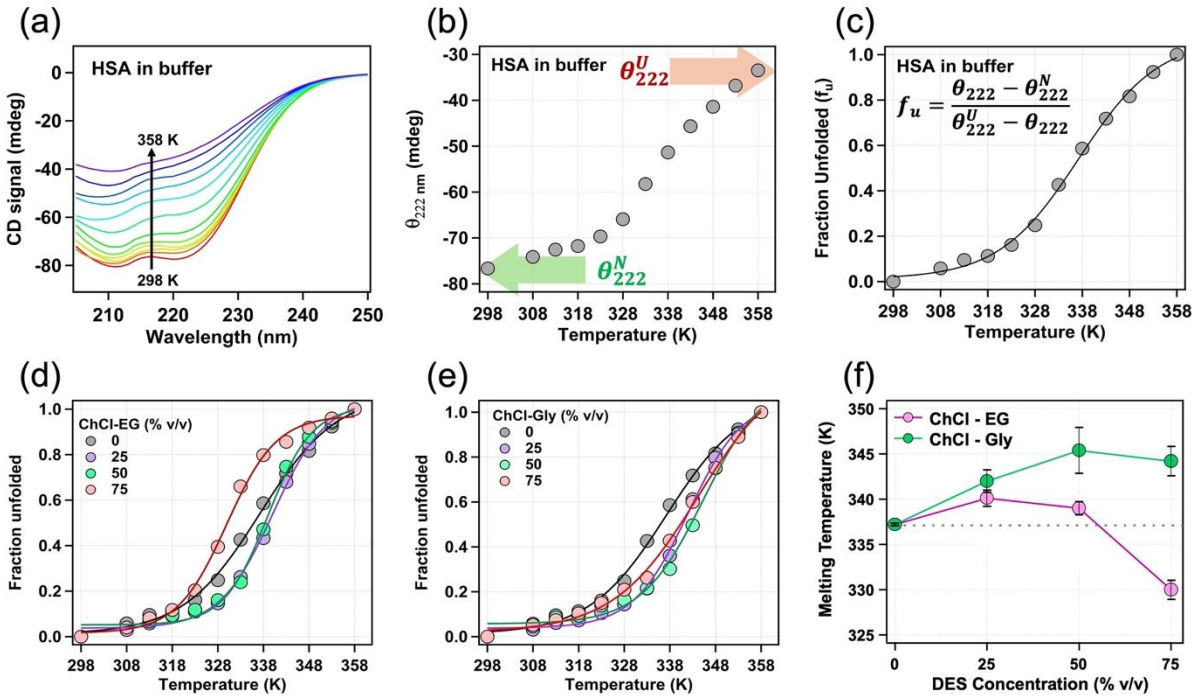

Figure 1. Thermal stability of HSA using circular dichroism spectroscopy. (a) Representative circular dichroism (CD) spectra of HSA in buffer at different temperatures (298 – 358 K). (b) Temperature-dependent changes in the CD signal at 222 nm. (c) Variation of fraction unfolded

(f_u), which has been calculated using the equation mentioned in the inset, as a function of temperature. Comparison of the thermal unfolding curve for different concentrations of (d) choline chloride-ethylene glycol (ChCl-EG), and (e) choline chloride-glycerol (ChCl-Gly) DES. Each melting curve was fitted using the sigmoidal function to get the melting temperature of HSA at each DES concentration. (f) Comparison of the melting temperature (T_m) of HSA in the presence of different concentrations of ChCl-EG and ChCl-Gly DES.

Comparison of the thermal unfolding curves of HSA for varying concentrations of ChCl-EG (Figure 1d) and ChCl-Gly (Figure 1e) clearly indicates a non-monotonic change in the melting temperature (Figure 1f). Data reveals that at 25% (v/v) DES, the thermal stability of HSA improves in both systems. For higher ChCl-Gly DES concentration, the thermal stability of HSA keeps increasing and tends to saturate. On the other hand, the effect of high concentration of ChCl-EG on HSA is found to be completely opposite, where a destabilisation of HSA has been observed (Figure 1f). Park *et al.* reported that the enhanced thermal stability of lysozyme in choline chloride-based DES positively correlates with the number of -OH groups in hydrogen bond donors [21]. Different DESs with sugars and polyols also showed similar observations for other proteins [28,58,59]. Consistent with this trend, a higher stability is observed for ChCl–Gly compared to ChCl–EG. This observation might be attributed, at least in part, to the additional –OH group present in glycerol. While specific interactions and hydrogen bonding between DES components and protein are typically considered to be the primary stabilizing factors, they fail to explain the concentration-dependent reversal of thermal stability of HSA in ChCl-EG. Moreover, viscosity-driven stabilization cannot account for this trend, as higher DES concentrations (which exhibit increased viscosity) result in reduced protein stability.

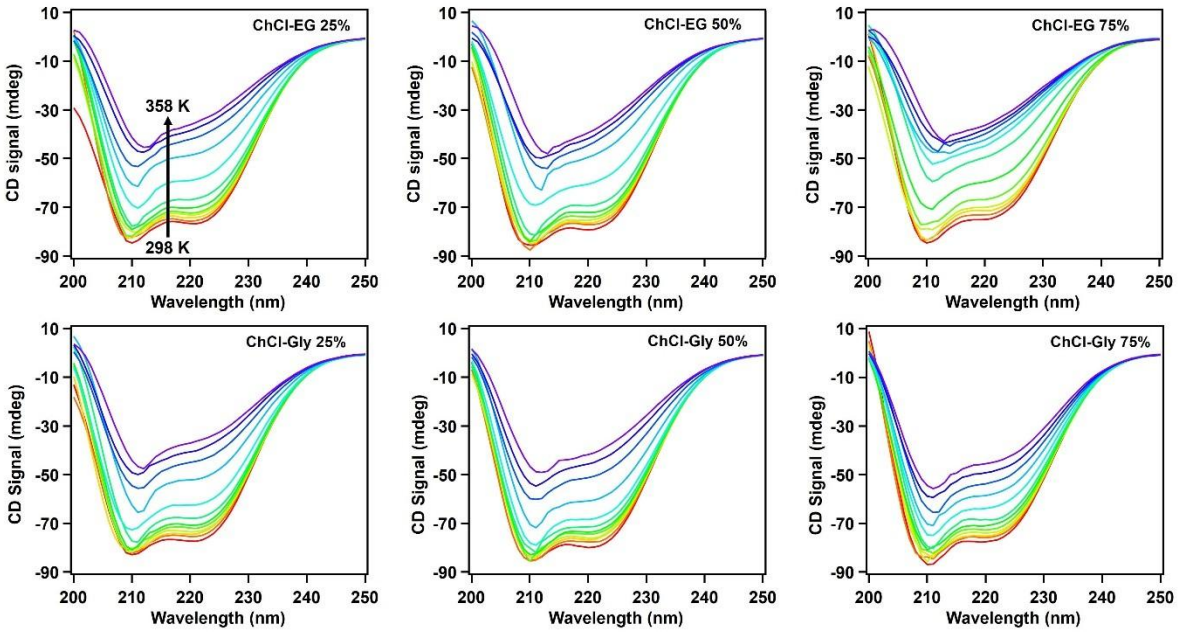

Figure 2. Representative circular dichroism (CD) spectra of HSA in the presence of different concentrations of ChCl-EG and ChCl-Gly DESs (the concentrations are mentioned in each figure itself) at different temperatures (298 – 358 K).

6.2.2. Recognition of Individual Entropic and Enthalpic Terms of Thermal Stabilization and Entropy-Enthalpy Compensation: To gain further insights into the thermal stability of HSA in the presence of choline chloride-based DESs, we sought to individually recognize the entropy (ΔS) and enthalpy (ΔH) of thermal unfolding at each DES concentration. According to our proposed associated water stabilization mechanism (AWSM) [35,48,60,61], thermodynamic changes in protein systems might be interpreted through the modulation of the dynamics of associated water molecules. Specifically, additive-induced entropic destabilization associated with enthalpic stabilization is expected to result in an increase in the flexibility of the associated water molecules. In contrast, entropic stabilization and enthalpic destabilization in the presence of additives are predicted to retard the water dynamics (Scheme 2). This relationship can be understood by the modulation of the water-protein hydrogen-bond network measured through its dynamics [45]. Enhanced flexibility in water dynamics implies a weakened hydrogen-bond network, which

increases the configurational entropy of water relative to that in the buffer environment. This results in a net positive change in entropy as,

$$\Delta\Delta S = \Delta S_{additive} - \Delta S_{buffer} > 0 \quad (6.3)$$

indicating entropic destabilization of the system. The reduction in hydrogen-bond strength requires energy input, typically in the form of heat. This corresponds to a positive enthalpic contribution leading to enthalpic stabilization.

$$Q_P > 0; H = Q_P = \left(\frac{dE}{dT}\right)_P dT \quad (6.4)$$

$$\Delta\Delta H = \Delta H_{additive} - \Delta H_{buffer} > 0 \quad (6.5)$$

Together, these suggest that associated water dynamics play a critical role in modulating the thermodynamic stability of proteins.

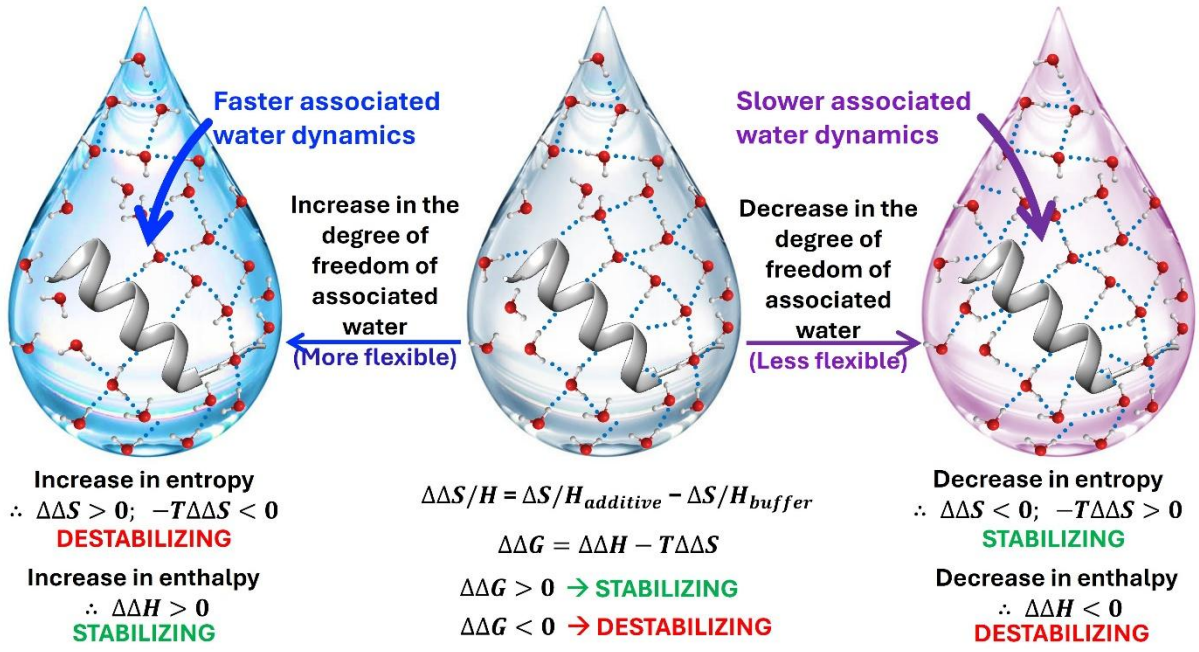

Scheme 2. Associated water reorganization is a critical factor that modulates protein Stability in the presence of any additives (here DES). This scheme has been represented based on the previous reports from our group [35,48,49].

Using the thermal melting curves and a two-state thermodynamic model (Figure 3a), we have calculated the temperature-dependent free energy of unfolding (ΔG) of HSA across different concentrations of ChCl-EG and ChCl-Gly DESs in buffer (Figures 3b-c). By applying the Gibbs-Helmholtz equation, we extracted entropic and enthalpic components of thermal unfolding at each DES concentration. Further, we computed the differential entropy ($\Delta\Delta S$) and enthalpy ($\Delta\Delta H$) of stabilization compared to that in buffer to delineate the positive or negative effect of DES on the protein in an individual entropic and enthalpic manner. The differential free energy of unfolding of the enzyme can be written as,

$$\Delta\Delta G = \Delta G_{DES} - \Delta G_{buffer} = \Delta\Delta H - T\Delta\Delta S \quad (6.6)$$

A positive value of $\Delta\Delta H$ contributes positively to the $\Delta\Delta G$, which implies that DES contributes to the enthalpic stabilization of HSA, whereas a positive value of $\Delta\Delta S$ (consequently, a negative value of $-T\Delta\Delta S$ that contributes negatively to the $\Delta\Delta G$) suggests entropic destabilization. The concentration-dependent differential entropy and enthalpy of stabilization of HSA in the presence of ChCl-EG and ChCl-Gly DESs are presented in Figures 3d and 3e, respectively. Up to 50% (v/v) of both ChCl-EG and ChCl-Gly DESs in buffer, we observed a steady increase in the entropic destabilization and enthalpic stabilization. However, at 75% (v/v) ChCl-EG and ChCl-Gly DES, the extent of both drastically reduces. Further, a plot of $\Delta\Delta H$ vs $-T\Delta\Delta S$ gives a straight line with slope ~0.85 and 0.83 for ChCl-EG and ChCl-Gly DESs, respectively, suggesting a strong entropy-enthalpy compensation in the presence of both the DESs (Figure 3f). Additionally, the enthalpy effect dominates in the overall stabilization process of HSA in the presence of both DESs.

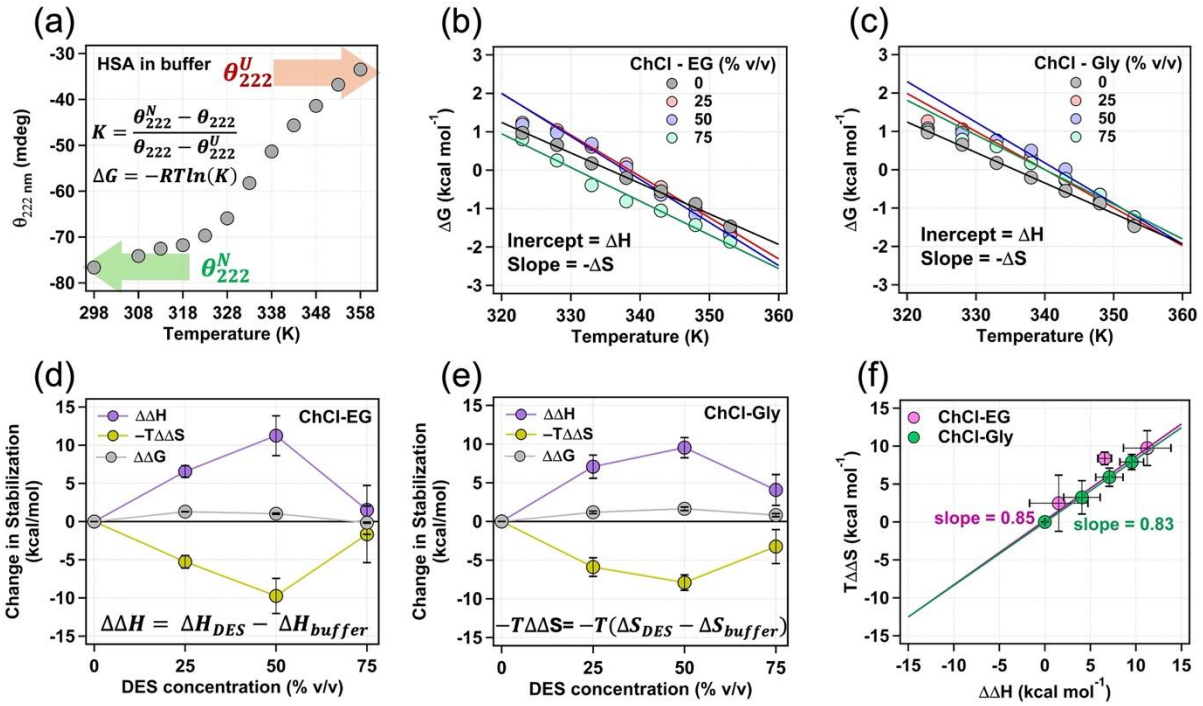

Figure 3. Individual entropic and enthalpic components might be positive or negative, depending on the type and concentration of the DESs. (a) Variation of the CD signal of HSA in buffer at 222 nm with temperature. The equation for calculating the equilibrium constant and the native and denatured state signals is mentioned in the figure. Plot of unfolding free energy of HSA as a function of the temperature in the presence of various concentrations of (b) ChCl-EG, and (c) ChCl-Gly DES. Plot of differential free energy ($\Delta\Delta G$) at 298 K, differential entropic component ($-T\Delta\Delta S$), and differential enthalpic component ($\Delta\Delta H$) for thermal unfolding of HSA in the presence of various concentrations of (d)ChCl-EG, and (e) ChCl-Gly DES. Here, $\Delta\Delta H$ *or* $\Delta\Delta G = \Delta H_{DES}$ *or* $\Delta G_{DES} - \Delta H_{buffer}$ *or* ΔG_{buffer}, and $-T\Delta\Delta S = -T(\Delta S_{DES} - \Delta S_{buffer})$ respectively. (f) Plot between entropic and enthalpic terms of thermal stability of HSA in the presence of various concentrations of both ChCl-EG (violet) and ChCl-Gly (green) DES. The black line is a linear fit, and a near-unity slope indicates entropy–enthalpy compensation.

Entropy-enthalpy compensation is a widely observed phenomenon in biochemical processes [48,49,62,63]. In a recent study, we reported a similar compensation effect for bromelain when exposed to acetamide-urea-sorbitol hydrated DES [35]. We proposed that water, being a common factor, modulates both entropic and enthalpic contributions in an opposing manner (Scheme 2) [35,48,49]. Specifically, we found that less flexible associated water in the presence of the DES stabilizes bromelain through entropy but destabilizes it through enthalpy, while flexible associated water dynamics result in an opposite thermodynamic outcome (Scheme 2). A similar

compensatory effect has been observed in the presence of macromolecular crowders, where modulation of water-protein hydrogen bonds (probed through the associated water dynamics) plays a critical role in protein stability [48,49]. Since associated water interacts directly with the protein surface, it likely exerts a significant influence on enzyme stability, and our previous studies support this mechanism [48–50].

To validate the mechanism (i.e., AWSM) further, we aim to investigate solvation dynamics around the protein. We employed fluorescence-based red edge excitation shift (REES) to estimate site-specific solvation dynamics at two different domains of HSA. This approach enables us to generate a residue-specific solvation dynamics map, providing mechanistic insights into the interplay between associated dynamics and protein stability in DES environments.

6.2.3. Measurement of red edge excitation shift (REES) as an indicator of solvation dynamics: While NMR and X-ray crystallography can provide insights into the water dynamics, their applicability is limited [64–67]. X-ray crystallography primarily reveals only the bound water molecules in the protein crystal [66–68], while NMR spectroscopy is generally restricted to small proteins such as calmodulin and lysozyme [69–71]. Other advanced techniques, such as Raman and infrared (IR) spectroscopy, terahertz spectroscopy, neutron scattering, and dielectric relaxation spectroscopy, offer valuable information on solvation dynamics [72–77]. However, these methods are often constrained by complex instrumentation and analysis, intricate sample preparation, and the requirement of high sample concentrations (chances of aggregation), making them less ideal for studying large protein systems [78–81].

In contrast, red edge excitation shift (REES) is a fluorescence-based method that is both experimentally simple and highly sensitive to solvation dynamics at site-specific fluorophore locations [51–54,82,83]. Unlike other spectroscopic techniques, REES requires only micromolar protein concentrations, making it experimentally accessible for a wide range of biological studies [51,54,55,84]. Moreover, high spatial

resolution of fluorescence makes REES particularly valuable for investigating solvent interactions in large and complex enzymes [51,54,85,86].

The occurrence of REES depends on the timescale of solvent relaxation relative to the fluorescence lifetime [84,87,88]. When the stabilization of the excited state by the surrounding solvent occurs much faster than its fluorescence lifetime ($\tau_S \ll \tau_f$), emission predominantly takes place from the fully solvated state, regardless of the excitation wavelength, and no REES is observed. However, if solvent relaxation is comparable or slower than the excited-state lifetime ($\tau_S \geq \tau_f$), emission occurs before complete solvent stabilization, and REES can be observed (Scheme 3) [88].

Since REES only manifests under the conditions of restricted solvent mobility, it serves as a sensitive probe for solvation dynamics around a fluorophore. Additionally, changes in the magnitude of REES in the presence of an additive suggest modulation of solvation dynamics within the system. Specifically, increased REES indicates slower solvation dynamics, revealing critical insights into solvent-protein interactions in diverse environments.

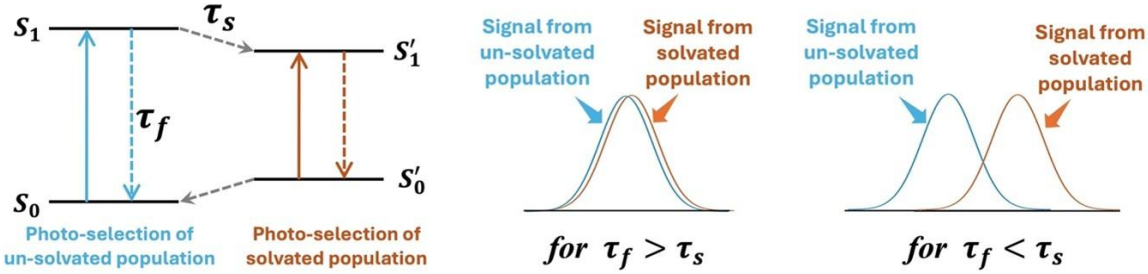

Scheme 3. Schematic representation of red edge excitation shift (REES). In a heterogeneous distribution of the environment around the fluorophore, photoexcitation at different wavelengths excites molecules to different excited states (S_1, S_1'). When the solvation dynamics (τ_s) is faster than the emission lifetime (τ_f), i.e., $\tau_f > \tau_s$, then irrespective of the excitation wavelength, molecules excited from both un-solvated (S_0) and solvated (S_0') ground states have sufficient time to reach the same fully relaxed excited state (S_1'). Consequently, signals from the unsolvated and solvated populations will merge together, and no REES can be observed. However, when the solvation dynamics is slower or comparable to the emission lifetime, i.e., $\tau_f < \tau_s$, it does not permit the solvent dipolar realignment before the emission. In this case, excitation of the unsolvated population leads to emission from a high-energy, unrelaxed state, while excitation at the red edge selectively targets the already solvated population, leading to emission from a lower-energy, relaxed state. As a result, signals from the unsolvated and

solvated populations will not merge, and red-shifted emissions spectra with longer wavelength of excitation (REES) will be observed.

Several reports have proposed that the network-like structure of DES forms a unique solvation shell around the protein, thereby influencing protein stability and dynamics [19,21–23,89]. Our group previously demonstrated that even at high concentrations of hydrated acetamide/urea/sorbitol DES, the immediate solvation environment of HSA remains unperturbed [36]. Additionally, using bromelain in the same DES system, we experimentally established that modulation of solvation (associated water) dynamics plays a critical role in determining both stability and activity [35]. In the present study, we aimed to estimate associated water dynamics through the measurement of REES.

REES has previously been recognized as a reliable indicator of dynamics across diverse protein systems [51,52,55,82,83,85,86,90,91]. Raghuraman *et al.* created a hydration dynamics mapping of K+ channels in their activated and inactivated form employing REES [52]. Very recently, More *et al.* used site-specific REES to develop a solvation dynamics map of TDP-43 protein during misfolding and aggregation [51]. The fluorescence lifetime of CPM-tagged HSA (domain I) and NPCE-tagged HSA (domain III) in buffer was reported to be around 3.6 ns [55] and 3.7 ns [56], and the solvation time was around 2.2 ns [36] and 1.32 ns [56], respectively. Because of the comparable solvation time and fluorescence lifetime, an appreciable amount of REES has been observed for both domains of HSA. Our group previously reported domain-specific REES changes in HSA during chemical denaturation with guanidine hydrochloride (GnHCl), demonstrating the effect of environmental rigidity on solvent relaxation dynamics [55]. Other groups also reported the REES of serum albumin protein [92,93].

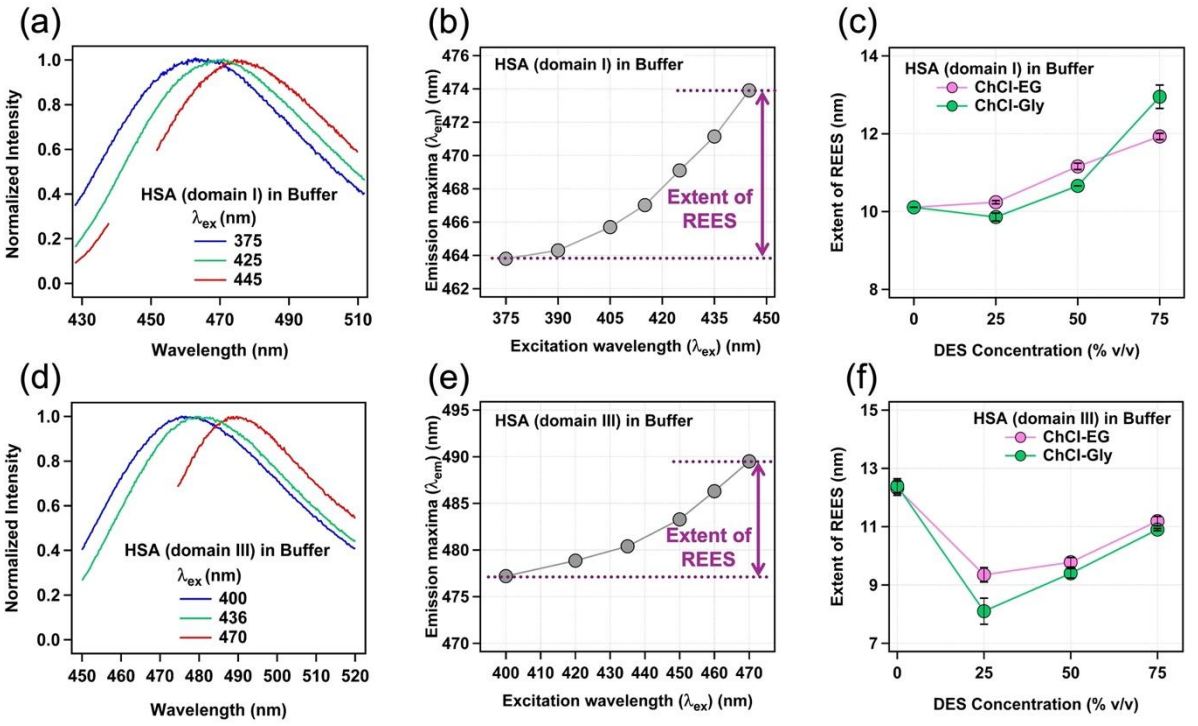

Figure 4. Modulation of hydration dynamics employing REES at different domains of HSA. (a) Excitation wavelength-dependent emission spectra of CPM tagged to HSA (domain I) in buffer. (b) Shift of the emission maxima of CPM tagged to HSA (domain I) with the change in the excitation wavelength. (c) Extent of REES of CPM tagged to HSA (domain I) in the presence of various concentrations of ChCl-EG (pink) and ChCl-Gly (green) DES. (d) Excitation wavelength-dependent emission spectra of NPCE tagged to HSA (domain III) in buffer. (e) Shift of the emission maxima of NPCE tagged to HSA (domain III) with the change in the excitation wavelength. (f) Extent of REES of NPCE tagged to HSA (domain III) in the presence of various concentrations of ChCl-EG (pink) and ChCl-Gly (green) DES.

Following our previous reports [36,49,55,56], we have selectively tagged two domains of the HSA protein with suitable fluorophores. The excitation wavelength dependent emission spectra of CPM-tagged HSA (domain I) and NPCE-tagged HSA in buffer show a clear red shift with the increase in the excitation wavelength (see Figure 4a and Figure 4d, respectively), and the corresponding excitation wavelength dependent emission maxima is plotted in Figure 4b and Figure 4e, respectively, from which the extent of REES is calculated. All the other raw data, except for buffer and relevant plots, are incorporated in Figures 5 and 6.

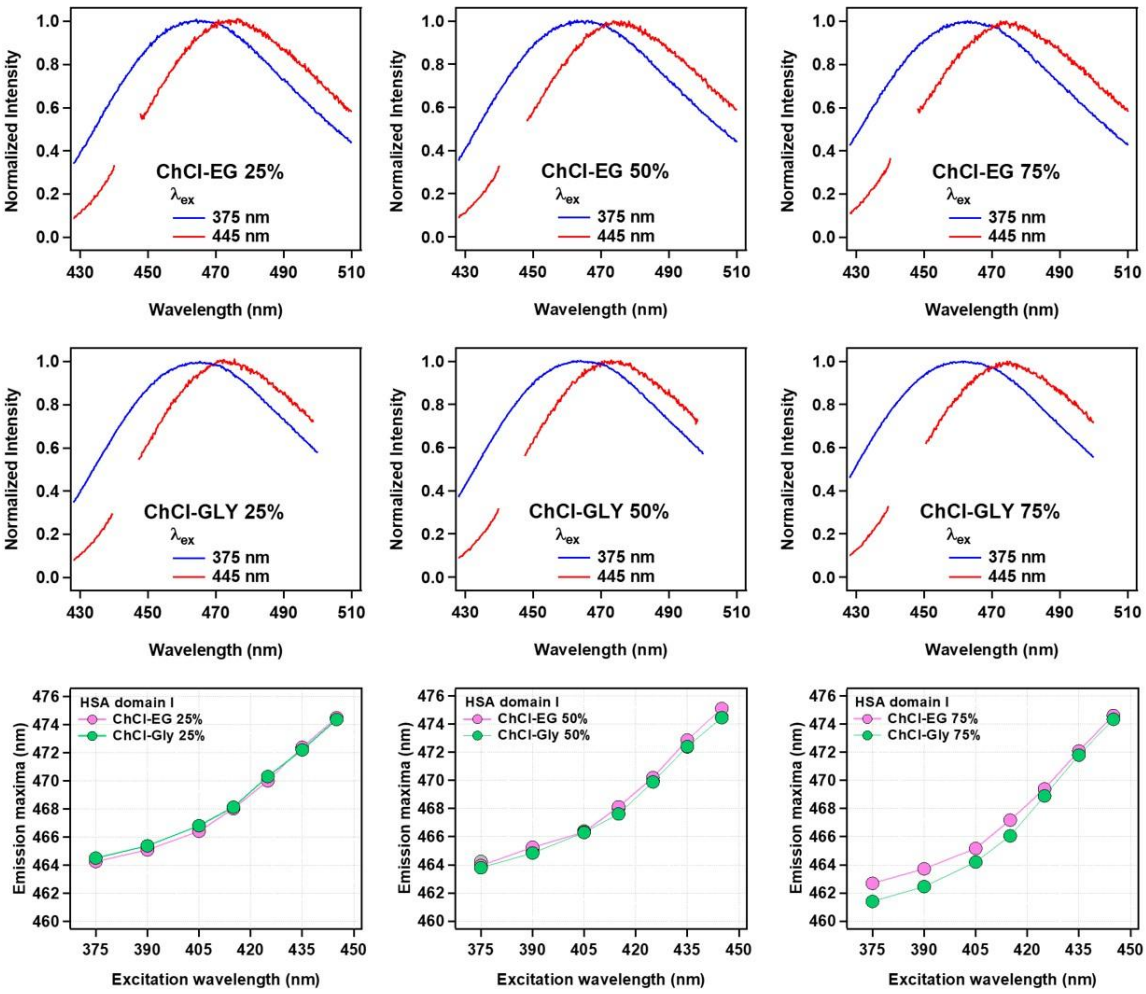

Figure 5. Excitation wavelength-dependent emission spectra of CPM tagged to HSA (domain I) in different concentrations of hydrated ChCl-EG (Upper panel) and ChCl-Gly (middle panel). (lower panel) Shift of the emission maxima with the change in the excitation wavelength in various concentrations of hydrated ChCl-EG (pink) and ChCl-Gly (green) DES. The concentrations of the DES are mentioned in each figure itself.

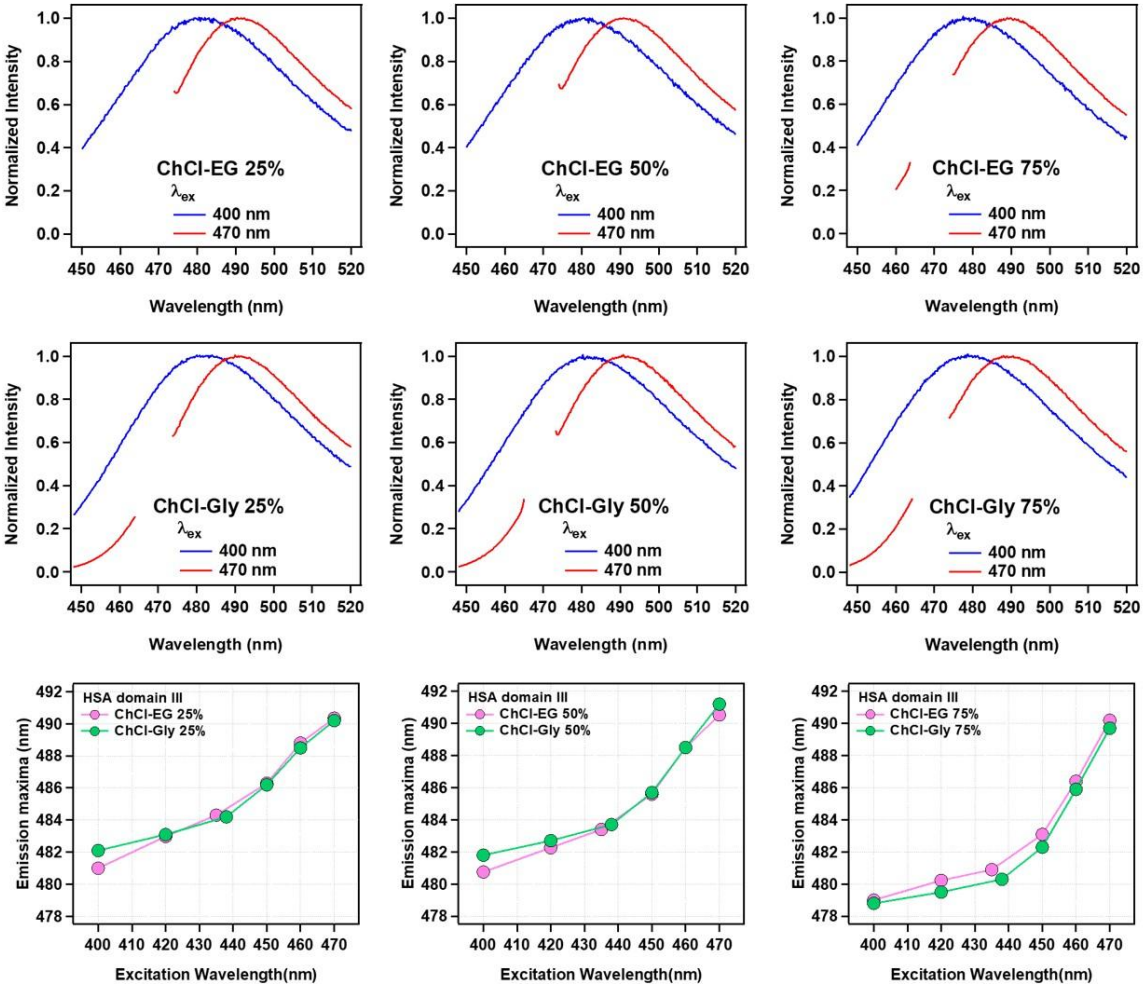

Figure 6. Excitation wavelength-dependent emission spectra of NPCE tagged to HSA (domain III) in different concentrations of hydrated ChCl-EG (Upper panel) and ChCl-Gly (middle panel). (lower panel) Shift of the emission maxima with the change in the excitation wavelength in various concentrations of hydrated ChCl-EG (pink) and ChCl-Gly (green) DES. The concentrations of the DES are mentioned in each figure itself.

The extent of REES for CPM tagged to domain-I of HSA is found to increase progressively with an increase in the DES concentration for both ChCl-EG and ChCl-Gly systems (Figure 4c). In contrast, the REES for NPCE tagged to domain-III of HSA exhibits a non-monotonic trend (Figure 4f) in the presence of both ChCl-EG and ChCl-Gly DESs. At low DES concentrations (25% v/v), REES of domain-III decreases, indicating increased flexibility in the nearby water molecules of the protein. At higher DES concentrations (50–75% v/v), REES increases again, suggesting a restricted solvent environment. The observed domain-specific

difference in REES modulation suggests that domain-I experiences progressive solvation retardation, whereas domain-III undergoes an initial increase in the associated water flexibility, followed by somewhat rigidification at higher DES concentrations.

6.2.4. Correlation between entropy and enthalpy of stabilization and associated water dynamics of HSA estimated through REES: To examine the correlation between the associated water dynamics around the protein and its thermal stability, we used $\Delta REES$, defined as,

$$\Delta REES = REES_{DES} - REES_{buffer} \quad (6.7)$$

A positive $\Delta REES$ value indicates retardation of the dynamics near the probe site. Conversely, a negative $\Delta REES$ suggests a more flexible solvent environment, indicating faster associated water dynamics (Figure 7a). According to the hypothesized associated water stabilization mechanism (AWSM), the entropic stabilization ($\Delta\Delta S < 0\ and\ -T\Delta\Delta S > 0$) and concomitant enthalpic destabilization ($\Delta\Delta H < 0$) will be associated with less flexible water dynamics than a buffer, and consequently a positive $\Delta REES$ must be observed (Figure 7b). On the other hand, the entropic destabilization ($-T\Delta\Delta S < 0$) and associated enthalpic stabilization ($\Delta\Delta H > 0$) will be linked to the flexible water dynamics than in the buffer, and consequently, a negative $\Delta REES$ will be observed (Figure 7b).

Figure 3 suggests a negative $\Delta REES$ at low DES concentrations (up to 50% v/v), while higher concentrations (75% v/v) of DES should yield less negative or even positive $\Delta REES$. The REES experiment of domain-III of HSA in the presence of both the DESs, yields expected results with a negative $\Delta REES$ at low DES concentrations (25–50% v/v), which become less negative at 75% v/v of DES (Figures 7c,f). In contrast, domain-I of HSA exhibited a different trend. In this case, $\Delta REES$ is found to be positive across all DES concentrations, indicating slower solvation dynamics in the

presence of both DESs (Figures 7c,f). Moreover, the magnitude of $\Delta REES$ increased with increasing DES's concentration, suggesting a progressive restriction of hydration dynamics in domain-I of HSA. These findings highlight the domain-specific modulation of hydration dynamics in DES environments. While domain-III experiences an increase in the associated water flexibility for low DES concentrations and then retards with high DES concentrations, domain-I portrays a monotonic retardation of the associated water dynamics.

To further analyze the relationship, we plotted differential entropic and enthalpic changes as a function of $\Delta REES$. Domain-I shows no correlation between $\Delta REES$ and components of thermal stabilization in either ChCl-EG or ChCl-Gly DESs (Figures 7d, g). The negative adjusted R^2 values in Figures 7d, g indicate that $\Delta REES$ of domain-I does not correlate with the overall entropic or enthalpic component of unfolding. However, for domain-III, $\Delta REES$ and differential entropic and enthalpic terms are somehow correlated (Figures 7e, h).

6.2.5. Necessity of domain-specific thermal unfolding of HSA via site-specific fluorescence spectroscopy: The unfolding of multi-domain proteins is inherently complex as different domains fold and unfold independently, contributing to the global structure [94–97]. Understanding domain-specific unfolding is therefore crucial to elucidate protein stabilization mechanisms [98–100]. Human serum albumin consists of three distinguishable domains [101]. Among which, REES of domains I and III are probed in the present study through selective fluorescent tags. Fortunately, through these domain-selective fluorescent tags, domain-specific thermal unfolding can also be measured.

Our previous research demonstrated that domain-III of HSA unfolds first, followed by domains-I and II, when exposed to guanidine hydrochloride (GnHCl) [98–100,102,103]. Mohan *et al.* even reported the domain-specific solvation dynamics of HSA in the presence and absence of sucrose during unfolding, revealing different modulation of the hydration dynamics across domains [104]. Other studies have explored domain-specific secondary structure and binding properties of HSA [101]. Inspired by these

studies, we aimed to measure domain-specific stabilization of HSA in the presence of ChCl-EG and ChCl-Gly DESs.

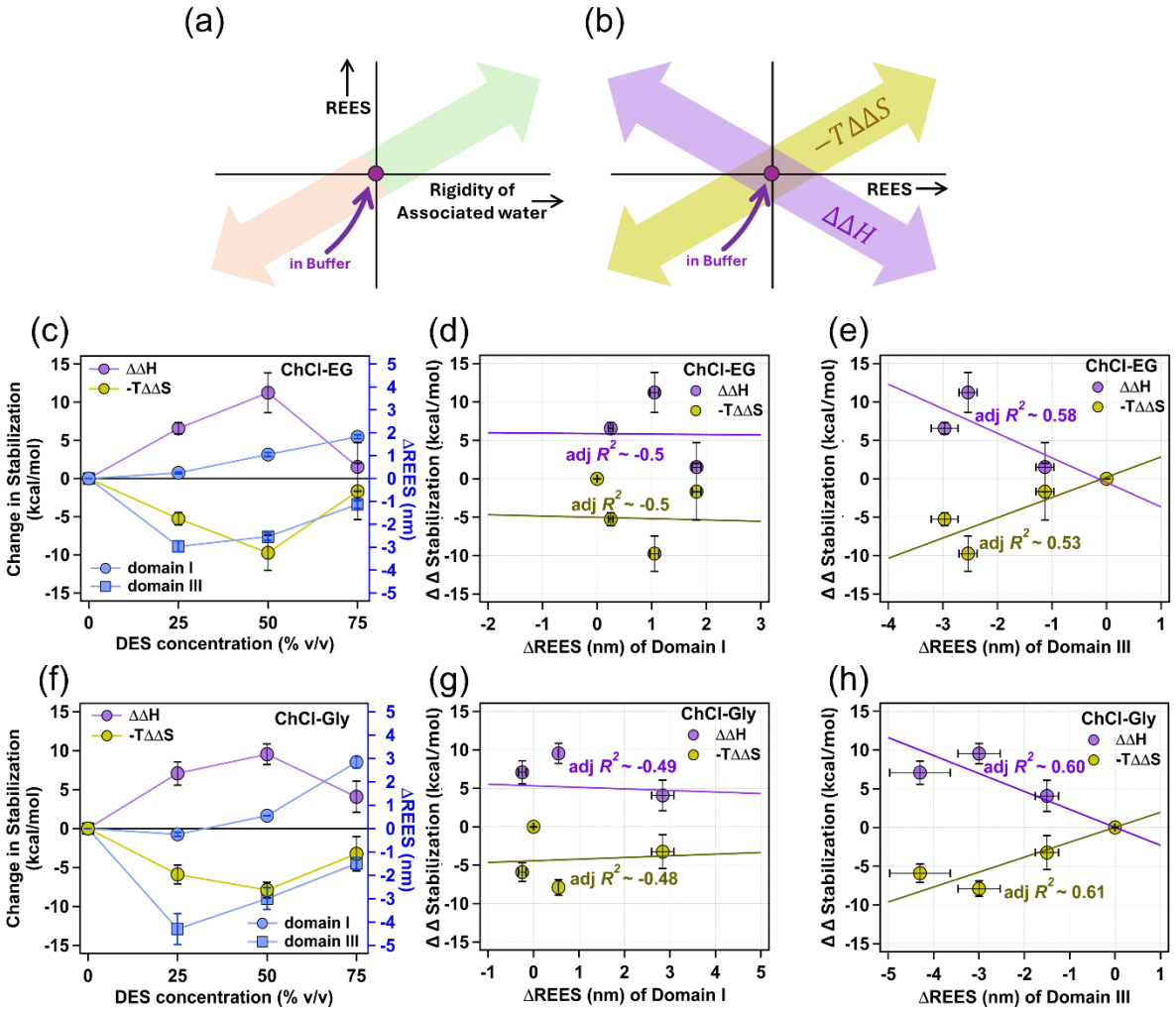

Figure 7. Correlation between the thermal stability of HSA and modulation of REES of two different domains of HSA. (a) Schematic representation of the relation between $\Delta REES$ and the modulation of solvation/hydration dynamics with respect to the buffer. (b) a schematic representation of our hypothesis, where entropic destabilization and associated enthalpic stabilization suggest faster hydration dynamics (negative $\Delta REES$) and the opposite thermodynamic outcome, which is entropic stabilization and associated enthalpic destabilization, suggests slower hydration dynamics, i.e., positive $\Delta REES$. (c) Differential entropic component ($-T\Delta\Delta S$) and enthalpic component ($\Delta\Delta H$) of thermal unfolding of HSA and the differential REES ($\Delta REES = REES_{DES} - REES_{buffer}$) of Domain-I and Domain-III in the presence of various concentrations of ChCl-EG. Plot of differential stability components ($\Delta\Delta H$ and $-T\Delta\Delta S$) of thermal unfolding of HSA in the presence of various concentrations of ChCl-EG DES as a function of the $\Delta REES$ of (d) Domain-I, and (e) Domain-III. (f) Differential entropic component ($-T\Delta\Delta S$) and enthalpic component ($\Delta\Delta H$) of thermal unfolding of HSA and the differential REES ($\Delta REES$) of Domain-I and Domain-III in the presence of various concentrations of ChCl-Gly DES. Plot of differential stability components ($\Delta\Delta H$ and $-T\Delta\Delta S$)

of thermal unfolding of HSA in the presence of various concentrations of ChCl-Gly DES as a function of the $\Delta REES$ of (g) Domain-I, and (h) Domain-III. No correlation was found in the case of $\Delta REES$ of Domain-I for both the DESs.

Thermal unfolding of domain-I of HSA is monitored through the change in the emission characteristics of CPM dye tagged to domain-I of HSA. CPM is a solvatochromic dye having high sensitivity to its microenvironment. In native HSA, CPM is buried within hydrophobic regions of domain-I, leading to a blue-shifted emission. However, upon protein unfolding, CPM becomes exposed to aqueous surroundings, causing a red-shifted emission (Figures 8a,b) as its excited-state dipole gets stabilized through the polar solvent (water) relaxation [105]. This environment-dependent spectral shift makes CPM fluorescence a sensitive indicator of protein unfolding.

From the thermal unfolding curve of domain-I of HSA in the absence and presence of different concentrations of the two DESs, we determined the free energy of the unfolding employing a two-state model (Section 1.1.4.2). Using the Gibbs–Helmholtz equation, we recognized the individual entropic and enthalpic terms of the thermal unfolding (see Figure 8c for buffer, Figure 8d for varying concentrations of ChCl-EG, and Figure 8g for varying concentrations of ChCl-Gly). We then calculated the differential entropy and enthalpy of thermal unfolding, taking the entropy and enthalpy of unfolding in buffer as a baseline. In Figures 8e and 8h, we have plotted differential entropy and enthalpy of domain-I unfolding alongside $\Delta REES$, across different concentrations of ChCl-EG and ChCl-Gly DESs, respectively. Clearly, with the entropic stabilization ($-T\Delta\Delta S > 0$) and concomitant enthalpic destabilization ($\Delta\Delta H < 0$), a positive $\Delta REES$ is observed, which suggests a retarded associated water dynamics. Moreover, the highest DES concentrations yielded the strongest positive $\Delta REES$, reinforcing the hypothesis that restriction in the associated water contributes to thermal stabilization. Consequently, a very strong correlation between differential entropy and enthalpy with $\Delta REES$ has been observed in the case of both the DESs

(Figures 8f and 8i), which was previously absent when correlated with the entropy and enthalpic components of overall stabilization (Figures 7d, 7g).

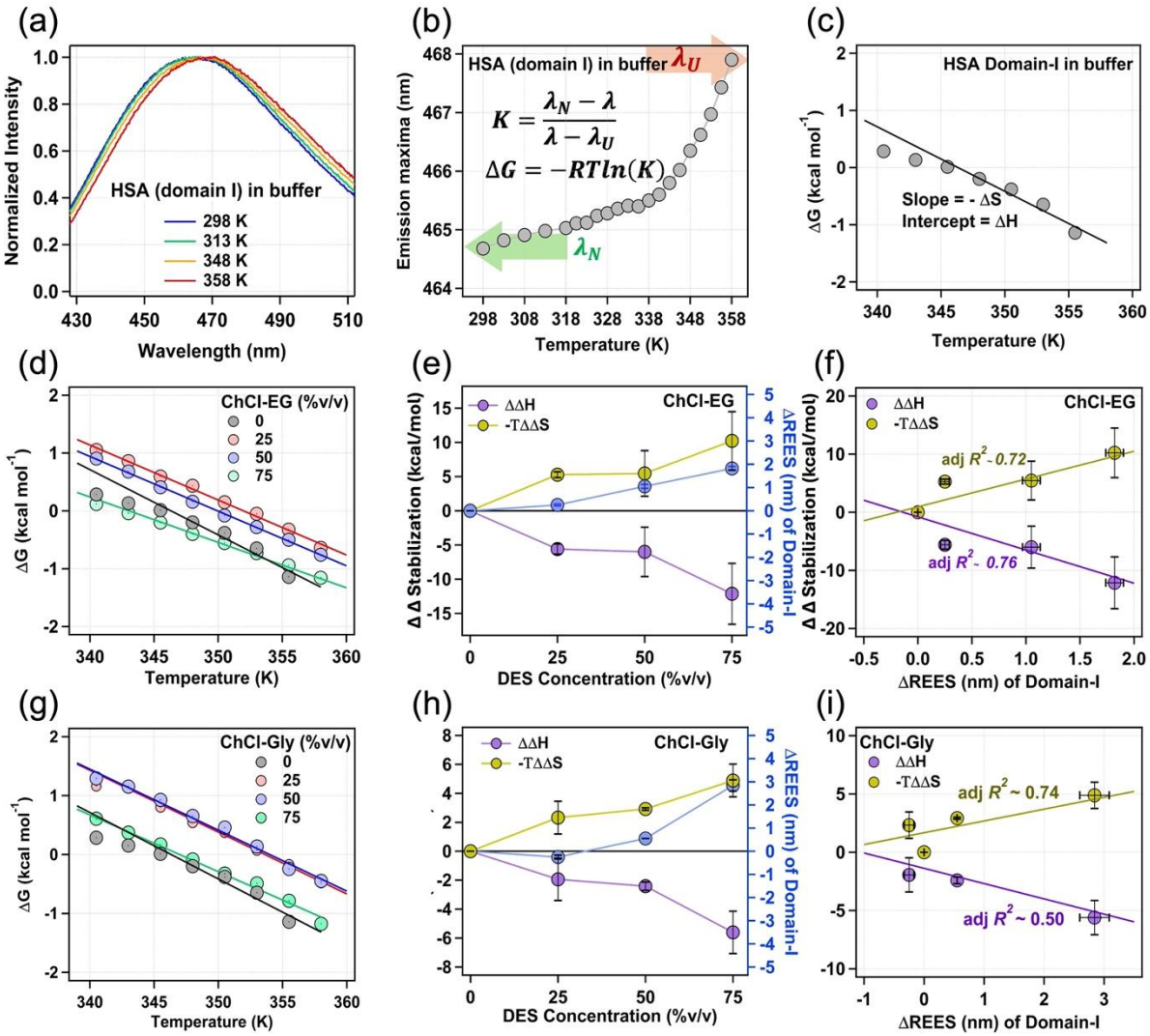

Figure 8. Thermal unfolding of Domain-I of HSA and its correlation with modulation of REES of Domain-I in the presence of different DES. (a) Representative steady-state fluorescence spectra of CPM-tagged HSA (domain I) in buffer at different temperatures. (b) Variation of emission maxima of CPM-tagged HSA in buffer as a function of temperature. (c) Schematic for estimating the change in the entropy and the enthalpy from the slope and the intercept, respectively, from the unfolding free energy of HSA in buffer. Plot of unfolding free energy of domain-I of HSA in the presence of various concentrations of (d) ChCl-EG, (g) ChCl-Gly DES as a function of the temperature. Differential entropic component ($-T\Delta\Delta S$) and enthalpic component ($\Delta\Delta H$) of thermal unfolding of Domain-I of HSA and the differential REES ($\Delta REES = REES_{DES} - REES_{buffer}$) of Domain-I in the presence of various concentrations of (e) ChCl-EG, (h) ChCl-Gly DES. Plot of differential stability components ($\Delta\Delta H$ and $-T\Delta\Delta S$) of thermal unfolding of HSA as a function of the $\Delta REES$ of Domain-I in the presence of various concentrations of (f) ChCl-EG, (i) ChCl-Gly DES.

To explore the stabilization of domain-III of HSA, we used the solvatochromic feature of NPCE tagged to domain-III of HSA. The temperature-dependent emission spectra and the shift of emission maxima of NPCE-tagged HSA in buffer are represented in Figures 9a and 9b, respectively. Employing the Gibbs-Helmholtz equation in the free energy of unfolding vs temperature plots, we have extracted the entropy and enthalpy of unfolding in buffer and at each experimental concentration of the two DESs (Figures 9c, 9d, and 9g). In figures 9e and 9h, we have plotted differential entropy and enthalpy of domain-III unfolding along with the $\Delta REES$ of that domain, in the presence of different concentrations of ChCl-EG and ChCl-Gly DES, respectively. Negative $\Delta REES$ is consistently observed across all DES concentrations, confirming that the associated water dynamics around domain-III become more flexible in DES environments. Also, the differential entropy and enthalpy are well correlated as a function of $\Delta REES$ (Figures 9f and 9i) and the adjusted R^2, which indicates that the goodness of fit substantially increases.

These findings reinforce the hypothesis that associated water dynamics significantly influence protein thermal stability, consistent with prior observations in other DESs and macromolecular crowders [35,48–50]. Moreover, these observations suggest a need for domain-specific measurement of thermal unfolding and solvation dynamics in the case of multidomain proteins.

The domain-specific thermal unfolding curves in the presence of different concentrations of ChCl-EG and ChCl-Gly DESs for both domains are presented in Figure 10.

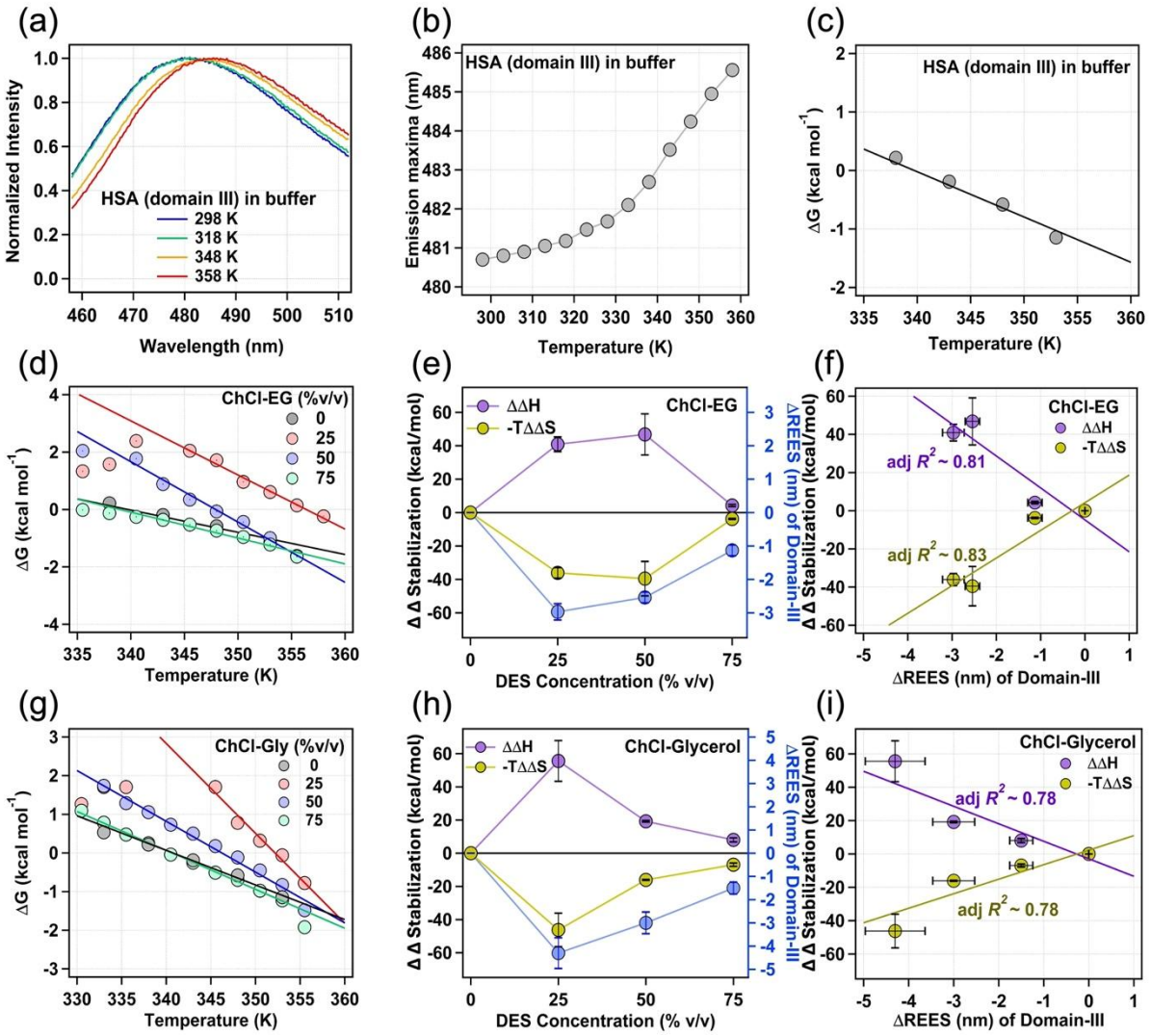

Figure 9. Thermal unfolding of Domain-III of HSA and its correlation with modulation of REES of Domain-III in the presence of different DES. (a) Representative steady-state fluorescence spectra of NPCE-tagged HSA (domain III) in buffer at different temperatures. (b) Variation of emission maxima of NPCE-tagged HSA in buffer as a function of temperature. (c) Schematic for estimating the change in the entropy and the enthalpy from the slope and the intercept, respectively, from the unfolding free energy of HSA in buffer. Plot of unfolding free energy of domain-III of HSA in the presence of various concentrations of (d)ChCl-EG, (g) ChCl-Gly DES as a function of the temperature. Differential entropic component ($-T\Delta\Delta S$) and enthalpic component ($\Delta\Delta H$) of thermal unfolding of Domain-III of HSA and the differential REES ($\Delta REES = REES_{DES} - REES_{buffer}$) of Domain-III in the presence of various concentrations of (e)ChCl-EG, (h) ChCl-Gly DES. Plot of differential stability components ($\Delta\Delta H$ and $-T\Delta\Delta S$) of thermal unfolding of HSA as a function of the $\Delta REES$ of Domain-III in the presence of various concentrations of (f)ChCl-EG, (i) ChCl-Gly DES.

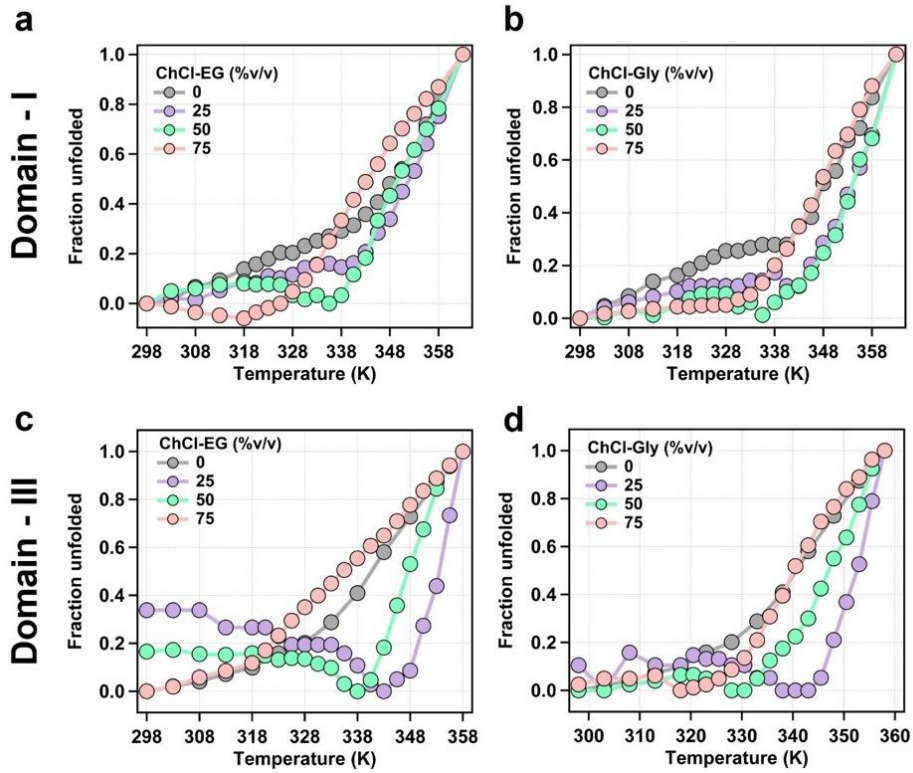

Figure 10. Domain-wise thermal unfolding curve for different concentrations of DESs. The upper panel represents the thermal unfolding curve for CPM-tagged (domain I) HSA in the presence of different concentrations of (a) ChCl-EG and (b) ChCl-Gly DES. The lower panel represents the thermal unfolding curve for NPCE-tagged (domain-III) HSA in the presence of different concentrations of (c) ChCl-EG and (d) ChCl-Gly DES.

6.2.6. Role of protein conformation in modulating the REES of HSA: Thus far, we have demonstrated a correlation between individual entropic and enthalpic terms of the domain-wise stability of HSA and the modulation of associated water dynamics around that domain probed through REES. However, changes in the protein conformations due to the addition of DES can also influence the thermal stability and the associated water dynamics. Also, if the protein conformations change significantly due to the DES addition, it might affect the extent of REES as well. Protein unfolding generally leads to increased water interaction that accelerates the associated water dynamics [99,102,104]. Our group previously reported that increasing GnHCl concentrations resulted in the unfolding of domain-I and domain-III of HSA with a significant decrease in the extent of REES [55]. Thus, one needs to be assured of the minimal structural changes of the

protein in the presence of different hydrated DES to comment on any relationship present between stability and REES, and consequently, associated water dynamics.

To examine whether DES affects the secondary structure of HSA, we performed circular dichroism (CD) spectroscopy at different DES concentrations. No significant spectral changes were observed with increasing ChCl-EG or ChCl-Gly DES concentrations, indicating no substantial alterations in protein conformation (Figures 11a, 11b, and 11c). To further assess any DES-induced global tertiary structural changes, we used single-molecular level fluorescence correlation spectroscopy (FCS) to determine the hydrodynamic radii of HSA in the presence of different concentrations of both the hydrated DESs (see Figures 11d-f). We found no significant change in the hydrodynamic radii in the presence of ChCl-EG. However, a slight compaction in the structure (decrease in the hydrodynamic radius) at 75% (v/v) of ChCl-Gly hydrated DES (Figure 11f) is observed. These results collectively confirm that structural changes do not play a significant role in DES-mediated domain-specific stabilization of HSA and further validate associated water dynamics modulation as the key factor influencing protein stability in DES media.

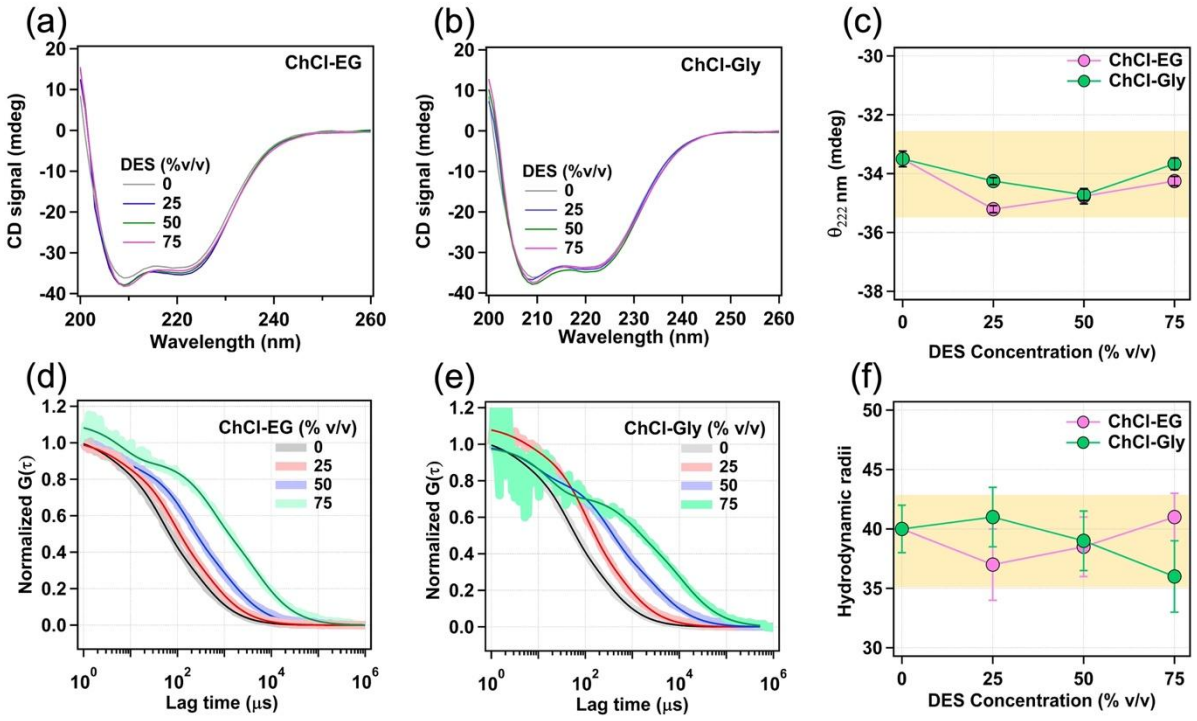

Figure 11. No significant conformational change of HSA in the presence of both ChCl-based DES. CD spectra of HSA at different concentrations of (a) ChCl-EG, and (b) ChCl-Gly hydrated DES. (c) experimental intensity of CD spectra at 222 nm at each DES concentration, which shows that the secondary structure is not significantly perturbed throughout the concentration range of DES. The normalized correlation function obtained using FCS for TMR-tagged (domain I) of HSA in the presence of different concentrations of (d) ChCl-EG, and (e) ChCl-Gly hydrated DES. (f) Modulation of hydrodynamic radii of HSA with the concentrations of hydrated DES.

6.3. Summary and Conclusion

This study elucidates the critical role of hydration dynamics in modulating protein stability within hydrated deep eutectic solvents, using human serum albumin (HSA) as a model system. By employing circular dichroism (CD) spectroscopy, fluorescence-based red-edge excitation shift (REES), and fluorescence spectroscopy, we systematically investigated the interplay between solvation dynamics, entropy-enthalpy compensation, and protein stability in the presence of choline chloride-based hydrated DESs (ChCl-EG and ChCl-Gly).

Our findings reveal that, firstly, hydration dynamics can be measured through a simple fluorescence-based technique, REES. More importantly, hydration dynamics rather than protein conformational changes dictate the thermal stability of HSA in choline chloride-based hydrated DESs.

Secondly, domain-specific unfolding is an important measurement to understand the intricate relationship between enzyme stability and hydration dynamics. Strong correlations between hydration dynamics ($\Delta REES$) and stability components ($-T\Delta\Delta S$ and $\Delta\Delta H$) affirm hydration-induced protein stabilization in DESs. Domain-specific REES changes directly correlate with stability trends, reinforcing the mechanistic link between hydration dynamics and entropy-enthalpy compensation.

Thirdly, Domain-specific hydration modulation governs the entropy-enthalpy balance of protein stabilization. Domain-I exhibits retarded associated water dynamics (positive $\Delta REES$), leading to enthalpic destabilization and entropic stabilization while Domain-III experiences hydration flexibility (negative $\Delta REES$), resulting in enthalpic stabilization and entropic destabilization.

Fourthly, ChCl-Gly DES exerts a stronger stabilizing effect than ChCl-EG, which might be due to differences in hydrogen bond donor interactions owing to a higher number of -OH groups present in glycerol relative to ethylene glycol.

Our results provide a fundamental understanding of protein-DES interactions by identifying hydration dynamics as a key determinant of protein stability. The findings hold broad implications in the field of biocatalysis, pharmaceutical formulations, and protein preservation in DES environments. Future studies should explore how hydration modulation can be fine-tuned for optimizing enzyme activity and stability in such unconventional solvent systems.

6.4. References

(1) Stepankova, V.; Bidmanova, S.; Koudelakova, T.; Prokop, Z.; Chaloupkova, R.; Damborsky, J. Strategies for Stabilization of Enzymes in Organic Solvents. *ACS Catal* **2013**, *3* (12), 2823–2836. https://doi.org/10.1021/cs400684x.

(2) Arnold, F. H. Directed Evolution: Bringing New Chemistry to Life. *Angew. Chem. Int. Ed.* **2018**, *57* (16), 4143–4148. https://doi.org/10.1002/ANIE.201708408.

(3) Kan, S. B. J.; Lewis, R. D.; Chen, K.; Arnold, F. H. Directed Evolution of Cytochrome c for Carbon-Silicon Bond Formation: Bringing Silicon to Life. *Science (1979)* **2016**, *354* (6315), 1048–1051. https://doi.org/10.1126/SCIENCE.AAH6219/SUPPL_FILE/KAN.SM.PDF

(4) van Rantwijk, F.; Sheldon, R. A. Biocatalysis in Ionic Liquids. *Chem. Rev.* **2007**, *107* (6), 2757–2785. https://doi.org/10.1021/cr050946x.

(5) Pätzold, M.; Siebenhaller, S.; Kara, S.; Liese, A.; Syldatk, C.; Holtmann, D. Deep Eutectic Solvents as Efficient Solvents in Biocatalysis. *Trends Biotechnol* **2019**, *37* (9), 943–959. https://doi.org/10.1016/j.tibtech.2019.03.007.

(6) Sheldon, R. A. Biocatalysis in Ionic Liquids: State-of-the-Union. *Green Chem.* **2021**, *23* (21), 8406–8427. https://doi.org/10.1039/d1gc03145g.

(7) Florindo, C.; Lima, F.; Ribeiro, B. D.; Marrucho, I. M. Deep Eutectic Solvents: Overcoming 21st Century Challenges. *Curr. Opin. Green Sustain. Chem.* **2019**, *18*, 31–36. https://doi.org/10.1016/j.cogsc.2018.12.003.

(8) Smith, E. L.; Abbott, A. P.; Ryder, K. S. Deep Eutectic Solvents (DESs) and Their Applications. *Chem Rev* **2014**, *114* (21), 11060–11082. https://doi.org/10.1021/cr300162p.

(9) Paiva, A.; Craveiro, R.; Aroso, I.; Martins, M.; Reis, R. L.; Duarte, A. R. C. Natural Deep Eutectic Solvents - Solvents for the 21st Century. *ACS Sustainable Chem. Eng.* **2014**, *2* (5), 1063–1071. https://doi.org/10.1021/sc500096j.

(10) Płotka-Wasylka, J.; de la Guardia, M.; Andruch, V.; Vilková, M. Deep Eutectic Solvents vs Ionic Liquids: Similarities and Differences. *Microchemical Journal* **2020**, *159*, 105539. https://doi.org/10.1016/j.microc.2020.105539.

(11) Domínguez de María, P.; Maugeri, Z. Ionic Liquids in Biotransformations: From Proof-of-Concept to Emerging Deep-Eutectic-Solvents. *Curr. Opin. Chem. Biol.* **2011**, *15* (2), 220–225. https://doi.org/10.1016/j.cbpa.2010.11.008.

(12) Yadav, N.; Venkatesu, P. Current Understanding and Insights towards Protein Stabilization and Activation in Deep Eutectic Solvents as Sustainable Solvent Media. *Phys. Chem. Chem. Phys.* **2022**, *24* (22), 13474–13509. https://doi.org/10.1039/D2CP00084A.

(13) Kist, J. A.; Zhao, H.; Mitchell-Koch, K. R.; Baker, G. A. The Study and Application of Biomolecules in Deep Eutectic Solvents. *J Mater Chem B* **2021**, *9* (3), 536–566. https://doi.org/10.1039/d0tb01656j.

(14) Juneidi, I.; Hayyan, M.; Hashim, M. A.; Hayyan, A. Pure and Aqueous Deep Eutectic Solvents for a Lipase-Catalysed Hydrolysis Reaction. *Biochem Eng J* **2017**, *117*, 129–138. https://doi.org/10.1016/j.bej.2016.10.003.

(15) Sanchez-Fernandez, A.; Jackson, A. J. Proteins in Deep Eutectic Solvents: Structure, Dynamics and Interactions with the Solvent. In *Advances in Botanical Research*; Academic Press Inc., 2021; Vol. 97, pp 69–94. https://doi.org/10.1016/bs.abr.2020.09.003.

(16) Toledo, M. L.; Pereira, M. M.; Freire, M. G.; Silva, J. P. A.; Coutinho, J. A. P.; Tavares, A. P. M. Laccase Activation in Deep Eutectic Solvents. *ACS Sustain Chem Eng* **2019**, *7* (13), 11806–11814. https://doi.org/10.1021/acssuschemeng.9b02179.

(17) Huang, Z. L.; Wu, B. P.; Wen, Q.; Yang, T. X.; Yang, Z. Deep Eutectic Solvents Can Be Viable Enzyme Activators and Stabilizers. *Journal of Chemical Technology and Biotechnology* **2014**, *89* (12), 1975–1981. https://doi.org/10.1002/jctb.4285.

(18) Tian, Y.; Zhu, M.; Hu, T.; Liu, C. Natural Deep Eutectic Solvent—A Novel Green Solvent for Protein Stabilization. *Int. J. Biol. Macromol.* **2023**, *247*, 125477. https://doi.org/10.1016/J.IJBIOMAC.2023.125477.

(19) Monhemi, H.; Housaindokht, M. R.; Moosavi-Movahedi, A. A.; Bozorgmehr, M. R. How a Protein Can Remain Stable in a Solvent with High Content of Urea: Insights from Molecular Dynamics Simulation of Candida Antarctica Lipase B in Urea: Choline Chloride Deep Eutectic Solvent. *Phys. Chem. Chem. Phys.* **2014**, *16* (28), 14882–14893. https://doi.org/10.1039/c4cp00503a.

(20) Zeng, C. X.; Qi, S. J.; Xin, R. P.; Yang, B.; Wang, Y. H. Synergistic Behavior of Betaine-Urea Mixture: Formation of Deep Eutectic Solvent. *J. Mol. Liq.* **2016**, *219*, 74–78. https://doi.org/10.1016/j.molliq.2016.02.076.

(21) Park, K.; Ham, B. Y.; Li, K.; Kang, S.; Jung, D.; Kim, H.; Liu, Y.; Hwang, I.; Lee, J. Insights into the Enhanced Thermal Stability of Lysozyme with Altered Structure and Activity Induced by Choline Chloride-Based Deep Eutectic Solvents Containing Polyols and Sugars. *J. Mol. Liq.* **2022**, *349*, 118143. https://doi.org/10.1016/j.molliq.2021.118143.

(22) Cao, J.; Wu, R.; Zhu, F.; Dong, Q.; Su, E. Enzymes in Nearly Anhydrous Deep Eutectic Solvents: Insight into the Biocompatibility and Thermal Stability. *Enzyme Microb. Technol.* **2022**, *157*, 110022. https://doi.org/10.1016/j.enzmictec.2022.110022.

(23) Mamashli, F.; Badraghi, J.; Delavari, B.; Lanjanian, H.; Sabbaghian, M.; Hosseini, M.; Saboury, A. A. Improvement of Versatile Peroxidase Activity and Stability by a Cholinium-Based Ionic Liquid. *J. Mol. Liq.* **2018**, *272*, 597–608. https://doi.org/10.1016/j.molliq.2018.09.128.

(24) Pal, S.; Roy, R.; Paul, S. Potential of a Natural Deep Eutectic Solvent, Glyceline, in the Thermal Stability of the Trp-Cage Mini-Protein. *J. Phys. Chem. B* **2020**, *124* (35), 7598–7610. https://doi.org/10.1021/ACS.JPCB.0C03501/ASSET/IMAGES/MEDIUM/JP0C03501_M002.GIF.

(25) Olivares, B.; Martínez, F.; Rivas, L.; Calderón, C.; M. Munita, J.; R. Campodonico, P. A Natural Deep Eutectic Solvent Formulated to Stabilize β-Lactam Antibiotics. *Scientific Reports 2018 8:1* **2018**, *8* (1), 1–12. https://doi.org/10.1038/s41598-018-33148-w.

(26) Gomes, I.; Galamba, N. Protein Stability in a Natural Deep Eutectic Solvent: Preferential Hydration or Solvent Slaving? *J. Chem. Phys.* **2023**, *159* (23). https://doi.org/10.1063/5.0177095/2929736.

(27) Sanchez-Fernandez, A.; Poon, J.-F.; Leung, A. E.; Prévost, S. F.; Dicko, C. Stabilization of Non-Native Folds and Programmable Protein Gelation in

Compositionally Designed Deep Eutectic Solvents. *ACS Nano* **2024**, *18* (28), 18314–18326. https://doi.org/10.1021/acsnano.4c01950.

(28) Sun, H.; Xin, R.; Qu, D.; Yao, F. Mechanism of Deep Eutectic Solvents Enhancing Catalytic Function of Cytochrome P450 Enzymes in Biosynthesis and Organic Synthesis. *J Biotechnol* **2020**, *323*, 264–273. https://doi.org/10.1016/j.jbiotec.2020.07.004.

(29) Das, N.; Khan, T.; Subba, N.; Sen, P. Correlating Bromelain's Activity with Its Structure and Active-Site Dynamics and the Medium's Physical Properties in a Hydrated Deep Eutectic Solvent. *Phys. Chem. Chem. Phys.* **2021**, *23* (15), 9337–9346. https://doi.org/10.1039/d1cp00046b.

(30) Esquembre, R.; Sanz, J. M.; Wall, J. G.; Del Monte, F.; Mateo, C. R.; Ferrer, M. L. Thermal Unfolding and Refolding of Lysozyme in Deep Eutectic Solvents and Their Aqueous Dilutions. *Phys. Chem. Chem. Phys.* **2013**, *15* (27), 11248–11256. https://doi.org/10.1039/c3cp44299c.

(31) Kumari, P.; Kumari, M.; Kashyap, H. K. How Pure and Hydrated Reline Deep Eutectic Solvents Affect the Conformation and Stability of Lysozyme: Insights from Atomistic Molecular Dynamics Simulations. *J. Phys. Chem. B* **2020**, *124* (52), 11919–11927. https://doi.org/10.1021/ACS.JPCB.0C09873/ASSET/IMAGES/LARGE/JP0C09873_0006.JPEG.

(32) Dhiman, D.; Marques, A. S. C.; Bisht, M.; Tavares, A. P. M.; Freire, M. G.; Venkatesu, P. Unveiling the Potential of Deep Eutectic Solvents to Improve the Conformational and Colloidal Stability of Immunoglobulin G Antibodies. *Green Chem.* **2023**, *25* (2), 650–660. https://doi.org/10.1039/D2GC03415H.

(33) Yadav, N.; Bhakuni, K.; Bisht, M.; Bahadur, I.; Venkatesu, P. Expanding the Potential Role of Deep Eutectic Solvents toward Facilitating the

Structural and Thermal Stability of α-Chymotrypsin. *ACS Sustain Chem Eng* **2020**, *8* (27), 10151–10160. https://doi.org/10.1021/acssuschemeng.0c02213.

(34) Papadopoulou, A. A.; Efstathiadou, E.; Patila, M.; Polydera, A. C.; Stamatis, H. Deep Eutectic Solvents as Media for Peroxidation Reactions Catalyzed by Heme-Dependent Biocatalysts. *Ind Eng Chem Res* **2016**, *55* (18), 5145–5151. https://doi.org/10.1021/acs.iecr.5b04867.

(35) Khan, T.; Das, N.; Bhowmik, S.; Negi, K. S.; Sen, P. Critical Role of Water beyond the Media to Maintain Protein Stability and Activity in Hydrated Deep Eutectic Solvent. *J. Phys. Chem. B* **2024**, *129*, 175. https://doi.org/10.1021/ACS.JPCB.4C07039/ASSET/IMAGES/LARGE/JP4C07039_0010.JPEG.

(36) Khan, T.; Das, N.; Negi, K. S.; Bhowmik, S.; Sen, P. Understanding the Intricacy of Protein in Hydrated Deep Eutectic Solvent: Solvation Dynamics, Conformational Fluctuation Dynamics, and Stability. *Int. J. Biol. Macromol.* **2023**, *253*, 127100. https://doi.org/10.1016/j.ijbiomac.2023.127100.

(37) Sanchez-Fernandez, A.; Edler, K. J.; Arnold, T.; Alba Venero, D.; Jackson, A. J. Protein Conformation in Pure and Hydrated Deep Eutectic Solvents. *Phys. Chem. Chem. Phys.* **2017**, *19* (13), 8667–8670. https://doi.org/10.1039/c7cp00459a.

(38) Durand, E.; Lecomte, J.; Baréa, B.; Villeneuve, P. Towards a Better Understanding of How to Improve Lipase-Catalyzed Reactions Using Deep Eutectic Solvents Based on Choline Chloride. *European Journal of Lipid Science and Technology* **2014**, *116* (1), 16–23. https://doi.org/10.1002/ejlt.201300246.

(39) Durand, E.; Lecomte, J.; Baréa, B.; Dubreucq, E.; Lortie, R.; Villeneuve, P. Evaluation of Deep Eutectic Solvent-Water Binary Mixtures for Lipase-Catalyzed Lipophilization of Phenolic Acids. *Green Chem.* **2013**, *15* (8), 2275–2282. https://doi.org/10.1039/c3gc40899j.

(40) Choi, Y. H.; van Spronsen, J.; Dai, Y.; Verberne, M.; Hollmann, F.; Arends, I. W. C. E.; Witkamp, G. J.; Verpoorte, R. Are Natural Deep Eutectic Solvents the Missing Link in Understanding Cellular Metabolism and Physiology? *Plant Physiol.* **2011**, *156* (4), 1701–1705. https://doi.org/10.1104/pp.111.178426.

(41) Wang, X.; Sheng, Y.; Cui, H.; Qiao, J.; Song, Y.; Li, X.; Huang, H. Corner Engineering: Tailoring Enzymes for Enhanced Resistance and Thermostability in Deep Eutectic Solvents. *Angew. Chem. Int. Ed.* **2024**, *63* (2), e202315125. https://doi.org/10.1002/ANIE.202315125.

(42) Soltani-Nezhad, Z.; Zaboli, M.; Mortazavi, M.; Torkzadeh-Mahani, M. Enhancing Stability and Catalytic Activity of Urate Oxidase Using Natural Deep Eutectic Solvent: Insights from Experimental and Computational Approaches. *J Biomol Struct Dyn* **2025**, 1–18. https://doi.org/10.1080/07391102.2025.2486444.

(43) Sanchez-Fernandez, A.; Basic, M.; Xiang, J.; Prevost, S.; Jackson, A. J.; Dicko, C. Hydration in Deep Eutectic Solvents Induces Non-Monotonic Changes in the Conformation and Stability of Proteins. *J. Am. Chem. Soc.* **2022**, *144* (51), 23657–23667. https://doi.org/10.1021/jacs.2c11190.

(44) Bhattacharyya, K. Nature of Biological Water: A Femtosecond Study. *Chemical Communications* **2008**, No. 25, 2848–2857. https://doi.org/10.1039/b800278a.

(45) Bagchi, B. Water Dynamics in the Hydration Layer around Proteins and Micelles. *Chem Rev* **2005**, *105* (9), 3197–3219. https://doi.org/10.1021/cr020661+.

(46) Bellissent-Funel, M. C.; Hassanali, A.; Havenith, M.; Henchman, R.; Pohl, P.; Sterpone, F.; Van Der Spoel, D.; Xu, Y.; Garcia, A. E. Water Determines the Structure and Dynamics of Proteins. *Chem Rev* **2016**, *116* (13), 7673–7697. https://doi.org/10.1021/acs.chemrev.5b00664.

(47) Ball, P. Water as an Active Constituent in Cell Biology. *Chem Rev* **2008**, *108* (1), 74–108. https://doi.org/10.1021/cr068037a.

(48) Khan, T.; Halder, B.; Das, N.; Sen, P. Role of Associated Water Dynamics on Protein Stability and Activity in Crowded Milieu. *J Phys Chem B* **2024**, *128*, 8672–8686. https://doi.org/10.1021/acs.jpcb.4c04337.

(49) Das, N.; Tarif, E.; Dutta, A.; Sen, P. Associated Water Dynamics Might Be a Key Factor Affecting Protein Stability in the Crowded Milieu. *J. Phys. Chem. B* **2023**, *127* (14), 3151–3163. https://doi.org/10.1021/acs.jpcb.2c09043.

(50) Negi, K. S.; Das, N.; Khan, T.; Sen, P. Osmolyte Induced Protein Stabilization: Modulation of Associated Water Dynamics Might Be a Key Factor. *Phys. Chem. Chem. Phys.* **2023**, *25* (47), 32602–32612. https://doi.org/10.1039/d3cp03357k.

(51) More, S. R.; Jha, S. K. Multi-Site Red-Edge Excitation Shift Reveals the Residue-Specific Solvation Dynamics during the Native to Amyloid-like Transition of an Amyloidogenic Protein. *J. Phys. Chem. B* **2025**, *129*, 176–193. https://doi.org/10.1021/acs.jpcb.4c07067.

(52) Raghuraman, H.; Islam, S. M.; Mukherjee, S.; Roux, B.; Perozo, E. Dynamics Transitions at the Outer Vestibule of the KcsA Potassium Channel

during Gating. *Proc. Natl. Acad. Sci. USA* **2014**, *111* (5), 1831–1836. https://doi.org/10.1073/pnas.1314875111.

(53) Brahma, R.; Raghuraman, H. Novel Insights in Linking Solvent Relaxation Dynamics and Protein Conformations Utilizing Red Edge Excitation Shift Approach. *Emerg. Top. Life Sci.* **2021**, *5* (1), 89–101. https://doi.org/10.1042/ETLS20200256.

(54) Chattopadhyay, A.; Haldar, S. Dynamic Insight into Protein Structure Utilizing Red Edge Excitation Shift. *Acc. Chem. Res.* **2014**, *47* (1), 12–19. https://doi.org/10.1021/ar400006z.

(55) Das, N.; Sahu, S.; Khan, T.; Sen, P. Site-Specific Heterogeneity of Multi-Domain Human Serum Albumin and Its Origin: A Red Edge Excitation Shift Study. *Photochem. Photobiol.* **2023**, *99* (2), 538–546.

(56) Sengupta, B.; Acharyya, A.; Sen, P. Elucidation of the Local Dynamics of Domain-III of Human Serum Albumin over the Ps–Ms Time Regime Using a New Fluorescent Label. *Phys. Chem. Chem. Phys.* **2016**, *18* (41), 28548–28555. https://doi.org/10.1039/C6CP05743H.

(57) Yadav, R.; Sengupta, B.; Sen, P. Conformational Fluctuation Dynamics of Domain i of Human Serum Albumin in the Course of Chemically and Thermally Induced Unfolding Using Fluorescence Correlation Spectroscopy. *J. Phys. Chem. B* **2014**, *118* (20), 5428–5438. https://doi.org/10.1021/jp502762t.

(58) Chakravorty, P.; Das, A. B. Impact of Choline Choride and Sugar Natural Deep Eutectic Solvents on Structure and Functionality of Treebean (Parkia Timoriana) Seed Protein. *Sci. Rep.* **2025**, *15* (1), 1–10. https://doi.org/10.1038/s41598-025-87890-z.

(59) Zhou, P.; Wang, X.; Yang, B.; Hollmann, F.; Wang, Y. Chemoenzymatic Epoxidation of Alkenes with Candida Antarctica Lipase B and Hydrogen

Peroxide in Deep Eutectic Solvents. *RSC Adv* **2017**, *7* (21), 12518–12523. https://doi.org/10.1039/c7ra00805h.

(60) Das, N.; Sen, P. Shape-Dependent Macromolecular Crowding on the Thermodynamics and Microsecond Conformational Dynamics of Protein Unfolding Revealed at the Single-Molecule Level. *J. Phys. Chem. B* **2020**, *124* (28), 5858–5871. https://doi.org/10.1021/acs.jpcb.0c03897.

(61) Das, N.; Sen, P. Size-Dependent Macromolecular Crowding Effect on the Thermodynamics of Protein Unfolding Revealed at the Single Molecular Level. *Int. J. Biol. Macromol.* **2019**, *141*, 843–854. https://doi.org/10.1016/j.ijbiomac.2019.09.029.

(62) Sukenik, S.; Sapir, L.; Harries, D. Balance of Enthalpy and Entropy in Depletion Forces. *Curr Opin Colloid Interface Sci* **2013**, *18* (6), 495–501. https://doi.org/10.1016/J.COCIS.2013.10.002.

(63) Sukenik, S.; Sapir, L.; Gilman-Politi, R.; Harries, D. Diversity in the Mechanisms of Cosolute Action on Biomolecular Processes. *Faraday Discuss* **2013**, *160*, 225–237. https://doi.org/10.1039/c2fd20101a.

(64) Denisov, V. P.; Jonsson, B. H.; Halle, B. Hydration of Denatured and Molten Globule Proteins. *Nat Struct Biol* **1999**, *6* (3), 253–260. https://doi.org/10.1038/6692.

(65) Li, C.; Liu, M. Protein Dynamics in Living Cells Studied by In-Cell NMR Spectroscopy. *FEBS Lett* **2013**, *587* (8), 1008–1011. https://doi.org/10.1016/J.FEBSLET.2012.12.023.

(66) Svergun, D. I.; Richard, S.; Koch, M. H. J.; Sayers, Z.; Kuprin, S.; Zaccai, G. Protein Hydration in Solution: Experimental Observation by x-Ray and Neutron Scattering. *Proc. Natl. Acad. Sci. USA* **1998**, *95* (5), 2267–2272. https://doi.org/10.1073/PNAS.95.5.2267/ASSET/57408DDB-7494-4973-AA54-A00B6878F29C/ASSETS/GRAPHIC/PQ0482604004.JPEG.

(67) Gerstein, M.; Chothia, C. Packing at the Protein-Water Interface. *Proc. Natl. Acad. Sci. USA* **1996**, *93* (19), 10167–10172. https://doi.org/10.1073/PNAS.93.19.10167;WGROUP:STRING:PUBLICATION.

(68) Burling, F. T.; Weis, W. I.; Flaherty, K. M.; Brünger, A. T. Direct Observation of Protein Solvation and Discrete Disorder with Experimental Crystallographic Phases. *Science (1979)* **1996**, *271* (5245), 72–77. https://doi.org/10.1126/SCIENCE.271.5245.72.

(69) Smith, L. J.; Bowen, A. M.; Di Paolo, A.; Matagne, A.; Redfield, C. The Dynamics of Lysozyme from Bacteriophage Lambda in Solution Probed by NMR and MD Simulations. *ChemBioChem* **2013**, *14* (14), 1780–1788. https://doi.org/10.1002/CBIC.201300193;PAGEGROUP:STRING:PUBLICATION.

(70) Marlow, M. S.; Dogan, J.; Frederick, K. K.; Valentine, K. G.; Wand, A. J. The Role of Conformational Entropy in Molecular Recognition by Calmodulin. *Nature Chemical Biology 2010 6:5* **2010**, *6* (5), 352–358. https://doi.org/10.1038/nchembio.347.

(71) Frederick, K. K.; Marlow, M. S.; Valentine, K. G.; Wand, A. J. Conformational Entropy in Molecular Recognition by Proteins. *Nature* **2007**, *448* (7151), 325–329. https://doi.org/10.1038/NATURE05959;KWRD=SCIENCE.

(72) Nandi, N.; Bagchi, B. Dielectric Relaxation of Biological Water. *J. Phys. Chem. B* **1997**, *101*, 10954–10961.

(73) Nandi, N.; Bhattacharyya, K.; Bagchi, B. Dielectric Relaxation and Solvation Dynamics of Water in Complex Chemical and Biological Systems. *Chem Rev* **2000**, *100* (6), 2013–2045. https://doi.org/10.1021/cr980127v.

(74) Russo, D.; Murarka, R. K.; Copley, J. R. D.; Head-Gordon, T. Molecular View of Water Dynamics near Model Peptides. *J. Phys. Chem. B* **2005**, *109* (26), 12966–12975. https://doi.org/10.1021/jp051137k.

(75) Lorenz-Ochoa, K. A.; Baiz, C. R. Ultrafast Spectroscopy Reveals Slow Water Dynamics in Biocondensates. *J. Am. Chem. Soc.* **2023**, *145* (50), 27800–27809. https://doi.org/10.1021/JACS.3C10862/ASSET/IMAGES/LARGE/JA3C10862_0005.JPEG.

(76) Laage, D.; Elsaesser, T.; Hynes, J. T. Water Dynamics in the Hydration Shells of Biomolecules. *Chem. Rev.* **2017**, *117* (16), 10694–10725. https://doi.org/10.1021/ACS.CHEMREV.6B00765/ASSET/IMAGES/LARGE/CR-2016-00765X_0014.JPEG.

(77) Dopfer, O.; Fujii, M. Probing Solvation Dynamics around Aromatic and Biological Molecules at the Single-Molecular Level. *Chem. Rev.* **2016**, *116* (9), 5432–5463. https://doi.org/10.1021/ACS.CHEMREV.5B00610/ASSET/IMAGES/LARGE/CR-2015-006102_0027.JPEG.

(78) Pignataro, M. F.; Herrera, M. G.; Dodero, V. I. Evaluation of Peptide/Protein Self-Assembly and Aggregation by Spectroscopic Methods. *Molecules 2020, Vol. 25, Page 4854* **2020**, *25* (20), 4854. https://doi.org/10.3390/MOLECULES25204854.

(79) Fogarty, A. C.; Duboué-Dijon, E.; Sterpone, F.; Hynes, J. T.; Laage, D. Biomolecular Hydration Dynamics: A Jump Model Perspective. *Chem Soc Rev* **2013**, *42* (13), 5672–5683. https://doi.org/10.1039/C3CS60091B.

(80) Levy, Y.; Onuchic, J. N. Water Mediation in Protein Folding and Molecular Recognition. *Annu Rev Biophys Biomol Struct* **2006**, *35* (1), 389–415.

https://doi.org/10.1146/ANNUREV.BIOPHYS.35.040405.102134/CITE/REFWORKS.

(81) Leitner, D. M.; Gruebele, M.; Havenith, M. Solvation Dynamics of Biomolecules: Modeling and Terahertz Experiments. *HFSP J* **2008**, *2* (6), 314–323. https://doi.org/10.2976/1.2976661.

(82) Chattopadhyay, A. Exploring Membrane Organization and Dynamics by the Wavelength-Selective Fluorescence Approach. *Chem. Phys. Lipids* **2003**, *122* (1–2), 3–17. https://doi.org/10.1016/S0009-3084(02)00174-3.

(83) Mishra, P.; Jha, S. K. Slow Motion Protein Dance Visualized Using Red-Edge Excitation Shift of a Buried Fluorophore. *J. Phys. Chem. B* **2019**, *123* (6), 1256–1264. https://doi.org/10.1021/ACS.JPCB.8B11151/ASSET/IMAGES/LARGE/JP-2018-111517_0005.JPEG.

(84) Demchenko, A. P. The Red-Edge Effects: 30 Years of Exploration. *Luminescence*. 2002, pp 19–42. https://doi.org/10.1002/bio.671.

(85) Demchenko, A. P. Fluorescence Molecular Relaxation Studies of Protein Dynamics: The Probe Binding Site of Melittin Is Rigid on the Nanosecond Time Scale. *FEBS Lett* **1985**, *182* (1), 99–102. https://doi.org/10.1016/0014-5793(85)81162-5.

(86) Demchenko, A. P. On the Nanosecond Mobility in Proteins: Edge Excitation Fluorescence Red Shift of Protein-Bound 2-(p-Toluidinylnaphthalene)-6-Sulfonate. *Biophys Chem* **1982**, *15* (2), 101–109. https://doi.org/10.1016/0301-4622(82)80022-7.

(87) Demchenko, A. P. Weber's Red-Edge Effect That Changed the Paradigm in Photophysics and Photochemistry. **2016**, 95–141. https://doi.org/10.1007/4243_2016_14.

(88) Das, N.; Khan, T.; Sen, P. The Shift of Excitation Spectra at Blue Edge of Emission (BEEmS) as a New Methodology to Probe Heterogeneity. *Chem. Phys.* **2024**, *577*, 112138. https://doi.org/10.1016/J.CHEMPHYS.2023.112138.

(89) Chen, G.; Zhang, Q.; Lu, Q.; Feng, B. Protection Effect of Polyols on Rhizopus Chinensis Lipase Counteracting the Deactivation from High Pressure and High Temperature Treatment. *Int. J. Biol. Macromol.* **2019**, *127*, 555–562. https://doi.org/10.1016/j.ijbiomac.2019.01.082.

(90) Rao, C. M.; Rao, S. C.; Rao, P. B. RED EDGE EXCITATION EFFECT IN INTACT EYE LENS. *Photochem Photobiol* **1989**, *50* (3), 399–402. https://doi.org/10.1111/J.1751-1097.1989.TB04176.X,.

(91) Rao, S. C.; Rao, C. M. Red Edge Excitation Shifts of Crystallins and Intact Lenses: A Study of Segmental Mobility and Inter-Protein Interactions. *FEBS Lett* **1994**, *337* (3), 269–273. https://doi.org/10.1016/0014-5793(94)80206-8.

(92) Muthu, S. A.; Jadav, H. C.; Srivastava, S.; Pissurlenkar, R. R. S.; Ahmad, B. The Reorganization of Conformations, Stability and Aggregation of Serum Albumin Isomers through the Interaction of Glycopeptide Antibiotic Teicoplanin: A Thermodynamic and Spectroscopy Study. *Int. J. Biol. Macromol.* **2020**, *163*, 66–78. https://doi.org/10.1016/J.IJBIOMAC.2020.06.258.

(93) Patra, S. K.; Pal, M. K. Red Edge Excitation Shift Emission Spectroscopic Investigation of Serum Albumins and Serum Albumin-Bilirubin Complexes. *Spectrochim Acta A Mol Biomol Spectrosc* **1997**, *53* (10), 1609–1614. https://doi.org/10.1016/S1386-1425(97)00098-X.

(94) Batey, S.; Clarke, J. The Folding Pathway of a Single Domain in a Multidomain Protein Is Not Affected by Its Neighbouring Domain. *J. Mol. Biol.* **2008**, *378* (2), 297. https://doi.org/10.1016/J.JMB.2008.02.032.

(95) Santorelli, D.; Marcocci, L.; Pennacchietti, V.; Nardella, C.; Diop, A.; Pietrangeli, P.; Pagano, L.; Toto, A.; Malagrinò, F.; Gianni, S. Understanding the Molecular Basis of Folding Cooperativity through a Comparative Analysis of a Multidomain Protein and Its Isolated Domains. *J. Biol. Chem.* **2023**, *299* (3), 102983. https://doi.org/10.1016/J.JBC.2023.102983.

(96) Varshney, A.; Ahmad, B.; Khan, R. H. Comparative Studies of Unfolding and Binding of Ligands to Human Serum Albumin in the Presence of Fatty Acid: Spectroscopic Approach. *Int. J. Biol. Macromol.* **2008**, *42* (5), 483–490. https://doi.org/10.1016/J.IJBIOMAC.2008.03.004.

(97) Muzammil, S.; Kumar, Y.; Tayyab, S. Anion-Induced Stabilization of Human Serum Albumin Prevents the Formation of Intermediate during Urea Denaturation. *Proteins: Structure, Function, and Bioinformatics* **2000**, *40* (1), 29–38. https://doi.org/10.1002/(SICI)1097-0134(20000701)40:1<29::AID-PROT50>3.0.CO;2-P.

(98) Yadav, R.; Sen, P. Mechanistic Investigation of Domain Specific Unfolding of Human Serum Albumin and the Effect of Sucrose. *Protein Science* **2013**, *22* (11), 1571–1581. https://doi.org/10.1002/pro.2357.

(99) Mohan, V.; Sengupta, B.; Acharyya, A.; Yadav, R.; Das, N.; Sen, P. Region-Specific Double Denaturation of Human Serum Albumin: Combined Effects of Temperature and GnHCl on Structural and Dynamical Responses. *ACS Omega* **2018**, *3* (8), 10406–10417. https://doi.org/10.1021/acsomega.8b00967.

(100) Santra, M. K.; Banerjee, A.; Rahaman, O.; Panda, D. Unfolding Pathways of Human Serum Albumin: Evidence for Sequential Unfolding and Folding of Its Three Domains. *Int. J. Biol. Macromol.* **2005**, *37* (4), 200–204. https://doi.org/10.1016/J.IJBIOMAC.2005.10.009.

(101) Dockal, M.; Carter, D. C.; Rüker, F. The Three Recombinant Domains of Human Serum Albumin: STRUCTURAL CHARACTERIZATION AND LIGAND BINDING PROPERTIES. *J. Biol. Chem.* **1999**, *274* (41), 29303–29310. https://doi.org/10.1074/JBC.274.41.29303.

(102) Yadav, R.; Sengupta, B.; Sen, P. Effect of Sucrose on Chemically and Thermally Induced Unfolding of Domain-I of Human Serum Albumin: Solvation Dynamics and Fluorescence Anisotropy Study. *Biophys Chem* **2016**, *211*, 59–69. https://doi.org/10.1016/j.bpc.2016.02.005.

(103) Ahmad, B.; Ahmed, M. Z.; Haq, S. K.; Khan, R. H. Guanidine Hydrochloride Denaturation of Human Serum Albumin Originates by Local Unfolding of Some Stable Loops in Domain III. *Biochimica et Biophysica Acta (BBA) - Proteins and Proteomics* **2005**, *1750* (1), 93–102. https://doi.org/10.1016/J.BBAPAP.2005.04.001.

(104) Mohan, V.; Sengupta, B.; Das, N.; Banerjee, I.; Sen, P. Domain-Specific Stabilization of Structural and Dynamic Responses of Human Serum Albumin by Sucrose. *Protein Pept Lett* **2019**, *26* (4), 287–300. https://doi.org/10.2174/0929866526666190122115702.

(105) Senisterra, G.; Chau, I.; Vedadi, M. Thermal Denaturation Assays in Chemical Biology. *Assay Drug Dev Technol* **2012**, *10* (2), 128–136. https://doi.org/10.1089/ADT.2011.0390

Chapter 7

Role of Associated Water Dynamics on Protein Stability and Activity in Crowded Milieu

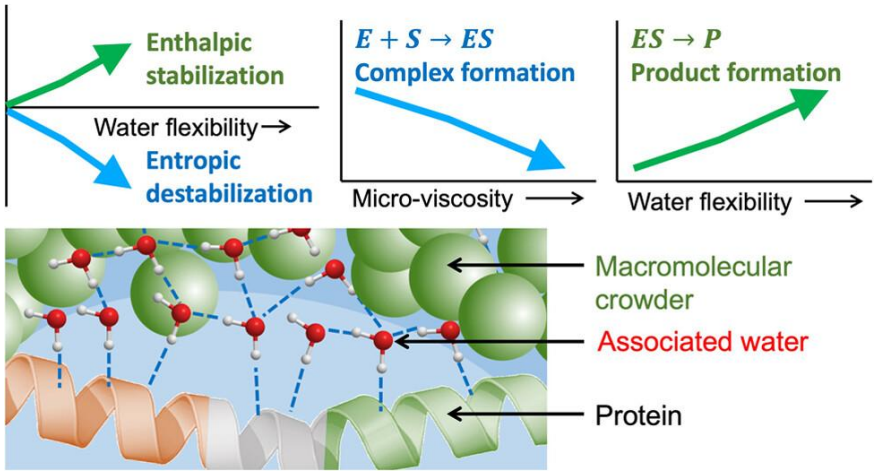

Tanmoy Khan, Bisal Halder, Nilimesh Das*, and Pratik Sen*

J. Phys. Chem. B **2024**, 128, 8672–8686

Abstract:

Macromolecular crowding bridges *in-vivo* and *in-vitro* studies by simulating cellular complexities such as high viscosity and limited space, while maintaining the experimental feasibility. Over the last two decades, the impact of macromolecular crowding on protein stability and activity has been a significant topic of study and discussion, though still lacking a thorough mechanistic understanding. This article investigates the role of associated water dynamics on protein stability and activity within crowded environments, using bromelain and Ficoll-70 as the model systems. Traditional crowding theory primarily attributes protein stability to entropic effects (excluded volume) and enthalpic interactions. However, our recent findings suggest that water structure modulation plays a crucial role in the crowded environment. In this report, we strengthen the conclusion of our previous study, i.e. rigid-associated water stabilizes proteins via entropy and destabilizes them via enthalpy, while flexible water has the opposite effect. In the process, we addressed previous shortcomings with a systematic concentration dependent study using a single-domain protein and component analysis of solvation dynamics. More importantly, we analyse bromelain's hydrolytic activity using the Michaelis-Menten model to understand kinetic parameters like maximum velocity (V_{max}) achieved by the system and the Michalis-Menten coefficient (K_M). Results indicate that micro-viscosity (not the bulk viscosity) controls the enzyme-substrate (ES) complex formation, where an increase in the micro-viscosity makes the ES complex formation less favourable. On the other hand, flexible associated water dynamics were found to favour the rate of product formation significantly from the ES complex, while rigid associated water hinders it. This study improves our understanding of protein stability and activity in crowded environments, highlighting the critical role of associated water dynamics.

7.1. Introduction

Macromolecular crowding: A vital component of cellular complexity:

The cellular environment is much more complex than the buffer solution that is typically used for biochemical studies [1]. Macromolecular crowding is probably the most essential component of such complexity as it mimics two of the most important cellular properties: increased viscosity and reduced accessible space in the cell [1,2]. Over the past two decades studies have shown that every protein property is affected by macromolecular crowding [3–28]. At the same time, like in any research field, efforts have been dedicated to understanding the mechanism of the macromolecular crowded induced alteration of the properties [14,19,29–31]. However, because of the enormous complexity of the system, an appropriate physical insight with predictive power is yet to be achieved. This report aims to gain this crucial mechanistic insight into two important protein properties, i.e. stability and activity, in a crowded environment.

Traditional vs. modern theories on protein stability in a crowded milieu:

Protein stability in the crowded milieu results from a delicate balance between stabilizing entropic effects and stabilizing/destabilizing enthalpic contributions [32]. The origin of the entropic effect is associated with the excluded volume. This stems from the fact that two solutes cannot access the same space at the same time, thus, in the presence of macromolecular crowder a protein can access lesser volume as compared to when no macromolecular crowder is present [9,33]. The excluded volume effect shifts protein unfolding in a direction where protein occupies a lesser volume, leading to protein compaction/stabilization [9,30,34]. The excluded volume effect remains the main pillar, even today, to explain protein stability in a crowded milieu [1,2,33,35–37]. However, many observations of protein destabilization in the crowded environment indicate the importance of interaction between the protein and the crowder [25,26,38–41]. Such interactions have an enthalpic component notwithstanding the entropic term [38,42].

In recent times, many reports individually recognized the entropic and enthalpic components of stabilization [24,26,39,43–46]. Such experiments sometimes yield two interesting observations, namely- negative entropic component and entropy-enthalpy compensation [26,43,45,47], which cannot be explained by traditional crowding theory (excluded volume effect + interaction). There are some hints, mainly from simulation studies, that water structure modulation could explain such observations [30,36,48]. Taking human serum albumin (HSA) and different crowders, we recently demonstrated that indeed the consideration of water structure modulation explains these two anomalies for protein stability in the crowded milieu [49]. Further, we suggested that the relationship between the protein stability and the associated water structure should be better understood in terms of individual entropic and enthalpic components, instead of overall stability [49].

Shortcomings of the previous study:

However, the generalization of such claims requires a huge effort, taking different crowders, proteins, and at a wide concentration range of the crowder. Moreover, a correlation of associated water dynamics with the function of the protein is expected, which is missing in the literature. Further, our previous study had limitations like- (i) used crowders were of different building blocks, meaning their interactions with the protein may vary. Therefore, directly linking the water structure modulation to stability modulation is risky in this context. (ii) Mechanism-wise, though it is quite expected that there would be a change in the property as one moves from lower to higher crowder concentrations [50–52], the same was not done in the previous study. (iii) We used multi-domain HSA, which anyway has a very complicated energy landscape with domains being independent folding units [53,54], makes the analysis quite challenging. We wanted to move forward with a simpler protein with systematic changes in the concentration of the crowder used and also to understand how the activity is altered in presence of macromolecular crowding.

Protein activity: The most important and least understood protein behaviour in crowded milieu:

Protein activity in the crowded milieu is also poorly understood despite many studies showing changes in protein function under such conditions [55–64]. This hurdle arises because protein functions often involve multiple steps, and various factors collectively influence activity of a protein in a crowded medium. Excluded volume effect, crowder-substrate interactions, changes in the effective concentration of enzyme and substrate, altered diffusion coefficient of the enzyme and substrate, and critical concentration of crowder are a few of such factors [59,65–71]. As a result, protein activity can increase, decrease, or remain the same in the presence of macromolecular crowders [59,62,64,66–68,70,71]. In 2017, Pielak and co-workers reviewed protein activity in crowded environments and found no consistent trend: nine reports showed increased activity, six showed decreased activity, and another six showed no change [65]. This inconsistency underscores the need for a deeper mechanistic understanding of protein behaviour in crowded milieus.

Our effort in this report to understand protein stability and activity in crowded milieu:

Herein, using bromelain as the model protein and Ficoll-70 as the synthetic crowders we (i) aimed to eliminate the shortcomings of our previous report and generalize the mechanism of protein stability in a crowded milieu that considers the important role of associated water, and (ii) also aims to provide mechanistic insights into protein activity in crowded milieu by correlating maximum velocity (V_{max}) and Michalis-Menten coefficient (K_M) with important protein and medium properties [60,61,69,72]. We have schematically presented the aim for this work in scheme 1.

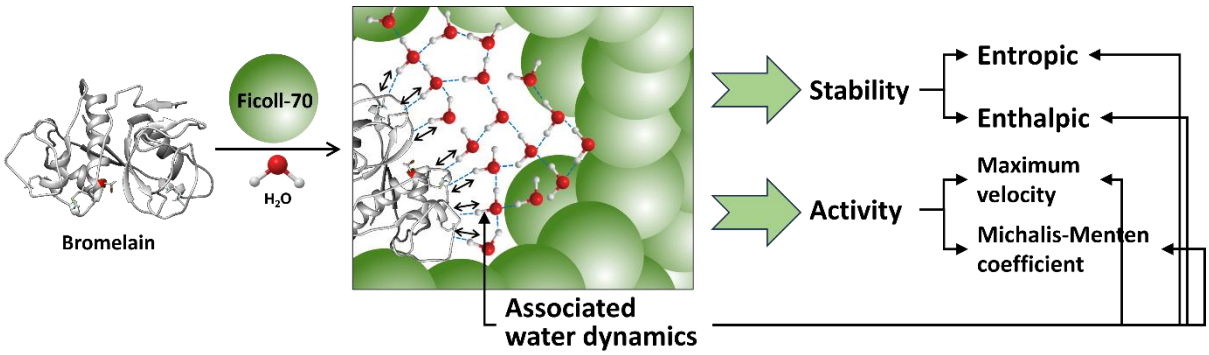

Scheme 1. Our effort in this report: Concentration-dependent effect of Ficoll-70 on the stability and activity of bromelain. We individually recognized the components of stability and activity and tested how solvent structure modulation controls them.

We find that rigid associated water structure stabilizes protein through entropy and destabilizes it through enthalpy. Further, micro-viscosity (and not the bulk viscosity) controls enzyme-substrate complex formation, while associated water significantly influences the rate of product formation. This study enhances our understanding on protein stability and activity in crowded environments, highlighting the critical role of associated water.

7.2. Results and Discussion

7.2.1. Modulation of associated water structure with macromolecular crowding:

The nature of the water near a protein, known as associated water or biological water, differs significantly from the bulk water [73–76]. This water interacts directly with the protein surface, and any changes in its structure can profoundly impact the biophysical processes [75–78]. In the present study, we took bromelain as our model protein and tagged it site-selectively with a solvent-sensitive fluorescent molecule 7-diethylamino-3-(4′-maleimidylphenyl)-4-methylcoumarin (CPM) to measure the water dynamics modulation around it using time-dependent fluorescence Stokes shift (TDFSS) method in the presence of different Ficoll-70 concentrations. TDFSS

has certain advantages over other techniques for the measurement of water dynamics. Firstly, the time resolution of this method is much superior to the other techniques like NMR [79,80], dielectric relaxation [81], etc., and secondly, it gives information about the solvent molecules present in the immediate vicinity of the fluorescent probe, those might interact directly with the protein, compared to the other techniques, where the information of bulk water and associated water are averaged out [76,82]. In TDFSS, the solvatochromic probe molecule undergoes a significant dipole moment change upon photoexcitation, causing surrounding solvents to compensate for this change by rearranging themselves. This rearrangement time is roughly a measure of the solvation dynamics [83,84].

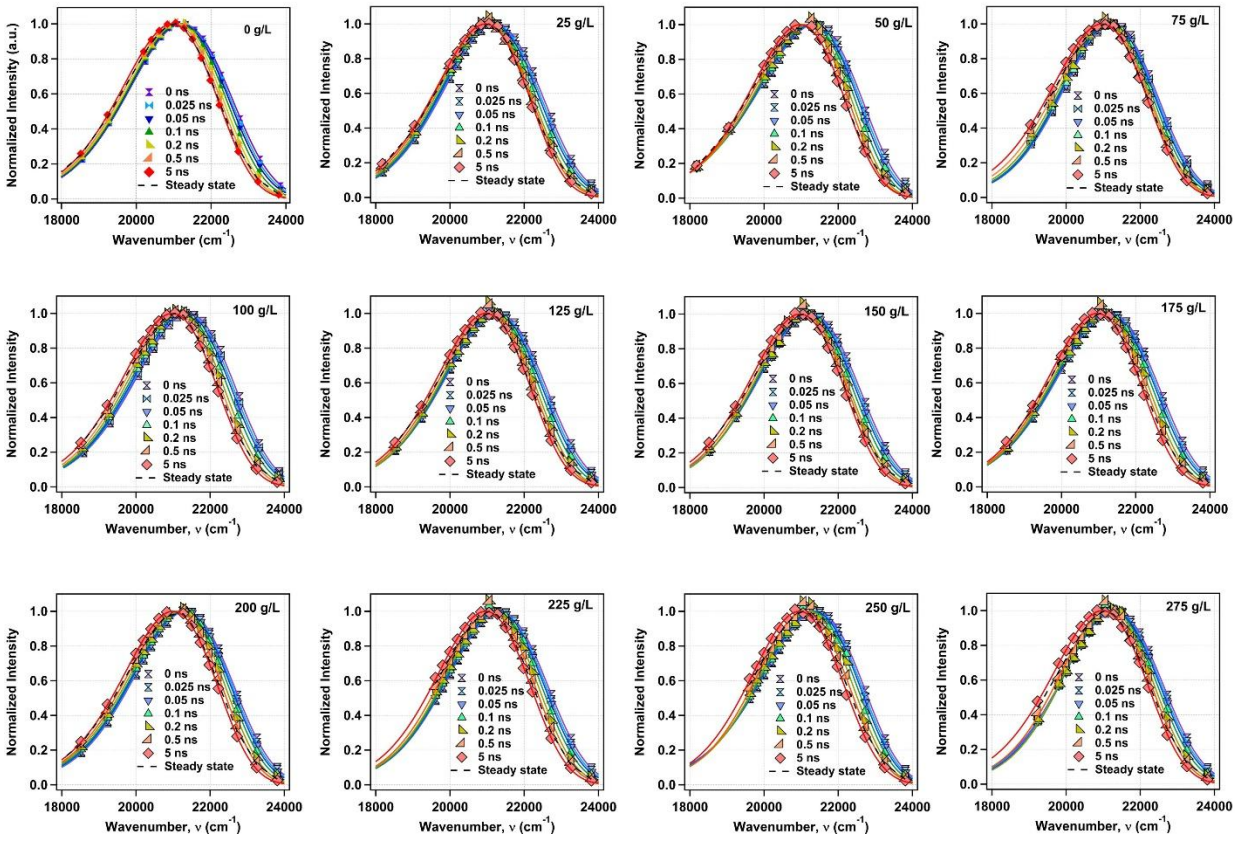

Figure 1. Time-resolved emission Spectra (TRES) of CPM-tagged Bromelain in the buffer and various concentrations of ficoll 70. Here, a few representative time points have been shown at each ficoll 70 concentration to provide clear visualization.

In the TDFSS method, one constructs the time-resolved emission spectra (TRES) and derives the solvent response function (S(t)), which is fitted to a multi-exponential function. For the present case, all the TRES of CPM-tagged bromelain with different Ficoll-70 concentrations are given in Figure 1. The TRES and the time-dependent shift of the emission maximum of CPM-tagged bromelain in the buffer are shown explicitly in Figure 2a and 2b, respectively, as a representative example of how to make the S(t) (Figure 2c) from TRES data. For each cases, the constructed S(t) is fitted to a bi-exponential function (Figures 2c-d), yielding τ_{s1}, τ_{s2}, a_1, a_2, τ_{avg}, which are tabulated in Table 1 and plotted in Figure 2e-h against the Ficoll-70 concentration.

We observed a decrease in the average solvation time (τ_{avg}) with an increase the Ficoll-70 concentration up to 100 gL^{-1}, and then increases. The result is rather unexpected as an increase in the concentration of Ficoll-70 increases the viscosity of the medium, however, the average solvation time decreases for the initial concentration range (see Table 1). The faster solvation component (τ_{s1}) decreases up to 100 gL^{-1} Ficoll-70 and then progressively increases. On the other hand, the slower solvation component (τ_{s2}) gradually increases with an increase in the crowder concentration, especially beyond ~75 gL^{-1}. Additionally, the contribution of the faster time component (a_1) increases up to 125 gL^{-1} Ficoll-70 and then decreases. An exact reverse trend is observed for a_2. Additionally, $a_1\tau_{s1}$ and $a_2\tau_{s2}$ follow a similar trend as τ_{s1} and τ_{s2}. Generally, a large portion (~70% in this present study) of solvation dynamics is always missed while measuring it through ps-TCSPC. However, the missing percentage remains fairly constant over the entire concentration range, especially in the lower Ficoll-70 concentration range, where a surprising decrease in solvation time was observed (see Table 1). Thus, it will probably not impact our conclusion.

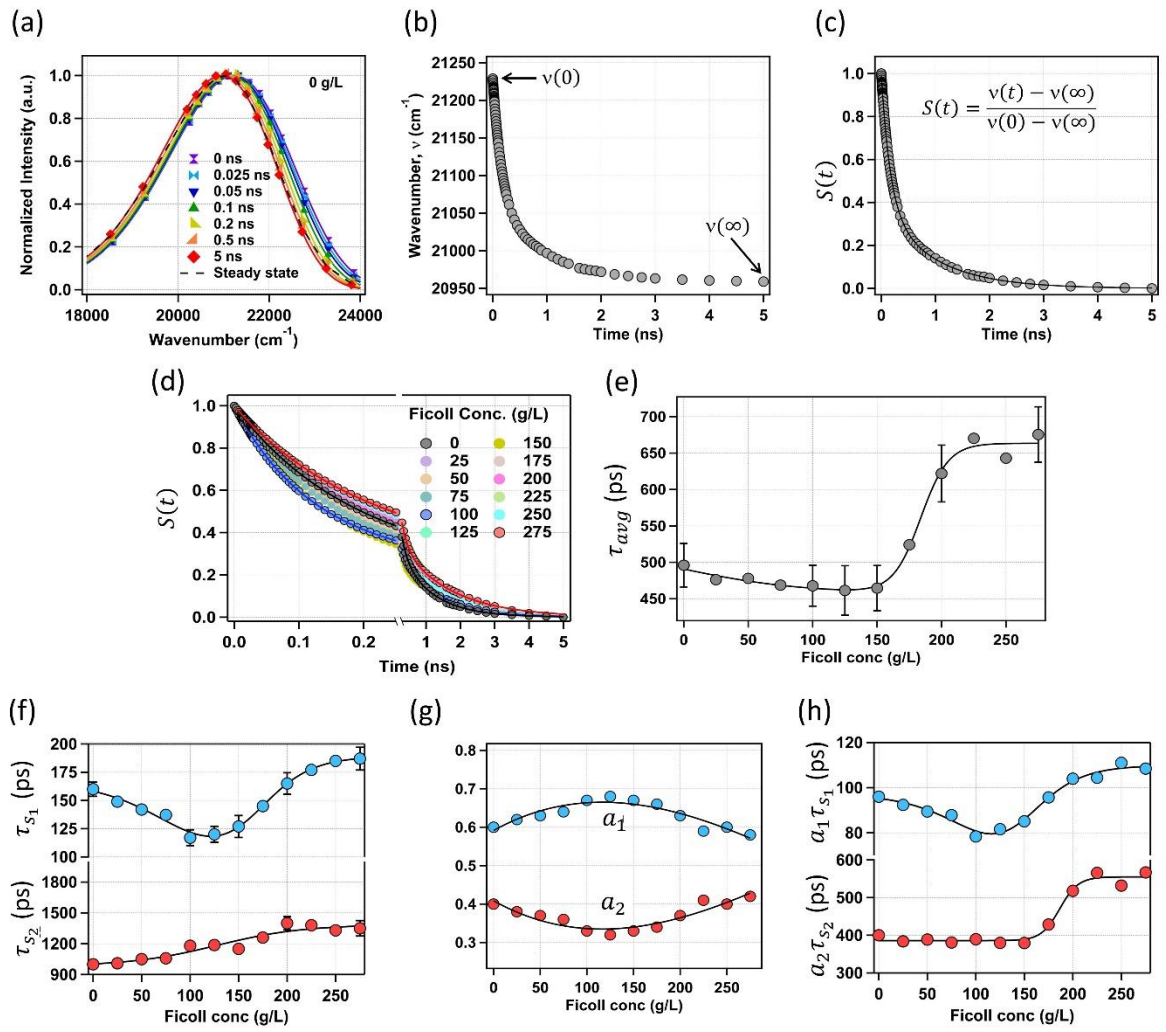

Figure 2. Solvation dynamics around bromelain become faster at lower Ficoll-70 concentrations, and then it increases. (a) Time-resolved emission spectra (TRES) of CPM-tagged bromelain in buffer (only a few representative time points have been shown to provide clear visualization). (b) Time-dependent shift of emission maxima of CPM-tagged bromelain in the buffer. (c) Solvent correlation function, S(t), of CPM-tagged bromelain in the buffer. The equation to form the function is mentioned in the inset. (d) Comparison of S(t)s in presence of different Ficoll-70 concentrations. (e) Comparison of the average solvation time (τ_{avg}) of CPM-tagged bromelain in presence of different Ficoll-70 concentrations. (f) Comparison of the faster time component, τ_{s1} (upper panel), and the slower time component, τ_{s2} (lower panel) of solvation dynamics in presence of different Ficoll-70 concentrations. (g) Contribution of the faster time component, a_1 (upper panel), and slower time component, a_2 (lower panel) of solvation dynamics for various Ficoll-70 concentrations. (h) Variation of $a_1\tau_{s1}$ (upper panel) and $a_2\tau_{s2}$ (lower panel) for different Ficoll-70 concentrations. The error bar represents the standard deviation of the mean of three independent experiments.

Table 1. Biexponential fitting parameters of solvent correlation function (S(t)) for CPM-tagged bromelain in the presence of various concentrations of Ficoll-70.

Ficoll-70 (gL^{-1})	a_1	τ_{s1} (ps)	a_2	τ_{s2} (ps)	τ_{avg} (ps)	$a_1\tau_{s1}$ (ps)	$a_2\tau_{s2}$ (ps)	Missing %
0	0.60	160	0.40	1000	496	96	400	73.0
25	0.62	150	0.38	1010	476	92	384	74.0
50	0.63	140	0.37	1050	478	89	389	70.0
75	0.64	140	0.36	1060	469	88	381	72.9
100	0.67	120	0.33	1180	468	78	389	70.5
125	0.68	120	0.32	1190	461	82	380	70.0
150	0.67	130	0.33	1150	465	85	380	71.3
175	0.66	145	0.34	1260	524	96	428	67.2
200	0.63	165	0.37	1400	622	104	518	65.8
225	0.59	180	0.41	1380	670	104	566	63.0
250	0.6	185	0.4	1330	643	111	532	58.0
275	0.58	185	0.42	1350	675	108	567	59.0

7.2.2. A control experiment to confidently assign modulation of solvation time to the modulation of the associated water structure around bromelain:

As already mentioned, not only water but any hydrophilic group, including protein side chains, can participate in the solvation process [76,84,85]. Thus, to verify whether structural alteration of bromelain plays a significant role in lowering the solvation time, we measured the secondary structural content of bromelain at each Ficoll-70 concentration employing CD spectroscopy (Figure 3). We found that the secondary structure of bromelain remains almost intact upon the addition of Ficoll-70, and thus it is concluded that the structural change of bromelain does not play a significant role in its stability and associated water dynamics modulation. Furthermore, if Ficoll-70 itself were the dominant contributor to bromelain's solvation-time changes, one might expect a monotonic increase or decrease in the solvation time with an increase in the Ficoll-70 concentration, which is not the case here. These observations therefore support a predominant role for modulation of the associated water near the protein, while not excluding weak or non-monotonic polymer–protein

interactions, particularly at higher Ficoll-70 concentrations. The rest of the part will explain how associated water structure modulation impacts the stability and activity of bromelain in the presence of Ficoll-70.

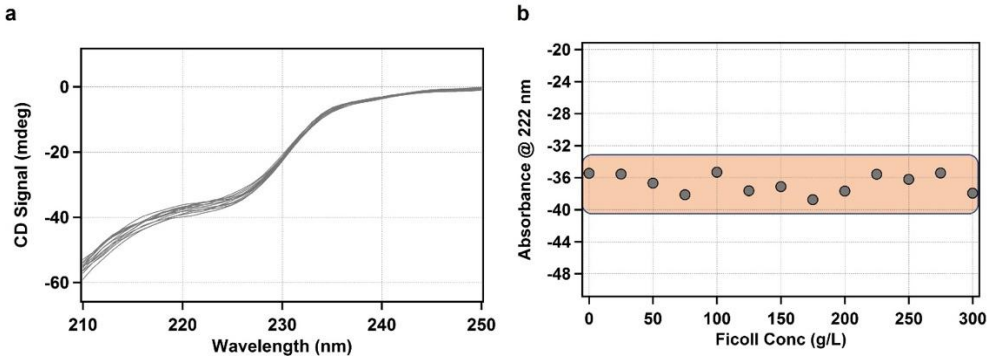

Figure 3. Ficoll-70 does not alter the secondary structure of bromelain. (a) CD spectra of Bromelain at each Ficoll-70 concentration. (b) Absorbance at 222 nm at each Ficoll-70 concentration, which shows that the secondary structure remains intact throughout the concentration range of Ficoll-70.

7.2.3. Thermal stability of bromelain:

Using circular dichroism (CD) spectroscopy, we contemplated the thermal unfolding of bromelain at different Ficoll-70 concentrations (Figure 4a) [86–88]. We have plotted the negative peak at 222 nm as a measure of α-helicity against the temperature (Figure 4b) and determined the fraction unfolded at each temperature using the equation mentioned in the figure (Figure 4c) [86,87]. Figure 4d shows the thermal unfolding curves of bromelain at various Ficoll-70 concentrations. Each unfolding curve is fitted with a sigmoidal function to determine the melting temperature (T_m) (see section 4.8 for details). Figure 4e depicts that the melting temperature (T_m) of bromelain remains fairly constant throughout the Ficoll-70 concentrations used in the study. This result is surprising because the traditional excluded volume theory predicts a gradual increase in protein stability with an increase in the crowder concentration.

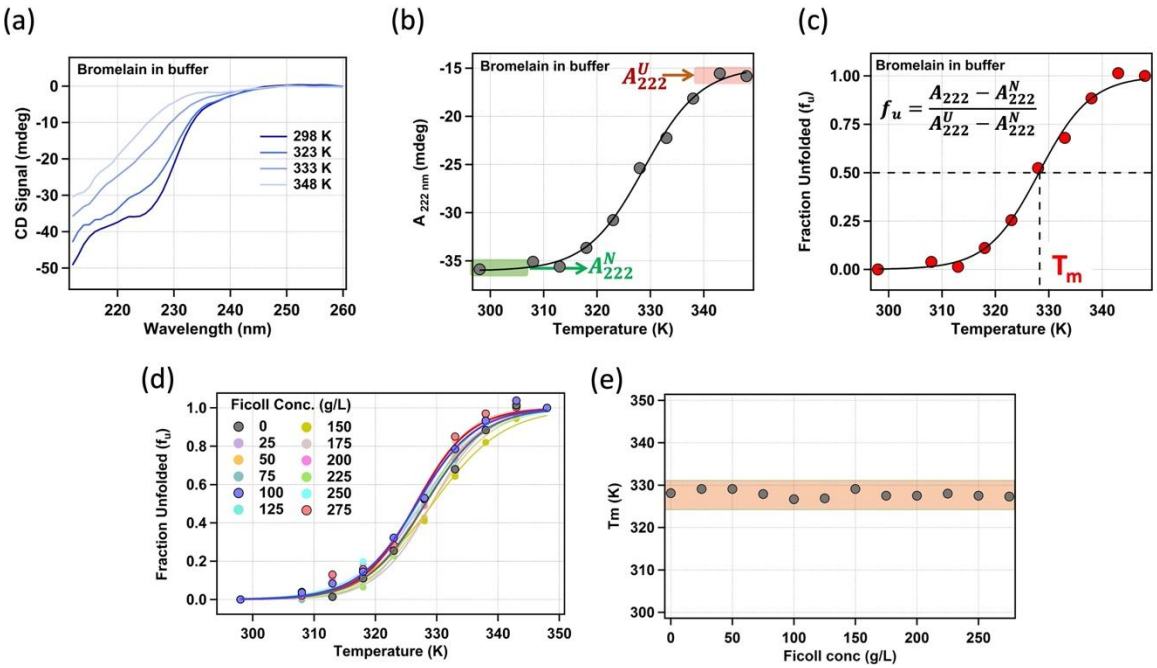

Figure 4. The thermal stability of bromelain does not change with Ficoll-70. (a) Representative circular dichroism (CD) spectra of bromelain in buffer at different temperatures. (b) Variation of CD signal of bromelain in buffer at 222 nm with temperature. (c) Variation of fraction unfolded (f_u), which has been calculated using the equation mentioned in the inset, as a function of temperature. (d) Comparison of the thermal unfolding curve for different Ficoll-70 concentrations. Each curve was fitted using the sigmoidal function (equation 12). (e) Comparison of the melting temperature (T_m) of bromelain in the presence of different Ficoll-70 concentrations.

7.2.4. Recognition of individual entropic and enthalpic terms of thermal stabilization and inadequacy of traditional crowding theory to explain bromelain stability with Ficoll-70:

From the unfolding data, we determined the free energy of unfolding (Figure 5a) for bromelain across Ficoll-70 concentrations using the equations mentioned in Figure 5, and the free energy of unfolding is found to be almost constant throughout the Ficoll-70 concentrations (Figure 5b). Traditional excluded volume effect, even more modern and routinely used scaled particle theory (SPT) could not explain such trend as shown in Figure 5b.[88]

According to the scaled particle theory,

$$\Delta G/RT = -\ln(1-\varphi) + \left(\frac{\varphi}{1-\varphi}\right)(z^3 + 3z^2 + z) + \left(\frac{\varphi}{1-\varphi}\right)^2 \left(3z^3 + \frac{9}{2}z^2\right) + \left(\frac{\varphi}{1-\varphi}\right)^3 (3z^3) \quad (7.1)$$

Where, $z = {r_f}/{r_c}$ is the ratio of the effective radius of the macromolecular crowder (r_c) and the radius of the folded conformation of the protein (r_f) and φ is the volume occupancies of crowding agents.

The volume occupancy can be calculated using Equation 2,

$$\varphi = \frac{4\pi(R_H)^3 N_A C}{3M_W} \quad (7.2)$$

Where, N_A is Avogadro's number, M_W is the molecular weight of the crowder, and C is the concentration (w/v) of the crowding agent.

Using equations 1 and 2, we calculated the free energy of protein in the folded state in the presence and absence of crowders and then calculated the differential free energy as,

$$\Delta\Delta G = \Delta G^{crowder} - \Delta G^{buffer} \quad (7.3)$$

Following our previous report [49], we felt that individual recognition of entropic and enthalpic components of stability might provide additional insights in this case as

well and determined the same using the Gibbs-Helmholtz equation, as shown in Figure 5c. We observed that at lower Ficoll-70 concentrations, the enthalpic effect stabilizes bromelain, while at higher concentrations, it destabilizes bromelain (Figure 5d). Surprisingly, the entropic component is destabilizing in the initial concentration range of Ficoll-70 (Figure 5e), which completely contradicts the classical crowding theory.

As the overall stability remains unchanged across Ficoll-70 concentrations, one expects the entropic effect (due to excluded volume) to be perfectly compensated by the enthalpic effect (due to interaction). Indeed, Figure 5f shows a linear relationship between $\Delta\Delta H^0$ and $-T\Delta\Delta S^0$ with a slope ~0.90, indicating this compensation across all crowder concentrations. Additionally, a subtle enthalpic excess in the overall stabilization process of bromelain in the presence of the DES was observed. This small enthalpic bias could arise from weak polymer–protein interaction at higher crowder concentrations. In most biophysical experiments, including those in crowded environments, entropy-enthalpy compensation is often observed [89,90]. However, the physical origin of such compensation cannot be explained using the traditional crowding theory. It hints that some common factor modulates both the entropic and the enthalpic terms. Water is present in almost all biochemical processes, and in our previous report, we have hypothesized how modulation of water-protein hydrogen bonds can originate in compensating entropy and enthalpy in such systems [49].

7.2.5. Associated water structure modulation explains stability of bromelain at different Ficoll-70 concentrations:

Water strongly interacts with protein and is an active and essential participant in deciding the stability, structure, dynamics, and function of biomolecules [49,74–76,91,92]. In our previous report, we proposed that the associated water reorganization is crucial for protein stability [49]. Because of this water rearrangement, the interacting

water molecules (associated water) might have a higher or lower degree of freedom. If the water molecules become flexible, the entropy increases, leading to entropic destabilization with a concomitant stabilizing enthalpy [49].

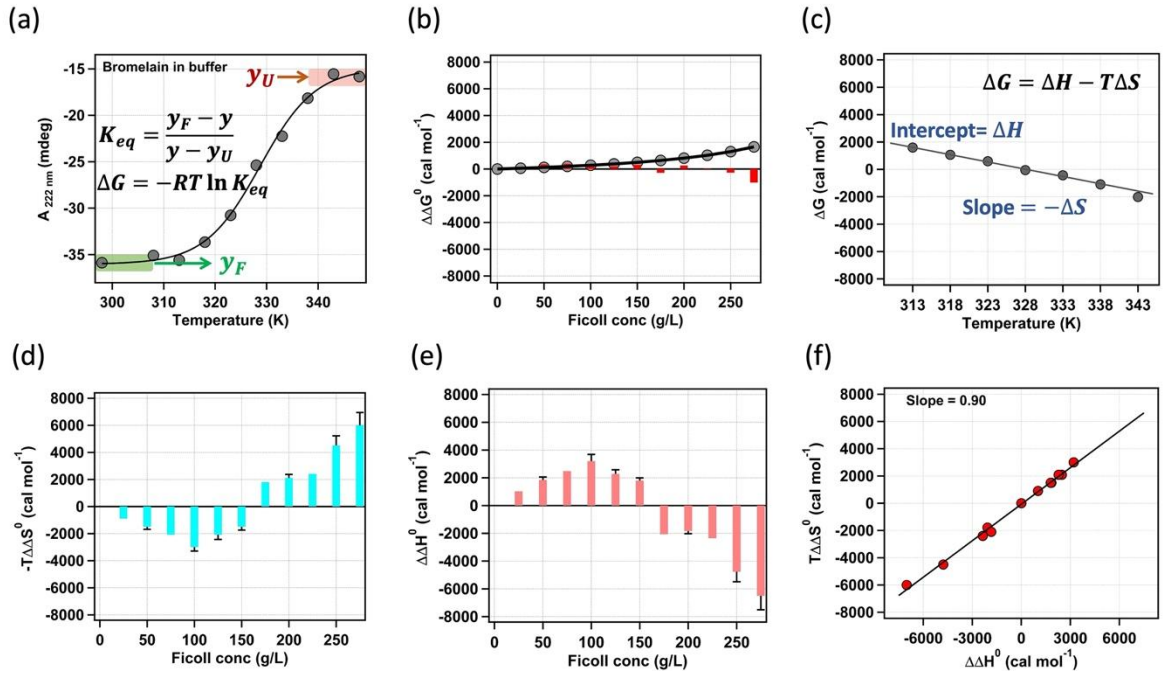

Figure 5. Individual entropic and enthalpic components might be positive or negative depending on Ficoll-70 concentrations. However, they compensate for each other and change with Ficoll-70 concentrations. (a) Variation of bromelain's CD signal at 222 nm as a function of temperature. The equation for calculating the equilibrium constant and the native and denatured state signals are mentioned in the figure. (b) Overall free energy change ($\Delta\Delta G$), where, $\Delta\Delta G = \Delta G_{ficoll} - \Delta G_{buffer}$. The grey circles (where the black bold line is the eye guide) represent the overall free energy change predicted by scaled particle theory (SPT) concerning the excluded volume effect only. (c) Schematic for estimating the change in the entropy and the enthalpy from the slope and the intercept, respectively, from the unfolding free energy. (d) Differential entropic component ($-T\Delta\Delta S^0$), where $\Delta\Delta S = -T(\Delta S_{ficoll} - \Delta S_{buffer})$ for thermal stabilization of bromelain in the presence of different concentrations of Ficoll-70. (e) Differential enthalpic component ($\Delta\Delta H^0$), where, $\Delta\Delta H = \Delta H_{ficoll} - \Delta H_{buffer}$ for thermal stabilization of bromelain in the presence of different concentrations of Ficoll-70. (f) Plot between entropic and enthalpic terms of stability. The black line is a linear fit indicating entropy-enthalpy compensation.

A quick look at Figures 5d and 5e reveals that at low Ficoll-70 concentrations, bromelain is destabilized by entropy, and the associated water dynamics around bromelain show a hint of more flexibility. Figures 2f and 2h highlight this for the faster solvation component. At the higher concentration range, the opposite behaviour is observed in both stability and associated water dynamics, indicating a correlation between water structure modulation and stability. To explore this further, we plotted entropic and enthalpic changes as a function of average solvation time, τ_{avg} (Figure 6a), faster component of solvation time, τ_{s1} (Figure 6b), $a_1\tau_{s1}$ (Figure 6d), τ_{s2} (Figure 6c) and $a_2\tau_{s2}$ (Figure 6e). We observed a strong correlation between τ_{avg} and individual entropic (adjusted R^2~0.89) or enthalpic terms (adjusted R^2~0.85), supporting our hypothesis on the importance of water structure modulation. More importantly, we get a better correlation between the faster component of solvation and entropy (adjusted R^2~0.90) or enthalpic component (adjusted R^2 ~ 0.87) of stability.

To gain a physical insight into the correlations between the average solvation time (and its components) and protein stability, we introspect into the origins of these timescales. Although the precise meaning of the individual time components is largely debated, a widely accepted theory provided by Bagchi and co-workers suggests that the 1-5 ps component originates from the reorientation dynamics of water molecules in the hydration layer [93,94]. There might be another component of 20-200 ps arising from the restructuring of the associated water, the water molecules residing in the first solvation shell [93–96]. The sub-nanosecond to nanosecond region is connected to the motion of the secondary structure of the protein, including the backbone, side chains and turns, surface, and the core of the protein [76]. In the present case, the two observed time constants are somewhat well distinguished, and the problem of mixing the time components is minimal. In our study, the faster component (τ_{s1}) significantly influences protein stability, aligning with the theoretical expectations. On the other hand, we observed a weak correlation between the longer solvation time component and protein stability (with adjusted R^2 ~ 0.47

for entropic and ~0.44 for the enthalpic term) (see Figure 6c). This may result from the exchange between associated and bulk water, the involvement of protein internal motion on water dynamics, and so on. Our future studies will investigate these aspects further.

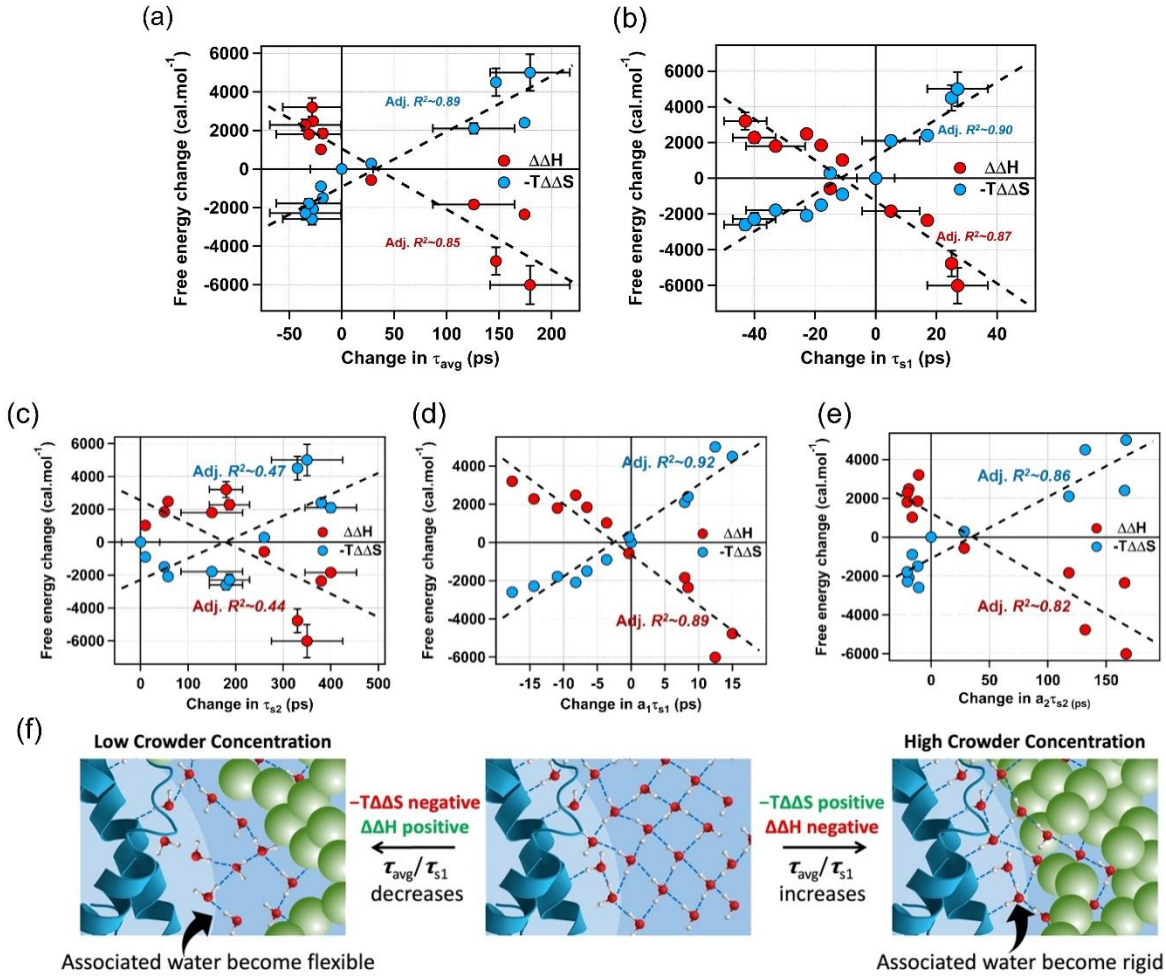

Figure 6. Associated water structure modulation is a key that controls the stability of bromelain. Correlation of individual stability components ($\Delta\Delta H$ and $-T\Delta\Delta S$) with (a) average solvation time, τ_{avg}, (b) the faster component of the solvation dynamics (τ_{s1}), (c) the slower component of solvation dynamics, τ_{s2}, (d) weighted slower solvation time, $a_1\tau_{s1}$, and (e) weighted faster solvation time, $a_2\tau_{s2}$. Broken lines are the linear fits. (f) Associated water dynamics modulation explains bromelain stability across Ficoll-70 concentrations. At initial concentrations of Ficoll-70, the associated water structure becomes more flexible, destabilizing bromelain through entropy, which is compensated by stabilizing enthalpy. Similarly, at higher Ficoll-70 concentrations, the associated water structure becomes more rigid, stabilizing bromelain through entropy with a concomitant enthalpic destabilization.

In section 2.2, we also showed that protein conformation remains consistent across Ficoll-70 concentrations, which eliminates any prominent role of structural alteration of protein in dictating its stability and solvation dynamics in the presence of Ficoll-70. Therefore, this result suggests that the water in the immediate vicinity of the protein (known as the protein hydration layer, PHL), becomes more flexible at initial concentrations of Ficoll-70, and that might play a key role in destabilizing bromelain at lower Ficoll-70 concentrations through entropy, which is compensated by stabilizing enthalpy. Basically, at lower Ficoll-70 concentrations the associated water around bromelain becomes more flexible, indicating a weaker hydrogen-bond network. In such cases, the water molecules gain higher degrees of freedom, and thus, the entropy is gained, leading to entropic destabilization. Concomitantly, the weaker hydrogen-bond network engenders a positive enthalpic change leading to enthalpic stabilization (recall energy expression from the equipartition principle and $\Delta H = Q_P = \left(\frac{dE}{dT}\right)_P dT$). Physically, weakening of the hydrogen-bonded network requires some energy, making Q_P positive and leading to enthalpic stabilization. Conversely, at higher Ficoll-70 concentrations, the associated water becomes more rigid, forming a tighter hydrogen-bond network. This rigidity stabilizes the system through entropic loss of the medium but leads to a negative enthalpic change, causing enthalpic destabilization.

We have schematically represented this correlation between the modulation of entropic and enthalpic components of stability with the changes in associated water structure/dynamics for low and high concentrations of Ficoll-70 in Figure 6f. Overall, our results support the hypothesis demonstrating that associated water structure modulation explains bromelain stability across Ficoll-70 concentrations. Component analysis of solvation (which was not possible in our previous report because of the convergence problem) provides additional insights. This study also overcomes previous limitations by employing a concentration dependent approach

with bromelain, a small, single-domain protein. It provides clearer insights into solvation dynamics and protein stability, addressing the issues faced in our earlier research (see section 1.4).

While there is a continuous exchange between bulk water and associated water, their modulation might not be similar to a given perturbation. For example, in this particular case, whereas the associated water dynamics around bromelain become more flexible with 100 gL^{-1} Ficoll-70, overall water dynamics become more rigid at this condition. This highlights the need to focus on associated water, not just the overall water dynamics, when explaining biological phenomena. Note that, at the same condition, the associated water around human serum albumin (HSA) becomes more rigid [49]. unlike bromelain. Interestingly, HSA is stabilized by entropy and destabilized by enthalpy, which is the opposite of bromelain's response. This result points towards the generality of our proposal and could explain protein-specific effects.

7.2.6. Modulation of the hydrolytic activity of bromelain with macromolecular crowding: We also investigated bromelain's hydrolytic activity towards *p*-nitrophenyl acetate (*p*NPA) (Figure 7a) in the presence of different Ficoll-70 concentrations. We observed a gradual decrease in the overall activity with an increase in the Ficoll-70 concentration (Figure 7b). At lower Ficoll-70 concentrations (up to 100 gL^{-1}), the decrease in bromelain's activity was minimal. Despite significant measurement error, this trend aligns with previous studies, such as those by Pielak and Chowdhury group, which reported similar effects with other proteins with varying crowder concentrations [56,57,65].

As mentioned earlier, understanding protein activity in the crowded milieu is difficult as it does not follow any specific trend [65]. Reports suggest that protein activity can increase, decrease, or remain the same in the presence of macromolecular crowders [22,50,58,59,66,97,98]. Factors e.g. excluded volume effect,

changes in the effective concentration of enzyme and substrate, decreased diffusion of the enzyme and the substrate, size and shape of crowder, crowder-substrate interactions, critical concentration of crowder, etc. can collectively influence the enzymatic activity making the situation more complex [22,50,58,59,62,66,97–99]. However, we thought that recognition of the individual steps of the enzymatic reaction (as has been done in the case of stability) might provide additional insights.

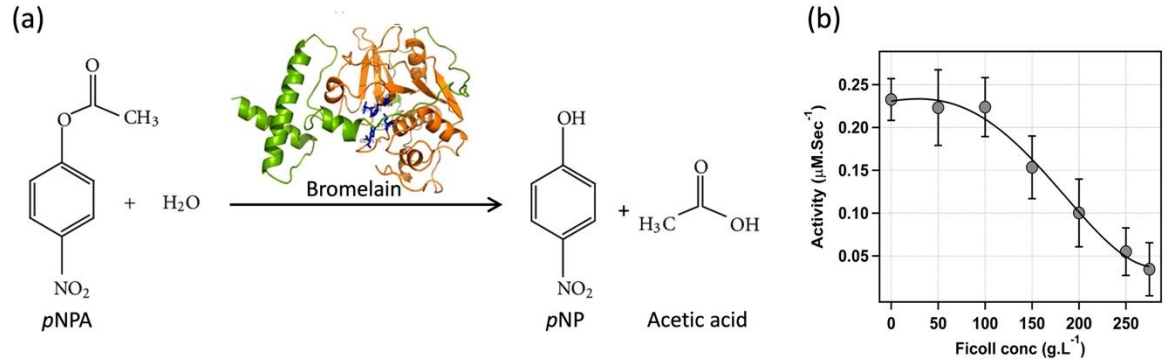

Figure 7. (a) Schematic representation of bromelain catalyzed para-nitrophenyl acetate (pNPA) hydrolysis, (b) Change in hydrolytic activity of bromelain with increasing Ficoll-70 concentration. The solid line is the eye guide.

7.2.7. Michaelis-Menten equation and determination of K_M and V_{max} to gain better insights: We applied the simplest and widely used Michaelis-Menten model to gain mechanistic insights into the enzymatic activity of bromelain in the presence of Ficoll-70 (see sections 4.10 and 4.11 for details) [60,69,71]. According to this model, the inverse of the initial rate is written as

$$\frac{1}{V_0} = \frac{K_m}{V_{max}}\frac{1}{[S]} + \frac{1}{V_{max}} \qquad (7.4)$$

where, $K_m = \frac{K_{-1}+K_2}{K_1}$ and $V_{max} = K_2[E]_0$, where, $[E]_0$ and $[S]$ are the enzyme and substrate concentrations, respectively. A higher value of K_m describes that the coming together of enzyme and substrate to form the enzyme-substrate complex is less favourable, leading to a loose binding. On the other hand, the maximum velocity (V_{max}) achieved by the system or K_2 (the turnover number) signifies the rate at which enzyme-substrate complex dissociates to form the product.

We have estimated V_0 from the time-dependent formation of the product monitored through the absorbance measurement for different substrate concentrations (Figure 8a). A plot of $\frac{1}{V_0}$ vs. the inverse of substrate concentrations $\left(\frac{1}{[S]}\right)$, the Lineweaver-Burk plot produces a straight line (Figure 8b), suggesting the correctness of applying the Michaelis-Menten equation in the present case (Figure 8c). K_m and V_{max} are determined from the slope and intercept, respectively. An increase in the enzymatic reaction rate is generally associated with an increase in the V_{max} and a decrease in the K_m value [69]. On the other hand, a decrease in enzymatic reaction rate is characterized by a decrease in the V_{max} and an increase in the K_m value [69,71].

Figures 8d and 8e represent the variation in relative V_{max} and K_m with increasing Ficoll-70 concentration. It represents an interesting case. At higher concentrations of Ficoll-70, V_{max} decreases and K_m increases. However, at initial concentrations of Ficoll-70, K_m increases, but V_{max} also surprisingly increases. Similar trends were observed in a few previous reports as well, for example, Basso group reported that for reductase activity V_{max} increases up to 100 gL^{-1} concentration of PEG [100].

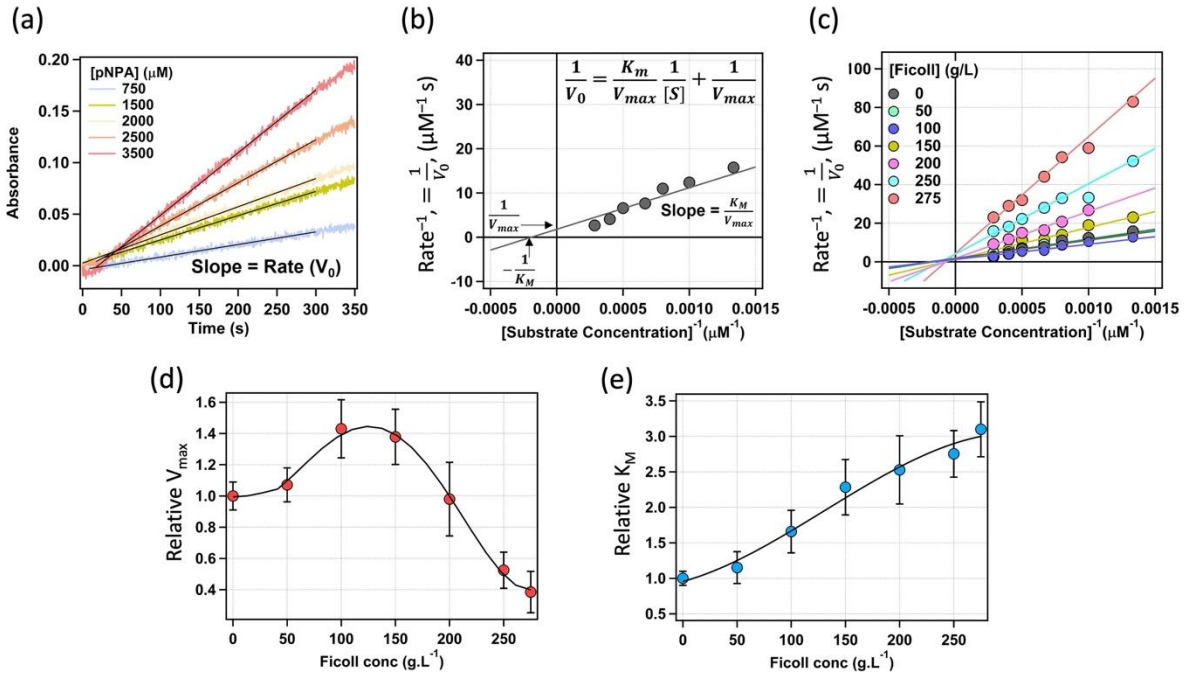

Figure 8. Individual recognition of K_m and V_{max} in hydrolysis of pNPA catalysed by bromelain with and without Ficoll-70. (a) Change in the absorbance of the product (pNP) formed with time in the presence of bromelain in buffer at varying substrate (pNPA) concentrations. (b) Representative Lineweaver-Burk plot between the inverse of the initial reaction rate of bromelain in buffer and the inverse of substrate concentration where V_{max} and K_M can be calculated from the intercept and the slope of the linear fit. (c) Lineweaver-Burk plot in the presence of different Ficoll-70 concentrations. (d) Variation of relative V_{max} with increasing Ficoll-70 concentration. (e) Variation of relative K_M with increasing Ficoll-70 concentration.

7.2.8. K_M prominently depends on micro viscosity:

The general scheme of Michaelis-Menten enzyme kinetics can be written as

$$E + S \underset{k_{-1}}{\overset{k_1}{\rightleftarrows}} ES \overset{k_2}{\rightarrow} ES^{\ddagger} \rightarrow E + Product \qquad (7.5)$$

The enzyme-substrate complex dissociation constant (K_d) for a high value of k_{-1} is related to K_M as

$$K_d = \frac{k_{-1}}{k_1} \approx K_M \quad (7.6)$$

The corresponding free energy of the process is given by

$$\Delta G_M = -RTln\frac{1}{K_d} \approx \text{RT ln } K_m \quad (7.7)$$

ΔG_M can be referred to as the "entrance channel" of the substrate in which the *ES* complex is formed [60,71]. A negative value of ΔG_M (see Table 2 and Figure 9a) ensures the process is energetically favourable [60,71]. With increasing Ficoll-70 concentration, the ΔG_M increases suggesting that enzyme-substrate complex formation becomes progressively less favourable with crowding, and concomitantly, the dissociation of the enzyme-substrate complex becomes more and more feasible.

Table 2. Kinetics and energetics of bromelain catalyzed hydrolysis of pNPA at various concentrations of Ficoll-70.

Ficoll-70 (g/L)	$\boldsymbol{K_M}$ **(μM)**	**Relative** $\boldsymbol{K_M}$	$\boldsymbol{\Delta G_M}$ **(kcal mol^{-1})**	$\boldsymbol{k_2}$ **(s^{-1})**	**Relative** $\boldsymbol{k_2}$	$\boldsymbol{\Delta G^{\ddagger}}$ **(kcal mol^{-1})**
0	5165	1.00	-3.11	0.057	1.00	19.15
50	5948	1.15	-3.02	0.061	1.07	19.11
100	8569	1.66	-2.81	0.082	1.43	18.94
150	11791	2.28	-2.62	0.079	1.38	18.97
200	13057	2.53	-2.56	0.056	0.98	19.17
250	14222	2.75	-2.51	0.030	0.52	19.54
275	16011	3.10	-2.44	0.022	0.38	19.72

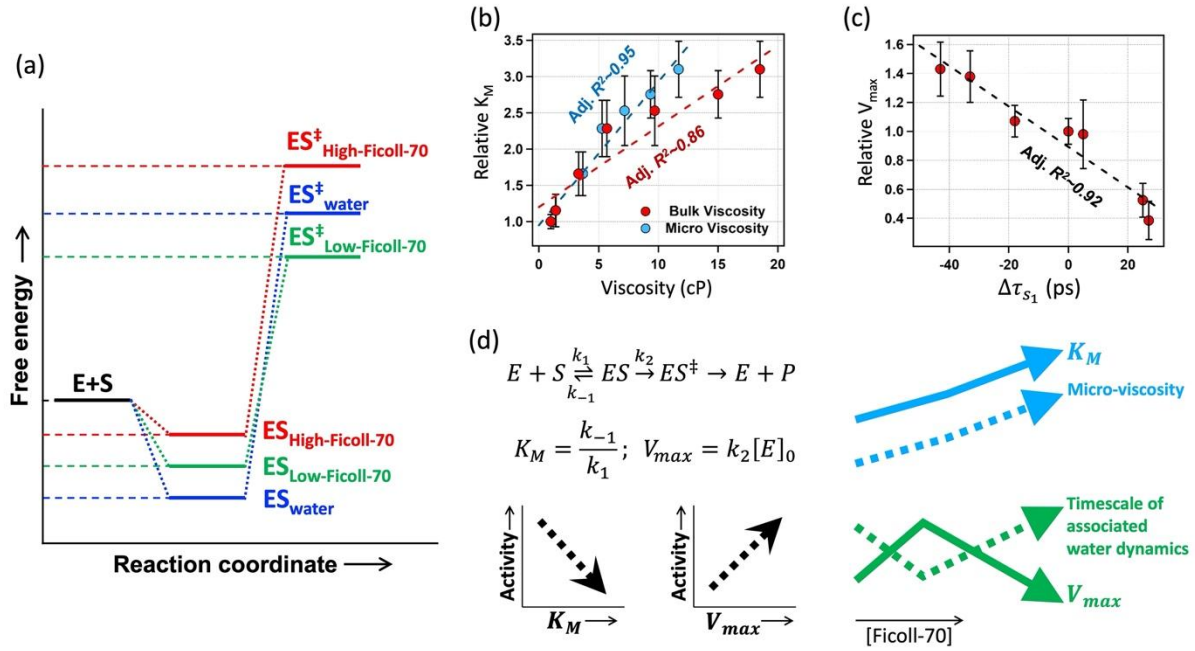

Figure 9. K_M and V_{max} prominently depends on micro viscosity and associated water dynamics, respectively. (a) Schematic representation of free energy changes during bromelain catalysed hydrolysis of para-nitrophenyl acetate (pNPA) in the absence and presence of Ficoll-70 derived from Michaelis–Menten model. (b) Correlation of K_M with the bulk and micro-viscosity of the solution. (c) Correlation of V_{max} with faster time component of solvation dynamics. (d) Relation of activity, K_M, V_{max} with microviscosity and associated water dynamics.

Various factors can alter K_m. The two most important factors in the present case could be excluded volume effect and increased viscosity with crowding. If the role of excluded volume is prominent, then with increasing crowding, the enzyme-substrate complex formation would be more energetically favourable. Earlier, Pal and co-workers observed similar observations in the case of enzymatic reaction of chymotrypsin in the presence of a PEG as a macromolecular crowder [71]. However, in the present case, we see exactly the opposite effect, i.e. an increasing trend of K_m with increasing Ficoll-70 concentration.

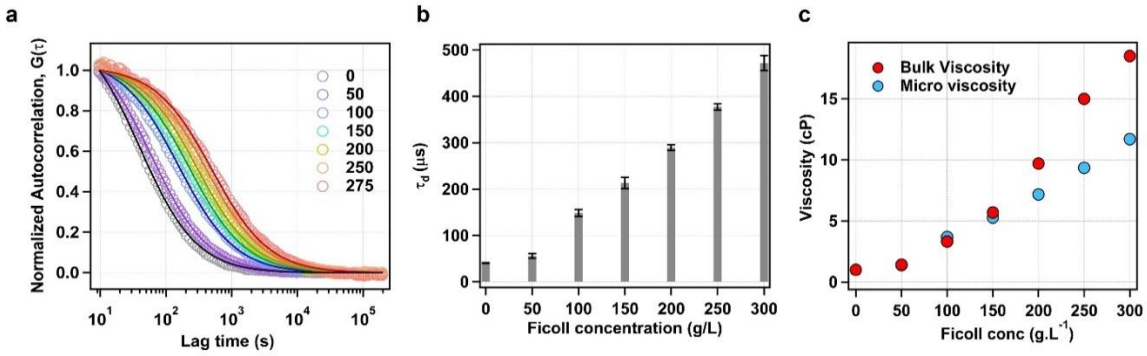

Figure 10. (a) Normalized intensity autocorrelation function of rhodamine 6G (R6G) dye at various Ficoll-70 concentrations, (b) diffusion time of R6G dye with the concentration of Ficoll-70, and (c) Bulk and microviscosity of the Ficoll-70 concentrations where activity is measured.

We have measured the microviscosity of the crowder solution employing fluorescence correlation spectroscopy and found an expected trend of increasing viscosity with an increase in the Ficoll-70 concentration. Briefly, we measured the diffusion time of a standard fluorophore (rhodamine 6G in the present study) in buffer and in different concentrations of Ficoll-70 employing FCS. According to the Stokes-Einstein equation [101], diffusion coefficient, $D_t = \frac{k_B T}{6\pi\eta r}$; where k_B is the Boltzmann constant, η is the viscosity, r is the spherical radius of the probe molecule. The diffusion coefficients can be related to the inverse of the diffusion times (τ_D) as $D_t \propto 1/\tau_D$. This means, $\tau_D \propto \eta$. Thus, the ratio of diffusion time in any solution in which viscosity is to be measured and a solution media of known viscosity (in this case, water) can give the viscosity of the unknown solution [102].

$$\frac{\tau_{D,Ficoll-70}}{\tau_{D,water}} = \frac{viscosity\ of\ Ficoll-70}{viscosity\ of\ water} \qquad (7.8)$$

The increased viscosity due to Ficoll-70 (see Figure 10) might slow down the ES complex formation, leading to an increase in K_m. Therefore, there might be a

correlation between K_m and viscosity. We have also measured the bulk viscosity using a viscometer. A plot of relative K_m vs. bulk viscosity (Figure 9b) indicates a hint of correlation but is not very strong (adjusted $R^2 \sim 0.86$). This might be because solute diffusion in crowded media does not generally follow bulk viscosity [103–105].

The length scale of translational diffusion (through which bromelain and pNPA should come together) occurs in the micrometer (μm) range [106]. Fluorescence correlation spectroscopy measures the diffusion dynamics of a fluorophore in the μm length scale [85,107–109], and therefore, we used FCS to measure the microviscosity (i.e., viscosity at micrometer length scale) and plotted it against K_m (Figure 9b). All the related raw data are provided in Figure 10. To our delight, we observe a stronger correlation (adjusted R^2~0.95) between microviscosity and K_m. This result signifies that enzyme-substrate complex formation definitely has some dependency on the solution microviscosity (see Figure 9d). However, a direct correlation of the micro-viscosity of the solution to a bulk thermodynamic property, K_m, at this point is not totally explainable and might be a little far-fetched. Future studies with different systems might give better insights.

7.2.9. V_{max} prominently depends on the associated water dynamics:

As discussed in the previous sections, the associated water structure of the protein becomes more flexible (manifested through faster solvation dynamics) in the same concentration range where V_{max} increases. Thus, it may be speculated that the associated water structure of protein might play a significant role in controlling the rate of product formation from the enzyme-substrate complex. Figure 9c illustrates the correlation between the change in the faster time component of solvation and V_{max} (adjusted R^2~0.92).

To understand the physical basis of this correlation, we need to understand what V_{max} basically signifies. Maximum velocity (V_{max}) is related to the rate constant of

the reaction in which the intermediate complex (ES) reaches the transition state ($ES^{\ddagger}$) at the expense of free energy $\Delta G^{\ddagger}$ and then eventually forms the product (equation 5) [60,71]. From the transition state theory, $\Delta G^{\ddagger}$ can be written as

$$\Delta G^{\ddagger} = -RT\ ln\left(\frac{h}{K_B T} K_2\right) \tag{7.9}$$

Here, $\Delta G^{\ddagger}$ refers to the exit channel in which the product is formed by dissociating the enzyme-substrate complex [60,71]. $\Delta G^{\ddagger}$ is positive. Its value decreases up to 100 gL^{-1} Ficoll-70 and increases thereafter (see Table 2 and Figure 9a), suggesting that Ficoll-70 facilitates the exit channel at lower Ficoll-70 concentrations but restricts the same at higher Ficoll-70 concentrations. We propose that the higher flexibility of associated water at lower Ficoll-70 concentrations makes the exit channel favourable at lower Ficolll-70 concentrations, whereas, at higher Ficoll-70 concentrations, the greater rigidity of associated water hinders such exit (Figure 9d).

7.3. Summary and Conclusions:

In this article, we examined the effect of macromolecular crowding on the stability and activity of enzyme with a focus on how these depend on associated water dynamics. Traditional crowding theory attributes protein stability as an interplay between stabilising entropic effects (excluded volume) and stabilising or destabilising enthalpic interactions. However, it fails to explain observations like destabilising entropic contribution and entropy-enthalpy compensation. Recently, we proposed that water structure modulation might play a crucial role in dictating protein stability in a crowded environment, which also explains these anomalies. However, our proposal needed generalization. In this article, we addressed the issues and deciphered that the role of associated water dynamics on bromelain's stability

and activity in presence of Ficoll-70. Surprisingly, up to 100 gL^{-1} of the Ficoll-70, the associated water becomes flexible, and then it increasingly rigidifies. Recognizing individual entropic and enthalpic components of thermal stabilization, we found low Ficoll-70 concentrations cause entropic destabilization and enthalpic stabilization, while higher concentrations have the opposite effect. Overall, we proposed that rigid associated water stabilizes bromelain via entropy and destabilizes via enthalpy, while flexible associated water has the opposite effect (Scheme 3). In the process, we addressed previous shortcomings with a systematic concentration-dependent study using a single-domain protein, bromelain, and component analysis of solvation dynamics.

More importantly, here, we provide mechanistic insight into the disputed topic of enzymatic activity in crowded media. Unlike other properties, protein activity does not follow a general trend in crowded environments, as the protein function often involves multiple steps and various factors collectively influence them. We observed that the hydrolytic activity of bromelain remains constant at low Ficoll-70 concentrations but decreases as concentration increases. For further insight, we analysed the activity using the Michaelis-Menten model and determined the maximum velocity (V_{max}) achieved by the system and Michalis-Menten coefficient (K_M). Results indicate that with an increase in the Ficoll-70 concentration, the Michalis-Menten coefficient increases, hindering the formation of the enzyme-substrate complex. This contradicts the traditional crowding theory, which predicts easier formation due to reduced volume. Our results suggest that the micro-viscosity, and not the bulk viscosity, dictates the process of enzyme-substrate complex formation (Scheme 2). Additionally, V_{max} increases up to 100 gL^{-1} Ficoll-70 and then decreases. Interestingly, this trend aligns with associated water dynamics, resulted in a strong correlation between V_{max} and associated water dynamics. We proposed that flexible associated water dynamics at low Ficoll-70 concentration favour the rate of product formation from the enzyme-substrate complex, while the

rigid associated water dynamics at high Ficoll-70 concentration impede the same (Scheme 2).

Overall, our study highlights the critical role of water in dictating protein stability and activity in a crowded environment, which is often overlooked. For protein stability in crowded milieu, our work can explain observations where traditional crowding theory falls short. We should consider the modulation of associated water structure, where rigid water stabilizes protein by entropy and destabilizes it through enthalpy, and flexible water has the opposite effect. For protein activity in crowded media, there was only a little understanding. Our study bridged this gap through conclusions like microviscosity of the medium controls enzyme-substrate complex formation, and flexible water dynamics favour product formation, whereas rigid water dynamics impede it.

This report enhances our understanding of protein behaviour in crowded environments, offering a novel perspective on the relationship between protein stability, activity, and associated water dynamics. While further research is needed to generalize the mechanism, this study provides a foundation for exploring how water dynamics influence protein function, potentially sparking extensive future research in this area.

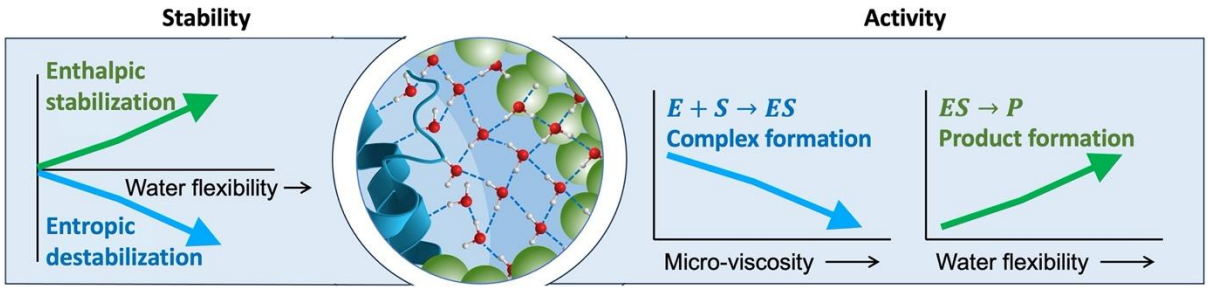

Scheme 2. The critical role of water beyond protein and macromolecular crowders to explain protein stability and activity in a crowded milieu. In the case of protein stability, one should consider the modulation of associated water structure, where rigid water stabilizes protein by entropy and destabilizes through enthalpy, whereas the flexible water has the opposite effect. Micro-viscosity of the medium controls the formation of enzyme-substrate complex, however,

the modulation of associated water controls the product formation from the enzyme-substrate complex, where flexibility of associated water favours the process.

7.4. References:

(1) Ellis, R. J. (2001) Macromolecular crowding: An important but neglected aspect of the intracellular environment. *Curr Opin Struct Biol 11*, 114–119.

(2) Ellis, R. J. (2001) Macromolecular crowding: Obvious but underappreciated. *Trends Biochem Sci 26*, 597–604.

(3) Bhakuni, K., and Venkatesu, P. (2019) Does macromolecular crowding compatible with enzyme stem bromelain structure and stability? *Int J Biol Macromol 131*, 527–535.

(4) Rajapaksha, A., Stanley, C. B., and Todd, B. A. (2015) Effects of macromolecular crowding on the structure of a protein complex: A small-angle scattering study of superoxide dismutase. *Biophys J 108*, 967–974.

(5) Wang, Y., Sarkar, M., Smith, A. E., Krois, A. S., and Pielak, G. J. (2012) Macromolecular crowding and protein stability. *J Am Chem Soc 134*, 16614–16618.

(6) Stagg, L., Christiansen, A., and Wittung-Stafshede, P. (2011) Macromolecular crowding tunes folding landscape of parallel α/β protein, apoflavodoxin. *J Am Chem Soc 133*, 646–648.

(7) Dhar, A., Samiotakis, A., Ebbinghaus, S., Nienhaus, L., Homouz, D., Gruebele, M., and Cheung, M. S. (2010) Structure, function, and folding of phosphoglycerate kinase are strongly perturbed by macromolecular crowding. *Proc. Natl. Acad. Sci. 107*, 17586–17591.

(8) Kumar, S., Sharma, D., and Kumar, R. (2017) Role of Macromolecular Crowding on Stability and Iron Release Kinetics of Serum Transferrin. *Journal of Physical Chemistry B 121*, 8669–8683.

(9) Beg, I., Minton, A. P., Islam, A., Hassan, M. I., and Ahmad, F. (2018) Comparison of the thermal stabilization of proteins by oligosaccharides and monosaccharide mixtures: Measurement and analysis in the context of excluded volume theory. *Biophys Chem 237*, 31–37.

(10) Zhou, H. X. (2013) Influence of crowded cellular environments on protein folding, binding, and oligomerization: Biological consequences and potentials of atomistic modeling. *FEBS Lett 587*, 1053–1061.

(11) Minton, A. P. (2001) The Influence of Macromolecular Crowding and Macromolecular Confinement on Biochemical Reactions in Physiological Media. *Journal of Biological Chemistry 276*, 10577–10580.

(12) Harada, R., Sugita, Y., and Feig, M. (2012) Protein crowding affects hydration structure and dynamics. *J Am Chem Soc 134*, 4842–4849.

(13) Gao, M., Estel, K., Seeliger, J., Friedrich, R. P., Dogan, S., Wanker, E. E., Winter, R., and Ebbinghaus, S. (2015) Modulation of human IAPP fibrillation: Cosolutes, crowders and chaperones. *Physical Chemistry Chemical Physics 17*, 8338–8348.

(14) Speer, S. L., Stewart, C. J., Sapir, L., Harries, D., and Pielak, G. J. (2022) Macromolecular Crowding Is More than Hard-Core Repulsions. *Ann. Rev. Biophys. 51*, 267–300.

(15) Cheng, K., Wu, Q., Zhang, Z., Pielak, G. J., Liu, M., and Li, C. (2018) Crowding and Confinement Can Oppositely Affect Protein Stability. *ChemPhysChem 19*, 3350–3355.

(16) Guseman, A. J., Goncalves, G. M. P., Speer, S. L., Young, G. B., and Pielak, G. J. (2018) Protein shape modulates crowding effects. *Proc Natl Acad Sci U S A 115*, 10965–10970.

(17) Nguemaha, V., Qin, S., and Zhou, H. X. (2019) Transfer free energies of test proteins into crowded protein solutions have simple dependence on crowder concentration. *Front Mol Biosci 6*, 438616.

(18) Gorensek-Benitez, A. H., Smith, A. E., Stadmiller, S. S., Perez Goncalves, G. M., and Pielak, G. J. (2017) Cosolutes, Crowding, and Protein Folding Kinetics. *Journal of Physical Chemistry B 121*, 6527–6537.

(19) Guseman, A. J., Speer, S. L., Perez Goncalves, G. M., and Pielak, G. J. (2018) Surface Charge Modulates Protein-Protein Interactions in Physiologically Relevant Environments. *Biochemistry 57*, 1681–1684.

(20) Biswas, S., and Chowdhury, P. K. (2015) Unusual domain movement in a multidomain protein in the presence of macromolecular crowders. *Physical Chemistry Chemical Physics 17*, 19820–19833.

(21) Samanta, N., Luong, T. Q., Das Mahanta, D., Mitra, R. K., and Havenith, M. (2016) Effect of Short Chain Poly(ethylene glycol)s on the Hydration Structure and Dynamics around Human Serum Albumin. *Langmuir 32*, 831–837.

(22) Samanta, N., Das Mahanta, D., Patra, A., and Mitra, R. K. (2018) Soft interaction and excluded volume effect compete as polyethylene glycols modulate enzyme activity. *Int J Biol Macromol 118*, 209–215.

(23) Yu, I., Mori, T., Ando, T., Harada, R., Jung, J., Sugita, Y., and Feig, M. (2016) Biomolecular interactions modulate macromolecular structure and dynamics in atomistic model of a bacterial cytoplasm. *Elife 5*, 19274.

(24) Das, N., and Sen, P. (2019) Size-dependent macromolecular crowding effect on the thermodynamics of protein unfolding revealed at the single molecular level. *Int. J. Biol. Macromol. 141*, 843–854.

(25) Das, N., and Sen, P. (2022) Macromolecular crowding: how shape and interaction affect the structure, function, conformational dynamics and relative domain movement of a multi-domain protein. *Phys. Chem. Chem. Phys. 24*, 14242–14256.

(26) Das, N., and Sen, P. (2020) Shape-Dependent Macromolecular Crowding on the Thermodynamics and Microsecond Conformational Dynamics of Protein Unfolding Revealed at the Single-Molecule Level. *J. Phys. Chem. B 124*, 5858–5871.

(27) Das, N., and Sen, P. (2018) Structural, Functional, and Dynamical Responses of a Protein in a Restricted Environment Imposed by Macromolecular Crowding. *Biochemistry 57*, 6078–6089.

(28) Nandy, A., Chakraborty, S., Nandi, S., Bhattacharyya, K., and Mukherjee, S. (2019) Structure, Activity, and Dynamics of Human Serum Albumin in a Crowded Pluronic F127 Hydrogel. *Journal of Physical Chemistry B 123*, 3397–3408.

(29) Pastore, A., and Temussi, P. A. (2022) Crowding revisited: Open questions and future perspectives. *Trends Biochem Sci 47*, 1048–1058.

(30) Zhou, H. X., Rivas, G., and Minton, A. P. (2008) Macromolecular crowding and confinement: Biochemical, biophysical, and potential physiological consequences. *Annu Rev Biophys 37*, 375–397.

(31) Stadmiller, S. S., and Pielak, G. J. (2021, February 1) Protein-complex stability in cells and in vitro under crowded conditions. *Curr Opin Struct Biol*. Elsevier Ltd.

(32) Minton, A. P. (2013) Quantitative assessment of the relative contributions of steric repulsion and chemical interactions to macromolecular crowding. *Biopolymers 99*, 239–244.

(33) Minton, A. P. (1981) Excluded volume as a determinant of macromolecular structure and reactivity. *Biopolymers 20*, 2093–2120.

(34) Silverstein, T. P., and Slade, K. (2019) Effects of Macromolecular Crowding on Biochemical Systems. *J Chem Educ 96*, 2476–2487.

(35) Ellis, R. J., and Minton, A. P. (2003) Join the crowd. *Nature 425*, 27–28.

(36) Majumdar, S., Rastogi, H., and Chowdhury, P. K. (2024) Bridging Soft Interaction and Excluded Volume in Crowded Milieu through Subtle Protein Dynamics. *Journal of Physical Chemistry B 128*, 716–730.

(37) Zhou, H. X. (2004) Loops, Linkages, Rings, Catenanes, Cages, and Crowders: Entropy-Based Strategies for Stabilizing Proteins. *Acc. Chem. Res. 37*, 123–130.

(38) Sarkar, M., Li, C., and Pielak, G. J. (2013) Soft interactions and crowding. *Biophys. Rev. 5*, 187–194.

(39) Benton, L. A., Smith, A. E., Young, G. B., and Pielak, G. J. (2012) Unexpected effects of macromolecular crowding on protein stability. *Biochemistry 51*, 9773–9775.

(40) Schlesinger, A. P., Wang, Y., Tadeo, X., Millet, O., and Pielak, G. J. (2011) Macromolecular crowding fails to fold a globular protein in cells. *J Am Chem Soc 133*, 8082–8085.

(41) Samanta, N., Mahanta, D. Das, Hazra, S., Kumar, G. S., and Mitra, R. K. (2014) Short chain polyethylene glycols unusually assist thermal unfolding of human serum albumin. *Biochimie 104*, 81–89.

(42) Makhatadze, G. I., and Privalovt, P. L. (1992) Protein Interactions with Urea and Guanidinium Chloride A Calorimetric Study. *J. Mol. Biol 226*, 491–505.

(43) Senske, M., Törk, L., Born, B., Havenith, M., Herrmann, C., and Ebbinghaus, S. (2014) Protein stabilization by macromolecular crowding through enthalpy rather than entropy. *J Am Chem Soc 136*, 9036–9041.

(44) Dupuis, N. F., Holmstrom, E. D., and Nesbitt, D. J. (2014) Molecular-crowding effects on single-molecule RNA folding/unfolding thermodynamics and kinetics. *Proc Natl Acad Sci U S A 111*, 8464–8469.

(45) Sung, H. L., and Nesbitt, D. J. (2021) Effects of Molecular Crowders on Single-Molecule Nucleic Acid Folding: Temperature-Dependent Studies Reveal True Crowding vs Enthalpic Interactions. *Journal of Physical Chemistry B 125*, 13147–13157.

(46) Sung, H. L., Sengupta, A., and Nesbitt, D. (2021) Smaller molecules crowd better: Crowder size dependence revealed by single-molecule FRET studies and depletion force modeling analysis. *Journal of Chemical Physics 154*, 155101.

(47) Sharp, K. (2001) Entropy--enthalpy compensation: Fact or artifact? *Protein Science 10*, 661–667.

(48) Stewart, C. J., Olgenblum, G. I., Propst, A., Harries, D., and Pielak, G. J. (2023) Resolving the enthalpy of protein stabilization by macromolecular crowding. *Protein Science 32*, e4573.

(49) Das, N., Tarif, E., Dutta, A., and Sen, P. (2023) Associated Water Dynamics Might Be a Key Factor Affecting Protein Stability in the Crowded Milieu. *J. Phys. Chem. B 127*, 3151–3163.

(50) Xu, S., Wang, J., and Dong, J. (2023) Nonspecific interaction and overlap concentration influence macromolecular crowding effect on glucose oxidase activity. *Int J Biol Macromol 241*.

(51) Zosel, F., Soranno, A., Buholzer, K. J., Nettels, D., and Schuler, B. (2020) Depletion interactions modulate the binding between disordered proteins in crowded environments. *Proc. Natl. Acad. Sci. 117*, 13480–13489.

(52) Adams, L. M., Andrews, R. J., Hu, Q. H., Schmit, H. L., Hati, S., and Bhattacharyya, S. (2019) Crowder-Induced Conformational Ensemble Shift in Escherichia coli Prolyl-tRNA Synthetase. *Biophys. J. 117*, 1269–1284.

(53) Mishra, V., and Heath, R. J. (2021) Structural and biochemical features of human serum albumin essential for eukaryotic cell culture. *Int J Mol Sci 22*, 8411.

(54) Yadav, R., and Sen, P. (2013) Mechanistic investigation of domain specific unfolding of human serum albumin and the effect of sucrose. *Protein Science 22*, 1571–1581.

(55) Shahid, S., Hassan, M. I., Islam, A., and Ahmad, F. (2017) Size-dependent studies of macromolecular crowding on the thermodynamic stability, structure and functional activity of proteins: in vitro and in silico approaches. *Biochim Biophys Acta Gen Subj 1861*, 178–197.

(56) Rastogi, H., and Chowdhury, P. K. (2021) Understanding enzyme behavior in a crowded scenario through modulation in activity, conformation and dynamics. *Biochim Biophys Acta Proteins Proteom 1869*, 140699.

(57) Rastogi, H., Singh, A., and Chowdhury, P. K. (2023) Towards the energy landscape of adenylate kinase in crowded milieu: Activity, conformation, structure and dynamics in sequence. *Arch Biochem Biophys 743*, 109658.

(58) Das, N., Yadav, S., Negi, K. S., Tarif, E., and Sen, P. (2022) Does Microsecond Active-Site Dynamics Primarily control Proteolytic Activity of Bromelain? Clues from Single Molecular Level Study with a Denaturant, a Stabilizer and a Macromolecular Crowder. *BBA Advances 2*, 100041.

(59) Vöpel, T., and Makhatadze, G. I. (2012) Enzyme activity in the crowded Milieu. *PLoS One 7*, e39418.

(60) Kamal, J. K. A., Xia, T., Pal, S. K., Zhao, L., and Zewail, A. H. (2004) Enzyme functionality and solvation of Subtilisin Carlsberg: From hours to femtoseconds. *Chem. Phys. Lett. 387*, 209–215.

(61) Warshel, A., and Bora, R. P. (2016) Perspective: Defining and quantifying the role of dynamics in enzyme catalysis. *Journal of Chemical Physics 144*, 180901.

(62) Minton, A. P. (1983) The effect of volume occupancy upon the thermodynamic activity of proteins: some biochemical consequences. *Mol Cell Biochem 55*, 140.

(63) Agarwal, P. K. (2019) A Biophysical Perspective on Enzyme Catalysis. *Biochemistry 58*, 438–449.

(64) Testa, A., Dindo, M., Rebane, A. A., Nasouri, B., Style, R. W., Golestanian, R., Dufresne, E. R., and Laurino, P. (2021) Sustained enzymatic activity and flow in crowded protein droplets. *Nat Commun 12*, 6293.

(65) Acosta, L. C., Perez Goncalves, G. M., Pielak, G. J., and Gorensek-Benitez, A. H. (2017) Large cosolutes, small cosolutes, and dihydrofolate reductase activity. *Prot. Sci. 26*, 2417–2425.

(66) Pozdnyakova, I., and Wittung-Stafshede, P. (2010) Non-linear effects of macromolecular crowding on enzymatic activity of multi-copper oxidase. *Biochim Biophys Acta Proteins Proteom 1804*, 740–744.

(67) Schneider, S. H., Lockwood, S. P., Hargreaves, D. I., Slade, D. J., Loconte, M. A., Logan, B. E., McLaughlin, E. E., Conroy, M. J., and Slade, K. M. (2015) Slowed Diffusion and Excluded Volume Both Contribute to the Effects of Macromolecular Crowding on Alcohol Dehydrogenase Steady-State Kinetics. *Biochemistry 54*, 5898–5906.

(68) Aumiller, W. M., Davis, B. W., Hatzakis, E., and Keating, C. D. (2014) Interactions of macromolecular crowding agents and cosolutes with small-molecule substrates: Effect on horseradish peroxidase activity with two different substrates. *Journal of Physical Chemistry B 118*, 10624–10632.

(69) Silverstein, T. P. (2019) When both Km and Vmax are altered, Is the enzyme inhibited or activated? *Biochemistry and Molecular Biology Education 47*, 446–449.

(70) Popielec, A., Ostrowska, N., Wojciechowska, M., Feig, M., and Trylska, J. (2020) Crowded environment affects the activity and inhibition of the NS3/4A protease. *Biochimie 176*, 169–180.

(71) Verma, P. K., Rakshit, S., Mitra, R. K., and Pal, S. K. (2011) Role of hydration on the functionality of a proteolytic enzyme α-chymotrypsin under crowded environment. *Biochimie 93*, 1424–1433.

(72) Verma, P. K., Kundu, A., and Cho, M. (2018) How Molecular Crowding Differs from Macromolecular Crowding: A Femtosecond Mid-Infrared Pump-Probe Study. *J. Phys.Chem. Lett. 9*, 6584–6592.

(73) Nandi, N., and Bagchi, B. (1997) Dielectric Relaxation of Biological Water. *J. Phys. Chem. B 101*, 10954–10961.

(74) Pal, S. K., and Zewail, A. H. (2004) Dynamics of water in biological recognition. *Chem. Rev. 104*, 2099–2124.

(75) Pal, S. K., Peon, J., Bagchi, B., and Zewail, A. H. (2002) Biological water: Femtosecond dynamics of macromolecular hydration. *J. Phys. Chem. B 106*, 12376–12395.

(76) Bhattacharyya, K. (2008) Nature of biological water: a femtosecond study. *Chem. Commun.* 2848.

(77) Guo, F., and Friedman, J. M. (2009) Osmolyte-induced perturbations of hydrogen bonding between hydration layer waters: Correlation with protein conformational changes. *Journal of Physical Chemistry B 113*, 16632–16642.

(78) Khan, T., Das, N., Negi, K. S., Bhowmik, S., and Sen, P. (2023) Understanding the intricacy of protein in hydrated deep eutectic solvent: Solvation dynamics, conformational fluctuation dynamics, and stability. *Int. J. Biol. Macromol. 253*, 127100.

(79) Denisov, V. P., Jonsson, B. H., and Halle, B. (1999) Hydration of denatured and molten globule proteins. *Nat Struct Biol 6*, 253–260.

(80) Otting, G., Liepinsh, E., and Wüthrich, K. (1991) Protein hydration in aqueous solution. *Science (1979) 254*, 974–980.

(81) Nandi, N., Bhattacharyya, K., and Bagchi, B. (2000) Dielectric relaxation and solvation dynamics of water in complex chemical and biological systems. *Chem. Rev. 100*, 2013–2045.

(82) Mondal, S., Mukherjee, S., and Bagchi, B. (2017) Protein hydration dynamics: Much ado about nothing? *J. Phys. Chem. Lett. 8*, 4878–4882.

(83) Fleming, G. R., Gijzeman, O. L. J., Freed, K. F., and Lin, S. H. (1975) Theory for time resolved emission spectra. *Journal of the Chemical Society, Faraday Transactions 2: Molecular and Chemical Physics 71*, 773–780.

(84) Maroncelli, M., and Fleming, G. R. (1987) Picosecond solvation dynamics of coumarin 153: The importance of molecular aspects of solvation. *J. Chem. Phys. 86*, 6221–6239.

(85) Lakowicz, J. R. (2006) Principles of fluorescence spectroscopy. *Principles of Fluorescence Spectroscopy*. Springer.

(86) Sanchez-Fernandez, A., Basic, M., Xiang, J., Prevost, S., Jackson, A. J., and Dicko, C. (2022) Hydration in Deep Eutectic Solvents Induces Non-monotonic Changes in the Conformation and Stability of Proteins. *J. Am. Chem. Soc. 144*, 23657–23667.

(87) Shil, S., Das, N., Sengupta, B., and Sen, P. (2018) Sucrose-Induced Stabilization of Domain-II and Overall Human Serum Albumin against Chemical and Thermal Denaturation. *ACS Omega 3*, 16633–16642.

(88) Dupuis, N. F., Holmstrom, E. D., and Nesbitt, D. J. (2014) Molecular-crowding effects on single-molecule RNA folding/unfolding thermodynamics and kinetics. *Proc Natl Acad Sci U S A 111*, 8464–8469.

(89) Sukenik, S., Sapir, L., and Harries, D. (2013) Balance of enthalpy and entropy in depletion forces. *Curr Opin Colloid Interface Sci 18*, 495–501.

(90) Sukenik, S., Sapir, L., Gilman-Politi, R., and Harries, D. (2013) Diversity in the mechanisms of cosolute action on biomolecular processes. *Faraday Discuss 160*, 225–237.

(91) Bagchi, B. (2005) Water dynamics in the hydration layer around proteins and micelles. *Chem. Rev. 105*, 3197–3219.

(92) Qiu, W., Zhang, L., Okobiah, O., Yang, Y., Wang, L., Zhong, D., and Zewail, A. H. (2006) Ultrafast solvation dynamics of human serum albumin: Correlations with conformational transitions and site-selected recognition. *J. Phys. Chem. B 110*, 10540–10549.

(93) Mondal, S., Mukherjee, S., and Bagchi, B. (2017) Origin of diverse time scales in the protein hydration layer solvation dynamics: A simulation study. *Journal of Chemical Physics 147*, 154901.

(94) Mondal, S., Mukherjee, S., and Bagchi, B. (2017) Decomposition of total solvation energy into core, side-chains and water contributions: Role of cross correlations and protein conformational fluctuations in dynamics of hydration layer. *Chem Phys Lett 683*, 29–37.

(95) Houston, P., Macro, N., Kang, M., Chen, L., Yang, J., Wang, L., Wu, Z., and Zhong, D. (2020) Ultrafast Dynamics of Water-Protein Coupled Motions around the Surface of Eye Crystallin. *J. Am. Chem. Soc. 142*, 3997–4007.

(96) Zhang, L., Wang, L., Kao, Y.-T., Qiu, W., Yang, Y., Okobiah, O., and Zhong, D. (2007) Mapping hydration dynamics around a protein surface. *Proc. Natl. Acad. Sci. USA 104*, 18461–18466.

(97) Yon, J. M., Perahia, D., and Ghélis, C. (1998) Conformational dynamics and enzyme activity. *Biochimie 80*, 33–42.

(98) Tzeng, S. R., and Kalodimos, C. G. (2012) Protein activity regulation by conformational entropy. *Nature 488*, 236–240.

(99) Berg, O. G. (1990) The influence of macromolecular crowding on thermodynamic activity: Solubility and dimerization constants for spherical and dumbbell-shaped molecules in a hard-sphere mixture. *Biopolymers 30*, 1027–1037.

(100) Rotta, M., Timmers, L. F. S. M., Sequeiros-Borja, C., Bizarro, C. V., De Souza, O. N., Santos, D. S., and Basso, L. A. (2017) Observed crowding effects on Mycobacterium tuberculosis 2-trans-enoyl-ACP (CoA) reductase enzyme activity are not due to excluded volume only. *Sci Rep 7*, 6826.

(101) Khan, T., Tarif, E., Awano, Y., Lozada, L. S., Das, N., Tominaga, K., and Sen, P. (2023) Multiple evidences for molecular level heterogeneity in a non-ionic biocatalytic deep eutectic solvent. *J. Mol. Liq. 389*, 122882.

(102) Chung, S., Lerner, E., Jin, Y., Kim, S., Alhadid, Y., Grimaud, L. W., Zhang Irina X, Knobler, C. M., Gelbart, W. M., and Weiss, S. (2019) The effect of macromolecular crowding on RNA polymerase. *Nucleic Acids Res 47*, 1440–1450.

(103) Junker, N. O., Vaghefikia, F., Albarghash, A., Höfig, H., Kempe, D., Walter, J., Otten, J., Pohl, M., Katranidis, A., Wiegand, S., and Fitter, J. (2019) Impact of Molecular Crowding on Translational Mobility and Conformational Properties of Biological Macromolecules. *J. Phys. Chem. B 123*, 4477–4486.

(104) Kusova, A. M., Rakipov, I. T., and Zuev, Y. F. (2023) Effects of Homogeneous and Heterogeneous Crowding on Translational Diffusion of Rigid Bovine Serum Albumin and Disordered Alfa-Casein. *Int J Mol Sci 24*.

(105) Lee, H. B., Cong, A., Leopold, H., Currie, M., Boersma, A. J., Sheets, E. D., and Heikal, A. A. (2018) Rotational and translational diffusion of size-dependent fluorescent probes in homogeneous and heterogeneous environments. *Phys. Chem. Chem. Phys. 20*, 24045–24057.

(106) Zorrilla, S., Hink, M. A., Visser, A. J. W. G., and Lillo, M. P. (2007) Translational and rotational motions of proteins in a protein crowded environment. *Biophys Chem 125*, 298–305.

(107) Das, N., Khan, T., Subba, N., and Sen, P. (2021) Correlating Bromelain's activity with its structure and active-site dynamics and the medium's physical properties in a hydrated deep eutectic solvent. *Phys. Chem. Chem. Phys. 23*, 9337–9346.

(108) Subba, N., Das, N., and Sen, P. (2020) Partial Viscosity Decoupling of Solute Solvation, Rotation, and Translation Dynamics in Lauric Acid/Menthol Deep Eutectic Solvent: Modulation of Dynamic Heterogeneity with Length Scale. *J. Phys. Chem. B 124*, 6875–6884.

(109) Wohland, T., Maiti, S., and Macháň, R. (2020) An Introduction to Fluorescence Correlation Spectroscopy. IOP Publishing.

This page left blank intentionally

Chapter 8

Conclusions and Future Outlooks

8.1. Summary of Chapter 3:

In this chapter we have measured the spatial and dynamic heterogeneity of a novel non-ionic DES, 0.5Ac/0.3Ur/0.2Sor DES, using a range of spectroscopic techniques. Additionally, we have compared the heterogeneity of our DES with the already reported acetamide based non-ionic DESs. The key observations from this study are outlined below.

Principal observations and insights of this chapter

i) Although deep eutectic solvents (DESs) are widely recognized for their inherent spatial and dynamic heterogeneity, most existing studies have primarily focused on ionic DESs. This is largely due to the ease of their formation, driven by strong ionic interactions between constituent molecules. However, from an application standpoint, non-ionic DESs are particularly valuable, especially due to their enhanced ability to solubilize hydrophobic compounds, making them highly relevant in areas such as drug delivery, extraction, and sustainable chemistry. Among these, the acetamide–urea system is one of the most extensively studied non-ionic DESs; however, its lack of liquidity at room temperature limits broader applicability. Interestingly, the addition of sorbitol to the acetamide–urea mixture results in a ternary DES (0.5Ac/0.3Ur/0.2Sor DES) that remains liquid even at temperatures as low as 280 K, significantly enhancing its usability. In this chapter, I examine this novel sorbitol-based ternary DES, synthesized by our group, and investigate its spatial and dynamic heterogeneity using a combination of spectroscopic techniques.

ii) To probe the structural characteristics of the ternary DES system (0.5Ac/0.3Ur/0.2Sor), we employed a comprehensive set of spectroscopic techniques, including red-edge excitation shift (REES), solvation dynamics,

rotational relaxation, dielectric relaxation, and single-molecule fluorescence correlation spectroscopy (FCS). Our findings reveal clear evidence of both spatial and dynamic heterogeneity within this system. Notably, the significant shift in the excitation wavelength-dependent emission maxima of the solvatochromic dye Coumarin 153 (C153) highlights pronounced spatial heterogeneity in the local microenvironments of the DES.

iii) The fractional viscosity decoupling of average solvation time ($p \approx 0.4$) indicates pronounced dynamic heterogeneity in the nanometer length and picosecond–nanosecond timescale of solvation dynamics. Dielectric relaxation (DR) measurements probing the medium's inherent dynamics similarly show substantial decoupling ($p \approx 0.41$). The average rotational time of the probe, reflecting anisotropy on the nanometer and nanosecond scale, also exhibits viscosity decoupling ($p \approx 0.6$), suggesting a definite but comparatively weaker dynamic heterogeneity. In contrast, translational dynamics measured by single-molecule FCS, operating at micrometer length and microsecond–millisecond timescales—revealed the strongest viscosity decoupling ($p \approx 0.3$), indicating pronounced heterogeneity at larger spatiotemporal scales. Collectively, these findings highlight that the observed dynamic heterogeneity is strongly dependent on both the length and timescale of the measurement technique.

iv) I have also compared the extent of heterogeneity across three acetamide-based non-ionic DESs: acetamide–urea (0.66Ac/0.33Ur), acetamide–urea–PEG (0.55Ac/0.36Ur/0.09PEG), and acetamide–urea–sorbitol (0.5Ac/0.3Ur/0.2Sor). Among these, the sorbitol-based DES exhibited the highest degree of decoupling in all dynamic measurements, followed by the PEG-containing system, while the binary acetamide–urea DES showed the least. These findings suggest an additive induced heterogeneity as both sorbitol (a solid additive) and PEG-300 (a liquid additive) enhance dynamic

heterogeneity in the Ac/Ur matrix. However, the effect is significantly more pronounced with sorbitol, highlighting its stronger influence on the structural and dynamic complexity of the system.

v) Although dynamic heterogeneity has long been observed in ionic liquids and DESs, its relevance to biocatalysis and reaction mechanisms remains underexplored. When an enzyme exhibits activity, it typically relies on the diffusion of large biomolecules, a process expected to be significantly hindered by the high viscosity of DESs. However, our findings suggest otherwise. The lowest viscosity coupling parameter ($p \approx 0.33$) for translational motion indicates that solutes experience much reduced resistance, implying that medium viscosity may not hinder diffusion as expected. To probe deeper, we analyzed solvation dynamics by separating fast and slow components. The shorter time component, which is attributed to the immediate solvation shell, shows strong viscosity decoupling ($p \approx 0.16$), suggesting this local environment remains intact even in viscous DES. This may explain why DESs, despite their high viscosity, can still support efficient biocatalysis: they preserve the enzyme's microenvironment while modulating bulk physical properties, thereby maintaining both stability and activity.

Limitations and future directions

i) While our study demonstrates that additive-induced heterogeneity is more pronounced with the inclusion of a solid component (sorbitol) compared to a liquid additive (PEG 300), literature reports suggest that liquid additives can also lead to greater decoupling. Therefore, such conclusions should not be generalized based on limited data. More comprehensive research is needed to systematically explore additive-induced heterogeneity, especially

since incorporating water or other solvents into a DES is a common practice in the field.

ii) This study reveals a length- and timescale-dependent heterogeneity, consistent with observations in other DESs and ionic liquids. However, the underlying origins of this behavior remain poorly understood, highlighting the need for more extensive and systematic investigations.

iii) The component-wise analysis of solvation dynamics and the observed viscosity decoupling across all dynamic measurements suggest a possible explanation for the remarkable stability and activity of proteins in viscous DES. However, to validate this hypothesis, studies involving real enzymes are essential. Future research incorporating actual biocatalysts may offer deeper insights into the molecular basis of this phenomenon.

8.2. Summary of Chapter 4:

In this chapter, I have investigated solvation dynamics, conformational fluctuation dynamics, and stability of human serum albumin (HSA) in hydrated 0.5Ac/0.3Ur/0.2Sor DES of varying concentrations to understand the intricacy of protein behaviour in DES. The main findings of this study are summarized below.

Principal observations and insights of this chapter

i) In our previous work, viscosity decoupling and solvation dynamics analysis indicated an unperturbed solvent environment around the probe. This is particularly relevant for proteins, where the integrity of the immediate solvent environment (known as biological water) is crucial for stability and function. Despite significant changes in bulk properties like viscosity and

polarity upon DES addition, the local solvation environment appears largely unaffected. In this chapter, solvation dynamics around domain I of HSA slowed only marginally, even with an ~83-fold increase in viscosity at 90% 0.5Ac/0.3Ur/0.2Sor DES, supporting this observation.

ii) The fast hundreds of picosecond solvation component arises from coupled motion between water molecules near the protein surface known as associated/ biological water, and side chain motion, while the slower component reflects protein-side chain motions and polar residue dynamics. In this study with HSA, the fast component remains unchanged despite increasing DES concentration. Moreover, its near-zero slope in a log-log plot against viscosity confirms viscosity independence, indicating that water dynamics in the immediate solvation shell remain intact even up to 70% (v/v) DES. This suggests the protein experiences an aqueous-like environment, which may explain the preserved stability and activity of enzymes in DESs, offering important implications for biocatalysis.

iii) Using transient absorption spectroscopy, we measured solvation dynamics of the hydrated DES media in the absence of protein and found that the average solvation time closely follows medium viscosity, unlike the case with protein. This contrast highlights the unique, tunable nature of DES environments.

iv) This chapter also addresses the debated question of whether the DES network is preserved in hydrated systems. By measuring micro viscosity using FCS, we compared hydrated DES with a simple aqueous mixture of its components at identical concentrations. From 30% (v/v) DES onward, distinct differences in micro viscosity emerge, indicating above this threshold, a DES network is retained which cannot be achieved just by mixing the constituents in water.

v) Although the component mixture and hydrated DES differ in micro viscosity, the solvation dynamics of HSA domain I show similar behaviour in both, highlighting the critical role of associated water in preserving protein behaviour regardless of the additive.

vi) An important but underexplored aspect in DES research is the microsecond-scale conformational fluctuation dynamics that governs protein activity. In this study, domain I of HSA shows unperturbed fluctuations up to ~30% DES, beyond which the dynamics gradually slow, likely due to increased viscosity and a corresponding rise in protein size.

vii) The thermal stability of HSA decreases with increasing DES concentration, with a more pronounced effect in the component solution than in the corresponding hydrated DES. This suggests that the structured network of DES may offer some protection against thermal stress.

Limitations and future directions

i) Despite observing an unperturbed immediate solvent environment, this study found a gradual decrease in the thermal stability of HSA with increasing DES concentration. This may be attributed to slight conformational changes or partial unfolding of the protein at higher DES levels (above 30% v/v). However, this interpretation remains speculative. Future studies should focus on systems where protein conformation remains unchanged upon DES addition, allowing for more definitive conclusions.

ii) Although the preservation of associated water around the protein in DES was clearly demonstrated in this study, the implication of this observation in

protein behaviour has not been observed. A proper mechanism where how the modulation of this associated water will influence the protein stability in the presence of DES is required.

iii) Protein function is one of the most important parameters that has been affected by DES or hydrated DES. However, this study does not address that aspect. Future work should aim to uncover the mechanistic basis of how DESs modulate protein function, providing a more comprehensive view of their utility in biocatalysis.

8.3. Summary of Chapter 5:

In this chapter, I have tried to address the limitations of the previous chapter. Herein, using bromelain as the model enzyme and hydrated 0.5Ac/0.3Ur/0.2Sor as the model DES, we provide experimental evidence that modulation of associated water plays a key role in dictating protein stability and activity in hydrated DES. The major conclusions drawn from this chapter are listed below.

Principal observations and insights of this chapter

i) Using femtosecond fluorescence up conversion (TDFSS technique) this study reveals, in hydrated 0.5Ac/0.3Ur/0.2Sor DES, associated water around bromelain becomes more flexible at lower DES concentrations (≤30% v/v) and rigidifies at higher concentrations (>40% v/v), highlighting a non-monotonic modulation.

ii) Contrary to previous literature, bromelain stability decreased at higher DES concentrations despite the rigidity of associated water, challenging the assumption that rigid hydration always enhances stability. This suggests a

need to re-evaluate stability in terms of entropic and enthalpic contributions rather than overall stability.

iii) The rigid associated water at higher DES concentrations (beyond 40% v/v) stabilizes bromelain through entropy but destabilizes it through enthalpy. On the other hand, flexible associated water dynamics at lower DES concentrations result in an opposite thermodynamic outcome. The work suggests a plausible mechanism of enthalpy–entropy compensation through DES-induced changes in associated water dynamics.

iv) No correlation was found between bromelain behaviour and bulk water solvation dynamics, affirming the dominant influence of the water near the protein surface (associated water).

v) This is the first study to experimentally correlate associated water dynamics with both protein stability and proteolytic activity in a DES environment. Bromelain activity increases in flexible hydration environments (low DES) and decreases with retarded hydration (high DES), reinforcing the role of associated water in facilitating enzymatic function.

vi) The effects of DESs or any additives on protein stability and activity are highly specific to both the protein and the additive. The same DES may stabilize one enzyme while destabilizing another, and different DESs can have varying impacts on the same protein. However, since our hypothesis centres on the role of associated water, which is the water that are directly interacting with the enzyme surface, it offers a unifying framework to explain these protein- and DES-specific behaviours.

Limitations and future directions

i) The findings are based on a single enzyme (bromelain) in a single hydrated DES. Broader studies across diverse protein and various DESs are required for generalizing our hypothesis. Future works should focus on this.

ii) While correlations between hydration dynamics and protein function are shown, the poorer correlation for activity suggests additional factors are at play. Also, the precise mechanism by which associated water influences catalysis remains speculative. More comprehensive kinetic studies like Michaelis-Menten analysis and controlled hydration environments may clarify this.

iii) Although from the modulation of associated water dynamics, we are suggesting the modulation of the hydrogen bonding network of the enzyme, this is an indirect measurement. The hypothesis on hydrogen-bond network alteration remains unquantified. Methods like FTIR, 2D-IR, or computational hydrogen-bond analysis could offer more direct evidence.

8.4. Summary of Chapter 6:

In the previous two chapters, I examined HSA and the enzyme bromelain in the same hydrated DES system, 0.5Ac/0.3Ur/0.2Sor DES. As we stated, our hypothesis lacks from a generalization with different DESs. To address this, the current chapter explores two of the most widely studied DESs, choline chloride–glycerol (1:2) and choline chloride–ethylene glycol (1:2), using HSA as the model protein. By employing red edge excitation shift (REES), which captures the excitation-dependent shift in emission maxima, we investigated the solvation dynamics around the protein and correlated them with its stability in these distinct DES environments. The main findings of this study are summarized below.

Principal observations and insights of this chapter

i) Both the DESs, ChCl-glycerol and ChCl-ethylene glycol stabilizes the protein up to 50% (v/v) DES. However, at higher DES concentrations (75% v/v), ChCl-EG shows some detrimental effects whereas ChCl-Gly continues to stabilize the protein.

ii) REES results reveal that Domain-I of HSA experiences progressive solvation retardation (positive $\Delta REES$ with respect to buffer), while Domain-III shows a non-monotonic trend—initial hydration flexibility (negative $\Delta REES$ with respect to buffer) followed by rigidification at higher DES concentrations.

iii) Recognition of individual entropy-enthalpy of thermal unfolding shows clear entropy–enthalpy compensation. The correlation between solvation dynamics and stability was strong in Domain-III but absent in Domain-I when only global unfolding data was considered. This highlights the need for domain-specific analysis in multidomain proteins.

iv) The modulation of solvation dynamics correlates well with the entropic and enthalpic components of domainwise thermal unfolding. The study finds that hydration flexibility around Domain-III (reflected in negative ΔREES) leads to enthalpic stabilization and entropic destabilization, while rigid hydration (positive ΔREES) around Domain-I produces the opposite thermodynamic trend reinforcing the mechanistic role of surrounding water in protein unfolding.

v) Even within the same protein, hydration dynamics and their thermodynamic consequences vary by domain. This finding is significant for understanding

enzyme behaviour in DES media, especially in proteins with multiple functional or folding domains.

vi) This chapter also reinforces the simple fluorescence-based REES as a sensitive, low-sample, site-specific approach to map hydration shell dynamics around proteins.

vii) Most importantly, this chapter extends the hypothesis from Chapter 5 (on bromelain in Ac/Ur/Sor DES) by confirming that hydration shell dynamics modulate protein stability across different proteins and DES systems, establishing this principle as potentially generalizable.

viii) Unlike in other chapters, structural analyses using CD and FCS confirm that HSA retains its native conformation in both ChCl-EG and ChCl-Gly DESs. This reinforces our conclusion that thermal stability changes are primarily driven by alterations in hydration dynamics.

Limitations and future directions

Although this chapter generalizes the hypothesis of associated water modulation in controlling protein behaviour in DESs and covers the limitations of the previous chapters to a certain extent, some limitations still exist.

i) Both ChCl-glycerol and ChCl-ethylene glycol DESs primarily stabilize the protein. Including a DES with contrasting, destabilizing behavior would serve as a valuable negative control to further validate the hydration-based stabilization mechanism.

ii) Although hydration shell dynamics are inferred and correlated with stability, they were assessed indirectly through REES. Direct measurement of

solvation timescales using time-resolved techniques such as TDFSS could offer deeper mechanistic insight and strengthen the conclusions.

iii) This chapter centres on protein stability. However, incorporating enzymatic activity would reveal whether hydration dynamics similarly influence function in ChCl-based DESs.

iv) Furthermore, while this chapter suggests higher thermal stabilization of HSA with the greater number of hydroxyl groups in glycerol versus ethylene glycol, the precise origin of this effect remains to be definitively proven. This could be elegantly achieved by designing experiments that compare DESs with the same effective number of hydroxyl groups but different constituents, such as 1:2 choline chloride:glycerol and 1:3 choline chloride:ethylene glycol. Such a study would provide more definitive, molecular-level insight into how HBD-HBA stoichiometry truly governs the protein's microenvironment and stability.

v) While hydration dynamics are highlighted, specific interactions between DES constituents and protein amino acid residues are not probed. MD simulations or other experimental studies could clarify these interactions.

vi) The study infers hydration behaviour from dynamic measurements but does not directly visualize hydrogen bonding networks. Future work incorporating computational simulations, vibrational spectroscopy, advanced NMR (NOESY, HOESY), and/or small-angle neutron scattering techniques might provide structural perturbations of hydration shells in the presence of DESs.

8.5. Summary of Chapter 7:

To further generalize the hypothesis that associated water modulation governs protein stability and activity, this chapter explores a biologically relevant system using macromolecular crowding. Crowding mimics the intracellular environment, making this study not only a conceptual extension but also biologically meaningful. Here, bromelain and Ficoll-70 (MW ~70,000 Da) were used as the model enzyme and crowder, respectively. Enzyme stability and activity were assessed across varying concentrations of Ficoll-70, while associated water dynamics near the active site were measured using time-dependent fluorescence Stokes shift (TDFSS) and correlated with both functional and structural parameters.

Principal observations and insights of this chapter

i) The solvation time around bromelain first decreases (indicating more flexible water) with increasing Ficoll-70 up to ~100 g/L, then increases again (indicating rigidification) with increasing crowder concentrations.

ii) The melting temperature of bromelain remains nearly constant, but a decomposition into enthalpic and entropic components reveals that at low Ficoll-70 concentrations, stabilization is enthalpic and destabilization is entropic, while at high concentrations, the trend reverses. This entropy–enthalpy compensation cannot be explained by classical crowding theory.

iii) The faster solvation time (ps scale), attributed to associated water dynamics, correlates strongly with both enthalpy and entropy changes reinforcing the mechanistic link between water structure and stability. Consistent with the previous chapters, this study reinforces the conclusion of our previous study, i.e., rigid-associated water stabilizes proteins via entropy and destabilizes them via enthalpy, while flexible water has the opposite effect.

iv) This chapter addresses two key observations, namely, negative entropic contributions and entropy–enthalpy compensation in the presence of crowders through the lens of associated water dynamics. These phenomena cannot be fully explained by classical crowding theories based on excluded volume and interaction effects, reinforces the need to consider hydration shell modulation. Moreover, CD spectroscopy confirms that bromelain's secondary structure is preserved across the full range of Ficoll-70 concentrations, indicating observed changes arise from hydration dynamics, not conformational shifts.

v) This chapter also provides mechanistic insights into one of the underexplored phenomena of protein activity in crowded milieu. By distinguishing the steps of enzyme catalysis through Michaelis-Menten analysis and correlating them with microviscosity and associated water, the study offers rare mechanistic clarity on why enzymatic activity varies so unpredictably in crowded media.

vi) Michaelis-Menten analysis of bromelain activity reveals that the increasing Ficoll-70 concentration leads to an increase in K_M, indicating hindered enzyme-substrate complex formation which is more closely correlated with micro viscosity measured via FCS than the bulk viscosity. Another parameter from the analysis is V_{max}, which shows a non-monotonic modulation with crowder concentration. V_{max} increases at low Ficoll-70 concentrations (where associated water is more flexible) and decreases at high concentrations (where associated water becomes rigid), suggesting that flexible associated water facilitates the catalytic step of product release.

vii) Most importantly, this chapter validates that regardless of additive type (synthetic crowders or DESs), protein stability and function is critically

modulated by the flexibility or rigidity of the hydration shell, and this effect can explain both the protein and additive specific effect.

Limitations and future directions

Although this chapter addresses several limitations of the previous ones and helps generalize the hypothesis, certain constraints still remain and can be resolved through future investigations.

i) Although this study itself is a generalization of the proposal but still some scopes left unattended. The study focuses on one protein (bromelain) and one synthetic crowder (Ficoll-70). Generalizing the findings requires testing with multiple proteins and different crowder types (e.g., PEG, proteins, polysaccharides).

ii) The strong correlation between microviscosity and K_M, and between hydration flexibility and V_{max}, is well-documented here, but the mechanistic link, especially how viscosity and local water dynamics affects the protein needs further theoretical exploration. Systematic studies by keeping one parameters constant (viscosity or dynamics) at each time could provide meaningful insights.

iii) While solvation dynamics are measured with TDFSS, the structural changes in the hydration shell (e.g., hydrogen bond networks) are inferred, not directly visualized. Future studies using neutron scattering or ultrafast IR techniques could provide higher-resolution insights. MD simulations could strengthen the proposed mechanism by visualizing the hydration shell under varying crowding conditions. Integrating computational results would provide molecular-level confirmation of experimental findings.

Through the collective insights presented in Chapters 3 to 7, this thesis advances a unified understanding of how associated water dynamics, rather than bulk solvent properties or conformational changes, critically govern protein stability and activity in complex environments like deep eutectic solvents (DESs) and crowded media. Beginning with the characterization of a novel non-ionic DES, we established that dynamic heterogeneity, especially at the nanoscale, is intrinsic to DES systems and can preserve local environments conducive to protein function. Building on this, the role of associated water was elucidated in both DESs and macromolecular crowders, revealing consistent entropy–enthalpy compensation and hydration modulation as fundamental determinants of protein behavior. Importantly, these findings were shown to transcend specific systems—validated in different DES types, with two different proteins, and in biologically relevant crowded conditions. Despite these advances, the complexity of hydration shell dynamics still presents open questions. A key limitation of this work is that it provides an indirect, dynamic picture of the solvation shell; therefore, a top priority for future work must be to obtain a direct, molecular-level visualization of its composition. Future studies integrating advanced structural techniques, such as NOESY NMR, SANS, with molecular dynamics (MD) simulations will be instrumental in refining this framework by explicitly quantifying the relative abundance of water versus DES components at the protein interface. Ultimately, this work lays the groundwork for rational design of DESs and biomimetic environments tailored for protein stabilization and biocatalysis.

This page left blank intentionally

List of Publications

 # are included in the thesis

(§ represents equal contribution)

#17. Site-Specific Water Dynamics Drives Protein Stability in Hydrated Deep Eutectic Solvents.
Tanmoy Khan, Kuntal Debnath, Kuldeep Singh Negi, Pratik Sen*
Biophys. J., **2025**, *124,* 1-18.

16. Dissecting the role of substrate folding in enzymatic digestion.
Nilimesh Das[§], **Tanmoy Khan**[§], Soumya Chaudhury, Bhaswati Sengupta, Pratik Sen*
Biointerphases, **2025**, *20*, 051001.

15. Interplay of Protein Fluctuation and Associated Water Dynamics in Osmolyte-induced Stabilization.
Kuldeep Singh Negi, Subhajit Rana, **Tanmoy Khan**, Dipankar Mondal, Pratik Sen*
Biophys. J., **2025**, *124*, 1-10.

#14. Critical Role of Water beyond the Media to Maintain Protein Stability and Activity in Hydrated Deep Eutectic Solvent.
Tanmoy Khan, Nilimesh Das, Suman Bhowmik, Kuldeep Singh Negi, Pratik Sen*
J. Phys. Chem. B, **2025***, 129,* 162–175.

13. Macromolecular Crowding Effects on Protein Dynamics.
Nilimesh Das, **Tanmoy Khan**, Bisal Halder, Shreya Ghosh, Pratik Sen*
Int. J. Biol. Macromol., **2024***, 281,* 136248.

#12. Role of Associated Water Dynamics on Protein Stability and Activity in Crowded Milieu.
Tanmoy Khan, Bisal Halder, Nilimesh Das,* Pratik Sen*
J. Phys. Chem. B, **2024***, 128,* 8672–8686.

11. Tracking Heterogeneous Protein Aggregation at Nanoscale through Fluorescence Correlation Spectroscopy.
Bisal Halder[§], Shreya Ghosh[§], **Tanmoy Khan[§]**, Subhendu Pal[§], Nilimesh Das*, Pratik Sen*
Photochem. Photobiol., **2024***, 100,* 989-999.

10. Osmolytes Induced Protein Stabilization: Modulation of Associated Water Dynamics Might be a Key Factor.
Kuldeep Singh Negi, Nilimesh Das, **Tanmoy Khan**, Pratik Sen*
Phys. Chem. Chem. Phys., **2023**, *25*, 32602-32612.

9. The Shift of Excitation Spectra at Blue Edge of Emission (BEEmS) as a New Methodology to Probe Heterogeneity.
Nilimesh Das, **Tanmoy Khan**, Pratik Sen*
Chemical Physics, **2024***, 577,* 112138.

#8. Understanding the Intricacy of Protein in Hydrated Deep Eutectic Solvent: Solvation dynamics, Conformational Fluctuation Dynamics, and Stability.
Tanmoy Khan, Nilimesh Das, Kuldeep Singh Negi, Suman Bhowmik, Pratik Sen*
Int. J. Biol. Macromol., ***2019****, 141, 843-854.*

#7. Multiple Evidences for Molecular Level Heterogeneity in a Non-ionic Biocatalytic Deep Eutectic Solvent.

Tanmoy Khan[§], Ejaj Tarif[§], Yuto Awano, Lou Serafin Lozada, Nilimesh Das, Keisuke Tominaga, Pratik Sen*
J. mol. liq., **2023***, 389,* 122882.

6. Site-specific Heterogeneity of Multi-domain Human Serum Albumin and its Origin: A Red Edge Excitation Shift Study.
Nilimesh Das, Subhrasmita Sahu, **Tanmoy Khan**, and Pratik Sen*
Photochem. Photobiol., **2023***, 99,* 538-546.

5. Massive Amplification of Photoluminescence and Exceptional Water Stability of $MAPbBr_3$ Nanocrystals through Core–shell Nanostructure Formation in a Self-Defence Mechanism.
Shovon Chatterjee, **Tanmoy Khan**, Arghya Sen, Nilimesh Das,* and Pratik Sen*
Mater. Adv., **2022***, 3,* 7360-7369.

4. Correlating Bromelain's Activity with its Structure and Active-site Dynamics and the Medium's Physical Properties in a Hydrated Deep Eutectic Solvent.
Nilimesh Das, **Tanmoy Khan**, Navin Subba and Pratik Sen*
Phys. Chem. Chem. Phys., **2021**, 23, 9337-9346.

3. A Novel Quinoline Derivative for Selective and Sensitive Visual Detection of PPB Level Cu^{2+} in Aqueous Solution.
Nilimesh Das, **Tanmoy Khan**, Aritra Das, Vipin Kumar Jain, Joydev Acharya, Md. Serajul Haque Faizi, Joseph Daniel, Pratik Sen*
Curr. Anal. Chem., **2022**, 18, 196-203

2. Highly Selective and Sensitive (PPB Level) Quinolin-Based Colorimetric Chemosensor for Cu (II).

Vaisakh Mohan, Nilimesh Das, Vipin K Jain, **Tanmoy Khan**, Sarvesh K Pandey, Md Serajul H Faizi, Joseph Daniel, Pratik Sen*
Chem. Select, **2020**, 5, 9435-9442.

1. Plasmonic Bi Nanoparticle Decorated $BiVO_4$/rGO as an Efficient Photoanode for Photoelectrochemical Water Splitting.
Palyam Subramanyam, **Tanmoy Khan**, Gudipati Neeraja Sinha, Duvvuri Suryakala, Challapalli Subrahmanyam*
Int. J. Hydrogen. Energy, **2020***, 45,*7779-7787

Unpublished works / Manuscript under preparation

1. Associated Water Stabilization Mechanism (AWSM) Reconciles the Enigmatic Differential Response of Proteins to a Single Osmolyte.
Kuldeep Singh Negi, **Tanmoy Khan**, and Pratik Sen*

2. Crucial Role of Hydrophobicity in Determining the Synergism and Heterogeneity in Binary Solvent Mixture.
Tanmoy Khan, Kuntal Debnath, Soumya Chaudhury, and Pratik Sen*

3. Solvation Dynamics through Steady-State Fluorimetry.
Nilimesh Das, **Tanmoy Khan**, and Pratik Sen*

4. Modulation of Associated Water Determines the Protein Stability in Hydrated Deep Eutectic Solvents.
Tanmoy Khan, Soumya Chaudhury, and Pratik Sen*

6. A Multi-Spectroscopic Study of Tanford Transition in β-Lactoglobulin.
Tanmoy Khan, Akash Rana, and Pratik Sen*